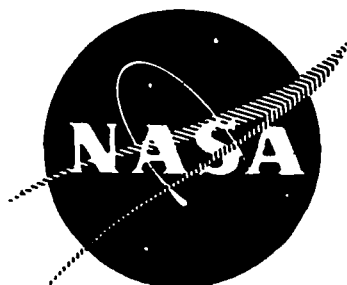


N 7 3 2 4 5 1 6

NASA CR-120976

R-9078



HIGH-PERFORMANCE SPACE SHUTTLE
AUXILIARY PROPELLANT VALVE PROGRAM

By
G. M. Smith

**CASE FILE
COPY**

ROCKETDYNE DIVISION
ROCKWELL INTERNATIONAL

prepared for
NATIONAL AERONAUTICS AND SPACE ADMINISTRATION

NASA-Lewis Research Center
NAS3-14350
Rudy E. Grey, Project Manager

NOTICE

This report was prepared as an account of Government-sponsored work. Neither the United States, nor the National Aeronautics and Space Administration (NASA), nor any person acting on behalf of NASA:

- A. Makes any warranty of representation, expressed or implied, with respect to the accuracy, completeness, or usefulness of the information contained in this report, or that the use of any information, apparatus, method, or process disclosed in this report may not infringe privately-owned rights; or
- B. Assumes any liabilities with respect to the use of, or for damages resulting from the use of, any information, apparatus, method or process disclosed in this report.

As used above, "person acting on behalf of NASA" includes any employee or contractor of NASA, or employee of such contractor, to the extent that such employee or contractor of NASA or employee of such contractor prepares, disseminates, or provides access to any information pursuant to his employment or contract with NASA, or his employment with such contractor.

Requests for copies of this report should be referred to

National Aeronautics and Space Administration
Scientific and Technical Information Facility
P.O. Box 33
College Park, Md. 20740

1 Report No NASA CR-120976	2 Government Accession No	3 Recipient's Catalog No	
4 Title and Subtitle HIGH-PERFORMANCE SPACE SHUTTLE AUXILIARY PROPELLANT VALVE PROGRAM		5 Report Date June 1973	
		6 Performing Organization Code	
7 Author(s) G. M. Smith		8 Performing Organization Report No R-9078	
9 Performing Organization Name and Address Rocketdyne Division, Rockwell International Canoga Park, California 91304		10 Work Unit No	
		11 Contract or Grant No NAS3-14350	
12 Sponsoring Agency Name and Address National Aeronautics and Space Administration Washington, D. C. 20546		13 Type of Report and Period Covered Contractor Report	
		14 Sponsoring Agency Code	
15 Supplementary Notes Project Manager, Rudy E. Grey, NASA-Lewis Research Center, Cleveland, Ohio			
16 Abstract Several potential valve closures for the space shuttle auxiliary propulsion system (SS/APS) have been investigated analytically and experimentally in a modeling program. The most promising of these were analyzed and experimentally evaluated in a full-size functional valve test fixture of novel design. The engineering investigations conducted for both model and scale evaluations of the SS/APS valve closures and functional valve fixture are described. Preliminary designs, laboratory tests, and overall valve test fixture designs are presented, and a final recommended flightweight SS/APS valve design is presented.			
17 Key Words (Suggested by Author(s)) Valve Closures Long Life Fast Response Low Leakage		18 Distribution Statement	
19 Security Classif (of this report) Unclassified	20 Security Classif (of this page) Unclassified	21 No of Pages 326	22 Price*

Page Intentionally Left Blank

CONTENTS

<u>Introduction</u>	3
<u>SS/APS Valves Program</u>	5
<u>Analysis and Conceptual Design</u>	5
Trade Study	5
Analytical Leakage Model	17
<u>Sealing Closure Screening Tests</u>	47
Sealing Closures	47
Closure Screening Tester	52
Testing	71
Test Results	89
<u>Valve Test Fixture</u>	129
Objective	129
Valve Preliminary Design	129
Fabrication	144
Testing	149
<u>Discussion of Results</u>	181
Introduction	181
Sealing Closures Results	181
Test Fixture Results	184
Flightweight Design	187
<u>Conclusions and Recommendations</u>	197
<u>References</u>	201
<u>Appendix A</u>	
APS Valve Closure Concepts - Model Layouts	203
<u>Appendix B</u>	
Simplified Description of Closure Screening Tester Operation	213
<u>Appendix C</u>	
Laminar Flow Leakage Correlation	219
<u>Appendix D</u>	
Valve Size Tradeoffs	231
<u>Appendix E</u>	
Design and Static Analysis, Valve Concept No. 3	237
<u>Appendix F</u>	
DAP4H Analysis of Design Concepts No. 1, 2, and 3	251
<u>Appendix G</u>	
APS Valve Fixture Tolerances	293
<u>Appendix H</u>	
APS Pilot Valve Design	297
<u>Appendix I</u>	
New Technology	303
<u>Appendix J</u>	
Distribution List (NAS3-14390)	315

Page Intentionally Left Blank

ABSTRACT

Several potential valve closures for the space shuttle auxiliary propulsion system (SS/APS) have been investigated analytically and experimentally in a modeling program. The most promising of these were analyzed and experimentally evaluated in a full-size functional valve test fixture of novel design.

The engineering investigations conducted for both model and scale evaluations of the SS/APS valve closures and functional valve fixture are described. Preliminary designs, laboratory tests, and overall valve test fixture designs are presented, and a final recommended flightweight SS/APS valve design is presented.

SUMMARY

The proposed use of hydrogen and oxygen propellants in the Space Shuttle Auxiliary Propulsion System (SS/APS) established unique requirements for low-leakage, fast-response, long-life shutoff valves. With as many as 50 thrusters to be ignited rapidly (<0.050 second), and reliably up to 1×10^6 times with zero or minimum maintenance, a novel approach in valve closures and mechanisms was required to satisfy the mission requirements of the space shuttle vehicle.

On 15 September 1970, Rocketdyne initiated an analytical experimental program aimed at developing SS/APS valve closures and valve designs capable of meeting the mission requirements. The objective of this program was to develop and demonstrate design criteria for the flight-type gaseous hydrogen-gaseous oxygen propellant shutoff valves which would be utilized on the SS/APS thrusters, and to complete design layouts of flightweight valves based on program results.

The program was comprised of five basic tasks: Task I - Valve Subcomponent Analysis and Conceptual Design; Task II - Valve Preliminary Design; Task III - Fabrication and Testing; A. Sealing Closure Screening, B. Valve Subcomponent Evaluation; Task IV - Valve Design; and Task V - Extended Valve Cycle Testing. Interrelationships of these tasks resulted in the program being performed in three distinct phases: Analysis and Conceptual Design, Sealing Closure Screening Tests, and Valve Test Fixture Evaluation.

Analysis and Conceptual Design was initiated with a thorough review of the SS/APS valves design requirements and a trade study of basic valve types to determine the best approach. These studies identified a poppet-type valve as the most feasible approach to satisfy the SS/APS mission requirements. Drawing upon Rocketdyne's extensive valve closure programs with the Air Force Rocket Propulsion Laboratory (AFRPL), six model valve closures were analyzed and designed which would be applicable to poppet-type valves. These model closures utilized a flat 440C poppet on flat 440C seat, flat gold seat, grooved gold seat, captive plastic seat, then flat carbide poppet on sharp carbide seat, and 440C nose poppet on beryllium copper disk seat. In addition, a unique closure screening tester was analyzed and designed to allow testing of the model closures. This tester allows three controlled modes of closing the poppet and seat: clamped (parallel), clamshell (hinge-type closing), and scrubbing (lateral motion at poppet-seat interface).

Upon completion of fabrication of the closure screening tester and the model closures, an extensive series of sealing closure screening tests was performed. The various closures mentioned above were subjected to tests with controlled impact loads, cyclic rates, and precise interfacial motions. Over 23×10^6 cycles of operation were accumulated during the entire series. The flat 440C poppet on the captive plastic seat (captive plastic closure concept) and the flat carbide poppet on sharp carbide seat (hard-sharp carbide closure concept) proved to be the most durable, best performing closures, the others having been incapable of meeting the leakage specification limit for 1×10^6 cycle life. These two concepts were chosen for analysis, design, and fabrication into full-size SS/APS valve closures. The closures were designed for use in the full-size SS/APS valve test fixture which evolved from the concept established in the early conceptual design phase.

The SS/APS valve test fixture, a 90-degree piloted poppet valve using propellant gas to operate, was subjected to initial contract testing (140,000 cycles) with the result that the captive plastic closure concept proved that it could meet the low leakage requirement of less than 0.102 scim (100 scc/hr) helium leakage at 450 psia (310.3 N/cm²) and 200 R (111 K). The hard-sharp carbide closure concept failed due to overstressing as a result of rapid valve closing to meet required valve actuation times (<30 milliseconds, signal to open, or signal to close). The SS/APS valve test fixture and the captive plastic closure were then subjected to an additional 900,000 cycles of testing. The final closure leakage was 0.001 scim (0.98 scc/hr) helium at 450 psia (310.3 N/cm²) and 530 R (294 K).

A flightweight design layout was produced of a valve identical in features and operation to that tested. It has been trimmed for weight reduction, and repackaged slightly to overcome some deficiencies discovered in the valve test fixture. The basic program objectives were met. The feasibility of a SS/APS valve for 1×10^6 cycles with low leakage has been demonstrated. The captive plastic closure was evaluated and demonstrated long life with leakage several orders of magnitude lower than conventional valve closures in use on today's rocket engine systems.

INTRODUCTION

The selection of gaseous hydrogen and gaseous oxygen propellants for the SS/APS presented a unique challenge to advance the state of the art in valve design. Never had valves of the size required been asked to actuate in less than 30 milliseconds, last 1×10^6 cycles, and leak less than 100 scc/Hr helium at minimum temperature and maximum inlet pressure throughout their entire life. The program discussed in this report concentrates on valves for the SS/APS thrusters, although the technology obtained can be applied more extensively. The purpose of the program was to advance, by means of analyses, design, and evaluations, the state of the art in valves and valve closures so that SS/APS thruster valves fully meeting the space shuttle mission requirements could be designed, fabricated, and delivered when the need arises.

At the initiation of this program, both high-pressure and low-pressure SS/APS systems were being considered and valve concepts for each system were being investigated. Later, the high-pressure system was selected and all efforts were then concentrated in meeting this requirement. However, the low-pressure valve was concluded with the preliminary design based on work completed to that point.

The auxiliary propulsion systems of previous vehicles used cold-gas systems, monopropellants, or hypergolic bipropellant systems, with valves of limited life capability. Larger pump-fed engines using liquid oxygen and hydrogen utilize valves of limited life and moderately low leakage performance. However, the fast-response requirements, extremely low allowable leakages, longer life requirements, and the problems of weight and power consumption dictated the investigation of new concepts for satisfaction of the SS/APS requirements.

During a series of Air Force contracts with Air Force Rocket Propulsion Laboratory (AFRPL), Rocketdyne had completed investigations into the field of low-leakage valve closures. In addition, early work with the captive plastic closure concept had been performed by its inventor at the Rocketdyne field laboratories. It was from these early works that the current contract effort extended the technology which has been investigated and demonstrated. The purpose of this report is to document the effort conducted during the performance of this contract.

The sequence of the program is illustrated in Fig. 1. The initial effort consisted of analysis and conceptual design to establish program direction and approach by means of selection of a valve type and closure concepts for evaluation. The closures selected were screened in the second phase of the program using a unique tester. Finally, in phase three of the program, the selected closure concepts (captive plastic and hard-sharp carbide) were mated with the valve test fixture to prove the program designs and analysis.

Appendix A through H give various design or analytical details performed during the program and are introduced in the main text as appropriate. Appendix J presents the New Technology Items developed during the performance of the program.

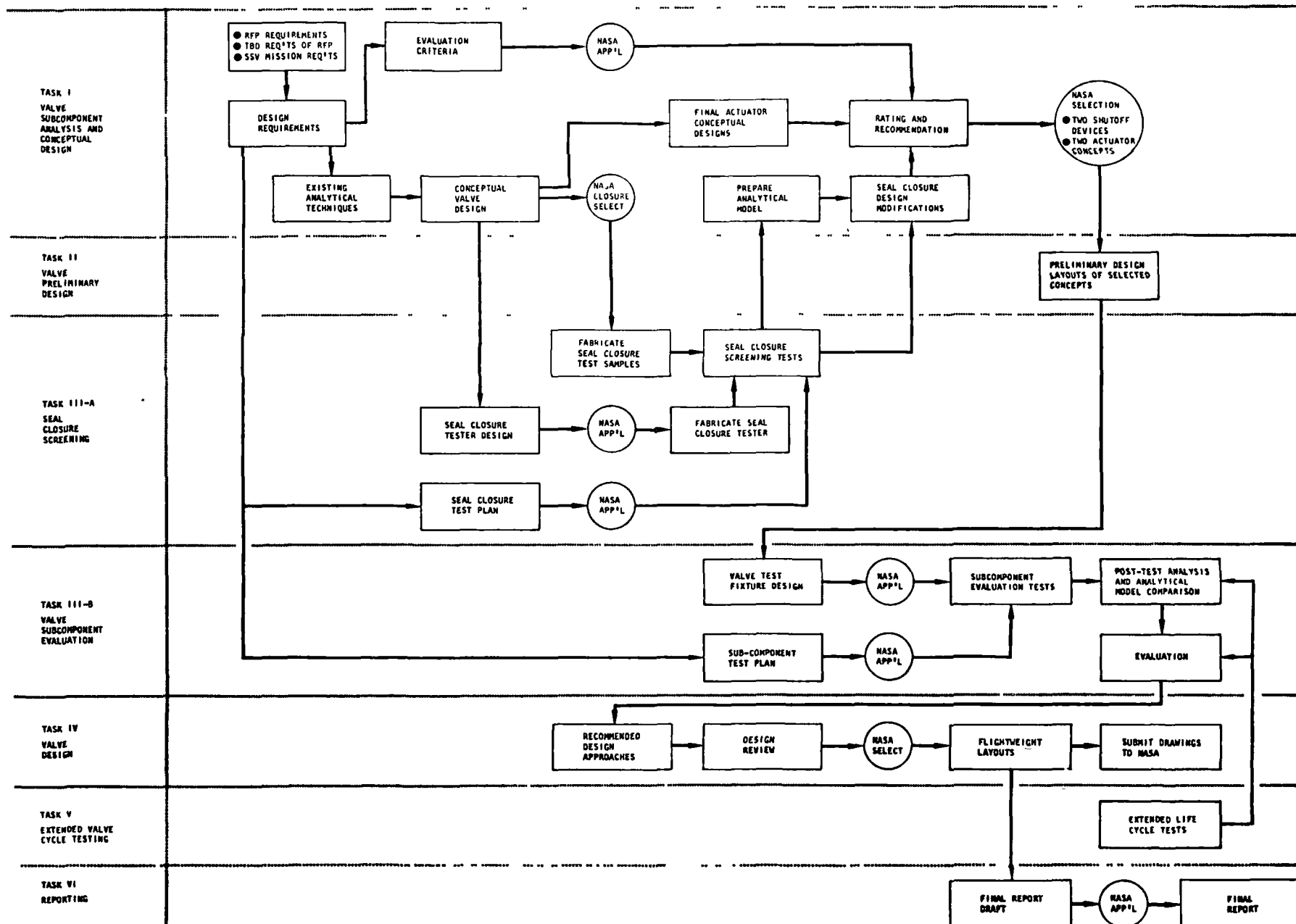


Figure 1. Logic Flow Diagram

SS/APS VALVES PROGRAM

ANALYSIS AND CONCEPTUAL DESIGN

The design requirements of Table I established the need for: (1) basic valve mechanism and closure concept studies and (2) an initial valve design trade study from which the contract effort would draw its direction. Based on these results, model closure concepts were analyzed and designed along with a unique closure screening tester to enable an evaluation of merit of the various closure concepts. These initial analyses and conceptual designs, then, pointed the way for a logical progression of effort toward the final program objectives: SS/APS lightweight valve design.

TRADE STUDY

Valving Concepts Study

A trade study covering past and potential performance of closures, actuators, seals, and other related supporting parts was initially a major item of effort. The trade study used the design requirements of Table I on a "no exceptions" basis to establish evaluation criteria for use in review of the various concepts. These criteria consisted of primary criteria selected on the basis of fundamental requirements, avoiding specific constraints that would limit the scope of a preliminary trade study. Secondary criteria were compiled on the basis of hardware and operational considerations for a more refined screening of candidate design concepts. Design concepts reviewed were listed in broad categories of single poppet valves, single rotary valves, miscellaneous valves, and bipropellant valves.

The actual valving types considered in the trade study are shown in Table II, with corresponding actuation concepts shown in Table III. Conventional butterfly, ball, and blade valves could not meet the long-life, low-leakage requirements because of seal wear factors. The diaphragm materials available would not meet the temperature requirements, and the spool valve basically will leak too much to be considered. Electric motors for the size and response required are too cumbersome and heavy and a direct solenoid of the size needed is not feasible from power, weight, and response considerations.

The question of monopropellant versus bipropellant valves was then considered. In any discussion of linked bipropellant and monopropellant valves, one of the primary topics involves weight of the respective valves. Typically, a bipropellant valve assembly will weigh less than two monopropellant valves for the same service. An immediate reduction in complexity and weight is achieved with a linked bipropellant valve since it uses a single pilot valve, a single housing, a single actuator, and a single position indicator, as opposed to two each for two monopropellant valves. For fast-response hydrogen and oxygen service, a bipropellant valve will use hydrogen for actuation, the pilot being intermediate in size between a pilot for a hydrogen monopropellant valve and a pilot for an oxygen monopropellant valve. Additionally, a bipropellant valve, even with its mechanical linkage, will represent fewer total parts than two monopropellant valves.

TABLE I - DESIGN REQUIREMENTS

Valve Type	Single or bipropellant
Propellants	Hydrogen (1) Oxygen (2)
Operating Temperature Range	200 to 850 R (111 to 472 K)
Propellant Temperature Range	
Hydrogen	200 to 800 R (111 to 444.5 K)
Oxygen	250 to 800 R (139 to 444.5 K)
Propellant Pressures at Valve Inlet	
High-Pressure System	400 \pm 50 psia (276 \pm 34.5 N/cm ²)
Low-Pressure System	20 \pm 5 psia (13.8 \pm 3.5 N/cm ²)
Pressure Drop (Maximums).	
High Pressure	
Fuel	5 psi at 0.69 lb/sec and 540 R (3.5 N/cm ² at 0.313 kg/sec and 300 K)
Oxidizer	5 psi at 2.76 lb/sec and 540 R (3.5 N/cm ² at 1.25 kg/sec and 300 K)
Low Pressure	
Fuel	1 psi at 1.14 lb/sec and 540 R (0.69 N/cm ² at 0.52 kg/sec and 300 K)
Oxidizer	1 psi at 2.86 lb/sec and 540 R (0.69 N/cm ² at 1.3 kg/sec and 300 K)
Actuation Requirements	
Pneumatic Pressure	TBD (to be determined)
Hydraulic	TBD
Electrical	TBD
Opening and Closing Response	Total time (delay and travel) from signal to end of motion = 30 milliseconds maximum Travel (motion) = 15 milliseconds maximum
Internal Leakage	0.102 scim (100 scc/hr) with gaseous helium at operating pressure and temperature per items 4 and 5
External Leakage	3.66 x 10 ⁻⁶ scim (1 x 10 ⁻⁶ scc/sec) with gaseous helium at operating pressures and temperature
Operating Life (Goal)	1,000,000 cycles
Environmental Conditions	
Vibration	TBD
Acceleration Loads	TBD
Acoustic	TBD
Maintenance - There shall be no maintenance of components during the design life period	
Size and Weight - Design to minimum	
Proof Pressure - 1.5 times operating pressure	
Burst Pressure - 1.33 times proof pressure	
Failure Criteria - The valve shall fail-safe close under normal operating conditions	
Gaseous hydrogen derived from the vaporization of liquid hydrogen per MIL-P-27201	
Gaseous oxygen derived from the vaporization of liquid oxygen per MIL-P-25508A	

TABLE II - VALVE CONCEPTS

- Butterfly
- Ball
- Blade
- Butterfly or Ball
(Retracting Seat)
- Poppet
- Diaphragm
- Spool

TABLE III - ACTUATION CONCEPTS

- Electric Motor
- Direct Solenoid
- Hydraulic
- Pneumatic (Helium)
- Pneumatic (Propellant)

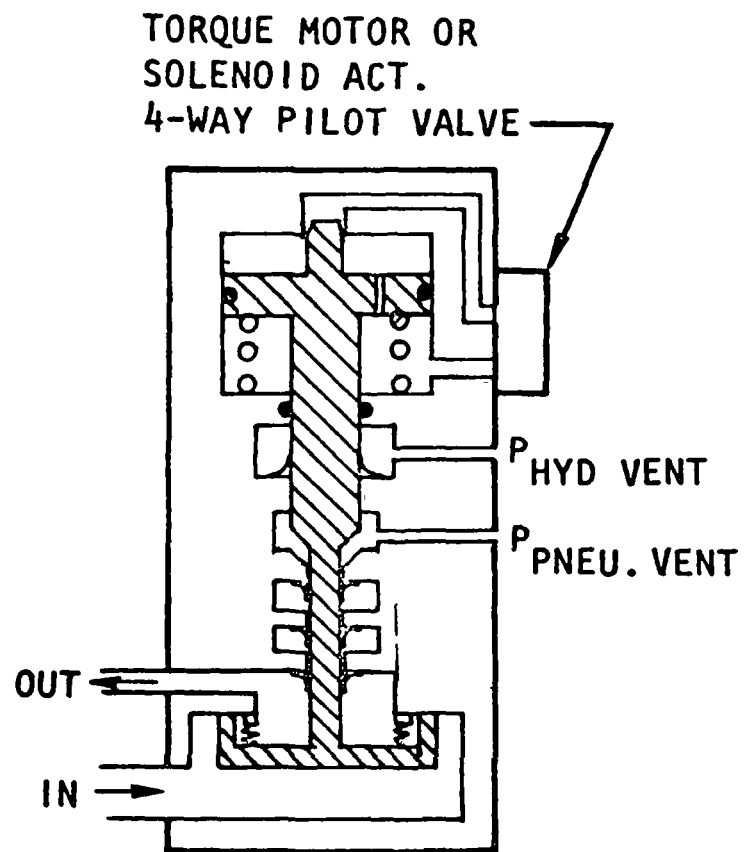
These considerations also lead to some other conclusions. Replacement of a single valve can be accomplished with a monopropellant valve configuration, so that a single valve failure replacement is simple. However, the bipropellant valve with its single pilot, indicator, and housing represents a simple installation from a total valve standpoint.

Sequencing of propellants is another important area of consideration. The bipropellant valve, due to its mechanical linkage, provides *positive* propellant sequencing. This is not possible with two independently actuated monopropellant valves. For propellant-actuated monopropellant valves, timing of one valve relative to the other will vary if propellant temperatures vary with respect to each other. Monopropellant valves, therefore, require thermal compensation to maintain timing; even so, this does not ensure *positive* sequencing as achieved with a linked bipropellant valve.

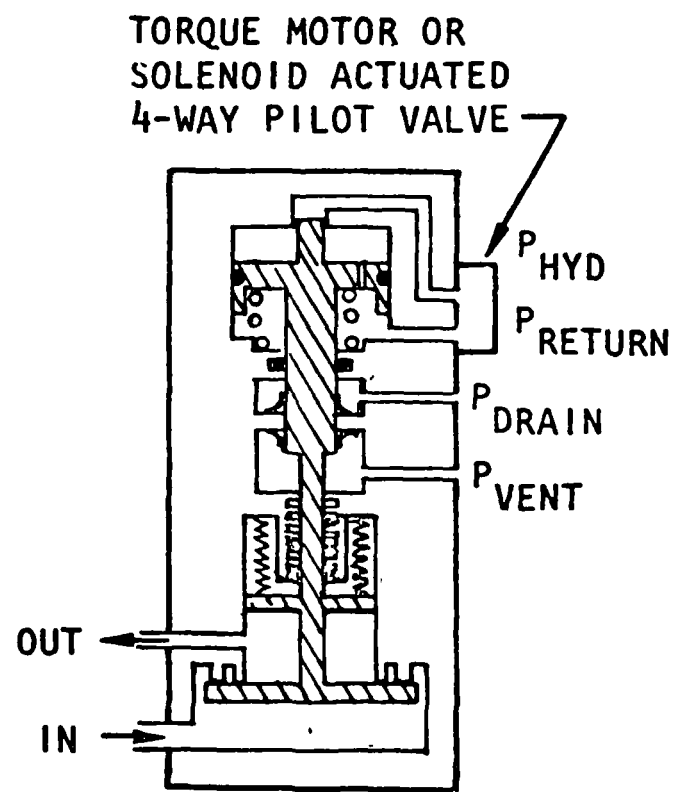
Monopropellant valves can accommodate a gross change of fuel or oxidizer lead or lag; the bipropellant valve is much less flexible. The most important aspect of the entire sequencing discussion, however, is the fact that *positive* mechanical linking of a bipropellant valve precludes thruster damage or destructive due to delay or fail to open of one of the propellant valves. In addition, the linked bipropellant valve will produce the optimum integrated mixture ratio for pulse performance, giving better pulse performance with less total propellant consumption.

Only certain concepts of monopropellant valves require bellows, diaphragms, or dynamic seals for operation. However, a linked bipropellant valve of any design will require a bellows or a zero leak dynamic shaft seal to achieve positive propellant isolation for explosion safety. For long-life capability, considerably more bellows technology effort will be required to ensure a reliable bipropellant valve design. In addition to the problem of propellant isolation for explosion safety, thermal isolation must be maintained between gaseous hydrogen and gaseous oxygen propellants since cold gaseous hydrogen in near proximity to gaseous oxygen would result in liquefaction of a portion of the gaseous oxygen. This condition would be extremely hazardous at thruster startup.

Because of the problems associated with propellant isolation and bellows technology, the "no exceptions" approach to the APS design requirements favored an hydraulically actuated poppet valve design concept with flat metal-to-metal closure seat-seal for the high-pressure system, while an hydraulically actuated valve with radial-arc displacement, a flexible metal seal, and metal seat was favored for the low-pressure system. The favored concepts are shown in Fig. 2 and 3, respectively.



(a)



(b)

Figure 2. Preliminary High-Pressure Trade Study Configurations

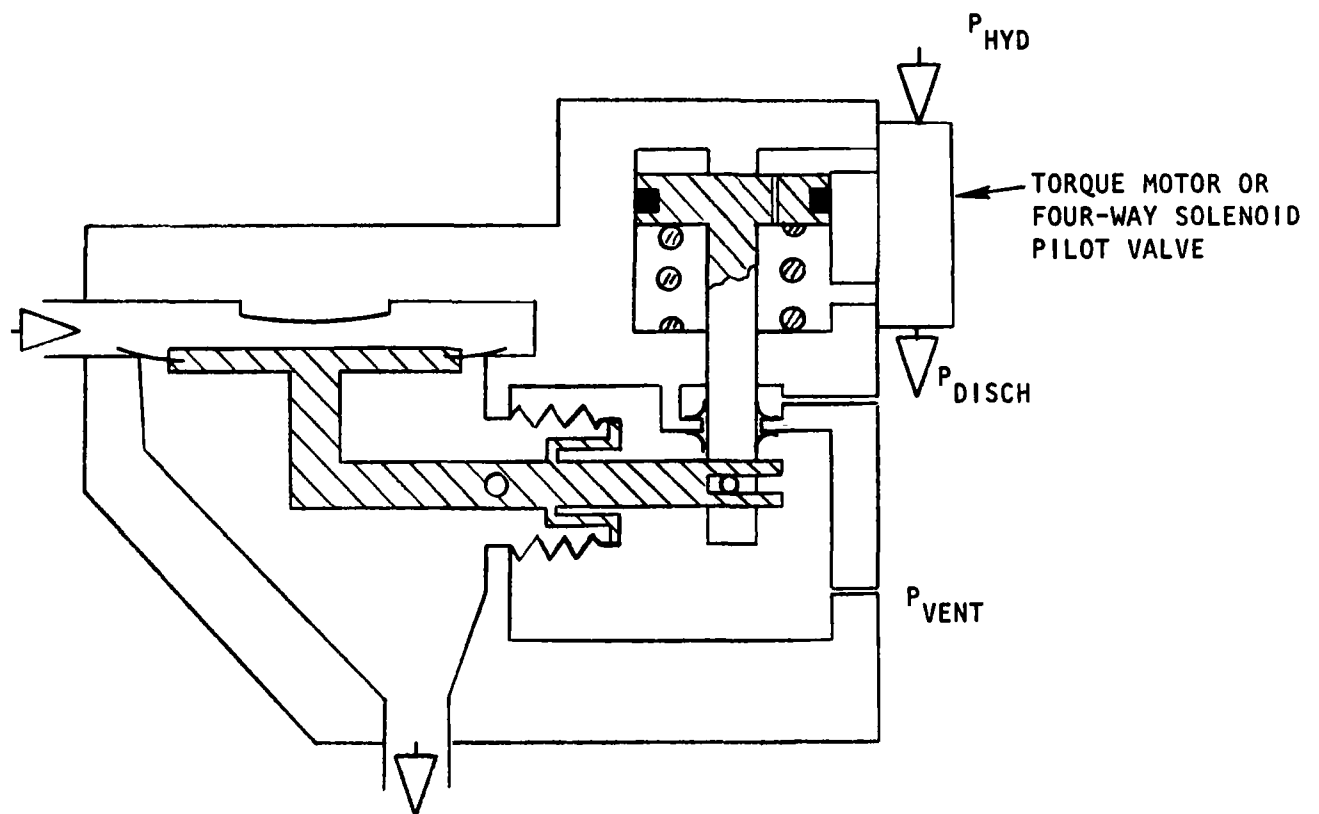


Figure 3. Preliminary Low-Pressure Trade Study Configuration

The design concept shown schematically in Fig. 2b has the same hydraulic actuator and impact-snubbing features as the concept of Fig. 2a. With the valve in or near its closed position, a contoured pintle attached to the actuator piston restricts the flow passage between the opening side of the piston and the pilot valve. When the main valve is beginning to open, or when it is approaching its seat during a closing transient, the restricted flow passage limits the hydraulic fluid volumetric displacement and, consequently, limits the initial valve-opening velocity as well as the valve-closing impact velocity against the poppet seat and mechanical stop.

The velocity-snubbing features at and near each end of the valve stroke do not impede the attainment of high velocities at intermediate valve displacements, as required for satisfying the response-timing requirements. The poppet stem dynamic seal is a metal bellows with an all-metal labyrinth seal for redundancy. The flat-faced poppet seat has an inner annular surface for sealing and an outer annular surface for absorbing impact energy.

Poppet valve full stroke is limited by a piston displacement stop in the hydraulic actuator. When the piston is at or near full stroke, the piston skirt restricts the pilot valve flow passage in the cylinder wall to restrict hydraulic fluid flow and, consequently, limit piston displacement velocity. The piston mechanical stop can be designed with a relatively large contact surface area and high impact momentum absorption capacity, compared to the poppet and seat, and can be designed so that minor deformation at the stop does not impair actuator functional integrity. Velocity snubbing is, therefore, less critical in the opening direction than in the closing direction, and less precision is required for opening impact velocity control.

Use of a contoured pintle attached to the piston, for impact velocity snubbing when the valve is closing, provides for adequate precision in closing-velocity contouring for as great a percentage of the piston full stroke as is required in obtaining full stroke within 0.015 second but with the slowest obtainable poppet-to-seat impact velocity.

Use of a high-pressure hydraulic operating fluid and a double-acting piston actuator contributes to minimizing the mass of the moving parts to minimize impact momentum, and contributes to precise control of velocity profiles in both directions of motion. The load stiffness and dashpot damping characteristics inherent in hydraulic actuators minimize rebound and repeated contact at the poppet closure seal.

When propellant inlet pressure is applied, it acts against the poppet seat cross section to increase the net closing force. Maximum poppet seat stress for sealing is obtained at maximum inlet pressure. As the valve begins to open and flow, the resulting increase in outlet pressure acts on the differential between seat cross-section area and bellows seal effective area to supply an opening force that increases as valve displacement increases. This regenerative-force assisting actuation ensures positive, continuous, chatter-free stroking in the presence of dynamic flow forces. As the valve begins to close, and outlet flow is throttled by the poppet, the reduction in outlet pressure decreases the net force opposing deactuation, and smooth closing is ensured.

During tests and checkouts with inlet pressures not applied, propellant pressure regenerative forces are not present, and the hydraulic differential pressure acting on the piston is different during checkouts from what it is during system operation. However, with hydraulic actuation, the piston can be sized to minimize variations in piston differential pressure related to variations in seal friction and to temperature-related variations in mechanical spring rates. Variations in response timing and in impact momentum can thereby be minimized throughout the full envelope of test and operating conditions.

The poppet valve stem primary dynamic seal is an internally vented metal bellows. The bellows is shielded from direct impingement of valve effluent and from direct exposure to effluent turbulence by locating the bellows in a semi-enclosed cavity. Acting as the primary dynamic seal, the bellows provides for compliance with the program design requirement for essentially zero external leakage.

Because a bellows seal will be vulnerable to fatigue failure in a valve designed for 1,000,000 full-stroke, 0.015-second, on-off cycles in a not-yet-defined vibration environment, the poppet stem guide is designed as a secondary dynamic seal. The guide is shown schematically as a series of close-fitting lands with small intermediate gas expansion volumes. An alternate stem seal concept appears in Fig. 2a. Secondary seal design emphasis would be on long cycle-life with minimum leakage in the event of a bellows leakage failure.

As the stem dynamic seals are isolated from propellant inlet pressure, a primary stem seal leakage failure would result in closely limited leakage only when the valve is in operation. A seal leakage failure will not result in a valve operational failure.

Figure 2b illustrates a flat-faced, metal-to-metal poppet and seat with two concentric seat lands. Contact between the poppet and the inner land provides the closure seal. When the poppet is seated on the inner land, there is a few ten-thousandths of an inch clearance between the poppet and the outer land. When the valve is open and is stroking to the closed position, angularity between the plane of the poppet sealing surface and the plane of the inner seat land sealing surface results in impact at the seat outer land. The potential for sealing surface impact deformation or abrasion is thereby minimized. This poppet and seat concept places the design emphasis on poppet guiding to minimize scuffing of the poppet against the seat as seating occurs.

Figure 3 illustrates a design concept for an hydraulically actuated, normally closed shutoff valve with a closure seal designed for low pressure. Valve closure sealing is effected by an initially flat, thin, annular metal section, deflected in contact with a seat in the valve housing.

The actuator is isolated from the propellant flow path by a metal bellows dynamic seal attached to a pivoted rocket arm in the valve lifting mechanism. A relatively large-diameter, low-lift valve with radial-arc displacement is indicated.

When the valve is open and flowing, the bellows dynamic seal is pressurized internally. As bellows elements have lower allowable pressure differentials with the internal pressure higher than they do with the external pressure higher, the concept of Fig. 3 is more applicable to the low-pressure propellant system than it is to the high-pressure system.

Additionally, the valve closure-seal design concept is more applicable to the low-pressure propellant system than it is to the high-pressure system.

Relatively high actuation forces related to large valve sizes are accompanied by relatively low actuation velocities related to low valve lifts. Use of an hydraulic actuator provides for fast response with relatively high power levels, and impact velocity snubbing can be obtained.

When propellant inlet pressure is applied, it acts against the valving element to increase the closing force. Maximum closure-seal stress for sealing is obtained at maximum inlet pressure. As the valve begins to open and flow, the resulting pressure increase in the valve body cavity that is ported for outflow acts against the valving element in the opening direction. This supplemental force (as a function of displacement) ensures positive, continuous, chatter-free actuation. Similarly, when the valve is open and flowing and begins to close, throttling of the valve flow results in a displacement-related reduction in pressure force opposing closing, and smooth deactuation is ensured.

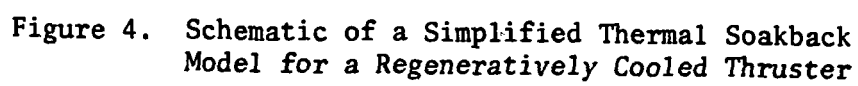
Because a bellows seal will be vulnerable to fatigue failure in a valve designed for 1,000,000, full-stroke, 0.015-second, on-off cycles in a not-yet-defined vibration environment, the vent cavity to which the bellows is exposed is designed for a restricted outflow. A bellows seal leakage failure will result in limited external leakage only when the valve is in operation. A seal-leakage failure will not result in a valve operational failure.

The actuator piston ring seal is for leakage deterrance only, and appreciable degradation of that seal is tolerable. Minor degradation of the piston rod seal with extensive cycling may be tolerable provided that the seal drain cavity and wiper seals are designed to prevent hydraulic leakage into the valve body vent cavity.

Heat Soakback and Venting

In order to ensure that the use of non-metallics in the valves was a safe approach, a thermal analysis of the thrusters was performed. A preliminary system soakback analysis was conducted for a typical thruster assembly to determine the transient temperature response of various components after shutdown. In particular, the effect of soakback to the fuel and oxidizer valves was studied using a simplified thermal model.

A simplified soakback model of the thruster assembly can be used advantageously for preliminary screening of valve-chamber-injector interaction. A typical schematic of such a simplified thermal model is shown in Fig. 4 for the double-wall, regeneratively cooled thruster concept.



In essence, the thruster assembly is represented by a nodal network comprised of the various components or subcomponents necessary to provide accurate soak-back temperature response results. In the selected simplified model, the thrust chamber is represented by the combustion-gas liner and outer shell. The injector is divided into face and body subcomponents and the igniter is also divided into hot-wall liner and outer body. Each of the valves is represented individually.

The thermal resistances between the various nodes (components) are calculated based on the relative geometries, wall thickness, and materials of the various components. In particular, the thermal resistance between the injector and valves can be readily varied to simulate the effects of close-coupled or stand-off valves on the resultant valve soakout temperatures.

The results of the analysis for close-mounted (but not integrated) valves are presented in Fig. 5, assuming a regeneratively cooled, double-wall thrust chamber. The hydrogen valve temperature increases about 100 F (311 K) within 1 hour after shutdown. The oxygen valve temperature increases about 70 F (294 K) in a similar time period. The primary heat input is from the thrust chamber hot-wall NARloy-Z liner, which is seen to cool down from its initial soakout value of 600 F (589 K) to -100 F (200 K) in 1 hour. The injector face plate also contributes to the head load to the valve. The initial temperatures at shutdown are based on nominal average steady-state operating temperatures of the various components.

It was apparent from this preliminary investigation that the magnitude of the soakback could be reduced by thermally isolating the chamber from the injector and/or by isolating the valves from the injector manifold. Studies into the impact of valve isolation were also made and showed very promising results. For this initial analysis, it was assumed that a 1-inch-long (2.54 cm), 0.5-inch (1.27 cm) -diameter steel bellows with 0.010-inch (0.0254 cm) wall thickness was integrated between the valve and injector body. The equivalent line length of the bellows was taken as 6 inches (15.24 cm). The resulting effective thermal resistance between valve and injector was about a factor of 100 higher than for the close-mounted valves.

The resulting soakback temperature response is presented in Fig. 6. It is apparent that in 6 hours (21,600 seconds), the hydrogen and oxygen valve temperature increases by only 15 and 10 F (264 and 261 K), respectively. Thus the use of non-metallics such as Teflon was considered a safe approach.

In the event that the gaseous propellants themselves would be used as the valve(s) actuating fluid, it was necessary to ensure that no adverse effects would occur as a result of venting those fluids. Initial investigation revolved around venting the propellant gas into a lower-pressure area on the thruster manifolds. However, this created the situation that as manifold pressure rose to near valve inlet pressures, a large valve actuator was needed to maintain force balances necessary for valve full-open conditions. In turn, these large actuators caused the response of the valves to be slowed by time-consuming venting and pressurizing of the larger actuator cavities. Computer studies with the DAP4H system (to be discussed later in this report) showed that

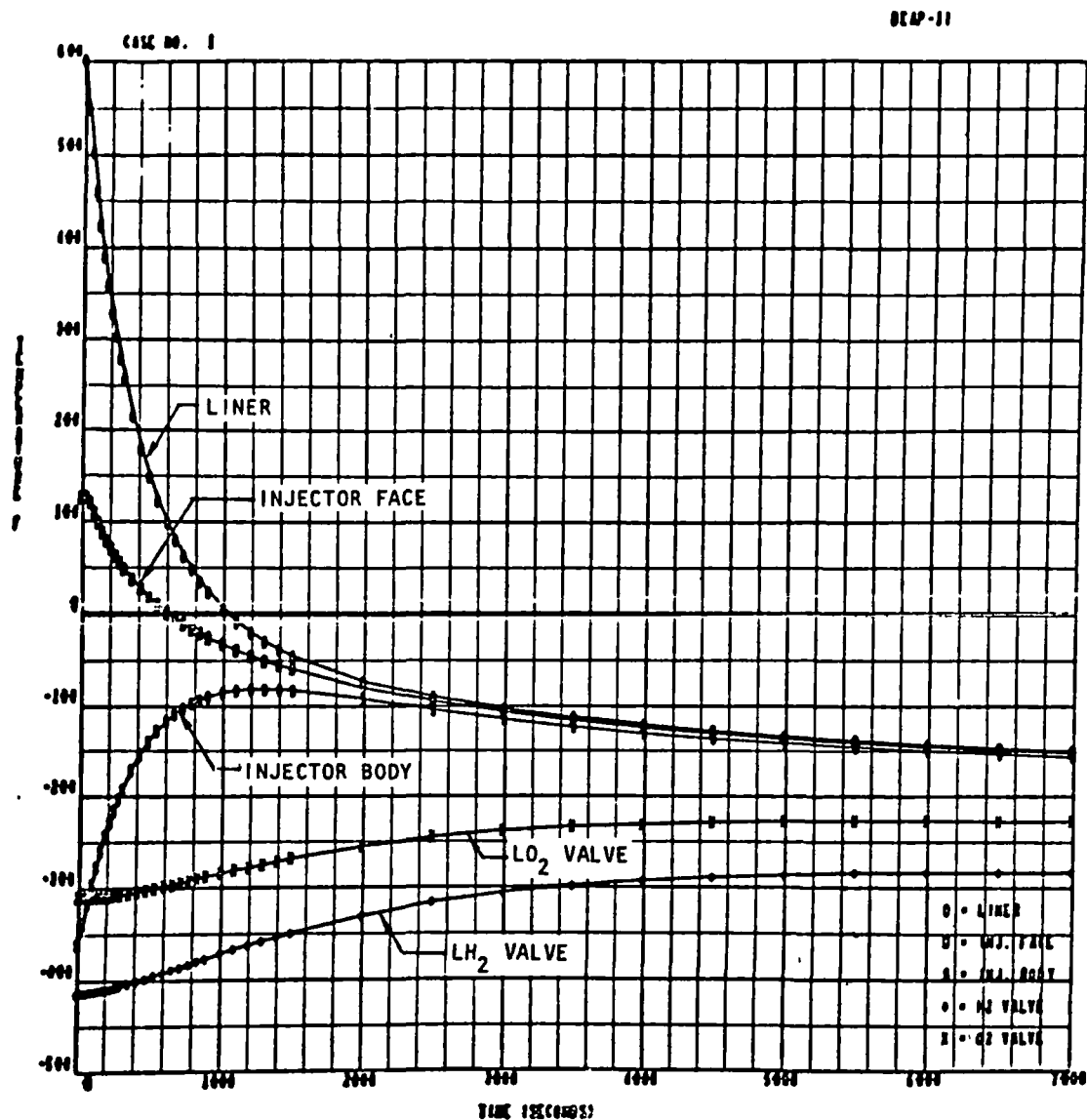


Figure 5. The Effect of Soakback on the Temperature of Various Thruster Components (Close-Mounted Valves)

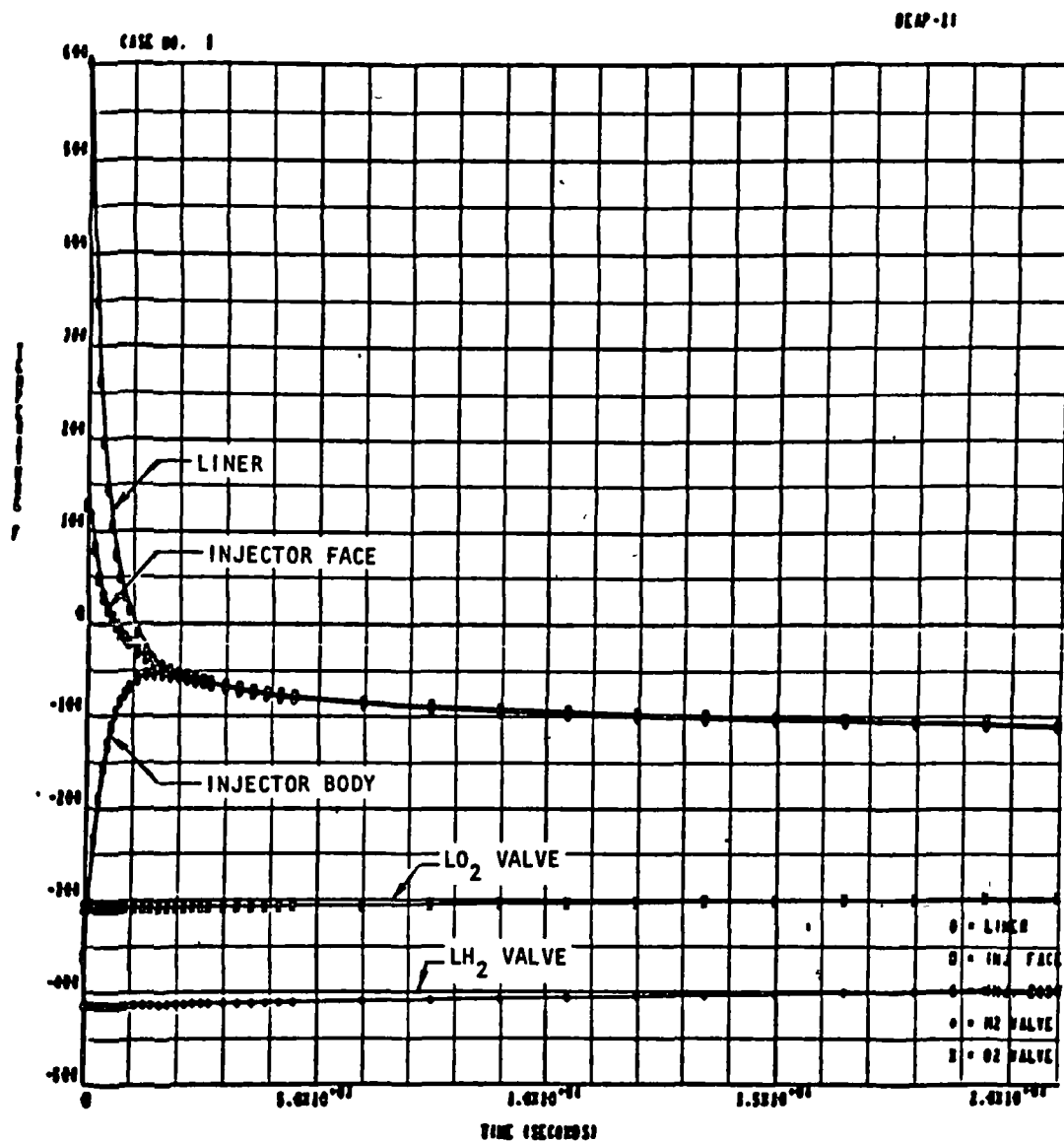


Figure 6. The Effect of Soakback on the Temperature of Various Thruster Components (Standoff Valves)

sonic nozzles could be incorporated into the injector just downstream of the valves, giving a low-pressure area for actuation gas venting, and also giving good pressure recovery for proper injection pressures. Thus, the valve actuators were not required to be so large, and response could be met. Venting into the respective propellant ducts prevents the hazardous situation of possible mixing of propellants. Thus, it was determined that on any flighweight engine, this approach could be used successfully.

ANALYTICAL LEAKAGE MODEL

Leakage past valve seats results from a combination of leakage paths consisting of surface roughness, surface flaws (scratches, nodules, etc.), deviation from pure geometrical surfaces (e.g., flat, sphere, cone) and non-conformance between sealing lands due to entrapped contamination, unsymmetrical loading, or warpage from temperature change or stress. Some of these factors can be analytically treated by comparison of measured and predicted leakage for idealized models. The value in this approach is that sealing performance can be related to specific causes through surface inspection tracers and microscopic examination using interference techniques. Relating cause and effect thereby provides the basis for design modification and improvement.

A variety of valve poppet and seat configurations have been tested and results correlated with measured surface conditions (Ref. 1 through 4 and 6). For aerospace applications, leakage is in the laminar-molecular range with surface roughness for metal-to-metal closures less than 2 microinches AA (5.08×10^{-6} cm). Even with entrapped solid particles causing sealing land separation, leakage is laminar except for contaminants normally termed "foreign objects." Significant variation from expected leakage can usually be traced to one or more of the aforementioned causes for increased gap.

Several attempts have been made to provide a theoretical basis to relate valve seat load with leakage (Ref. 1, 6, and 7). While allowing a better understanding of the problem, these attempts have failed because there is not a sufficiently accurate means to measure the myriad "real world" surface and geometrical features and, even if they could be measured, the strain interaction between these features would require a costly three-dimensional finite element stress analysis. Wear-related surface changes present an even more complex problem because existing wear data are not related to surface texture (Ref. 8). Consequently, each valve seat of a type or configuration must be load-leakage tested and cycled to characterize its performance. With multiple tests to establish a mean or normal condition, the correlation of leakage with geometry, before and after specific tests, will provide a basis to define overall limitations and capabilities.

The following paragraphs present a general discussion of valve seat geometry and means for predicting leakage through various flaws. The flow equations are presented with a typical example and the section is concluded with flow curves of theoretical model seat leakage versus gap, or height.

Nomenclature

Nomenclature used in subsequent discussion and analyses is as follows:

A	= area, sq in.
C	= discharge coefficient
D	= hydraulic diameter, inches
D _e	= effective pressure balance diameter
D _s	= mean seat diameter
f	= friction coefficient
g	= gravitational acceleration constant, 1.39×10^6 in./min ² (3.5306×10^6 cm/min ²)
h _o	= taper height, inches
h _e	= equivalent parallel plate channel height, inches
h _p	= parallel plate channel height, inches
k	= ratio of specific heats
L or X	= channel length, inches
M	= entrance Mach number
P	= static pressure, psia
Q	= volumetric flow at standard conditions of temperature (T _s = 530 R, 294 K) and pressure (P _s = 14.7 psia, 10.13 N/cm ²), in. ³ /min, or for compressible flow, scim
R _i	= inside diameter, inches
R _o	= outside diameter, inches
R	= gas constant, in./R
Re	= Reynolds number
T	= static temperature, R
V	= velocity, in./min
W	= channel width or perimeter, inches

Greek Symbols

ω	= weight flowrate, lb/min
μ	= viscosity, lb-min/in. ²
ρ	= density, lb/in. ³
λ'	= mean molecular free path, inches
β	= pressure profile factor

Subscripts

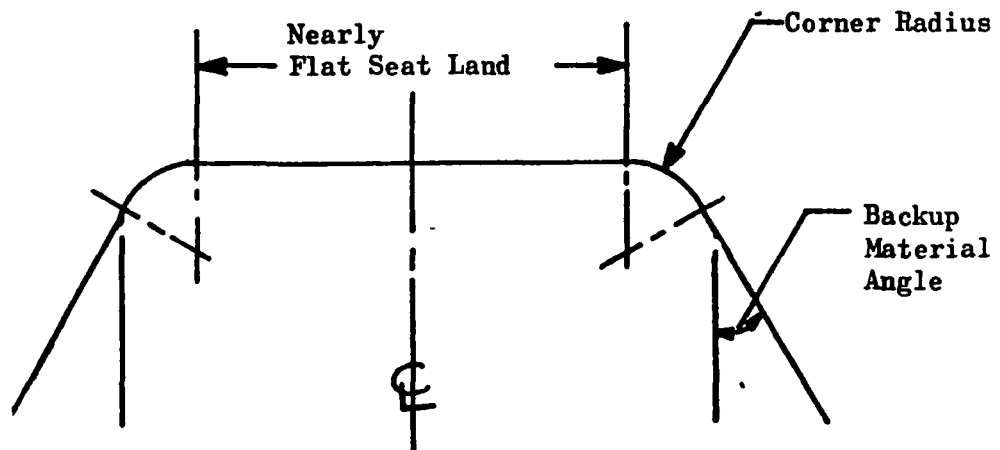
- 1 = inlet or entrance conditions
- 2 = outlet or discharge conditions
- o = stagnation conditions
- s = standard conditions
- i = incompressible
- c = compressible

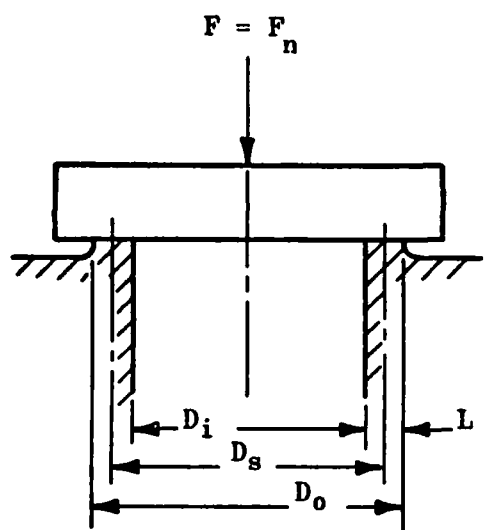
Geometry of Valve Seating

The performance of a valve seat is intimately related to the geometrical configuration of the seating surfaces. While a large variety of configurations are employed, the fundamental flat, conical, and spherical geometries can be identified in most cases. This stems from the simplicity of these shapes which are attendant with natural fabrication processes. The three configurations are shown in Fig. 7 with the parameters and equations combining basic geometry and load for the definition of apparent seat stress (S).

Superimposed upon real valve seating surfaces is a variety of other smaller geometries which often have a greater influence on the closure than the more obvious gross configuration. Most apparent is surface texture which includes the machining errors of roughness, waviness, pits, nodules, and scratches. However, often overlooked and of more subtle influence is the geometry of the seat land. While a seat land may be specified by engineering drawing or fabrication process, perfect conformability of mating surfaces is impossible and deviations are difficult to define or prove precisely; hence, the actual contact dimensions may be quite different than planned and also may change with seat load. Because leakage is inversely dependent upon real contact land dimensions, it follows that variation of these dimensions will also have an effect on leakage.

Land geometry is identical in cross section for the flat and conical configurations. For spherical seating, the only difference is the definition of a land width on a curved surface which is usually narrow; thus, except for this one difference, the seat land is the same for all three configurations. The land, which may be on the seat, poppet or both, is composed of three basic parts as illustrated below:



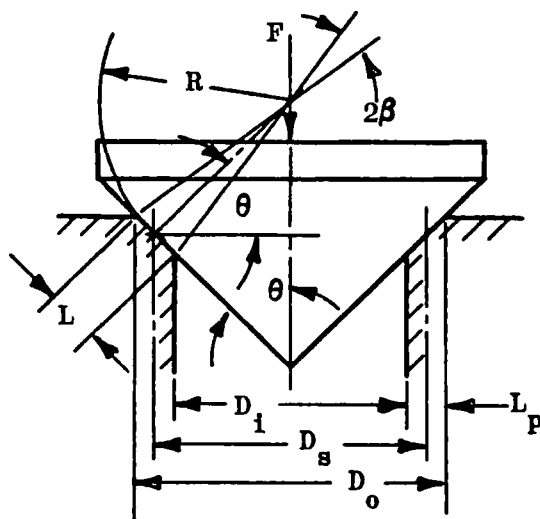


$$L = 1/2 (D_o - D_i)$$

$$D_s = 1/2 (D_o + D_i) = D_i + L$$

$$A_s = \pi D_s L$$

$$S \equiv \frac{F}{A_s} \equiv \frac{F}{\pi D_s L}$$



$$L_p = 1/2 (D_o - D_i) = L \sin \theta$$

$$L = 2R \tan \theta \approx 2\beta R$$

$$D_s = D_i + L_p$$

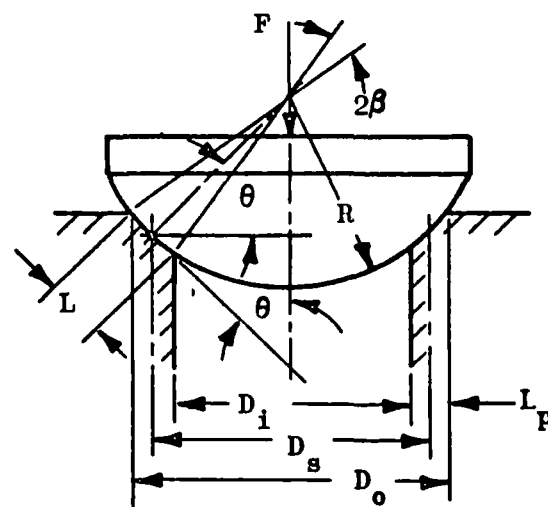
$$A_s = \pi D_s L$$

$$A_{sp} = \pi D_s L_p$$

$$F_n = F / \sin \theta$$

$$F_r = F / \tan \theta$$

$$S \equiv \frac{F}{A_{sp}} \equiv \frac{F_n}{A_s}$$



$$L = 2\beta R$$

$$L_p = 1/2 (D_o - D_i) \approx L \sin \theta$$

$$D_s = 2R \cos \theta$$

$$A_s = \pi D_s L$$

$$A_{sp} = \pi D_s L_p$$

$$S \equiv \frac{F_n}{A_s} \equiv \frac{F}{A_{sp}}$$

Figure 7. Flat, Conical, and Spherical Seating Equations

Each of these parts may take many forms and combinations too numerous to depict. The backup material angle on most flat seats is zero (but may approach 90 degrees) whereas for 45-degree conical or spherical seating, it is normally 45 degrees (but also may approach 90 degrees). The "flat land" may be flat, concave, or convex with symmetry near its own centerline or to the seat diameter. Corner radii also vary over a considerable range from a mere ragged discontinuity formed by intersecting surface roughnesses to the opposite extreme of a complete sphere (ball in cone).

Seating Gap

The seating gap under a no-load condition is a result of variation in the above land geometry combined with dimensional and positional errors. In many cases, the real length of land contact is a complex function of the load, being formed elastically with each contact. The seat land may have been developed through plastic flow of an initially sharp edge with subsequent deformations predominantly elastic. Where the land is plastically formed, the resultant contact shape is largely indeterminate. With defined simple curved shapes, however, a Hertz stress analysis may be used to predict the elastically loaded configuration. In any case, a definite land length does exist under the slightest load, and the term "sharp seat" is a relative generalization.

Dimension errors result in deviations from true form and nonconformity between poppet and seat lands. Symmetrical errors may create only a taper gap with full contact at the roughness level around the periphery; however, errors of roundness always result in a through-gap. Even with symmetrical errors, as exemplified by differential radii in spherical seating, a finite load must be applied to establish a minimal land for adequate sealing or else leakage could be in the nozzle regime and, thus, much greater than for the laminar condition.

It is notable that unlike the flat poppet and seat (for which it is relatively simple to obtain near-perfect conformity), the conical and spherical designs necessitate a match of physical dimensions, i.e., the included angle for the cone and radius for the sphere. As a result, these configurations will almost always have a taper gap from a few microinches to thousandths of an inch, depending upon size and fabrication and measurement precision. For constrained flat and conical seats, parallelism and axis tilt are usual positional errors. Freedom from this error is the advantage of the spherical seat.

Superimposed upon the seat land, and causing gaps which may only be reduced but never closed, are the surface textural errors of roughness, waviness, modules, pits, and scratches. Thus, a variety of geometrical errors cause conformal gaps in seating which must be reduced through load deformation of the "high" material.

Equivalent Flow Paths for Surface Deviations

The deviations of seating geometry that result in leakage may be broadly divided into the following:

1. Gross abnormalities of geometry such as out-of-parallel plates; broad curvatures measured as a deviation from a flat plane; and spherical, out-of-round, or tapered mating surfaces

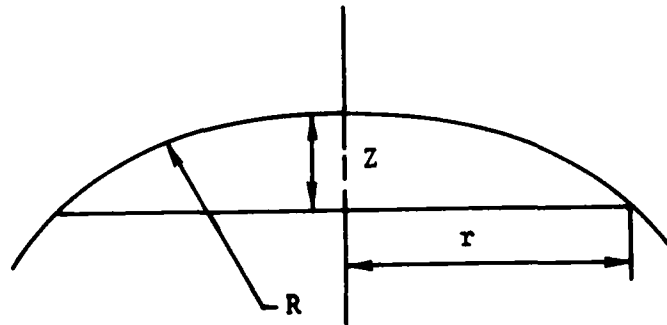
2. Parameters of surface texture, i.e., roughness, waviness, nodules, pits, and scratches

The leakage flow through these various surface deviations may be indirectly approximated by computing the equivalent flow path of each deviation for that portion of the seating surface it occupies. Valve seat leakage takes place mainly in the laminar and, to a lesser extent, in the molecular flow regimes. In laminar flow between parallel plates, the defining parameters are the channel length or the radial land width (L), peripheral width ($W = \pi D_s$), and separation height cubed (h^3). The same conditions hold for molecular flow except the separation height is squared (h^2).

Because the surface deviations considered herein are very close approximations of parallel plates, the flow may be imagined to travel through discrete radial channels of varying height which may be integrated to arrive at an equivalent parallel plate separation (h_e).

In these calculations, advantage is taken of the fact that the majority of flow occurs through the larger spaces so that small nonradial flows may be neglected. It has also been assumed that the seat land width is sufficiently narrow with respect to the ID to neglect radial flow divergence.

Simplified Chordal Equations. In analyses of various curved geometries, the expression for the chordal height often occurs as shown below:



The equation defining this geometry is:

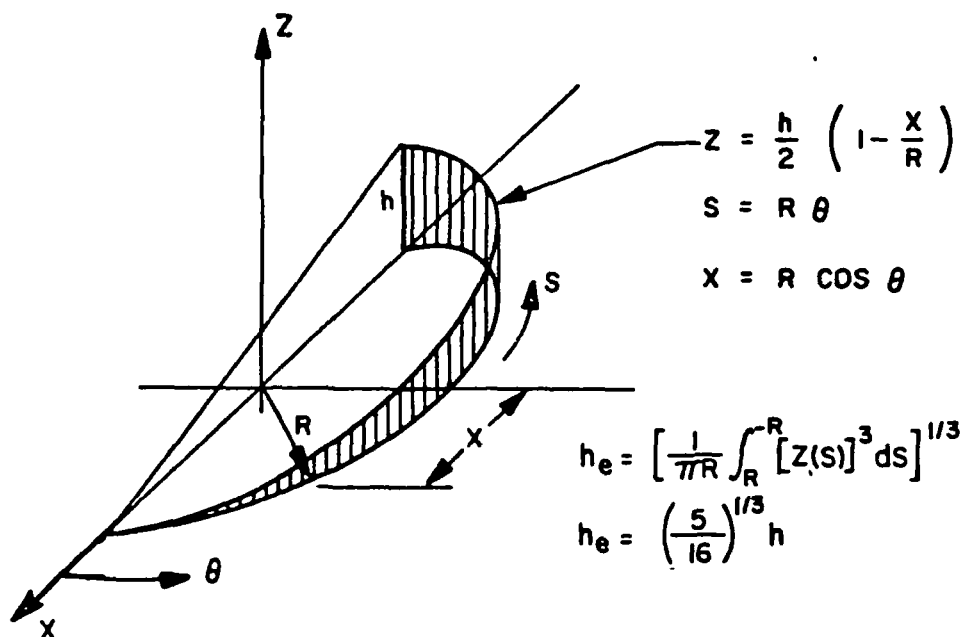
$$r = \sqrt{2RZ - Z^2} \approx \sqrt{2RZ}$$
$$Z \approx \frac{r^2}{2R}$$

For most analyses herein, R is much larger than Z; therefore, the approximate relation may be used with small error as shown below:

R/Z	Error, percent
25.4	1.0
5.4	5.0
2.9	10.0

Gross Geometry Deviations. Valve seat leakage caused by gross separations in the interface is mainly laminar, but may be turbulent channel or nozzle flow. While a large number of surface deviations are possible, there is a great similarity between the various gap shapes which allows the consideration of maximum gap and equivalent height to be reduced to a reasonable few. These may often be superimposed to obtain approximate results for composite shapes. In the case of taper gaps (h_0), a physical separation of the seating surfaces (h_p) is assumed to exist due to surface texture or other errors.

Out-Parallel Flat Poppet and Seat. For this case, the seating surfaces are assumed perfectly smooth and flat with flow perfectly radial. The flow may be imagined to follow a large but finite number of radial stream channels which may be summed to obtain the total flow through the gap. Because laminar flow varies as the height cubed, it follows that the predominant flow path is through the widest gap. The analytical model and describing equations are shown below:



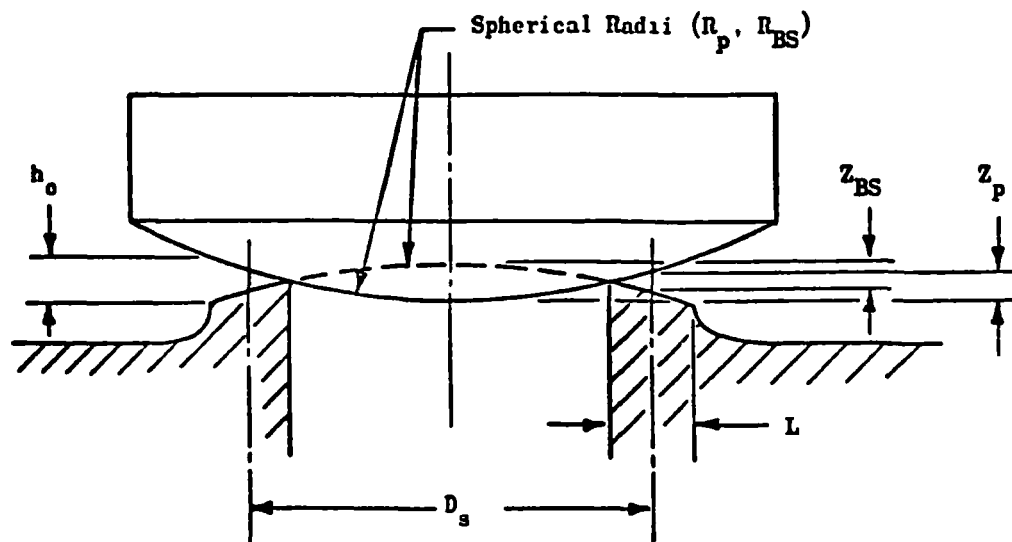
As curve Z is one-half of a sine wave when unwrapped, the same result is obtained by integrating Z over the length πR . It can be shown for this model that the assumption of perfect radial flow results in small error because more than 90 percent of the total flow discharges from the wide 180 degrees of the periphery, leaving less than 10 percent of the flow involved in the contact regions where the flow is partially circumferential.

Sinusoidal Gap Separations. The flat poppet and seat have one or both surfaces cylindrically out-of-flat (egg-shaped poppet) and, also, out-of-round conical, and spherical seating surfaces all have gaps which are basically sinusoidal regardless of the number of lobes. Consequently, integration of these shapes yields the same results obtained for the flat out-of-parallel case above, i.e.:

$$h_e = \left(\frac{5}{16} \right)^{1/3} h$$

where h is the maximum gap.

Axially Symmetrical Tapered Seating. Taper between poppet and seat is usual for nearly all forms of seating involving matching surfaces. It results in flat seating from customary convex (or, to a lesser extent, concave) machining errors, as schematically shown below:

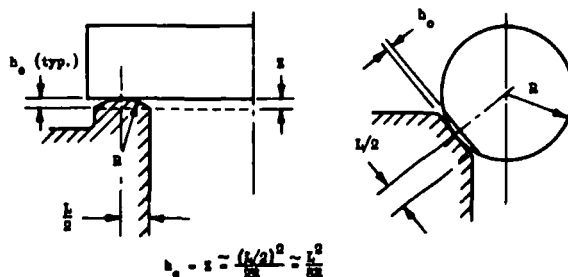


For flatness errors (Z_1 and Z_2) measured nominally at the mean seat diameter (D_s), the taper gap (h_o) is derived from the simplified chordal equation as:

$$h_o \approx \frac{4L}{D_s} (Z_p + Z_{BS})$$

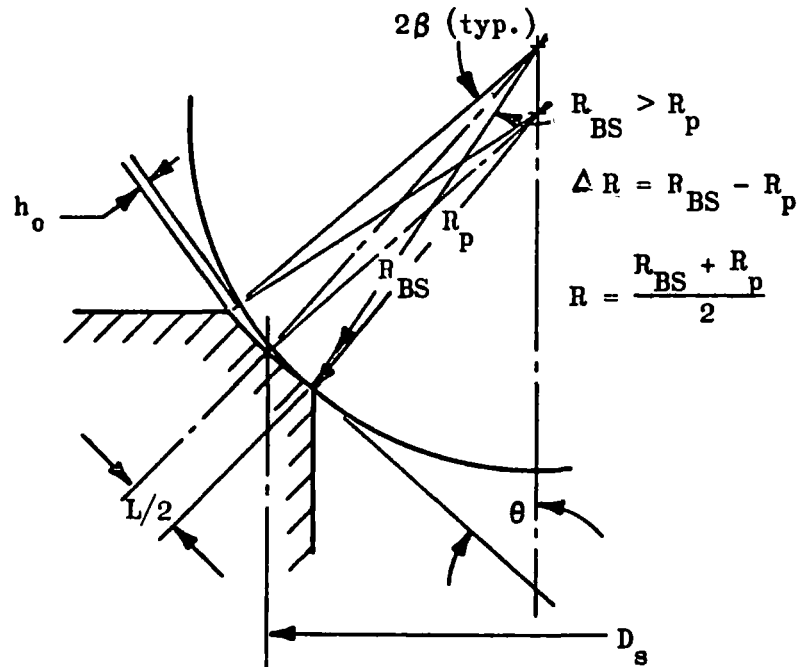
with the appropriate sign applied to Z for concave or convex conditions.

A more unusual symmetrical form error is the crowned surface which might occur from excessive polishing of a flat, conical, or even spherical seat, thus dubbing the edges. Although the actual shape is often elliptical, the geometry may be approximately described by the chordal equation. A similar seating configuration occurring naturally is the ball in a wide conical seat (elastic contact only). Taper gaps from these configurations are shown below:



As previously noted, a more serious problem exists for the conical and spherical surfaces because of the conformal dependence upon physical dimensions. For conical seating, the seat gap is a function of the land width (L) and differential seating or half angle ($\Delta\theta$) between poppet and seat; thus, $h_o = \Delta\theta L$.

With spherical seating, the taper gap is related to the differential (ΔR) between the poppet (R_p) and ball seat (R_{BS}) spherical radii. The exact equation is cumbersome in that small differences necessitate a computer solution. However, simplification is possible for seating half-angle (θ) between 15 and 75 degrees, and land with (L) is small with respect to the basic spherical radius (R). Applicable terms are shown in the following sketch for the case where (R_{BS}) is greater than (R_p). The approximate solution for (h_o) is derived from the sine law with (L) assumed a straight line.



$$h_o \approx \frac{\Delta R L}{R_p \tan(\theta \pm \beta)} = \frac{\Delta D L}{D \tan(\theta \pm \beta)}$$

$$\beta \approx \frac{L}{2R} : (+) \text{ for } R_{BS} > R_p; (-) \text{ for } R_p > R_{BS}$$

$$\theta = \arccos \frac{D_s}{2R}$$

In terms of the differential between ball and seat spherical diameters (ΔD) and mean seat diameter (D_s):

$$h_o \approx \frac{\Delta D L \cos \theta}{D_s \tan(\theta \pm \beta)} = \Delta\theta L$$

Taper gap data are plotted in Fig. 8 in terms of the taper angle ($\Delta\theta$). Consideration of experimental data has shown that the usual tolerance angular differential of 1/2 to 1.0 degree would, in most cases, result in unacceptable large taper gaps.

The problem now is to describe the taper gap (h_o) in leakage parameter terms. For the ideal case of perfectly smooth, flat, or round surfaces, there would be no leakage. Roughness and/or geometry errors do, however, cause a separation which, due to the very narrow contact land, may be assumed to offer negligible resistance to flow (unless the taper gap is very large, in which case the leakage would result from a nozzle flow condition). With some gap, the problem is resolved to one of simple tapered flow. The equivalent separation for this case will be presented in the Leakage Flow Analysis section. The simple integration averaging process may not be used for channel height varying along the flow direction. Comparison of laminar flow factors is illustrated in Fig. 9 for two cases noted as "linear" and "taper" flow. For the linear case, h does not vary in the direction of land width (L), and the cubical average (h_e) is obtained as previously shown. For taper flow, the basic flow equation must be integrated with L to obtain an equivalent path height. There is a small difference between the two flow factors at (h_p/h_o) ratios greater than one; thus, the more universal M_L factor may be used to approximate complex surface geometry. Below this value, however, taper flow should be considered as the defining parameter and N_L used to compute the flow.

Surface Texture Deviations. Except in rare instances, loaded on-seat leakage will be laminar and, for gases, may reach molecular levels. The basic leak path is through the interstices formed by contacting waviness and/or roughness. Additional leakage components of possible significance may be through nodule created gaps, radial scratches, or a density of interconnecting pits. As with gross geometry deviations, weighted averages of the maximum spacing height (h) can be computed for various regular geometric wave forms.

Surface Roughness and Waviness. The geometrical terms and equations used to describe model surfaces are summarized in the sinusoidal representation shown in Fig. 10. The height (h) and wave length (λ) can be assumed to represent various other wave forms and exist as waviness or roughness, or a combination of both. For example, a sinusoidal curve of smaller (h) and (λ) can be superimposed upon the sine wave shown. In addition, these waves can be imagined to be either linear into the paper or undulating in a similar fashion as that indicated resulting in a three-dimensional series of "hills and valleys" which contain a smaller version of the same. For the fine surfaces under consideration ($h = 0.5$ to 20 microinches [1.27×10^{-6} to 50.8×10^{-6} cm]), the average asperity angle (Φ) will seldom exceed 4 degrees, and sharp lapping scratches do not have slope angles much greater than 10 degrees.

Various averages have been computed from the equations shown in Fig. 10 for a number of regular geometric wave forms (Fig. 11). These factors may be used to estimate the variations between surfaces and the possible effects on leakage performance.

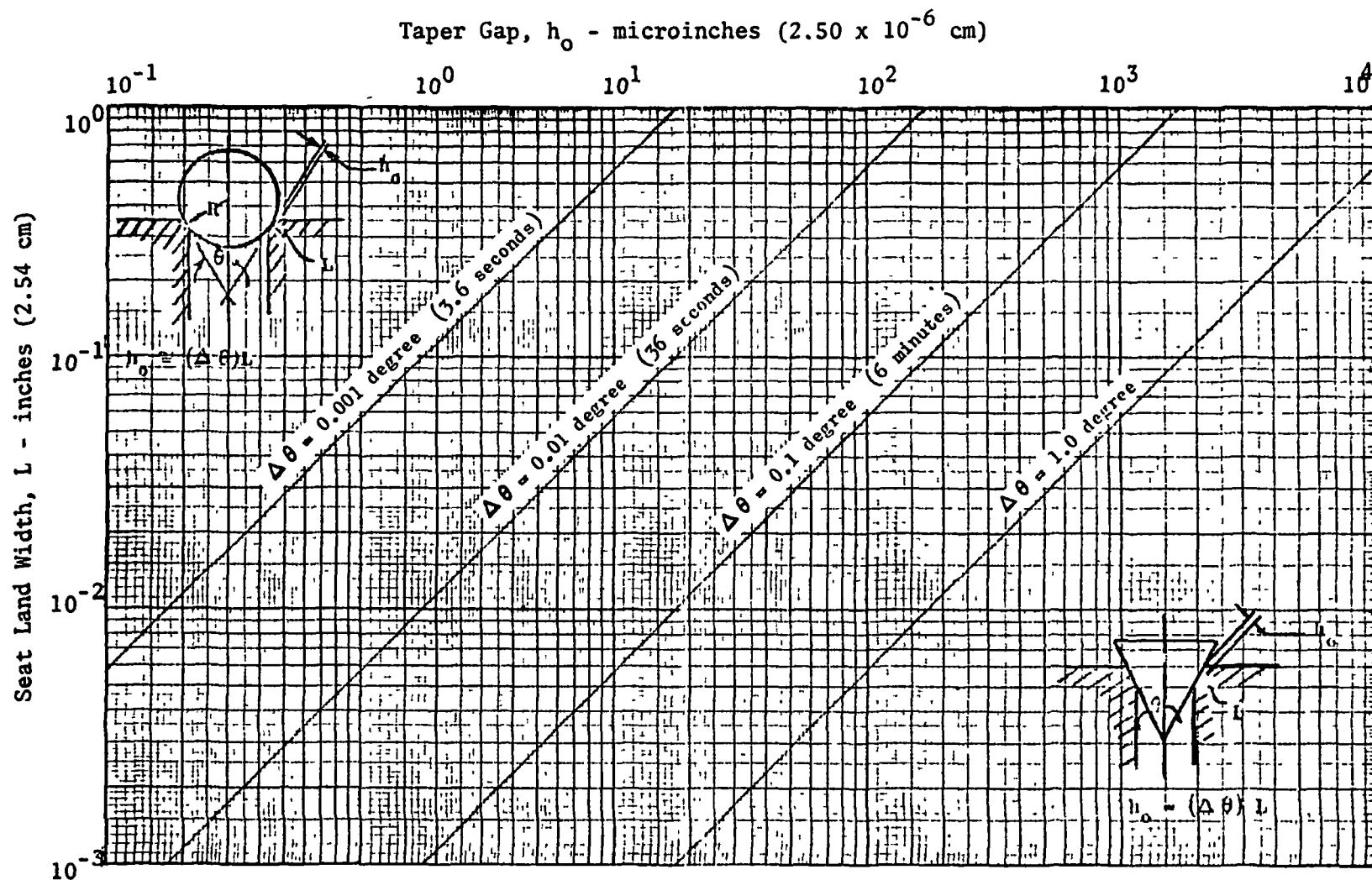


Figure 8. Taper Gap for Flat, Conical, and Spherical Seating

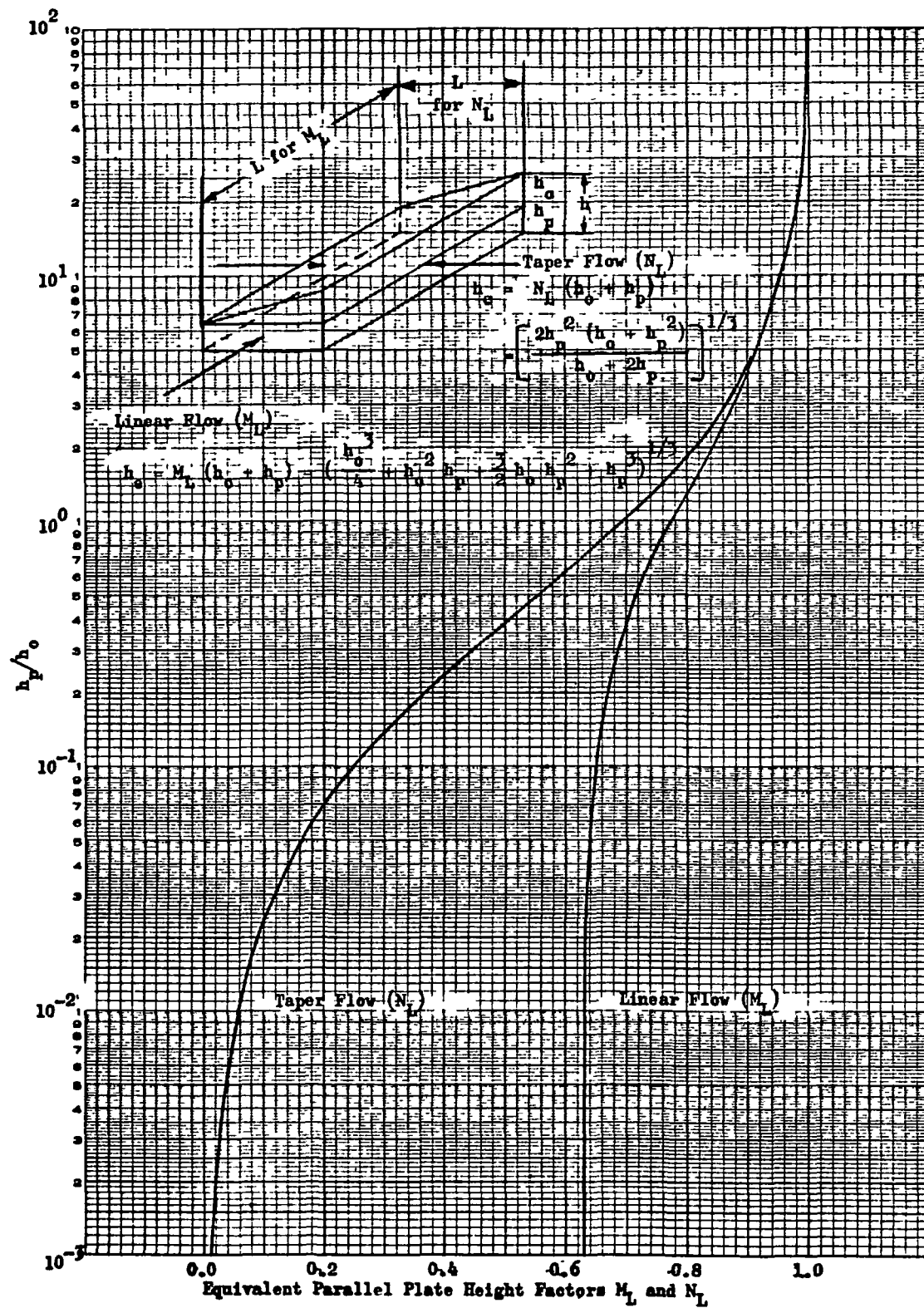
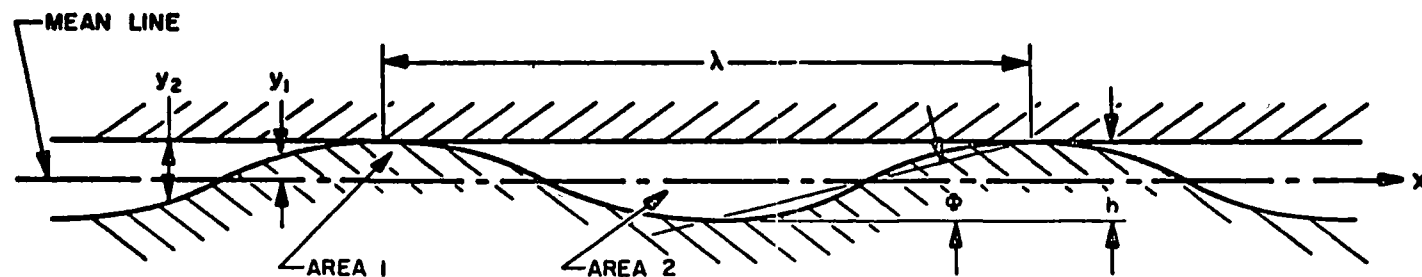


Figure 9. Laminar Flow Factors



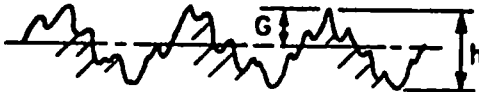



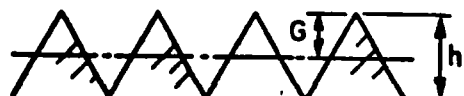
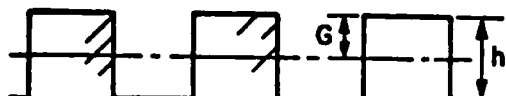
$$AA = \frac{1}{\lambda} \int_0^{\lambda} |y_1| dx ; \text{rms} = \left[\frac{1}{\lambda} \int_0^{\lambda} y_1^2 dx \right]^{1/2}$$

$$h_{eL} = \left[\frac{1}{\lambda} \int_0^{\lambda} y_2^3 dx \right]^{1/3} ; h_{eM} = \left[\frac{1}{\lambda} \int_0^{\lambda} y_2^2 dx \right]^{1/2}$$

$$\text{Average Asperity Angle } \Phi \approx \frac{2h}{\lambda}$$

Location of Mean Line Defined by Area 1 = Area 2

Figure 10. Model Surface Geometry With Defining Equations

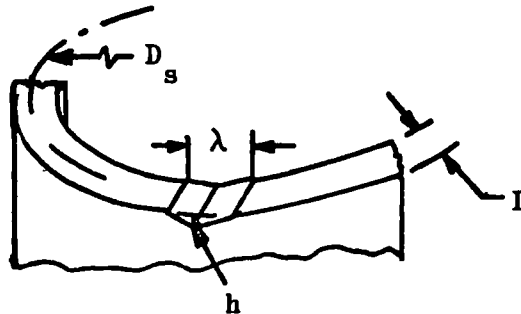
WAVE FORM: $h = 1$		M_L^*	M_M^*	AA	rms	$\frac{h}{AA}$	$\frac{h}{rms}$	$\frac{G}{h}$	$\frac{G}{AA}$	$\frac{rms}{AA}$
UNIFORMLY RANDOM		---	---	0.2	0.25	5.0	4.0	0.5	2.5	1.25
ROUND CRESTED PARABOLIC		0.523	---	0.256	0.298	3.91	3.36	0.333	1.29	1.16
SHARP CRESTED PARABOLIC		0.770	---	0.256	0.298	3.91	3.36	0.667	2.60	1.16
SINUSOIDAL		0.678	0.612	0.318	0.353	3.14	2.83	0.5	1.57	1.11
SAW TOOTH		0.630	0.578	0.25	0.289	4.0	3.46	0.5	2.0	1.16
SQUARE		1.0	1.0	0.5	0.5	2.0	2.0	0.5	1.0	1.0

$$*h_{eL} = M_L h; h_{eM} = M_M h$$

Figure 11. Average Height Values for Various Wave Forms

Scratches. The remaining surface defects pertinent to valve seating are scratches, nodules, and pits in decreasing significance. Because of the difficulty associated with defining these defects, they take on a much greater importance than is commensurate with their usual contribution to leakage. Of particular significance in this respect are scratches. The definition of the relative effect of scratches (and other defects) upon leakage may be estimated through comparison of their size-number contribution to total leakage as compared with other deviations.

The analytical model considered is the seat land having one radial scratch, as shown below:



The equivalent height for the sawtooth configuration from Fig. 11 is:

$$h_{eL} = 0.63 h \text{ and } h_{eM} = 0.58 h$$

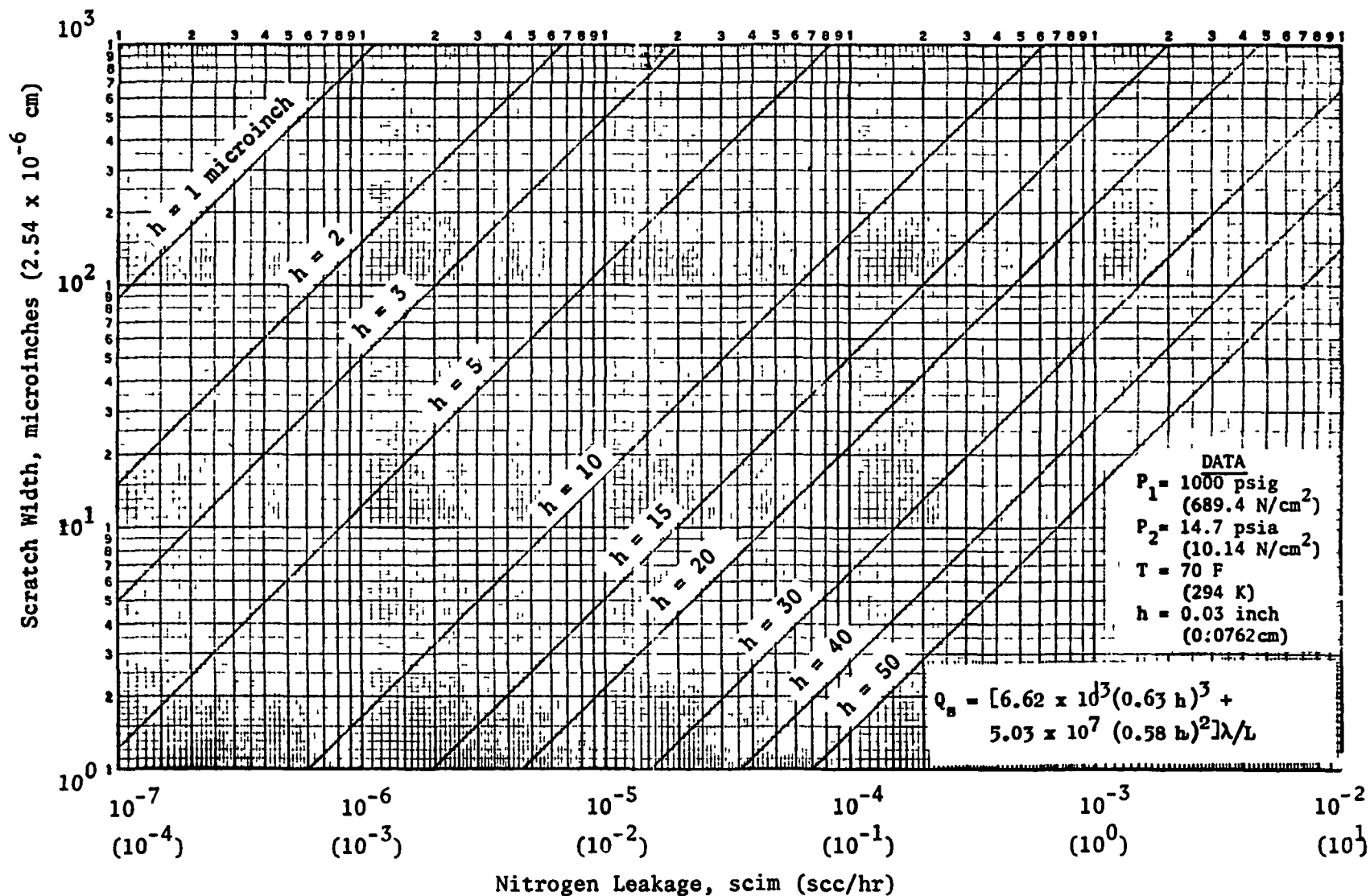
Scratch density (β_s) relates the one-radial-scratch model to the usual case of many radial scratches; thus:

$$\beta_s \equiv \frac{n\lambda}{\pi D_s} \text{ or } n = \frac{\pi D_s \beta_s}{\lambda}$$

where Q for many scratches of average width (λ) equals (n) times (Q_s) for one scratch. Scratch leakage, computed for correlation with experimental data, is shown in Fig. 12 with the reduced flow equation and applicable data.

Nodules. Contaminants and nodules have a highly load-sensitive effect on leakage due to their usually small contact area. Uniformly dispersed over the seating area, the separation height is merely the parallel plate configuration. However, one nodule will cause the out-of-parallel positional error previously discussed. In this case, contact will occur at the roughness height of the two surfaces and the equivalent height must be determined for the combined gaps (i.e., M_L in Fig. 9 where h_p is the equivalent combined roughness height, and h_o the out-of-parallel gap).

Pits. Few localized pits not bridging the seat land will have little effect on leakage. A uniform distribution of pits will tend to reduce the effective land width since they offer negligible flow resistance (large relative h).

Figure 12. Single Scratch Leakage, Q_s

Leakage Flow Analysis

In considering the leakage and flow across a valve seat, a number of equations must be taken into account. These range from the nozzle equation which generally applies to the wide open valve to the viscous and molecular flow equations applicable under seated conditions. The equations derived in this section are presented for compressible and noncompressible fluids for flow through parallel plates. The equations are equally applicable to flat, conical, and spherical valve configurations because the near and on-seated passage configurations approximate the parallel plate model. Because of the importance of the laminar flow regime, the special case of taper in the direction of flow is also considered.

A specific example of nitrogen flow through a model valve seat is presented which shows how each flow regime blends into the next to build the overall flow-leakage characteristic curve. As the flow regime boundaries are not sharply defined, the example additionally illustrates the range over which the various equations may be applied.

Nozzle Flow. The compressible and incompressible flow equations derive from the basic Euler momentum relationship. The Euler equation gives the following relationship between velocity, pressure, and density:

$$\frac{v^2}{2g} + \int \frac{dP}{\rho} = \text{constant}$$

For the incompressible consideration, density (ρ) is constant, and the resultant relationship is known as the Bernoulli equation. If the inlet velocity is neglected, the following equation evolves for flow of an incompressible fluid through a nozzle:

$$\omega = CA \sqrt{2 g \rho (P_1 - P_2)}$$

This equation requires a discharge coefficient (C) to correct the ideal frictionless flow to the actual case. The discharge coefficient is a function of the specific configuration being considered; therefore, it is derived from empirical data.

For the specific application of this equation to a valve configuration, area (A) is the minimum flow opening expressed as a function of the stroke height (h_p) and the minimum seat perimeter. This substitution can be made in the nozzle and the turbulent channel equations. For circular valve seats where the radial land width (L) is small with respect to the ID, it is convenient to assume a mean seat perimeter $W = \pi D_s$, where (D_s) is the mean seat diameter.

With compressible flow, the density is not constant and, therefore, the integral of dP/ρ must be evaluated for specific assumptions. For an adiabatic, frictionless process considering a perfect gas, the following equation is derived:

$$\omega = \frac{CAP_1}{\sqrt{RT_1}} \sqrt{gk \left(\frac{2}{k+1} \right)^{k+1/k-1}}$$

As in the case of the incompressible flow, a discharge coefficient is required to account for the irreversibility of flow. The above equation further assumes that choked or sonic flow exists across the nozzle.

In practice, leakage is most often expressed in terms of a volumetric flow. For compressible fluids, where density is a variable function of pressure and temperature, standard conditions (P_s , T_s , ρ_s) must be defined. The conversion relationship for all fluids is:

$$Q = \frac{\omega}{\rho_s} = \omega \frac{RT_s}{P_s}$$

Therefore, for both incompressible and compressible flow at standard conditions, the weight and volumetric flows differ by a constant.

The nozzle equations can be applied to a poppet valve configuration (similar to an orifice) from the wide-open condition to the near-seated position. When the valve closure height has decreased to the position where wall friction at the seating surface (and, thus, land length) is significant, the nozzle regime terminates and turbulent channel flow commences. There is no precise point at which nozzle flow terminates, the transition being a complex function of the particular channel geometry and Reynolds number. However, in general, if the length-to-height ratio is 10 or greater, channel flow is imminent.

Turbulent Channel Flow. In this flow regime, the same basic continuity and momentum considerations hold with the addition of a term for the effects of friction. In the case of an incompressible fluid, the basic Bernoulli equation is modified to the form:

$$\Delta P = \frac{fL}{D} \frac{\rho V^2}{2g}$$

where flow is defined by continuity as:

$$\omega = \rho A V$$

The first equation expresses differential pressure as a function of friction factor (f) and velocity (V). The friction factor is related to velocity through empirical parametric curves of friction versus Reynolds number and wall roughness. The solution to these equations is by trial and error.

The equations for flow in the turbulent channel regime were developed for flow-through circular tubes. To apply the equations to other channel configurations, the tube diameter in these equations must be expressed in terms of hydraulic diameter (D). Hydraulic diameter is defined as four times the ratio of the cross-sectional area to the wetted perimeter. For parallel plates, the hydraulic diameter is equal to twice the plate spacing ($2h_p$).

The equations used to compute compressible fluid flow in this regime are obtained from Shapiro (Ref. 9). They assume an adiabatic constant-area flow and include the effects of internal fluid and wall friction and fluid momentum. To compute the weight flowrate, two equations are required. The first is a relationship between entrance Mach number (M) and friction factor (f) for the condition of choked flow at the exit of the valve seat channel (M = 1):

$$\frac{fL}{D} = \frac{1-M^2}{kM^2} + \frac{k+1}{2k} \ln \frac{(k+1) M^2}{2(1+\frac{k-1}{2} M^2)}$$

As in the incompressible case, the solution of this equation is by trial and error. Shapiro's text gives considerable assistance in the solution of this equation by tabulating fL/D versus Mach number, thus permitting interpolation of desired information. For the subsonic solution, reference is made to Shapiro's text.

Once the entrance Mach number and density are determined, they are used in the continuity equation to compute the weight flowrate based on the inlet conditions:

$$\omega = \rho A M \sqrt{k g R T}$$

The equations in this section are confined to the turbulent flow regime, i.e., Reynold numbers greater than 2000. However, these equations can be extended into the initial portion of the laminar flow regime where fluid momentum is still an important consideration. In this case, the friction factor is a linear function of Reynolds number and is given for the parallel plate consideration as:

$$f = 96/Re \quad \text{and} \quad Re > 500$$

The defining equation for Reynolds number is:

$$Re = \frac{VD\rho}{\mu g}$$

As before, (D) refers to the hydraulic diameter for other than round configurations. For the parallel plate consideration of a circular valve seat, this equation may be reduced to:

$$Re = \frac{2\omega}{W\mu g}$$

Laminar Flow. The analysis of fluid flow in this regime assumes that the temperature is constant (isothermal), that the fluid momentum effects are negligible, and that viscous shear forces govern the flow, i.e., Reynolds number less than 500. These assumptions result in the Poiseuille equation for flow through stationary flat plates (Ref. 11):

$$-\frac{dP}{dX} = \frac{12 \mu V_{\text{average}}}{h^2}$$

By using the continuity equation, the relationship is reduced to express the viscous flow through flat plates:

$$\omega = \frac{\rho W h_p^3 (P_1 - P_2)}{12\mu L}$$

For a compressible gas, thermal effects are present; however, the assumption of isothermal condition can be made because of the small channel thickness and low velocity. The compressible version of the Poiseuille equation is obtained by integration of the pressure profile across the seat land and assumption of a perfect gas; therefore,

$$\omega = \frac{W h_p^3 (P_1^2 - P_2^2)}{24\mu L R T}$$

This same basic relationship can be derived for flow between circular flat plates. This equation contains the natural log of the radius ratio which accounts for radial divergence of the flow and is as follows:

$$\omega = \frac{\pi h_p^3}{12\mu \ln \frac{R_o}{R_i}} \left(\frac{P_1^2 - P_2^2}{R T} \right)$$

Normally, this divergence can be neglected as the R_o/R_i ratio is close to unity.

For the special case where convergent or divergent taper exists between seating surfaces, the equivalent parallel plate separation becomes:

$$h_e = \frac{2h_p^2 (h_o + h_p)^2}{h_o + 2h_p}$$

where (h_p) is the separation at the narrow end of the land (L) and $(h_o + h_p)$ the separation at the wide end. Thus, for $h_o = 0$, $h_e^3 = h_p^3$.

Transition and Molecular Flow. The determination of molecular flow involves the application of the kinetic theory of gases. A flow equation derived (Ref. 12) for the molecular regime is:

$$Q = \frac{4}{3} \frac{V_a}{L \int_o^L \frac{H}{A^2} dL} (P_1 - P_2)$$

This equation relates the flow (Q) to the mean molecular speed (V_a), differential pressure ($P_1 - P_2$), and geometry where (H) is the channel perimeter. When this basic relationship is applied to parallel planes, the equation has the form:

$$\omega = \frac{4}{3} \sqrt{\frac{2}{\pi}} \frac{W h_p^2}{L} \frac{(P_1 - P_2)}{\sqrt{\frac{RT}{g}}}$$

There exists a transition region where both molecular and laminar (viscous) flow effects are operating. The limits of these regions are approximately defined by the ratio of mean free path of the molecule (λ') to the characteristic dimension of the channel (h_p) when:

$\lambda'/h_p < 0.01$, flow is viscous

λ'/h_p is 0.01 to 1.0, transitional flow exists

$\lambda'/h_p > 1.0$, flow is molecular

From kinetic theory of gases, the mean free path of gas molecules is given as:

$$\lambda' \approx \frac{\delta \mu \sqrt{RTg}}{P}$$

where δ is a constant. At atmospheric pressure and 70 F (294 K) the computed value of δ is nearly constant (~ 1.8) for nitrogen, helium, argon, and hydrogen gases. Assuming at high pressures that P is the mean channel pressure, the average mean free path reduces to:

$$\bar{\lambda}' = \frac{3.6 \mu \sqrt{RTg}}{P_1 + P_2}$$

The separation at midtransition flow may be found by equating the molecular and laminar flow equations, and is given by:

$$h_p = \frac{25.5 \mu \sqrt{RTg}}{P_1 + P_2}$$

The corresponding ratio of $\bar{\lambda}'/h_p$ is 0.14. A modified equation proposed for flow in the transition region is:

$$\omega_{\text{total}} = \omega_{\text{viscous}} + \epsilon \omega_{\text{molecular}}$$

The molecular flow factor (ϵ) is generally close to unity. It takes into consideration such items as the difference in gases and physical properties of the passage walls. For simplicity and in lieu of explicit test data, (ϵ) has been assumed as unity.

Throughout the entire range of laminar and molecular flow, the flowrate computed from each of the specific equations will predominate in its applicable regime of flow. Thus, the summation equation above may be used without regard to regime boundary since the flow computed for the regime outside of its range will be negligible (see Sample Computation below).

Sample Computation

To illustrate how the previously developed flow equations are used, the following sample computation is presented. The seat model selected is the 1-inch configuration used in the off-seat leakage tests. A cross section of this seat configuration is shown in Fig. 13. Flow is from the inside (ID) to the outside (OD) of the 0.060-inch (0.1524 cm) flat seat land. Leakage has been computed for nitrogen gas at a 100-psig (68.95 N/cm²) inlet pressure, a 70 F (294 K) inlet gas temperature, and a 14.7-psia (10.14 N/cm²) outlet pressure.

Figure 14 presents the leakage spectrum for the sample computation. The various flow regimes, i.e., nozzle, turbulent channel, laminar, transitional, and molecular are identified on the curve. Also, the limits of each regime are shown. A range of theoretical parametric data has been computed for various pressures and gases and is presented with the Model Leakage section.

The following parameters are known values for this seat configuration and are used in the flow equations to compute the noted leakage characteristics:

Discharge Coefficient	$C = 0.95$
Gravitational Acceleration Constant	$g = 1.39 \times 10^6 \text{ in./min}^2$ $(3.5306 \times 10^6 \text{ cm/min}^2)$
Specific Heat Ratio	$k = 1.14$
Channel Length or Land Width	$L = 0.060 \text{ in. (0.1524 cm)}$
Inlet Pressure	$P_1 = 114.7 \text{ psia (79.07 N/cm}^2)$
Discharge Pressure	$P_2 = P_s = 14.7 \text{ psia (10.13 N/cm}^2)$
Gas Constant	$R = 663 \text{ in./R}$
Absolute Temperature	$T_1 = T_s = 530 \text{ R (294.4 K)}$
Channel Perimeter (πD_s)	$W = 2.95 \text{ in. (7.493 cm)}$
Absolute Viscosity	$\mu = 4.40 \times 10^{-11} \text{ lb-min/in.}^2$ $(7.944 \times 10^{-13} \text{ N-sec/cm}^2)$

Nozzle Flow. For a compressible fluid flowing sonically, the following equation is used:

$$Q = \frac{RT_s}{P_s} \left[\frac{C W_h P_1}{\sqrt{RT_1}} \sqrt{gk \frac{2}{k+1}}^{k+1/k-1} \right]$$

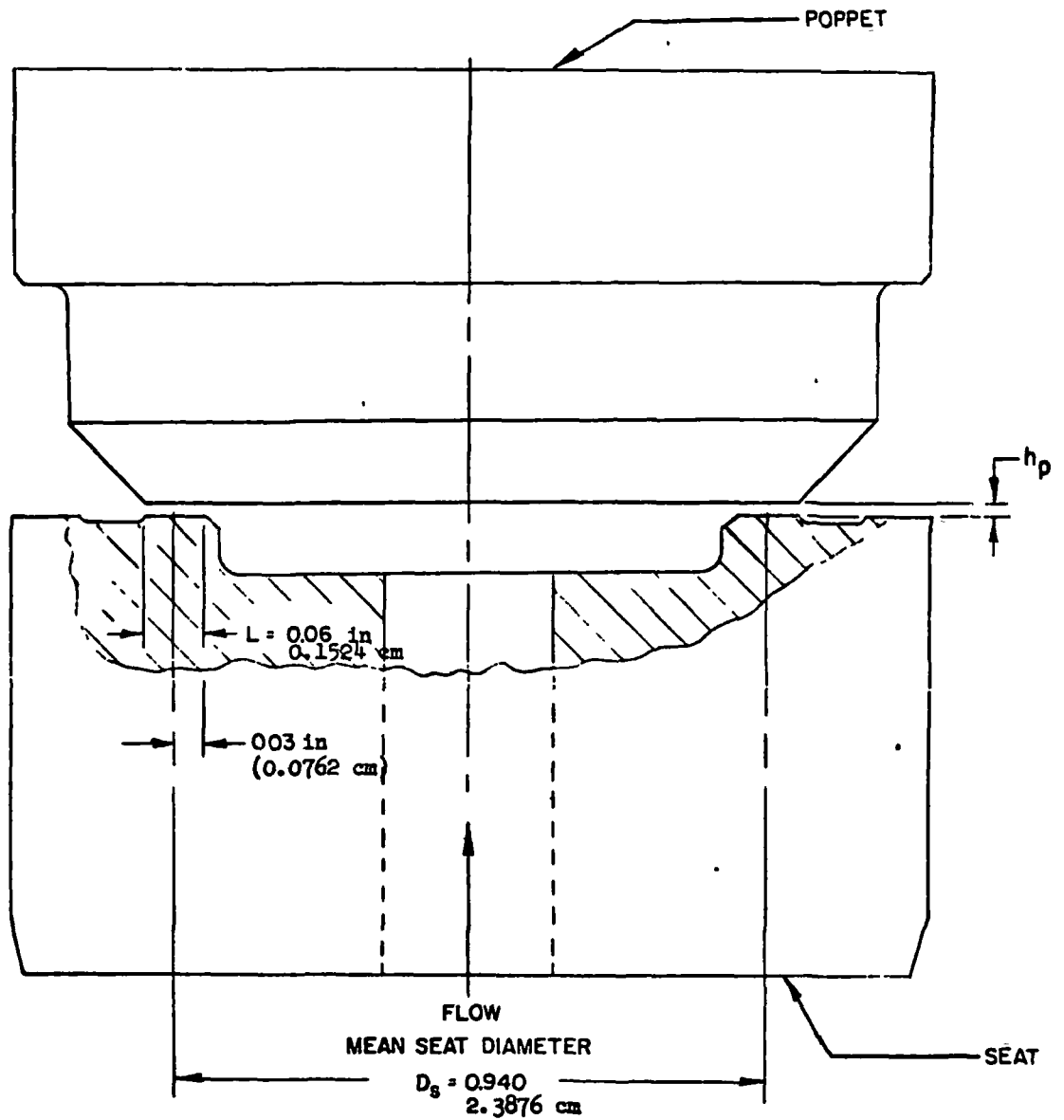


Figure 13. Typical 1.0-Inch (2.54 cm) Poppet and Seat Model

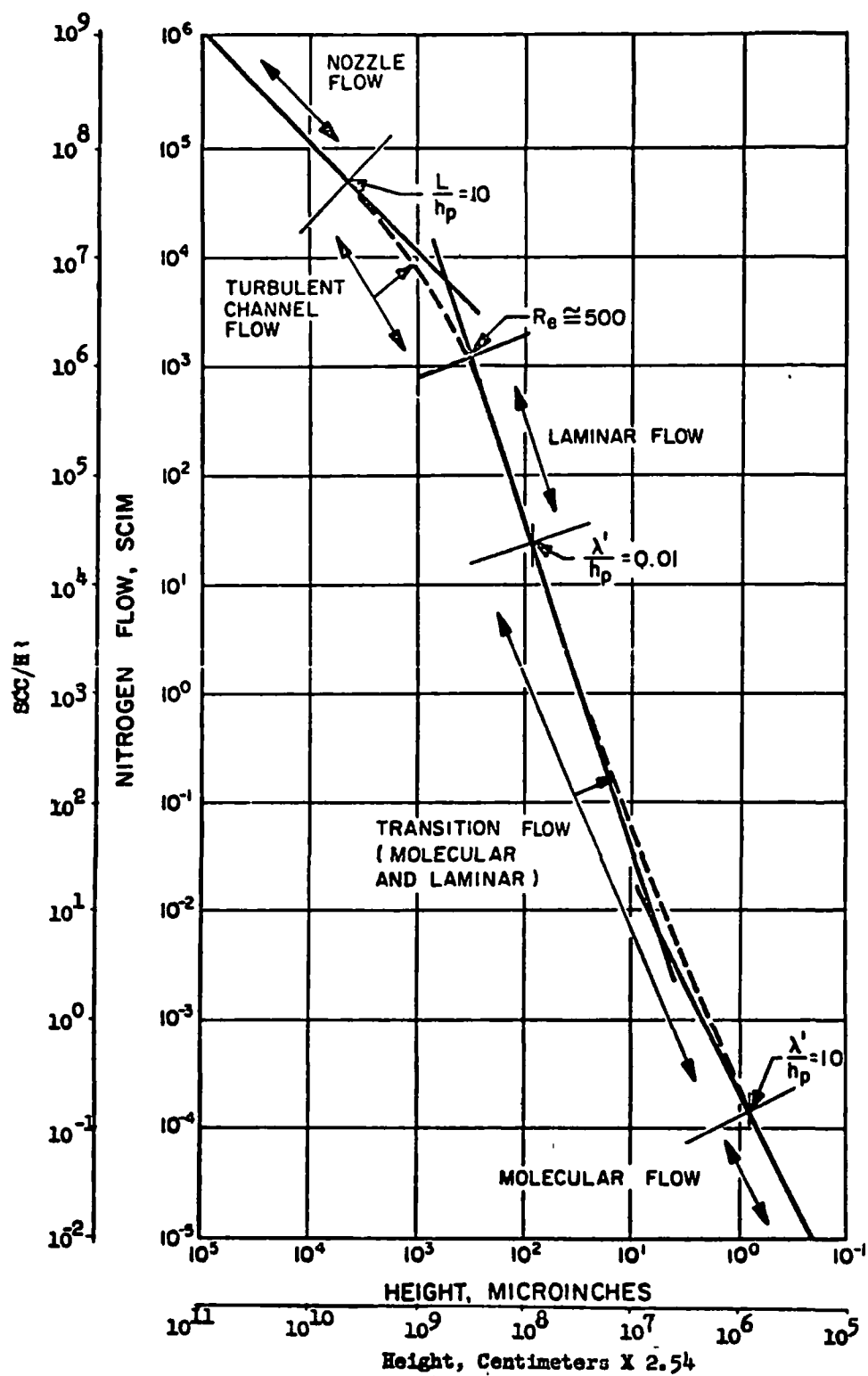


Figure 14. Theoretical Nitrogen Flow Through the Valve Model Shown in Fig. 13

Using the assumptions and data outlined:

$$Q = 1.045 \times 10^7 h_p$$

The orifice flow ceases, and turbulent channel flow commences at a height (h_p) of approximately 6×10^3 microinches 0.01524 cm (Fig. 14). The land width is 0.060 (0.1524 cm) inch, giving an L/h_p ratio of 10 for the break point.

Turbulent Channel Flow. Flow in this regime is defined by a curve on log-log paper; therefore, a sample calculation of one point will illustrate the method used. Leakage is computed for a stroke height (h_p) of 0.001 inch (0.00254 cm) in the following steps:

1. Hydraulic diameter, $D = 2h_p = 0.002$ inch (0.00508 cm)
2. A friction coefficient (f) is estimated at 0.040. This is the starting point for the trial and error solution; (f) will be verified at the conclusion of this computation.
3. Compute $fL/D = fL/2h_p = 1.20$
4. Using Table B-4, Ref. 9, and the equation:

$$\frac{fL}{D} = \frac{1 - M^2}{kM} + \frac{k+1}{2k} \ln \frac{(k+1) M^2}{2 \left(1 + \frac{k-1}{2} M^2\right)}$$

yields entrance Mach number (M_1) = 0.49.

5. Assuming an isentropic entrance condition, entrance static pressure (P_1) can be computed from the following equation (Ref. 9) where P_o is the stagnation (total) pressure of 114.7 psia (79.08 N/cm²) and M is the entrance Mach number:

$$\frac{P_o}{P_1} = \left(1 + \frac{k-1}{2} M^2\right)^{k/k-1}$$

therefore, static entrance pressure (P_1) = 97.3 psia (67.09 N/cm²)

6. Again, assuming isentropic conditions, the entrance static temperature (T_1) is computed from the following equation for a total temperature (T_o) of 530 R (294 K)

$$\frac{T_o}{T_1} = 1 + \frac{k-1}{2} M^2$$

therefore, static temperature (T_1) = 506 R (281 K)

7. The following series of equations are used to compute the flow (Q) in the channel:

$$V_1 = M \sqrt{kg RT_1}$$

$$\rho_1 = \frac{P_1}{RT_1}$$

$$A = Wh_p$$

$$\omega = \rho_1 AV_1$$

$$Q = \omega \frac{RT_s}{P_s}$$

from which the flow (Q) = 8090 scim (7.95×10^6 scc/hr)

8. To prove the flow computation, the originally estimated friction coefficient (f) is checked. Reynolds number is first computed:

$$Re = \frac{DV_1\rho_1}{\mu g} = 3.76 \times 10^3$$

Using the computed value for Reynolds number, a friction coefficient is determined from the Moody diagram. The friction coefficient determined from this curve is close enough to the original estimate of 0.040 so that a recomputation is not necessary.

The curve plotted from this and other data points is shown as a dashed line in Fig. 14. This flow regime extends into the initial portion of laminar flow, i.e., Re below 2000 where fluid momentum is still an important consideration.

Laminar Flow. Laminar flow for nitrogen gas is computed from the Poiseuille equation in the following form:

$$Q = \frac{RT_s}{P_s} \left[\frac{Wh_p^3 (P_1^2 - P_2^2)}{24 \mu L RT} \right]$$

Using the assumptions and data outlined:

$$Q = 4.08 \times 10^{13} (h_p^3)$$

Transition and Molecular Flow. The equation used to compute leakage in the molecular regime is as follows:

$$Q = \frac{RT_s}{P_s} \left[\frac{4}{3} \frac{2}{\pi} \frac{Wh_p^2 (P_1 - P_2)}{L \sqrt{RT/g}} \right]$$

Using the assumptions and data outlined:

$$Q = 2.49 \times 10^8 (h_p^2)$$

This flow regime is plotted on the lower right of Fig. 14. The dashed line connecting the laminar and molecular flow regimes is simply the sum of the two leakage values. Therefore, the transition equation is:

$$Q_{\text{transition}} = Q_{\text{laminar}} + Q_{\text{molecular}}$$

The boundaries of this transition regime are defined by the following limits:

$$\bar{\lambda}/h_p = 0.01 \text{ to } 1.0$$

The molecular mean free path (λ') is 3.61 (9.17×10^{-6} cm) microinches for nitrogen at standard conditions (70 F (294 K) and 14.7 (10.13 N/cm^2) psia). For a mean pressure of 50 psig, $\bar{\lambda}' = 0.82$ microinch (2.08×10^{-6} cm).

The corresponding height limitation of the transition regime is between 0.82 and 82 microinches (2.08×10^{-6} and 2.08×10^{-4} cm) with the point of equal laminar-molecular flow at 6.05 microinches 1.54×10^{-5} cm (Fig. 14).

Model Leakage

Theoretical nitrogen leakage for a flat poppet and seat model employed in screening tests is presented in Fig. 15 through 17. Helium leakage in the laminar regime will be nearly the same as nitrogen since the viscosity of nitrogen and helium are close.

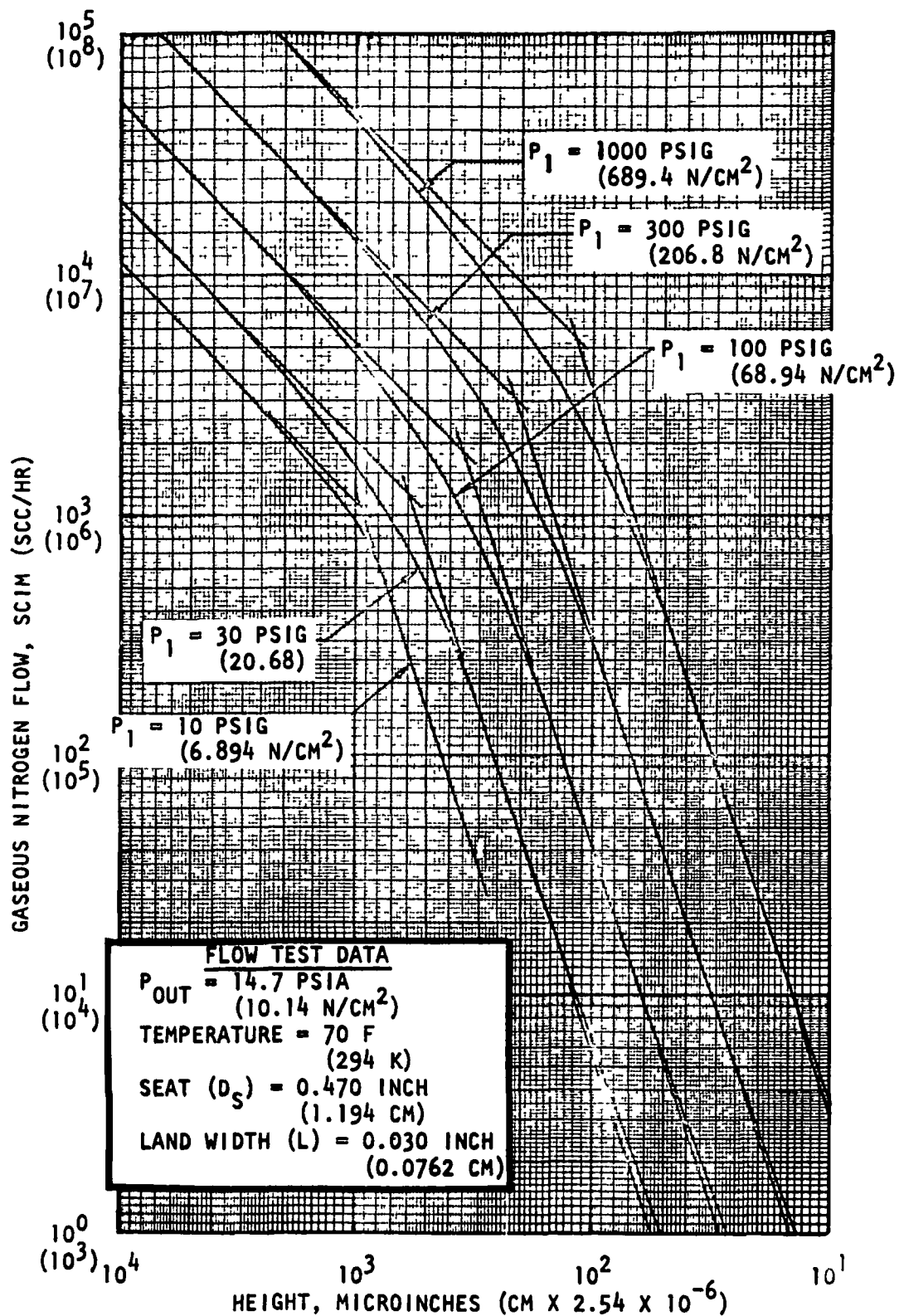


Figure 15. Theoretical Seat Leakage, Part 1

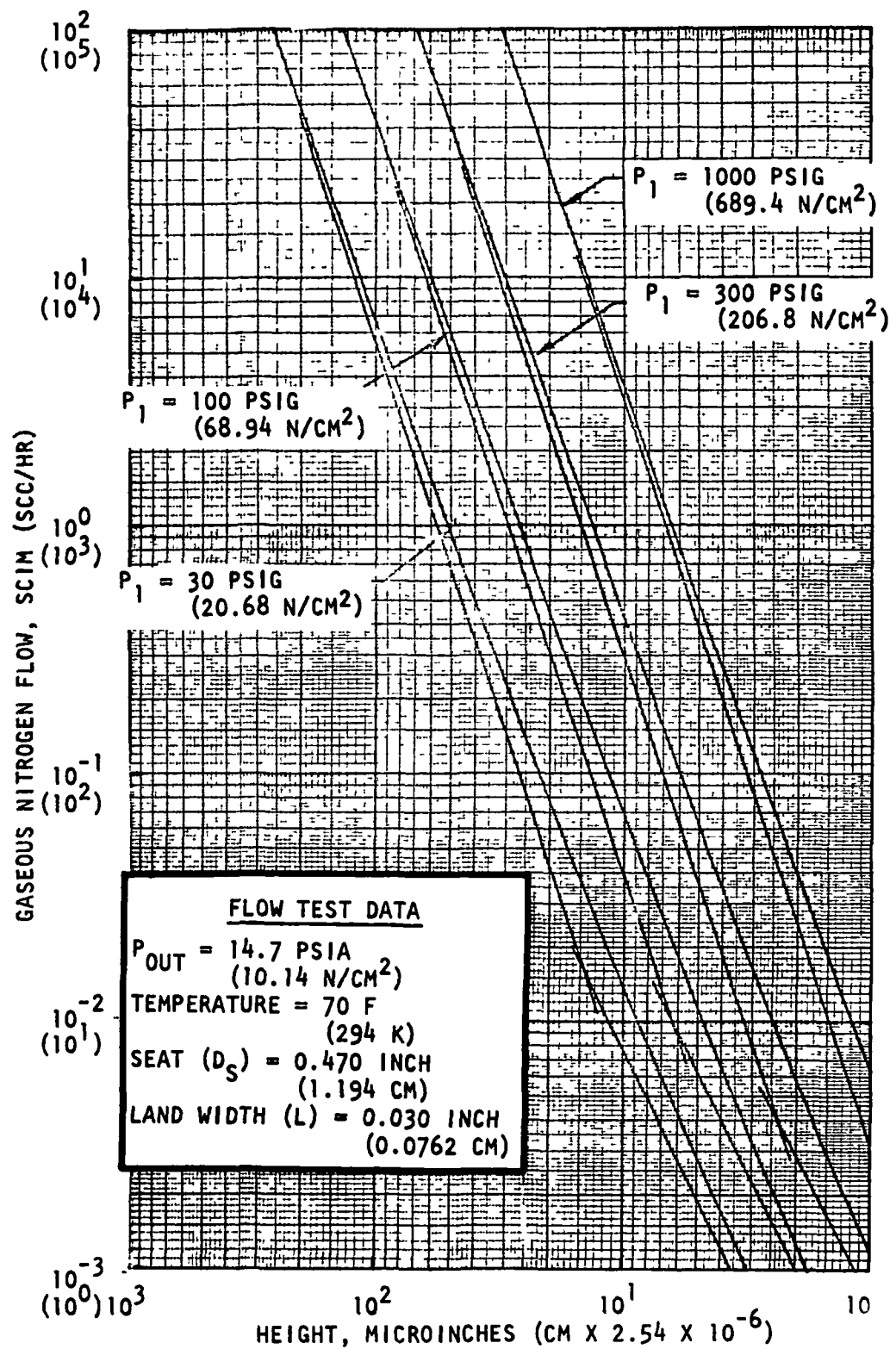


Figure 16. Theoretical Seat Leakage, Part 2

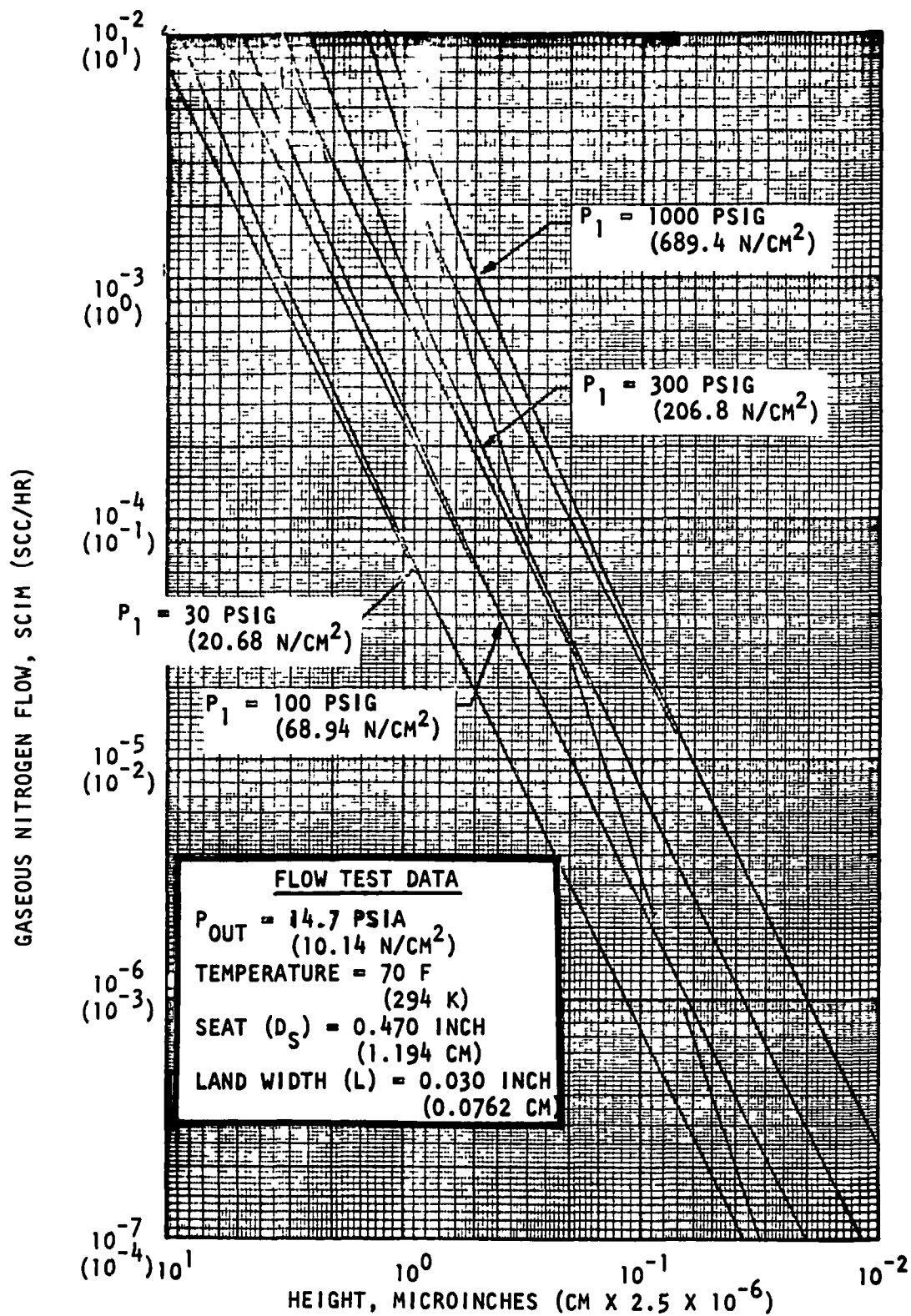


Figure 17. Theoretical Seat Leakage, Part 3

SEALING CLOSURE SCREENING TESTS

The preparation of the trade study and continuing effort on its refinements led to the selection of six valve closure concepts, which were designed and fabricated as model closures. A novel closure screening tester was designed and fabricated to allow selection of the best valve closure concepts based upon their test performance. These results were used in continuing the program progression toward its objectives: SS/APS flightweight valve design.

SEALING CLOSURES

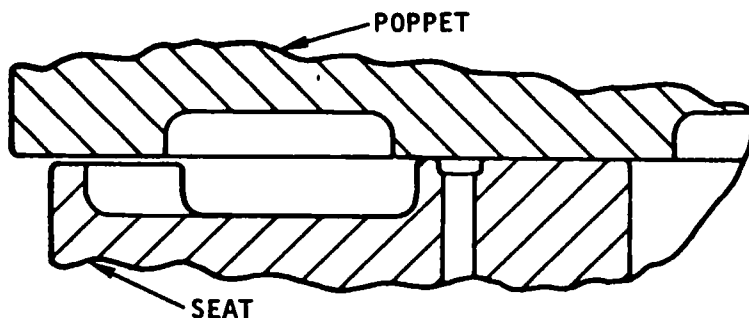
Selection

The basic concepts selected are: (1) flat 440C poppet on flat 440C seat, (2) flat 440C poppet on flat gold seat, (3) flat 440C poppet on grooved gold seat (all three shown in Fig. 18), (4) 440C nose poppet on beryllium copper disk seat, Fig. 19, (5) flat 440C poppet on captive plastic seat, Fig. 20, and (6) flat carbide poppet on sharp carbide seat (Fig. 21). The actual layouts are shown in Appendix A.

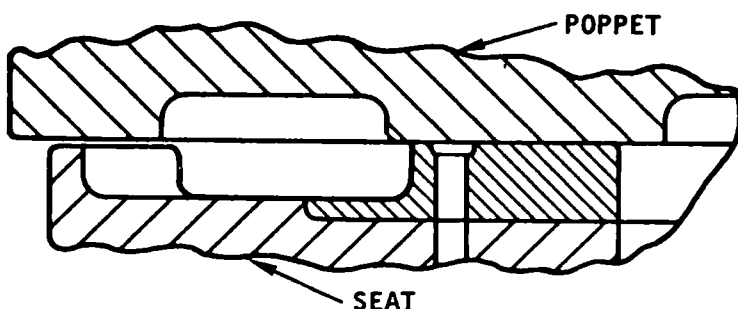
Flat 440C Poppet on Flat 440C Seat. This configuration was the major test vehicle for previous AFRPL programs (Ref. 1 through 4). It was readily fabricated and, because of lap finishing ease, had been thoroughly evaluated for sealing characteristics over a wide range of surface roughness conditions. The hardened 440C (R_c 58-62) also represented typical hard seating materials which were demonstrated to have very low leakage capability. Thus, a ready-made body of data existed to allow a comparison of the upcoming model testing with previously conducted experimental work.

Flat 440C Poppet on Flat Gold Seat. This test model was used to form the baseline static and dynamic test data for the hard-on-soft seating combinations. The original design from previous AFRPL contract testing had used work-hardened copper as the seating material; however, fabrication and testing results indicated the desirability of having a soft material to plastically flow for conformation to the poppet surface. Contaminants trapped within the wide soft land result in raised material, and the gold represented lower seating loads required to elastically and plastically deform the seating surface for poppet conformation and leakage shutoff.

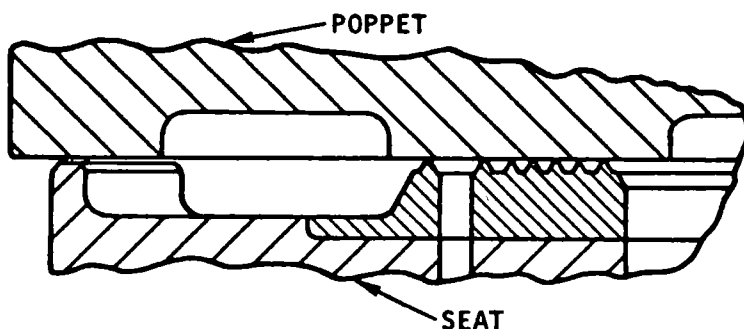
Flat 440C Poppet on Grooved Gold Seat. Consideration of particle effects observed from AFRPL tests indicated that raised metal from particle entrapment is minimal when the event occurs near a boundary. This is because the material has access to free space, i.e., can flow laterally with minimal restraint. Conversely, particles entrapped within a wide seat land must displace their volume through a combination of plastic and elastic deformation, resulting in relatively large amounts of material extruded vertically, with the general surrounding plane more gently raised. It follows that a valve seat composed of "all edges" would more readily envelop particles. Conventionally, a narrow land conical seat is thought to have favorable "particle-eating" properties, but just the opposite is true for very low leakage because a single particle can bridge the land. Combining these concepts, however, a flat or spherical seat land composed of concentric sealing annuli 0.001- to 0.002-inch (0.00254 to 0.00454 cm) wide,



CONCEPT 1 FLAT HARD POPPET ON FLAT HARD SEAT



CONCEPT 2 FLAT HARD POPPET ON FLAT SOFT SEAT



CONCEPT 3 FLAT HARD POPPET ON GROOVED SOFT SEAT

- EVALUATED IN AFRPL CONTRACTS AF04(611)-8392 & AF04(611)-9712

- CONTAMINANT SENSITIVE

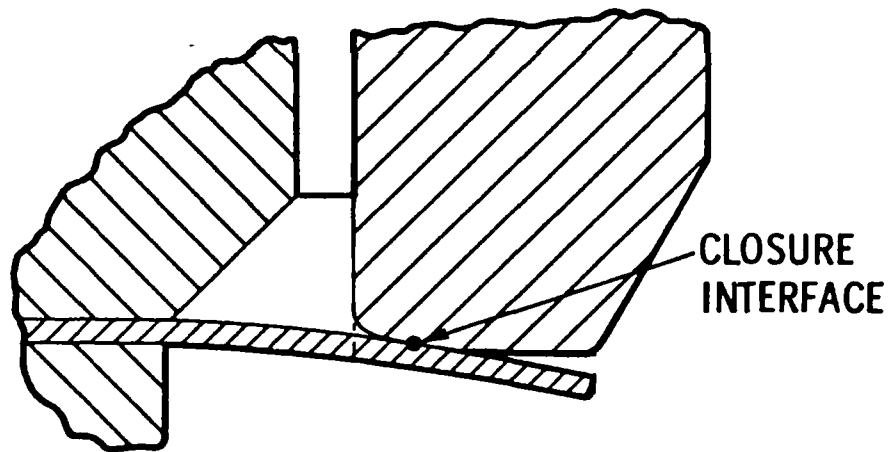
- EVALUATED IN AFRPL CONTRACT F04611-67-C-0085

- SOMEWHAT CONTAMINANT TOLERANT

- EVALUATED IN AFRPL CONTRACT F04611-67-0085

- VERY CONTAMINANT TOLERANT

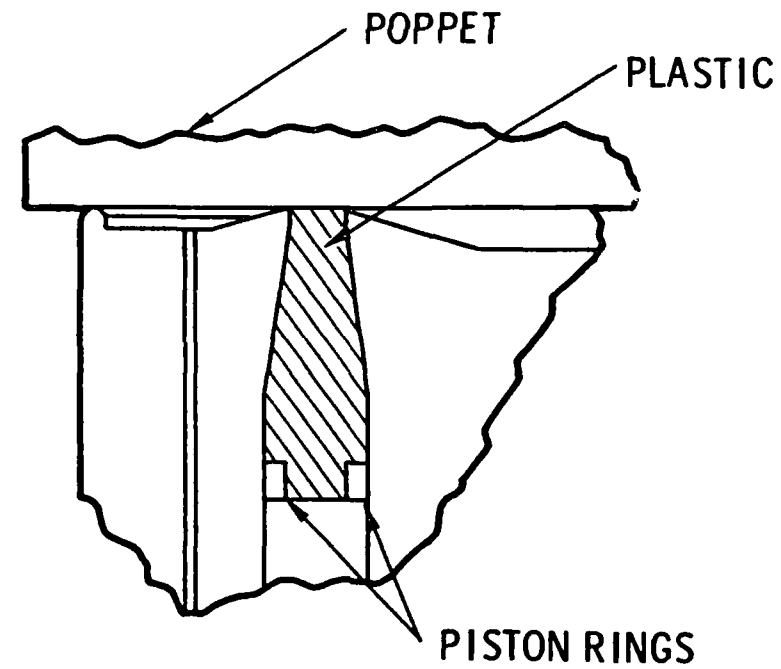
Figure 18. Closure Concepts



- USED ON J-2 ENGINE
- REDUCES INTERFACIAL ALIGNMENT REQUIREMENTS

CONCEPT 4 FLEXIBLE DISC SEAL

Figure 19. Closure Concepts

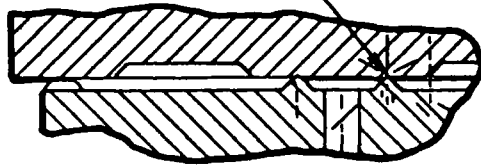


•
CONCEPT 5 CAPTIVE PLASTIC SEAL

- USED IN ROCKETDYNE FACILITY VALVES
- VERY CONTAMINANT TOLERANT

Figure 20. Closure Concepts

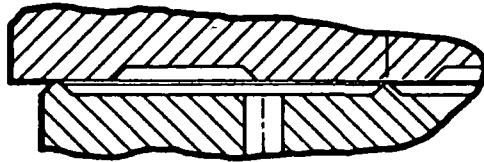
CLOSURE INTERFACE



- UNIQUE CONCEPT

- CONTAMINANT TOLERANT

- CONTAMINANT DESTROYER



ALTERNATE

CONCEPT 6 HARD-SHARP CARBIDE SEAL

Figure 21. Closure Concepts

separated by grooves of similar width and depth, appeared to be advantageous. The grooves provide a repository for displaced material and also particles. Multiple sealing annuli allow for the loss of one or more lands without serious increase in leakage.

440C Nose Poppet on Beryllium Copper Disk Seat. Of all the sealing concepts, this is the only one which was limited solely to the low-pressure SS/APS system. The two previous concepts, flat gold and grooved gold, were planned as being applicable to the low-pressure system as well, since the gold is soft and conforms readily to the poppet for sealing. The concept was chosen based on good performance of a similar seal design flight-qualified in the Rocketdyne J-2 program. The disk material used in the J-2 is elgiloy foil since the life cycle requirement is low. For the SS/APS application, beryllium copper was chosen since it is a material which has exhibited good wear capability in long-cycle tests.

Flat 440C Poppet on Captive Plastic Seat. The captive plastic seal concept is an application of an improvement on an earlier Rocketdyne patented sealing device (Ref. 10). A TFE Teflon seal ring is "captured" between inner and outer retainer rings, the model seat ram, and the 440C poppet. Piston rings are used as anti-extrusion devices to prevent TFE from extruding along the clearances between the seat ram, and the inner and outer retainer rings. Thus, the TFE Teflon ring becomes, in effect, a hydrostatic sealing member since the retaining rings are free to overtravel at valve closing, with the seat ram "pressurizing" the TFE seal ring against the mating poppet. This capability provides intimate sealing contact between the TFE and the model poppet, forming in essence a new seal at each closure. The closure is very contaminant resistant for that reason.

The TFE Teflon was chosen for use as a seal material in gaseous oxygen service because of the vast experience Rocketdyne had accumulated on TFE in LO₂ service. The TFE had been used in many engine applications to pressures several times higher than the SS/APS pressure. Batch compatibility-testing was performed in many cases to establish LOX compatibility.

Flat Carbide Poppet on Sharp Carbide Seat. The hard sharp carbide concept evolved from previous AFRPL program efforts to provide an "ultimate" contaminant-resistant closure. Unlike all previous designs wherein bearing stress was maintained reasonably low, the seat was loaded to approach the compressive yield strength of tungsten carbide. Particle resistance was provided by the ultrahard seat material being able to cut or break entrapped contaminants without permanent damage. The poppet is harder and stronger than the seat to maintain a flat reference geometry.

CLOSURE SCREENING TESTER

Design

In previous Air Force Rocket Propulsion Laboratory poppet and seat programs (Ref. 1 and 2), precision testers were utilized to evaluate the relationship between load, surface texture, and leakage for a large variety of metal-to-metal closures. (Axial load positioning and control were provided by a pressurized hydrostatic

bearing.) Some models were cycled one-million times with final leakage less than APS requirements. The AFRPL Poppet and Seat program was continued with contamination as a primary variable (Ref. 3 and 4), and tests were completed to evaluate closure models most resistant to solid particle entrapment through a combination of static (load) and life-cycle tests in a controlled contaminant environment. In these latter tests, it had been demonstrated that 50,000 impact cycles in Freon TF results in negligible sealing degradation of models currently meeting APS leakage requirements. This is attributed to the almost total lack of lateral scrubbing during closure provided by the tester design.

It was in recognition of this tester capability, which is not entirely possible to incorporate into a flightweight valve, that the decision was made to add closure lateral scrubbing control as a primary cyclic requirement of the APS closure screening tester.

Early investigations into various means for providing ball joint poppet closure indicated design feasibility, but with considerable interfacial sliding. Provision of a hinge joint at the seat interface corrected this problem, but at the sacrifice of ball joint scrubbing. A force balance analysis of the design showed that friction resulted in high seat forces (≈ 50 pounds; 222.4 N) during closure.

Even with little scrubbing, such high forces would likely cause excessive wear with many materials. Therefore, it was concluded that a design was necessary that would have the capability of causing failure through scrubbing, but that also could allow retreat to even more perfect closure control to eventually effect success, and thus define design criteria limits.

It was but a short step to provide complete rolling bearings for all poppet articulation, and this has been accomplished in the finalized design shown in Fig. 22 and 23. The following paragraphs present a summary of the tester design requirements, features, and results of the poppet force balance analysis.

Design Requirements. General design requirements were initially defined for the tester, and as design analysis proceeded, were finalized to provide a more precise definition of tester capabilities. These are summarized as follows:

Closure Interface Control. Controls applied to the tester are as follows:

1. Inlet pressure: Zero to 1000 psig (0 to 689.4 N/cm^2) (0.1 percent)
2. Static load: 1 to 2000 pounds (4.44 to 8896 N) (1.0 percent) with load application within 0.0005 inch (0.00127 cm) of seat center of pressure
3. Impact load: 100 to 1000 pounds (44.4 to 4448 N) (5.0 percent)
4. Closure mode
 - a. Clamped: poppet and seat parallel within 20 microinches (0.0000508 cm).
 - b. Clamshell: poppet axis angular rotation to closure variable from 0.0002 to 0.01 radians with 0.0004 inch (0.001 cm) maximum interfacial sliding (scrubbing) at 0.01 radians. Maximum closure load less than 15.0 pounds (66.72 N).

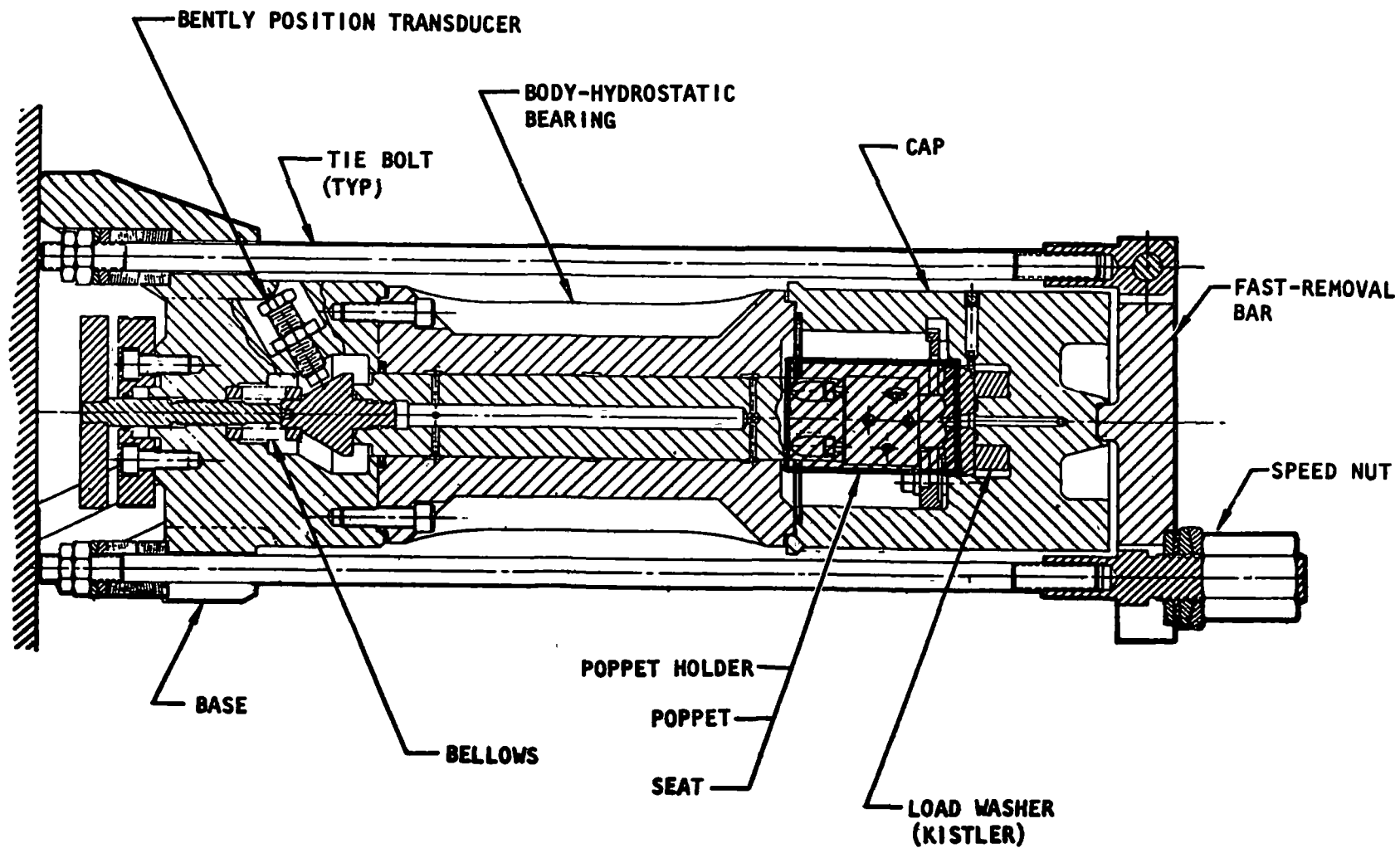


Figure 22. Closure Screening Tester

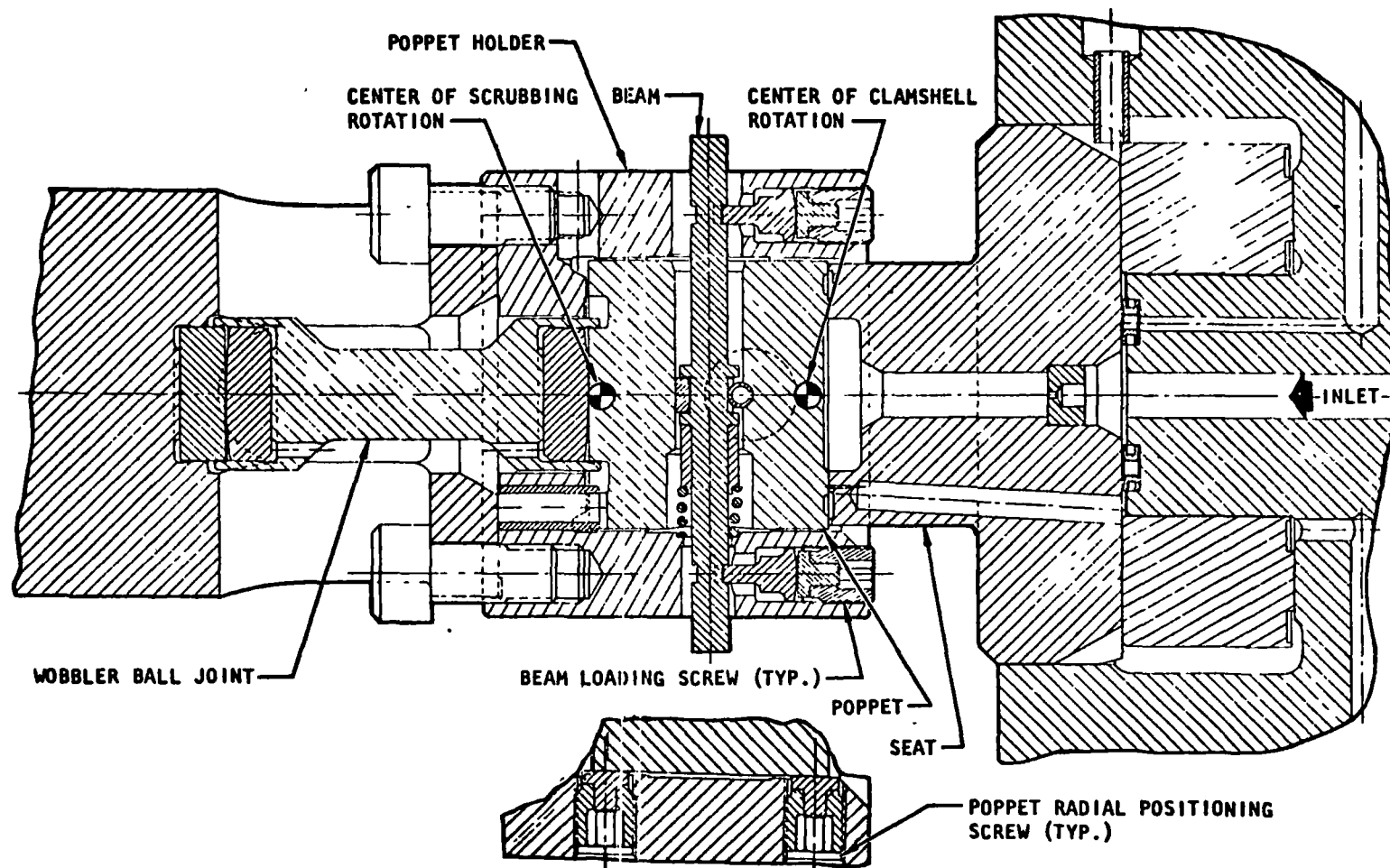


Figure 23. Poppet Articulation Detail

- c. Scrubbing: some angular limits as b., but with up to 0.0062 inch (0.0157 cm) interfacial sliding at 0.01 radians.
5. Removal repositioning: 0.0005 inch (0.00127 cm) maximum deviation from any position.

Tester Requirements. Requirements applied for the design were as follows:

1. Pressure: 1000 psig (689.4 N/cm²) inlet, 2000 psig (1378.8 N/cm²) load control.
2. Temperature: 140 to 850 R (77.8 to 472 K)
3. Cycle life: 10⁹
4. Negligible friction
5. Ultraclean inlet design
6. Gaseous nitrogen, helium, hydrogen operation
7. Solenoid cycling or unstable cycling from 10 to 100 Hz with impact loading to 1000 pounds (4448 N)
8. Measure low leakage (<0.061 sci/hr, <1.0 scc/hr) over temperature range
9. Measure static load within 1 percent
10. Measure impact load within 5 percent
11. Measure impact velocity within 5 percent
12. Proof that poppet does not separate from wobbler bearing during cycling
13. Measure surface scrubbing energy expended with each closure

Tester Design Features. Except for the poppet holder, the overall tester design was patterned after the AFRPL dynamic tester of Ref. 4 . Basic differences resulted from the requirement for operation at 140 R (77.8 K) and, as previously noted, poppet articulation. In general, the tester is simply a hydrostatic bearing with actuation force provided by gas pressure. Many detail features provide the facility for precise control and measurement of test variables.

Base. The tester incorporates a three-leg INCO 718 base which rests on a granite surface plate from which electronic gaging can be performed. The piston is forced against a 40-pitch ball joint screw by a bellows held to the base by externally removable set screws. The bellows thus provides return spring force and rotational orientation, while also allowing the piston to be rotated as a precision air bearing for poppet measurements. A pointer and 0.01-inch (0.0254 cm) machinists' scale provide axial control within 50 microinches (0.000127 cm) via the 40-pitch screw. The base also contains a Bently position transducer for axial velocity measurement during cycling and a port for applying piston load control pressure.

Hydrostatic Bearing-Body. The hydrostatic bearing and body are made of 440C stainless steel. Each part is held round and straight within 10 microinches (0.0000254 cm) to provide about 50 microinches (0.000127 cm) diametral clearance for the 1.250-inch (3.175 cm) basic diameter. The piston is flame sprayed with

tungsten carbide (for 140 R, 77.8 K, operation) rather than aluminum oxide as in the AFRPL testers. Stiff resistance to lateral motion and negligible friction will be obtained by pressurizing the central clearance with nitrogen or helium to 1000 psig (689.4 N/cm^2). Dual exhausts are provided to allow prechill purging during 140 R (77.8 K) cooldown.

Static seat load will be applied by pressurizing the piston end with hand control via 0.1 percent Heise gage and bottle regulator.

Cap. Rapid access to the poppet and seat are provided by a removable cap holding the seat. (In previous designs, the seat and poppet had to be carefully assembled into a limited access cavity. Sealing surfaces were easily damaged if bumped, so the design herein was incorporated.) This is accomplished by loosening one tie bolt nut, allowing the tie bolt and loading bar to be swung away and the cap removed. The seat is retained in the cap by a clamp spring, thus avoiding inlet line tie-down screw threads. Directly under the seat is a piezoelectric load washer (Kistler) for measuring static and dynamic loads. Calibration was obtained by piston loading. This device has proved exceptionally reliable and stable in past AFRPL programs. Seat repositioning is provided by pins between the cap and body.

The cap contains several ports for bleed and leakage measurement. Inlet pressure is supplied to the seat directly from a 1-inch (25 mm), 1/2-micron membrane filter integral with the cap. Supply pressure is isolated from the leakage measurement cavity by two K-seals separated by an overboard bleed. Volumetric leakage is measured from either of two ports depending upon the leak rate. All seats are designed with an integral low-volume seal cavity for leak collection which is ported directly out of the tester via a small hole. The cap also contains a burst diaphragm in the event excessive pressure is built up within the vent cavity.

All external ports are of the fitting type so that the tester can be submerged in liquid nitrogen without LN_2 entering the tester cavity.

Poppet Holder and Wobbler Bearings. This device is the heart of the tester. As shown in Fig. 23, the external holder positions the poppet on the wobbler bearing held within the piston. The wobbler is a lens shape because the more desirable sphere would be too long due to necessary large radii required to minimize bearing stress. Poppet centricity is controlled with 8 carbide button, 120-pitch screws located near each end of the poppet 45 degrees from the beam axis. Installation clearance will be 0.0002 inch (0.000508 cm) diametral. A beam loads the poppet (up to 40 pounds, 177.9 N) onto the wobbler via two end bearings and one center bearing. The end bearings are axially adjustable to vary beam deflection and, thereby, load. Except for a saddle shape over the beam, the end bearings are lens shaped similar to the wobbler bearing.

Clamped closure mode is obtained by removing the wobbler bearing. The poppet then rests directly on the holder face. Clamshell and scrubbing closure modes are obtained by backing off either the top or bottom two screws (opposite the coil spring) the desired amount. Gaging will be performed with an electronic indicator referencing opposite screws against the air bearing axis which will be rotated. Positioning will be within ± 50 microinches ($\pm 0.000127 \text{ cm}$).

A cocking load is produced by either a coil spring, as shown, or use of end bearings with offset radii. The latter will be employed for cocking up to 0.004 radians (0.002 inch, 0.00508 cm, over 0.500-inch (1.27 cm) outside seat diameter).

Poppet repositioning is provided by a pin between the poppet holder and poppet.

All wobbler bearings are a combination of tungsten carbide (6-percent cobalt) and 440C stainless steel. (All clearances have been evaluated for 140 R, 77.8 K, operation). The main bearing (1.5-inch, 3.81-cm radius) contact stress is 475,000 psi (327,501 N/cm²) at 2040 pounds (9074 N) load and 380,000 psi (262,001 N/cm²) at the maximum impact load of 1040 pounds (4626 N). End and center beam bearings are stressed to 250,000 psi (172,369 N/cm²) at the maximum beam load of 40 pounds (178 N).

For long life, the use of 440C is desirable and, therefore, the beam is made from this material but with a low bending stress of 100,000 psi (68,948 N/cm²).

Cyclic Operation. Unstable cyclic operation was accomplished by pressurizing the inlet seat (P_1) through a small (No. 80) orifice to provide a sustaining rebound force against a fixed-bias piston control pressure (P_C). By varying these two pressures, cyclic rate and impact force were adjusted. Typical values are 100 Hz and 250 pounds (1112 N) impact force.

Poppet Force Balance Analysis. As previously noted, excessive friction force with a simple ball joint instigated the wobble bearing design. The objective was to be able to load the poppet with up to 40 pounds (178 N), clamshell close with minimum scrubbing, and with edge seat load less than 15 pounds (67 N). Attainment of this objective necessitated several iterative design approaches to establish bearing radii, clearances, and spring force. A summation of the final results for the clamshell closure case is presented.

Dimensions and Limits. Dimensions and limits for the poppet holder are defined by the nomenclature of Fig. 24 and as follows:

$e = 0.001$ in. (0.00254 cm) max	$r_s = 0.250$ in. (0.64 cm)
$e_T = 0.002$ in. (0.00508 cm) max offset	$R_B = 0.25^{+0.05}_{-0}$ in. (0.64 ^{+0.127} ₋₀ cm)
$F_B = F_S/2$	$R_C = 0.25^{+0.05}_{-0}$ in. (0.64 ^{+0.127} ₋₀ cm)
$F_C = 7$ pounds (31.1 N) max	$R_{BB} = 0.035$ in. (0.0889 cm)
$F_S = 40$ pounds (178 N) max	$R_{CB} = 0.052$ in. (0.132 cm)
$l_o = 0.04$ in. (0.1 cm)	$R_T = 0.313$ in. (0.795 cm)
$l_1 = 0.344$ in. (0.87 cm)	$R_W = 1.50$ in. (3.81 cm)
$l_2 = 0.58$ in. (1.47 cm)	$S = 0.0001$ in. (0.000254 cm) to 0.0058 in. (0.0147 cm)
$l_B = 0.20$ in. (0.508 cm)	$\alpha = 0.01$ radians max
$l_T = 1.0$ in. (2.54 cm)	$\beta = 0.01$ radians max
$l_w = 1.0$ in. (2.54 cm)	$\mu = 0.1$ (friction)
$r_p = 0.375$ in. (0.95 cm)	

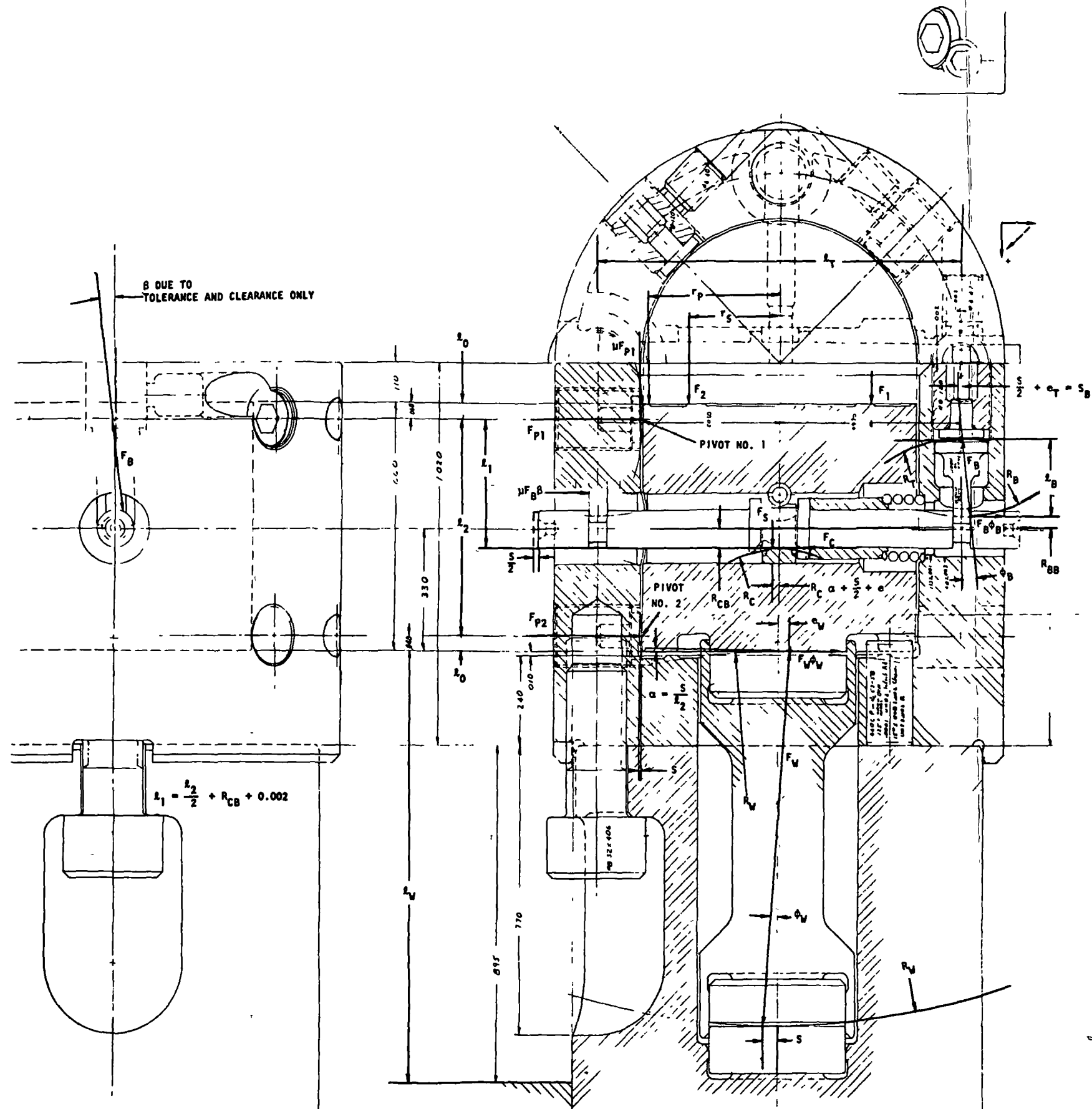


Figure 24. Load Analysis Diagram

Scrubbing Limits. Out-of-parallel gap at poppet and seat radii are given by:

$$\Delta_p = 2\alpha r_p, \Delta_s = 2\alpha r_s$$

Interface scrubbing is dependent on the pivot point and cocking angle (α) and is defined for clamshell closure as:

$$S_{C_1} = l_o \alpha$$

and scrubbing closure as:

$$S_{C_2} = (l_o + l_2)\alpha$$

Evaluation of these parameters for the previously defined limits is tabulated as follows with all dimensions in inches $\times 10^{-3}$ (i.e., mils)

<u>S</u>	<u>α, rad $\times 10^3$</u>	<u>Δ_p</u>	<u>Δ_s</u>	<u>S_{C_1}</u>	<u>S_{C_2}</u>
0.1	0.1724	0.1293	0.0862	0.0069	0.107
2.32	4.00	3.0	2.0	0.160	2.48
5.80	10.0	7.5	5.0	0.400	6.20

The following are tabulated in centimeters $\times 10^{-4}$ (i.e., microns).

<u>S</u>	<u>α, rad $\times 10^3$</u>	<u>Δ_p</u>	<u>Δ_s</u>	<u>S_{C_1}</u>	<u>S_{C_2}</u>
2.54	0.1724	3.284	2.189	0.1753	2.718
58.92	4.00	76.20	50.80	4.064	62.99
147.3	10.00	190.5	127.0	10.16	157.5

Wobbler Analysis. With reference to Fig. 24, as the poppet base swings about pivot No. 1 to the left to contact pivot No. 2, the main bearing base radius (R_w) rolls distance, S. Simultaneously, the upper radius contact moves to the right an amount, e_w , due to the rolling "lens effect" and also poppet angle, α . The result is a component force from angle ϕ_w , tending to oppose the described motion. An identical situation exists for the beam end post bearings. In the latter case, radii offsets can be built into the post bearings to supplement or replace the coil spring. The main bearing must remain centered, however, so that static and dynamic loading will be uniformly applied to the seat.

Analysis of the lens effect shows that the upper radius center along the wobbler axis follows the curve of a prolate cycloid with horizontal displacement given by:

$$b \cong \frac{S}{R} (R - l_w)$$

Vertical displacement with small angles is negligible relative to poppet position and beam load-deflection.

With poppet cocking an angle $\alpha \cong S/\ell_2$, the upper contact displacement is given by:

$$e_w \cong S \left(1 + \frac{R}{\ell_2} - \frac{\ell_w}{R} \right)$$

Force angle ϕ_w is found as:

$$\phi_w \cong \frac{S + e_w}{\ell_w} = \frac{S}{\ell_w} \left(2 + \frac{R_w}{\ell_2} - \frac{\ell_w}{R_w} \right)$$

Because the beam remains horizontal with translation, the cocking term is omitted. Beam deflection angle is neglected because it is cancelled. The end bearing force angle (ϕ_B) is given by:

$$\phi_B \cong \frac{S_B}{\ell_B} \left(2 - \frac{\ell_B}{R_B} \right)$$

Force Balance Analysis. With the preceding geometrical definitions, the force balance equations for the poppet can be defined. These equations are written with rotation about pivot No. 1:

$$\Sigma F_y = 0 = F_2 + \mu F_{p1} + F_s - F_w \quad (1)$$

$$\Sigma F_x = 0 = F_{p1} + F_{p2} + 2\mu F_B \beta + 2F_B \phi_B + F_w \phi_w - F_c \quad (2)$$

$$\begin{aligned} \Sigma T (\text{pivot No. 1}) = 0 = & F_2 (r_p - r_s) + \\ & F_s (r_p - R_c \alpha - \frac{S}{2} - e) - F_w (r_p + e_w) - \\ & F_{p2} \ell_2 - 2F_B \phi_B \ell_1 - F_w \phi_w (\ell_2 + \ell_o) + \\ & F_c \ell_1 - 2\mu F_B \beta \ell_1 \end{aligned} \quad (3)$$

Unknown variables are F_2 , F_{p1} , F_{p2} , and F_w .

In design, it was desired to know the required minimum cocking spring force (F_c) required to establish a positive (F_{p2}) force with the maximum beam spring force. As noted in the nomenclature, a complete eccentricity study of all tolerances indicated that the center bearing could be 0.001 inch (0.00254 cm) from true

position, and end bearings ± 0.002 inch (± 0.00508 cm). To counteract end bearing eccentricity, the R_B radius is defined to be offset from the part axis (defined by R_T) by 0.003 inch (0.00762 cm).

Solution of Eq. 1, 2, and 3 for:

$$\begin{aligned} S &= 0.0058 \text{ in. (0.0147 cm)} \\ \alpha &= 0.01 \text{ radians} \\ F_S &= 40 \text{ pounds (178 N)} \\ e_T &= 0.002 - 0.003 = -0.001 \text{ in. (-0.00254 cm)} \\ F_C &= 7 \text{ pounds (31.1 N)} \end{aligned}$$

yielded the following results:

$$\begin{aligned} F_{P_1} &= 4.642 \text{ pounds (20.65 N)} \\ F_{P_2} &= 0.8806 \text{ pounds (3.92 N)} \\ F_w &= 40.46 \text{ pounds (180 N)} \end{aligned}$$

With the noted conditions it was further computed that a seat force (F_2) of 12.43 pounds (55.29 N) was required to just close (i.e., $S = 0$, $F_1 = 0$).

The preceding parameters were design limits. To establish a nominal worst starting condition for test, a seat out-of-parallel dimension of 0.002 inch (0.00508 cm) was selected. Further evaluation of offset end bearing radii (R_B) led to the conclusion that an offset of 0.01 inch (0.0254 cm) could be allowed and still maintain a suitable Hz stress contact area within the 0.05-inch (0.127 cm) length. As a result, several sets of these bearings were fabricated with 0.003-in. (0.00762 cm) and 0.01-inch (0.0254 cm) offsets. Combinations can thereby be used with or without a coil spring to provide suitable cocking force. The following case was selected for analysis:

$$\begin{aligned} S &= 0.00232 \text{ in. (0.00589 cm)} \\ \alpha &= 0.004 \text{ radians} \\ F_S &= 20 \text{ pounds (88.96 N)} \\ e_T &= -0.01 \text{ in. (-0.0254 cm)} \\ F_C &= 0 \end{aligned}$$

These data gave:

$$\begin{aligned} F_{P_1} &= 0.9029 \text{ pounds (4.016 N)} \\ F_{P_2} &= 0.09758 \text{ pounds (0.4340 N)} \\ F_w &= 20.09 \text{ pounds (89.36 N)} \end{aligned}$$

Poppet assembly and wobbler weights were calculated and an estimate made of the force required to accelerate the assembly to contact pivot No. 2. Assuming one half the weight effective, it was computed that 0.03 pounds (0.13344 N) force was required to move the poppet and wobbler the 0.00232 inch (0.00589 cm) within 0.005 second; thus, adequate margin exists.

For the above-noted conditions, the maximum (F_2) seat force required to balance the poppet in the closed position is 1.942 pounds (8.638 N). With these data, it has been shown that a wide limit of tests can be performed with the capability to approach near-perfect closure with little scrubbing.

A simplified description of the closure screening tester operation is included as Appendix B.

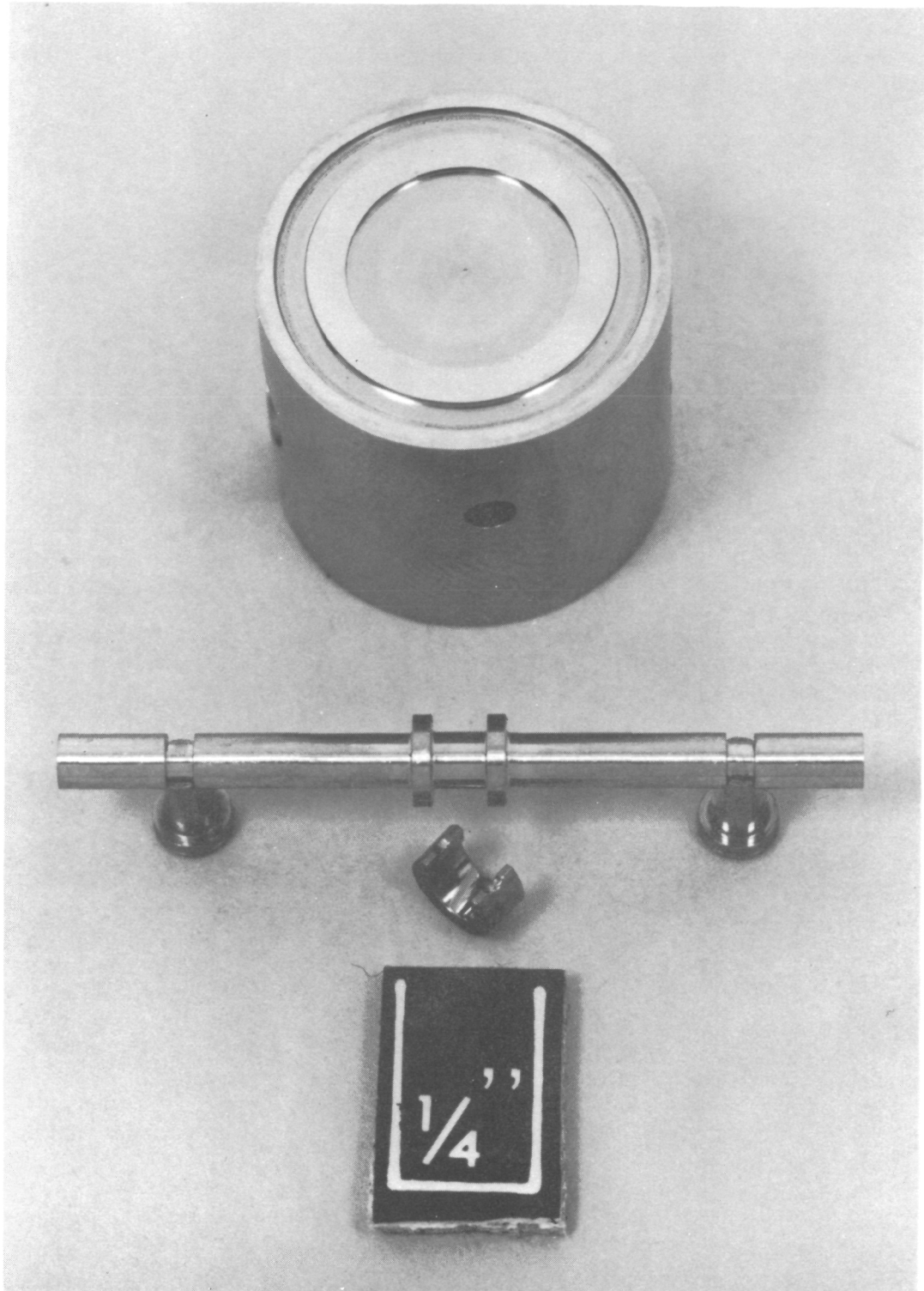
Fabrication

Fabrication of both the closure models and the closure screening tester was accomplished at L. A. Gauge Co., Inc., Sun Valley, California. The specialized capabilities of this vendor, as proved on the AFRPL programs, represented the minimum risk to fabricating hardware with the tolerances and finishes needed to satisfy SS/APS requirements. The detail parts of the closures and tester were fabricated using conventional machining and tool room techniques, with the exception of the items discussed below.

Figure 25 shows the 440C poppet along with the poppet loading beam and end and center bearings which will be discussed later. The poppet is fabricated with its sealing and bumper lands flat within 0.000010 inch (0.000025 cm) and parallel to the back face and perpendicular to the outside diameter within 0.000050 inch (0.000127 cm) total. The final effort on each poppet consisted of a diamond-lapping process which produced a finish of approximately 1 microinch AA (2.54×10^{-6} cm). The poppet is shown installed within the poppet holder in Fig. 26, and alongside the mating seat in Fig. 27.

The seat pictured in Fig. 27 is one of the grooved gold models, with a lapping ring in place on the seat. The lapping rings were made and serialized to each seat so that controlled lapping of the seat face could be performed. The lapping ring provides a larger area for lapping, preventing any "overturning" motion that would result in a crowned rather than a flat face on the seat. In Fig. 28, a completed flat 440C seat is shown installed within the top cap of the tester. The seat critical leakage measurement hole may be observed just inboard of the "gross" leakage slot. The gross leakage slot was provided in each seat to prevent pressure buildup outside the actual sealing area so that balance pressure and low seat load tests could be performed. The seat is held in place on the Kistler load washer by the spring clip arrangement.

Figure 29 shows the tester with the top cap removed. The end of the hydrostatic or "air" bearing piston and poppet holder are visible. Figure 30 shows the complete closure screening tester assembly readied for proof testing. Figure 31 shows the poppet loading beam, the two end or "saddle" bearings, and the center bearing mentioned earlier. The end bearings were fabricated as one part, with the pivot crown being ground and lapped on either end, then the center "saddle" formed by stick-lapping the center hole to form a controlled, double-bellmouth



1ST91-5/21/71-C1G

Figure 25. 440C Poppet With Loading Beam and Bearings

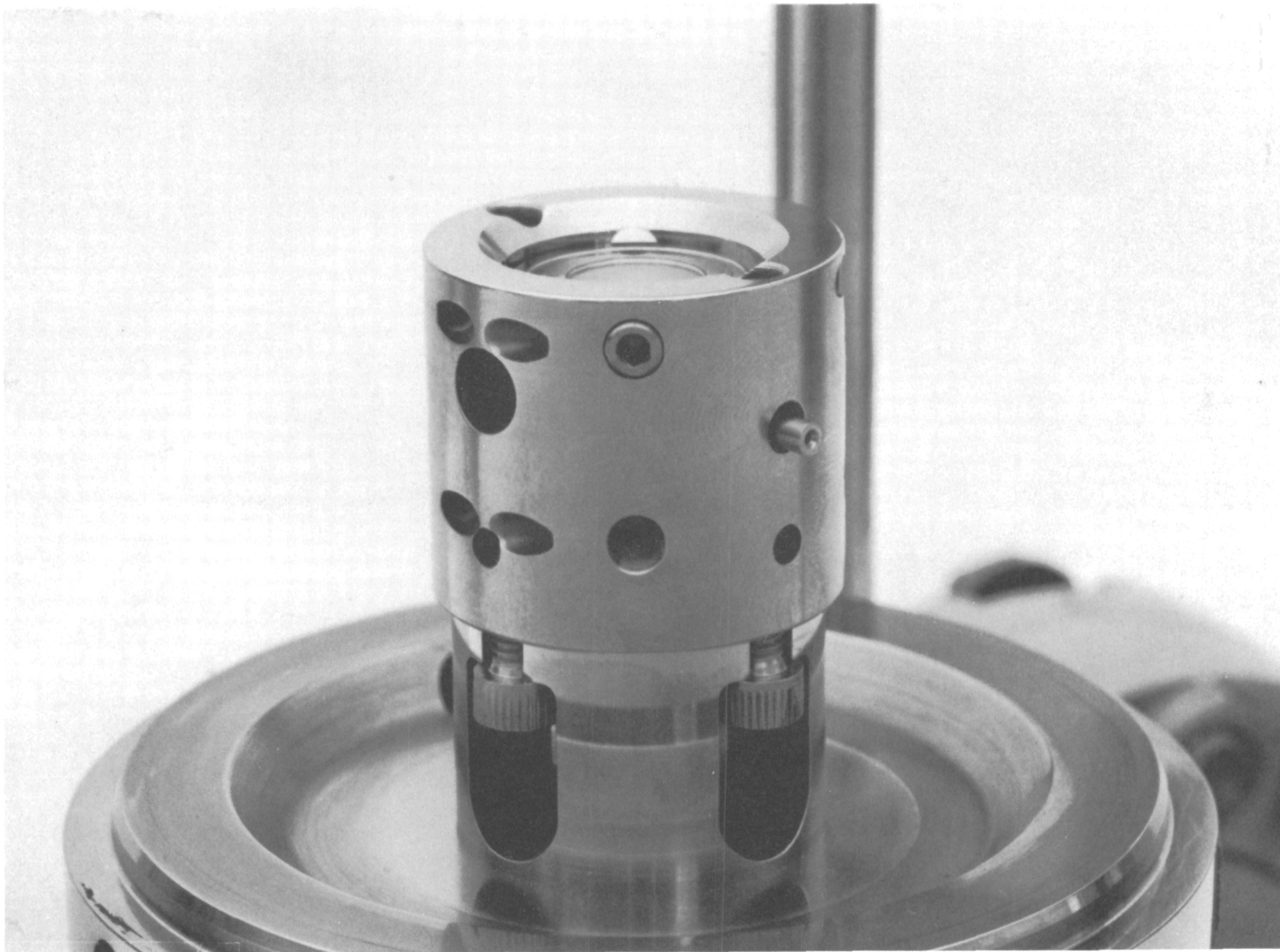
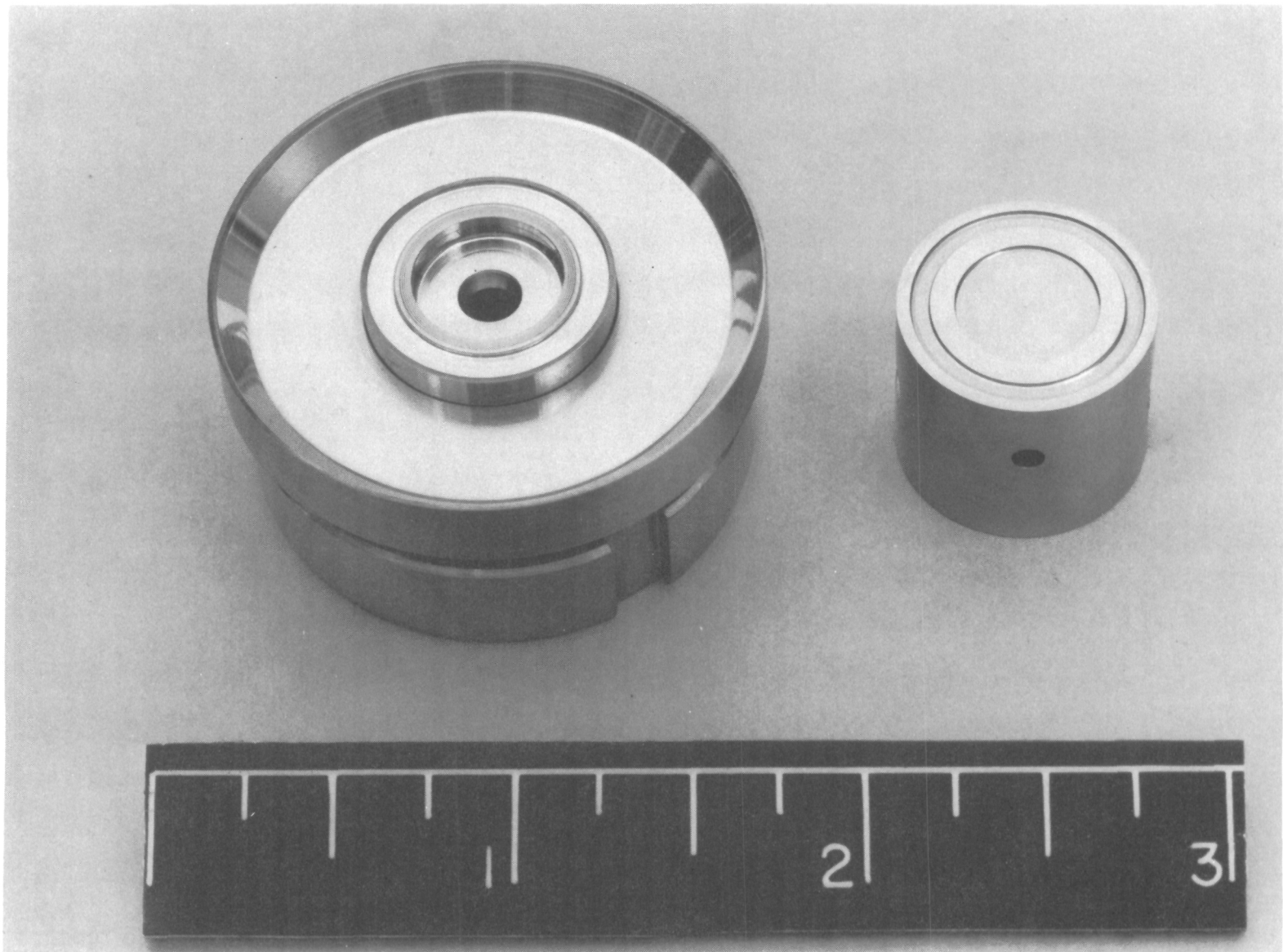


Figure 26. Poppet Holder Detail

1ST91-5/21/71-C1A



1ST91-5/21/71-C1C

Figure 27. Grooved Gold Seat in Lapping Ring and 440C Poppet

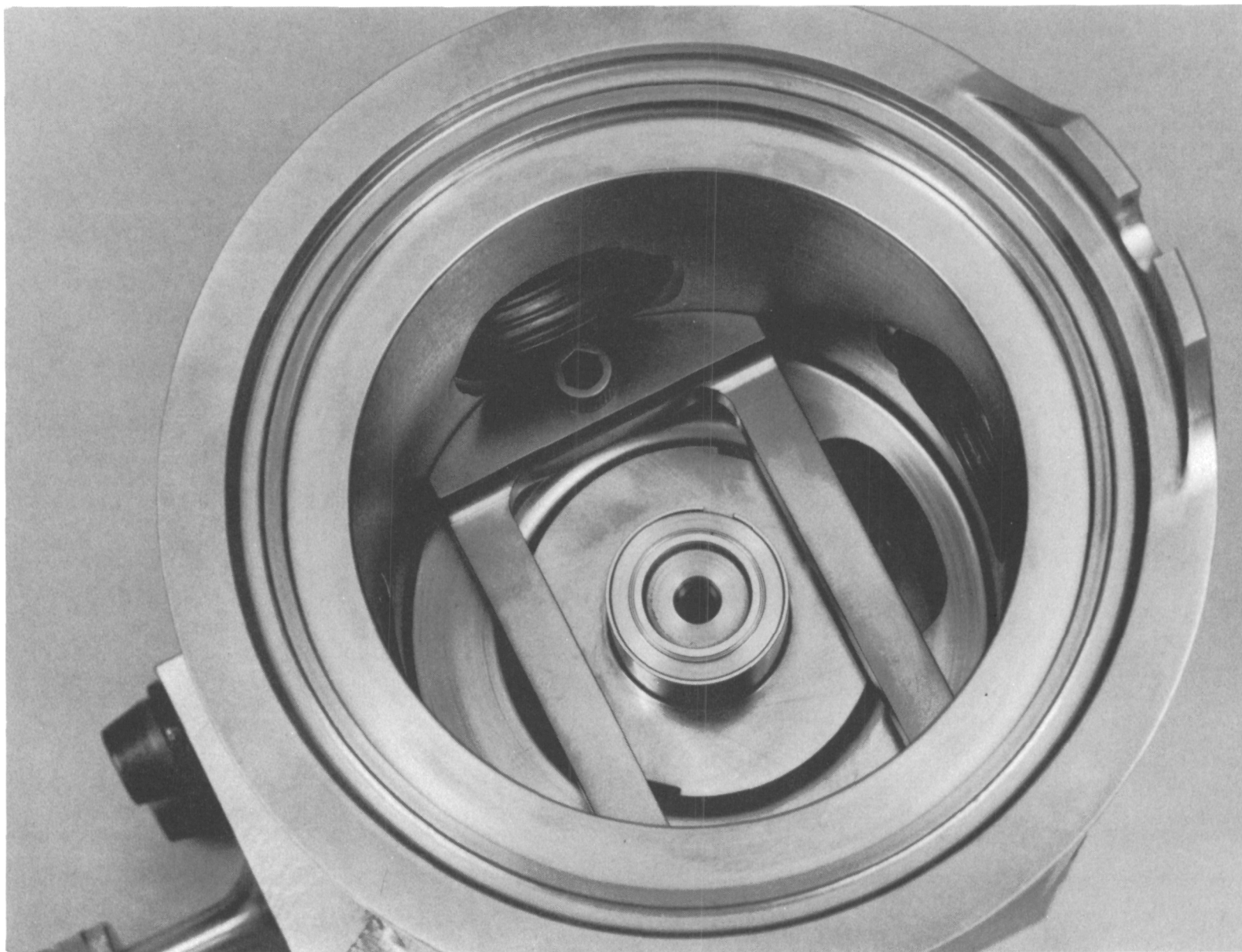
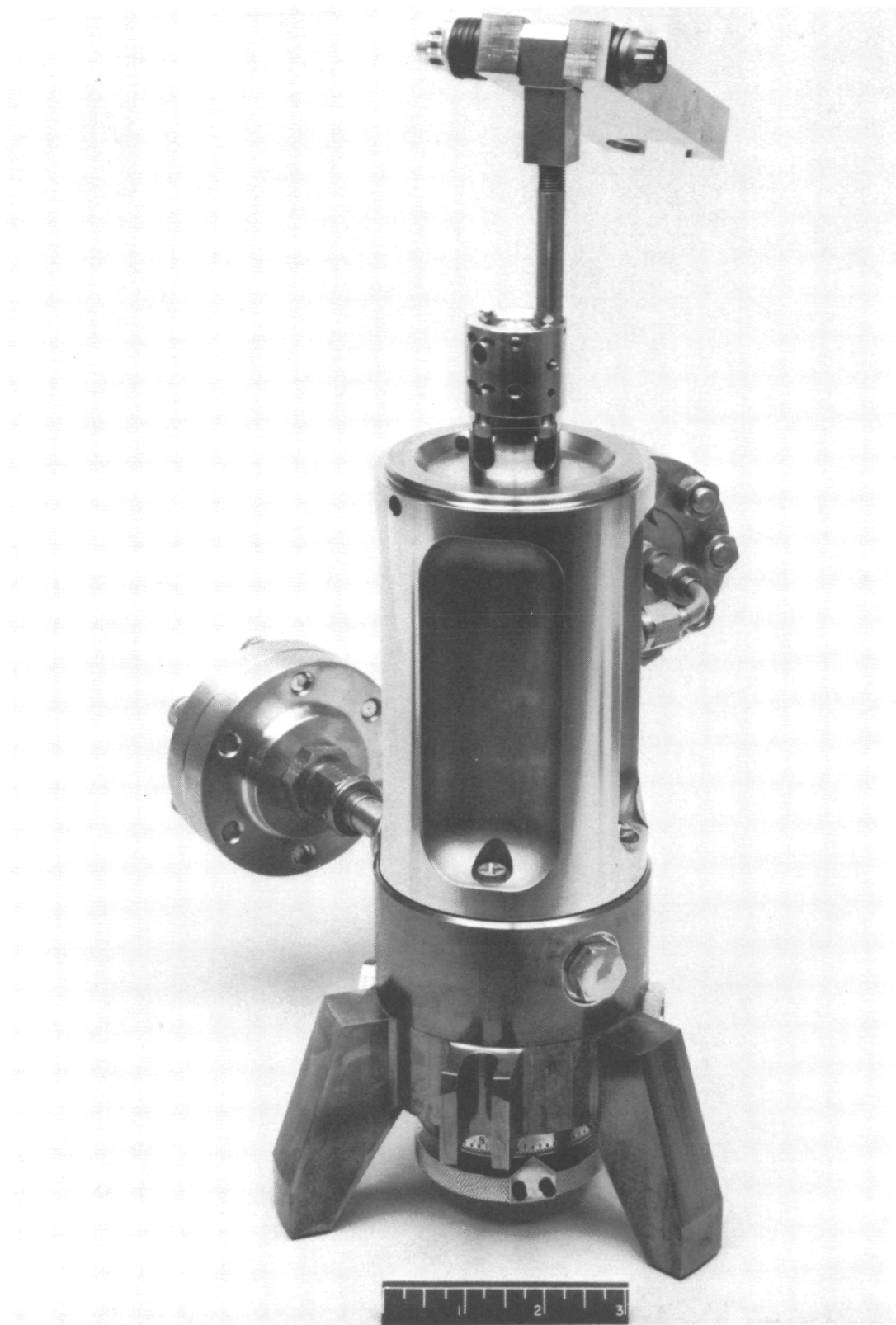


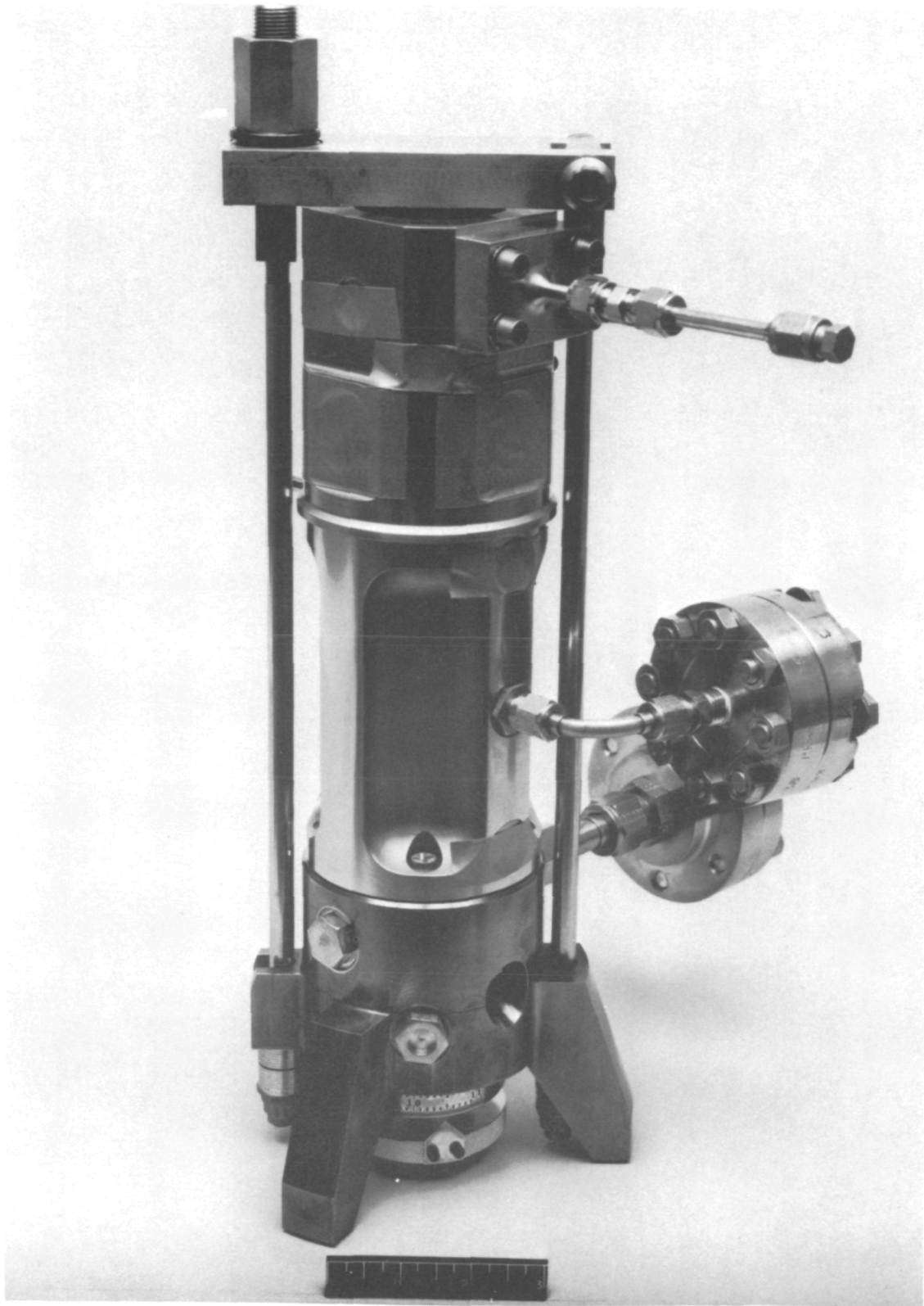
Figure 28. 440C Seat Installed in Top Cap

1ST91-5/21/71-C1D



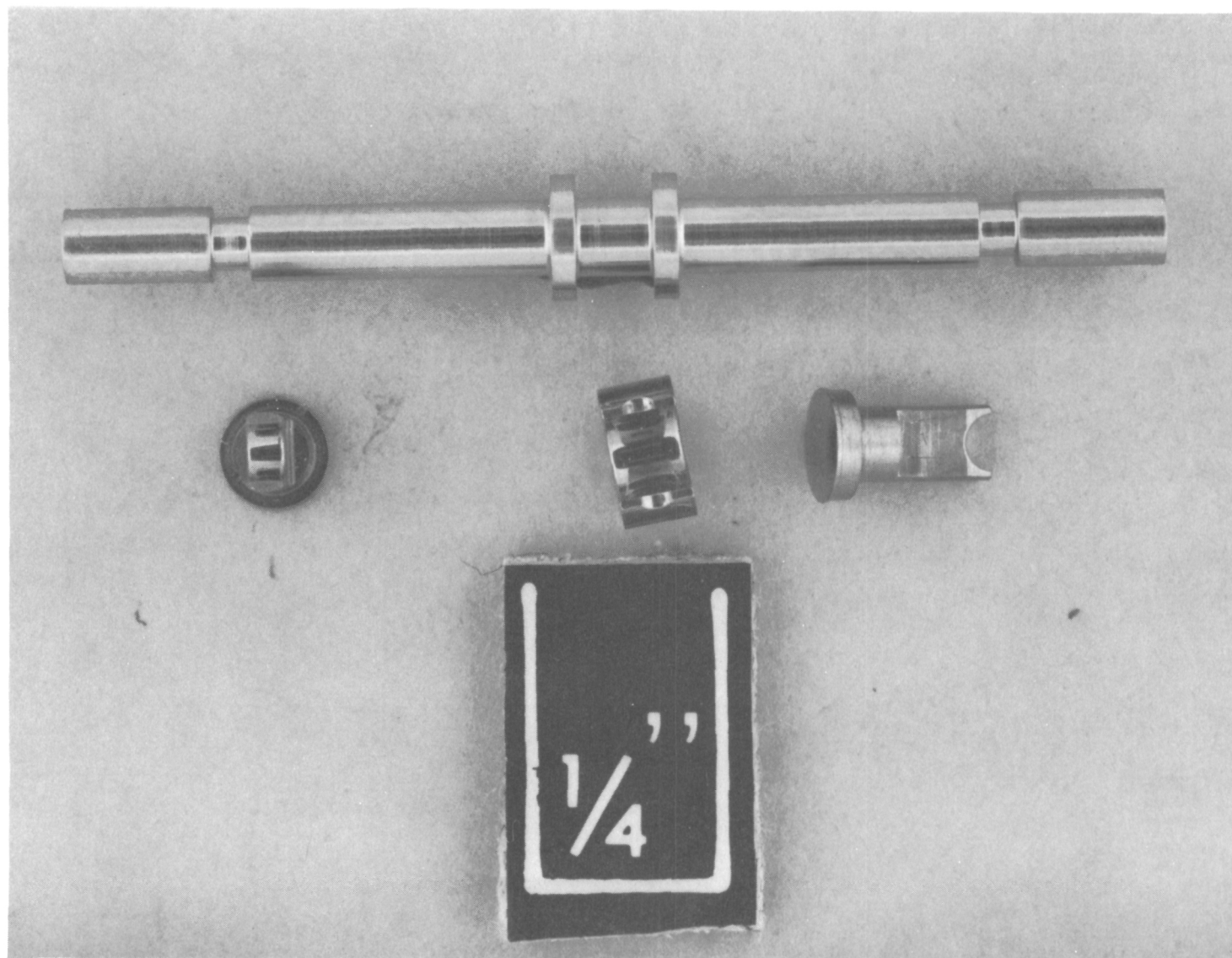
1ST91-5/21/71-C1E

Figure 29. Tester Without Top Cap



1ST91-5/21/71-C1F

Figure 30. Tester Assembly



1ST91-5/21/71-C1B

Figure 31. Poppet Loading Beam With End and Center Bearings

entry. After the proper radius and finish were obtained, the part was then ground into, forming two end bearings. The center bearing was stick-lapped in a similar manner, then slotted to fit the poppet loading beam, and a roll pin retention groove added. All these features may be observed more readily by observing the poppet articulation drawing presented as Fig. 23.

TESTING

The following sections will describe the tester, its test system, and initial checkout efforts.

Tester and System Information

Closure Tester Description. The closure tester is a multiple-feature fixture providing for closure mounting, loading, and leakage collection together with integral instrumentation for monitoring fundamental closure parameters. The basic structure consists of a pneumatically pressurized hydrostatic bearing (body and piston) which permits near-frictionless loading of closure test surfaces via pressure application to one end of the piston. The test closure poppet is retained at the opposite end of the piston. The mating test closure seat is located in a removable cap through which closure inlet pressure is directed and resulting leakage is captured. The tester is designed to operate in both static and dynamic modes. In the static application, tester function is to provide a means of positioning a closure poppet and seat in intimate contact with supply pressure applied, while incrementally varying closure interface load and monitoring leakage variation as a function of that load. In the dynamic mode, impact loads are applied to closure interfaces to simulate cyclic operating conditions found in actual valves.

The test device must provide significantly more precise control and information than is usual for valve evaluation and testing. In previous Air Force Rocket Propulsion Laboratory (AFRPL) poppet and seat programs Ref. 1 through 3), precision testers were utilized to evaluate the relationship between load, surface texture, and leakage for a variety of metal-to-metal closures. These testers also permitted investigation of contamination sensitivity and cyclic endurance of closure designs. However, the degree of precision built into the testers (fixed orientation; parallelism within 20 microinches, 0.000051 cm; etc.) exceeded that which is practicable for flightweight valves. Thus, the influence of abnormal motion during poppet and seal closure, experienced in most aerospace valves, was not investigated. In recognition of this problem, the capability of controlled articulation (nonparallel or clamshell, and scrubbing interfacial motions) was added to the APS closure tester.

Test System. The test system required to support closure screening tests is patterned after similar systems developed for Air Force closure evaluation programs (Ref. 1 through 3). While the innovations adopted in the APS closure tester necessitate instrumentation not previously used, pressure and leakage measurement subsystems remain fundamental to this tester concept. For ambient and elevated temperature testing, these subsystems did not require extensive buildup and checkout effort. Low-temperature investigations, however, did require supplemental subsystems to provide for: (1) dry test gas supply, (2) pre-chilling test and purge gases, and (3) additional instrumentation. Thus, test

system requirements resolved into two parts: a basic and a supplemental low-temperature test setup. These are described in the following paragraphs.

Basic Test System. While candidate closure configurations were evaluated at extreme temperature conditions, the bulk of preliminary investigations were performed at room temperature. Thus, a basic test system combining the closure tester and all equipment necessary for tester and closure evaluation under ambient conditions was fabricated initially. Figure 32 illustrates this system, which can be categorized into pressurization, leak measurement, and instrumentation subsystems.

Pressurization Subsystems. Four pressurization sources were used, three for tester operation and one for manual purging purposes. Pressure regulators were standard commercial bottle regulators (Hoke, Airco, etc.). These devices proved in previous programs to have exceptional stability under low-flow conditions and to provide pressure control within 0.1 psi (0.0689 N/cm²). For the critical applications of piston control (P_c) and closure supply (P_1) pressures, downstream bleed flow was utilized to enhance response.

Hydrostatic bearing pressure (film pressure, P_c) is directed to the tester through a 1/2-micron absolute-rating membrane filter element. To preclude rupture through inadvertent reverse pressurization, the element was mounted in a holder utilizing support screens in both flow directions. A conventional bottle regulator gage provided sufficient accuracy in setting this pressure to a nominal 600 psig (413 N/cm²) value.

Closure inlet pressure was supplied directly to the tester integral filter without prefiltration. A 0- to 1000-psig (0 to 689.5 N/cm²) Heise gage was used for inlet pressure measurement. This type of gage is temperature compensated, can be remotely zero set, and is accurate to 0.1 percent of full scale.

A 1/2-micron bidirectional-membrane micron-type filter was employed in the piston control pressure gas supply. To provide accuracy in the low closure load region (down to the order of 4.0 pounds, 17.8 N) a 0- to 300-psig (0 to 206.8 N/cm²), 0.1-percent Heise gage was used. A 0- to 2000-psig (0 to 1379 N/cm²) Heise gage provided for measurement of upper-level load applications.

The purge flow system was utilized primarily for removing dust particles (attendant with assembly) from closure sealing surfaces. No pressure monitoring device was necessary. The 1-inch (25-mm) size membrane filter is adequate for this function and, because reverse pressurization cannot occur, a unidirectional element holder sufficed.

Since all tester pressurization applications required relatively low flows, 1/4-inch OD (0.635 cm) lines were used. While flexible lines were employed upstream of test system filters to facilitate tester movement and access, all plumbing downstream of these filters was stainless-steel tubing. Flexible lines were cleaned by flushing with solvent. Hard lines were first scrubbed internally and then flushed with solvent.

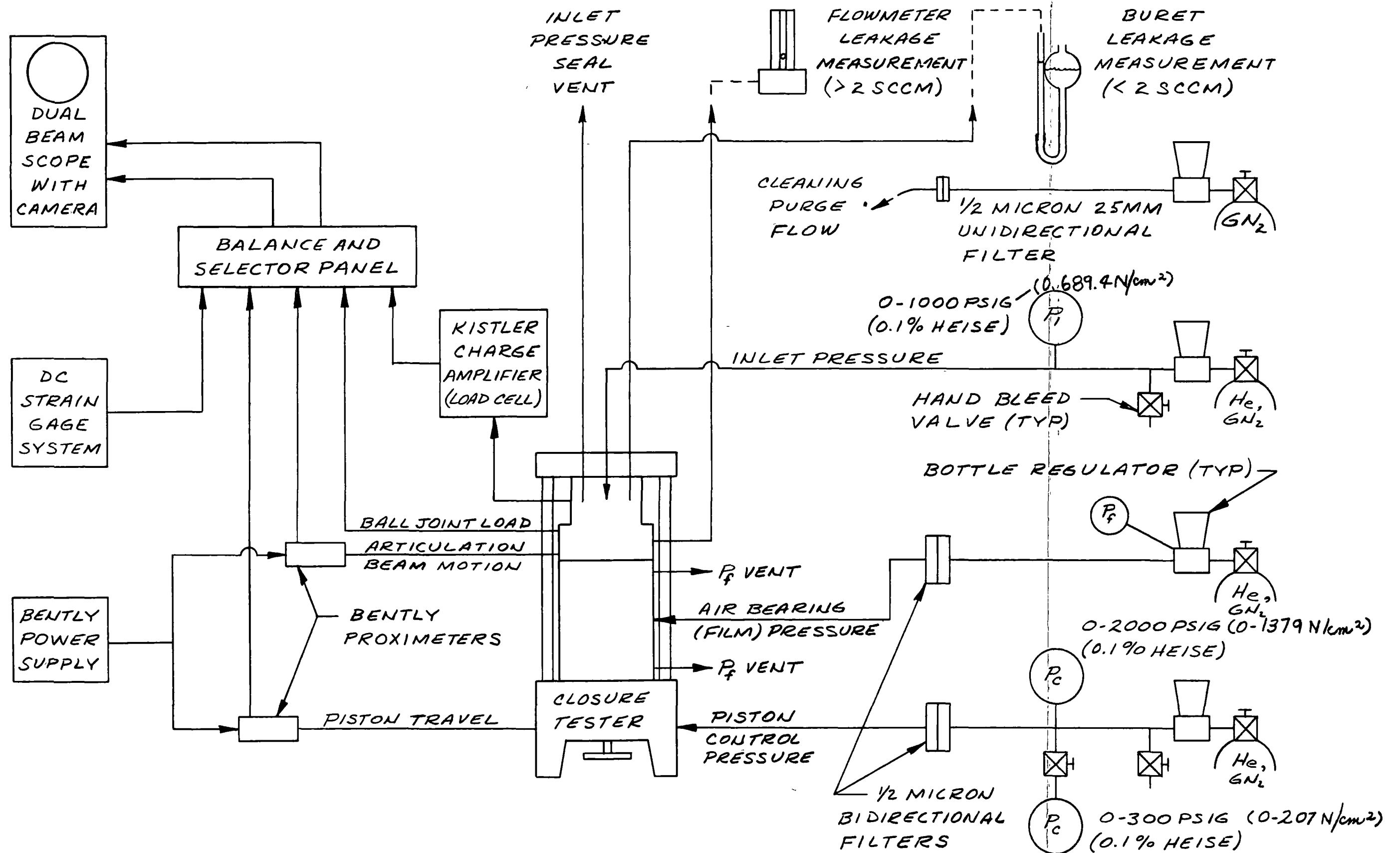


Figure 32. Basic APS Closure Test Schematic

Leakage Measurement. Two methods of leakage measurement were used. For leakage flows on the order of 0.126 scim (2 sccm) and greater, Pyrex ball-float rotameters were employed. These devices, particularly those with Brooks tubes, have demonstrated repeatable accuracy (less than 5-percent error) in past programs over periods ranging up to 3-1/2 years.

A leveling-bulb buret procedure was used to measure leakage less than 0.126 scim, 2 sccm (and down to the 6×10^{-6} scim, 10^{-4} sccm, region). This method differs from the conventional "bubble under" buret measurement concept in that the leak is introduced over the buret water column rather than through it. Investigations conducted during former programs indicated that bubble under measurement was unsatisfactory for low flows because backpressure created by the water head must first be overcome before measurement is initiated; a time-consuming process.

With the leveling-bulb method, leakage is introduced into the top of a 1-cc buret via small-diameter tubing (0.038-inch, 0.0965-cm ID). This tubing was kept short as possible to minimize the leak volume. A leveling bottle connected to the base of the buret, movable relative to the buret, provided a means of controlling both water level and internal pressure after leakage introduction. By lowering the bottle to match water column displacement as leakage is captured, the leak volume is maintained from atmospheric pressure to a slight negative head. Insertion of volume displaced and elapsed time into an expression which provides for temperature and vapor pressure compensation permits calculation of leakage flowrate.

Extensive use and analysis of the leveling-buret measurement system in former programs has indicated the procedure is accurate to ± 5 percent at the leakage rates down to 10^{-3} scim (0.016 sccm). From this level to the 10^{-5} scim (1.6×10^{-4} sccm) lower limit, the potential error increases to a predicted maximum of 41 percent. (The majority of this error stems from potential temperature variation during the leakage measurement run. However, numerous repeats of data points indicate a precision better than this, usually ± 10 to ± 30 percent. Also, overall data presentation accuracy is improved by simultaneously plotting load versus leakage data points during test; thus, nonrepeat points or those appearing in error can be rerun if necessary.)

Instrumentation. Displacement and load-monitoring instrumentation was required for the basic test system. Piston stroke and articulation beam motion were observed via Bently proximity transducers. These devices operate on an eddy current principle and are not directly coupled to the moving element. Ideally, the transducers are intended to "observe" a flat plane of specific optimum dimensions and material without influence of surrounding structures. In the closure tester, these ideal conditions are not practicably attainable; therefore, each transducer was calibrated in-place with travel versus output voltage recorded for discrete incremental displacements. With output signal displayed on a real-time basis, the position transducers were used for velocity measurements during cyclic tester operation. Transducer response capabilities range from dc to 100,000 Hz.

A primary parameter in dynamic testing is closure impact force. This was monitored by a piezoelectric load washer mounted internally in the tester. This unit, made by the Kistler Instrument Corp., was identical to one used with excellent results in previous programs. With this device, static or dynamic strain-induced crystal electrostatic charges are converted into an amplified d-c signal by the associated charge amplifier for subsequent readout. It has a compressive load range of 20,000 pounds (88,960 N) and has been used to discriminate loads as low as 10 pounds (44.5 N). Experiments indicate that, with proper signal amplification, loads less than 1 pound (4.45 N) can be accurately measured.

A strain gage was used to measure the load applied to the wobbler ball joint. In this application, wobbler loading during impact was observed to ensure that the poppet-wobbler surfaces did not separate.

The aforementioned instrumentation signals were fed into a balance and selector panel. This unit provided for amplifier balance operations and selection of signals to be monitored. During normal operations, simultaneous display of all instrumentation is not necessary. Thus, a dual-beam oscilloscope was used as the primary readout device. Permanent retention of typical data displays were obtained by Polaroid camera photographs.

Cryogenic Test System. The major problem in cryogenic testing is the delivery of dry, prechilled gas to the closure tester. Past experience in developing a disk seat valve design for the J-2 engine established icing in the seating area as a prime cause of leakage. It was found that additional drying of initial -100 F (200 K) dewpoint helium was necessary. In the solution of this problem, the dual-drying system shown in Fig. 33 evolved.

Storage bottle (high-pressure) supply was passed through a heat exchanger submerged in liquid nitrogen (LN₂). This performs the primary gas drying operation. Moisture in the gas is condensed in the form of ice particles which either adhere to the tubing walls or, if entrained in the flowing gas, are lodged in the tee trap and filter. The gas is then directed to a room-temperature heat exchanger for warming prior to entry into the system regulators (rubber diaphragms and seals, incompatible with low temperatures). Finally, regulated tester input pressures are passed through a second cryogenic heat exchanger for final dryout, filtration, and prechilling.

For cryogenic testing, a piston purge feed line was added. This subsystem provided a flow of chilled gas entering through one film pressure vent port, passing through the piston center passage, and exiting from the other film pressure vent. It accelerates chilldown of the thermally isolated piston.

While the basic system instrumentation sensors were suitable for cryogenic service, calibration and zero shifts occurred at extreme temperature conditions. This required recalibration effort during cryogenic investigations. In addition to the basic instrumentation, at least five thermocouples were utilized to monitor chilldown characteristics. One measured body temperature while the remaining units were used to determine piston, wobbler ball joint, and tie bolt differences. Temperatures were measured with a manually switched thermocouple bridge.

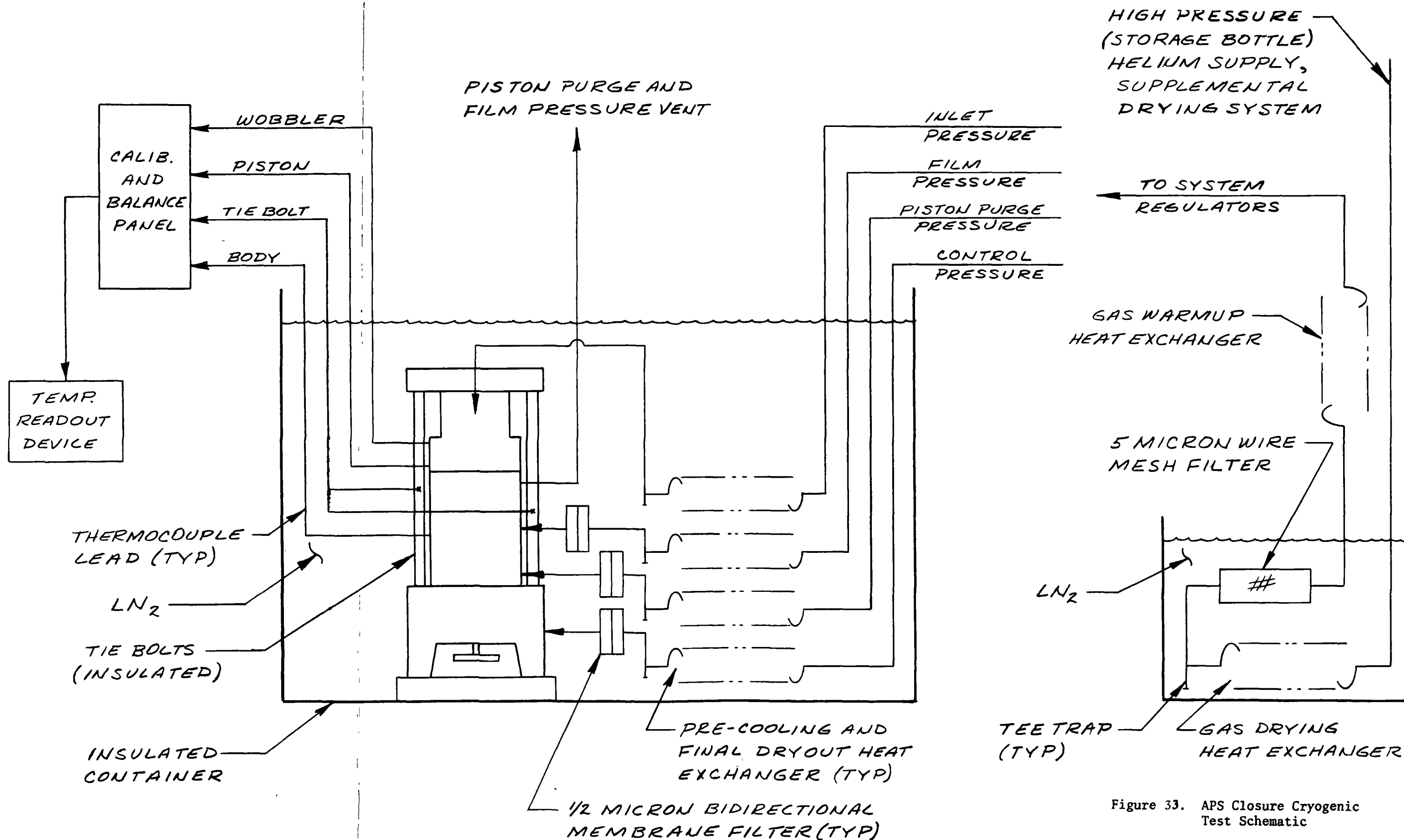


Figure 33. APS Closure Cryogenic Test Schematic

Analysis indicated that temperature differentials during chilldown should not exceed 560 R (311 K). Therefore, chilldown was accomplished gradually by discharging LN₂ or near-liquid vapors over heat exchanger coils and insulated or shrouded tester parts while monitoring tester temperatures. After the critical parts reached approximately 240 R (133 K), the container was filled with LN₂ to maintain temperature during test. (High-temperature testing was done in a temperature-controlled box and, while gas preconditioning heat exchangers were used, heating rate control was no problem.)

To prevent moisture entry into the tester and plumbing during chilldown and warmup phases, positive pressure was maintained on all pressure systems. Return of equipment to room temperature was accelerated by passing heated air over all components. No tester actuation occurred during temperature transient periods.

Tester Evaluation. The closure tester required development and evaluation effort prior to initiation of closure model investigations. This preliminary action encompassed basic assembly checkout, definition of operating parameters, evaluation of articulation mechanism capabilities, and extended into preliminary dynamic closure studies during evaluation of tester cyclic operation. This effort can be broadly categorized into general assembly, static, and dynamic checkout phases.

General Assembly. This portion of tester evaluation involved basic assembly, instrumentation setup, and determination of static operating parameters.

Hydrostatic Bearing. While the hydrostatic bearing concept had been successfully used on former program testers, none had operated at low temperature. Therefore, the APS closure tester hydrostatic bearing was cryogenically tested during the fabrication phase. The piston was finished to size and the body bore was matched to it with a targeted 50-microinch (0.000127 cm) diametral clearance. When this condition was approximated, bearing operation at a nominal 600 psig (413.7 N/cm²) and liquid nitrogen temperature was checked.

Inspection and Assembly. While all detail dimensions were inspected by the tester manufacturer, certain dimensional characteristics pertinent to closure testing were rechecked and documented during assembly. These included individual and stackup parallelism and concentricity values relative to poppet and seat positioning.

Each model tested required adjustment of poppet holder screws to establish concentric and offset conditions. Procedures and technique for this operation using multiple-range electronic indicators were developed. The tester hydrostatic bearing feature facilitated this adjustment by permitting rotation of the poppet holder in a precise fashion while individual screws were indicated and adjusted.

Instrumentation Setup and Calibration. Instrumentation facilities were set up concurrent with tester assembly phases. Although APS program personnel operated instrumentation equipment during closure testing, Rocketdyne instrumentation specialists were utilized for basic circuitry fabrication, initial debugging, and as consultants in establishing operating procedures.

The piston displacement transducer was installed in conjunction with dimensional checks to preclude actual contact with the piston assembly while still yielding maximum signal under stroked (seating contact) conditions. This transducer was calibrated by using both the micrometer thread handwheel and precision scale built into the tester base and a supplemental electronic indicator at the poppet end of the piston. Over the entire 0.100-inch (0.254 cm) stroke, calibration accuracy of ± 0.0005 inch (± 0.000127 cm) was achieved.

The articulation beam motion transducer monitored displacements much smaller than piston travel. An electronic indicator was used for calibration of beam motion within ± 50 microinch (± 0.000127 cm).

Load calibration of the ball joint wobbler strain gage and Kistler load washer were accomplished by incrementally pressurizing the tester piston. The piston area was determined with negligible error (diameter measured within ± 20 micro-inches, ± 0.000051 cm) and pressure levels were monitored with a 0.1-percent Heise gage which establishes basic accuracy.

Thermocouple instrumentation was set up when extreme temperature testing was initiated. Thermocouple leads and readout device overall accuracy were on the order of ± 3 percent.

Static Operation. Static checkouts involved establishment of assembly loads, articulation mechanism load-displacement characteristics, and the investigation of balance pressure variations and measurement.

Load-Position Tests. After initial assembly and installation problems were resolved, design parameter verification checks were performed. One of these was tie-bolt loading which must be sufficient to prevent cap-body interface separation under maximum seating forces. Initial load determination was established by calculation, based on measured bolt elongation on the order of 1500 pounds (6672 N) per bolt. A secondary check of bolt loads up to 2000 pounds total (8900 N) was performed by applying a small pressure internally to the cap and then pressurizing the piston until cap-body separation occurred as indicated by gas leakage.

Similarly, seat retention spring load was initially established using the load washer as a force indicator. When the desired 250- to 300-pound load (1110 to 1330 N) was set, the gap between spring and mounting surface was measured and a washer fabricated to provide a spring deflection positive stop for subsequent installation. The variations in seat flange thickness (± 0.001 inch; 0.0025 cm) did not significantly affect load, and instrumentation readout was not required for subsequent seat installations.

Articulation mechanism loads and displacements were evaluated. Given static beam loads established by calculation based on beam deflection were verified by ball joint wobbler strain gage readout. Then, via piston pressure application, the poppet was advanced toward the seat until initial contact occurred as indicated by load washer output. (A controlled piston motion is possible because the alignment bellows spring rate will provide a constantly increasing resistive load.) Additional piston pressure was then applied. This first overcomes the poppet adjustment screw friction forces and, ultimately, causes articulation motion to occur until full seat contact is achieved. The force expended in causing interfacial motion to closure was thus isolated at 2.5 pounds (11.12 N).

Balance Pressure Measurement. As discussed later, seat load versus leakage tests provide a prime indicator of closure sealing performance. To precisely define actual seat loads, however, all extraneous forces must be accounted for. This was accomplished by correlation of the piston balance pressure derived analytically with that obtained by model geometry (inspection data) and test.

Basically, the balance pressure test consisted of determining what piston control pressure was required to offset all opposing forces so that the seating interfaces contact just under a virtually no-load condition. Once balance control pressure (P_{cb}) is established as a datum point, incremental variation in seat loading is accomplished by incremental P_c changes ($P_{c\Delta}$) above the balance pressure level. These conditions can be defined as follows for the closure tester in the upright condition:

$$\sum F = 0 = P_c A_p - P_1 A_e - W - F_b - F_s$$

where

P_c = piston control pressure

A_p = piston area

P_1 = closure inlet pressure

A_e = closure effective seating area

W = weight of piston, poppet, and articulation mechanism

F_b = bellows spring force (negligible rate)

F = other forces

F_s = seat force

for

$$F_s = 0$$

$$P_{cb} = \frac{P_1 A_e + W + F_b + F}{A_p}$$

and

$$F_s = A_p (P_{cb} + P_{c\Delta}) - (P_1 A_e + W + F_b + F)$$

Combining these expressions gives:

$$F_s = P_{c\Delta} A_p$$

In previous AFRPL programs, seating closure occurred in a relatively parallel condition and balance pressure was defined in several ways. One method was to apply P_c until seat leakage, when converted to an equivalent parallel plate gap, indicated closure to within several microinches of total surface roughness gap. Another procedure utilized initiation of audible leakage and decrease in P_1 as an indicator. In both instances, the advantage of parallel closure with reasonably predictable A_e facilitated balance pressure definition.

In the APS tester, not only was closure nonparallel but articulation forces also affected balance pressure measurement. Other known variables were:

1. Gage error (P_1 and P_c)
2. Articulation loads
3. A_e variation with leakage flow (i.e., gap) and nonparallel seating surfaces
4. Balance pressure definition
5. Eccentric loading (ball joint load axis not on closure center)

The evaluation of these and any other potential variables were performed during initial tester checkout using a flat 440C closure.

APS closure balance pressure definition was evaluated. From a fully closed condition, P_c was decreased to a value where the poppet has opened sufficient to cause initiation of audible leakage. This, then, defines the balance pressure of each particular closure model.

Dynamic Operation. Flat 440C test models were used as test vehicles for confirmation of tester dynamic capabilities in three closure modes: clamped, clamshell, and scrubbing. While tester function was of prime importance, the effect of million-cycle operation on model surfaces was monitored as data preliminary to formal closure screening tests.

Clamped Closure Mode. This test served to establish basic tester capability for load cycling without the complexity of the articulation mechanism. The seat was preloaded to 250 to 300 pounds (1110 to 1330 N) against the load washer while the poppet was clamped to the piston (ball joint wobbler removed) with 20 to 40 pounds (88.9 to 178 N) beam load. Parallelism between the seat and cap-body joint face and the poppet to the same junction was adjusted to provide 20 microinches (0.00051 cm) maximum mismatch.

Using a No. 80 drill (0.013 inch, 0.0343 cm) seat orifice as a first approximation, control and inlet pressure levels were adjusted to establish requirements for: (1) 50 up to 150-Hz cyclic operation, and (2) 50 to 1000 pounds (222 to 4450 N) peak impact force. Cycling is caused by an unstable pressure balance condition at the seating interface. Increasing inlet pressure force acting over the effective seating diameter will gradually overcome the static control pressure-piston area force until seat interface separation occurs. Upon separation, inlet gas (between the orifice and seating interface) vents and piston force will effect closure again to reinitiate the cycle.

Using a target value of 100 Hz and 500 pounds (2220 N) impact force, a one-million cycle test was performed with the following determined:

1. Consistent frequency (test cycles will be counted on a timed basis)
2. Consistent impact force
3. Cycle stroke
4. Photographic procedures--lens and time settings for typical velocity and force data acquisition from oscilloscope display

Following cycling, the tester piston was checked for hydrostatic bearing effectiveness and free axial motion, and the tester was disassembled. Areas requiring particular inspection included all axial interfaces for evidence of fretting wear (indicating separation or interfacial motion), diametral guides and bearings for wear indications, and the bellows assembly for evidence of damage or incipient cracking failure. The tester was reassembled in preparation for clamshell testing. The test model used for clamped tester was inspected and refinished for further use.

Clamshell Closure Mode. For this test, the ball joint wobbler was installed and both wobbler strain gage and beam displacement instrumentation were employed. The refinished 440C model was installed and adjusted to give a 0.004 radian angular excursion to closure (0.00016-inch, 0.000407-cm interfacial scrubbing). Beam load was set to 20 pounds (88.9 N) for initial tests.

Using a nominal 500-pound (2220 N) impact load, a 62,000-cycle test was performed while monitoring tester and articulation mechanism instrumentation for evidence of abnormalities. After this test, the articulation mechanism components were inspected for cyclic effects and the model sealing surfaces were examined. Re-inspection of the tester bellows and critical bearing areas also was performed. The test was terminated due to galling of a poppet-positioning button screw. Further work will be discussed under Model Performance.

Scrubbing Closure Mode. This evaluation test was similar to the clamshell closure evaluation except that interfacial scrubbing or lateral closure motion will be adjusted for 0.00108 radian angular closure excursion. A new flat 440C closure model was used. Inspection of tester and articulation mechanism components and closure sealing surfaces followed the cycle test as with preceding evaluations.

Test Procedures and Closure Screening Tests. The goal of closure screening tests is to evaluate candidate closure configurations under variable operating conditions and in sufficient detail to permit optimization of APS valve closure design. The realization of maximum output data within schedule and budgetary limitations depended on efficient test methods. To that end, testing was directed toward establishment of standard sequences and methods. While deviations from "standard" procedures were expected as each new closure configuration was evaluated, basic testing consisted of static load versus leakage and dynamic test sequences. These are discussed in the following paragraphs together with acceptance leakage criteria, test variables, and a description of the closure screening test program.

Acceptance Leakage Criteria. To facilitate leakage measurement and provide ready comparison with previous AFRPL program data, the closure testing was conducted at 1000 psig (689.4 N/cm²) nitrogen or helium supply pressure. This condition was related to the APS valve design requirements in the following manner to permit definition of acceptance test leakage criteria.

The worst condition for APS valve leakage is at 200 R (111 K) regardless of configuration or supply pressure. Using laminar and molecular flow expressions developed in previous programs (Ref. 2) and in the analytical leakage model for this program, equivalent parallel plate seating gaps, h , were computed for three APS valve cases: (1) high-pressure system with a standard 0.03-inch (0.0762 cm) land width, (2) low-pressure system with the same land width, and (3) low-pressure system with a 0.001-inch (0.0025 cm) land width to accommodate the disk seal concept. The following given and anticipated APS valve parameters were utilized in these calculations.

- D_s = mean seat diameter
 = 1.00 in. (2.54 cm) for high-pressure system
 = 5.00 in. (12.7 cm) for low-pressure system
- L = seat land width
 = 0.03 in. (0.0762 cm) for high- and low-pressure systems except disk seal
 = 0.001-in. (0.0025 cm) disk seal contact width, low-pressure system
- P_1 = closure inlet pressure
 = 450 psia (310 N/cm²) high-pressure system
 = 25 psia (17.2 N/cm²) low-pressure system
- P_2 = closure discharge pressure
 = 0 psia (0 N/cm²) for both systems
- T = fluid temperature
 = 200 R (111 K) for both systems
- Q = helium leakage rate
 = 0.102 scim (100 scc/hr) for both systems

From these parameters and resulting parallel plate leakage gaps, equivalent leakage rates for the APS test closures were calculated. These were established for a variety of anticipated test conditions (temperatures, fluids, and pressures), as shown in Table IV. See Appendix C for further correlation data.

These data include not only allowable leakage variations at temperature extremes, but cyclic degradation of sealing performance as well. For new test models, some margin must be allowed for subsequent sealing surface damage. Therefore, new model ambient temperature acceptance leakage was defined as 10 percent of the maximum allowable full-service leakage at a seat load (excepting the disk seal concept) of 50 to 100 pounds (222 to 445 N). From this starting point, acceptable leakage during model cycling was defined as less than a factor of 2 increase after 100,000 cycles, and no more than a tenfold increase after 10⁻⁶ cycles (considering also fluid property and temperature-variation effects).

Static Test (Load Versus Leakage). This test is fundamental to closure evaluation and provides the most definitive measure of closure sealing performance. A typical load versus leakage test was performed in the following sequence:

1. Model Inspection
 - a. Assess sealing surface condition
 - b. Determine sealing land dimensions
 - c. Photograph typical sealing surface areas at 100X and 500X magnification
 - d. Prepare inspection data sheet

TABLE IV - APS VALVE AND EQUIVALENT TEST MODEL LEAKAGE CHARACTERISTICS

For High-Pressure System: $L = 0.03$ in., $h = 2.09 \times 10^{-6}$ in.
 (0.0762 cm) (5.3 x 10⁻⁶ cm)

Temperature, K F		Test Valve Leakage, scim (scc/hr) $P_1 = 450$ psia He (310 N/cm ²) $P_2 = 0$ psia (0 N/cm ²)	Test Model Leakage, scim (scc/hr), $P_2 =$ Ambient					
			P_1 , psig (N/cm ²) GN ₂			P_1 , psig (N/cm ²) He		
			100 (68.94)	450 (310)	1000 (689.4)	100 (68.94)	450 (310)	1000 (689.4)
77.8	-320							0.301 (296)
111	-260	0.102 (100)						
294.5	70	0.0382 (37.6)	0.00147 (1.45)	0.0112 (11.0)	0.0405 (39.8)	0.00373 (3.18)	0.0188 (18.5)	0.0566 (55.7)
472	390	0.0270 (26.6)						0.0354 (34.8)

For Low-Pressure System: $L = 0.03$ in., $h = 5.5 \times 10^{-6}$ in.
 (0.0762 cm) (13.97 x 10⁻⁶ cm)

Temperature, K F		Test Valve Leakage, scim (scc/hr) $P_1 = 25$ psia He (17.23 N/cm ²) $P_2 = 0$ psia (0 N/cm ²)	Test Model Leakage, scim (scc/hr), $P_2 =$ Ambient			
			P_1 , psig (N/cm ²) GN ₂		P_2 , psig (N/cm ²) He	
			25 (17.23)	1000 (689.4)	25 (17.23)	1000 (689.4)
77.8	-320				0.0157 (15.5)	4.84 (4760)
111	-260	0.102 (100)				
294.4	70	0.0564 (55.5)	0.00262 (2.58)	0.615 (605)	0.00564 (5.55)	0.707 (695)
472	390	0.0433 (42.6)			0.00424 (4.17)	0.157 (154)

TABLE IV (Concluded)

For Low-Pressure System: $L = 0.001$ in., $h = 1.07 \times 10^{-6}$ in.
 (0.0025 cm) (2.7 $\times 10^{-6}$ cm)

Temperature,		Test Valve Leakage, scim (scc/hr) $P_1 = 25$ psia (17.23 N/cm ²) $P_2 = 0$ psia (0 N/cm ²)	Test Model Leakage, scim (scc/hr), $P_2 = \text{Ambient}$	
			$P_1 = 25$ psig GN ₂ (17.23 N/cm ²)	$P_1 = 25$ psig He (17.23 N/cm ²)
77.8	-320			0.0123 (12.1)
111	-260	0.102 (100)		
294.4	70	0.061 (60.0)	0.0023 (2.26)	0.0058 (5.71)
472	390	0.0479 (47.1)		0.00454 (4.47)

2. Test Data Sheet

- a. Prepare data sheet
- b. Calculate balance pressure

3. Closure Assembly into Tester

- a. Install seat into cap
- b. Adjust poppet holder screws to produce desired clamshell or scrubbing motion
- c. Install poppet into holder and adjust beam load
- d. Install cap-seat assembly onto tester body and clamp with tie-bolt load

4. Balance Pressure Test

- a. Adjust handwheel to limit closure gap to approximately 0.001 inch (0.00254 cm)
- b. Apply P_c to a level slightly over calculated balance pressure value
- c. Apply 1000-psig inlet pressure (689.4 N/cm²)
- d. Decrease P_c and determine balance pressure
- e. Increase P_c to a differential pressure above balance pressure equivalent to approximately 4 pounds seat load (17.8 N)

5. Load Versus Leak Data

- a. Measure and record leakage at the previously set 4 pound (17.8 N) load
- b. Measure leakage at increasing incremental net seating load values of approximately 10, 20, 50, 100, 200, and 500 pounds (44.5, 89.0, 222.5, 445, 890, and 2225 N) and at similar values in a decreasing load sequence
- c. Plot load versus leakage curve (described in Data Presentation section) and repeat data points that do not appear correct
- d. Reduce P_c to near balance value; reduce P_1 and then P_c to zero

6. Review load versus leakage data for closure acceptance

The results of the load versus leakage test will determine if a given closure model is suitable for dynamic testing or must be refinished and retested. The basic data also form a frame of reference from which post-cycling performance can be assessed.

Dynamic Test. In considering a test matrix for closure evaluation, the number of potential variables poses a formidable problem. Major variables relating to dynamic testing are:

1. Clamshell closure angle, α
2. Scrubbing mode closure angle, α
3. Peak impact force
4. Beam load (poppet righting force)
5. Cycle rate (interfacial temperature)

A comprehensive investigation of candidate closures under all variable combinations far exceeds the scope of the screening effort. Consequently, restraints were placed on certain variables.

Closure angles for both the clamshell and scrubbing modes were upper-limited to 0.004 radians. Peak impact force was established at 500 pounds (2220 N). Beam load was limited to that amount determined in tester evaluation tests that prevented poppet-wobbler separation under cyclic rate, impact load, and closure modes to be considered: 20 pounds (89 N). Finally, cyclic rate was the maximum value commensurate with minimal interface heating effects, also determined during tester evaluation (about 100 Hz). These restraints represented target objectives. As each individual model configuration was evaluated, revisions to certain variable limits were required. However, the preceding permitted establishment of ground rules from which test plans were formulated.

Upon completion of a satisfactory load versus leakage test, candidate closures were evaluated dynamically. While preliminary procedures to establish a standard test condition varied (as subsequently discussed) the following summarizes a typical full-length dynamic test:

1. Satisfactory completion of load versus leakage test
2. Set piston stroke to a value greater than the unstable cycling stroke predetermined in initial parametric evaluation tests
3. Initiate cycling
 - a. Increase P_c to predetermined cycle requirement value
 - b. Increase P_1 to initiate cycling with final value set to produce desired peak impact force
 - c. Start elapsed-time clock to count cycles
 - d. Verify cycle frequency
4. Periodic leak check
 - a. Terminate cycling by reducing P_1
 - b. Increase P_c , then P_1 to values required for leak check (100 pounds seat load, 445 N; 1000 psig, 689.4 N/cm²)
 - c. Measure leakage and record
 - d. Leak check frequency: after 5000, 10,000, 50,000, 100,000, 200,000, 500,000 and one-million cycles, depending on sealing performance acceptance criteria
 - e. Return P_c and P_1 to former conditions and reinitiate cycling
5. Final load versus leakage test
6. Model disassembly and inspection

Data Presentation. Several forms of data presentation will be used in discussing, analyzing, and correlating the closure screening program.

Closure Identification. To readily discuss closure design performances, a system of identification was established for each test model. A test model is defined as a poppet and seat pair forming a unique combination of sealing surfaces. Should a model poppet or seat be replaced or refinished, a new model, again with unique sealing surfaces, is created. To maintain control and identification of test models, a three-digit numerical designation was used for each configuration with individual models sequentially numbered. Thus, for example, Model 101 would indicate the first poppet and seat combination of the 100-series configuration. Basic closure designs were designated as follows:

<u>Number Series</u>	<u>Configuration</u>
100	Flat 440C
200	Flat Gold
300	Flat, Grooved Gold
400	Hard-Sharp Carbide
500	Captive Plastic
600	Disk Seal

While various quantities of poppets and seat were fabricated for each configuration, test model numbers could exceed the number of sets made if parts are refinished for additional testing, interchanged, or otherwise altered.

In addition to model designations, each poppet and seat is permanently serialized. Inspection data sheets prepared for each detail part note this serial number. (These sheets form a raw data record of pertinent dimensions and inspection observations and will not be formally published. Abstracted information will, however, be compiled for later presentation.)

Inspection Data. Test models were subjected to a variety of sealing surface assessment and basic configuration geometry inspection procedures. The most important part of this inspection is the plain and interference microscopic examination of sealing surfaces from which sealing land dimensions, flatness, surface roughness, defects, and effects of cyclic closure will be determined.

Test Parameters. Basic fixed parameters such as configuration, model number, supply pressures, static temperatures, etc., were recorded on data sheets. Test variables such as piston control pressure (load) and leakage, which are manually observed, also were recorded. These data are utilized as appropriate in discussion of test model performance, preparation of load-leakage curves, and similar applications.

Dynamic test data such as impact velocity, peak impact loads, and articulation motion were observed on the oscilloscope screen. Photographs of typical characteristics were taken for reduction to numerical values and presentation in support of test result discussions.

Load Versus Leakage Data. The prime indication of test model performance capabilities is the relationship of applied seating load and resulting leakage at constant inlet pressures. This is graphically portrayed in the form of a load-leakage plot. Actual data points are plotted and interconnected by a best-fit curve.

TEST RESULTS

Closure Screening Results

The following section will discuss the results of the screening of the six model closure concepts.

Model Performance. Clamped mode tests were performed on a 440C poppet and seat to evaluate tester performance. The results of the test were satisfactory and verified the capability of the tester to be adjusted to provide the required closing mode, to cycle with controlled impact loads, to provide controlled loads for load-leakage data, and to permit accurate measurements of low-magnitude leakage. The tests were conducted at a 100-Hz cycling rate. Results of the tests are shown in Fig. 34.

The screening test program was initiated with ambient temperature clamshell mode tests using a 440C poppet and seat closure. This model was chosen as the baseline and several tests were performed to define the allowable angle between the poppet and seat on impact to provide a basis for screening.

The original nominal α angle as described in the Screening Test Plan was 0.004 radians. The test data of Model 103 (Fig. 35) indicated that 440C on 440C is very susceptible to fretting, and that the permissible angle between the poppet and seat at contact is very small. The large α resulted in one of the poppet adjustment screws galling against the poppet. Thus, the α of 0.00017 radians on Model 104 (Fig. 36) was used to try to establish a lower limit of clamshelling. The tests of Fig. 37 through 39 were performed to evaluate slightly larger α angles of clamshell motion.

Prior to test of Model 108 (Fig. 40), a conversation was held with the NASA-LeRC Project Manager in which he suggested we relate the nominal α clamshell and α scrubbing angles to the preliminary design concepts which will be discussed later in the report. The preliminary designs were reviewed for tolerances, allowing for the worst possible out-of-print conditions, and α_{\max} clamshelling was found to be equal to 0.0007 radians, while α_{\max} scrubbing was equal to 0.00108 radians. Other testing was to be performed at 2α radians clamshelling and scrubbing, and at $\alpha/2$ radians scrubbing. The tester geometry thus establishes the interfacial motion of the poppet with respect to the seat during closure. The values are:

$$S_{(\text{clamshell})}, \text{ interfacial motion, inches} = 0.04 \alpha_{\text{clamshell}}$$

$$(S_{\text{clamshell}}, \text{ interfacial motion, cm} = 0.1016 \alpha_{\text{clamshell}})$$

$$S_{(\text{scrubbing})}, \text{ interfacial motion, inches} = 0.62 \alpha_{\text{scrubbing}}$$

$$(S_{\text{scrubbing}}, \text{ interfacial motion, cm} = 1.5748 \alpha_{\text{scrubbing}})$$

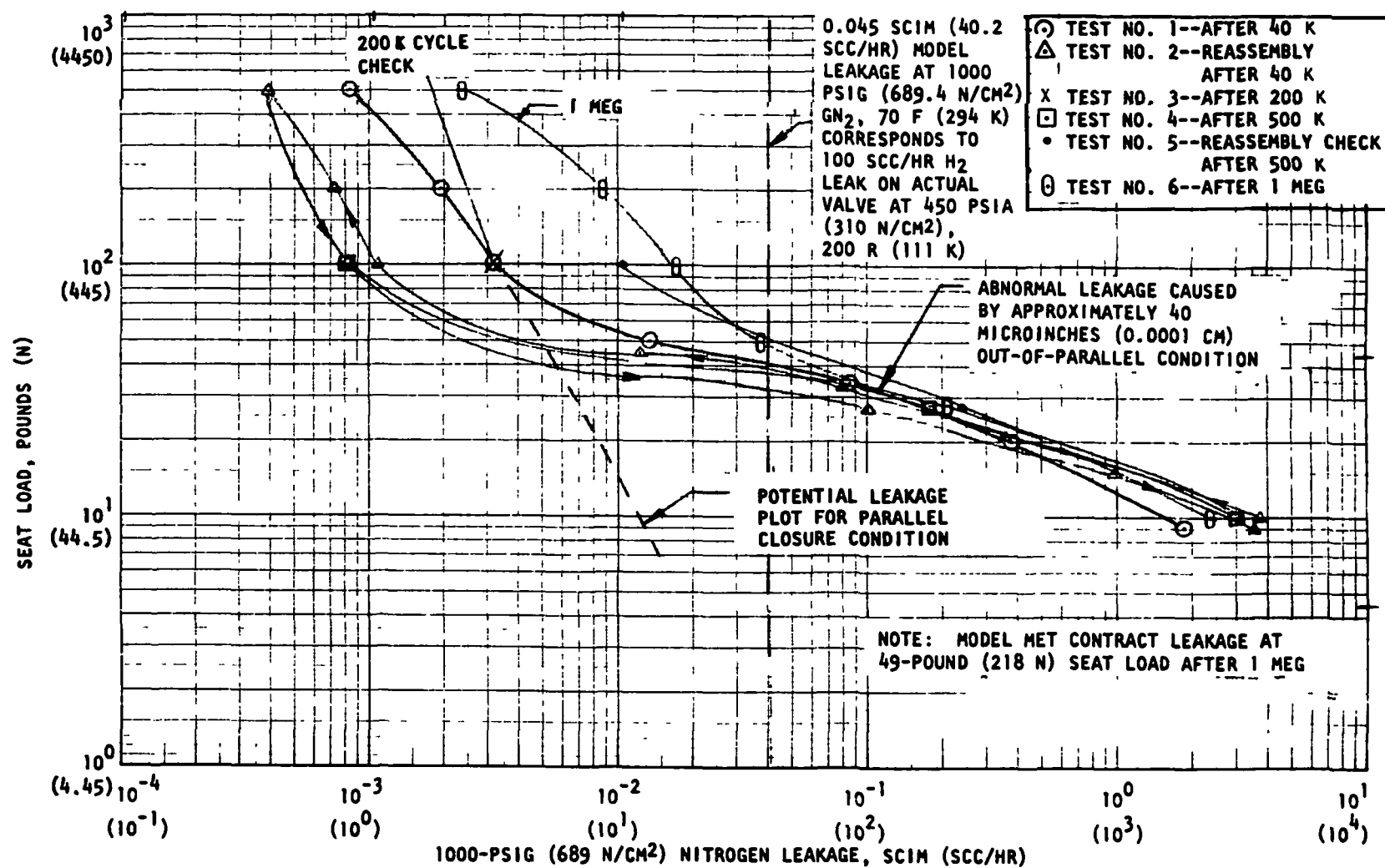


Figure 34. 440C on 440C Load-Leak Data for Preliminary Clamped Mode After 1,000,000-Cycle Test

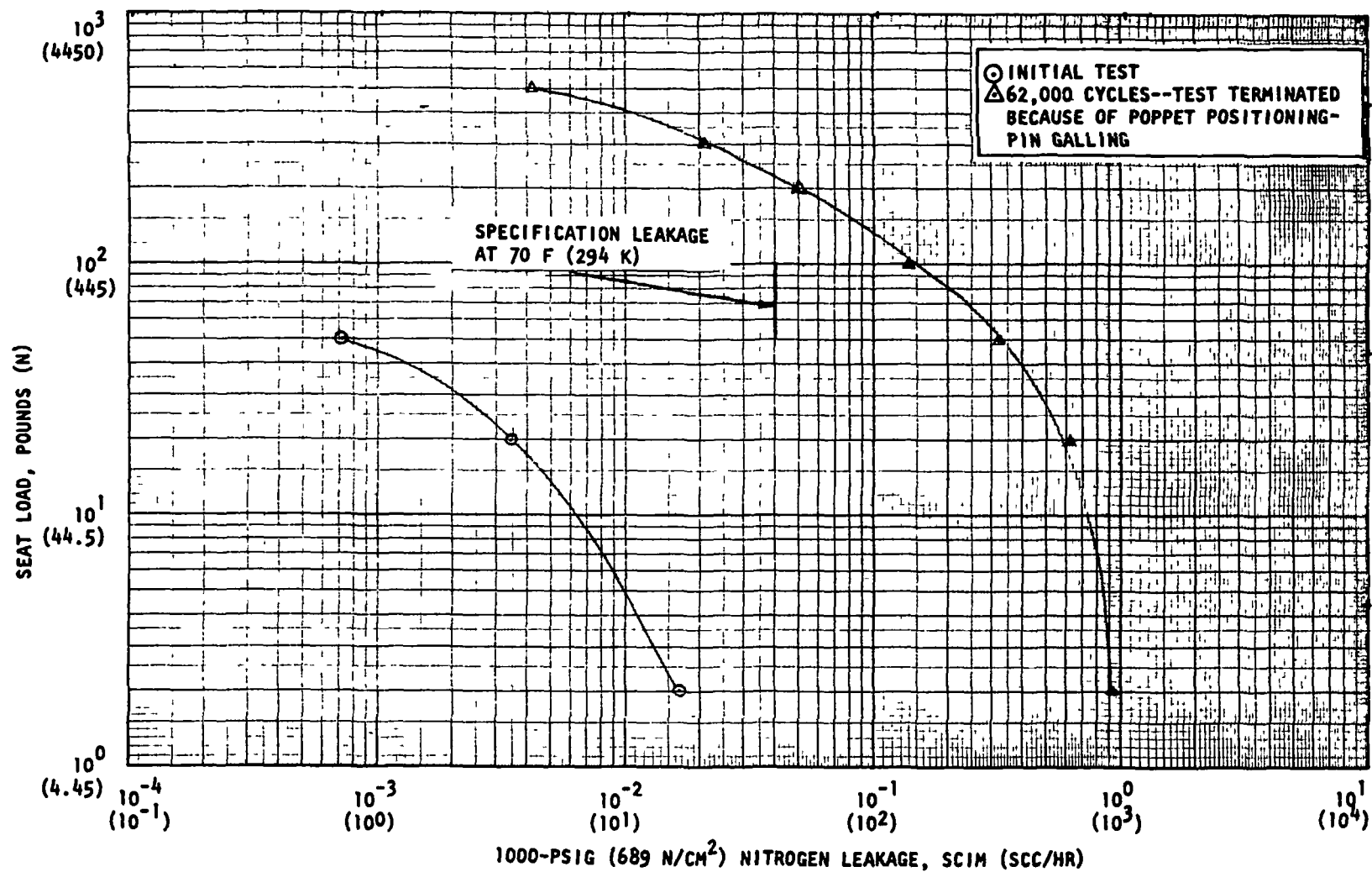


Figure 35. 440C on 440C Test Model 103, 0.004-Radian Clamshell

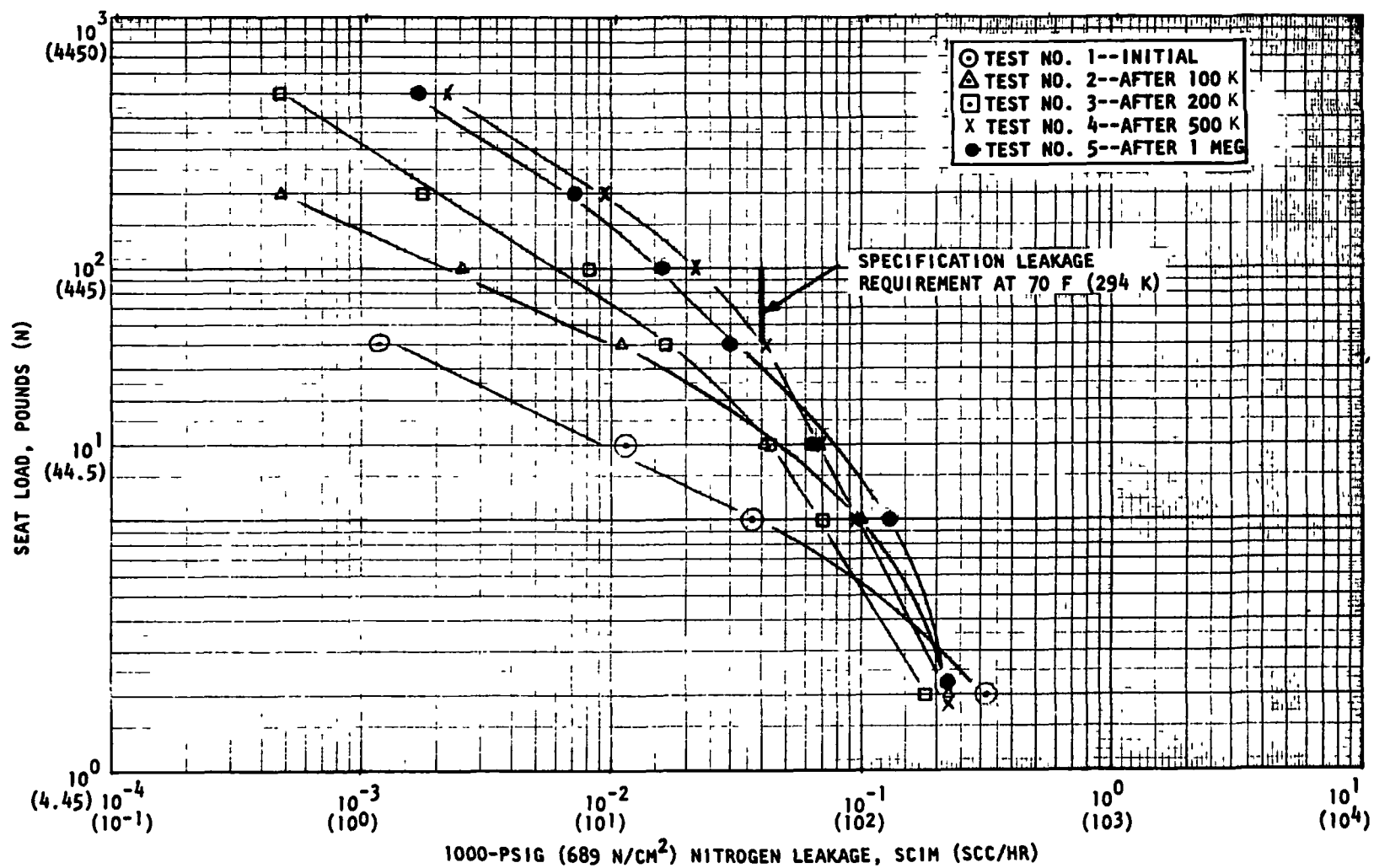


Figure 36. 440C on 440C Test Model 104, 0.00017-Radian Clamshell

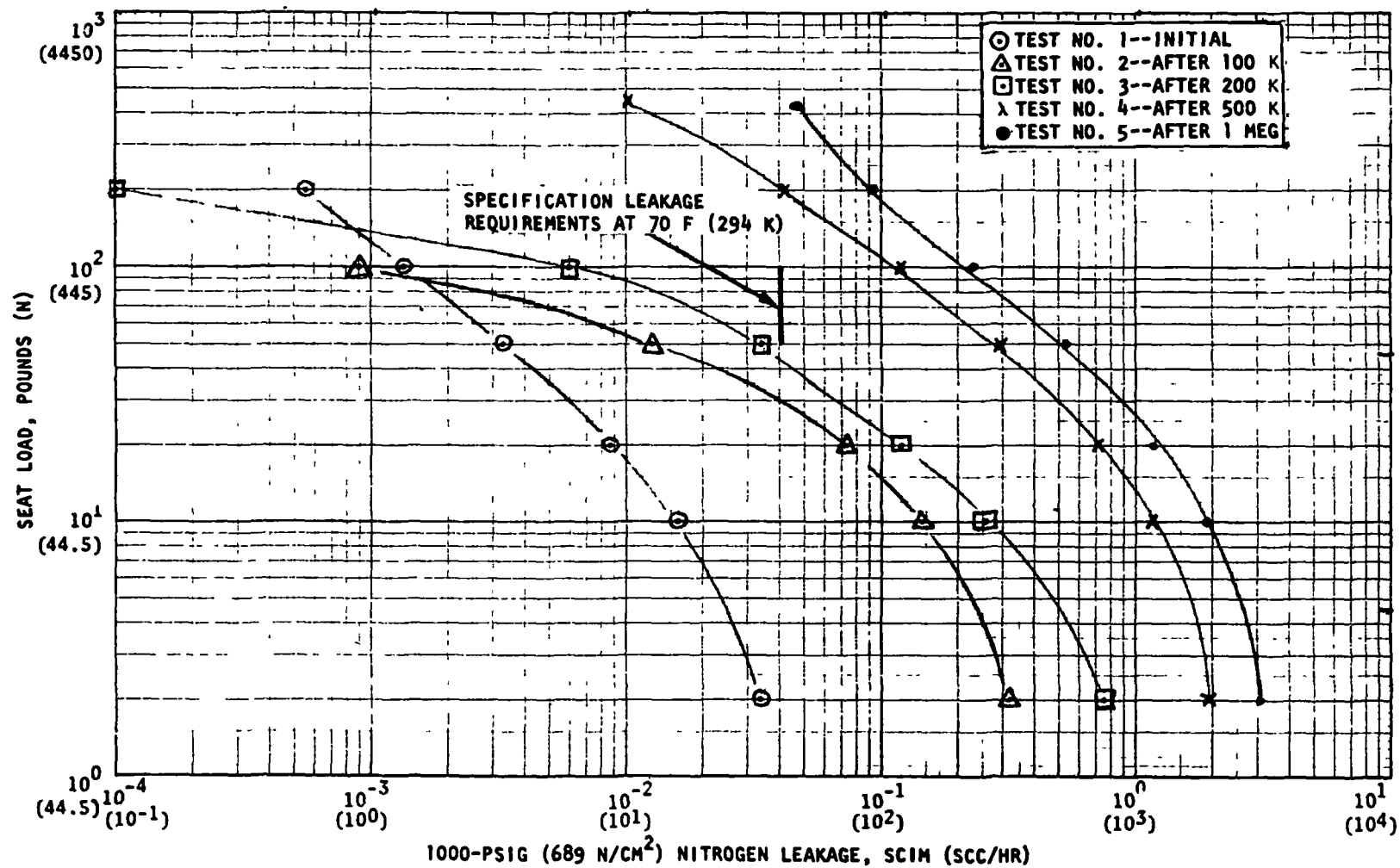


Figure 37. 440C on 440C Test Model 105, 0.0005-Radian Clamshell

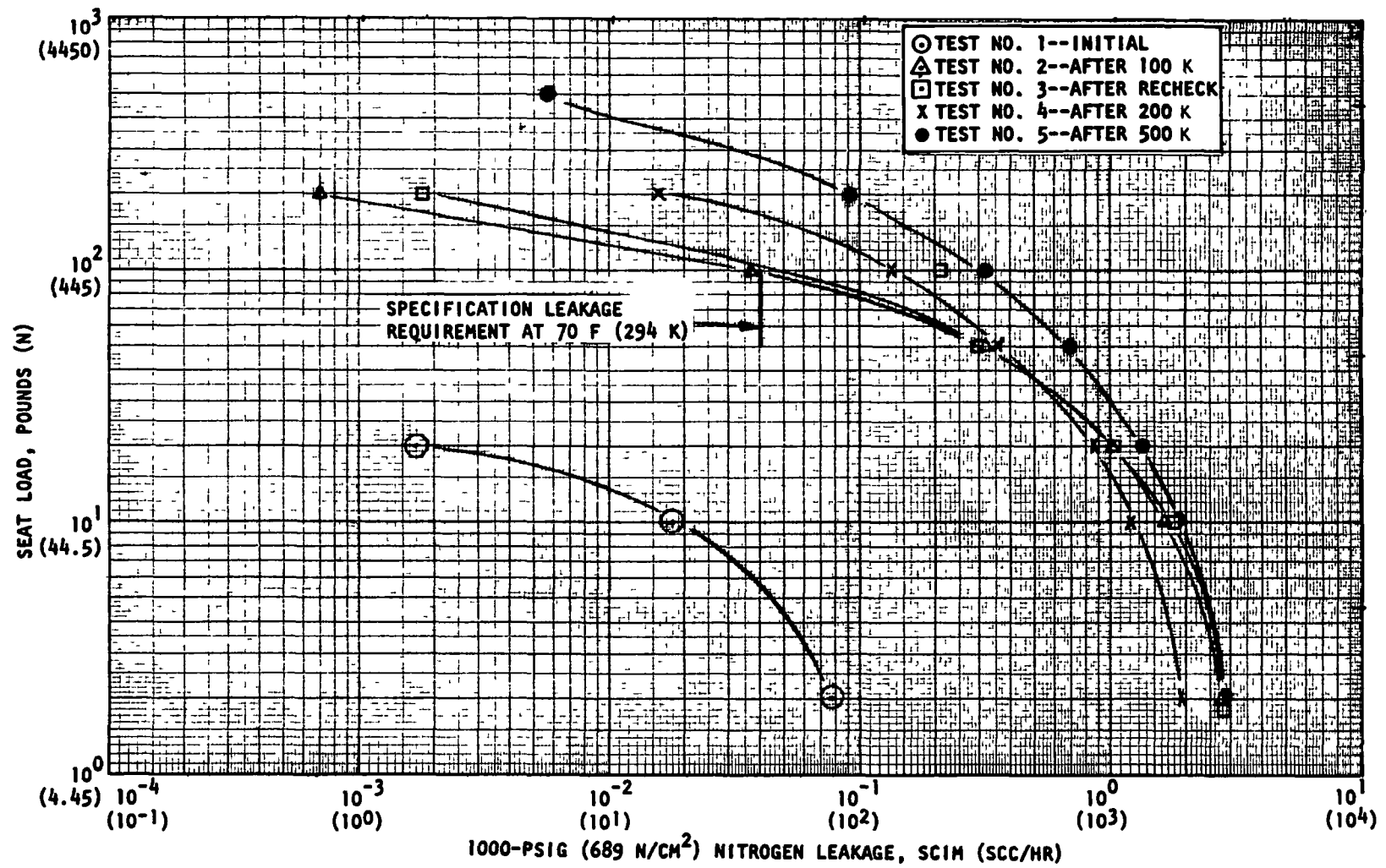


Figure 38. 440C on 440C Test Model 106, 0.0004-Radian Clamshell

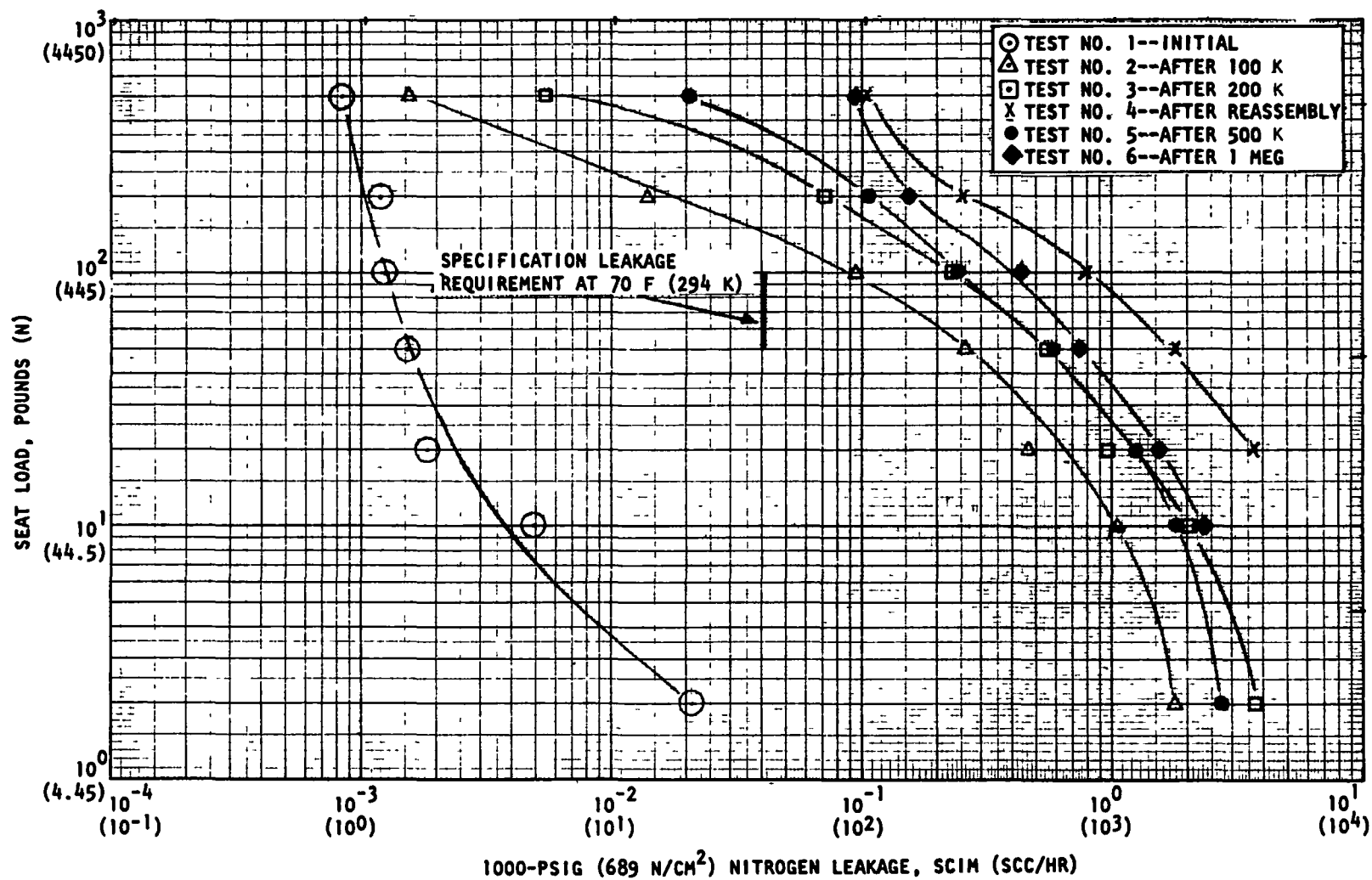


Figure 39. 440C on 440C Test Model 107, 0.0004-Radian Clamshell

As seen in Fig. 40, the 0.0007 radians clamshelling at 500 pounds (2220 N) peak impact load caused a failure condition of the 440C on 440C. Further analysis of the preliminary design concepts revealed that the maximum predicted impact load was approximately 100 pounds (445 N) at 40 inches/second (101.6 cm/sec) impact on the full-sized valve. Therefore, a peak impact load of 250 pounds (1110 N) was chosen for the balance of the closure screening tests to give a margin above that expected in the real valve.

The next testing was a series of 0.0007 radians clamshell closure on the grooved gold (Fig. 41), the captive plastic (Fig. 42), and the hard-sharp carbide (Fig. 43). Each of these concepts passed the leakage criteria as established from scaling down the 0.102 scim (100 scc/hr) leakage requirement on the valve at 200 R (111 K) to the closure model at the respective test temperature as shown on each graph.

The next test series was performed at 2α clamshell (0.0014 radians) on the hard-sharp carbide (Fig. 44), the grooved gold (Fig. 45), and the captive plastic (Fig. 46). Of these closures, the grooved gold (Fig. 45) failed to meet the leakage criteria; however, the leakage was not significantly (i.e., order of magnitude) greater than the specification limits. For this reason, it was decided to continue with the grooved gold concept into the scrubbing mode closure tests.

The scrubbing mode closure screening tests were preceded with a 440C on 440C test (Fig. 47) to establish, once again, baseline data for a known closure concept. By the end of 100,000 cycles, the closure had degraded significantly and, after 200,000 cycles, the test was terminated.

The scrubbing tests (0.00108 radians) were then performed on the captive plastic (Fig. 48), hard-sharp carbide (Fig. 49), and the grooved gold (Fig. 50). Again, the grooved gold failed to meet specification leakage, but did not fail in a decisive manner; therefore, it was decided to submit it to an $\alpha/2$ test at a later period.

The captive plastic (Fig. 51) and the hard-sharp carbide (Fig. 52) were subjected to a 2α (0.00216 radians) scrubbing test at ambient temperature. This produces interfacial motion of the poppet relative to the seat of 0.00134 inches (0.0034 cm). Both sealing concepts passed these tests, leaking well below the specification limit after 1,000,000 cycles. These two concepts, then, on the basis of their ambient performance, became the leading concepts for the final APS closures.

Before proceeding into the environmental tests, two $\alpha/2$ scrubbing tests (0.00054 radians) were performed to evaluate the grooved gold (Fig. 53) and the 440C on 440C (Fig. 54). The grooved gold seat concept passed the leakage specification after 1,000,000 cycles, even though it initially was not within specification limits. Even though the model did successfully pass, gold was transferred to the 440C poppet, and the low interfacial motion allowed "keying" of the sealing surface asperities, keeping the leakage low. This characteristics, combined with an earlier experience in which a fiber across the grooved gold seat completely wiped out all sealing capability, eliminated the grooved gold from any real contention as a final closure design. The 440C on 440C model (Fig. 54) failed to meet the leakage requirements, and was characterized by the fretting wear seen in earlier 440C tests.

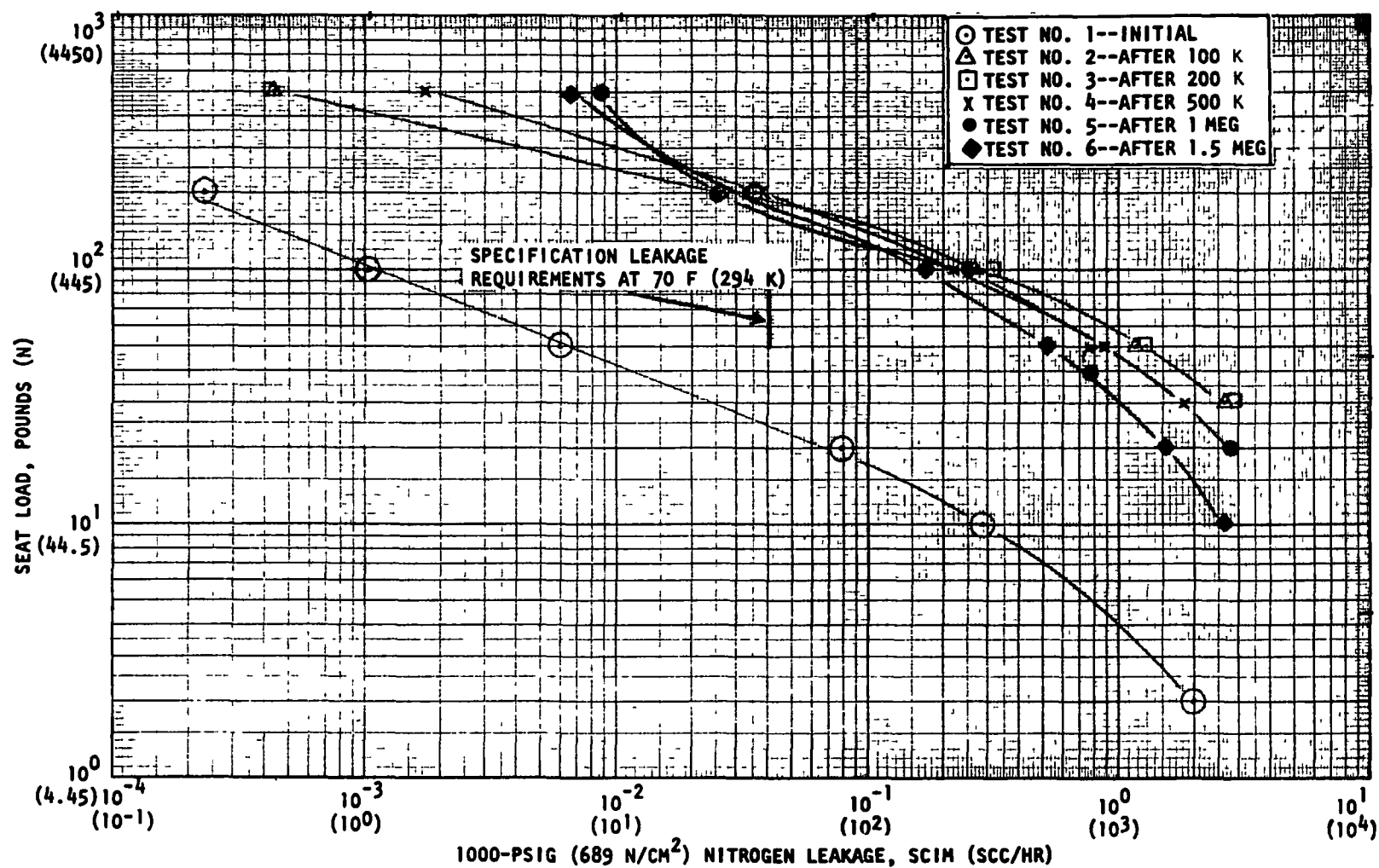


Figure 40. 440C on 440C Test Model 108, 0.0007-Radian Clamshell

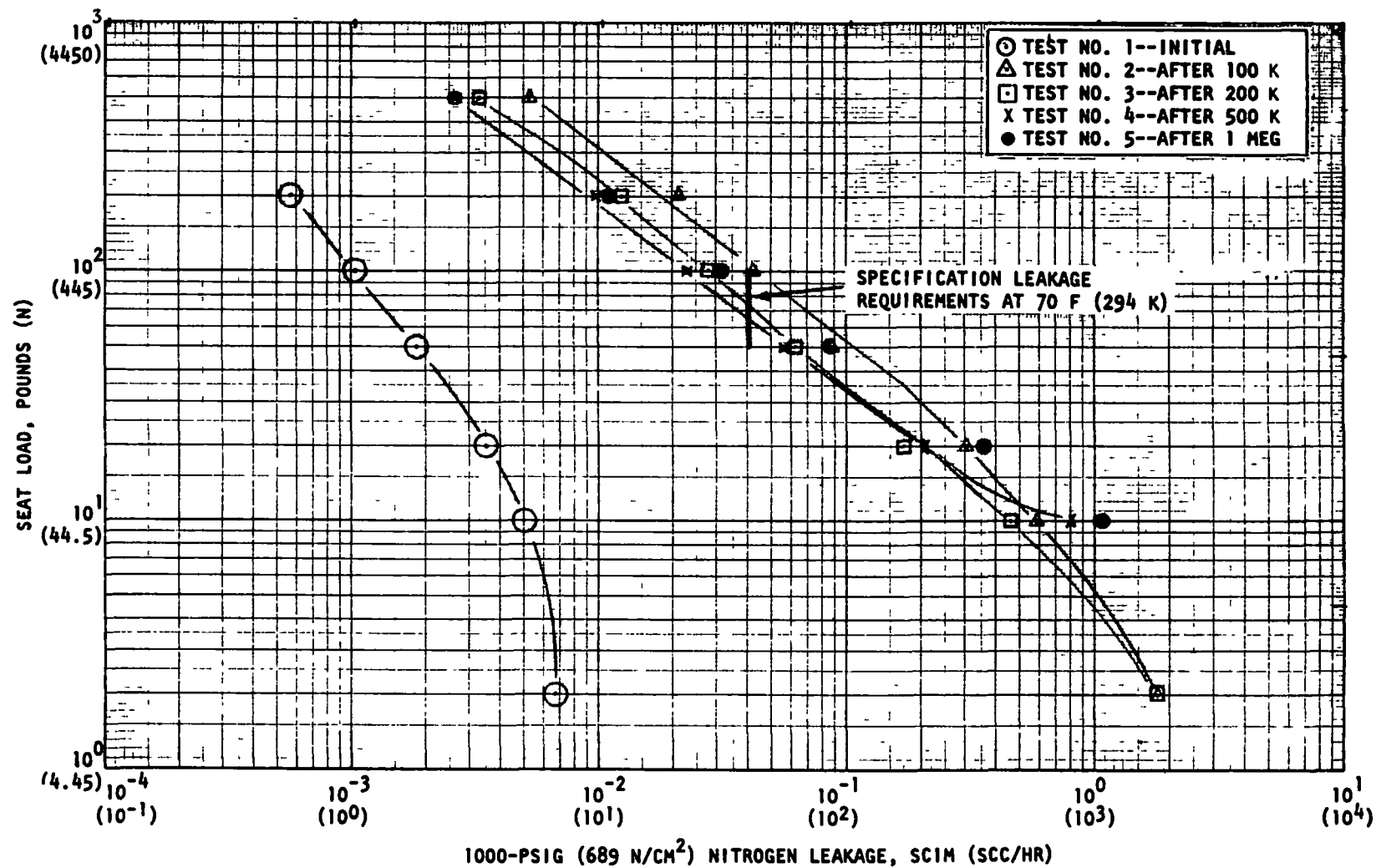


Figure 41. 440C on Grooved Gold, Test Model 302, 0.007-Radian Clamshell

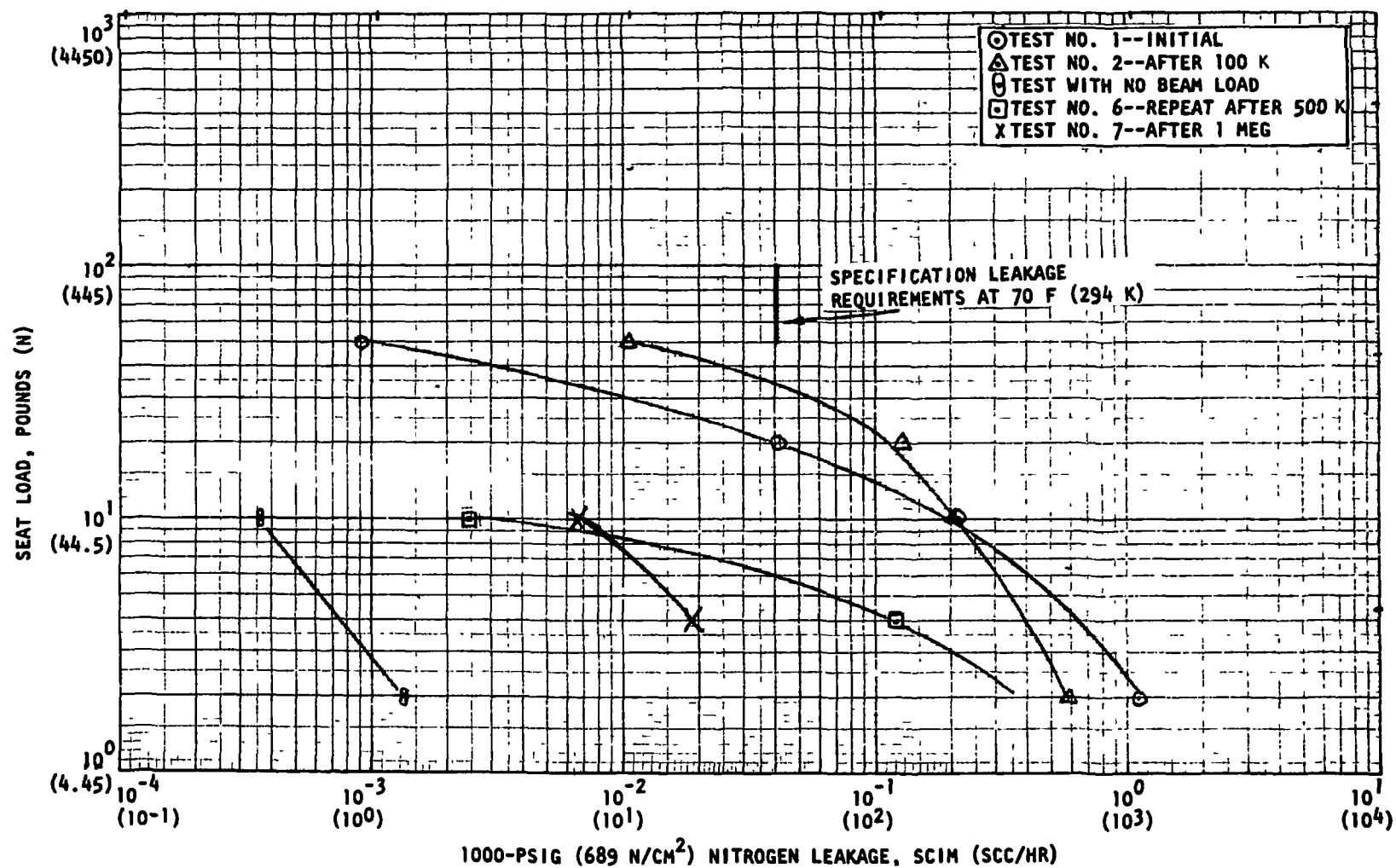


Figure 42. 440C on Captive Plastic, Test Model 501, 0.0007-Radian Clamshell

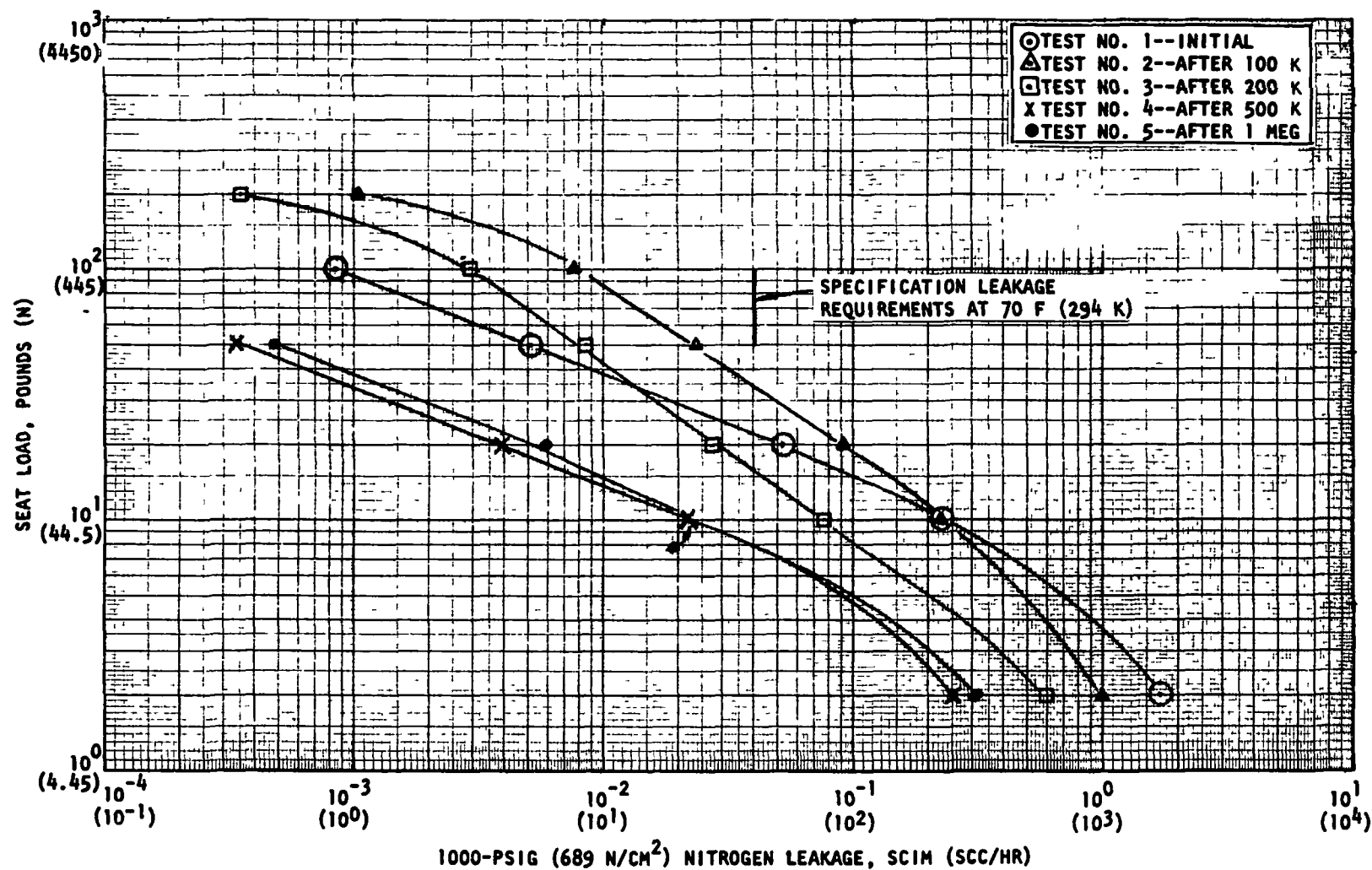


Figure 43. Carbide on Hard-Sharp Carbide, Test Model 401, 0.0007-Radian Clamshell

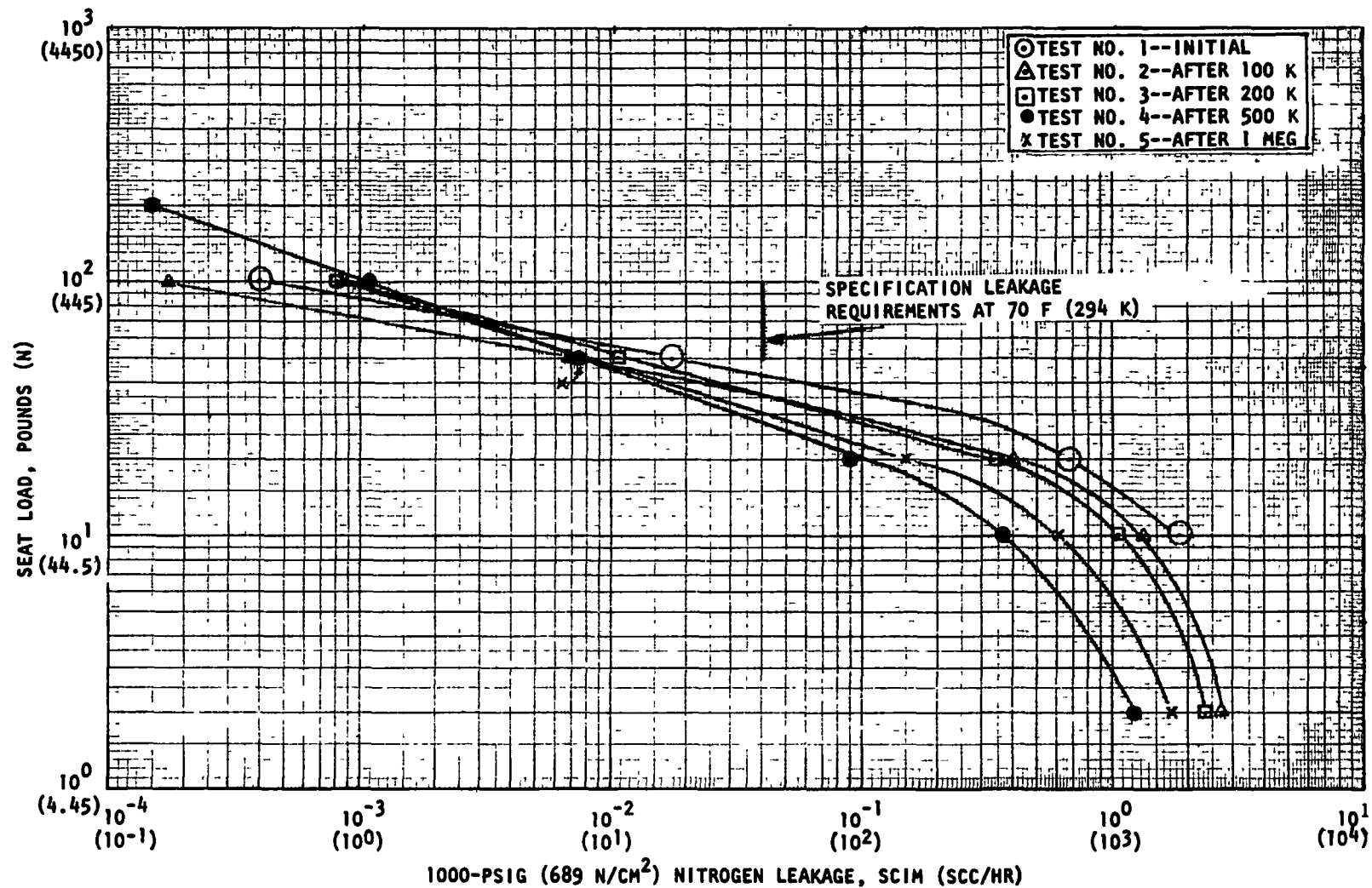


Figure 44. Carbide on Hard-Sharp Carbide, Test Model 401, 0.0014 Radian Clamshell

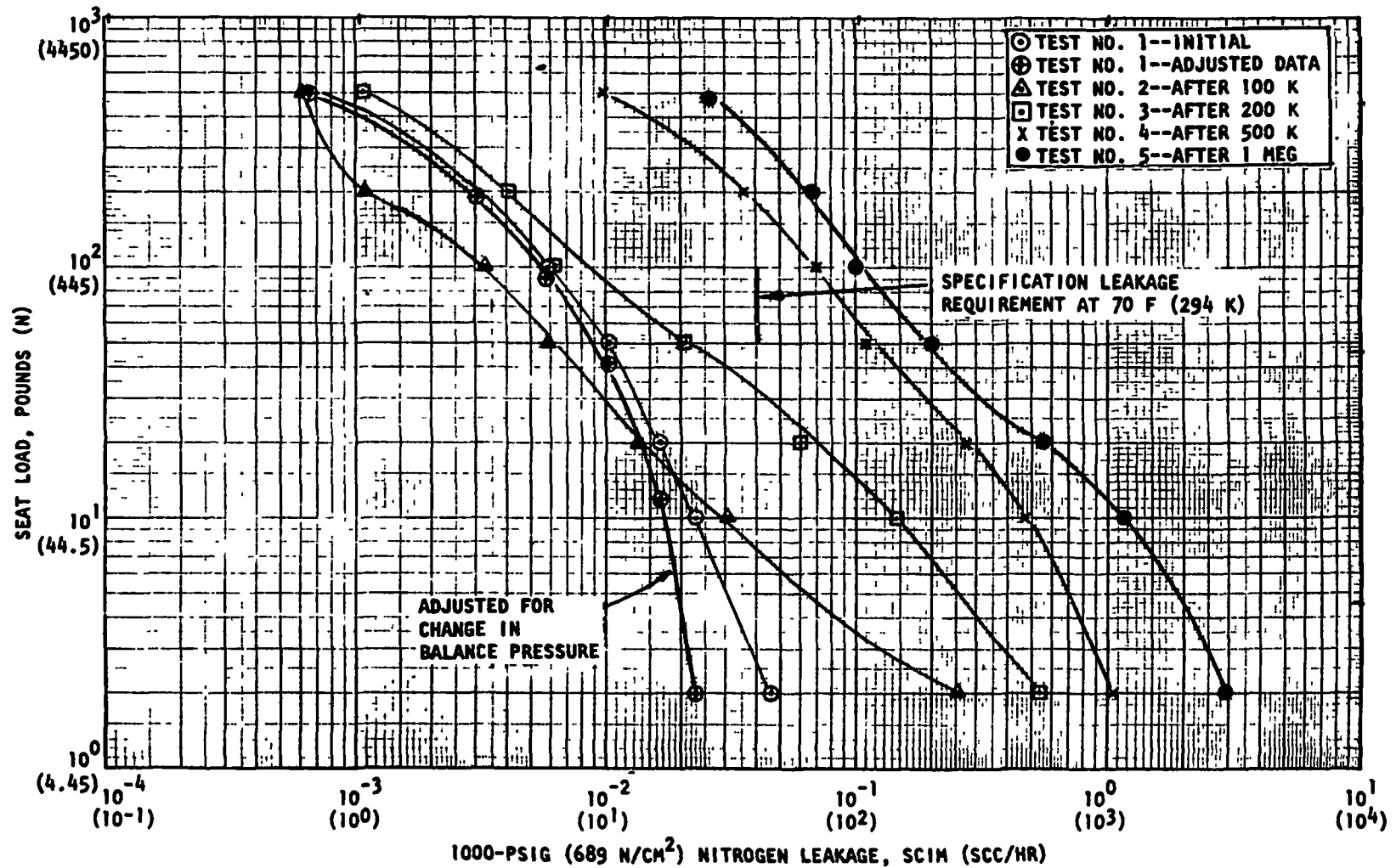


Figure 45. 440C on Grooved Gold, Test Model 303, 0.0014-Radian Clamshell

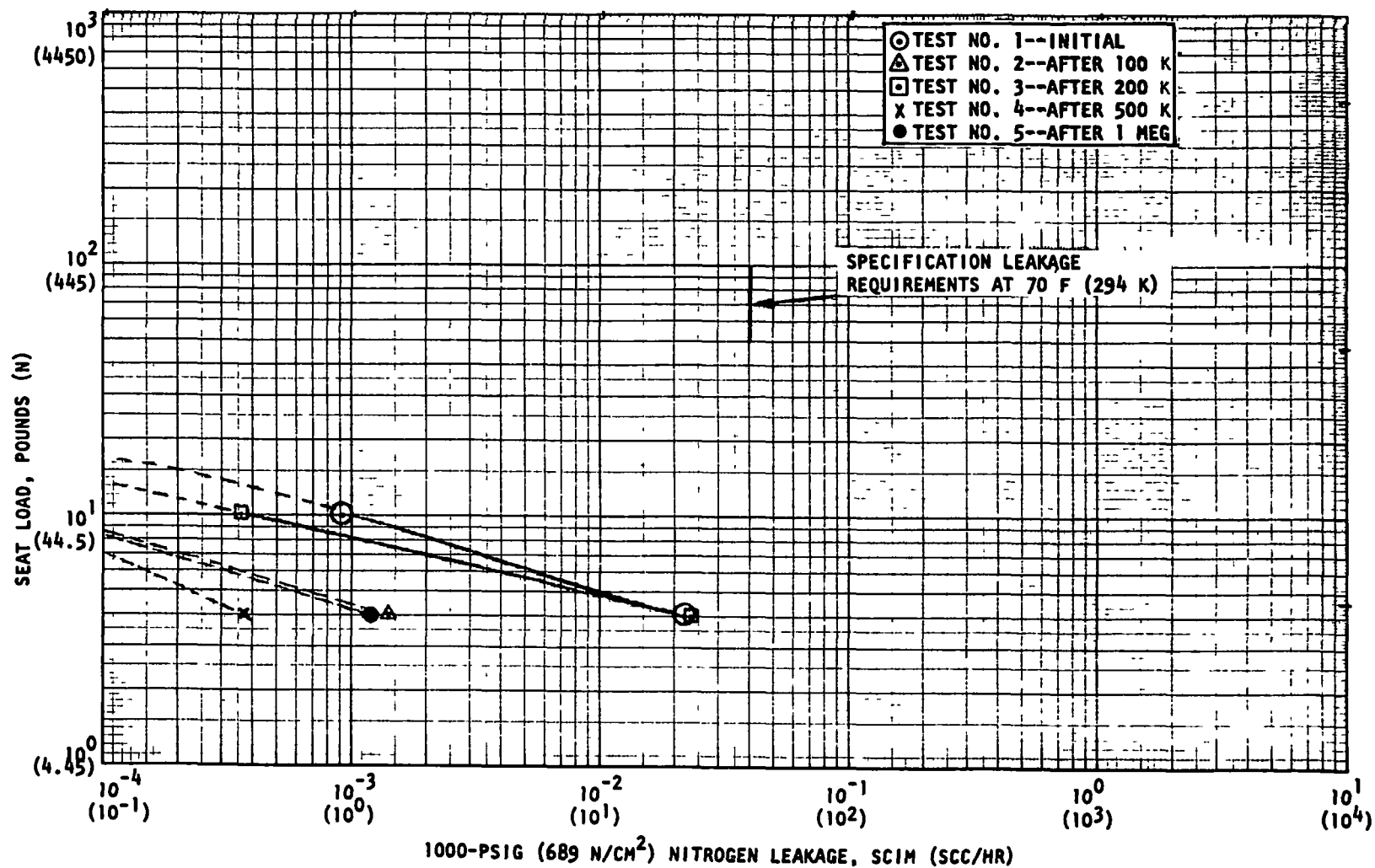


Figure 46.440C on Captive Plastic, Model 502, 0.004-Radian Clamshell

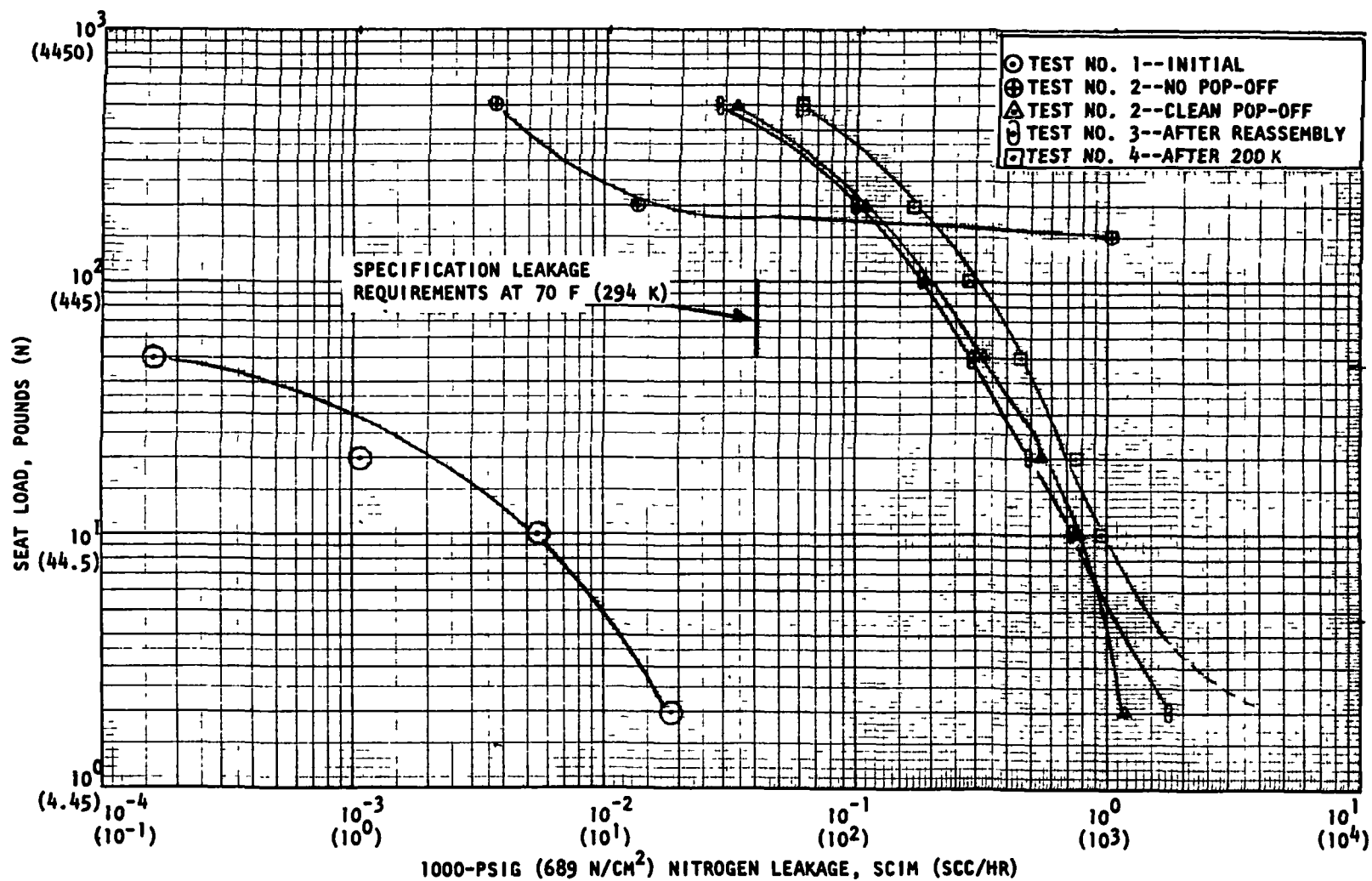


Figure 47. 440C on 440C Ambient, Test Model 109, 0.00108-Radian Scrubbing

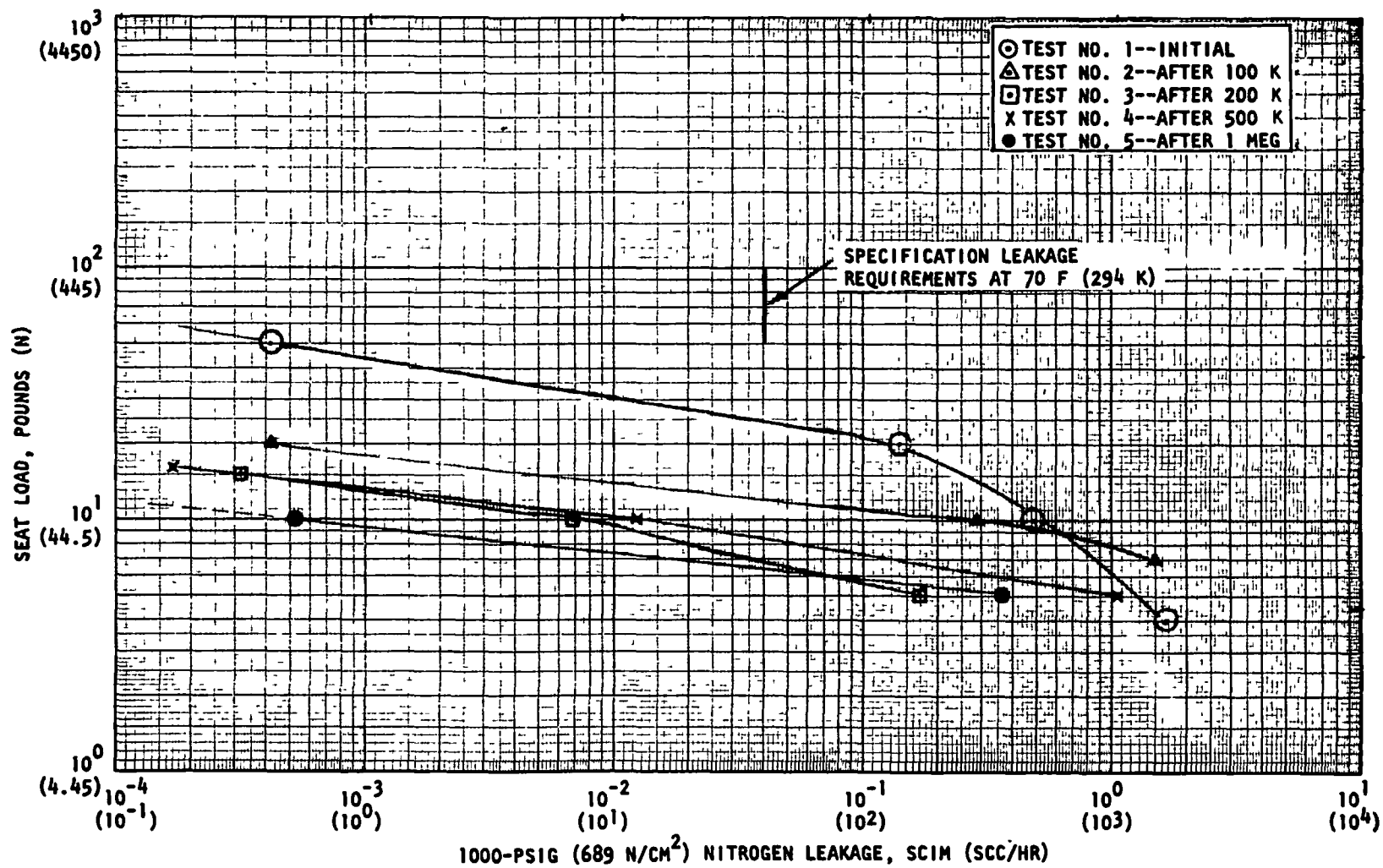


Figure 48. 440C on Captive Plastic, Test Model 503, 0.00127-Radian Scrubbing

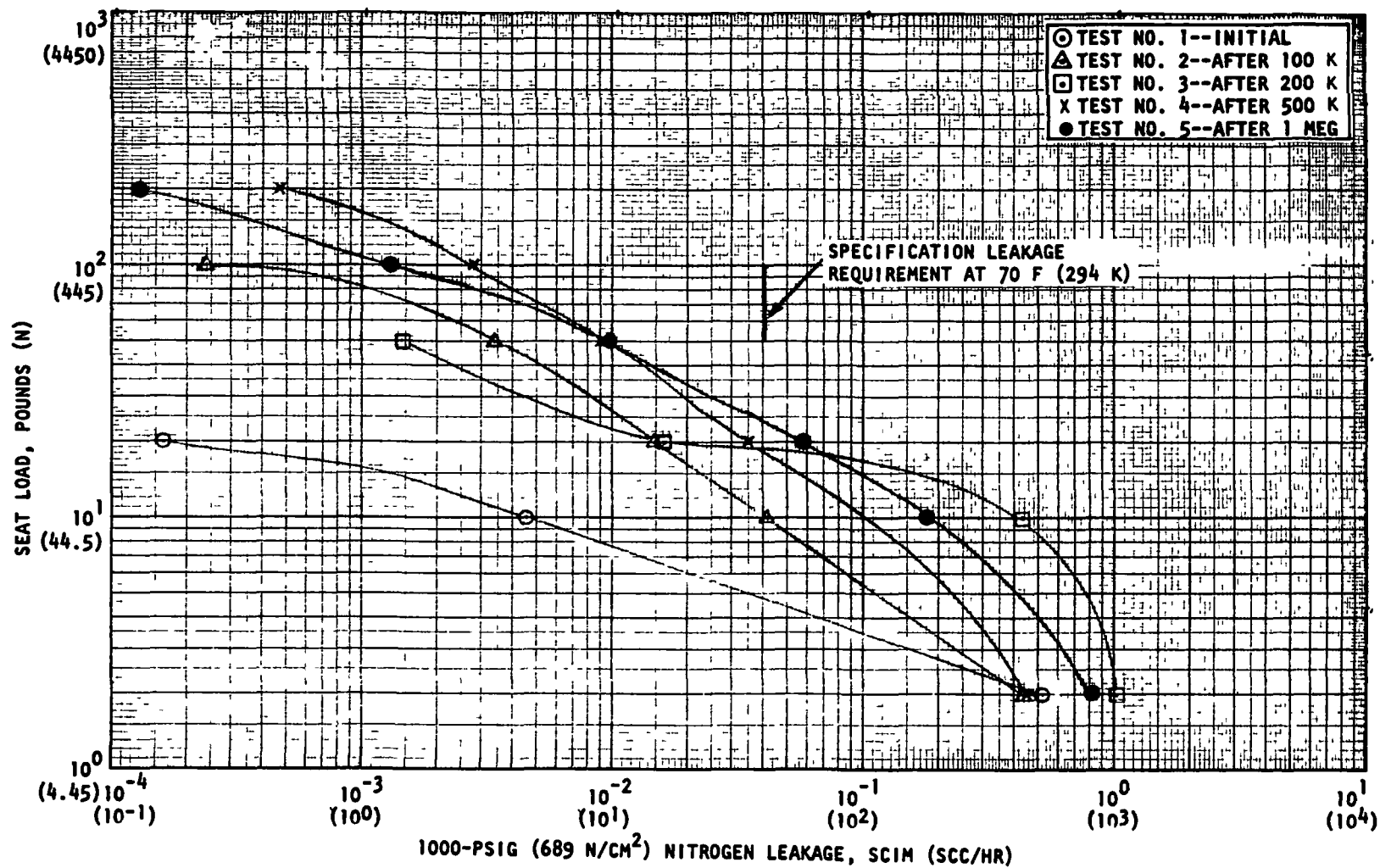


Figure 49. Carbide on Hard-Sharp Carbide, Test Model 403, 0.00108-Radian Scrubbing

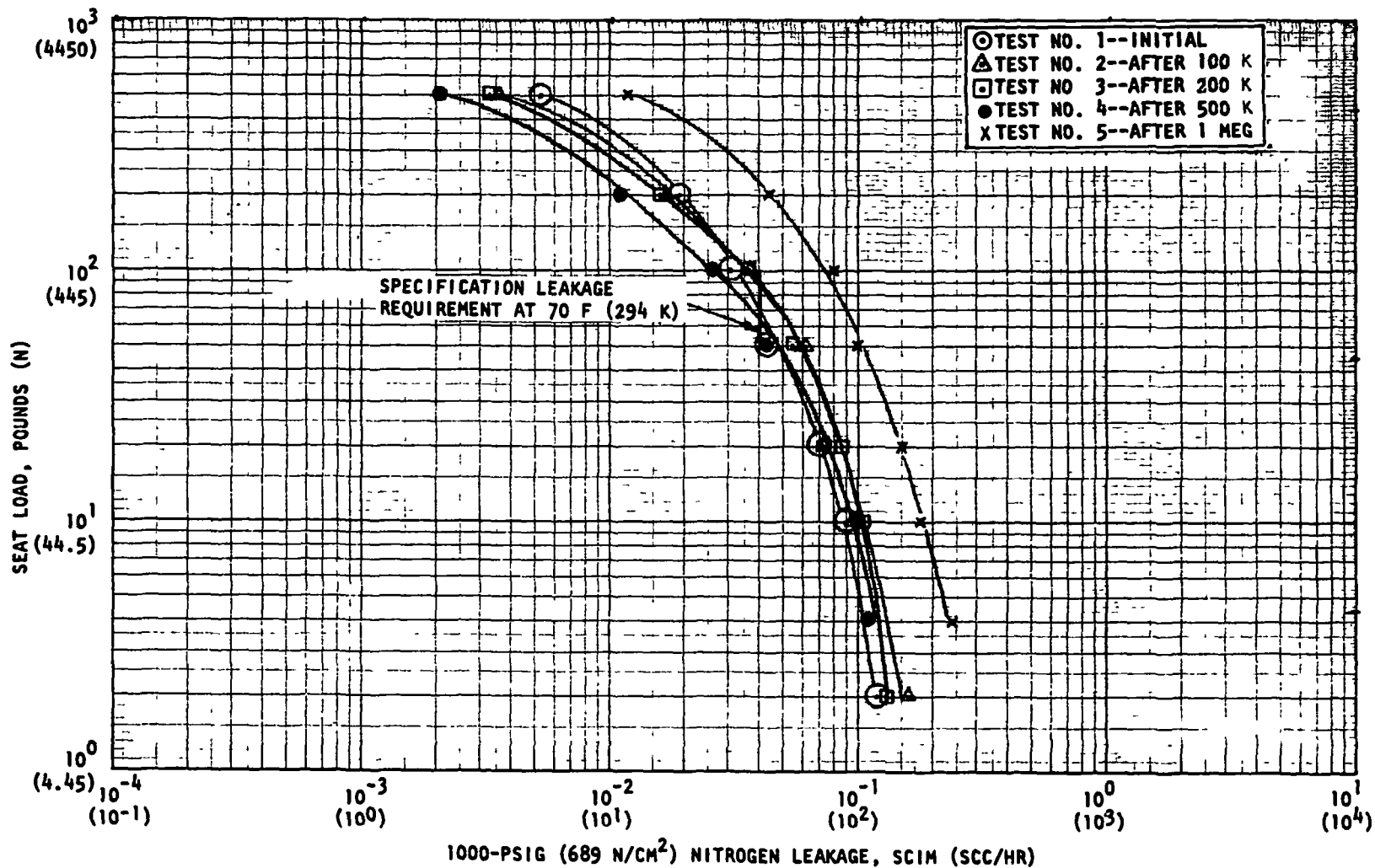


Figure 50. 440C on Grooved Gold, Model 304, 0.00108-Radian Scrubbing

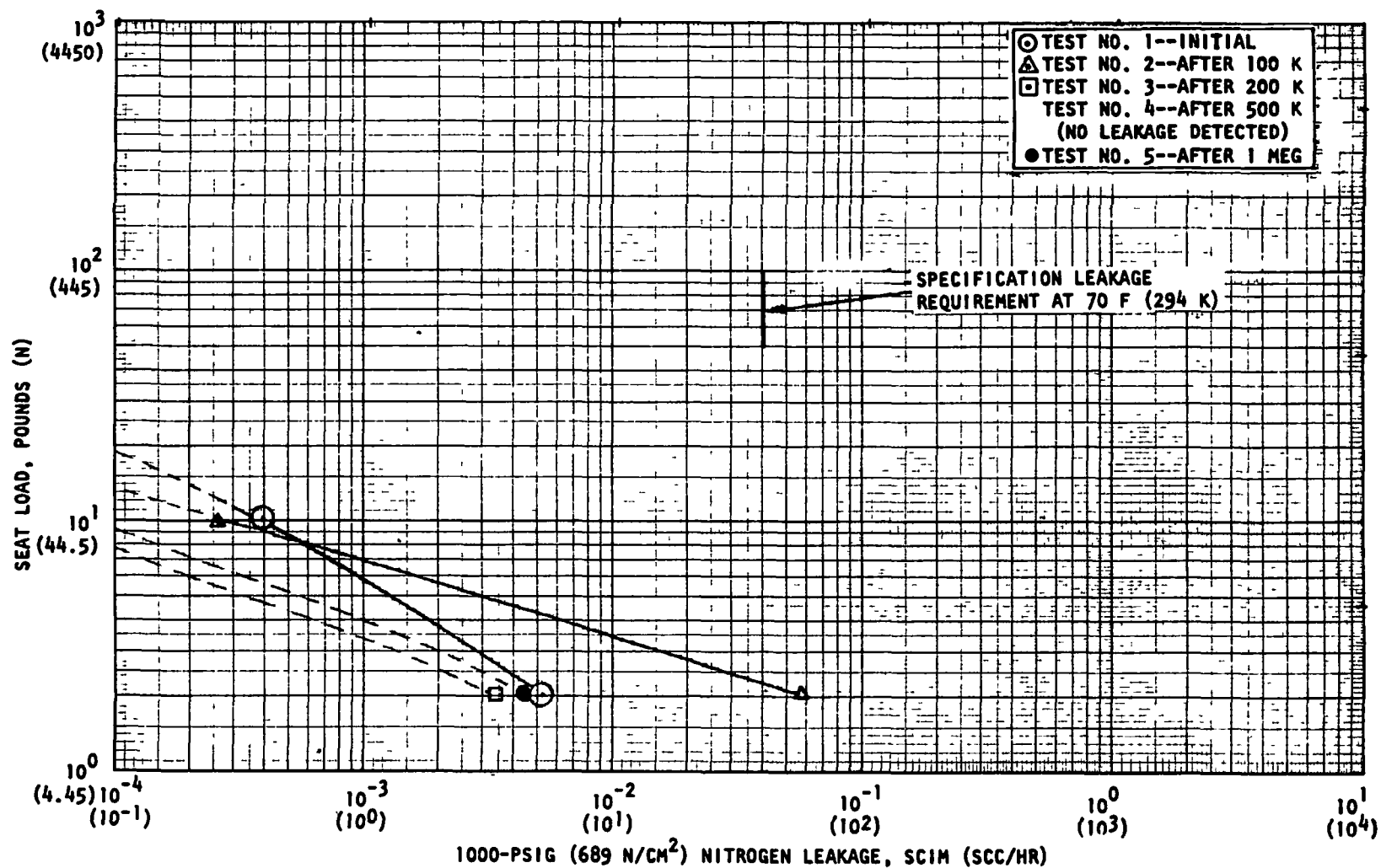


Figure 51. 440C on Captive Plastic, Model 504, 0.00216-Radian Scrubbing

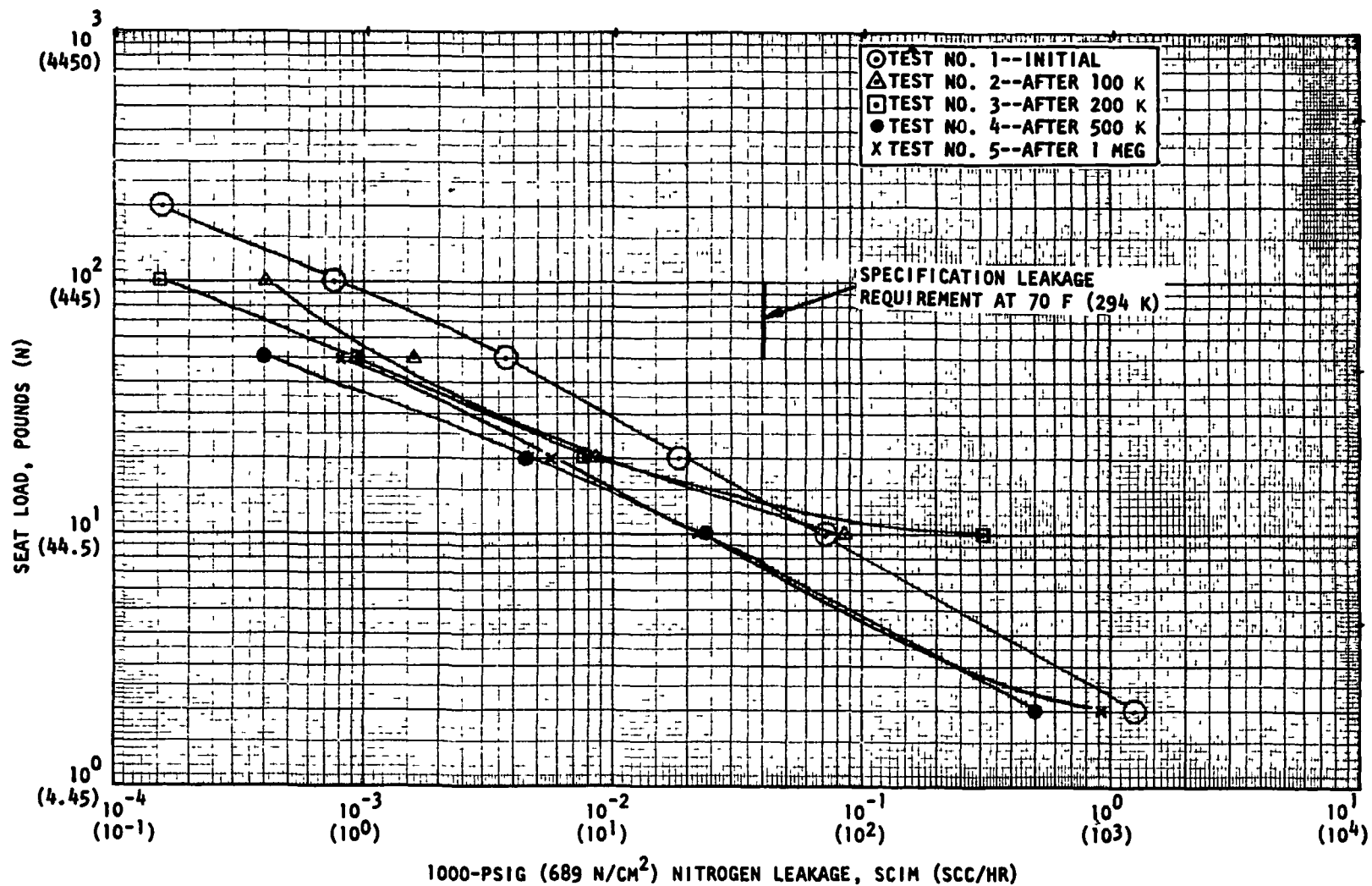


Figure 52. Carbide on Hard-Sharp Carbide, Model 404, 0.00216-Radian Scrubbing

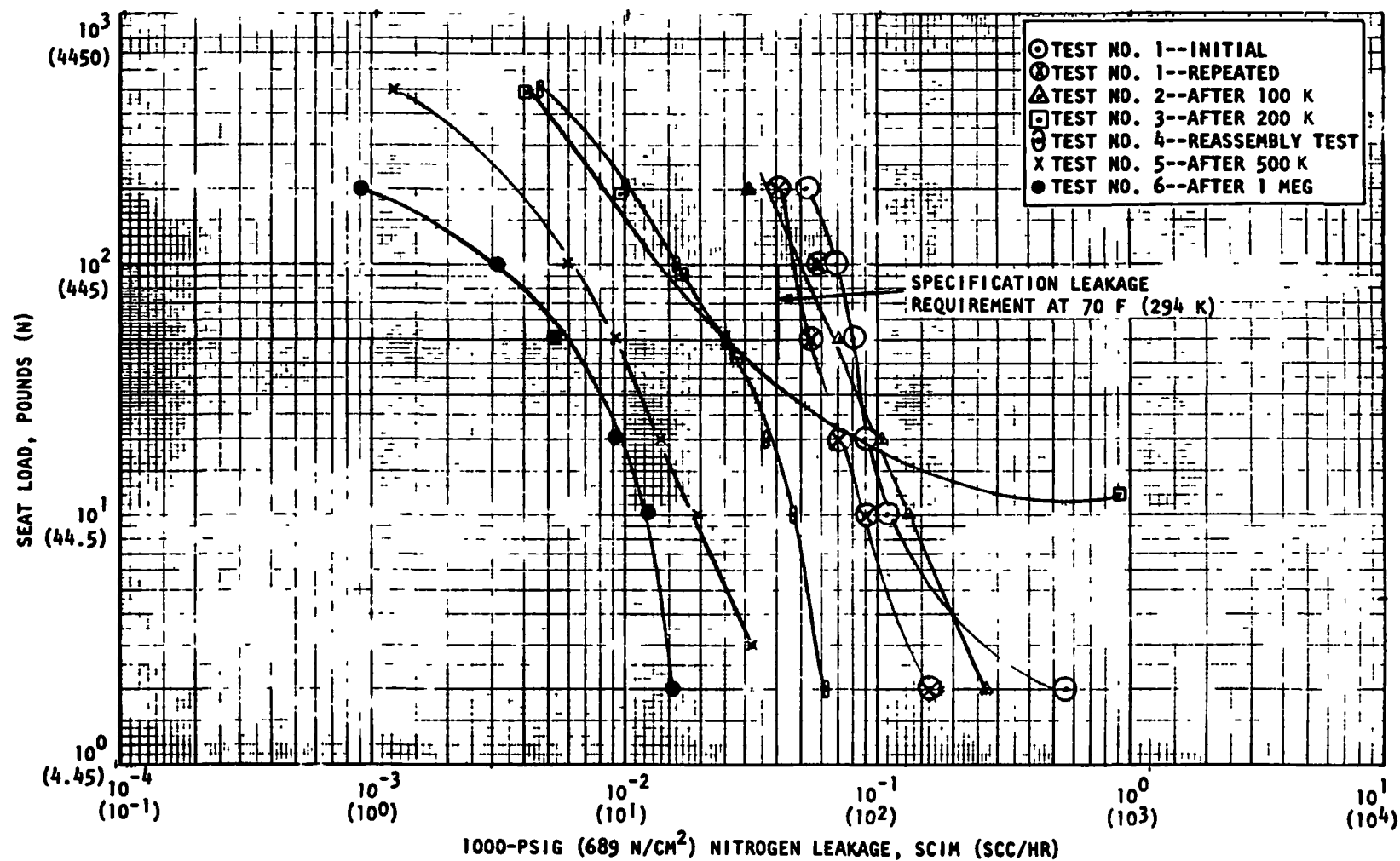


Figure 53. 440C on Grooved Gold, Model 305, $\alpha/2$ -Radian Scrubbing

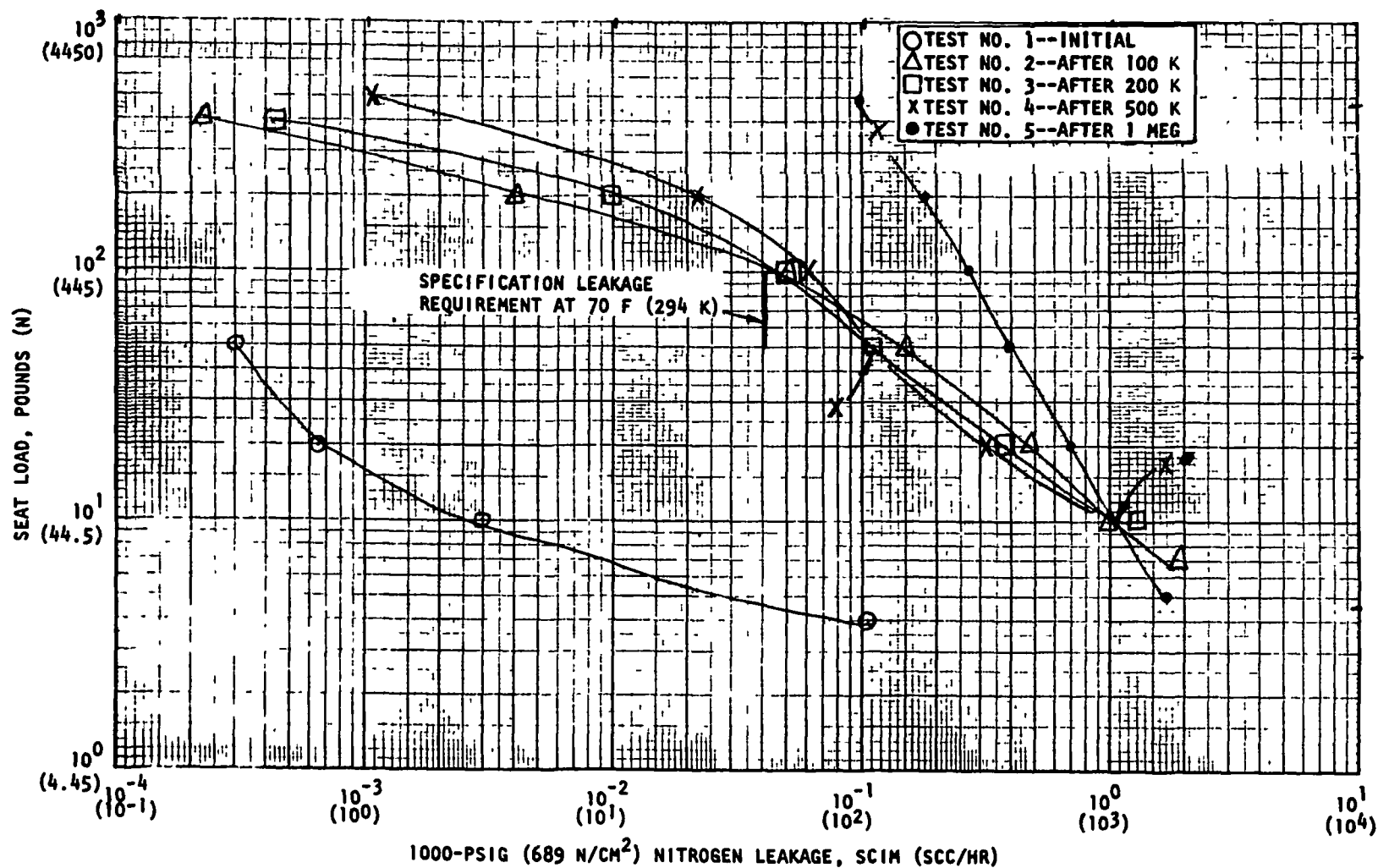


Figure 54. 440C on 440C Ambient, Model 110, 0.00054-Radian Scrubbing ($\alpha/2$)

Having narrowed the candidate closures down to two candidates, captive plastic and hard-sharp carbide, the closure screening tester was set up for the environmental tests. Early attempts at low-temperature (140 R, 77.7 K) cycling revealed a distortion-binding problem in the tester hydrostatic bearing area. For this reason, the high-temperature (850 R, 472 K) tests were performed first, prior to tester rework which corrected the earlier binding problem. The hard-sharp carbide (Fig. 55) was the first model to be subjected to the hot tests. The model was subjected to 500,000 cycles at an average temperature of 860 R (478 K). After 500,000 cycles, the initial indications, as seat load was being lowered to determine balance pressure, were that the leakage characteristics had not changed significantly from the initial hot test; however, no data were taken. When the balance pressure was reached, the pop-off occurred violently because the handwheel was not properly positioned to limit stroke, with the result that the closing impact was on the order of 2000 to 3000 pounds (8900 to 13,350 N). This severe impact crumbled a portion of the outer edge of the sealing land, resulting in the top leakage curve of Fig. 55. Even with the severe damage, the leakage was not grossly excessive, in that approximately 260 pounds (1157 N) of seat load brought the leakage below the specification limit. No ambient data were recorded with the damage because ambient leakage is typically lower than that at elevated temperature.

The captive plastic seat was tested next (Fig. 56) and successfully passed the leakage tests after 500,000 cycles at approximately 850 R (472 K). Upon disassembly, it was found that the plastic insert had extruded toward the inside diameter of the seat model. Analysis of the seat showed that the spring holding the inner retainer under load exerted enough force to produce a stress in the plastic at 850 R (472 K), approaching the compressive yield of the plastic. On the basis of this analysis, a new spring was obtained to use in a retest of the captive plastic seat at elevated temperature.

While awaiting the new spring for the captive plastic model, a special test was performed at the suggestion of the NASA-LeRC Project Manager. This test used the grooved gold seat in conjunction with the carbide poppet in a 2α radians high-temperature test (Fig. 57) to evaluate whether or not the gold would transfer to the carbide as it had in all the tests using 440C poppets. The test was terminated at 162,000 cycles because of a tester problem, but a load-leak tests at that point showed gross degradation of the model. Subsequent examination showed that the gold had transferred to the carbide to a considerable degree.

Upon receipt of the new spring for the captive plastic model, it was assembled and subsequently subjected to the hot test of Fig. 58. The captive plastic model performed very well during this test, and the extrusion over the inner retainer was not experienced.

In an effort to speed the testing schedule, a hard-sharp carbide model that had previously been tested for 1,000,000 ambient cycles was polished for the test of Fig. 59. The test was performed for 500,000 cycles cold, and the final cold and ambient leak checks showed a gross leakage. Examination at 500 power with the interference microscope revealed that the attempt at polishing the model had dubbed off the edges of the sealing land, leaving a crown where line-to-line contact existed. The 500,000 cycles of 250 pounds (1112 N) impact had slightly

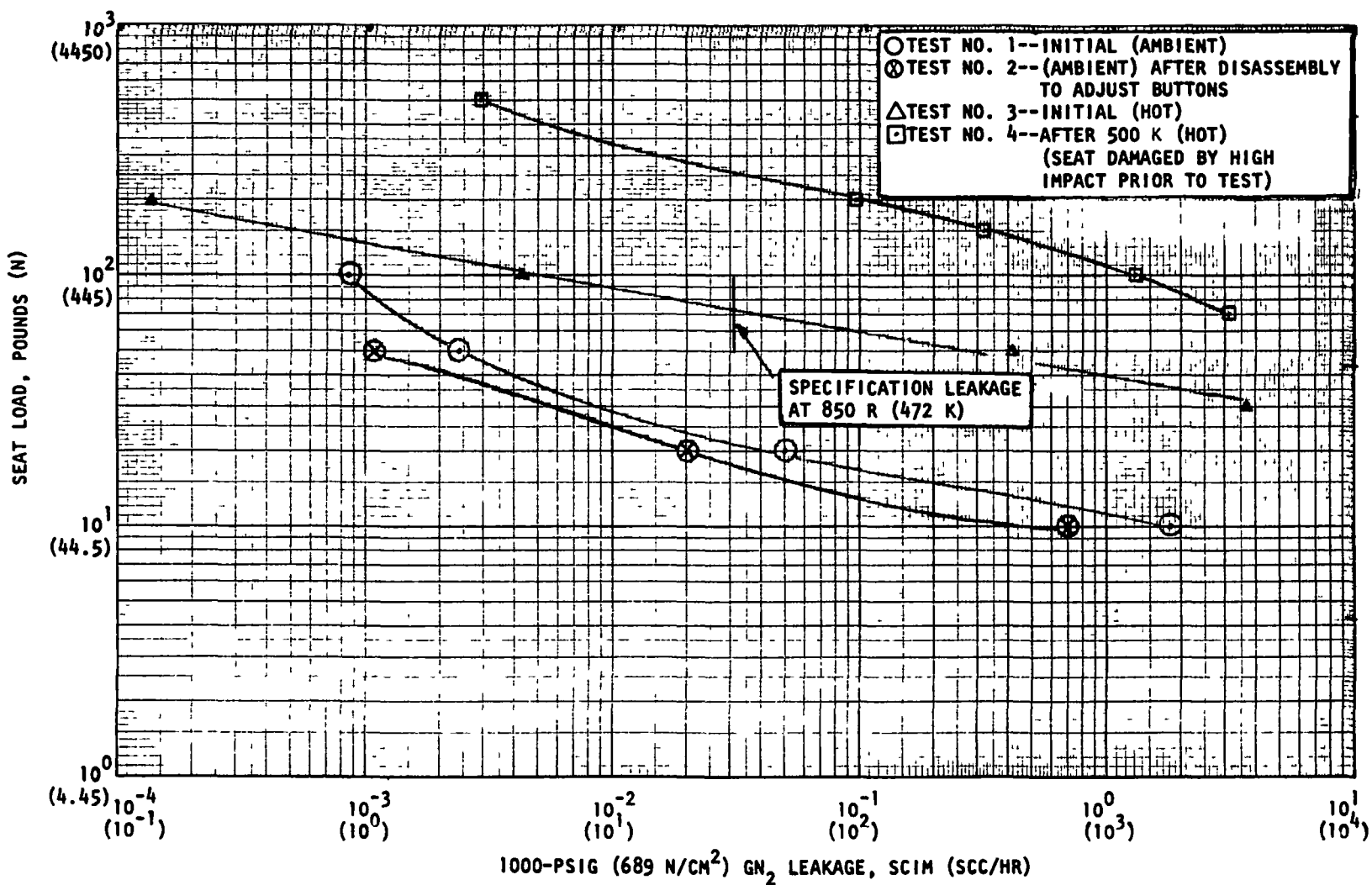


Figure 55. Carbide on Hard-Sharp Carbide, Model 405, High Temperature, 2α Scrubbing

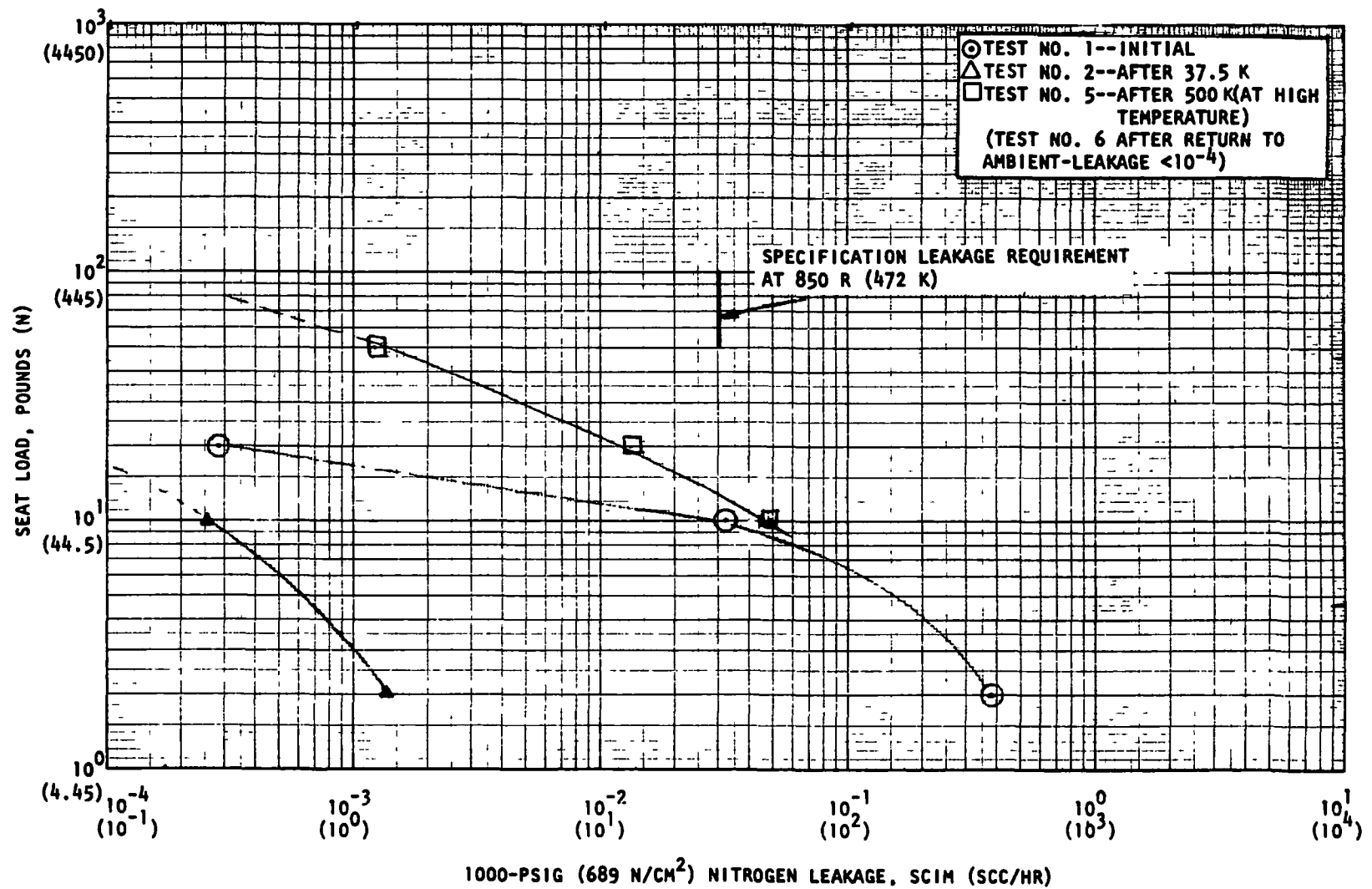


Figure 56. 440C on Captive Plastic, Test Model 505, High Temperature, 2α Scrubbing

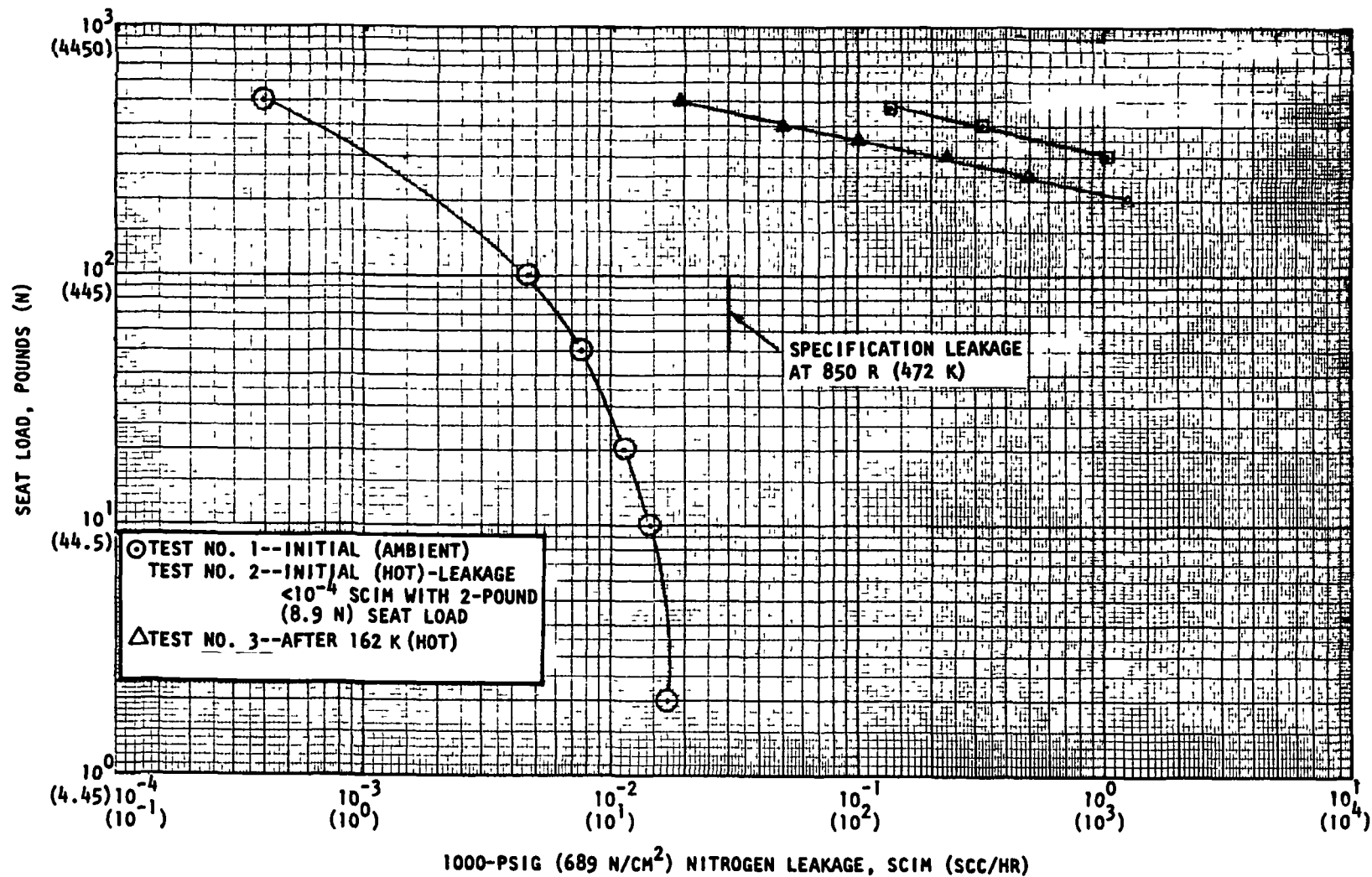


Figure 57. Carbide on Grooved Gold, Test Model 306, High Temperature, 2α Scrubbing

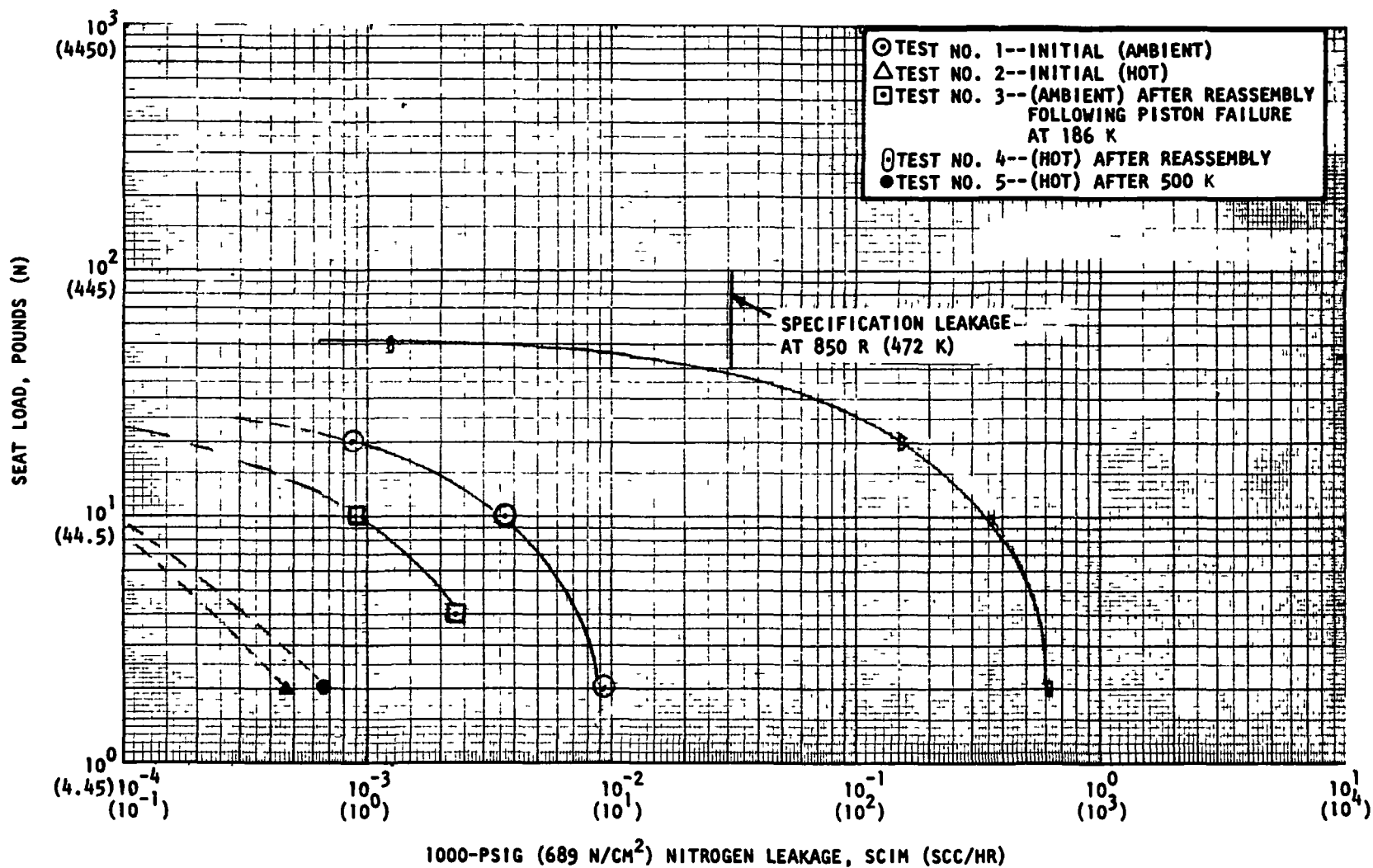


Figure 58. 440C on Captive Plastic, Test Model 506, High Temperature, 2α Scrubbing

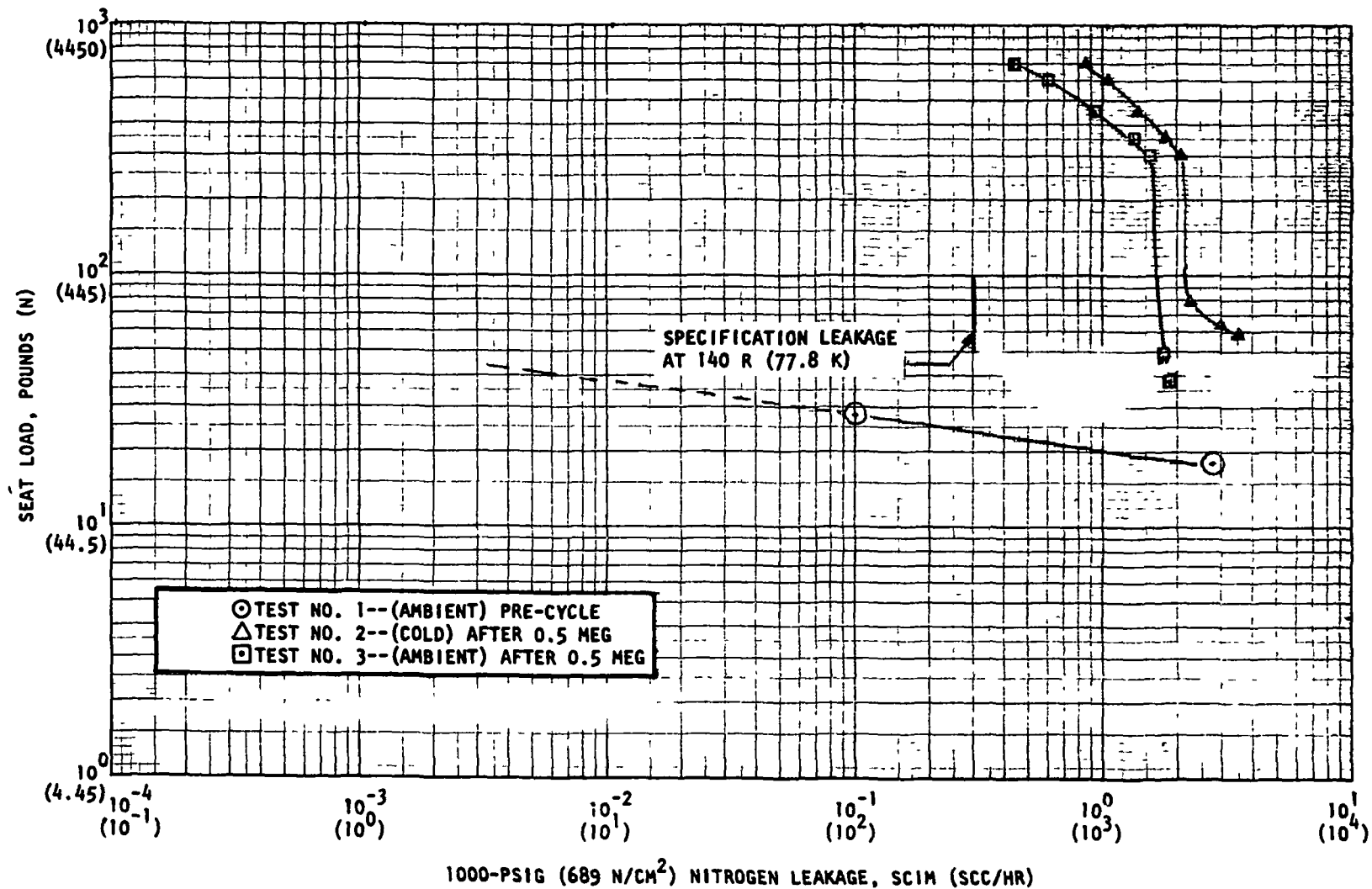


Figure 59. Carbide on Hard-Sharp Carbide, Test Model 406, 0.00216 Radian Scrubbing

impaired the crown producing the resultant leakage. The model was properly refinished to print dimensions, and later used for the contamination tests, then for a cold series as Model 408.

The captive plastic model (Fig. 60) was reassembled using some new beryllium copper outer retainer loading disks after a problem was experienced with the earlier disks. The inside diameter of the earlier disks in the deflected state was so near the outside diameter of the outer retainer load lip that the temperature differential experienced in reducing the tester to the cold condition caused the disks to snap over the outer retainer, thereby losing the retainer load. The new disks with a smaller inside diameter eliminated this problem. The model performed so well that great difficulty was experienced in detecting any leakage, i.e., at approximately 10 pounds (44.5 N) seat load, the leakage was less than 10^{-4} scim ($\approx 10^{-1}$ scc/hr) helium at 1000 psig (689 N/cm²) inlet pressure.

A brief series of tests was performed to determine general particle effects on the captive plastic and hard-sharp carbide models. These tests were limited to room temperature.

The results on the captive plastic model are shown in Fig. 61. The initial ambient leakage at 1000 psig (689 N/cm²) GN₂ inlet pressure was in the 10^{-4} scim (10^{-1} scc/hr) range at 4 pounds (17.8 N) seat load. The first test consisted of placing three 120-micron diameter R_C 23 nickel balls at 120-degree spacing, centered on the plastic insert. The balls were completely enveloped with leakage $<10^{-4}$ scim (10^{-1} scc/hr) at 4 pounds (17.8 N) seat load. Then, a human hair was used to bridge the entire seat. The result was an orifice-type leak, plotted in Fig. 61. The hair was removed using a human eyelash as a probe, and the resultant grooved seat retested. Again, the plastic healed its surface, the leakage being $<10^{-4}$ scim ($<10^{-1}$ scc/hr) at 4 pounds (17.8 N) seat load. Finally, one 60-micron diameter R_C 23 nickel ball was placed on the outer retainer adjacent to the plastic insert to purposely cause the retainer to be unable to contain the plastic at the outside diameter because the ball prevented the retainer from contacting the poppet face. Two leak tests showed an initial orifice-type leak, reducing to $<10^{-4}$ scim ($<10^{-1}$ scc/hr) by 100 pounds (445 N) seat load. An important facet demonstrated by this series of tests was the self-healing capability of the captive plastic concept. Where the contaminant is wholly in the plastic, it is enveloped. In a bridging-type contaminant, the extremely light forces required to remove the contaminant showed that the next cycle of flow would flush a contaminant from the seat. This capability is vitally important to a 1,000,000-cycle valve closure. Photomicrographs of seat damage are shown in Fig. 62 through 65.

Because the hard-sharp carbide seat was originally designed as a contamination destroyer, it was tested (Fig. 66) using typical bridging-type contaminants. The first test used a human hair with hardly noticeable effects. The hair was cut cleanly by the sharp carbide seat acting against the flat carbide poppet. The seat was then completely bridged by a 0.007-inch (0.0019 cm) diameter enameled copper wire. It, too, was cleanly cut with practically no effect on leakage. Subsequent examination of the seat and poppet at 500 power with the interference

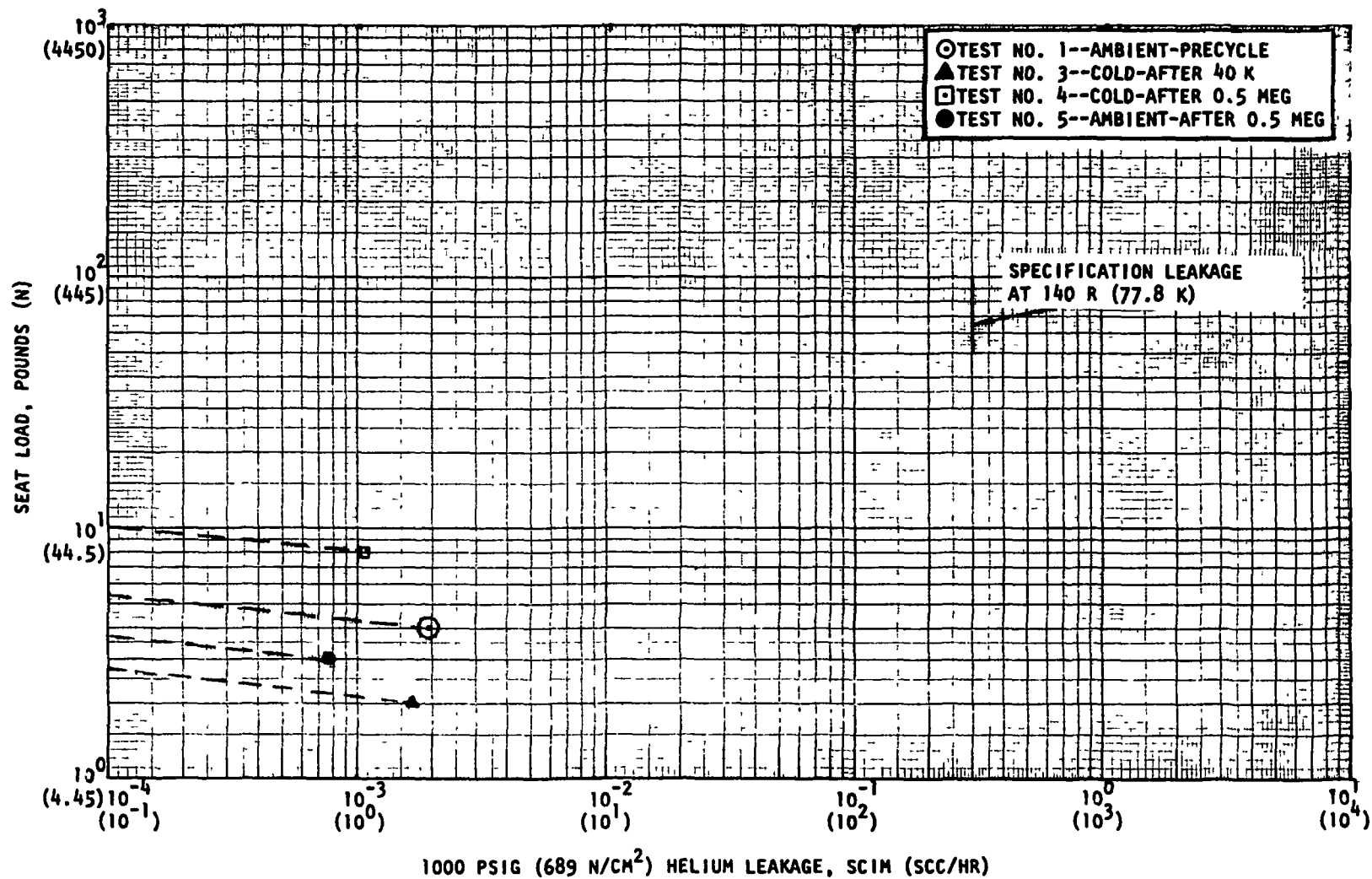


Figure 60. 440C on Captive Plastic, Test Model 508, 0.00216 Scrubbing, Low Temperature

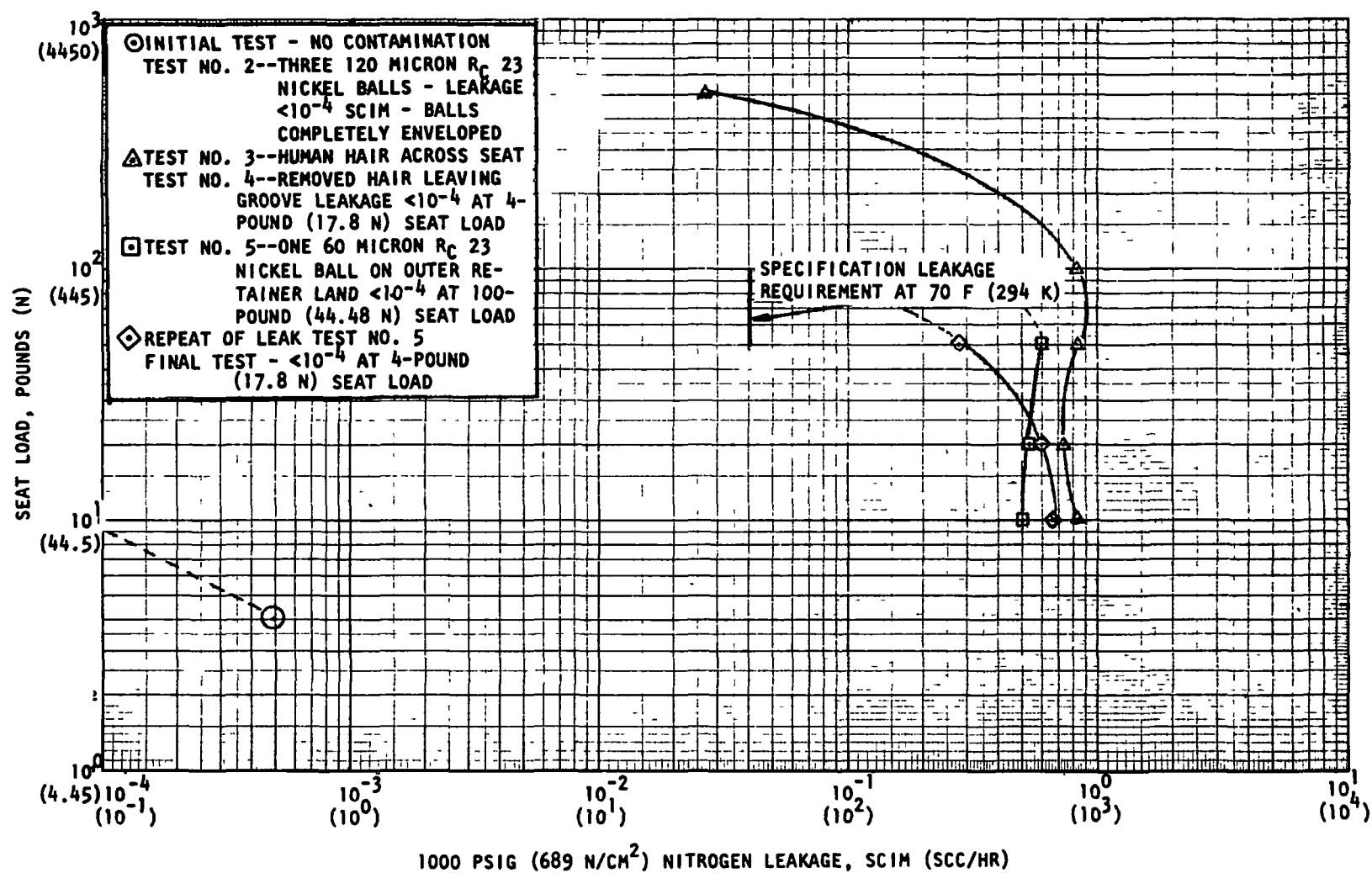


Figure 61. 440C on Captive Plastic, Test Model 509, Contamination Tests

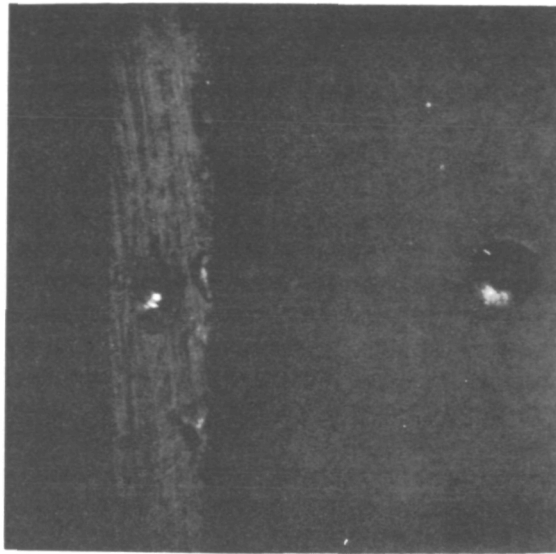


Figure 62. Model 509 Captive Plastic Seat With H60 Particles; Metal Land Particle Not Embedded (91X Plain Photo)

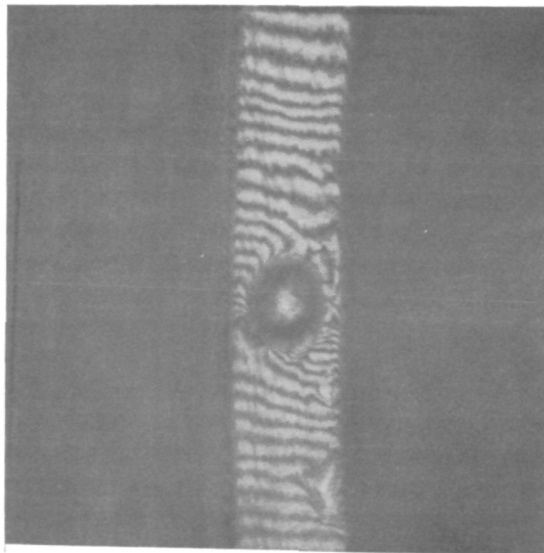


Figure 63. Model 509 Captive Plastic Seat Showing Indentation From H60 Particle (91X Interference Photo)

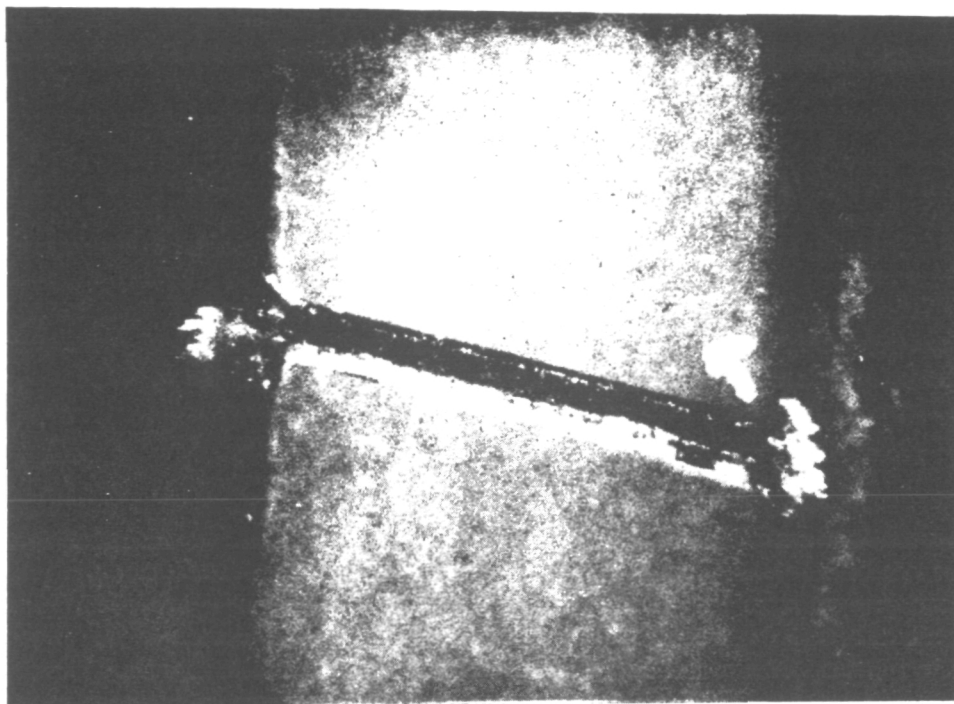


Figure 64. Model 509 Captive Plastic Seat
with Embedded Hair (91X Plain Photo)

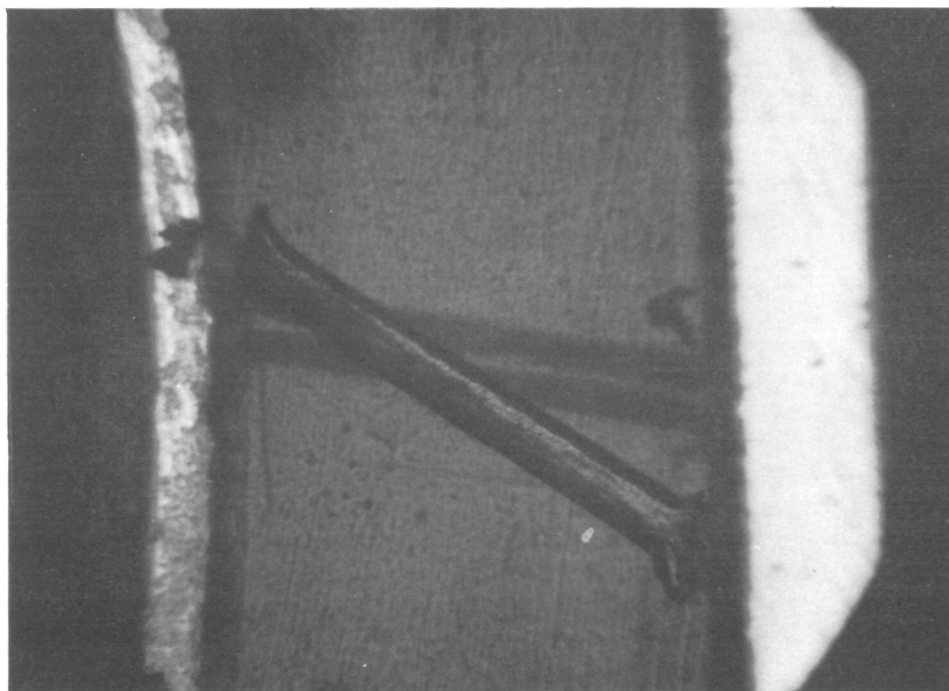


Figure 65. Model 509 Captive Plastic Seat
Showing Groove from Hair (91X Plain Photo)

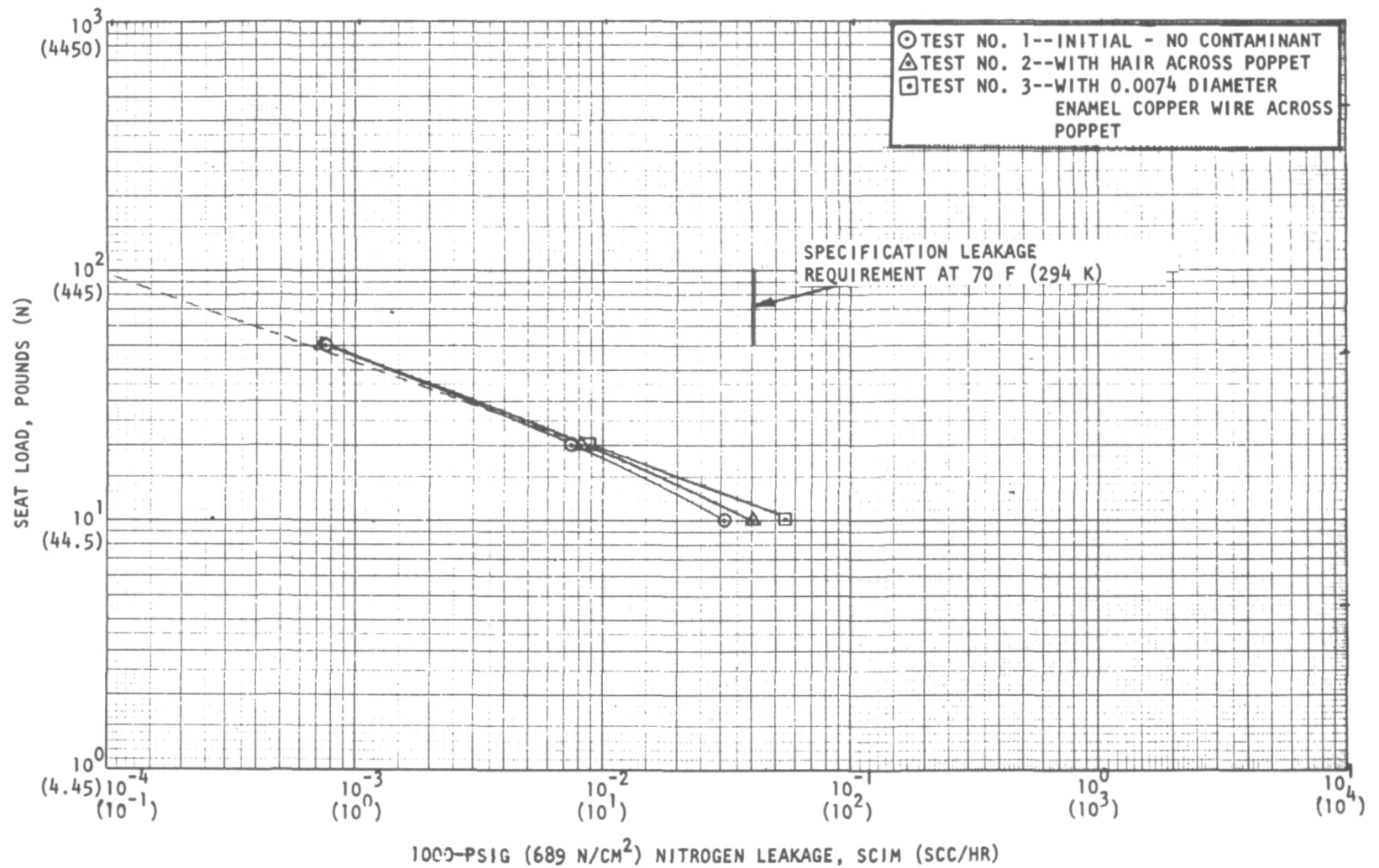


Figure 66. Carbide on Hard-Sharp Carbide, Test Model 407, Contamination Tests

microscope revealed no deformation of the model as a result of cutting these fibers. This test clearly illustrated the capability of the hard-sharp carbide seat to destroy contaminants. Figures 67 and 68 depict the results of the wire cutting.

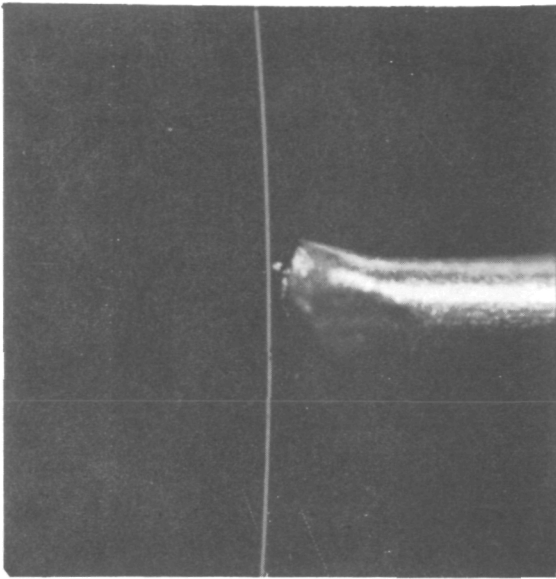


Figure 67. Model 407 Seat Showing Cut Wire (91X Plain Photo)

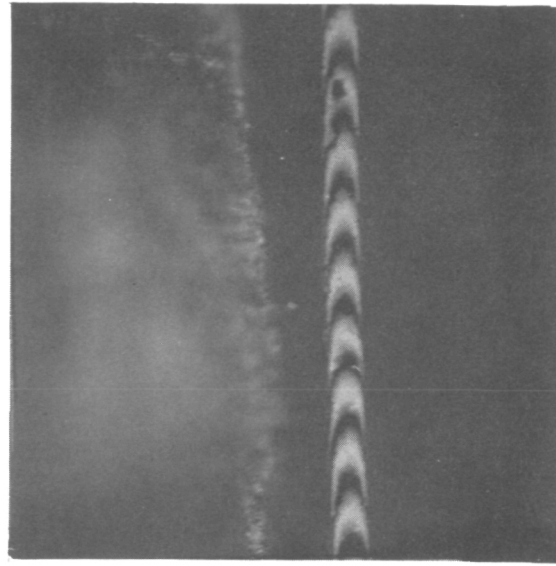


Figure 68. Model 407 Seat Showing Cut Wire (462X Interference Photo)

This same model was used to repeat the earlier cold test of the hard-sharp carbide which was invalid because of improper finishing of the model. With the model finished to drawing requirements, the data of Fig. 69 were obtained. After 500,000 cycles cold, the sealing characteristics hardly changed cold and, at ambient, leaked slightly less at very low loads and slightly more than initially at the higher loads.

The tests of Fig. 70 were performed to evaluate the need for preferential seating on each cycle of the hard-sharp carbide model. The 500,000 cycles were accumulated in the seat positions shown and demonstrated that the Task II design concept of using guide pins to prevent poppet rotation was not needed. The valve test fixture eliminated these guide pins, greatly simplifying the design, and eliminating a potential source of binding and friction.

The final test of the screening series evaluated the low-pressure disk seal concept. Because inlet pressure loads the disk seal independently of piston control pressure, the data of Fig. 71 is plotted as leakage versus inlet pressure as opposed to all the other model data. Progressive cycling of the model produced severe degradation and, at 500,000 cycles, had exceeded the leakage-measuring capacity of the low-leak system used in the APS tester. Because the leakage was so great, the data were not recorded using the high-leak system. The cycles were performed at a low inlet pressure during cycling, but at 250 pounds (1112 N) peak impact. Perhaps this impact level was too great for a low-pressure concept in a normal low-pressure valve, but would be representative of values to be expected in

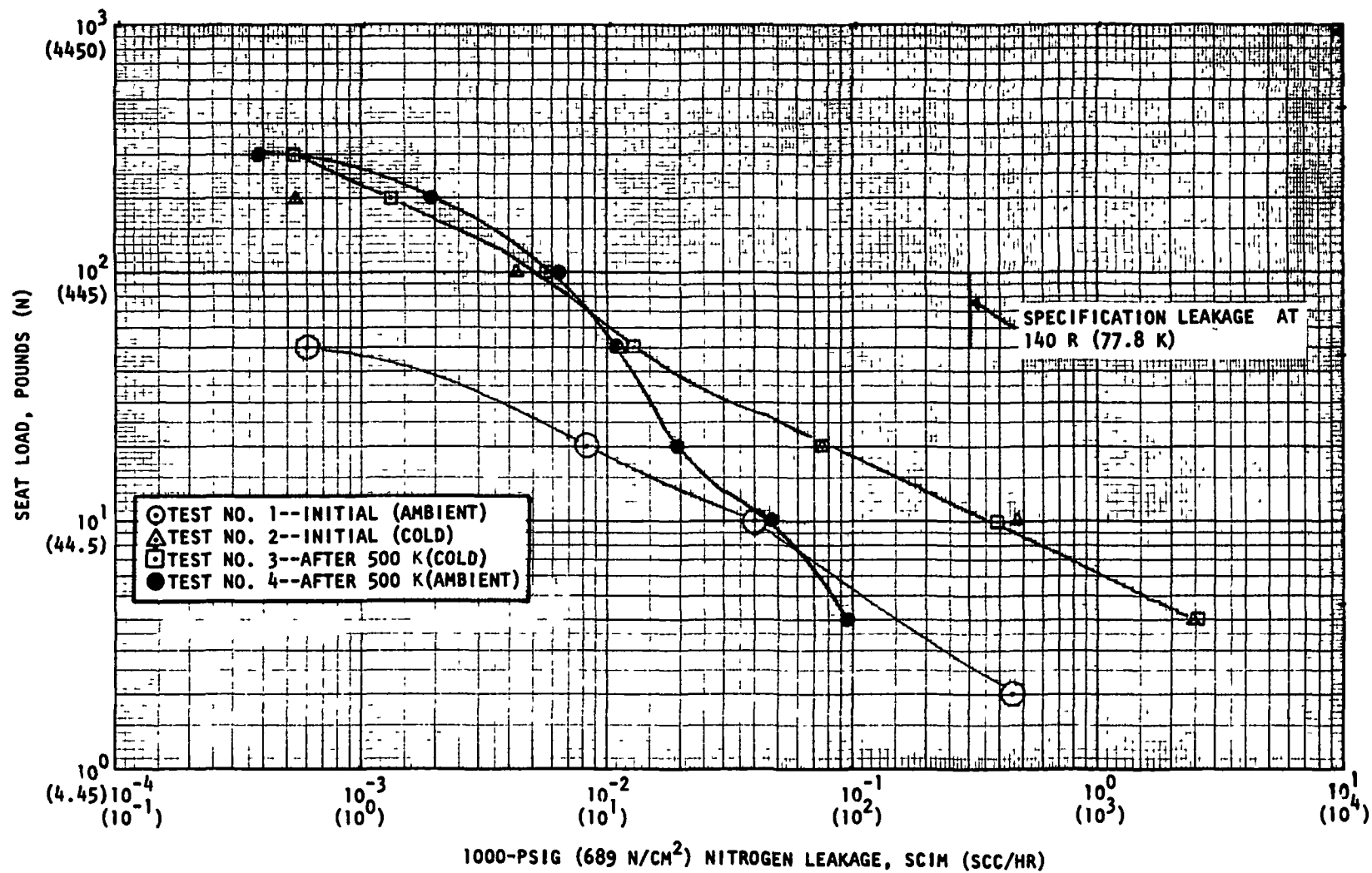


Figure 69. Carbide on Hard-Sharp Carbide, Test Model 408, Low Temperature, 2 α Scrubbing

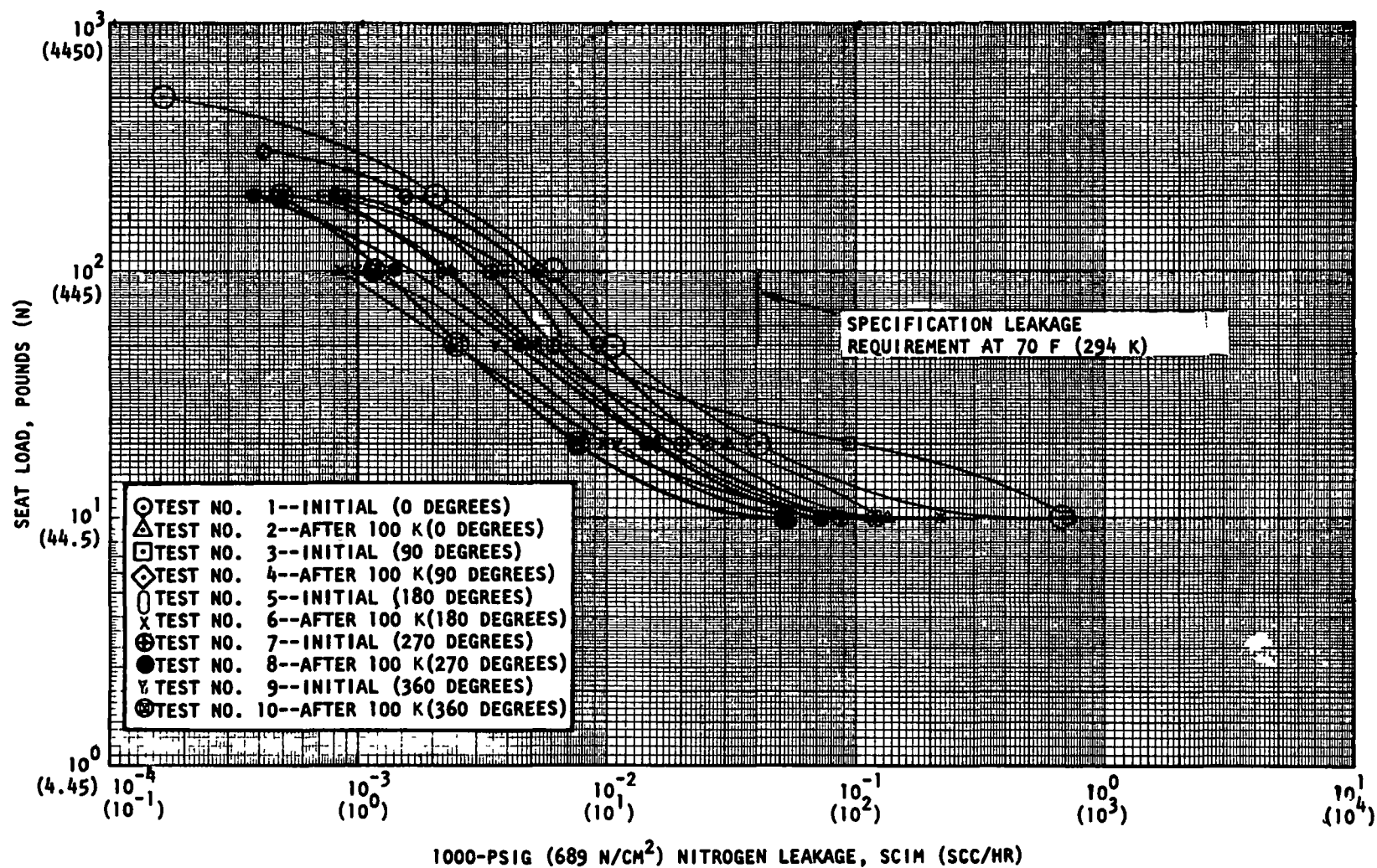


Figure 70. Carbide on Hard-Sharp Carbide, Test Model 409, Orientation Tests, 2α Scrubbing

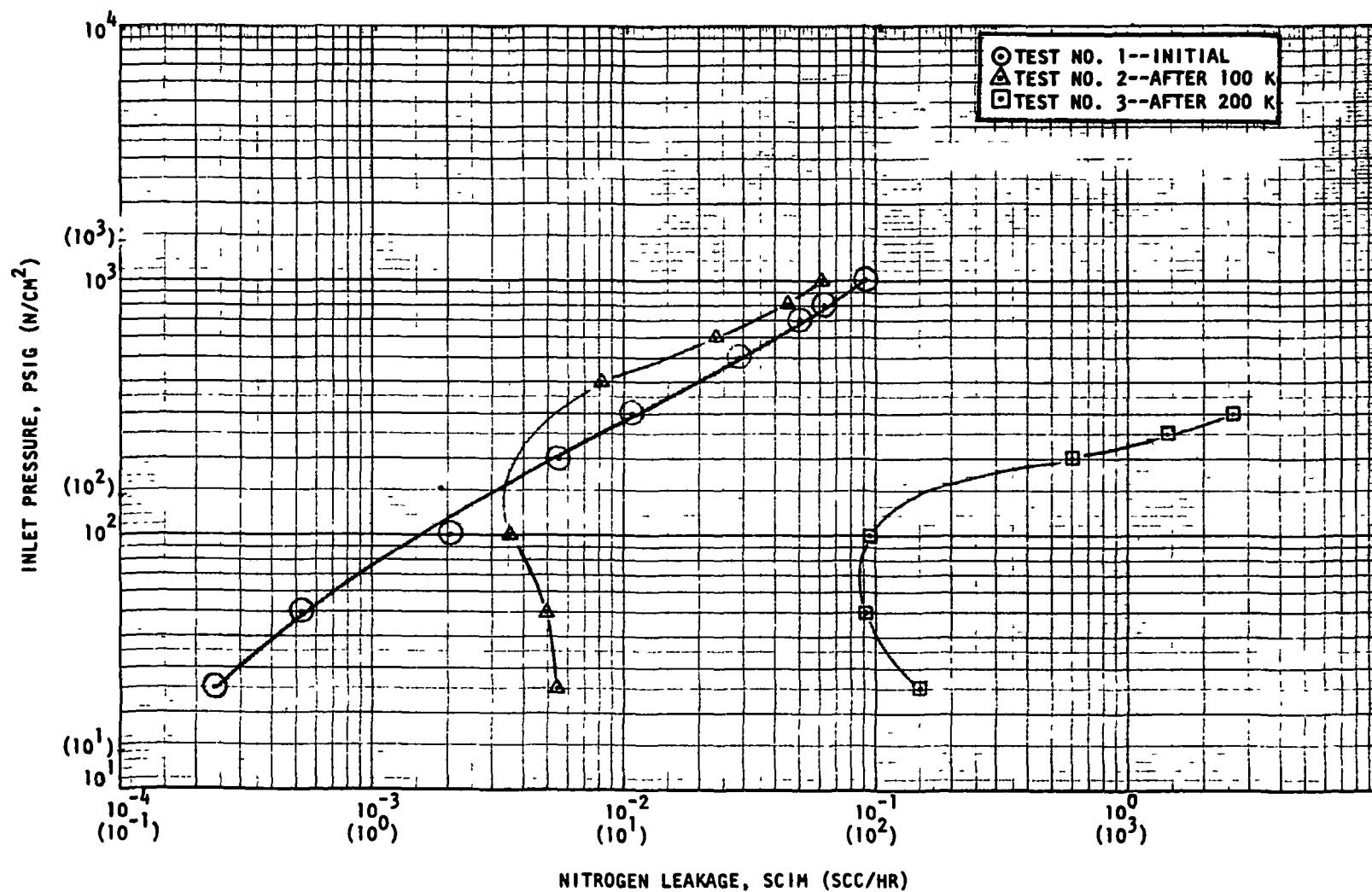


Figure 71. Disk Seal, Test Model 601, Initial Tests, Poppet Parallel Within 0.0001

a low-pressure valve meeting APS thruster timing requirements. Other low-pressure layouts were generated during the Task II effort which were superior to this concept in that liftoff seating was used. These concepts were provided to NASA-LeRC under separate cover, and not used for this report, because the emphasis had, by that time, shifted to the high-pressure system for APS.

As a final comment, it should be noted that the same captive-plastic insert was used for certain of the ambient, cold, and contamination tests, accumulating over 1,500,000 cycles successfully, and with capability for more cycles. Similarly, one of the carbide models accumulated over 3,500,000 cycles, the only rework being to relap the faces of the sharp crests prior to each test series to ensure a good baseline datum. Table V presents the test matrix performed using the APS Closure Screening Tester with the exception of the clamped 440C checkout tests. Thus, the hard-sharp carbide and the captive plastic closures were carried forward into the next portion of the contract effort as the two candidate designs.

TABLE V - TEST MATRIX

Mode	440C	Grooved Gold		Hard-Sharp Carbide			Captive Plastic		
	Ambient	Ambient	High Temp	Ambient	High Temp	Cold	Ambient	High Temp	Cold
Clamshell α	1.5M Fail	1.0M Pass	--	1.0M Pass	--	--	1.0M Pass	--	--
2 α	--	1.0M Fail	--	1.0M Pass	--	--	1.0M Pass	--	--
Scrubbing α	200K Fail	1.0M Fail	--	1.0M Pass	--	--	1.0M Pass	--	--
2 α	--	--	*162K Fail	1.0M Pass	0.5M Pass	0.5M Pass	1.0M Pass	0.5M Pass 0.5M Pass	0.5M Pass
$\alpha/2$	1.0M Fail	1.0M Pass	--	--	--	--	--	--	--

*With carbide poppet

VALVE TEST FIXTURE

OBJECTIVE

During the earlier program phases, it had been determined that the most feasible approach was the use of a poppet-type valve for both high- and low-pressure APS systems. Also, analysis followed by extensive closure screening testing had shown the captive plastic closure concept and the hard-sharp carbide closure concept to be superior in performance to the other models tested, and indeed, could meet the stringent leakage goal of less than 100 scc/hr helium after 1×10^6 cycles. The objective of this phase of the program was to prove, with a full-scale valve (valve test fixture) and closures, the conclusions reached in the earlier phases by demonstrating the long-life, low-leakage performance required for SS/APS.

VALVE PRELIMINARY DESIGN

During the early phases of the APS program, a preliminary trade study was made on a "no exceptions" basis to the design requirements. The results of the trade study indicated the use of an hydraulically actuated poppet valve with a bellows shaft seal and flat metal-to-metal closure for the high-pressure system. As the program progressed, with completion of the Task IIIA Closure Screening Tests, and work progressing on the Task II Preliminary Designs, it became apparent that the results of the preliminary trade study required modification. By this point in the program, two basic decisions had been reached: (1) the low-pressure system was no longer a SS/APS requirement, therefore it was eliminated from further consideration, and (2) hydraulic power would not be available during orbit for SS/APS valves actuation.

Therefore, the selection logic of Fig. 72 was formulated. The design requirements were reviewed, and technology factor assessments assigned as shown in Table VI. Using these factors, valve concepts pilot valves, actuation methods, mechanical elements, and closures were studied. The valve concepts of Table VII were considered in the re-evaluation of the basic requirements. From these studies, a qualitative valve concept comparison chart was prepared as shown in Table VIII. In addition to these factors, system adaptability was considered along with the various actuation methods, as shown in Table IX. The results of these studies indicated that a poppet-type valve, actuated by a pilot solenoid using the propellant gas as actuation media, was preferred over using stored pneumatic systems since this will produce the lightest weight system. Again, electric methods were unable to meet needed response times.

Also, studies being conducted on the APS thruster program indicated that valve ΔP could increase without performance penalty. This allowed a valve size decrease, resulting in a smaller, lighter weight package. The valve ΔP tradeoffs are shown in Appendix D.

The above-mentioned studies were being conducted during the closure screening tests. Preliminary designs were prepared so that the selected closures and preliminary designs could be chosen at a single design review with the NASA-LeRC Project Manager. The valve preliminary designs are discussed as follows.

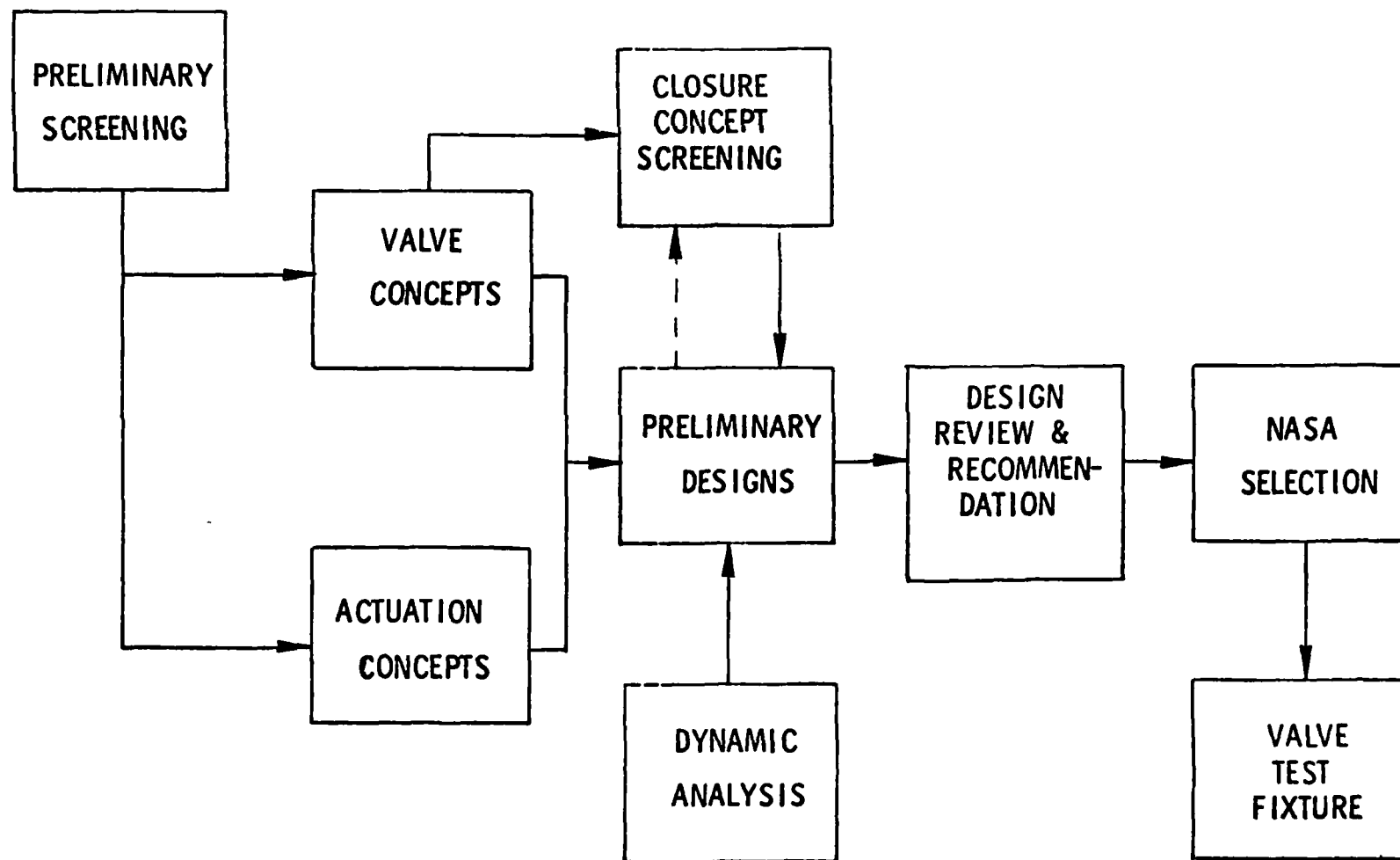


Figure 72. SS/APS Valves Program Selection Logic

TABLE VI - QUALITATIVE VALVE CONCEPT COMPARISON

Type	Weight	ΔP	Closure Life	Complexity	Development Risk	Contamination Insensitivity
Butterfly	Low	Medium	Medium	Medium	High	Low
Ball	Low	Low	Low	Medium	High	Low
Blade	High	Low	Low	Medium	High	Low
Butterfly/Ball (Retracting Seat)	High	Low	High	High	Medium	Medium
Poppet	Medium	Medium	High	Low	Low	High
Diaphragm	Available materials will not meet temperature requirements					
Spool	Will not meet leakage requirements					

TABLE VII - REQUIREMENT OVERVIEW

Requirement	Technology Factor
Response	2
Life	10
Fluid Compatibility	1.1
Fluid Pressure	1
Temperature	1.5
Leakage	10

TABLE VIII - VALVE CONCEPTS

<ul style="list-style-type: none"> • Butterfly • Ball • Blade • Butterfly or Ball (Retracting Seat) • Poppet • Diaphragm • Spool

Valve Preliminary Design

Design No. 1. The first design (Fig. 73) is a conventional, semibalanced, 90-degree poppet valve with some unique features to obtain long life. The valve is pneumatically opened by the propellant and is closed by a helical spring when a pilot valve vents the actuator.

TABLE IX - ACTUATION CONCEPTS

<ul style="list-style-type: none"> • Electric Motor • Direct Solenoid • Hydraulic • Pneumatic (Helium) • Pneumatic (Propellant)
--

All static seals in the valve are Teflon-coated metal O-rings. These were selected for their long service life (no age control required as with elastomer seals) and their resistance to corrosion. The piston and shaft seals, manufactured by Rudolf E. Krueger Co., were selected because of better wear characteristics than conventional lipseals and because they are able to compensate for thermal effects of the shaft.

The poppet/seat arrangement as shown in Fig. 73, is a grooved gold seat with a flat poppet. A captive plastic poppet with a flat seat can be incorporated into the same design. These concepts are two representative types of those which were tested under the closure screening test program. The seat assembly is an insert which "floats" on the two metal O-rings to compensate for temperature effects between the Inconel flange and aluminum body. This design also flexes the sealing surface toward the poppet. The poppet seal is attached to the bellows, but not rigidly attached to the shaft. Instead, a flexure disk is used to support the poppet to the shaft and prevent seat scrubbing due to shaft movement.

Wear prevention and particle generation from rubbing are of prime concern for long life characteristics. A Teflon bushing between the shaft and guide prevents metal-to-metal contact during valve actuation. The poppet bellows, which prevents shaft rotation, is of conventional design, but a shroud is used on the outside to protect it from particles in the flow stream and to prevent movement due to flow turbulence. A thrust bearing is used in the actuator cover to permit the poppet return spring to rotate during compression, thus preventing seat rotation.

Design No. 2. The second design (Fig. 74) is of an inverted, 90-degree poppet valve which, like the conventional semibalanced poppet valve (design No. 1), has some unique features to obtain long life. The valve is pneumatically opened by the propellant and is closed by a helical spring when a pilot valve vents the actuator.

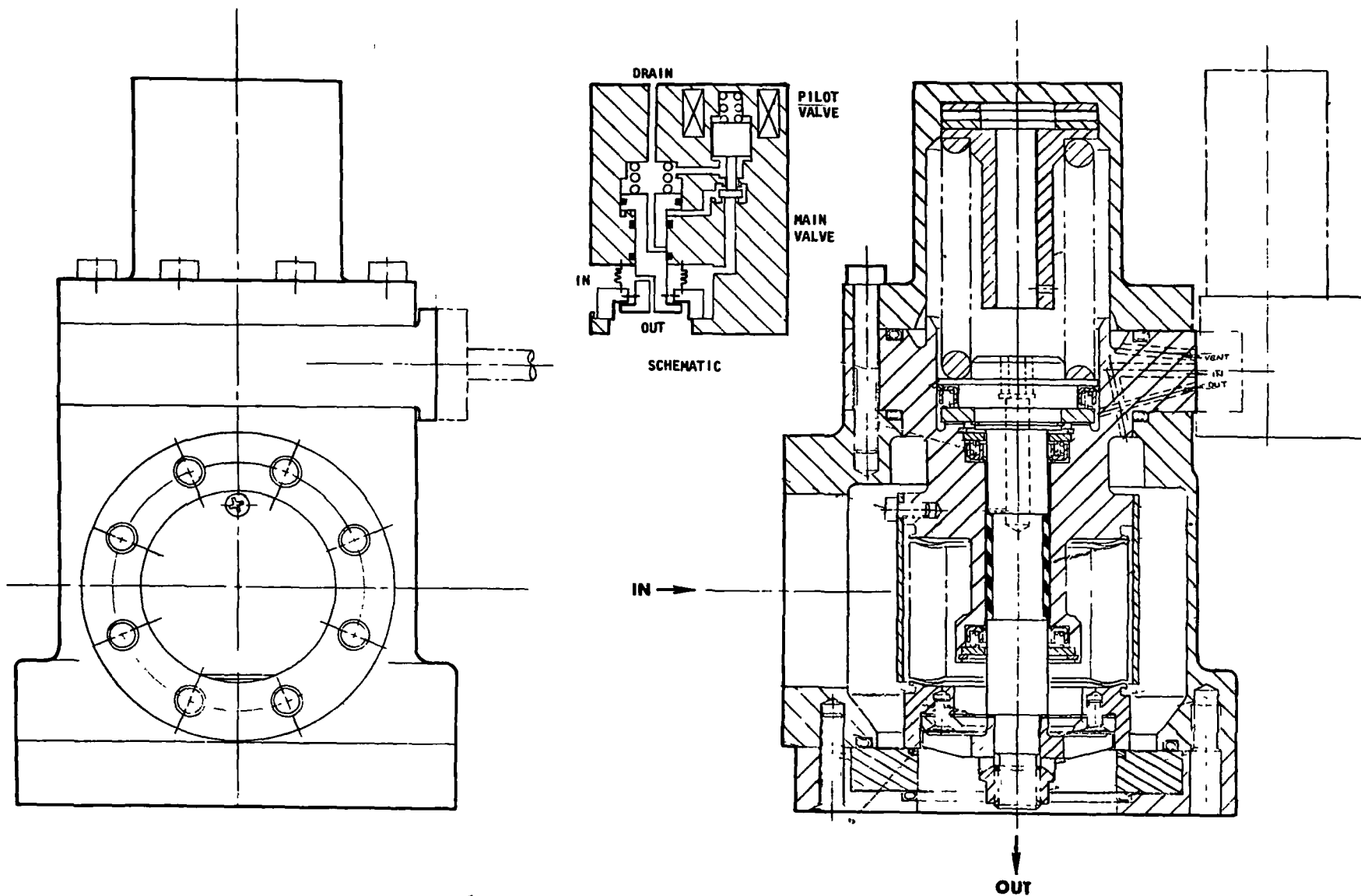


Figure 73. Conventional, Semibalanced 90-Degree Poppet Valve (Design 1)

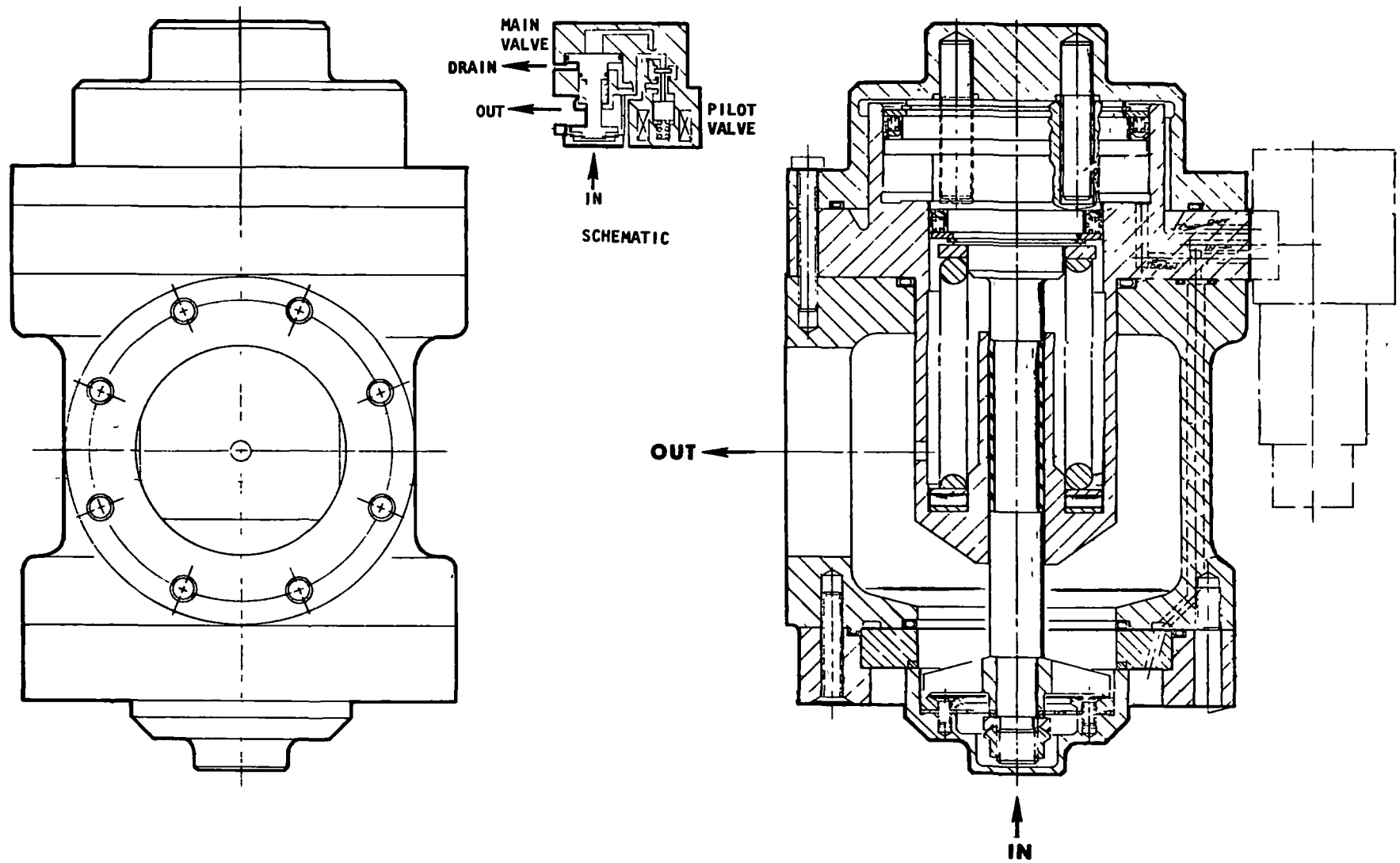


Figure 74. Inverted, 90-Degree Poppet Valve (Design 2)

All static seals in the valve are Teflon-coated metal O-rings. These were selected for their long service life (no age control required as with elastomer seals) and their resistance to corrosion. The piston and shaft seals, manufactured by Rudolf E. Krueger Co., were selected because of better wear characteristics than conventional lipseals, and because they are able to compensate for thermal effects of the shaft.

The poppet/seat arrangement, as shown in Fig. 74, is a grooved gold seat with a flat poppet, or could accommodate a captive plastic poppet with a flat seat. These concepts are two representative types of those tested under the closure screening test program. The seat assembly is an insert which "floats" on metal O-rings to compensate for temperature effects between the Inconel flange and aluminum body. This design also flexes the sealing surface toward the poppet. The poppet seal is attached to the poppet shaft by means of a flexure disk which prevents the seat from scrubbing due to shaft movement.

Wear prevention and particle generation from rubbing are of prime concern for long life characteristics. A Teflon bushing between the shaft and guide prevents metal-to-metal contact during valve actuation. A thrust bearing is nested in the housing to permit the poppet return spring to rotate during compression, thus preventing rotation of the seat. Unlike the conventional semibalanced poppet valve, which utilizes the bellows to prevent shaft rotation, the inverted poppet valve utilizes two guide pins, covered with Teflon bushings, on which the actuator piston is guided in a straight line motion.

To prevent the valve from slamming open after the initial opening has been initiated, an increased area is provided on the poppet shaft, on which the downstream pressure acts, thus providing a semibalanced poppet during the stroking of the poppet.

Design No. 3. The third design (Fig. 75) is of a piloted, 90-degree poppet valve which, like the conventional semibalanced poppet valve (design No. 1), has some unique features to obtain long life. The valve is opened by venting the propellant pressure from the back side of the actuator piston. The valve is closed by opening (de-energizing) a pilot valve, allowing propellant pressure into the actuator, and by the assistance of a helical spring.

All static seals in the valve are Teflon-coated metal O-rings. These were selected for their long service life (no age control required as with elastomer seals) and their resistance to corrosion. The piston seal, manufactured by Rudolf E. Krueger Co., was selected because of better wear characteristics than conventional lipseals, and because it is able to compensate for thermal effects of the piston.

The poppet/seat arrangement, as shown in Fig. 75 is a grooved gold seat with a flat poppet, or can be a captive plastic poppet with a flat seat. These concepts are two representative types of those which were tested under the closure screening test program. The seat assembly is an insert which "floats" on metal O-rings to compensate for temperature effects between the Inconel flange and aluminum body. This design also flexes the sealing surface toward the poppet. The poppet seal is attached to the poppet shaft by means of a flexure disk which prevents the seat from scrubbing due to shaft movement.

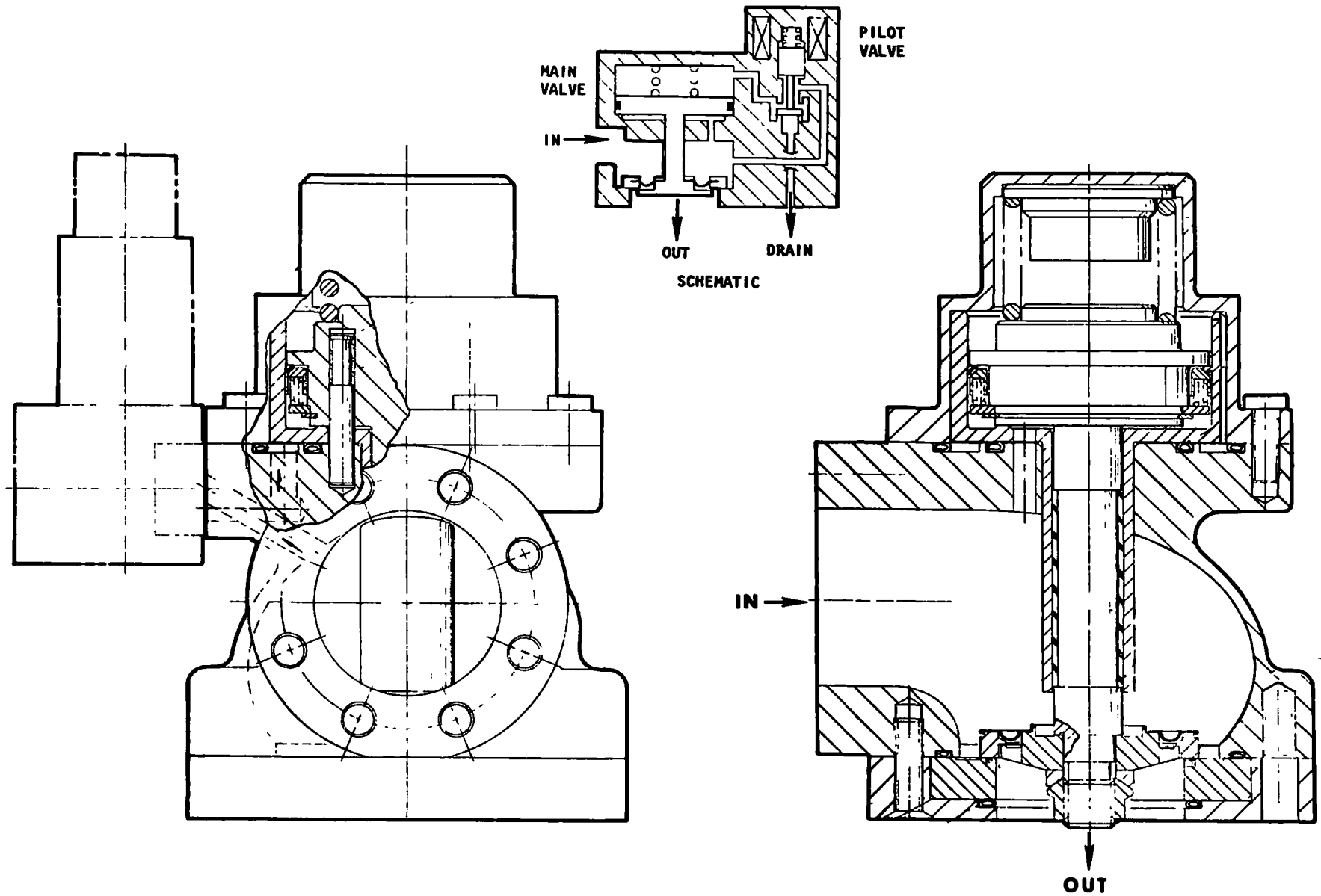


Figure 75. Piloted, 90-Degree Poppet Valve (Design 3)

Wear prevention and particle generation from rubbing are of prime concern for long life characteristics. A teflon bushing between the shaft and guide prevents metal-to-metal contact during valve actuation. Both designs No. 1 and 2 utilize a thrust bearing to permit the poppet return spring to rotate during compression, thus preventing particle generation from rubbing. Due to the low spring loads in this design the bearing was not required. To prevent scrubbing between the poppet and seat due to shaft rotation, two guide pins covered with Teflon bushings are used, like design No. 2, on which the actuator piston is guided in a straight line motion.

Design No. 4. In addition to the three poppet valve designs, a preliminary design for a retracting seal ball valve was completed (Fig. 76). This type of valve combines the low-pressure loss characteristics of the ball valve with the poppet valve translating seal which minimizes rubbing contact. The preliminary design incorporates a mechanism which lifts the seal from one side. This simplifies the mechanism at the expense of increased rubbing contact. A layout of the pilot valve was also completed and is partially shown in Fig. 77. This pilot valve is sized for use with GH_2 or GO_2 and with any of the designs presented. The solenoid valve of Fig. 78 is used to initiate action of the pilot valve.

The ball valve design was not favored because of the scrubbing inherent in its seat design. The first three designs were the subject of static analyses and then analysis by the DAP4H computer program. The static analysis for design No. 3 and the DAP4H analysis are presented in Appendices E and F, respectively. In the design review with NASA-LeRC personnel, design No. 3 with the pilot valve was selected for preparation of the APS Valve Test Fixture. The captive plastic and hard-sharp carbide closure were also selected as equals to pursue during the valve subcomponent tests.

Test Fixture Design. During the Design Review Meeting at NASA-LeRC 27 July 1971, certain areas of concern in the proposed subcomponent fixture design were expressed. The concerns were based on the review of the design 3 drawing previously presented.

The first item of interest was concern over poppet flexure diaphragm life expectancy. Subsequent to the review, further design investigations allowed the elimination of this diaphragm while still maintaining its two important advantages: self-aligning capability, and impact force damping as the valve closes.

Figure 79 illustrates the proposed subcomponent test fixture (valve) as designed. In the illustration, the poppet half to the left of the valve shaft centerline shows the hard-sharp carbide closure concept, while the right half shows the captive plastic closure concept. The valve shaft, and the coil spring which provides poppet preferential position under zero pressure conditions, are common to both closure concepts.

The hard-sharp carbide concept uses a Carmet CA-315 seat into which are ground the sharp annular crests typical of this concept. The poppet is DuPont Baxtron DBW, being a solid, shaped disk needing no flexures or other devices to effect a seal at a shaft juncture. The poppet is maintained in contact on the seat under zero inlet pressure conditions by a coil spring. The poppet and wave spring are held within a carrier which is assembled to the valve shaft by aligning its four slots

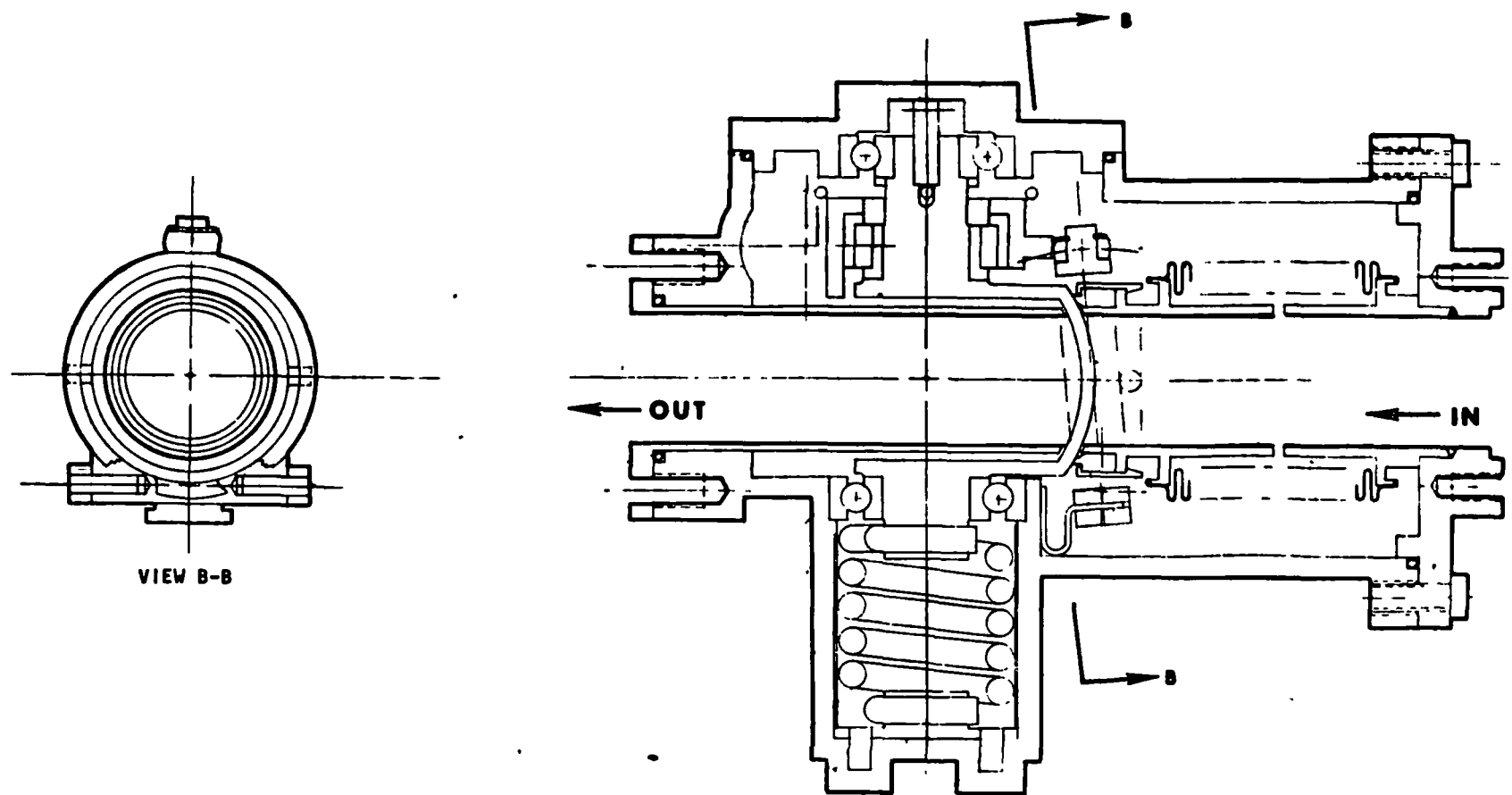


Figure 76. Retracting Seat Ball Valve (Design 4)

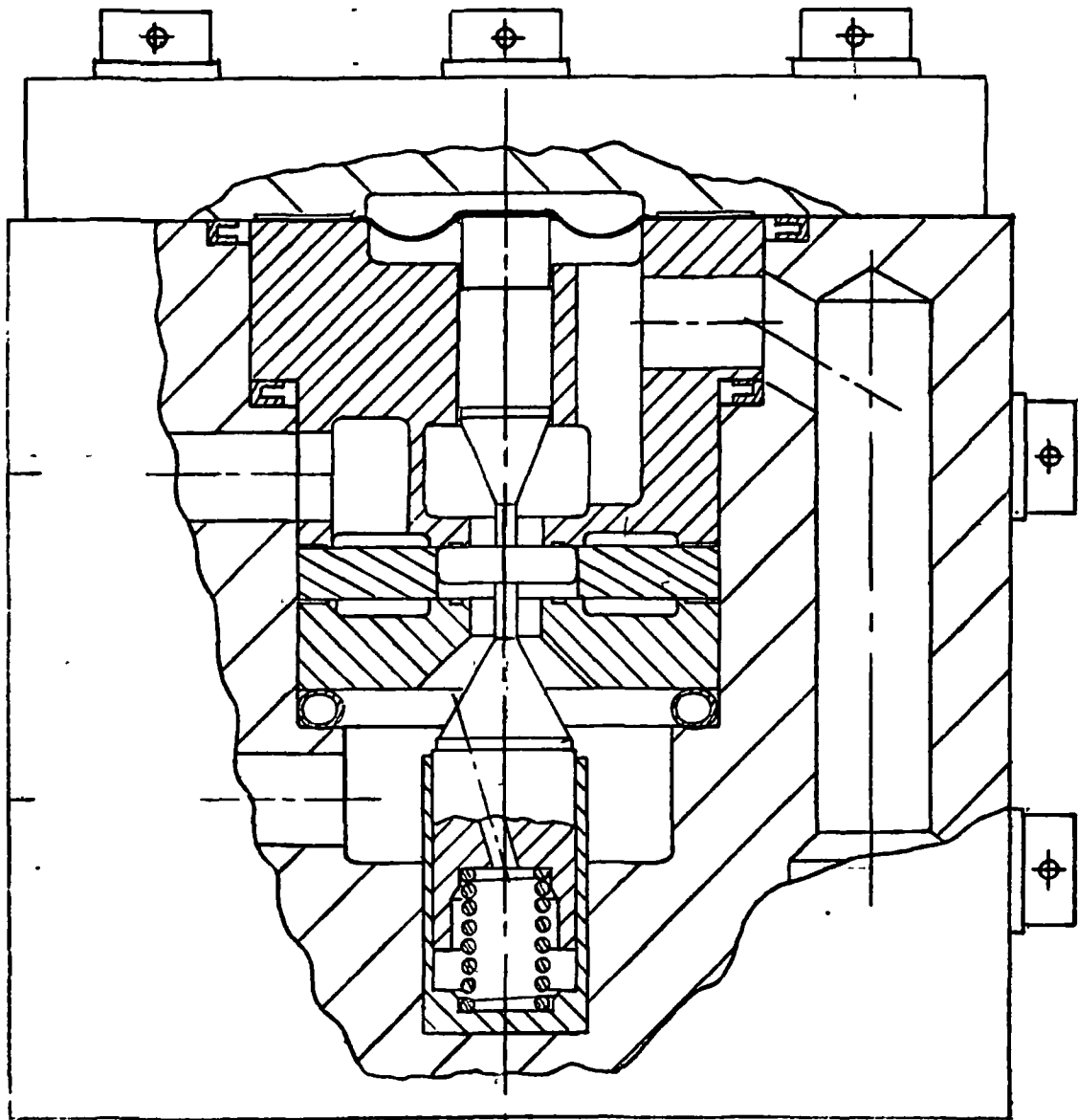
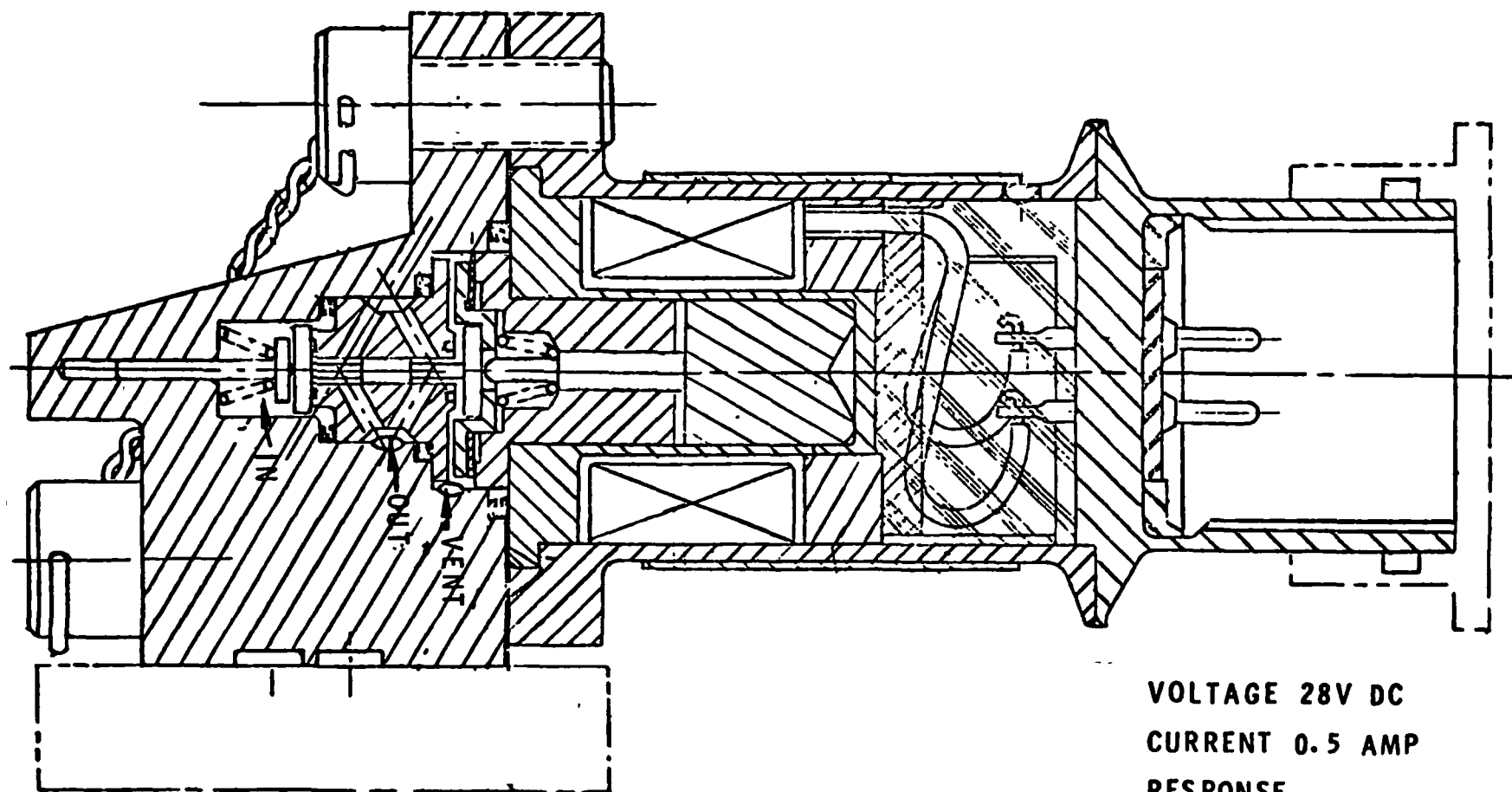


Figure 77. Pilot Valve



VOLTAGE 28V DC
CURRENT 0.5 AMP
RESPONSE

PULL IN 5.5MS
DROP OUT 1.5MS
EQUIV ORIFICE
 $CA=0.000475 \text{ IN.}^2$

Figure 78. Three-Way Solenoid Valve (NAS-27273)

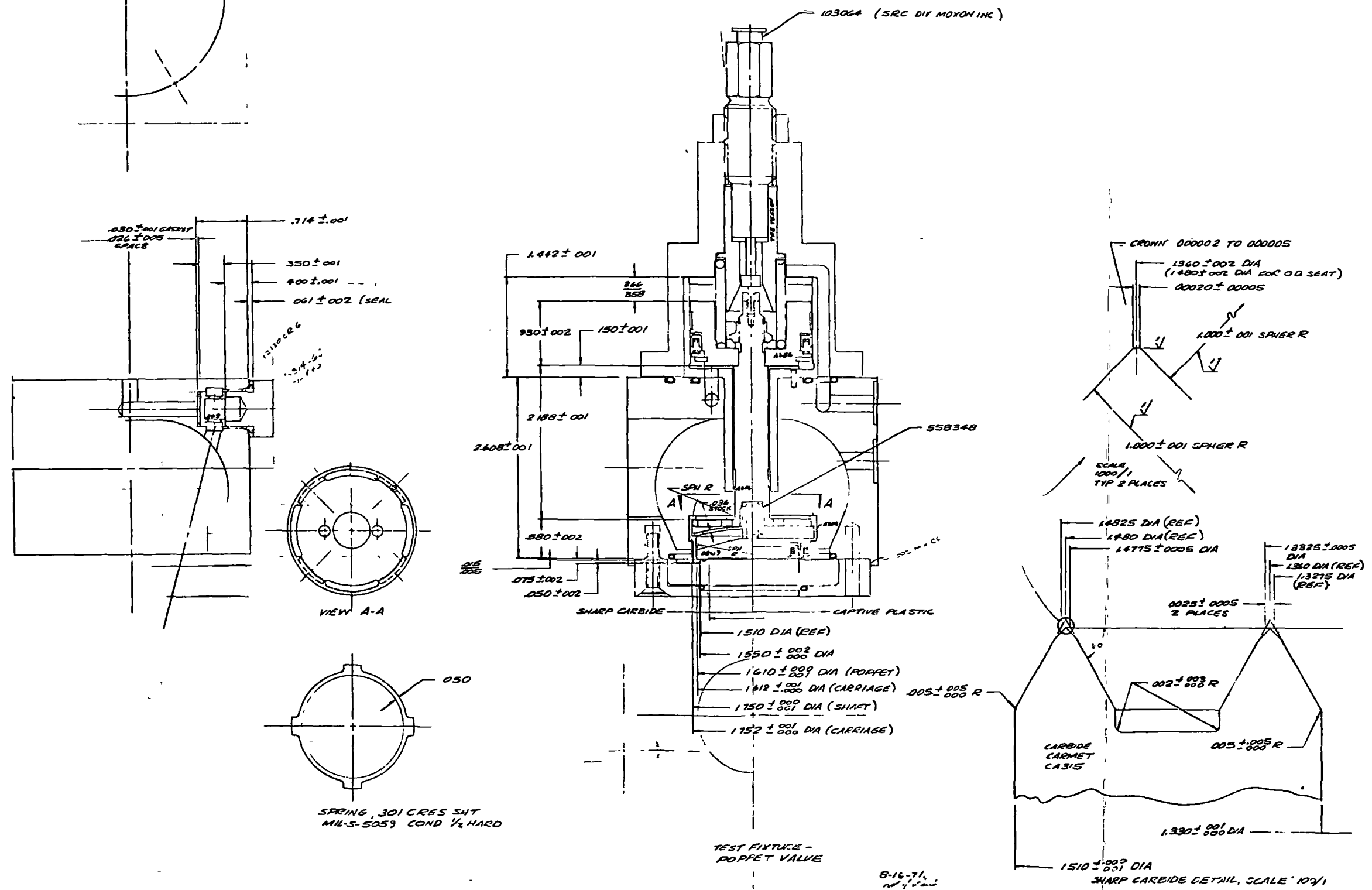


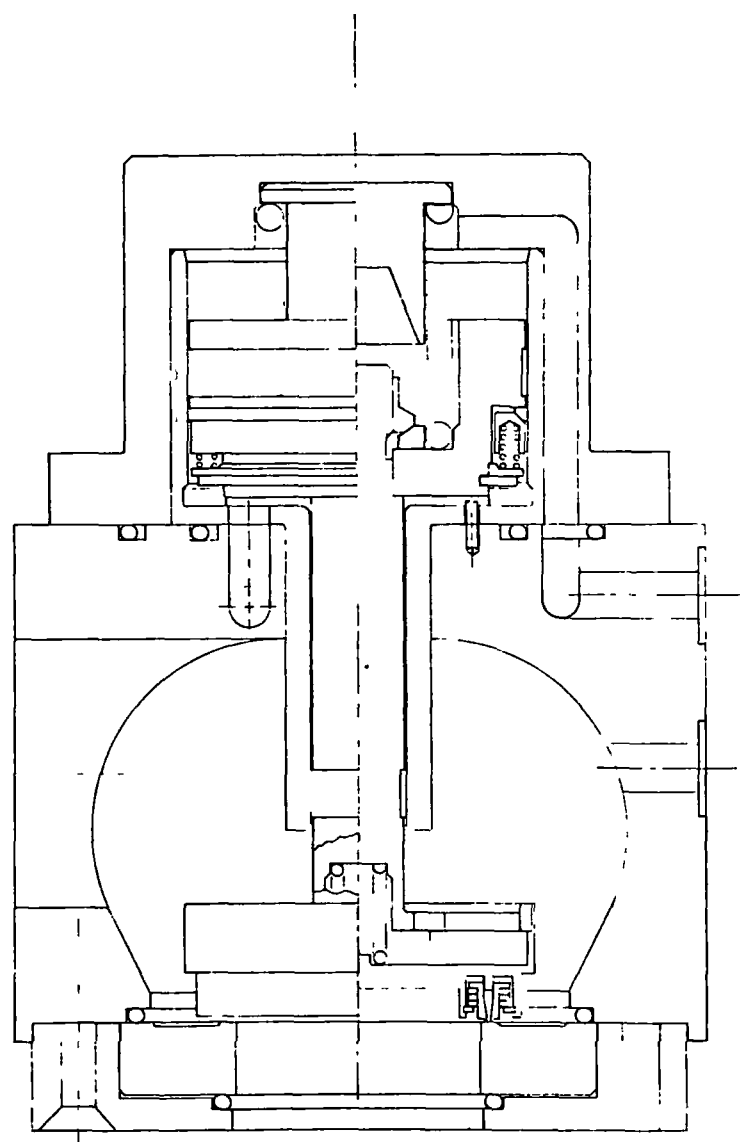
Figure 79. Test Fixture Layout

with the four shaft tabs, compressing the coil spring and wave washer, then rotating the carrier 45 degrees to allow the carrier pin to engage the slotted shaft tab. In the valve closed position, the wave spring provides a load to prevent carrier motion and pin disengagement, and in the valve open position, the coil spring adds to this force by forcing the poppet disk to ride on the lower lip of the carrier. The carrier does not contact the valve seat and, thus, the wave washer does not move during normal valve function; its only purpose is to prevent carrier motion and pin disengagement with the valve closed. As the valve closes, the poppet first contacts the seat, with only its mass and the pressure load contributing to the impact because the carrier, shaft, etc., continue to travel another 0.005 to 0.015 inch (0.0127 to 0.0381 cm) with the piston positively bottoming in the body. In turn, the Teflon-coated, metal O-ring under the seat may deflect slightly, helping to absorb the impact of the poppet. The amount of clamshelling and scrubbing which can occur in this concept are covered in detail in Appendix A, APS Valve Fixture Tolerances.

The captive plastic closure concept uses a Flat Carmet CA-315 seat. The poppet uses an A-286 carrier, Inconel 718 retainers, 301 CRES springs, and beryllium copper snap rings. The carrier is an integral part of this concept and is assembled to the shaft in an identical manner to the carbide carrier. Because the carrier is integral to the poppet, a wave washer is not necessary in this concept. As the poppet approaches the seat, initial contact results in the Inconel 718 retainers first overtraveling slightly, bringing the plastic into contact with the seat. The mass of the carrier-poppet plus the pressure loads determine the impact forces because, as with the carbide closure, the shaft moves another 0.005 to 0.015 inch (0.0127 to 0.0381 cm) until the piston stops in the valve body.

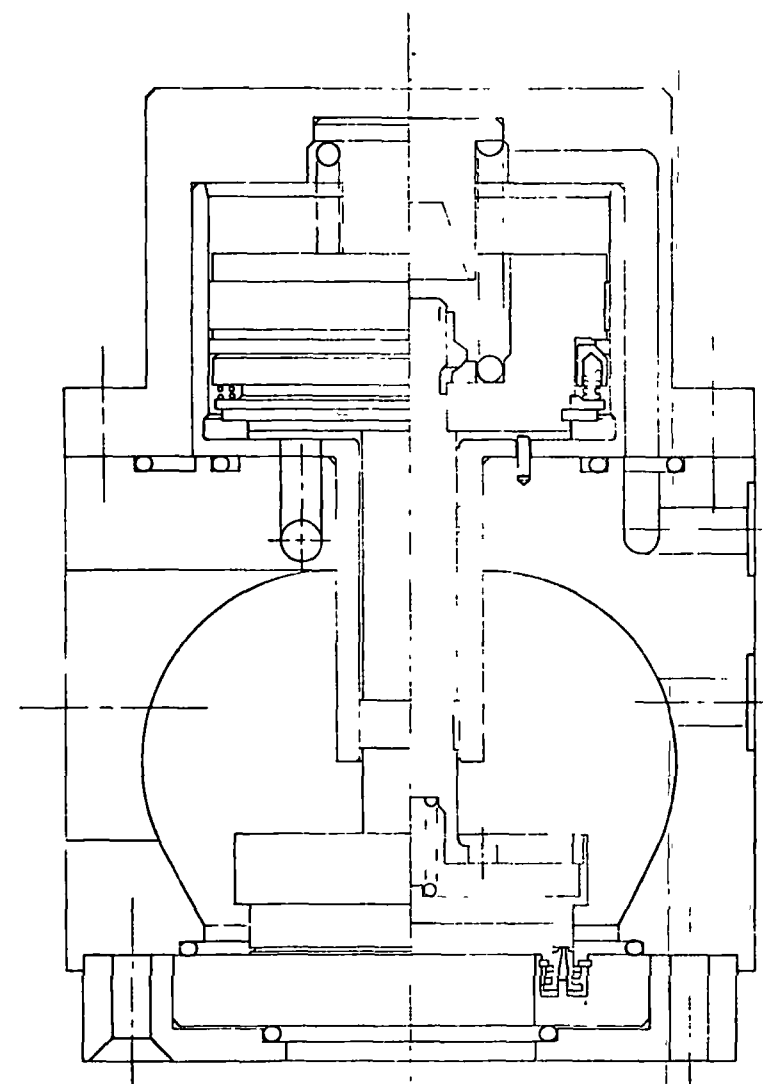
Use of these two approaches has eliminated the poppet flexure diaphragms shown in design 3. The need for diaphragm technology should not be overlooked, however. In the pilot valve, a beryllium-copper diaphragm is used as the actuator for the main pilot stage. This will allow some evaluation of diaphragms under simulated APS conditions with propellants, temperature variations, etc. Conventional piston-type actuation is provided as backup, however, in the event the diaphragm proves troublesome.

A second item of interest concerned the question of putting the captive plastic member of the closure into the valve body as a seat, rather than in the poppet as shown in the fixture. Figure 80 illustrates the consequences of this approach. The flow ΔP requirements dictate a valve outlet diameter of 1.33 inches (3.378 cm). With the captive plastic member in the poppet, this diameter is machined into a rather simple seat. However, putting the captive plastic member into the body requires that the inside diameter of the supporting structure be 1.33 inches (3.378 cm). As a consequence, the diameter of the captive plastic member increases to a mean of 1.678 inches (4.262 cm) versus the 1.408 inches (3.576 cm) if the captive plastic is in the poppet to allow room for the snap ring, spring, and retainer. This increase in mean seat diameter results in a 42 percent increase in seat load, requiring a matching increase in actuator area to maintain proper force ratio for valve operation. Because the actuator swept volume also increases 42 percent, larger pilot passages will be required, resulting in a pilot valve seat area increase of about 50 percent. The larger actuator and pilot produce a heavier valve estimated at a 0.5 pound (2.23 N) (estimated at



CAPTIVE SEAL IN POPPET

A



CAPTIVE SEAL IN SEAT

B

Figure 80. Captive Seal Placement Tradeoff

1.0 pounds (4.45 N) in the fixture) increase for a flightweight version. Because the proposed fixture design provides for ease of changing both the poppet and seat without valve disassembly, the lighter weight configuration was selected.

The third item of interest was the possibility of combining the two closure concepts by using a carbide inner retainer. Design studies show that an Inconel 718 or a carbide inner retainer could be designed to bottom out and seal at both ends reasonably well in the event of gross failure of the captive plastic member. Carbide has much lower ductility and elongation than Inconel 718 so that, to maintain the combination hoop compressive and bending stresses at a conservative level for 1,000,000 cycle life, the carbide cross section must increase over that of Inconel 718. This would increase the weight of the poppet considerably, and raise the valve closing impact forces; therefore, a carbide inner retainer was not incorporated into the test fixture design.

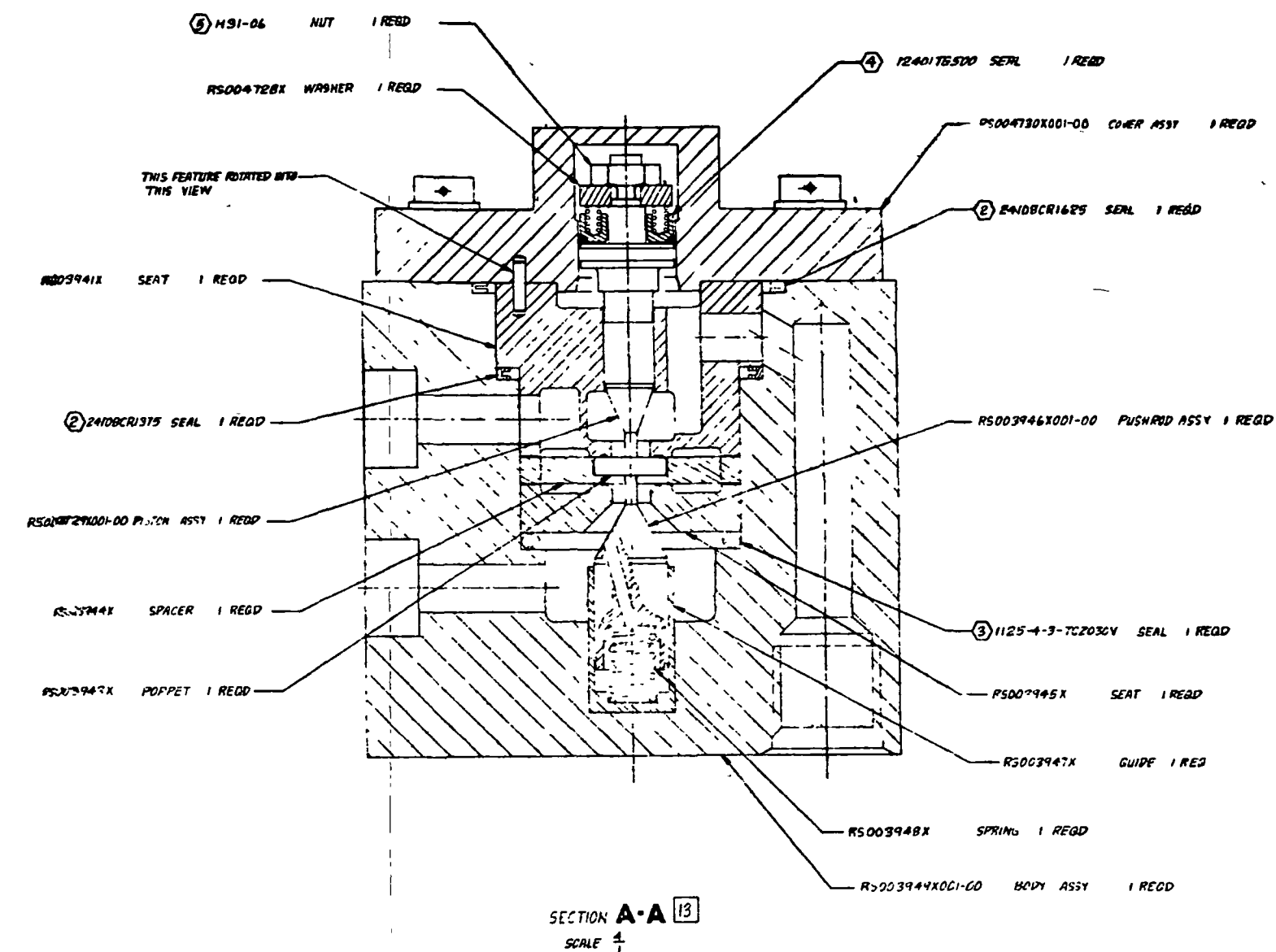
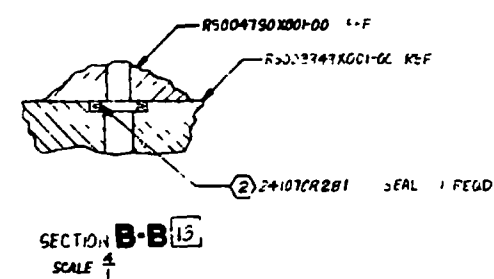
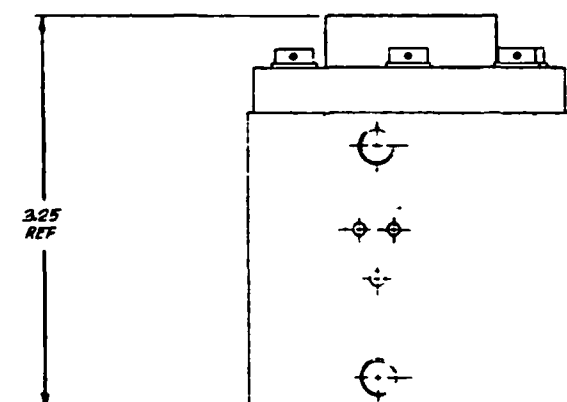
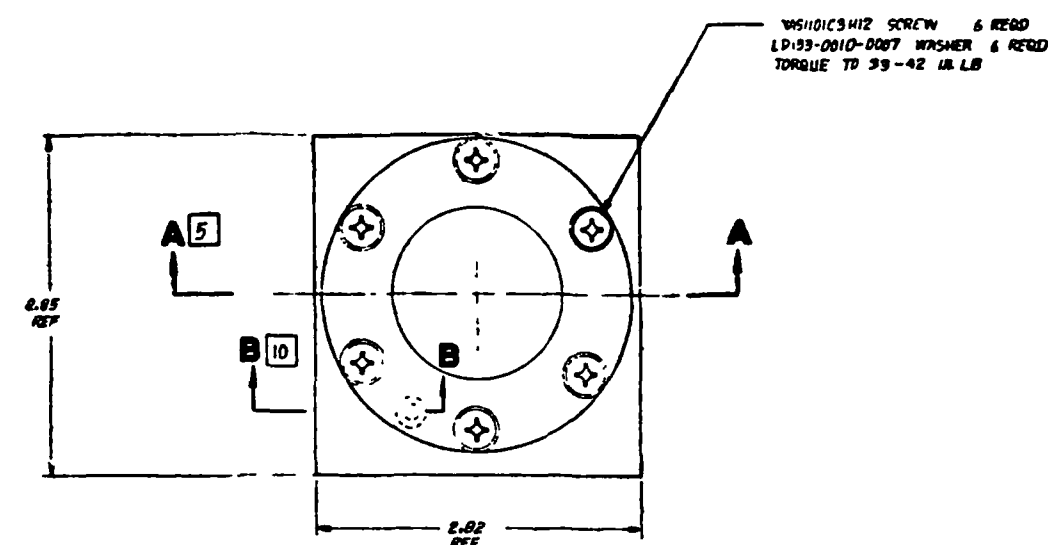
Vendors of solenoid valves were contacted in an effort to purchase a cryogenic solenoid valve for use with the SS/APS valve test fixture. Review of the designs offered indicated that no manufacturer currently has cryogenic solenoids available of the size, response, and low-leakage performance required. Therefore, the pilot valve was designed in-house. A brief portion of the design analysis is presented in Appendix H. The pilot valve is shown in Fig. 81. The areas of concern discussed above were the subject of conversations with the NASA-LeRC project manager, resulting in agreement and approval of the valve test fixture assembly presented in Fig. 82.

FABRICATION

Since the valve test fixture and its pilot valve represented the proof of the preceding program designs and analyses, it was of vital importance that the fabrication be of the highest quality obtainable. Thus, the very specialized capabilities of L.A. Gauge Co., Inc., were selected to fabricate the detail parts.

Pilot Valve

The pilot valve was the first component to be fabricated. In addition to the Krueger Delta seal actuator shown in Fig. 83, a separate cap, upper piston assembly, and beryllium copper actuator diaphragms were fabricated. In Fig. 83, the cap, diaphragm, and piston are laid out above the dynamic piston actuator parts which are in line with the remaining valve details. In Fig. 83, the TFE Teflon bushings on the upper and lower pistons are quite evident. The bushings prevent metal-to-metal contact of the sliding parts, thus minimizing self-generated contaminants. The bushings are somewhat novel in that they are made by installing heat-shrinkable TFE tubing over the metal parts, then oven-heating the detail to cause the TFE tubing to shrink into place within the machined recess provided on the metal parts. Finally, they are finish-machined to the required outside diameter. The assembled pilot valve fixture is shown assembled and attached to a checkout fixture in Fig. 84. The inlet and vent seats of the pilot valve are fabricated from 440C and lapped as a final finish. The small poppet is fabricated from DuPont Baxtron DBW micrograin tungsten carbide and lapped for final finish.



- 5 KAYMAR MFG CO. INC. LONG ISLAND CITY, N.Y.
4 RUDDOLPH E. KRUEGER CO. NEW PORT BEACH, CALIF.
3 ADVANCED PRODUCTS CO. NORTH HAVEN, CONN.
2 TECHNICAL INDUSTRIES INC. HARRISON MFG. CO. DIVISION, BURLINGAME, CALIF.
1 INITIAL INTENDED FASTENERS PER R-3101-002
NOTE: UNLESS OTHERWISE SPECIFIED

Figure 81. APS Pilot Valve Assembly

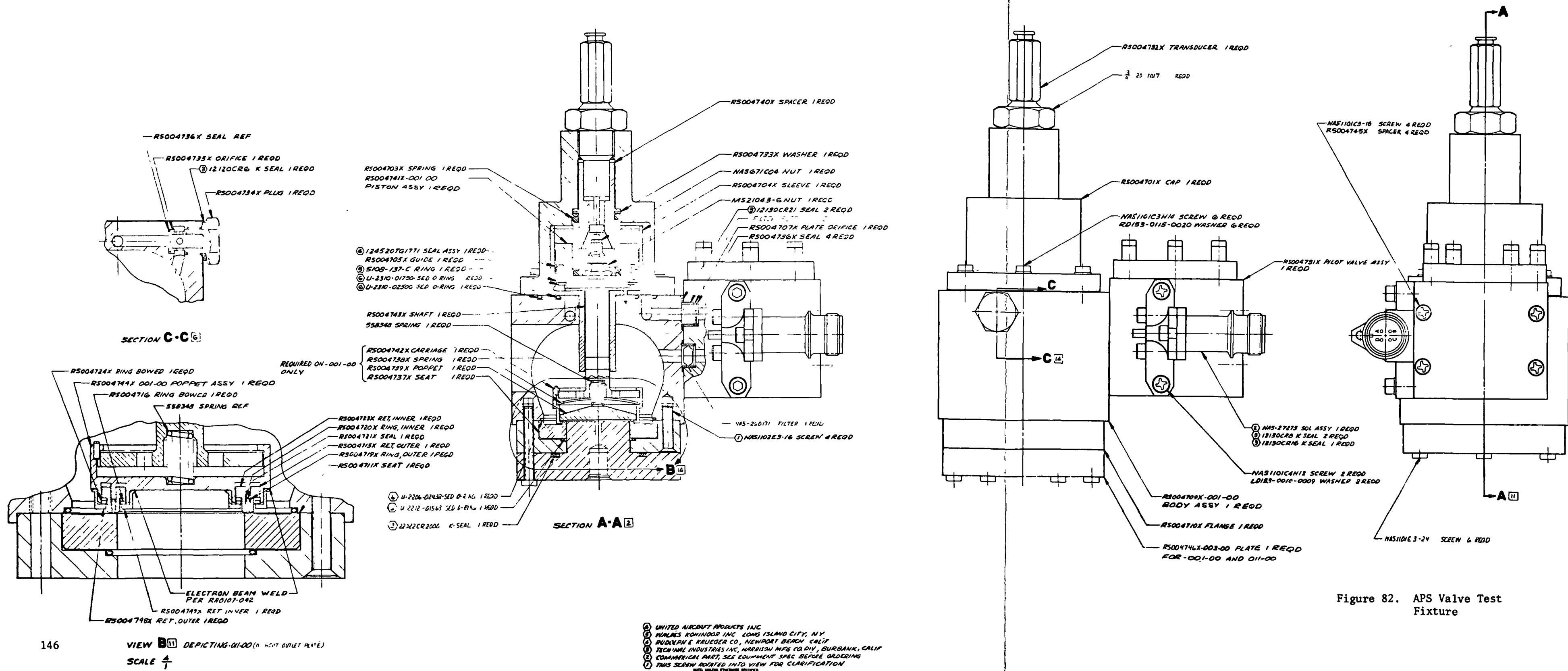
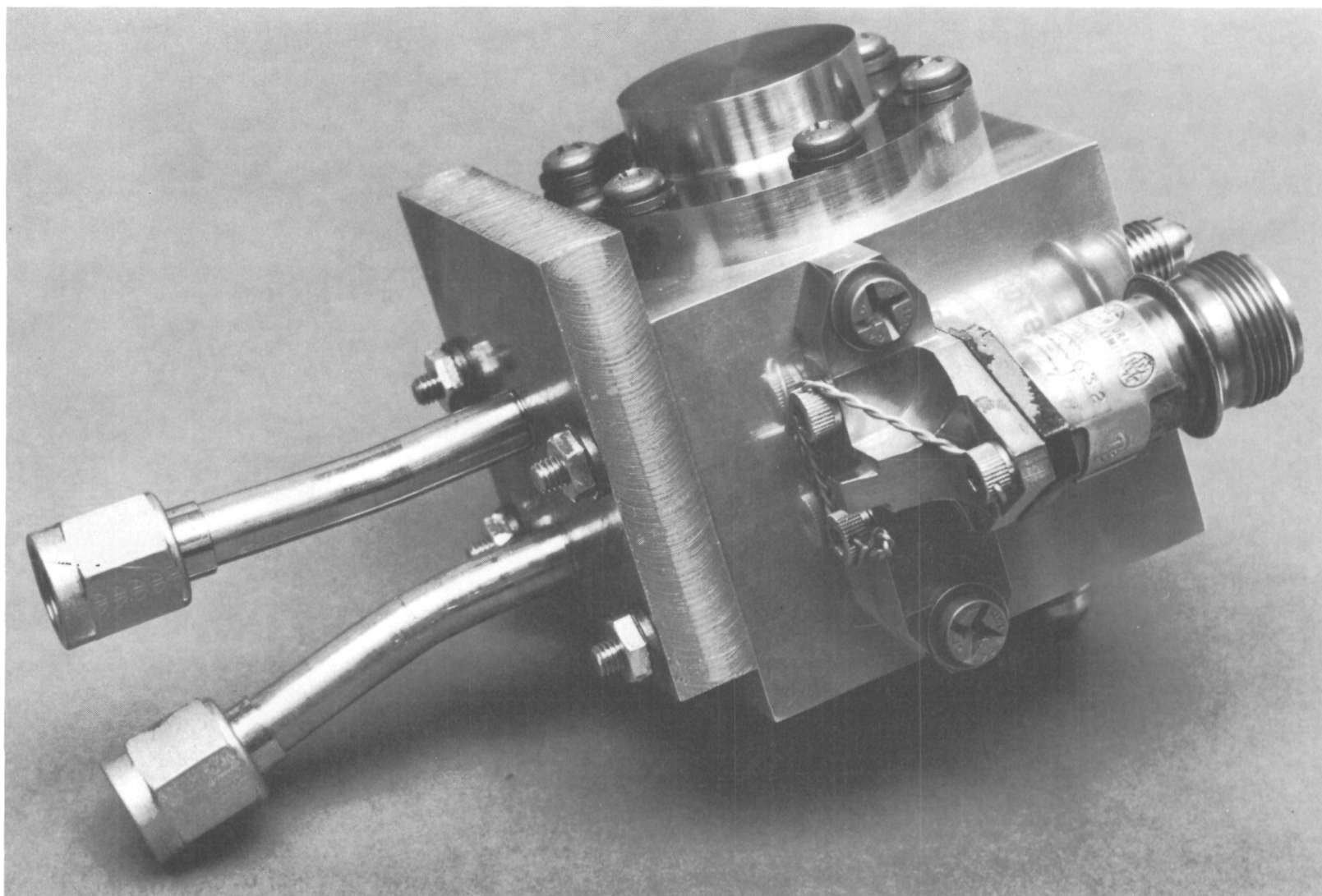


Figure 82. APS Valve Test Fixture



1XZ62-1-/19/1A-C1

Figure 84. APS Pilot Valve

Main Valve

The main valve test fixture was fabricated using somewhat standard manufacturing techniques available at L.A. Gauge. The micrograin carbide parts were fabricated using combinations of grinding, electrical discharge machining and, finally hand-lapping with fine diamond compound to achieve the finishes required for meeting the SS/APS leakage requirements. Again, the TFE Teflon bushing on the valve shaft was fabricated from heat-shrinkable tubing as mentioned above in discussing pilot valve fabrication. This bushing may be seen on the main shaft in Fig. 85. The TFE Teflon bushing on the piston outer diameter is made from conventional TFE bar stock because heat-shrinkable tubing in that size was not readily available. A similar approach in assembly was used, however, in that the bushing inside diameter was made to have a rather large diametral interference with the outside diameter of the piston in the bushing undercut area. Extra thickness of the TFE Teflon was provided, and the entire assembly placed in an oven, with the TFE ring on a tapered installation nose which mated to the piston. Heating the entire assembly to 860 R (478 K) allowed the TFE ring to be slipped downward into its recess within the piston, at which time the assembly was removed from the oven to cool. The TFE ring then shrank into place by attempting to return to its original dimensions. Thus, it gripped the piston and was then machined to the final required outside dimension.

The original detail parts of the captive plastic closure and its mating carbide seat are shown in Fig. 85, arranged above the hard-sharp carbide closure parts which are in line with the remaining valve details. The assembled pilot valve is shown positioned adjacent to the main valve body. The parts contained within the plastic bags are the seal ring and follower ring of the main piston Krueger Delta seal assembly. The assembled APS valve test fixture is shown in Fig. 86. The pilot valve is equipped with the flat cap used for the beryllium copper diaphragm actuator version.

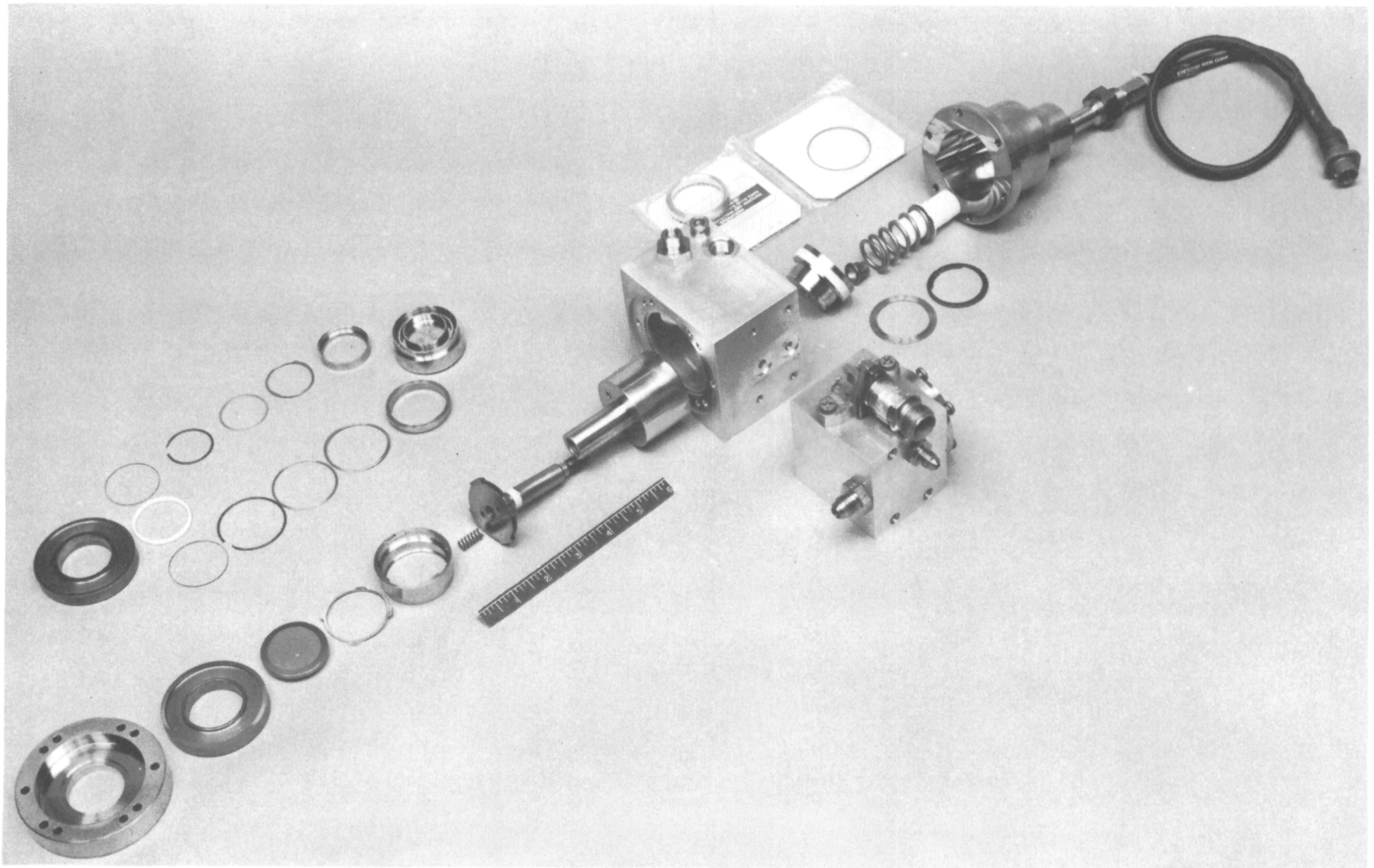
TESTING

The testing to be performed on the SS/APS valve test fixture represented the culmination of all the preceding program designs, analyses, and tests. Would the fixture be capable of 1×10^6 cycles? Would either the hard-sharp carbide or captive plastic closures be able to perform for 1×10^6 cycles and still leak less than 100 scc/hr helium? These were the questions to be answered; for, if successful, then the program objective of preparing a flightweight SS/APS valve design could be accomplished.

Pilot Valve

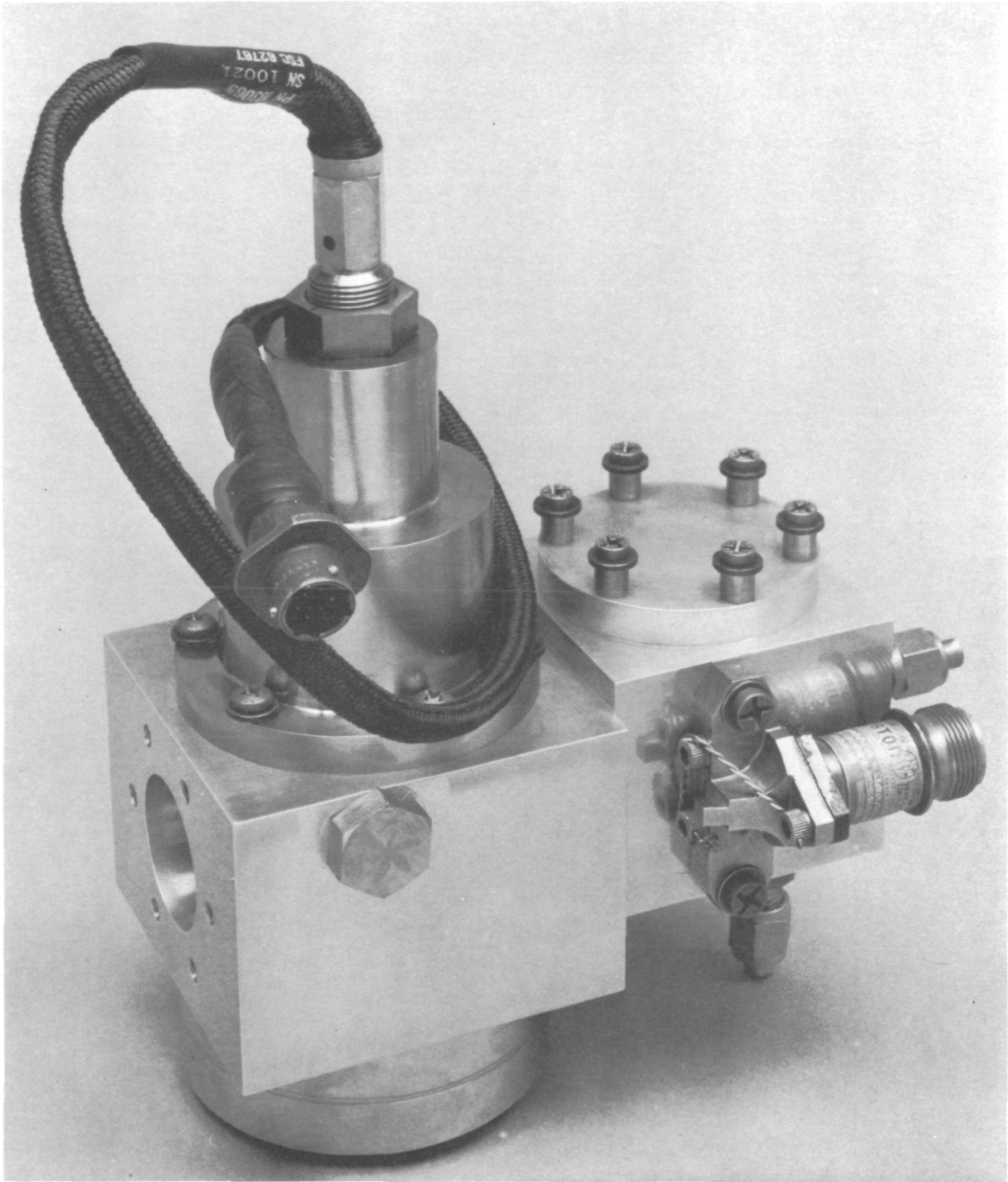
Because of the way drawings were released and detail parts fabricated, the SS/APS pilot valve was completed first. It was initially assembled as the Krueger Delta seal actuated version. Following proof testing, disassembly, and cleaning, the pilot valve was reassembled for a life cycle test. The Krueger seal actuator performed well for the initial 1000 cycles with leakages decreasing slightly during test.

The pilot valve was reassembled using the annealed beryllium copper diaphragm as the actuator. The first diaphragm failed after 240 cycles. The failure was



5AJ53-10/26/71-C1B*

Figure 85. APS Main Valve Fixture Details



1XZ61-11/4/71-C1*

Figure 86. Assembled APS Valve Test Fixture

characterized by radial wrinkles across the convolution, final failure being a crack along one of the wrinkles. A second annealed beryllium copper diaphragm was installed and cycled; failure as above occurred after 185 cycles. A third specimen was installed and cycled one time. Evidence of wrinkles was noted; four more cycles produced the typical pattern.

The use of annealed diaphragms was abandoned, and a heat-treated version was installed. The diaphragm performed for 1000 cycles with no evidence of failure, so an additional 1000 cycles were performed. The diaphragm still appeared good and did not leak. A fixture was designed that used lengths of tubing to simulate the main valve test fixture actuator volumes. The actuator volumes were calculated₃ from actual main valve detail part dimensions, and showed a volume of 1.926 in.³ (31.56 cm³) to vent to start the main valve opening, and a volume of 0.594 in.³ (9.73 cm³) to repressurize to start the main valve closing. One timing test was performed in which the latter volume was used to simulate the venting required for main valve opening to see what effect volume had on pressure decay. Runs also were made using the heat-treated beryllium copper diaphragm actuator. The pressures indicated are pressures which were derived from the DAP4H computer program simulating the main valve test fixture system. The 200-psig (137.9 N/cm²) level is where the main valve will start to open, and the 370-psig (255 N/cm²) level is where the main valve will start to close. The data are shown in Table X.

TABLE X - PILOT VALVE TIMING

Parameter	Piston Actuator			Heat-Treated Diaphragm Actuator	
	Actuate		Deactuate	Actuate	Deactuate
	0.594 in. ³ , (9.73 cm ³)	1.926 in. ³ , (31.56 cm ³)	0.594 in. ³ , (9.73 cm ³)	0.594 in. ³ , (9.73 cm ³)	0.594 in. ³ , (9.73 cm ³)
Signal to sole-noid actuation	2.8*	3.0	2.2	2.8	2.2
Signal to start of pressure change	5.2	5.7	5.4	4.0	3.2
Signal to pressure decay to 200 psig (137.9 N/cm ²)	6.8	9.1	---	6.0	---
Signal to pressure rise to 370 psig (255 N/cm ²)	---	---	9.4	---	6.9

*All values in milliseconds

As seen above, use of the diaphragm actuator does improve the response of the solenoid-pilot valve combination slightly because the pilot valve actuator volume pressurized by the Weston solenoid is much smaller than with the Krueger Delta seal actuated version. Also, the data indicate that a reduction in vented volume can significantly reduce time to main valve start to open (6.8 versus 9.1 milliseconds).

Flow tests were conducted on the pilot valve in which 400-psig (275.8 N/cm^2) gaseous nitrogen was flowed in the in-out direction (main valve closing) and in the out-vent direction (main valve opening). The flow data are shown in Fig. 87. Analysis of these data indicated a steady-state flow coefficient (C_D) of the pilot valve of 0.42. A C_D of 0.50 had been desired for use with the main valve test fixture. Later in the testing of the combined pilot valve-main valve fixture, the dynamic C_D was found by computer analysis of the actual test data to be approximately 0.24. This low flow coefficient was ultimately responsible for the inability to meet the 30-millisecond total response time with gaseous oxygen. Response on gaseous hydrogen was no problem due to its lower molecular weight, and control orifices were required to prevent the main valve from overspeeding during actuation.

Combined Fixture

With completion of the flow test facility, the combined fixture tests were begun after the valve test fixture was proof tested. The valve installed in the flow test facility is shown in Fig. 88, and Fig. 89 shows the precision gages used to record the pressures from the sonic orifice flowmeter. The fixture was designed to have a nominal 15 psi (10.34 N/cm^2) pressure drop at rated gaseous nitrogen flow of 2.57 lb/sec (1.166 kg/sec) at 540 R (300 K). This figure was agreed upon with the NASA-LeRC Project Manager during the period when the low-pressure system for SS/APS was deleted by mutual agreement. The equipment required for a low-pressure system appeared so bulky from the results of early trade studies that agreement was to concentrate that effort into additional testing of the two closure designs. The flow ΔP curve for the valve test fixture is shown in Fig. 90, and illustrates a valve pressure drop of 15.6 psi (10.75 N/cm^2) at rated flow.

The valve was then moved into the cycle test facility (Fig. 91) for the life cycle and timing tests. The captive plastic closure was the initial installation made for timing tests. The initial valve timing series was performed with ambient GN_2 at 450-psia (310.3 N/cm^2) inlet pressure. The timing data are presented below for GN_2 ; orifice designations are from the DAP4H computer program used to predict valve performance. DPV34 is the pilot valve-main valve interface orifice, and D15 is the damping orifice from the valve inlet to the opening side of the actuator.

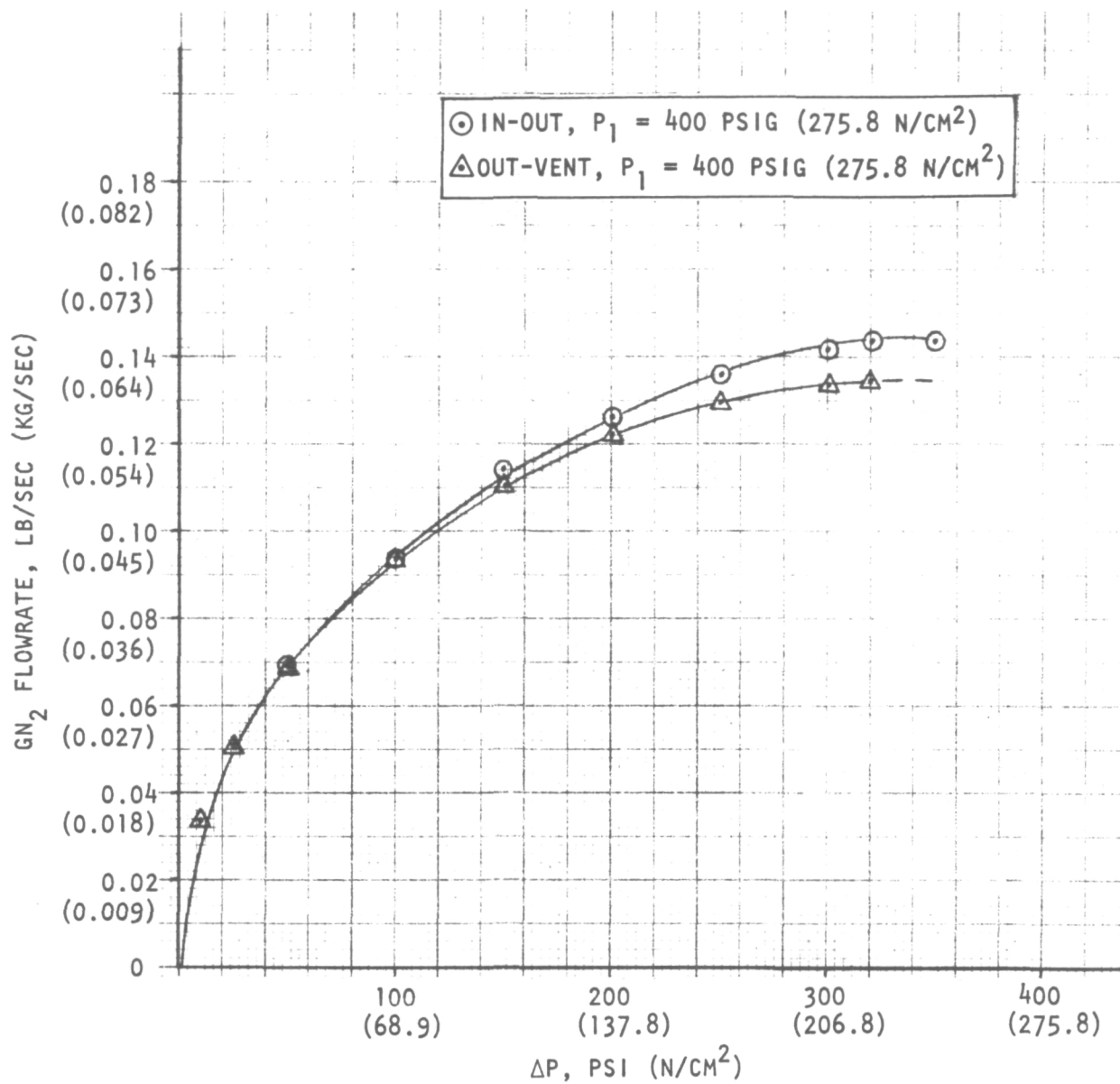
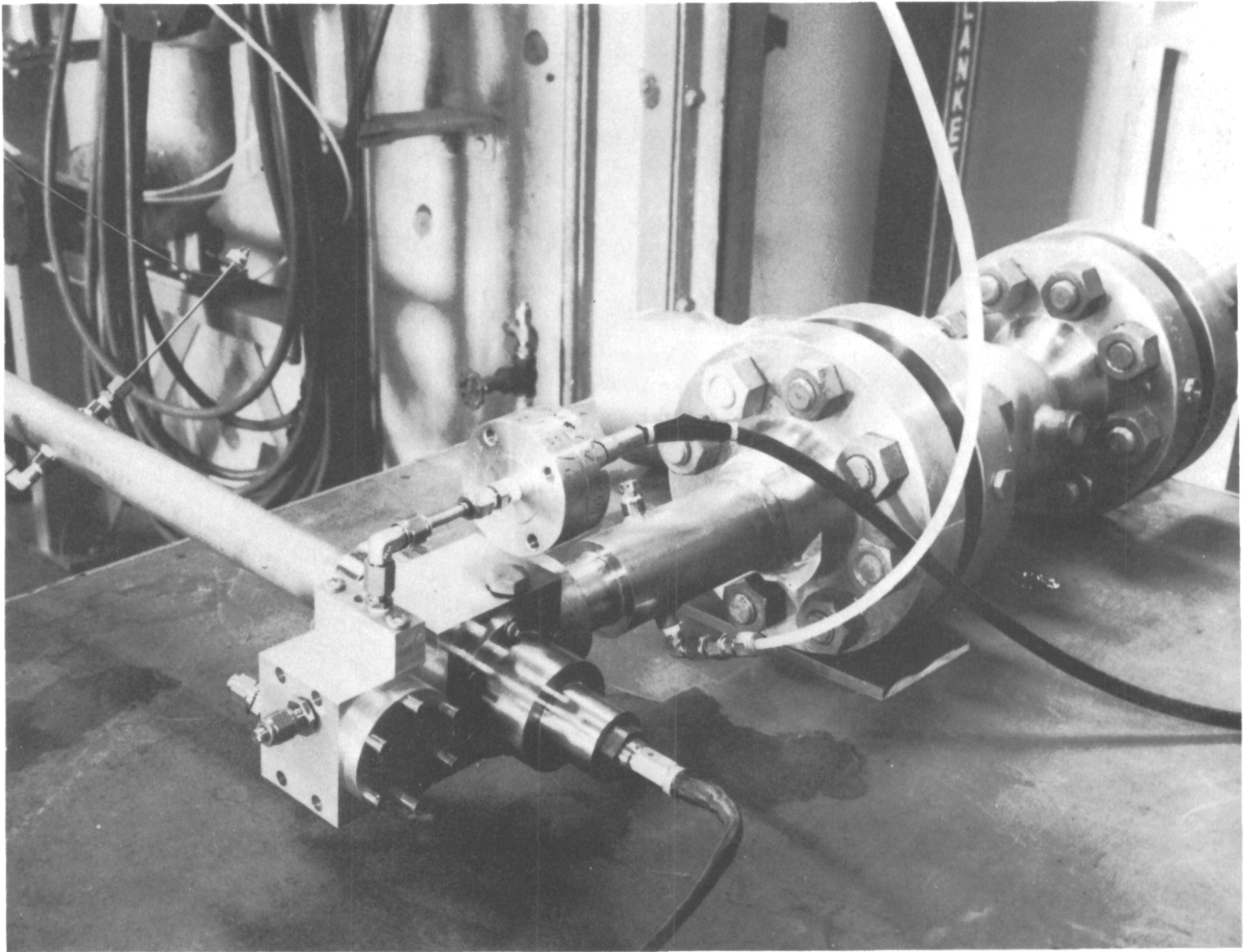
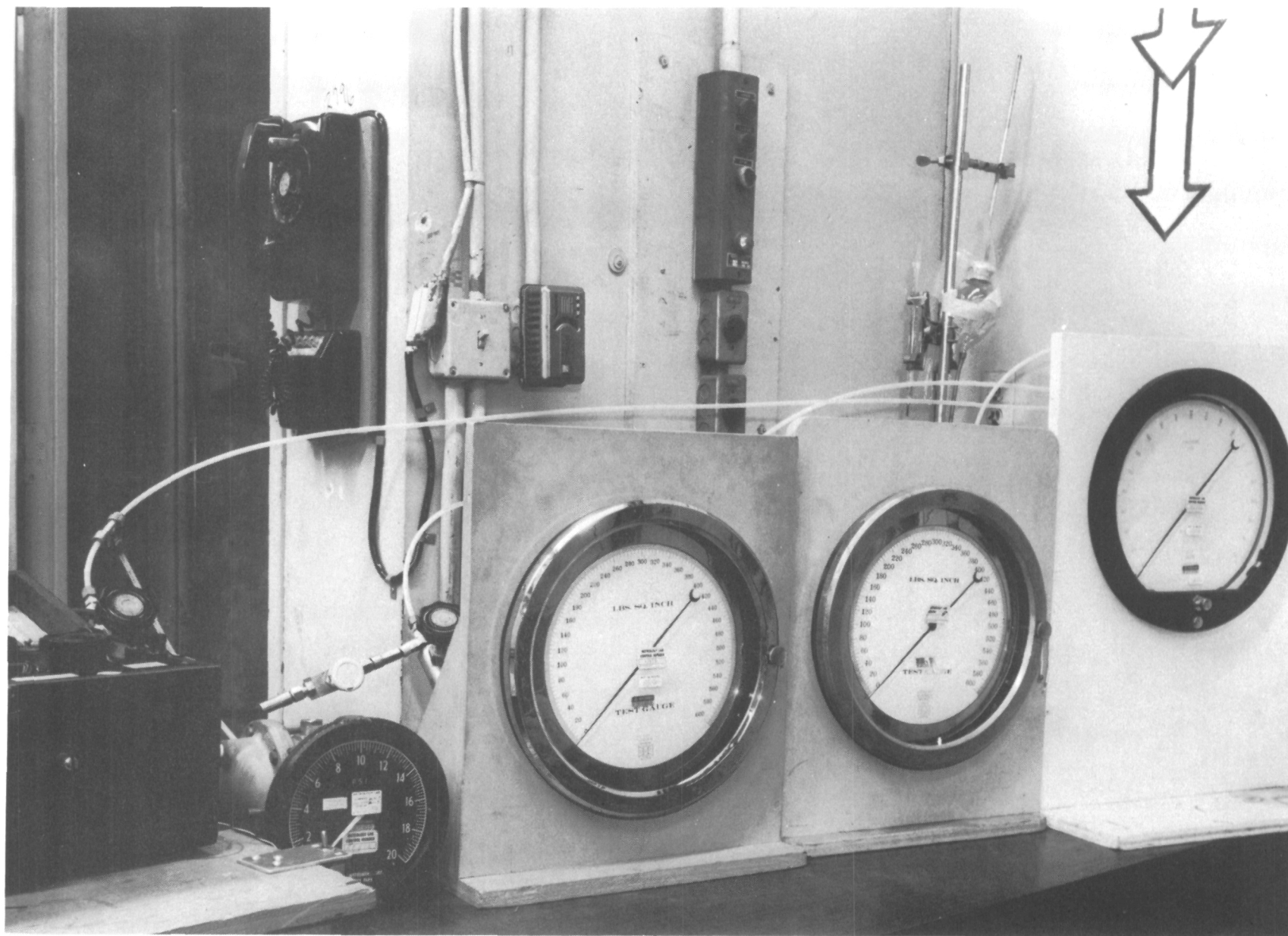


Figure 87. APS Pilot Valve Flow



7452-95-1C/12-10-71

Figure 88. Valve Test Fixture in Flow Facility



7452-95-1A/12-10-71

Figure 89. Flow Facility Gages

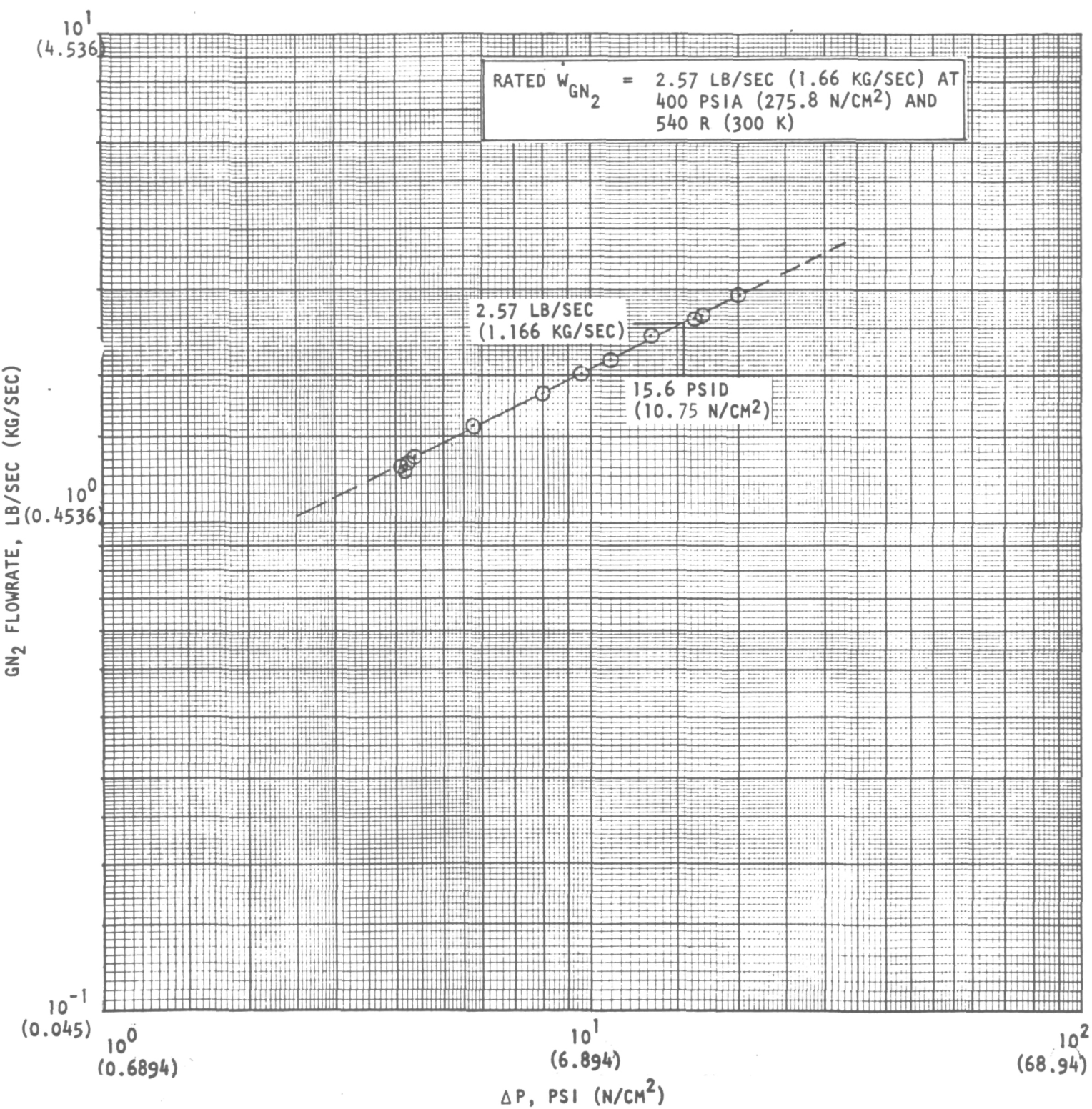


Figure 90. Flow-Delta Pressure Curve for the APS Valve Test Fixture

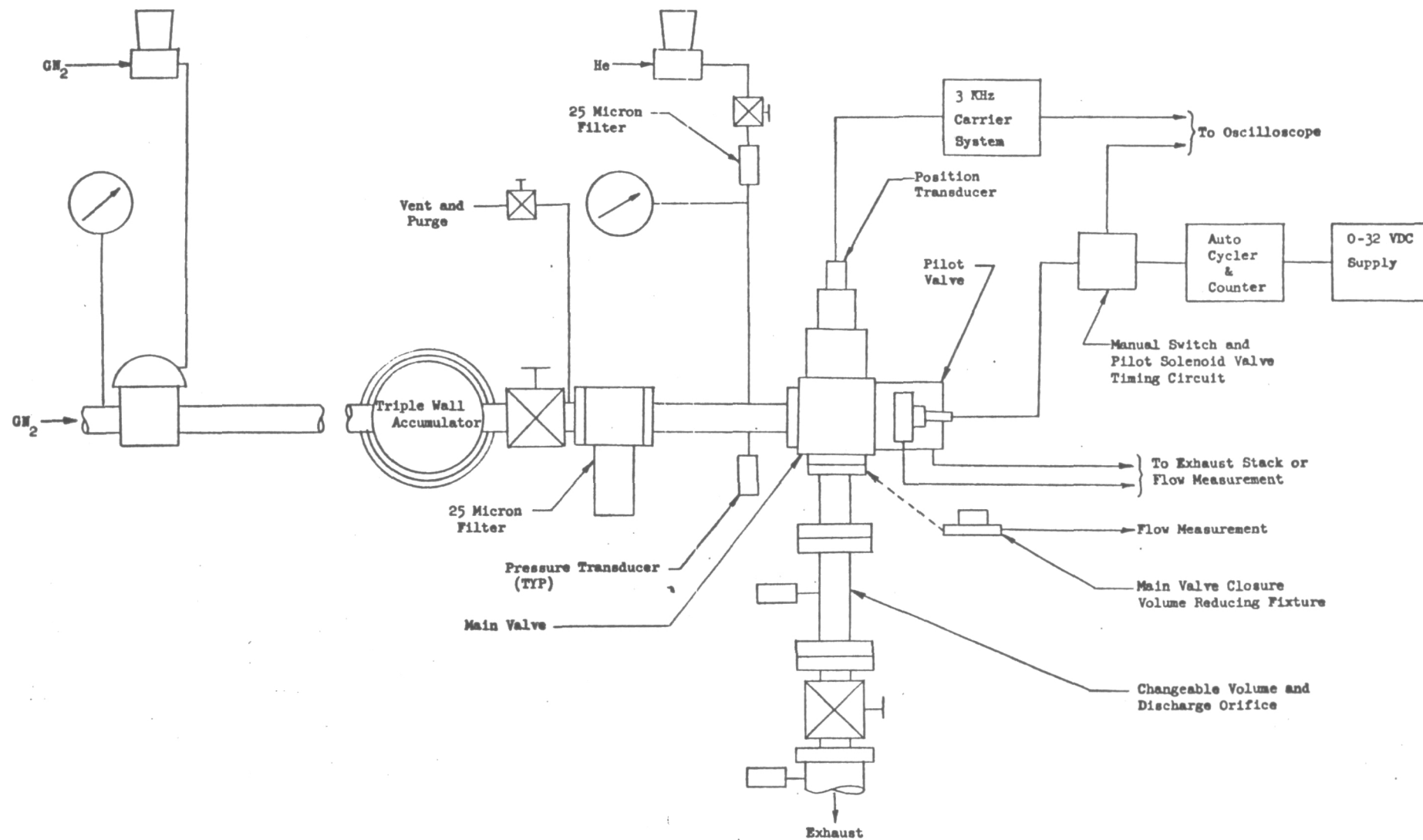


Figure 91. APS Test Fixture Cycle Test Schematic

Special Conditions as Noted	Orifice Diameter, Inches (cm)		Opening Times, Milliseconds		Closing Times, Milliseconds	
	DPV 34	D15	Stroke	Total	Stroke	Total
Discharge to ambient pressure	0.125 (0.3175)	0.125 (0.3175)	10.5	43.5	27.5	48.5
Discharge to vacuum	0.125 (0.3175)	0.125 (0.3175)	10.5	44.5	29.0	49.5
Discharge to ambient pressure	0.144 (0.366)	0.125 (0.3175)	10.0	41.0	26.0	45.5
	0.144 (0.366)	0.135 (0.343)	10.0	40.5	27.5	47.0
	0.150 (0.381)	0.145 (0.368)	9.0	38.5	25.5	44.0
	0.155 (0.394)	0.150 (0.381)	10.0	38.0	24.5	43.0
	Wide Open	0.150 (0.381)	10.0	37.5	24.0	41.5
Discharge to ambient pressure	Wide Open	Wide Open	8.5	36.0	20.0	39.0
Discharge to ambient pressure with pilot and solenoid vent lines and fittings removed	Wide Open	Wide Open	8.0	35.0	19.5	38.0

As seen from these data, the valve does not quite meet the 30-millisecond signal to open or closed criteria. However, the stroke time was as predicted by the DAP4H computer program. The delay in motion is caused by the pilot valve being slightly under capacity, as mentioned earlier. Since the valve stroke time was correct, the dynamic forces were proper, so the NASA-LeRC Project Manager concurred in a decision to proceed with testing.

In the changeover to GH₂ timing tests, it was discovered that the inner snap ring, bowed ring, and washer holding the inner captive plastic retainer had become disengaged. It was considered that improper installation was responsible, so new parts were installed, checked, and preparations for GH₂ testing continued.

The following GH₂ timing data were obtained, using 450-psia (310.3 N/cm²) inlet pressure, ambient GH₂. The GH₂ flow system is flow limited, so various means were explored to reduce inlet pressure dropoff, including use of a 1/2 flow discharge orifice.

	Orifice Diameter, inches (cm)		Opening			Closing		
			Inlet Pressure at Stroke End, psig (N/cm ²)	Stroke, milliseconds	Total, milliseconds	Inlet Pressure (avg during stroke), psig (N/cm ²)	Stroke, milliseconds	Total, milliseconds
	D15	DPV34						
(a)	0.081 (0.206)	0.073 (0.185)	337 (232)	7.5	33.0	164 (113)	16.0	24.0
(a)	0.081 (0.206)	0.073 (0.185)	329 (227)	8.0	29.5	161 (111)	16.0	23.0
(a)(c)	0.081 (0.206)	0.073 (0.185)	317 (219)	9.0	30.0	284 (196)	15.5	29.0
(a)	0.081 (0.206)	0.081 (0.206)	328 (226)	8.0	26.5	125 (86)	14.5	20.5
(a)	0.081 (0.206)	0.081 (0.206)	325 (224)	7.5	26.5	166 (114)	15.5	23.5
(a)(d)	0.081 (0.206)	0.081 (0.206)	327 (225)	8.0	27.0	327 (225)	15.5	26.5
(a)(d)	0.081 (0.206)	0.081 (0.206)	325 (224)	8.0	27.5	325 (224)	15.5	27.0
(b)	0.081 (0.206)	0.081 (0.206)	352 (243)	8.0	27.0	276 (190)	19.5	31.5
(b)(d)	0.081 (0.206)	0.081 (0.206)	343 (236)	7.5	27.5	367 (253)	21.0	32.0
(b)(d)	0.081 (0.206)	0.081 (0.206)	343 (236)	7.5	27.5	369 (254)	20.0	32.0
(b)(d)	0.081 (0.206)	0.081 (0.206)	345 (238)	7.0	26.5	371 (256)	19.5	32.5

(a) Full-flow downstream orifice

(b) Half-flow downstream orifice

(c) Sequencer used to reduce valve open time to 65 milliseconds

(d) Sequencer used to reduce valve open time to 35 milliseconds

Later, during actual cycling, the valve time was reduced to about 20 milliseconds valve open time, which improved the inlet pressure conditions considerably.

Disassembly of the downstream sections after GH₂ timing test revealed that the inner captive plastic snap ring, bowed ring, and washer had disengaged again. Dynamic forces at valve opening could result in unloading the snap rings. Accordingly, a redesign was initiated to install round snap rings and tapered washers to maintain a radial load on the rings. This is shown in Fig. 92.

Meanwhile, GH₂ timing tests using the hard-sharp carbide closure were in progress. The following timing data were obtained, using 450-psia (310 N/cm²) inlet pressure, ambient GH₂.

	Orifice Diameter, inches (cm)		Opening			Closing		
			Inlet Pressure at Stroke End, psig (N/cm ²)	Stroke, milli- seconds	Total milli- seconds	Inlet Pressure (avg during stroke), psig (N/cm ²)	Stroke, milli- seconds	Total, milli- seconds
	D15	DPV34						
(a)	0.081 (0.206)	0.081 (0.206)	349 (240)	8.0	27.0	241 (166)	19.0	29.0
(a)(c)	0.081 (0.206)	0.081 (0.206)	347 (239)	8.0	27.0	371 (256)	20.5	32.5
(a)(b)(c)	0.081 (0.206)	0.081 (0.206)	---	---	---	---	19.0	31.5
(b)	0.081 (0.206)	0.081 (0.206)	325 (224)	8.5	28.0	313 (216)	15.0	27.5
(b)	0.081 (0.206)	0.081 (0.206)	325 (224)	8.5	27.5	315 (217)	15.0	27.5
(b)	0.081 (0.206)	0.081 (0.206)	328 (226)	9.0	28.0	316 (218)	15.5	27.5
(b)	0.081 (0.206)	0.081 (0.206)	325 (224)	8.5	28.0	314 (216)	14.5	26.0

(a) Half-flow downstream orifice

(b) Full-flow downstream orifice

(c) Sequencer used to reduce valve on-time to 35 milliseconds

(d) Scope photo; closing only

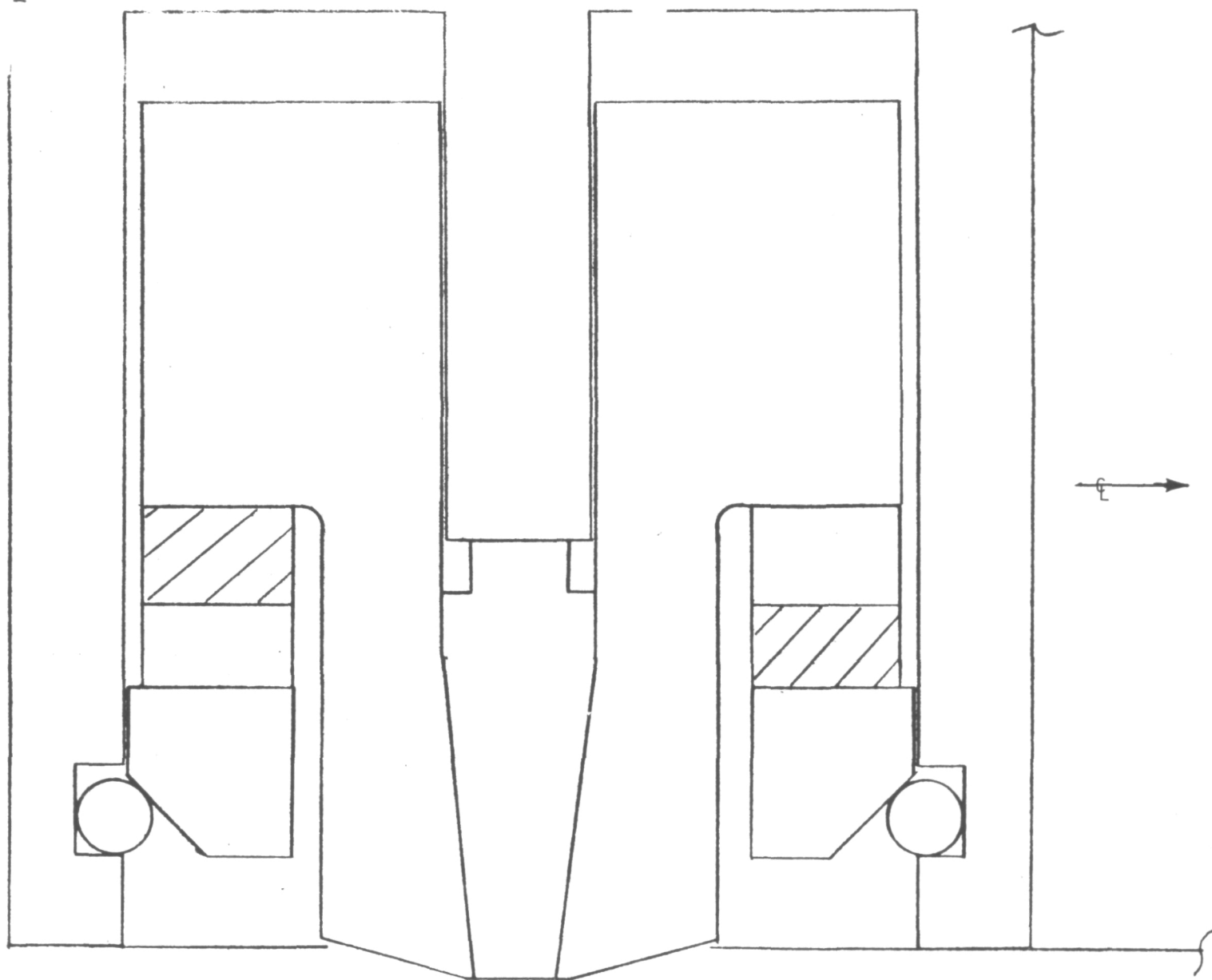


Figure 92. Circlip-Wedge Ring Configuration

Following these timing tests on the hard-sharp carbide closure, it was found that the closure leaked excessively. Disassembly of the valve revealed that the inner land of the hard-sharp carbide seat was contacted but not the outer land. This was shown by subsequent analysis to be the result of a ring-tension twist induced in the seat ring by the lower metal O-ring placement. Analysis and subsequent measurements reveal that this condition no longer existed. Instead of using the lower metal O-ring, a 0.0005-inch (0.00127 cm) thick sheet of FEP Teflon was heat and pressure bonded between the seat and the outlet flange.

Furhter effort was initiated to start the cycling tests with the redesigned captive closure of Fig. 92. During the actuations for control leakage tests, the closure was again subjected to loss of the inner rings. A conversation with the NASA-LeRC Project Manager resulted in an electron-beam welded assembly as shown in Fig. 93.

After the reworked captive plastic closure was installed in the valve, the valve was subjected to a heat soak at 700 R (389 K) with inlet pressure at 450 psia (310.3 N/cm²) to ensure that the Teflon seal ring had filled the voids in the closure. The initial leakages were as follows:

<u>Temperature</u>	<u>Main Seal Leakage, scim (scc/hr) He</u>
700 R (389 K)	Zero scim; 0.0037 scim (3.64 scc/hr) after one actuation open and closed
Ambient	Zero scim; 0.00877 scim (8.62 scc/hr) after one actuation open and closed
280 R (156 K)	0.00637 scim (6.26 scc/hr); 0.0374 scim (36.8 scc/hr) after one actuation open and closed

To minimize test interference, all the GN₂ cycles were run prior to any GH₂ and GO₂ testing. Table XI presents the test history of the captive plastic closure.

The method of taking accurate leakage measurements requires the installation of a special volume-reducing leak fixture in the valve outlet. Thus, the usual increase in leakage noted after one additional actuation is the result of extremely slow, soft valve closing due to severely restricting the downstream flow passage.

During the cyclic life tests of the captive plastic closure, failure of the heat-treated beryllium copper actuator diaphragm in the pilot valve was experienced after 4325 ambient GN₂ cycles. The diaphragm was replaced, with the replacement diaphragm failing after an additional 1460 cycles. These failures prompted a changeover to the Krueger-seal piston actuator for the pilot valve. No additional problems with the pilot valve were experienced during the 100,000 cycle test series.

Early in the cycling, the position indicator slug broke off the indicator shaft. The position indicator body was unscrewed and the slug removed. Cycling was continued until 60,000 cycles in ambient GN₂ had been accumulated. At that time, a new probe had been received and the valve cap was removed to install the new probe

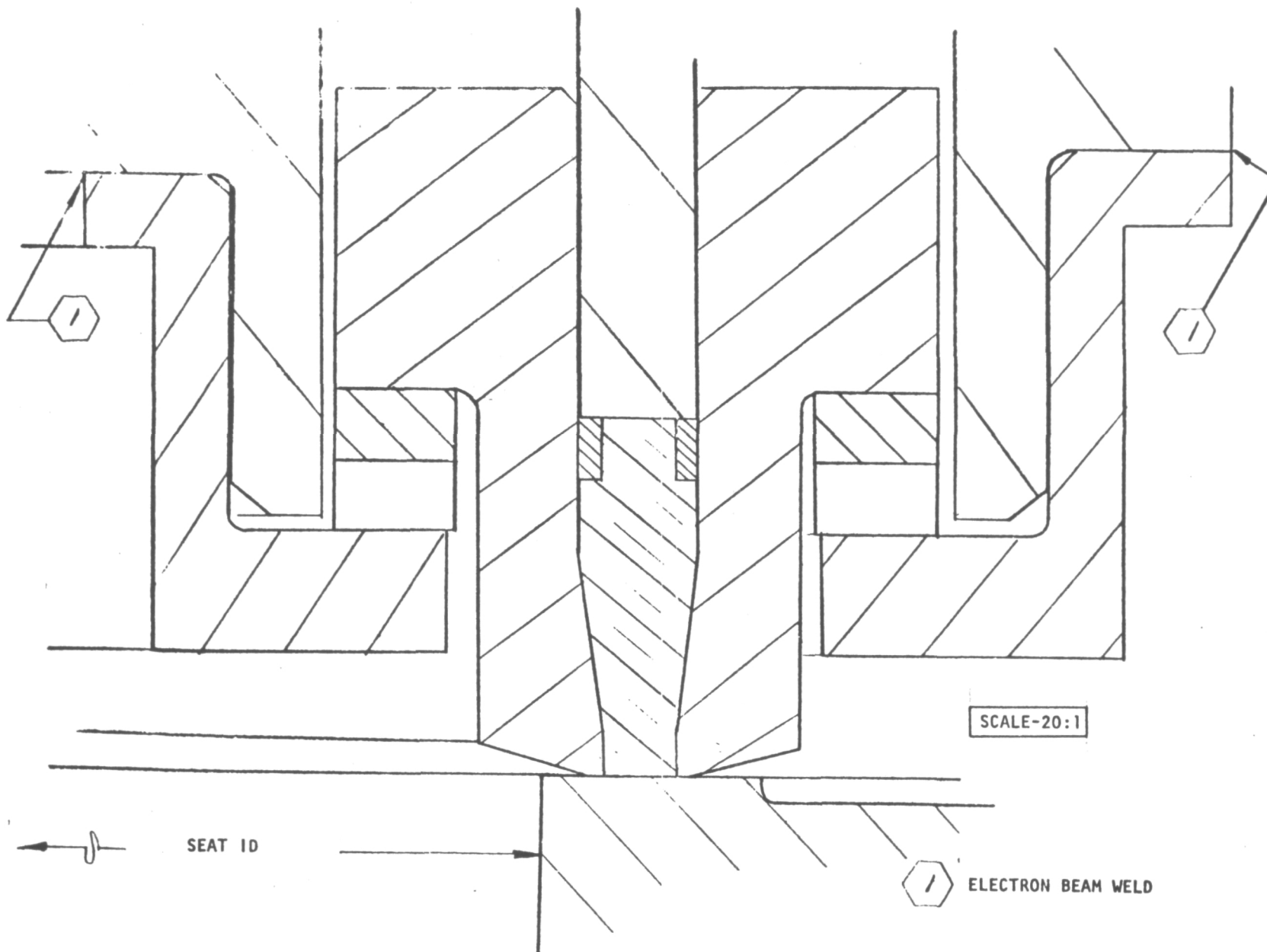


Figure 93. Electron Beam Welded Configuration

TABLE XI - INITIAL TESTING RESULTS

NUMBER OF CYCLES x 1000	ACCUMULATED CYCLES x 1000	TEST GAS	TEMPERATURE TEST °K	LEAKAGE, SCC/HR HELIUM AT 310.3 N/cm ²				
				MAIN SEAT x 1000	KRUEGER SEAL x 1000	PILOT INLET SEAT	PILOT VENT SEAT	
0.5	0.5	GN ₂	AMBIENT	ZERO	2.74	1.0	6.10	
0.5	1.0			ZERO	7.71	1.0	6.29	
9	10			10 ⁻⁵	-	-	2.86	
10	20			ZERO	-	-	2.80	
10	30	↓	↓		2.59	1.0	2.51	
10	40				3.90	-	2.91	
10	50				8.57	-	2.51	
10	60				26.2	-	2.10	
5	65			GH ₂		35.7	1.0	1.55
5	70					42.9		1.13
5	75	↓	389		133.		1.47	
5	80		144		381.		7.52	
5	85	GO ₂	AMBIENT	0.00134	667.		2.19	
5	90		AMBIENT	0.00787	714.		4.16	
5	* 95	↓	144	33.34	524.		10.3	
5	100		389	11.43	381.		10.0	

* OUTER ANTI-EXTRUSION RING FAILED

to verify GH₂ timing. It was found that the indicator shaft had further broken up and the pieces were lodged in the Teflon spacer which surrounds the probe. Some particles had impacted between the piston and the cap, and had entered the clearance between the piston diameter and the sleeve bore. These particles were no doubt responsible for the rapid seal wear noted after about 40,000 cycles as evidenced by increased Krueger seal leakage.

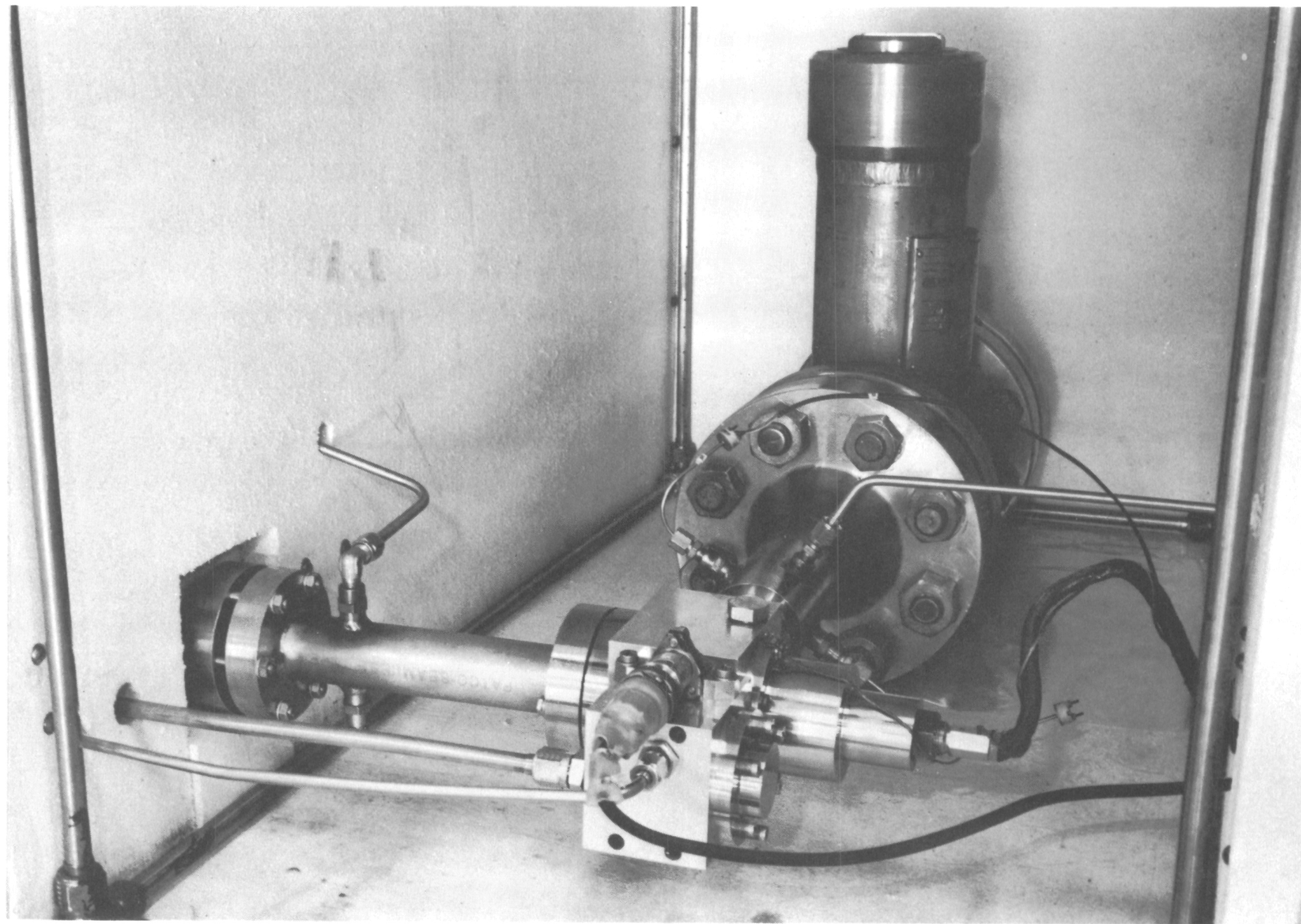
A new probe was installed and GH₂ timing was verified. After 755 cycles in GH₂, the valve ceased to cycle upon signal and a gross leakage through the main closure was evident. Disassembly of the downstream section revealed that the poppet carriage had disengaged from the main shaft due to the carriage roll pin having "backed out," thus no longer engaging the shaft to the poppet carriage. The roll pin was pushed back into its original position and a small heliarc tack weld was made between the pin and the upper surface of the poppet carriage.

The valve cycling was continued and the cycling accumulated as shown in Table IX. The high leakage was noted after 95,000 cycles total. A quick visual examination of the poppet did not reveal any unusual situation, so the valve was readied for the final hot GO₂ cycling. After the valve temperature had stabilized, the leakage was rechecked and had reduced to 7.0 scim (6.9×10^3 scc/hr) helium at 450-psia (310.3 N/cm^2) inlet. The last 5000 cycles were performed, with the results as shown in Table XI.

Figure 94 shows the valve test fixture installed within the environmental box which has a frame made from stainless tubing with small discharge holes. Hot GN₂ or LN₂ was introduced through the tubes, respectively, for heating or cooling the test valve. A controller reading the valve body and gas inlet temperatures maintained flow. The control center used is shown in Fig. 95, and Fig. 96 shows the overall test setup with various control valves, heat exchangers, heaters, accumulators, etc. The triple wall accumulator shown in Fig. 91 was used to help control inlet gas temperatures by using LN₂ in the middle jacket during cold tests, and hot GH₂ during hot tests.

After completion of the 100,000-cycle test of the captive plastic closure, the valve was disassembled to evaluate its condition prior to initiation of the hard-sharp carbide closure testing. The main actuator seal wear was severe as a result of the breakup of the position indicator probe. The metallic particles had not only severely damaged the seal, but had also scored the wall of the sleeve against which the seal travels. This wall was honed to remove the scratches in the wall; the diameter remained within drawing tolerances, so no change in Krueger seal basic size was required. The TFE bushing on the piston also was severely worn from these actions, so a new plastic bushing was installed on the piston. A Krueger seal of Vespel SP-21 was installed.

The poppet shaft TFE bushing was missing. No evidence of its loss was noted during cycling, so it may be surmised that it was lost during the final 5000 cycles. The loss of the bushing resulted in scoring of the inner guide diameter of the sleeve and of the shaft adjacent to the bushing. Examination of the shaft with a 200X comparator revealed that the undercut diameter for the bushing did not have sharp fillets and corners, as did the piston for a similar bushing. The sleeve diameter was honed to remain within drawing tolerances, while the shaft was remachined in the undercut to give sharp corners and fillets. This was accomplished



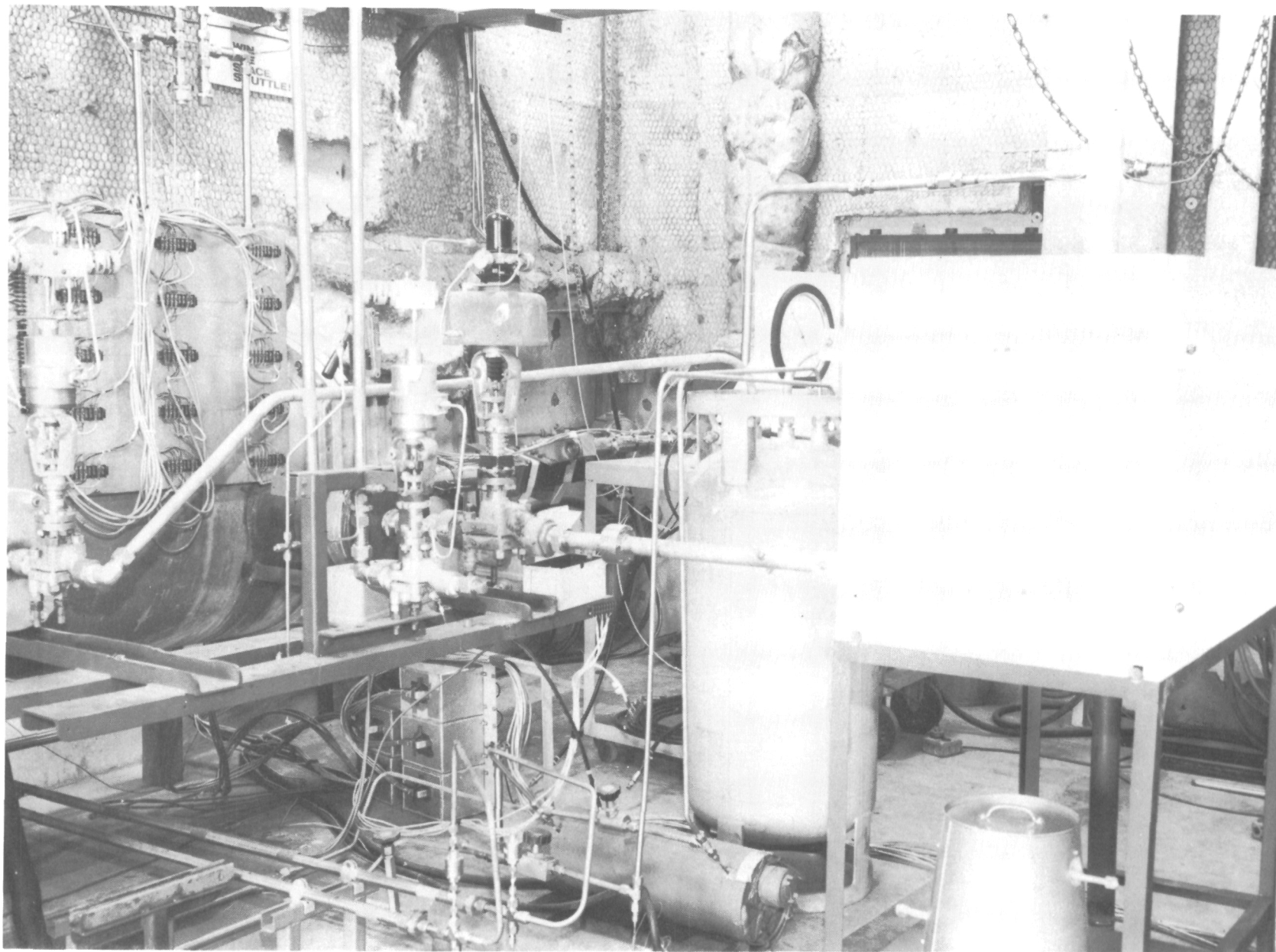
11034-95-2B/5-9-72

Figure 94. Valve Test Fixture Installed in Environmental Box



11034-95-2A/5-9-72

Figure 95. Control Center



7452-95-2A/1-10-72

Figure 96. Overall View of Test Facility

with less than 0.010 inch (0.025 cm) increase in bushing length. A new bushing was installed. The remaining items noted were of a very minimal nature except for wear of the poppet roll pin. In all subsequent tests, a solid pin was substituted.

The pilot valve was checked with the following leakage results at 450 psia (310.3 N/cm²) ambient helium:

<u>Measurement</u>	<u>Initial leakage, scim (scc/hr)</u>	<u>After 1000,000 cycles, scim (scc/hr)</u>
Pilot inlet seat	0.0357 (35)	0.93 (912)
Pilot vent seat	0.00428 (4.2)	0.0134 (13)
Solenoid inlet seat	0.0319 (31.3)	0.007 (6.9)
Solenoid vent seat	0.00456 (4.5)	0.004 (3.9)

These leakages were so minimal, that the pilot valve was not disassembled prior to starting the hard-sharp carbide closure tests. It should be noted that the pilot inlet seat is normally open, and would only leak when the valve is open.

The hard-sharp carbide closure was installed in the valve. As mentioned earlier, a metal O-ring was not used under the carbide seat ring. This eliminates the seat ring torsional twist. An 0.0005-inch (0.00127 cm) sheet of FEP Teflon was heat and pressure bonded between the seat ring and the outlet flange to serve as a seal. No leakage was detected at this joint during the cycling tests.

Initial testing of the hard-sharp carbide closure concept produced the following leakages with 450 psia (310.3 N/cm²) helium at the inlet.

<u>Temperature</u>	<u>Main Seal Leakage, scim (scc/hr)</u>
Ambient	zero (0)
260 R (144 K)	0.00115 (1.13)
700 R (389 K)	0.00407 (4)

Testing of the hard-sharp carbide closure proceeded with the results summarized as follows:

<u>Number of Cycles</u>	<u>Accumulated Cycles</u>	<u>Test Gas</u>	<u>Test Temperature</u>	<u>Main Seat Leakage After Last Cyclic Closure, scim (scc/hr) He</u>	<u>Main Seat Leakage After One Additional Actuation and Reseat, scim (scc/hr) He</u>
500	500	GN ₂	Ambient	0.0074 (7.25)	0.0067 (6.57)
500	1000	GN ₂	Ambient	0.00759 (7.44)	0.0087 (8.53)
9000	10,000	GN ₂	Ambient	Zero (0)	Zero (0)
10,000	20,000	GN ₂	Ambient	0.18 (176)	0.14 (137)
10,000	30,000	GN ₂	Ambient	450.0 (44 x 10 ⁴)	450.0 (44 x 10 ⁴)

The closure had exceeded the specification leakage limit at a total of 20,000 cycles; however, testing was continued to 30,000 total cycles where gross failure was evident by the leakage.

A failure analysis was initiated to determine the cause for failure. Examination of the seal revealed a progressive fatigue failure of the sealing lands. This was evidenced by the "crumbling" of the edges of the sealing lands. The material for the valve seat was the same Carmet CA-315 from which the model seat was made. Therefore, a program was initiated to evaluate the impact forces at valve closure.

A fixture was designed to nest the valve seat with a Kistler Model 904A load cell underneath to measure impact forces. An overall view of the test setup is shown in Fig. 97. The fixture is shown more closely in Fig. 98. The test gas discharges through the center of the impact force-measuring adapter to the cell atmosphere. Figure 99 shows typical forces measured in the hard-sharp carbide closure. The opening impact transmits a compression force of 1800 pounds (8010 N) into the seat via the valve structure. The force has no effect on the sealing lands. The closing impact force is measured directly as 2350 to 2400 pounds (10458 to 10680 N). Based on the projected sealing land areas of the valve seat, the apparent impact stress is 536,176 lb/in.² (369,640 N/cm²). Similarly, the apparent impact stress on the sealing lands of the models tested in Task IIIA was 225,752 lb/in.² (155,633 N/cm²). The almost 100-percent increase in impact stresses was caused by increasing valve speed to meet the 30-millisecond response time. Thus, for this program, no further development will be performed on the hard-sharp carbide closure concept.

As mentioned earlier, the analysis of the captive plastic closure had been initiated. Subsequent disassembly of the closure assembly revealed that the outer anti-extrusion ring had broken, twisted over the upper surface of the plastic seal ring, and had "jammed" the inner anti-extrusion ring downward into the tapered section of the inner retainer. This resulted in the assembly being relatively incapable of any movement, with the result that the plastic seal ring could not be "pressurized" against the valve seat.

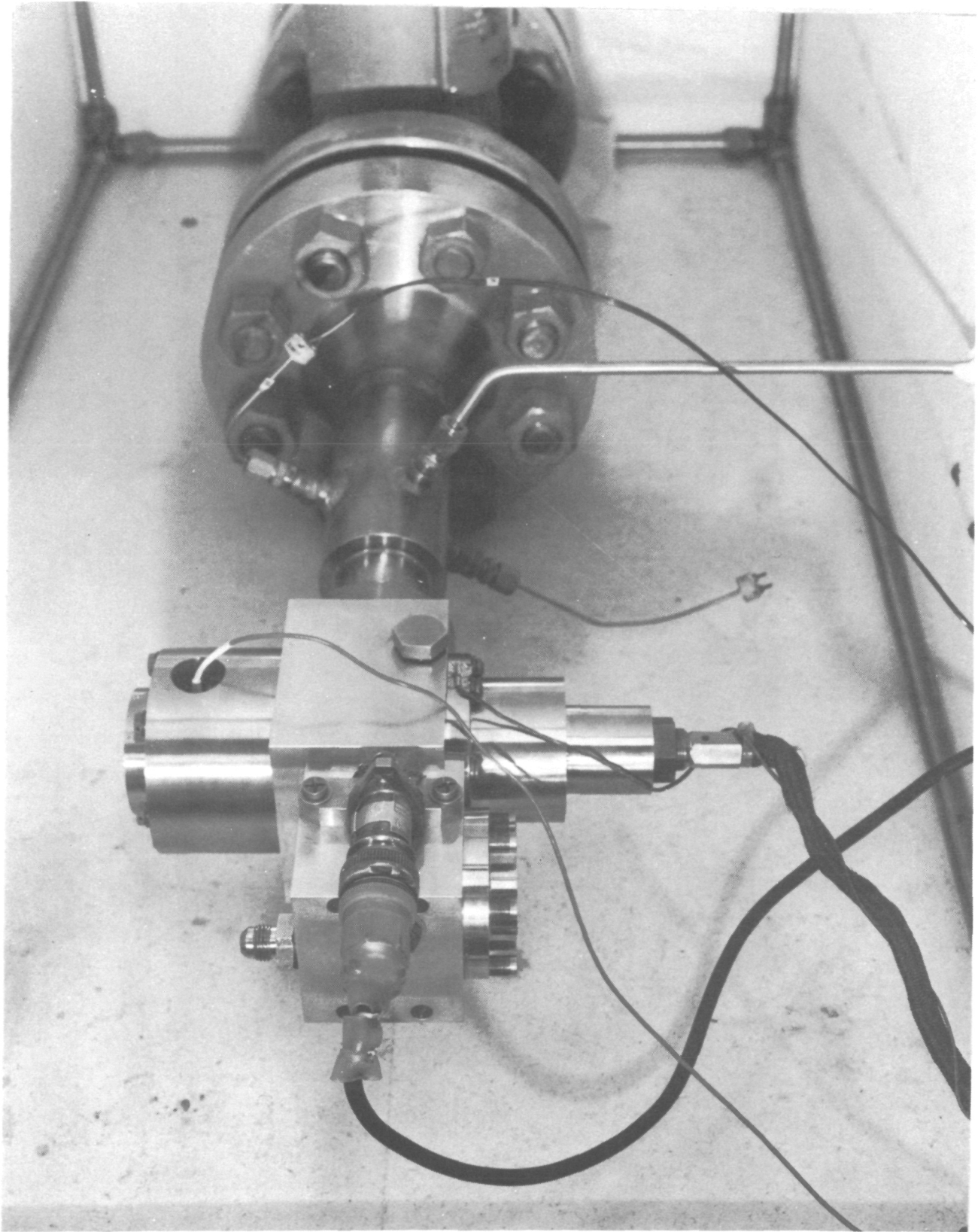
TFE Teflon extrusion tests using the closure parts were performed at 710 R (394 K) and at 10 times the design stresses in the plastic. These tests proved that the anti-extrusion rings are unnecessary, so they were eliminated from the design. In addition, the inner and outer retainer rings and the mating poppet ram were Microseal treated to help prevent the minor fretting seen from earlier tests. The TFE Teflon sealing ring was also formed at 710 R (394 K) and 2000 pounds (8900 N) load prior to final assembly to ensure that the plastic fills all the seal cavity voids. The configuration is shown in Fig. 100.

The reworked captive plastic closure was evaluated by a 10,000-cycle test in cold GO₂. The pretest leakage of the closure was <10⁻⁵ scim (<10⁻² scc/hr) helium at 450 psia (310.3 N/cm²), while the posttest leakage was zero. Following these cycles, the closure was disassembled to evaluate its condition. The plastic seal ring had not extruded between the poppet ram and the inner and outer retainers, so the elimination of the piston rings proved quite feasible. The Microseal treatment did wear away, however, and the resulting surfaces, while not galled, were bare of any coating.



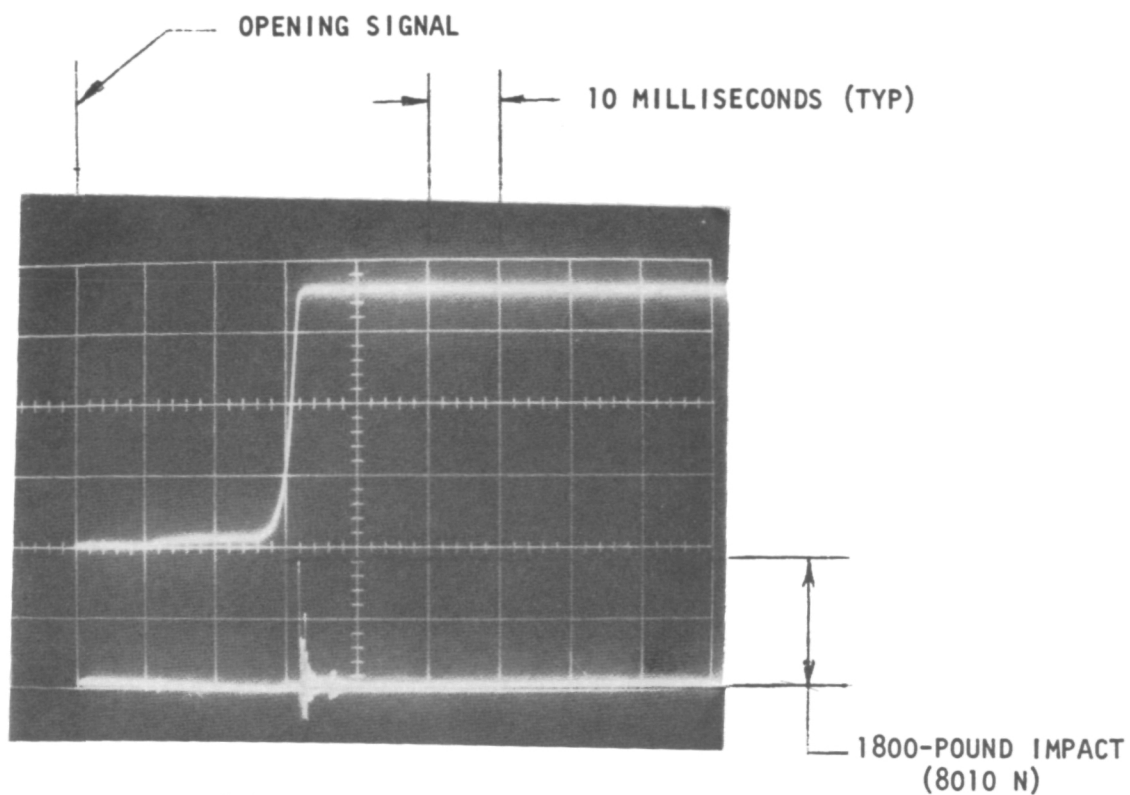
5-5-72/11034-95-1A

Figure 97. Impact Load Measuring Test Setup

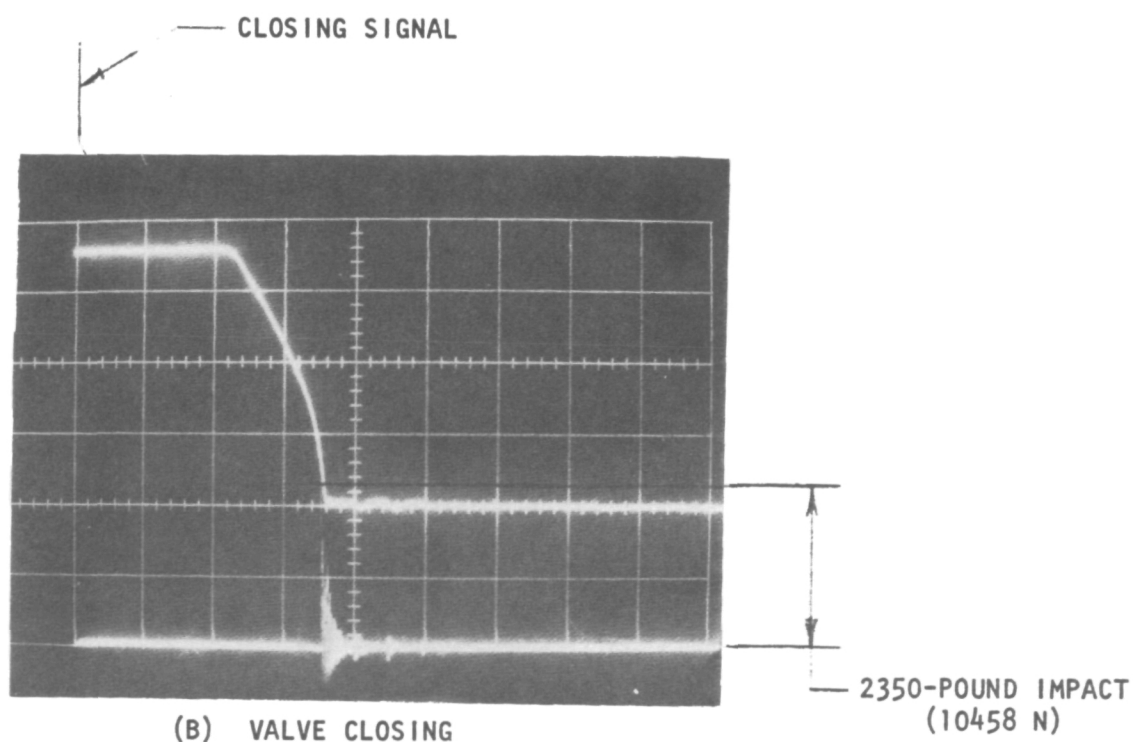


5-5-72/11034-95-1B

Figure 98. Impact Load Measuring Fixture Installed on Valve



(A) VALVE OPENING



(B) VALVE CLOSING

Figure 99. Impact Loads

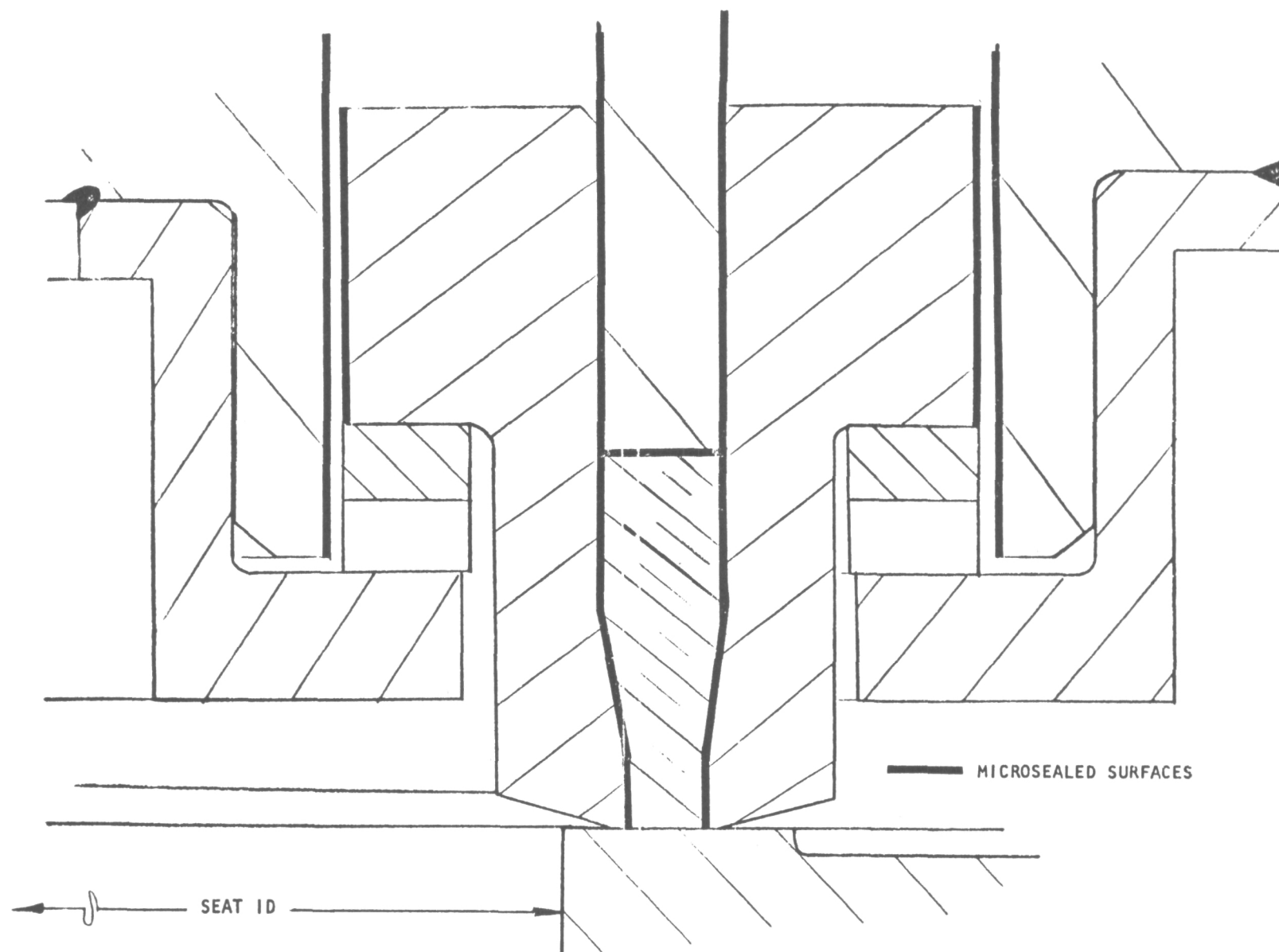


Figure 100. Reworked Captive Plastic Closure

The valve itself was again completely disassembled, having accumulated another 40,000 cycles during the hard-sharp carbide and cold captive plastic closure tests. Prior to disassembly, the following leakages were recorded at 450 psia (310.3 N/cm²) helium:

Main acutator Krueger seal	0.825 scim (811 scc/hr)
Pilot vent seat	0.0097 scim (9.5 scc/hr)
Pilot inlet seat	2.196 scim (2 x 10 ³ scc/hr)
Pilot Krueger seal	0.0442 scim (43.3 scc/hr)

The leakages experienced at the main actuator seal and at the pilot inlet seat occur only when the valve is open. In actual use, the leakages would be dumped into the flow stream downstream of the valve and would not represent overboard leakages.

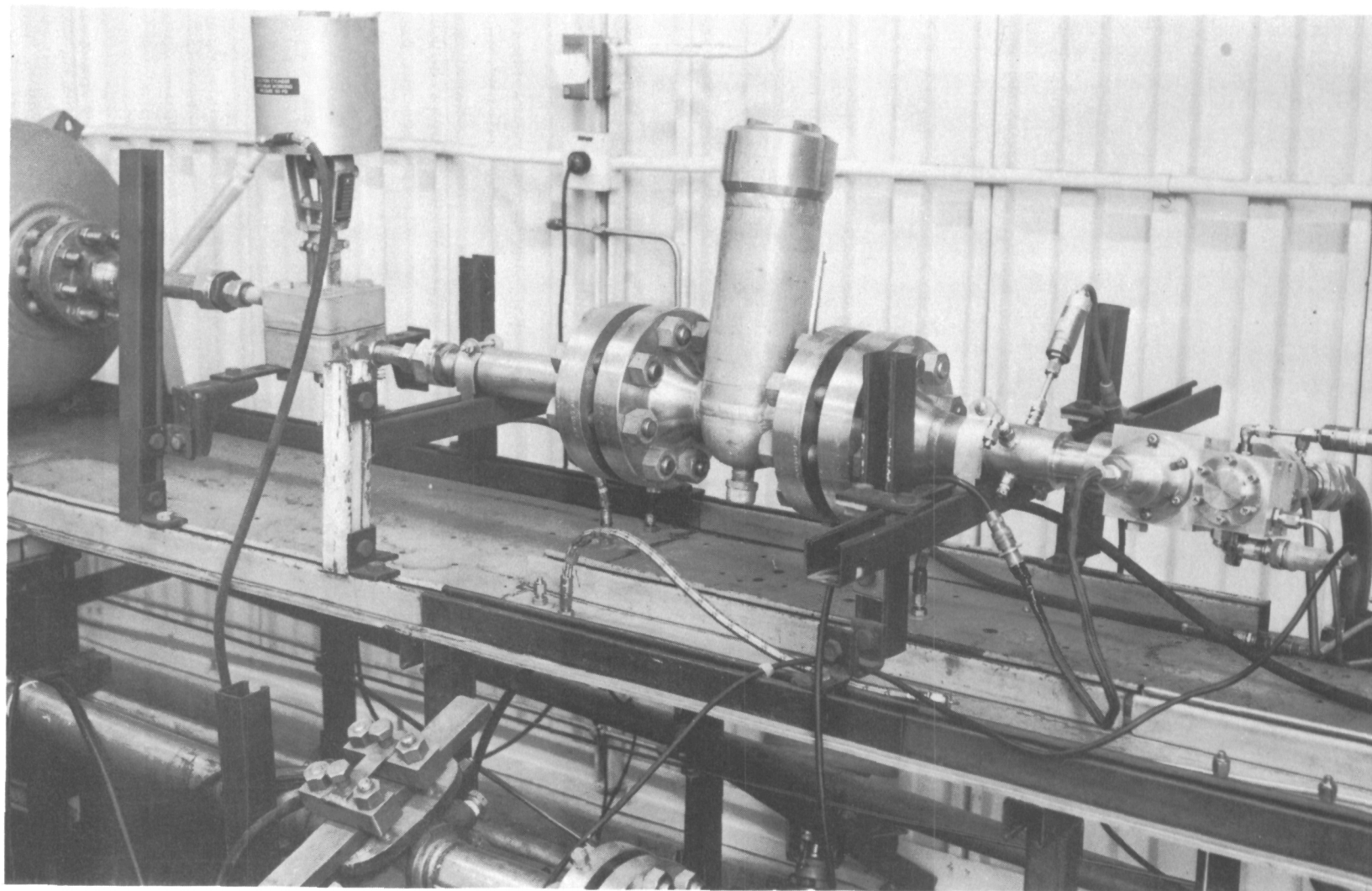
The pilot was also disassembled, and the seats relapped. A new graphite-filled TFE Krueger seal was installed. These reworks brought all pilot valve leakages to <10⁻⁴ scim (<10⁻¹ scc/hr) helium at 450 psia (310.3 N/cm²).

The main valve actuator Krueger seal was replaced even though the old one appeared quite good. Again, Vespel SP-21 material was used. The plastic bushing on the main piston is not a heat-shrink bushing as is the poppet shaft bushing. The poppet shaft bushing had worn less than 0.0001 inch (0.00025 cm) in diameter, and was not replaced. The piston bushing had worn 0.0004 inch (0.001 cm) in diameter and was replaced with a new bushing.

The captive plastic closure parts were stripped of the Microseal coating and a dry-film LOX compatible lube per NAO112-008 was applied. This dry-film was to be evaluated during the 800,000-cycle test.

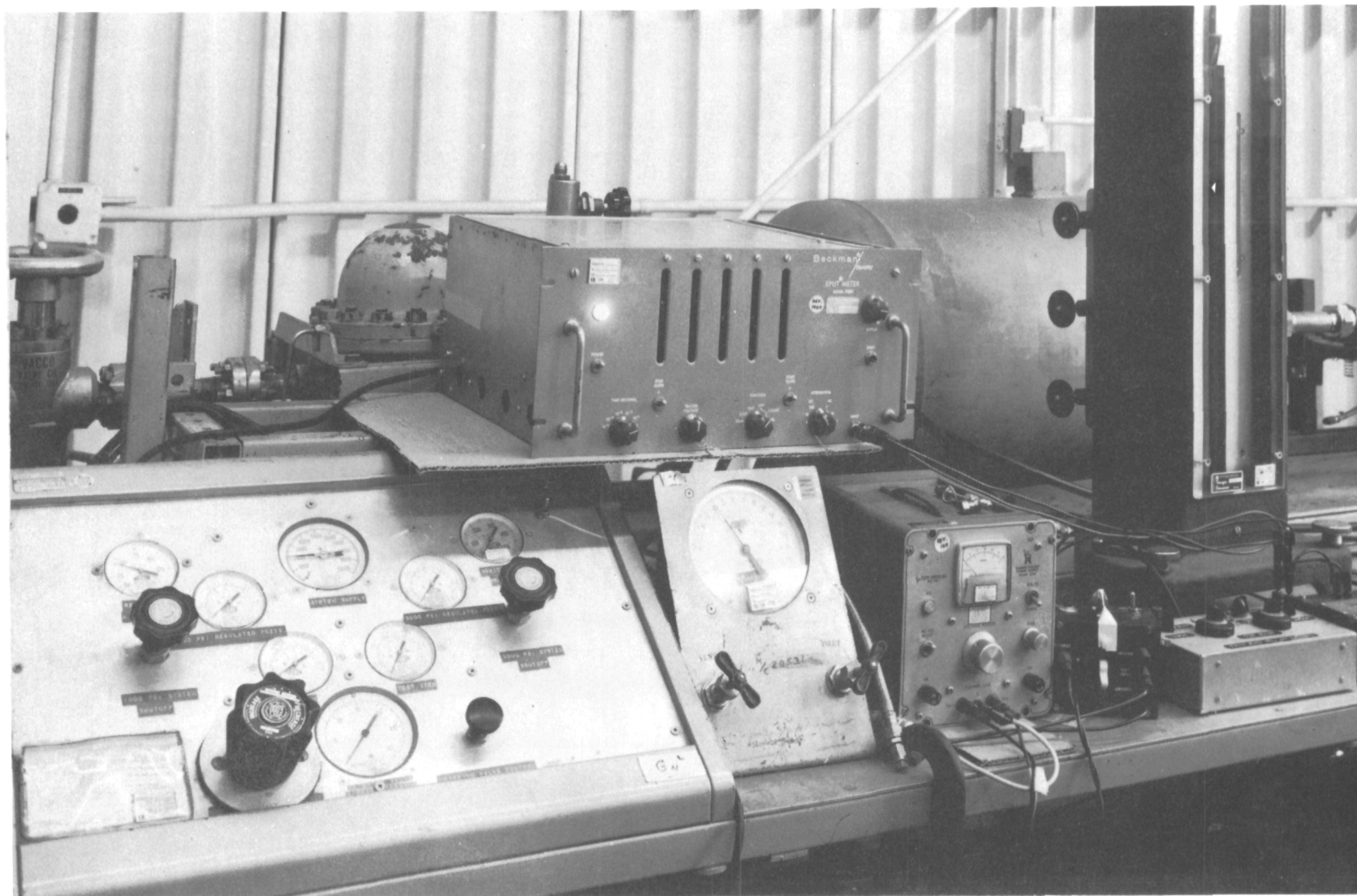
The original design goal for the SS/APS program was 1,000,000 cycles with final leakage less than 0.102 scim (100 scc/hr) helium. Toward the end of the testing effort described in the preceding paragraphs, the NASA-LeRC Project Manager solicited a bid by means of a request for proposal to do an additional 800,000 cycles as a life test of the valve concept and its captive plastic closure. Rocketdyne responded favorably and was awarded a small follow-on contract to do additional cycling of the valve test fixture.

The tests were performed at the Rocketdyne development laboratory using ambient gaseous nitrogen. The SS/APS valve test fixture is shown installed in the GN₂ flow bench in Fig. 101. The schematic is the same as Fig. 91 except that a triple wall accumulator was not used. Because the tests were with GN₂, a half-flow control orifice was used at the first joint downstream of the valve seat. This gives a simulated injector "dribble" volume of 12.5 in.³ (204.8 cm³). In earlier hydrogen testing, a volume of 50 in.³ (819.4 cm³) was used because these volumes matched Rocketdyne's thruster assembly design volumes. In Fig. 102, the cycling control equipment is shown. The valve was cycled with GN₂ at half-flow at an average cycle rate of 10 Hz. By "fine-tuning" the on-off time, the valve could follow 12.6 Hz, but the tests were run at 10 Hz. Leak tests and timing



1SU64-8/4/72-C1C

Figure 101. Extended Life Cycle Test Setup



1SU64-8/4/72-C1A

Figure 102. Control Equipment for Extended Life Cycling

tests were performed every 100,000 cycles. During the leak check after 300,000 cycles, it was noted that a large increase in main seat leakage was experienced. A quick check revealed that the spring which is inserted between the shaft and the poppet (to help provide self-alignment capability) had failed. Also, the main valve actuator spring had failed. The failure of the shaft-to-poppet spring had allowed the poppet to swing through a large angle during the unknown (<100,000) number of cycles it had accumulated after spring failure. This caused the outer retainer of the captive plastic seat to be driven back slightly. The closure was reworked to bring the retainer back into place, but using the same plastic (TFE Teflon) sealing member. The main actuator spring was replaced. A Kel-F spacer was fabricated to fit between the shaft and poppet to limit poppet overtravel and spring bottoming at valve opening stroke due to dynamic loads. The space was originally present only to allow the valve test fixture to accommodate both the hard-sharp carbide as well as the captive plastic closure concepts. The closure with the Kel-F spacer is shown in Fig. 103. The valve was actually cycled 900,000 times which, with the earlier testing, brought the total number of cycles on the fixture to 1,040,000 + cycles. The test data for the 900,000-cycle test are shown in Table XII.

Thus, the test program was successfully completed, proving that a fixture can endure 1,000,000 cycles. More importantly, the captive plastic closure leaked less than 10^{-3} scim (1.0 scc/hr) helium at 450 psia (310.3 N/cm²) at the end of the test.

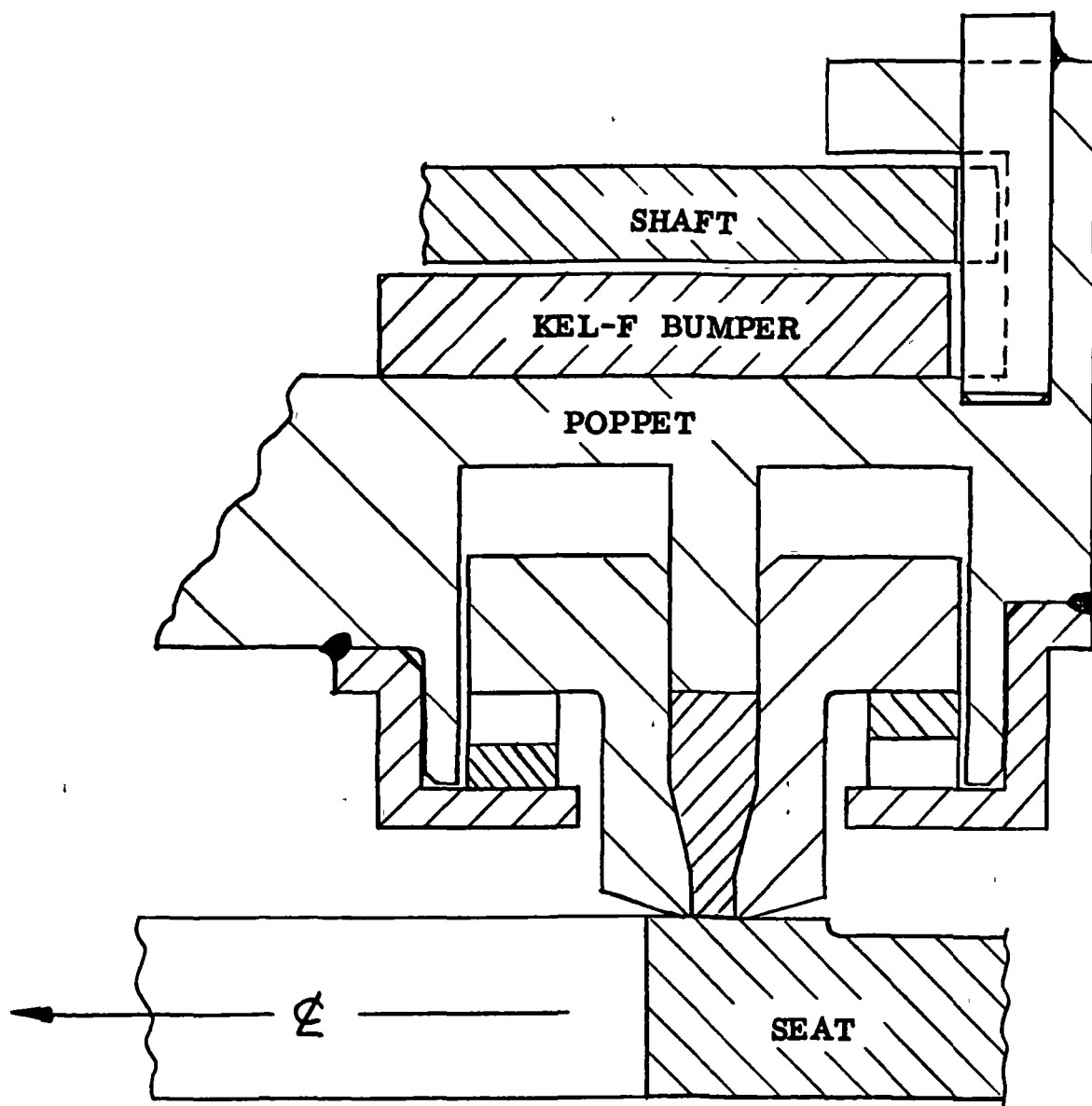


Figure 103. Captive Plastic Closure

TABLE XII - EXTENDED CYCLE TESTING RESULTS

Temperature, R (K)	Cycle Fluid	Number of Cycles Prior to Leakage Test	Helium Leakage Tests*, 450 psia (310.3 N/cm ²) Ambient Gas							Cumulative Cycles
			Main Valve		Main Seat, scim (acc/hr)	Main Actuator Seal, Pilot Actuator Seal, Pilot Normally Open Seat**, scim (acc/hr)	Pilot Normally Closed Seat, scim (acc/hr)	Solenoid		
			Closed	Open				Normally Open Seat, scim (acc/hr)	Normally Closed Seat, scim (acc/hr)	
530 (294)	--	Control Leak Tests	X		0.0023 (2.25)	--	<10 ⁻⁴ ($<10^{-1}$)	--	<10 ⁻³ (<1.0)	--
	GN ₂	1	X	X	--	<10 ⁻⁴ ($<10^{-1}$)	--	<10 ⁻⁴ ($<10^{-1}$)	--	1
		99,999	X	X	--	<10 ⁻⁴ ($<10^{-1}$)	--	<10 ⁻⁴ ($<10^{-1}$)	--	100,000
		100,000	X	X	--	7.9 (7.7 x 10 ³)	--	Zero	--	200,000
		100,000	X	X	--	85 (83.3 x 10 ³)	--	<10 ⁻³ (<1.0)	--	300,000
		100,000	X	X	0.084 (82.6)	--	<10 ⁻³ (<1.0)	--	0.47 (4.6 x 10 ²)	400,000
			X	X	--	10.4 x 10 ³ (1.01 x 10 ⁷)	--	<10 ⁻³ (<1.0)	--	500,000
			X	X	<10 ⁻³ (<1.0)	--	0.060 (58.8)	--	0.125 (1.2 x 10 ²)	600,000
			X	X	--	35 (34.3 x 10 ³)	--	<10 ⁻³ (<1.0)	--	700,000
			X	X	<10 ⁻³ (<1.0)	--	0.056 (54.9)	--	0.106 (1 x 10 ²)	800,000
			X	X	--	21.5 (21 x 10 ³)	--	<10 ⁻² (<10)	--	900,000
			X	X	<10 ⁻³ (<1.0)	--	0.040 (39.2)	--	0.019 (18.6)	--
			X	X	--	800 (78.4 x 10 ⁴)	--	<10 ⁻² (<10)	--	--
			X	X	<10 ⁻³ (<1.0)	--	0.062 (60.8)	--	0.019 (18.6)	--
			X	X	--	3.05 (7.9 x 10 ³)	--	<10 ⁻³ (<1.0)	--	--
			X	X	<10 ⁻³ (<1.0)	--	0.096 (94.1)	--	0.024 (23.5)	--
			X	X	--	290 (28.4 x 10 ⁴)	--	<10 ⁻² (<1.0)	--	--
			X	X	<10 ⁻³ (<1.0)	--	0.062 (60.7)	--	0.022 (21.6)	--
			X	X	--	0.85 (8.3 x 10 ²)	--	<10 ⁻² (<10)	--	--
		Control Leak Tests	X		0.001 (0.98)	--	0.10 (98.03)	--	0.0368 (36.07)	--
			X		--	7.06*** (6.9 x 10 ³)	--	0.0051 (5.0)	--	--

*P, precision burst leakage measurement, minimum volumes

**Pilot valve vent port leakage includes these three leakage sources Special test procedures including pilot and main valve separation are necessary to isolate these when required

***Main valve Krueger seal--7 0 scim (6 86 x 10³ acc/hr)

Pilot inlet seat--0 0616 scim (60 39 acc/hr)

DISCUSSION OF RESULTS

INTRODUCTION

The SS/APS valves design requirements established a need for valve technology which was truly "beyond the state of the art." No valve of the size required had ever been required to actuate so rapidly (<30 milliseconds), last so long (1×10^6 cycles), and leak so little (<0.102 scim; <100 scc/hr He). The results, then, of the valve program are outstanding in view of the initial goals.

This section of the report will discuss the results of the sealing closure screening tests, followed by a discussion of the valve test fixture testing results. Finally, the flightweight design which was prepared based upon the testing results will be discussed.

SEALING CLOSURES RESULTS

One of the initial tasks in this program was to develop closure design criteria and identify specific designs most capable of meeting APS valve requirements with contamination considerations. This was accomplished by analysis and test of closure model designs. A dynamic tester employing a hydrostatic gas bearing was designed to operate from 140 to 860 R (78 to 478 K), with cycling provided at 50 to 100 Hz by impact between poppet and seat and interacting piston control and inlet pressures.

A primary parameter examined in the closure screening tests was the amount of scrubbing occurring between sealing surfaces at closure impact. This parameter was controlled by an adjustable poppet holder which utilized a system of rolling carbide bearings that forced the poppet to either clamshell closed (hinge near the interface plane), or scrub closed by rotation below the interface plane.

Screening tests were performed on six closure designs. To provide an inter-connect and baseline performance with previous poppet and seat program results (Ref. 2), initial tests were performed on flat 440C poppet and seat models. The five other closure concepts tested were:

1. Flat gold with 440C poppet
2. Flat-grooved gold with 440C poppet
3. Metal disk seal
4. Captive plastic
5. Hard sharp carbide

Model screening tests were performed at 1000-psig (689 N/cm^2) inlet pressure with nitrogen (helium was used for cold cycling). Tolerance leakage was computed from the valve requirements as 4×10^{-2} scim (≈ 40 scc/hr) at 530 R (295 K) with 50 to 100 pounds (222.5 to 445 N) as net seat load limits.

The results of the screening tests have been completely described in an earlier section. However, in summary, the 440C and first three concepts exhibited excessive wear and leakage with cycling (to 1 million cycles). Some models passed the tests with minimum scrubbing but inspection revealed fretting on the 440C models and transfer of gold to 440C on the gold models. This also occurred on one test with a grooved gold seat and tungsten carbide poppet. The use of gold instead of copper for seating metal was based on corrosion observed on lapped copper seats. It may have been the lack of such corrosion that caused the poor wear condition on the gold seats. Additional tests are required to evaluate soft metal seats with scrubbing in a gaseous environment.

The disk seal model, consisting of a thin, flat beryllium copper washer on radiused 440C poppet, incurred excessive wear and was cycled only 500,000 times.

The variety of seat models tested, with their multitude of influences and parameters on leakage, presented insufficient data with which to update and modify the analytical leakage model. Since the modeling of wear-related factors in sealing closure models is a very complex task, it would require a vast number of controlled tests with models of many surface finish measurements to evaluate and understand the characteristics associated with any given material and closure model configuration. It was not the intent of the program to fully develop a wear-leakage model, but rather, by screening various models, to establish the identity of those models which had the probability of exceeding the required cycle life within leakage requirements.

The remaining two models met all requirements of the screening tests. More than five one-million cycle tests were performed on each model leakage. Several extreme temperature tests also were performed consisting of 500,000 cycles each at 160 and 850 R (89 to 477 K). The test program demonstrated the capability of the two model designs to sustain one million impact cycles with at least 0.002-inch (0.00508 cm) scrubbing at closure.

A brief series of tests were performed to determine general particle effects on the plastic and carbide models. These tests were limited to room temperature. Typical load-leakage results from one million cycle tests are presented in the following sections.

Captive Plastic Model

Data from a typical one-million cycle test were presented in Fig. 51. As shown, leakage above 10 pounds (44.5 N) seat load was below 10^{-3} scim (1 scc/hr) throughout the test. Similar results were obtained in cycle tests at extreme temperatures.

Contamination test results for the captive plastic model are shown in Fig. 61. The first test consisted of placing three 120-micron nickel balls (R_c 23) at 120-degree spacing, centered on the plastic insert. The balls were completely enveloped with leakage less than 10^{-4} scim (10^{-1} scc/hr) at 4 pounds (17.8 N) seat load. A 0.003-inch-diameter (0.00762 cm) human hair was then laid across

the seat centerline to bridge all lands. The result was an orifice-type leak up to 100 pounds (445 N) seat load (test 3). The hair was removed (with a human eyelash as a probe) and the seat retested; leakage was less than 10^{-4} scim (10^{-1} scc/hr) at 4 pounds (17.8 N) seat load.

For a final test, one 60-micron diameter R_C 23 nickel ball was placed on the outer retainer adjacent to the plastic insert to purposely cause the retainer to be unable to contain the plastic. Two leak tests showed an orifice-type leak, reducing to less than 10^{-4} scim (10^{-1} scc/hr) by 100 pounds (445 N) seat load. Upon removal of the ball, leakage was again less than 10^{-4} scim (10^{-1} scc/hr) at 1000-psig (689 N/cm²) inlet pressure with 4 pounds (17.8 N) seat load. Photomicrographs of seat damage were shown in Fig. 62 through 65.

This test series demonstrated the self-healing capability of the captive plastic concept. Where the contaminant is within the plastic it is enveloped. With soft contaminants that bridge the seat, subsequent cycles may flush the particle from the seat.

Hard Sharp Carbide Model

For systems requiring metal-to-metal closures with low leakage, the results obtained with the hard sharp carbide model design appeared quite promising. Contamination resistance is provided by both particle avoidance and particle destruction features. The probability of entrapping a spherical particle on the land is slight. Since most fibers are relatively soft, they should be easily cut. The obvious danger in the design is fracture due to the brittle nature of the material. Impact stresses must primarily be compressive. Temperature extremes pose holding problems because of very low expansion relative to steel.

The detail design was modified for test to press an outer bushing of tungsten carbide over a 440C seat base; an adhesive was used to seal between members. With limited testing, a range of seat land widths could not be explored; therefore, a slightly wider land than indicated by the detail was used (0.002 to 0.0004 inch; 0.000508 to 0.001016 cm).

Results of a typical one-million cycle test are shown in Fig. 52. Cycling was performed at 100 Hz and 250 pounds (1110 N) impact.

Since the carbide seat was designed as a contaminant destroyer, it was tested with typical bridging-type contaminants. An initial test with a human hair bridging all lands produced negligible effect (Fig. 66). This test was followed by placement of a 0.0075-inch-diameter copper wire across all lands. The wire was cleanly cut, as shown by Fig. 67 and 68, with no effect on leakage or the seat sealing surfaces (Fig. 66).

Previous program testing has indicated the desirability and, with some designs, the necessity for maintaining a close orientation between poppet and seat. The captive plastic seat did not have this requirement because of the soft sealing material. To evaluate reorientation effects on the carbide seat design, 500,000

cycles were accumulated with the poppet rotated on the seat 90 degrees with each 100,000 cycles. Leakage decreased throughout the test. It was concluded that for the nominal 10^{-2} scim (10^1 scc/hr) level requirement, seat orientation was not necessary.

These tests showed that the captive plastic and hard-sharp carbide seat concepts had considerable potential as contaminant-resistant closures. Like any design, the limitations of these designs needed exploring. Consequently, they were chosen as the full-size closures which would be fabricated for tests in the valve test fixture.

TEST FIXTURE RESULTS

The valve test fixture was designed based on the results of early trade studies, the Task II preliminary designs, and the closure screening test results. It was designed as a multiple-feature device capable of testing both the hard-sharp carbide closure and the captive plastic closure.

The valve was designed to have a nominal ΔP_{of} 15 psid (10.34 N/cm^2) at rated flow. The actual flow test performed with ambient GN_2 at 2.57 lb/sec (1.166 kg/sec) proved the valve to have a pressure drop of 15.6 psid (10.75 N/cm^2), extremely close to the design point.

Timing tests with the valve test fixture were performed in GN_2 , GO_2 , and GH_2 at hot, ambient, and cold conditions. These tests showed that the 30-millisecond response could be met on GH_2 at any condition, and also with hot GN_2 and GO_2 . However, the pilot valve fabricated for the program was slightly under capacity, with the result that 30 milliseconds response could not be achieved with ambient and cold GN_2 and GO_2 . This fact was input to the final flightweight design so that the condition could not exist.

Initially, the contract specified 100,000 cycles on the captive plastic closure and 100,000 cycles on the hard-sharp carbide closure. The captive plastic closure was tested first. Early problems with retention of the inner and outer retainer were solved by the use of an electron-beam welded assembly. The closure performed exceptionally well for over 90,000 cycles, when high leakage was noted at 95,000 cycles. Later, it was found that the outer anti-extrusion ring had broken and jammed the assembly in a manner that prevented the plastic from being "pressurized" against the valve seat. The test results for the initial captive plastic closure testing are shown in Table XIII. After disassembly of the valve, it was found that the shaft TFE bushing had been lost. Subsequent analysis showed that the shaft was improperly undercut for the bushing. This condition was corrected with no further problems experienced.

The hard-sharp carbide seat was then started into its 100,000 cycle test program. After 20,000 cycles in ambient GN_2 , it was found to be leaking 176 scc/hr helium, over the specification limit of 100 scc/hr. An additional 10,000 cycles were run, with leakage of 44,000 scc/hr. Testing of the hard-sharp carbide was discontinued at that point except for failure analysis testing. By means of impact load measurements it was found that, to meet the valve 30-millisecond response

TABLE XIII - INITIAL TESTING RESULTS (CAPTIVE PLASTIC CLOSURE)

NUMBER OF CYCLES x 1000	ACCUMULATED CYCLES x 1000	TEST GAS	TEST TEMPERATURE °K	LEAKAGE, SCC/HR HELIUM AT 310.3 N/CM ²	
				MAIN SEAT x 1000	KRUEGER SEAL x 1000
0.5	0.5	GN ₂	AMBIENT	ZERO	2.74
0.5	1.0			ZERO	7.71
9	10			10 ⁻⁵	-
10	20			ZERO	-
10	30	GH ₂	↓	↓	2.59
10	40				3.90
10	50				8.57
10	60				26.2
5	65	GO ₂	↓	↓	35.7
5	70				42.9
5	75		389		133.
5	80		144		381.
5	85	↓	AMBIENT	0.00134	667.
5	90		AMBIENT	0.00787	714.
5	* 95		144	33.34	524.
5	100		389	11.43	381.

* OUTER ANTI-EXTRUSION RING FAILED

- CAPTIVE PLASTIC CLOSURE

- 900,000 CYCLES

- AMBIENT GN_2

- RESULTS

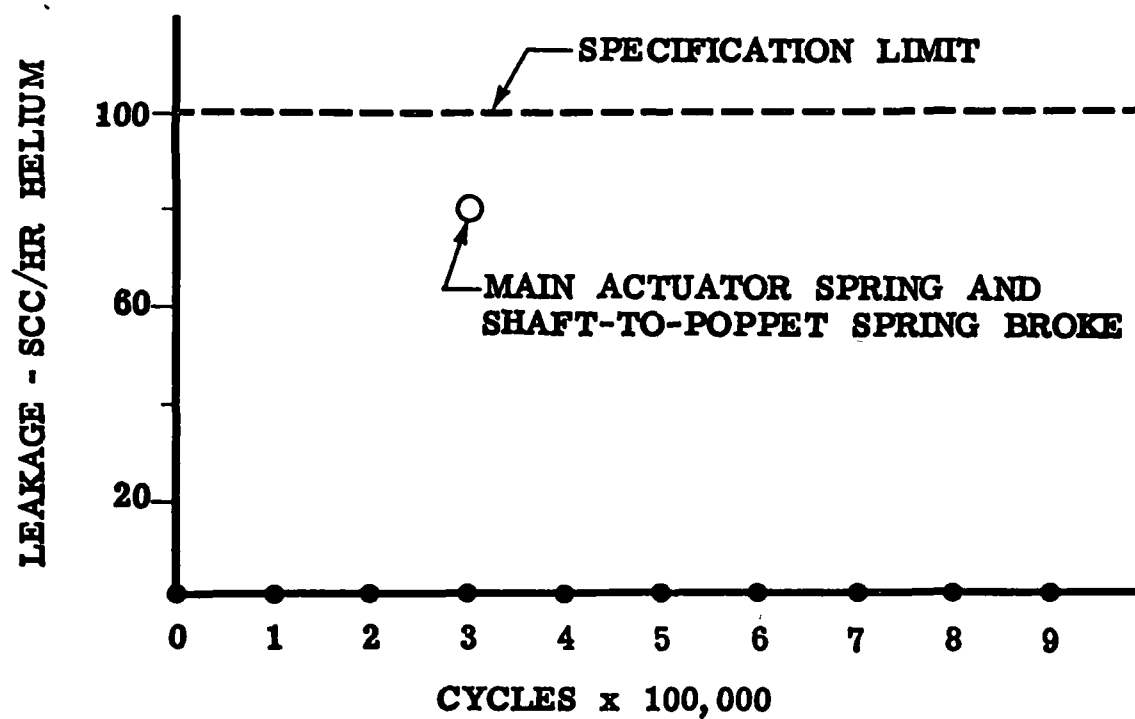


Figure 104. Extended Cycle Testing

time, the hard-sharp carbide poppet was being impacted at an apparent stress of 536,176 lb/in.² (369,640 N/cm²). The apparent impact stress on the hard-sharp carbide model seat was 225,752 lb/in.² (155,633 N/cm²). Thus, for this program, further development work on the hard-sharp carbide closure was suspended.

In the meantime, tests with the captive plastic closure had proved the anti-extrusion rings (which were responsible for the earlier high leakage) were unnecessary, so the closure was assembled with a new seal ring of TFE without anti-extrusion rings. The contract was then modified to add an extended cycle test of 800,000 cycles to prove the capability of the captive plastic closure.

The testing was performed in ambient GN₂ with the precision leakage test being performed every 100,000 cycles. During the leak check after 300,000 cycles, it was noted that a large increase in main seat leakage was experienced. A quick check revealed that the spring which is inserted between the shaft and the poppet (to help provide self-alignment capability) had failed. Also, the main valve actuator spring had failed. The failure of the shaft-to-poppet spring had allowed the poppet to swing through a large angle during the unknown (<100,000) number of cycles it had accumulated after spring failure. This caused the outer retainer of the captive plastic seat to be driven back slightly. The closure was reworked to bring the retainer back into place, but using the same plastic (TFE Teflon) sealing member. The main actuator spring was replaced. A Kel-F spacer was fabricated to fit between the shaft and poppet to limit poppet over-travel and spring bottoming at valve opening stroke due to dynamic loads. The space was originally present only to allow the valve test fixture to accommodate both the hard-sharp carbide as well as the captive plastic closure concepts. The valve was actually cycled 900,000 times which, with the earlier testing, brought the total number of cycles on the fixture to 1,040,000 + cycles. The test data for the 900,000-cycle test are shown in Fig. 104.

The failure of the two springs appears to show that the captive plastic closure can withstand very severe angulation and scrubbing during closure since the leakage was still less than the specification requirement even with the failed spring in place within the valve. During the 900,000 cycles, the TFE seal ring, originally 0.147 inch (0.373 cm) long was worn to 0.133 to 0.135 inch (0.338 to 0.343 cm) in length. Other areas of wear in the valve were not severe at all for the length of test performed. Minor fretting was observed at most bolted interfaces, and some heavier fretting was apparent between the valve shaft and poppet. The wear noted was not detrimental to function or response.

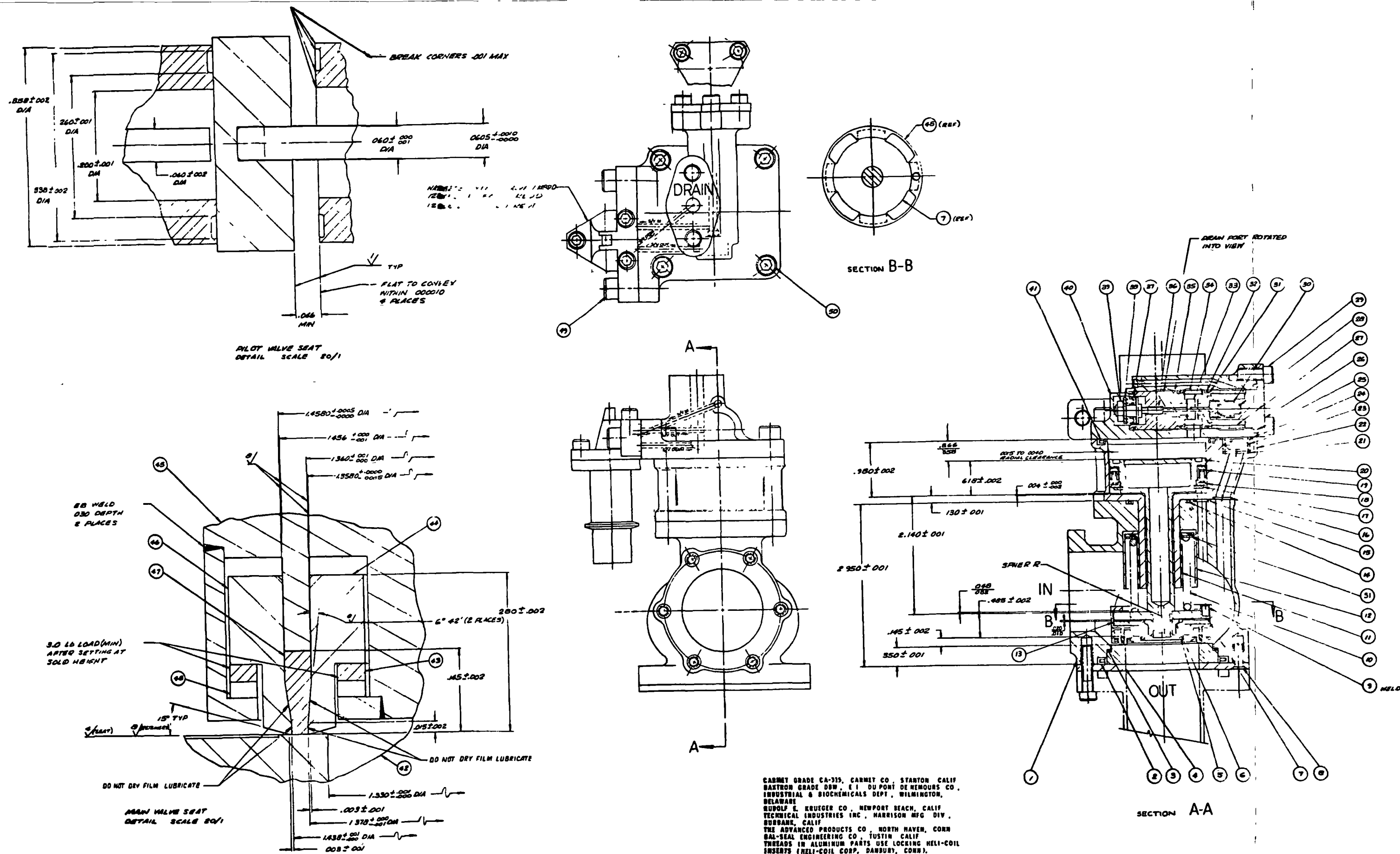
Thus, the test program was successfully completed, proving that a fixture can endure 1,000,000 cycles. More importantly, the captive plastic closure leaked less than 10⁻³ scim (1.0 scc/hr) helium at 450 psia (310.3 N/cm²) at the end of the test. The testing summary is shown in Table XIV.

FLIGHTWEIGHT DESIGN

Based on overall program results, the flightweight valve of Fig. 105 is presented. The valve reflects the improvements dictated by the findings during the test program. During the test program it was found that the pilot valve was under capacity for flow. Thus, the flightweight valve has an improved pilot

TABLE XIV - FIXTURE TESTING SUMMARY

REQUIREMENTS	RESULTS	COMMENTS
1. PRESSURE DROP - 15 PSID (10.34 N/CM ²)	15.6 PSID AT RATED FLOW (10.38 N/CM ²)	
2. PROPELLANT GAS ACTUATION	PROPELLANT GAS ACTUATION	
3. OPENING AND CLOSING RESPONSE - 30 MILLISECONDS GO ₂ AND GH ₂	ORIFICED TO 30 MS ON GH ₂ (COLD, AMBIENT, HOT) 60 - 32 MS ON GO ₂ (COLD TO HOT) OPENING 55 - 30 MS ON GO ₂ (COLD TO HOT) CLOSING	PILOT VALVE UNDER-SIZED, GIVING LARGE VENTING AND DE-PRESSURIZING DELAYS
4. INTERNAL LEAKAGE - 100 SCC/HR HELIUM	TYPICALLY <1.0 SCC/HR	CAPTIVE PLASTIC CLOSURE
5. OPERATING LIFE GOAL - 1,000,000 CYCLES	1,040,000 + CYCLES	1,010,000 ON CAPTIVE PLASTIC CLOSURE



31	1	WASHER	303 CRES	
30	4	SCREW	A286 CRES	
49	2	SCREW	A286 CRES	
43	1	SPRING, BOWED	BERYLLIUM COPPER	
42	1	SEAL	TFE	
46	1	RETAINER, OUTER	INCONEL 718	DRY FILM LUBRICATE
45	1	CARRIAGE	INCONEL 718	DRY FILM LUBRICATE
44	1	RETAINER, INNER	INCONEL 718	DRY FILM LUBRICATE
43	1	SPRING, BOWED	BERYLLIUM COPPER	
42	1	SEAL	TUNGSTEN CARBIDE	
41	1	SEAL "BAL"	TFE, 302 CRES	
40	1	COVER	A286 CRES	
39	1	NUT, LOCKING	A286 CRES	
38	1	WASHER	A286 CRES	
37	1	SEAL, "DELTA"	TFE, CRES	
36	1	PISTON	INCONEL 718, TFE	
35	1	SEAL, VENT	440C CRES	
34	1	SLEEVE, OUTLET	A286 CRES	
33	1	POPPET	TUNGSTEN CARBIDE	
32	3	SEAL, "BAL"	TFE, 302 CRES	
31	1	SEAL, INLET	440C CRES	
30	1	PUSHROD	INCONEL 718 TFE	
29	5	SCREW	A286 CRES	
28	1	SPRING	ELGILOY	
27	1	SLEEVE, INLET	6061-T631 AL ALLOY	
26	1	CAP	A286 CRES	
25	1	SEAL, "BAL"	TFE 302 CRES	
24	1	SEAL "K"	304 CRES	TFE COATING
23	1	FILTER	304 CRES	
22	1	SLEEVE	A286 CRES	
21	1	RING	TFE	
20	1	PISTON	INCONEL 718	
19	1	SEAL, "DELTA"	TFE, CRES	
18	1	GUIDE	A286 CRES	
17	1	RETAINING RING	BERYLLIUM COPPER	
16	1	SEAL, "K"	304 CRES	TFE COATING
15	1	SEAL, "K"	304 CRES	TFE COATING
14	1	SEAL, "BAL"	TFE, 302 CRES	
13	1	BUMPER	KEL-F	
12	1	SHROUD	A286 CRES	
11	1	BUSHING	TFE	
10	1	SPRING	ELGILOY	
9	1	PIN	440C CRES	
8	4	SCREW	A286 CRES	
7	1	LIFTER	INCONEL 718	DRY FILM LUBRICATE
6	3	NUT, LOCKING	A286	SILVER PLATE
5	1	SPRING	ELGILOY	
4	1	PLATE	A286 CRES	
3	1	SEAL, METAL "O" RING	321 CRES	TFE COATING
2	1	SEAL, "BAL"	TFE, 302 CRES	
1	1	HOUSING	6061-T631 AL ALLOY	SULPHURIC ACID ANODIZE
NO.	QTY	DESCRIPTION	MATERIAL	FINISH

Figure 105. Valve Layout

valve. The pilto has been integrated into the valve cap so that the flow passages can be very short and clean with minimum turns and interferences. Also, the pilot seat area has been increased by 12 percent in addition to the improved flow geometry. The volume pressurized and vented in the main valve piston has been reduced by moving the main return spring into the main valve body. TFE Teflon spring bumpers prevent metal-to-metal wear.

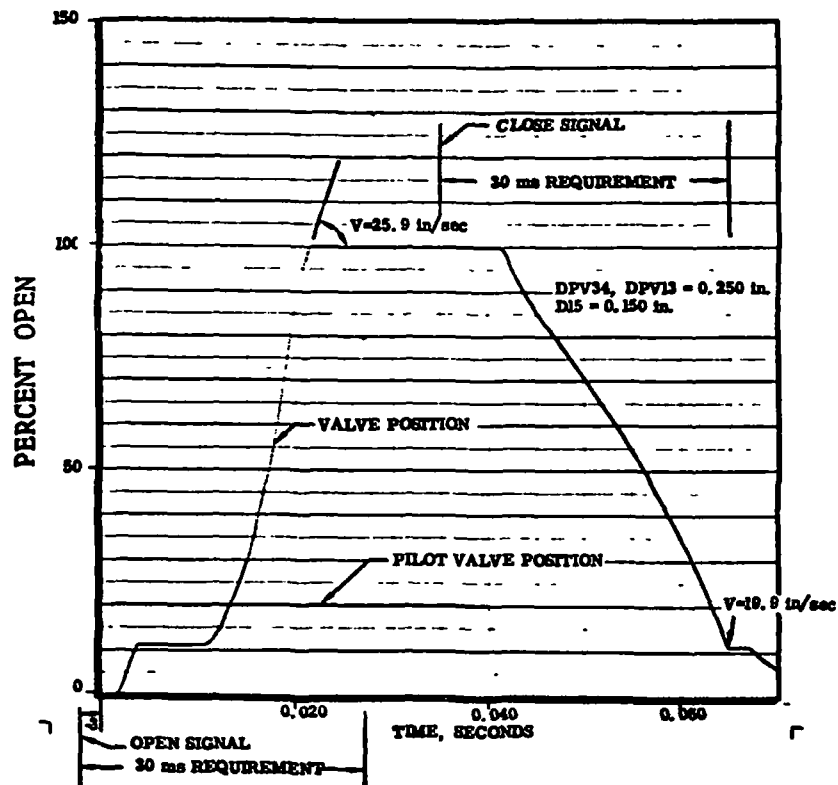
The main shaft bushing of heat-shrink TFE tubing has been increased in length to provide more area and reduce the possibility of metal-to-metal wear. The captive plastic seal assembly poppet has improved fabrication detail and is electron beam welded.

A Kel-F spacer prevents self-alignment spring bottoming and severe poppet articulation. A larger poppet-shaft retention pin has been added to improve its wear capability based on earlier test results. The weight of the valve assembly is estimated at 4.6 pounds (2.087 kilograms).

The flightweight design has been subjected to a considerable amount of dynamic analysis with the DAP4H program (Ref. 5). This program completely simulates the valve dynamics with gaseous flows, pressures, and temperature effects accounted for in the dynamic response. Figures 106 through 111 present the computerized summary of valve performance under cold, ambient, and hot gaseous flow conditions for GO_2 and GH_2 . The valve will meet the required response times at all temperature conditions without orificing changes and without exceeding impact velocities already tested in the valve test fixture. Note that the valve for GH_2 service has initially smaller orifice sizes that can be manufactured into the new valve, or the configuration can be built as a GO_2 valve and later orificed for GH_2 service.

As with any other new, unproved design, the SS/APS valve should be subjected to a complete component development test series with life cycle, vibration, etc., performed, followed by systems evaluation in conjunction with an APS thruster system.

VALVE POSITIONS



VALVE PRESSURES

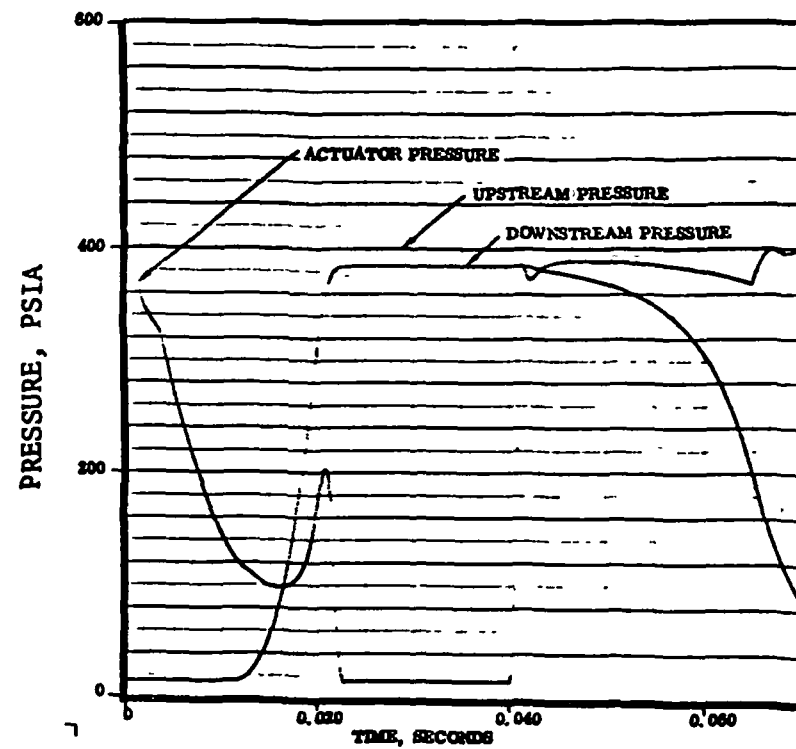
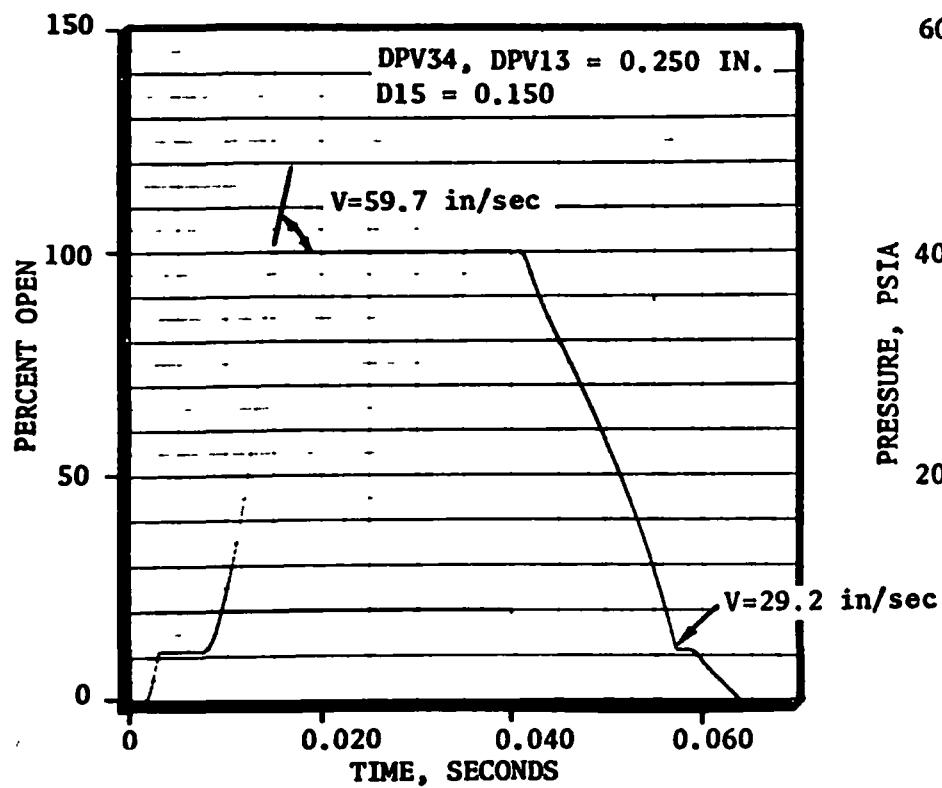
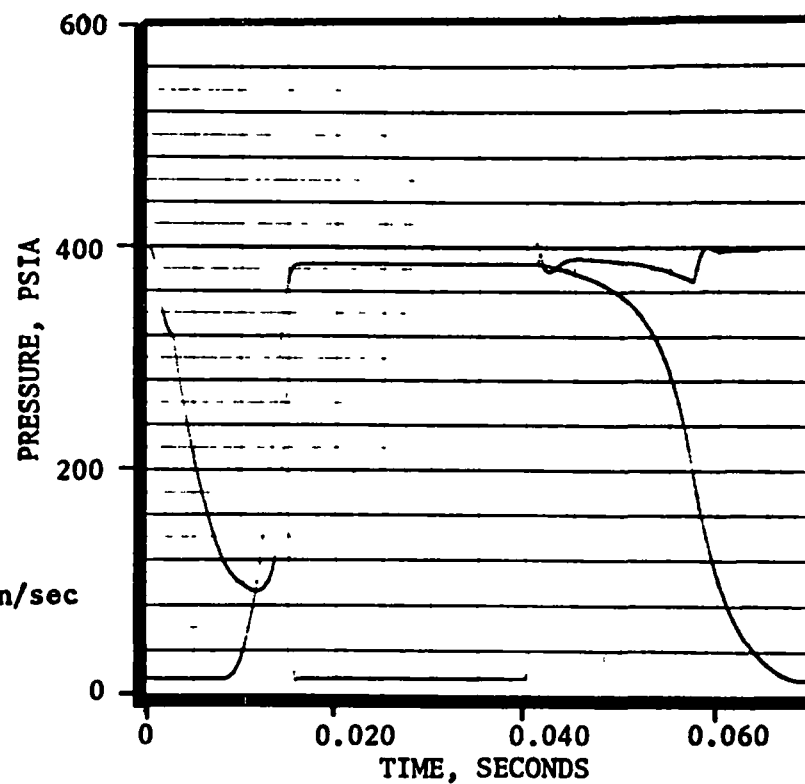


Figure 106. Cold GO_2 Performance

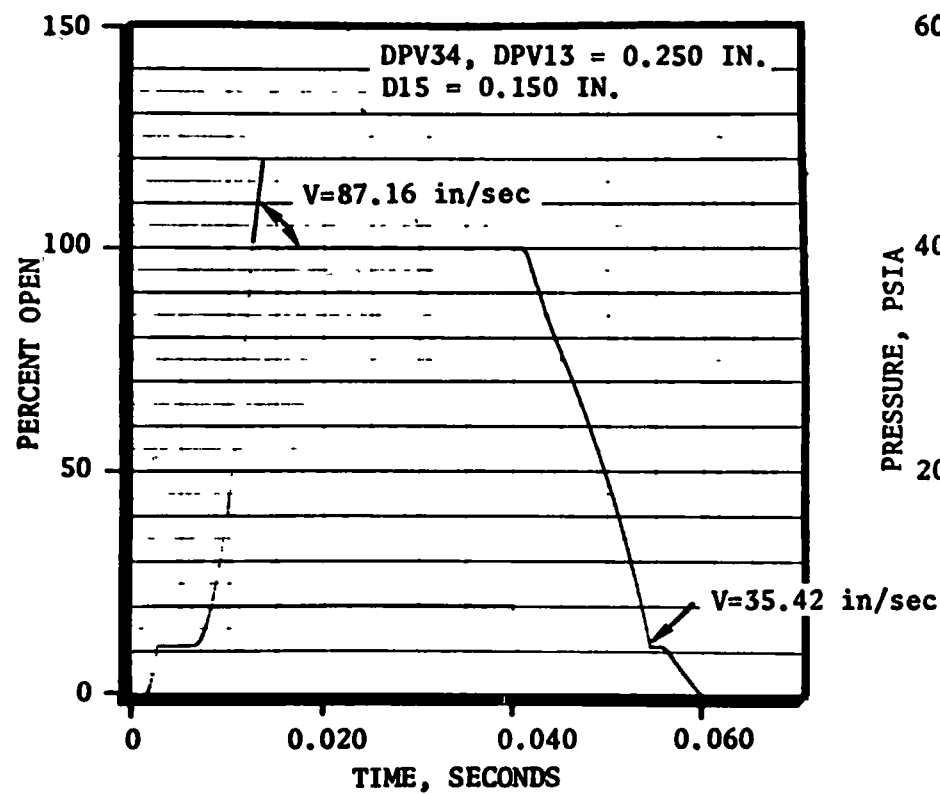
VALVE POSITIONS



VALVE PRESSURES

Figure 107. Ambient GO_2 Performance

VALVE POSITIONS



VALVE PRESSURES

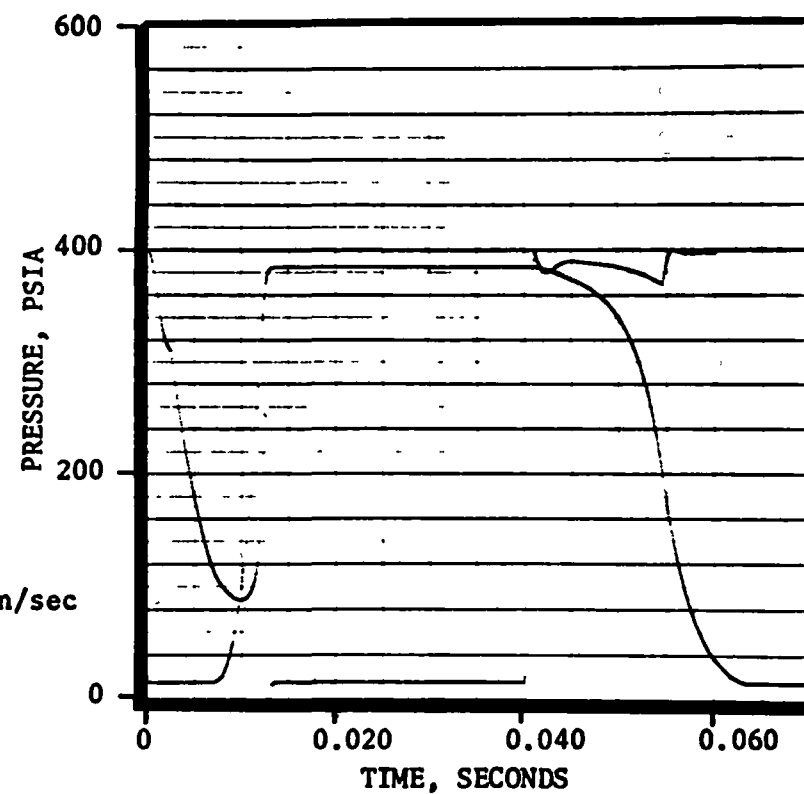
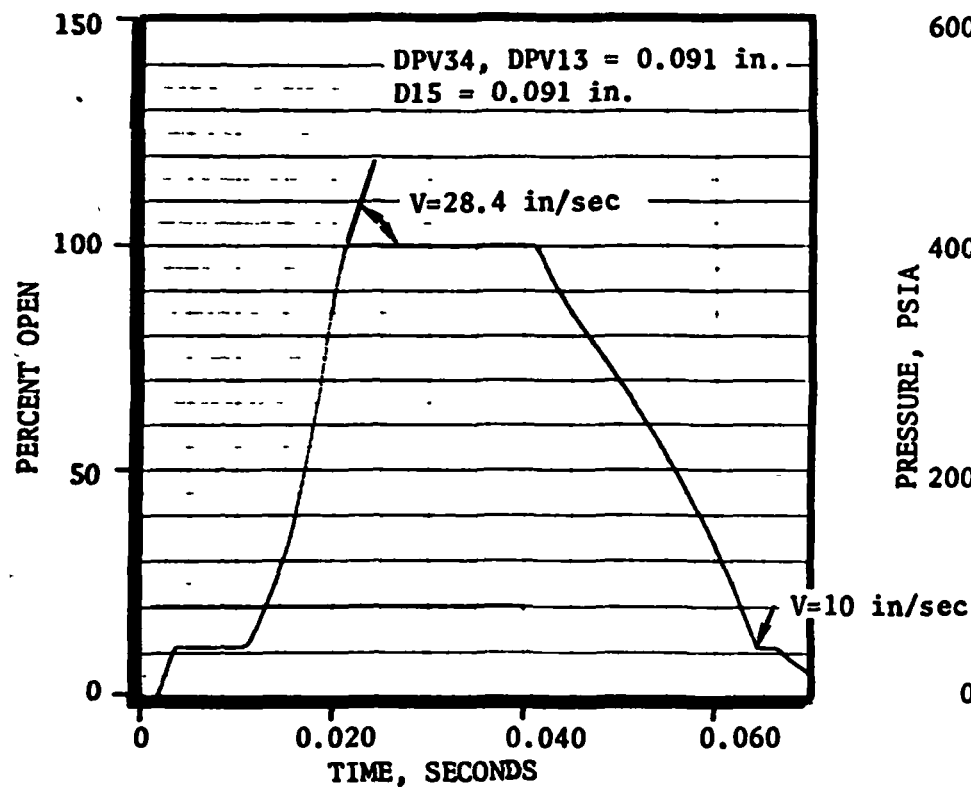
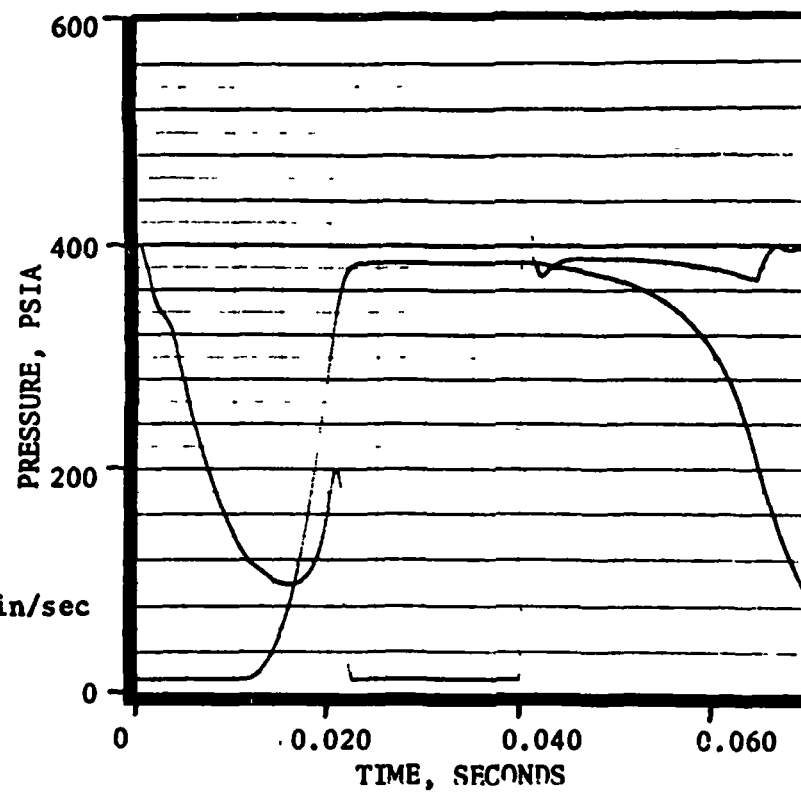


Figure 108. Hot GO_2 Performance

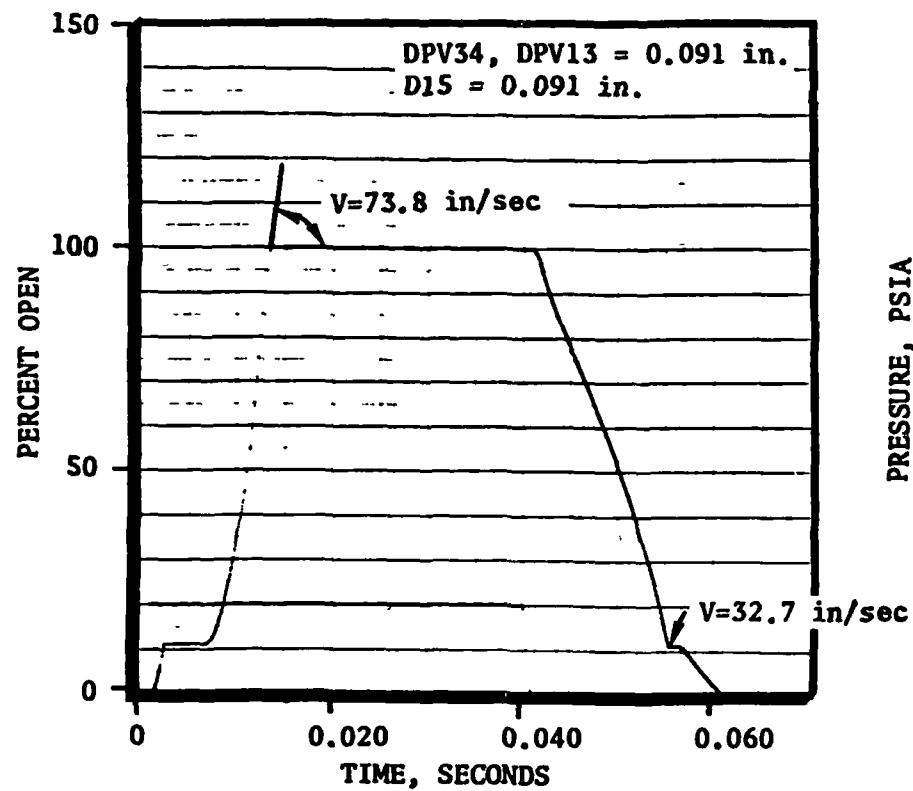
VALVE POSITIONS



VALVE PRESSURES

Figure 109. Cold GH_2 Performance

VALVE POSITIONS



VALVE PRESSURES

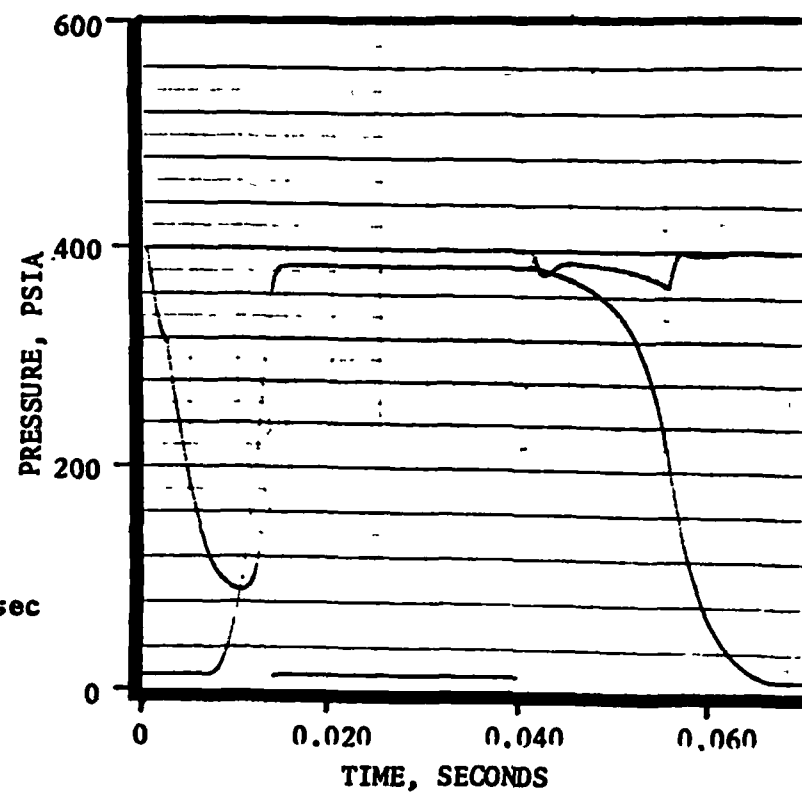
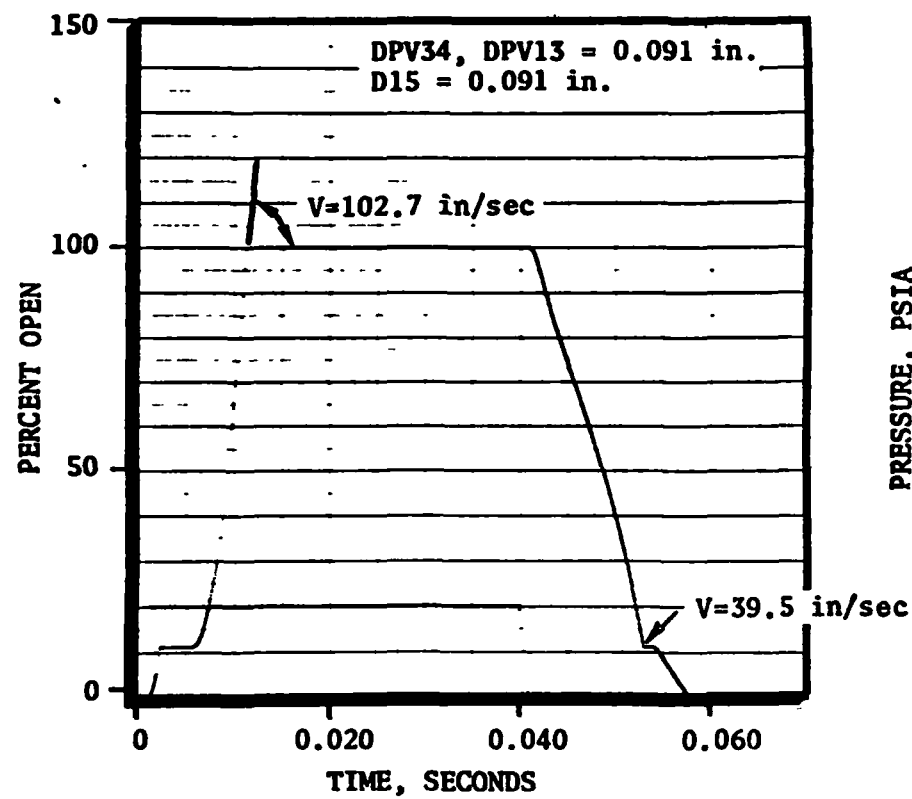
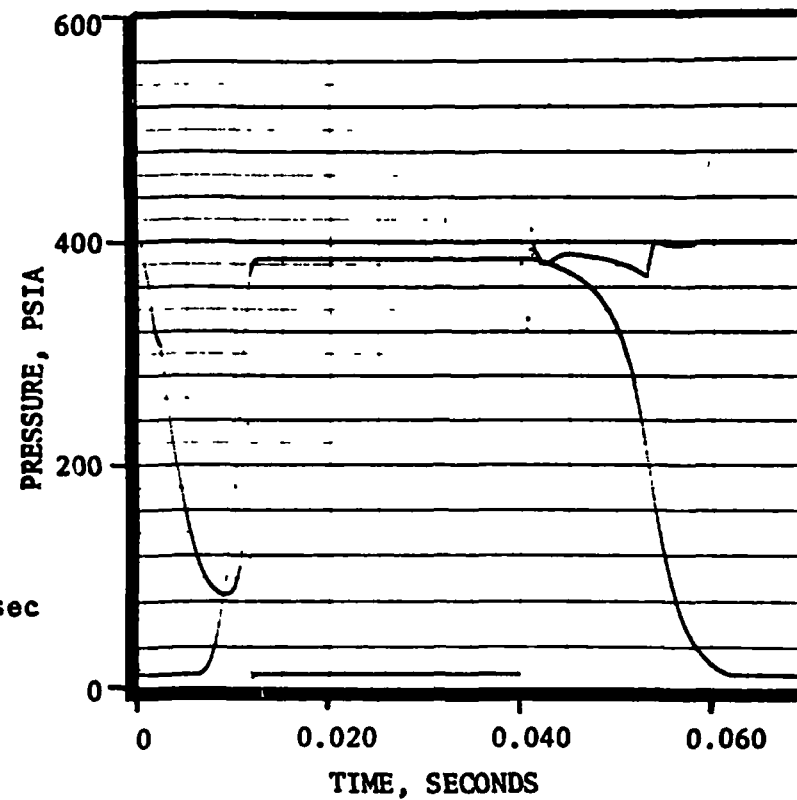


Figure 110. Ambient GH_2 Performance

VALVE POSITIONS



VALVE PRESSURES

Figure 111. Hot GH_2 Performance

CONCLUSIONS AND RECOMMENDATIONS

The SS/APS valves program has produced significant results in terms of concepts and hardware which enabled the achievement of the requirements originally responsible for the initiation of this program.

The screening tests of the closure models revealed several items of interest. Wear can be sustained without serious degradation of the sealing finish. Sealing ability of the hard-sharp carbide seat improved over 1×10^6 cycles, even with reorientation of the seat. Conversely, damaging wear was experienced by a flat-grooved gold seat cycled with a 440C poppet. The failure resulted from transfer of gold to the 440C poppet followed by adhesive wear of gold-on-gold. A similar failure occurred when the flat-grooved gold seat was cycled against a tungsten carbide poppet. The flat 440C models tested also failed from fretting wear. The results provide emphasis for the need to understand the physical chemistry of rubbing surfaces in the environment of interest.

The testing of the model closures indicate that the captive plastic and hard-sharp carbide closure concepts have considerable potential as contaminant resistant closures. Both closures demonstrated resistance to certain types of contaminants, however, additional tests would be required to compare them with AFRPL program results. It is known from the full-size closure tests, that the hard-sharp carbide closure is susceptible to damage from overstressing at closure. The concept, however, appears to have such a great potential as a "contaminant destroyer" that it should be more fully evaluated in models of different land widths, particle exposures, and impact environments.

A unique screening tester was designed and fabricated which allowed three modes of closure operation. Actual values used during the closure screening test are shown in Table XV. In addition, the larger articulation limits available would allow the tester to be used in the investigation of basic phenomena involved in friction and wear. Also, the tester can be adapted to screen many other types of valve model closures than were tested, so a basic research tool has been made available for use to further the art as required.

During the initial testing of the valve test fixture, the hard-sharp carbide closure failed because it was being overimpacted at valve closure. This was caused by the valve actuation speed needed to meet the 30-millisecond actuation time requirement since the pilot valve was under-capacity and used up most of the available 30 milliseconds in pneumatic delays. Initial testing also proved that anti-extrusion rings are not necessary in the captive plastic closure design within the load and temperature limits imposed during this program. A novel means of producing anti-wear bushings of heat-shrinkable TFE Teflon tubing was developed and will be used in future programs. Later testing showed that the captive plastic closure can withstand considerably greater clamshell motion at closure than tested during the model program and still seal effectively.

The basic program objectives have been met. The feasibility of a SS/APS valve for 1×10^6 cycles with low leakage has been demonstrated. A valve closure called the captive plastic closure has been evaluated and demonstrated long life

TABLE XV - POPPET ARTICULATION FEATURES

- **THREE CLOSURE MODES**

- **PARALLEL (CLAMPED)**
NO INTERFACIAL MOTION

- ***CLAMSHELL**
INTERFACE MOTION = 0.04 α INCH
= 0.000028 INCH
= 0.000071 CM

- ***SCRUBBING**
INTERFACE MOTION = 0.62 α INCH
= 0.00067 INCH
= 0.0017 CM

CONTROL
INTERFACIAL
MOVEMENT

- **LOW LEAKAGE MEASUREMENT**

* ACTUAL VALVE DESIGN ALLOWS: α (CLAMSHELL) = 0.0007 RADIANS
 α (SCRUBBING) = 0.00108 RADIANS
 MODEL TESTS WERE PERFORMED AT
 DOUBLE THESE VALUES TO ASSURE
 ADEQUATE DESIGN MARGIN

with leakage several orders of magnitude lower than conventional valve closures in use on today's rocket engine systems. This technology effort will provide the ground work input for SS/APS tradeoff studies and configuration decisions on an overall vehicle basis. It will ensure that specifications established for the APS are realistic and achievable and will provide the basis for an expeditious future engine development program.

Author's Note: The section of this report regarding design and selection of closure concepts included a brief description of Rocketdyne's rationale for use of TFE Teflon as the seal material in the Captive Plastic Closure Concept. Subsequent to the completion of contract technical effort, information regarding impact compatibility testing of TFE Teflon has been received from NASA-MSFC. Results of these high-pressure impact tests indicate zero detonations or flashes in 120 tests, thus supporting the choice of TFE Teflon as the impact-seal ring in the Captive Plastic Closure for the SS/APS valve.

Page intentionally left blank

REFERENCES

1. RPL-TDR-64-68, Rocket Engine Valve Poppet and Seat Design Data, Rocketdyne Division, Rockwell International Corporation, Canoga Park, California, May 1964.
2. Tellier, G. F.: Poppet and Seat Design Data for Aerospace Valves, AFRPL-TR-66-147, Rocketdyne Division, Rockwell International Corporation, Canoga Park, California, July 1966.
3. Tellier, G. F., et al.: Survey of Contamination in Rocket Propulsion Fluid Systems, AFRPL-TR-67-290, Rocketdyne Division, Rockwell International Corporation, Canoga Park, California, November 1967.
4. Tellier, G. F., et al.: Poppet and Seat Design Criteria for Contaminant-Particle Resistance, AFRPL-TR-70-1, Rocketdyne Division, Rockwell International Corporation, Canoga Park, California, April 1970.
5. NASA Tech Brief 67-10523. (Also, contact COSMIC, Computer Center, University of Georgia, for further information.)
6. Bauer, P.: Investigation of Leakage and Sealing Parameters, AFRPL-TR-65-153, ITT Research Institute, Chicago, August 1965.
7. Gitzendanner, L. G. and F. O. Rathburn,: Statistical Interface-Leakage Analysis and Feasibility of Superfinished Surfaces for Sealing, Contract NAS8-4012, General Electric Co., May 1965.
8. Wichmann, H.: Quarterly Progress Report for the Period of Sept. 1, 1971 through Nov. 30, 1971 for Contract NAS3-14349 Space Shuttle Auxiliary Propellant Valves, The Marquardt Co., March 1972.
9. Shapiro, A. H.: The Dynamics and Thermodynamics of Compressible Fluid Flow, Vol. 1, Ronald Press, New York 1953.
10. U. S. Patent No. 3572735, Captive Plastic Seal, Rocketdyne Division, Rockwell International Corporation, Canoga Park, California, March 1971.
11. Knudsen, J. G., et al.: Fluid Dynamics and Heat Transfer, McGraw-Hill Book Co., Inc., New York, 1958.
12. Dushman, S., et al.: Scientific Foundations of Vacuum Technique, John Wiley and Sons, New York, 1962.

Page intentionally left blank

APPENDIX A

APS VALVE CLOSURE CONCEPTS - MODEL LAYOUTS

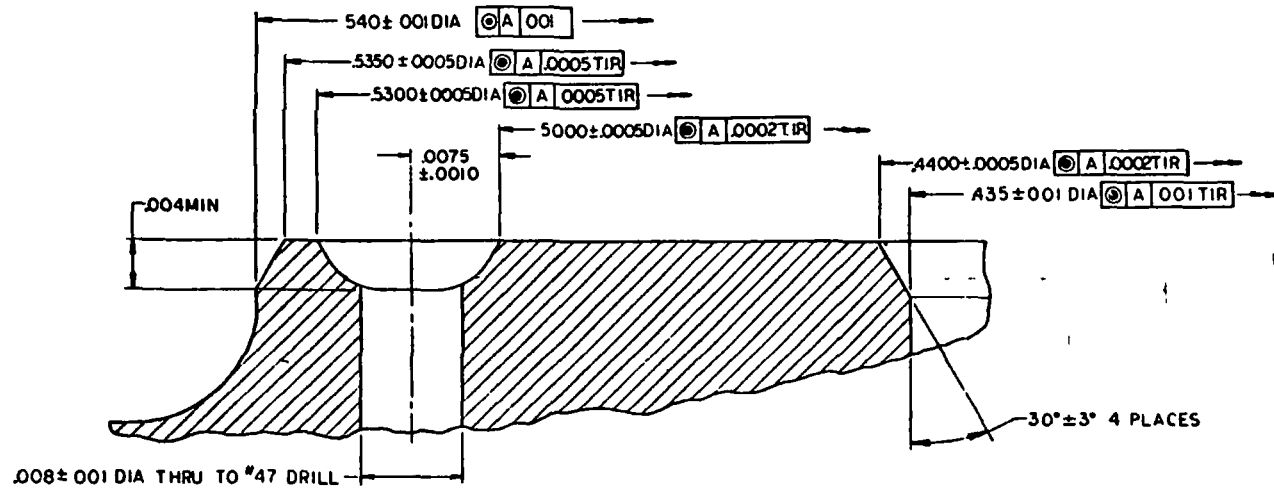
REVISONS		DATE	APP. #2
LT#	DESC. PRGM		
	1 MAY BE REWORKED	3 RECORD CHANGE	
	2 CANNOT BE REWORKED	4 MAY SHOP PRACTICE	
	5 PARTS MADE ON		
X	A		
X	1 ADDED -3		

Handwritten notes on the right margin:
 GUS
 11/10/80
 11/10/80

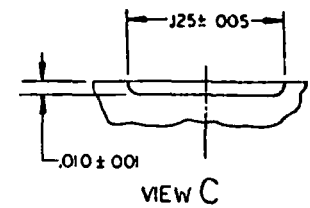
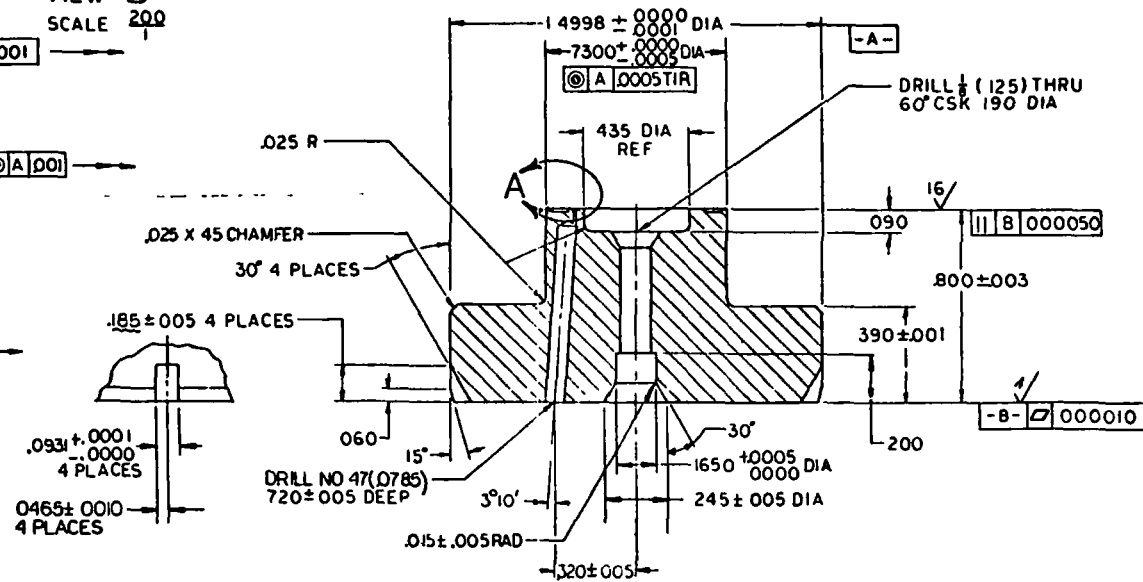
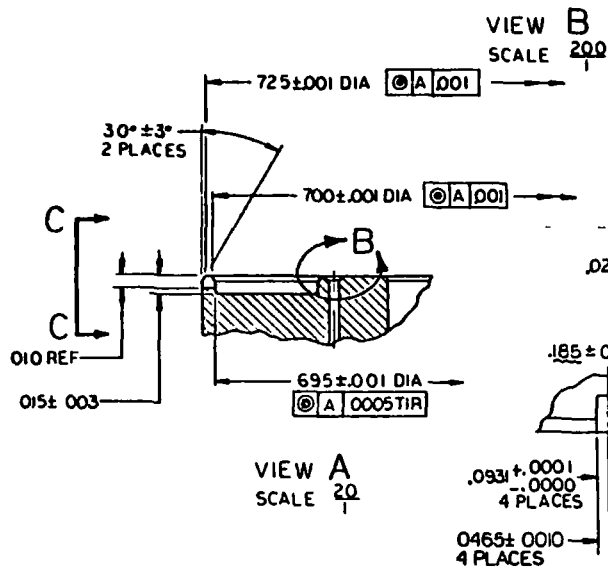
⑥ HEAT TREAT PER PF 605-14 EXCEPT MIN
FINAL TEMPER 350°F TO PRODUCE R_c58-62
⑤ CLEAN PER RA0110-C18
4 ³²/₃₂ ALL SURFACES
3 FILLET RADII 010 ± 025
2 BREAK CORNERS 001-010
1 MACHINE PER RA0103 002

NOTE: UNLESS OTHERWISE SPECIFIED

[illegible]



REVISIONS			
LTN	DESCRIPTION	DATE	APPROVED
1	1. NOT BE REWORKED		
2	2. RECORD CHANGE		
3	3. CANNOT BE REWORKED		
4	4. NOT SHOP PRACTICE		
5	5. PARTS MADE OK		



- 5 MACHINE PER RA0103-002
- 4 ALL FILLET RADII .005-.010
- 3 ALL SURFACE FINISH 32
- 2 BREAK CORNERS .001-.005
- 1 FOR NO RSOC3522X POPPET

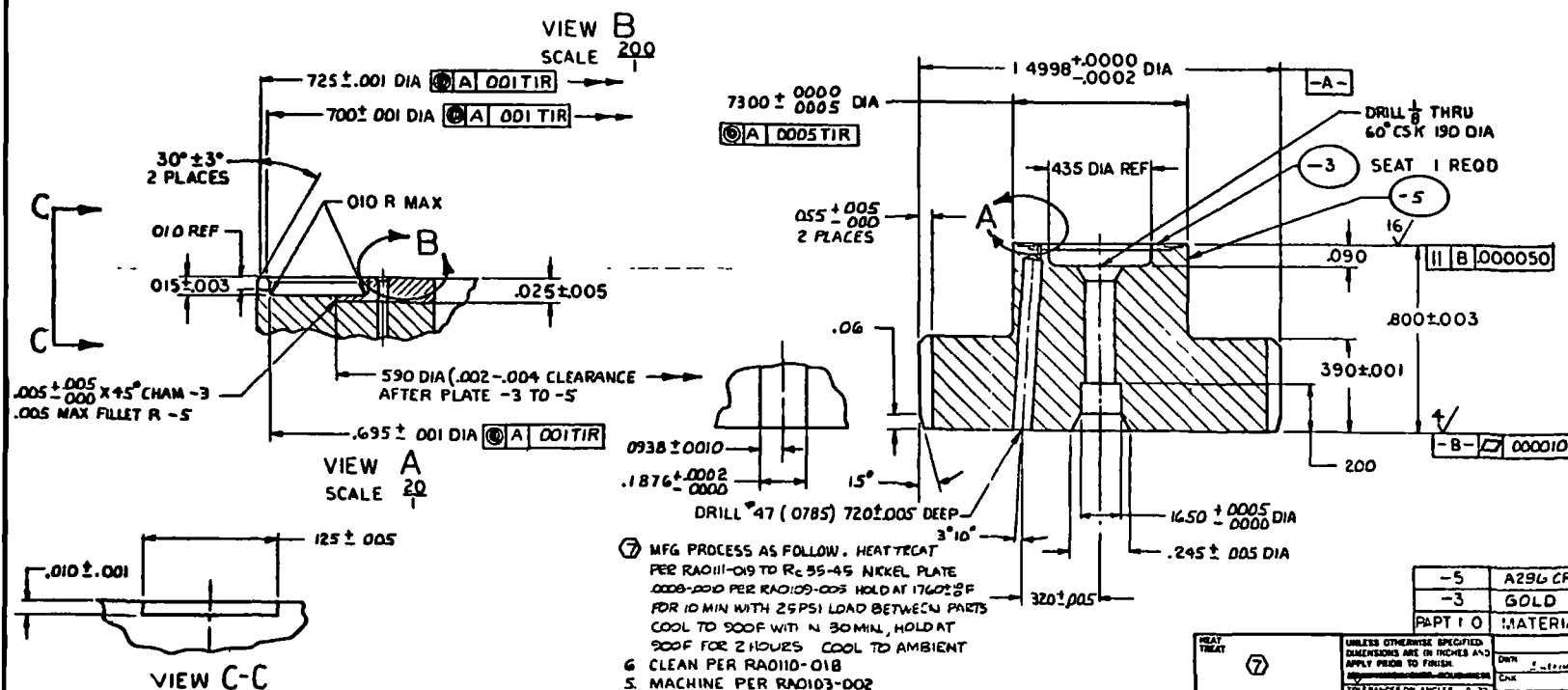
NOTE: UNLESS OTHERWISE SPECIFIED

HEAT TREAT	⑥	UNLESS OTHERWISE SPECIFIED, DIMENSIONS ARE IN INCHES AND APPLY PRIOR TO FINISH	DATE	DATE	SIGN	DATE	SCALE	FILE
FINISH	NONE	TOLERANCES ON ANGLES ± 0° 30'	MATERIAL	STRUCT	DESIGN	DATE	SCALE	FILE
MATERIAL	1 5/8 DIA X 4.00 PER 18016Q-151 (AC MILIT)	TOLERANCE	DATE	DATE	SIGN	DATE	SCALE	FILE
HEAT TREAT	⑥	UNLESS OTHERWISE SPECIFIED, DIMENSIONS ARE IN INCHES AND APPLY PRIOR TO FINISH	DATE	DATE	SIGN	DATE	SCALE	FILE
FINISH	NONE	TOLERANCES ON ANGLES ± 0° 30'	MATERIAL	STRUCT	DESIGN	DATE	SCALE	FILE
MATERIAL	1 5/8 DIA X 4.00 PER 18016Q-151 (AC MILIT)	TOLERANCE	DATE	DATE	SIGN	DATE	SCALE	FILE

- 7 CLEAN PER RA010-018
- ⑥ HEAT TREAT PER PR605-14 EXCEPT MIN FINAL TEMPER 350°F TO PRODUCE R_c 56-60

Rockwell North American Rockwell		Compass Rockwell In Greater Texas	
SEAT, FLAT 440C - CLOSURE TESTER (AFS)		SCALE 4/1	
D 02602		P3335-04	

REVISIONS				DATE	APPROVE
LEN	DESCRIPTION				
	1. MAY BE REMOVED	2. RECORD CHANGE			
	2. CANNOT BE REMOVED	4. NOW SHIP PRACTICE			
		5. PARTS SEND ON			

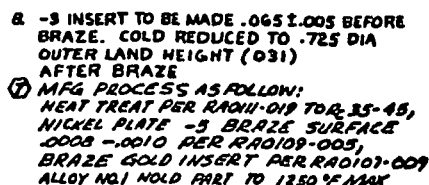
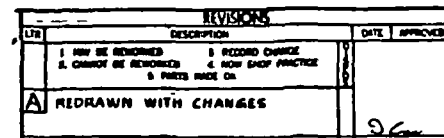


⑦ MFG PROCESS AS FOLLOW. HEAT TREAT
 PER RA0110-019 TO R. 35-45 NICKEL PLATE
 0008-000 PER RA0109-003 HOLD AT 1760±25F
 FOR 10 MIN WITH 25PSI LOAD BETWEEN PARTS
 COOL TO 500F WITH N 30MIN, HOLD AT
 500F FOR 21HOURS COOL TO AMBIENT
 6 CLEAN PER RA0110-018
 5. MACHINE PER RA0103-002
 4 ALL FILLET RA011 005-010
 3 ALL SURFACE FINISH 36/
 2 BREAK CORNERS 001-005
 1 FOR NO R5003522X POPPET

NOTE: UNLESS OTHERWISE INDICATED

-5		A296 CRES BAR	1.500 DIA X .85	AMS.5737
-3		GOLD	600 DIA X .065	LOVM 99.95 PURITY
PART 10		MATERIAL	SIZE	SPECIFICATION

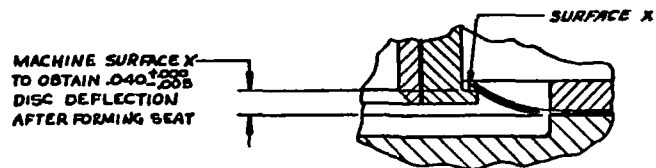
HEAT TREAT	⑦	UNLESS OTHERWISE SPECIFIED DIMENSIONS ARE IN INCHES AND APPLY FIRST TO FINISH	Rockwell C Non-Uniform Rockwell Country Park, California McGregor Tools
FINISH		TOLERANCES ON ANGLES = 0° ± 30' DECIMALS AS ± .01 AS ± .005 HOLES NOTED "H"	DWN <i>Engr</i> DATE DATE
NONE		OVER THRU TOLERANCE .000 + .0015 - .0015 .000 + .0015 - .0015 .1300 + .0015 - .0015 1.300 .2760 + .0045 - .0045 .2760 .8000 + .0040 - .0040 .5500 .7500 + .0070 - .0070 .7500 1.0000 + .0070 - .0070 1.0000 2.0000 + .0120 - .0120	DESGN STA. CT <i>51</i>
MATL	NOTED	DO NOT SCALE PRINT	SEAT, FLAT GOLD - CLOSURE - LASTER (MPS)
			1-1 ACTIVITY APMD DATE 1-1
			1-12 COLE IDENT NO D 02602
			CRANK NO. P0000021A
			SCALE 1:1 1/4"



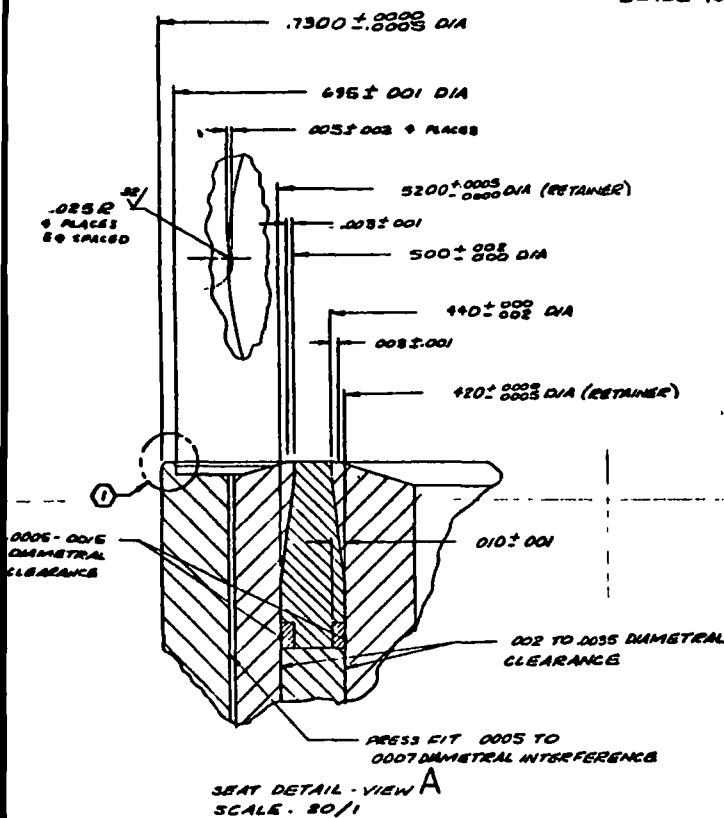
6. CLEAN PER RADIO-010
5. MACHINE PER RADIOS-002
4. ALL FILLET RADII .005-.010
3. ALL SURFACE FINISH $\frac{32}{\sqrt{}}$
2. BREAK CORNERS .001-.005
1. FOR NO R5003522X POPPET

100% LOW-CARB CARBONATED BEVERAGE

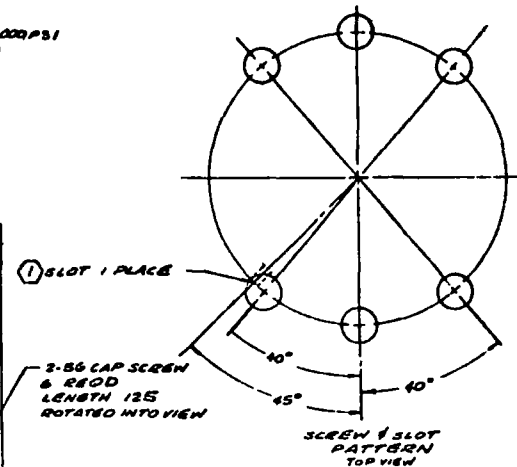
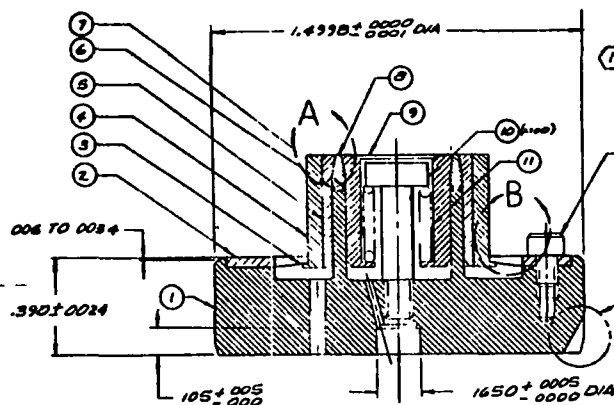
[illegible]



VIEW B
SCALE 10/1



HELICAL SPRING DATA
 O.D. .275 STRESS AT SOLID HT: 200,000 PSI
 I.D. .185 INSTALLATION HEIGHT: .809
 MATL: EL6140Y LOAD: 20 LB
 WIRE DIA: .045 RATE: 103 LB/IN
 ACTIVE COILS: 4 FREE HEIGHT: .503
 TOTAL COILS: 6
 SOLID HEIGHT: .270
 LOAD 24 LB



NO	DESCRIPTION	MATERIAL	QTY	REMARKS
11	SPRING, HELICAL	EL6140Y RBO170-097	MPS111001	PHYS1400V
10	SCREW	303 CRES CONL- DIC #414	(E)	PHYS1400V
9	RETAINER, INNER	INCOV8L 718 RBO170-101	RAD111-019	PHYS1400V
8	SEAL	TEFLON, TFE RBO130-008	-	PHYS1400V
7	RING, INNER	B3RILLIUM COPPER CONC A, CO-C-530	-	PHYS1400V
6	RING, OUTER	B3RILLIUM COPPER CONC A, CO-C-530	-	PHYS1400V
5	RETAINER, OUTER	INCOV8L 718 RBO170-101	RAD111-019	PHYS1400V
4	CYLINDER	INCOV8L 718 RBO170-101	RAD111-019	PHYS1400V
3	DISC	INCOV8L 718 (002 PM) CONC HT 00 C 533	R, 40-46	PHYS1400V
2	CLAMP	303 CRES CONC S 763	-	PHYS1400V
1	SEAT	440C CRES RBO160-151	R, 56-60	PHYS1400V
NO	DESCRIPTION	MATERIAL	QTY	REMARKS

2 REDUCE REOD THICKNESS AS SHOWN
 1 DETAIL AS SHOWN ON DWG RS008520X

HEAT TREAT	UNLESS OTHERWISE SPECIFIED DIMENSIONS ARE IN INCHES AND APPLY PRIOR TO FINISH TOLERANCES ON ANGLES ± 1° UNLESS OTHERWISE SPECIFIED	DATE	DATE
FINISH	100/ MACH SURF ROUGHNESS TOLERANCES ON ANGLES ± 1° UNLESS OTHERWISE SPECIFIED	DATE	DATE
MATL	100/ MACH SURF ROUGHNESS TOLERANCES ON ANGLES ± 1° UNLESS OTHERWISE SPECIFIED	DATE	DATE

DO NOT SCALE PRINT

Rockwell
North American Products
Chicago, Ill. 60604

TEST MODEL 4-51-11
PLASTIC SEAL

SIZE CODE IDENT NO. DRAWING NO.
02602
HSC005641

SCALE 1/1

FORM	DATE	DESCRIPTION	DATE	APPROVED
1	1	1	1	1
2	2	2	2	2
3	3	3	3	3
4	4	4	4	4
5	5	5	5	5



- NOTE: UNLESS OTHERWISE SPECIFIED

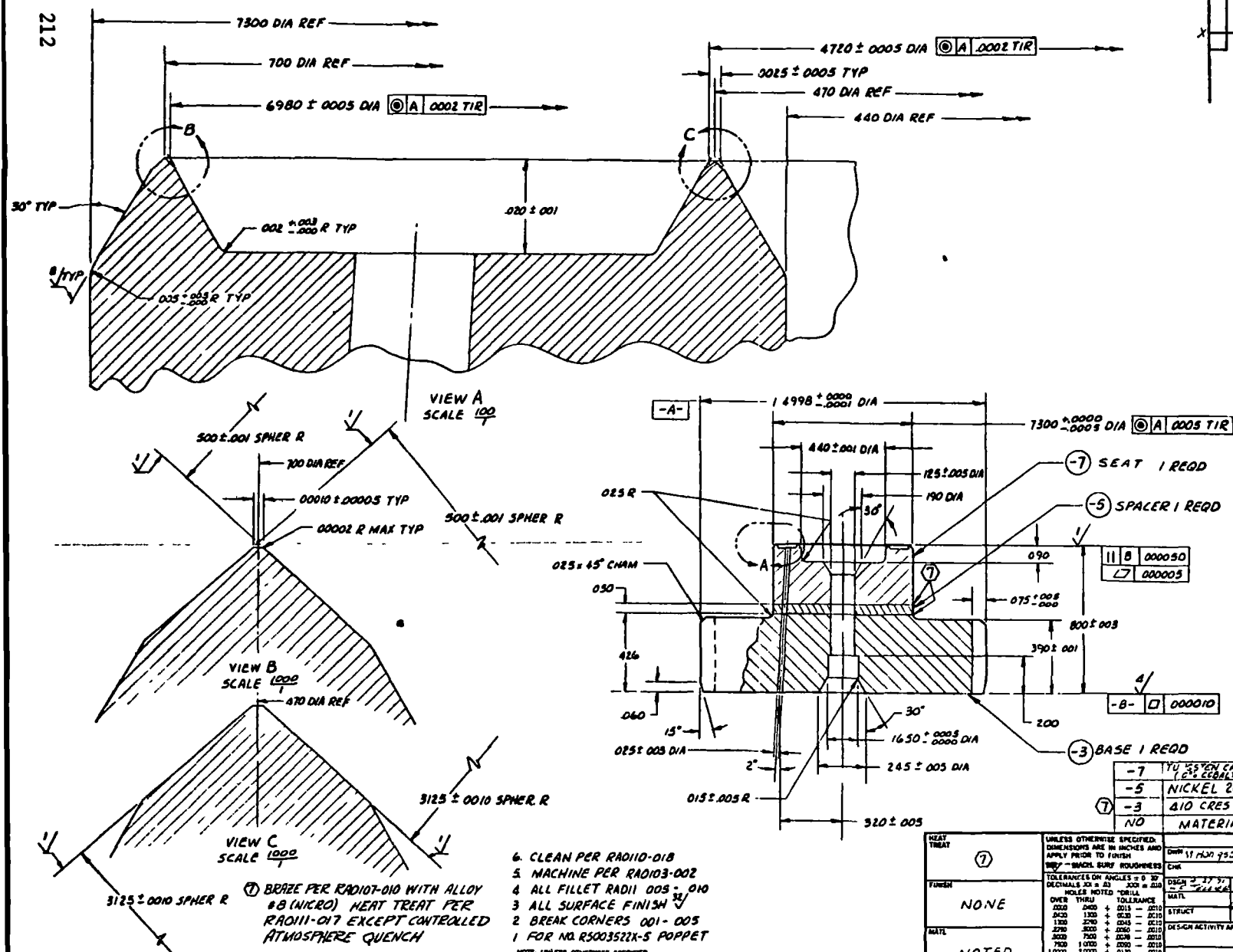
-7	440C (REF)	—	MALC = L.A. C-2-34221-3
-5	TUNGSTEN CARBIDE	76 DIA x .180	CONVEE. AC C-2A-3A
-3	TUNGSTEN CARBIDE	—	GE 303
PAR 12	11-2 A	SIZE	SPECIFICATION

[illegible]



NOTE: UNLESS OTHERWISE SPECIFIED

211



6. CLEAN PER RADIO-018
5. MACHINE PER RADIO-002
4. ALL FILLET RADII 005 - 010
3. ALL SURFACE FINISH $\frac{32}{\sqrt{16}}$
2. BREAK CORNERS 001 - 005
1. FOR NO. R5003522X-5 POPPET

NOTE: UNLESS OTHERWISE SPECIFIED

NOTE: UNLESS OTHERWISE SPECIFIED

MEAT TUNISH	UNLESS OTHERWISE SPECIFIED: DIMENSIONS ARE IN INCHES AND APPLY PRIOR TO FINISH ✓ - BANGS BURY ROUGHNESS	DATE 11 JUN 75 (07)	DATE 7	Rockwell North American Rockwell	Copyright © 1975 McGraw-Hill
⑦		CHK	DATE		
FRESH	TOLERANCES OF ANGLES = 30° ± 30° DECIMALS: 20 ± 20 HOLE NOTED "DRILL OVER THRU TOLERANCE 2400 ± 0.015 ± 0.010 2400 1200 ± 0.010 ± 0.010 1300 2700 ± 0.015 ± 0.010 2700 3000 ± 0.005 ± 0.010 3000 7500 ± 0.010 ± 0.010 7500 1.0000 ± 0.005 ± 0.010 1.0000 2.0000 ± 0.010 ± 0.010	DATE 27 75 N/A N/A		SEAT, FLAT SHARP CAGE DE - CLOSURE TESTER (APS)	
NONE		STRUCT			
DATE		DESIGN ACTIVITY APVD	DATE	SIZE D 02602	LEARNING NO. FSD033765X
NOTED	DO NOT SCALE PRINT			SCALE	1-INCH

APPENDIX B

SIMPLIFIED DESCRIPTION OF CLOSURE SCREENING TESTER OPERATION

APS CLOSURE TESTER

Purpose

The APS closure tester was designed to provide a research tool with which to investigate fundamental parameters affecting the cyclic life and sealing performance of valve seats and poppets. The tester provides the capabilities of varying impact loading of the poppet on the seat, while controlling the amount of relative motion between the sealing interfaces of the seat and poppet. This relative motion can be varied in three modes that will be discussed later. The net result of a given impact load at a given interface motion is wear of the sealing interface, and this wear is then translatable to valve seat and poppet cyclic life and sealing capability.

Description and Function

The APS closure tester is basically a hydrostatic bearing (although the bearing fluid used is a gas) which provides precisely controlled axial movement of the central piston in a near-frictionless manner. At one end of the piston, a valve poppet is mounted in near proximity to a valve seat while, at the other end of the piston, pneumatic pressure may be applied to drive the poppet into contact with the seat in a controlled impact. The valve poppet is carried in a poppet holder on the end of the piston; it is this poppet holder that allows the use of one of three modes of interface motion between the seat and the poppet. Refer to Fig. B-1 for a schematic representation of the APS closure tester.

The tester may be operated as shown in Fig. B-1; that is, with the poppet clamped by the poppet holder set screws so that the poppet interface is parallel with the seat interface. This is called the clamped mode, producing no relative interfacial motion between the seat and the poppet. Any wear produced is the result of impact forces sufficiently high to create Poissons stress deformations in the mating surfaces.

The next mode of operation is illustrated in Fig. B-2, and is called the clamshell (or hinge) mode. In this operation, only the poppet holder set screws nearest the seat-poppet interface are in contact with the poppet. A spring provides a small cocking load to the poppet, causing the poppet-wobbler combination to roll, with the center of the rotation being at the plane of the poppet holder set screws nearest the seat-poppet interface. When control pressure is applied to the piston, the poppet is moved into contact with the seat; further motion being the rotation of the poppet interface into full contact with the seat interface. If the plane of the set screws exactly matched the poppet interface plane, true clamshell or hinging action would occur, with no relative interfacial motion. In the APS closure tester, physical size limitations dictate a set screw plane slightly below the poppet interface so that a small relative interfacial motion is produced when the poppet-seat closure is effected. Thus, a small component of the closing impact is expended in interface motion, producing wear of the seat-poppet interfaces.

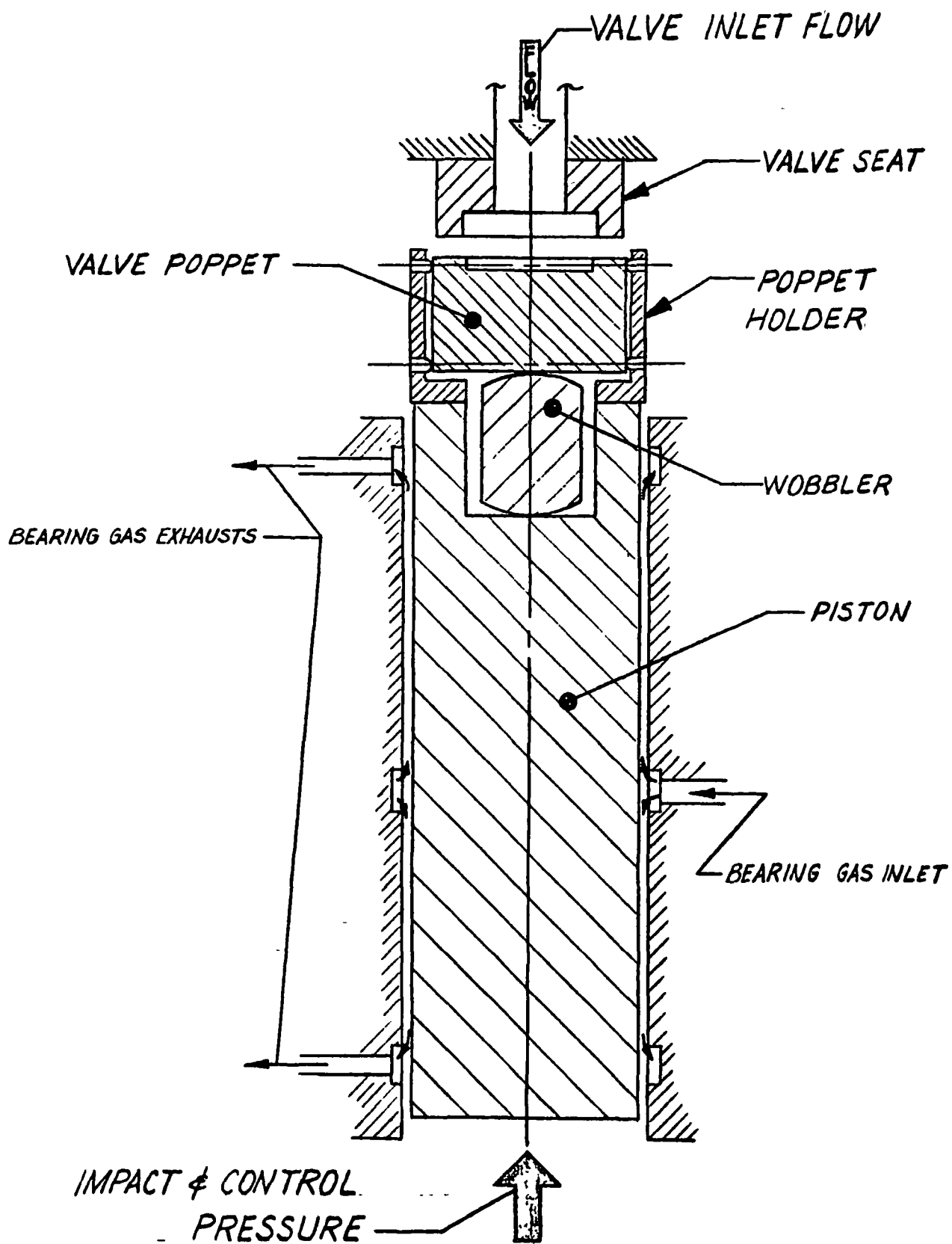


Figure B-1

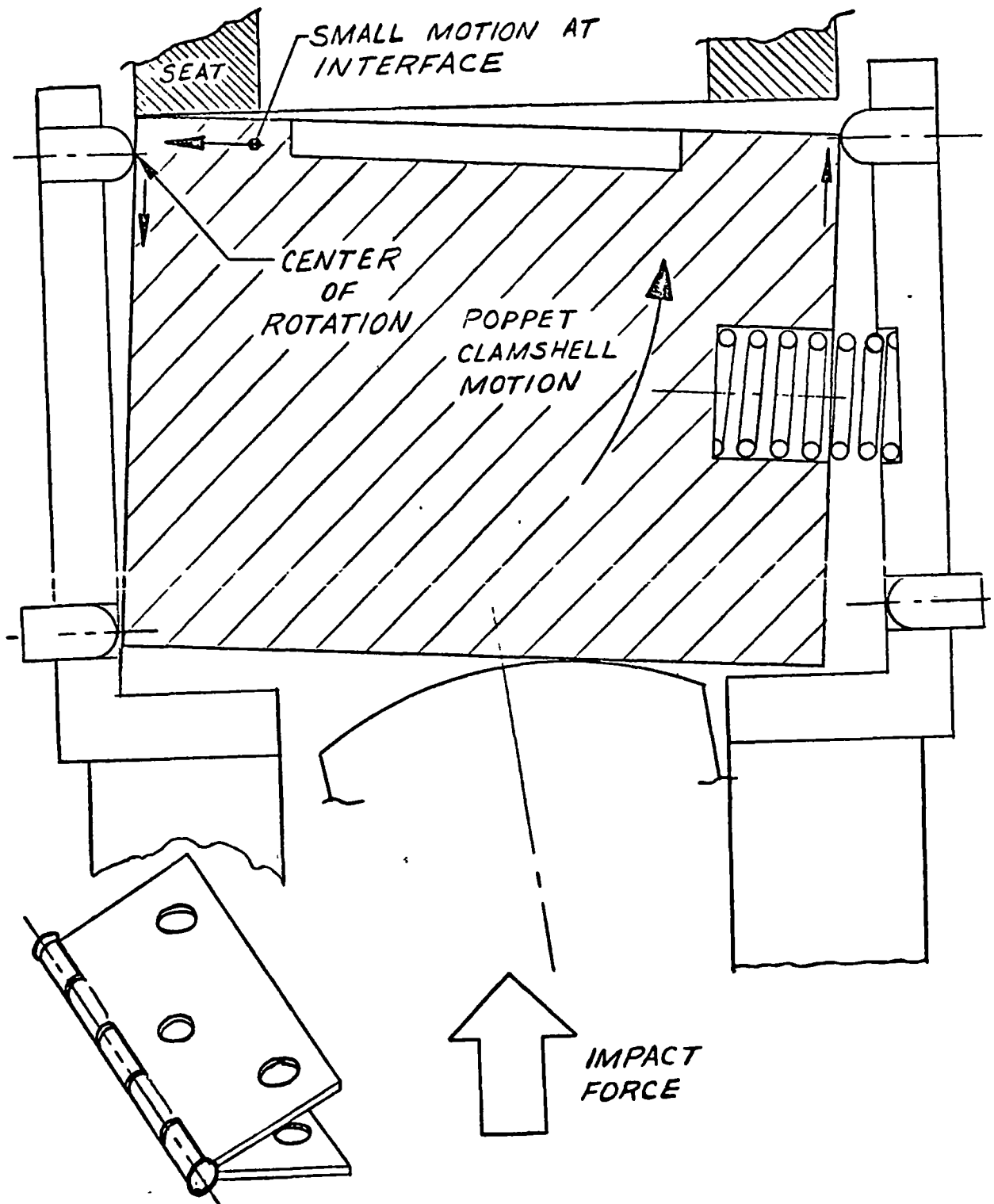


Figure B-2.

The third mode of operation (Fig. B-3) is called the scrubbing mode because it produces a much greater degree of relative motion between the seat-poppet interfaces as they are caused to close. In this mode, the poppet holder set screws farthest from the poppet interface contact the poppet, forcing the poppet-wobbler combination to roll (the center of rotation being at the plane of the poppet holder set screws farthest from the poppet interface). As before, a spring provides a small cocking load to the poppet. When control pressure is applied to the piston, the poppet is caused to contact the seat on one side first, the remaining motion being a combination scrubbing-sliding and rotational motion until the seat-poppet interfaces are in full contact. A larger component of the impact force is expended in interface motion, thus producing wear.

These features, then enable the testing of various material combinations, variations in impact loading, variations in rate of cycling, and control of the physical amount of relative interfacial motion. Correlation of these parameters allow an assessment of wear, cyclic life capability, and sealing performance. The tester is designed to allow direct measurement of the sealing performance at any point desired in the cyclic testing of a valve poppet and seat.

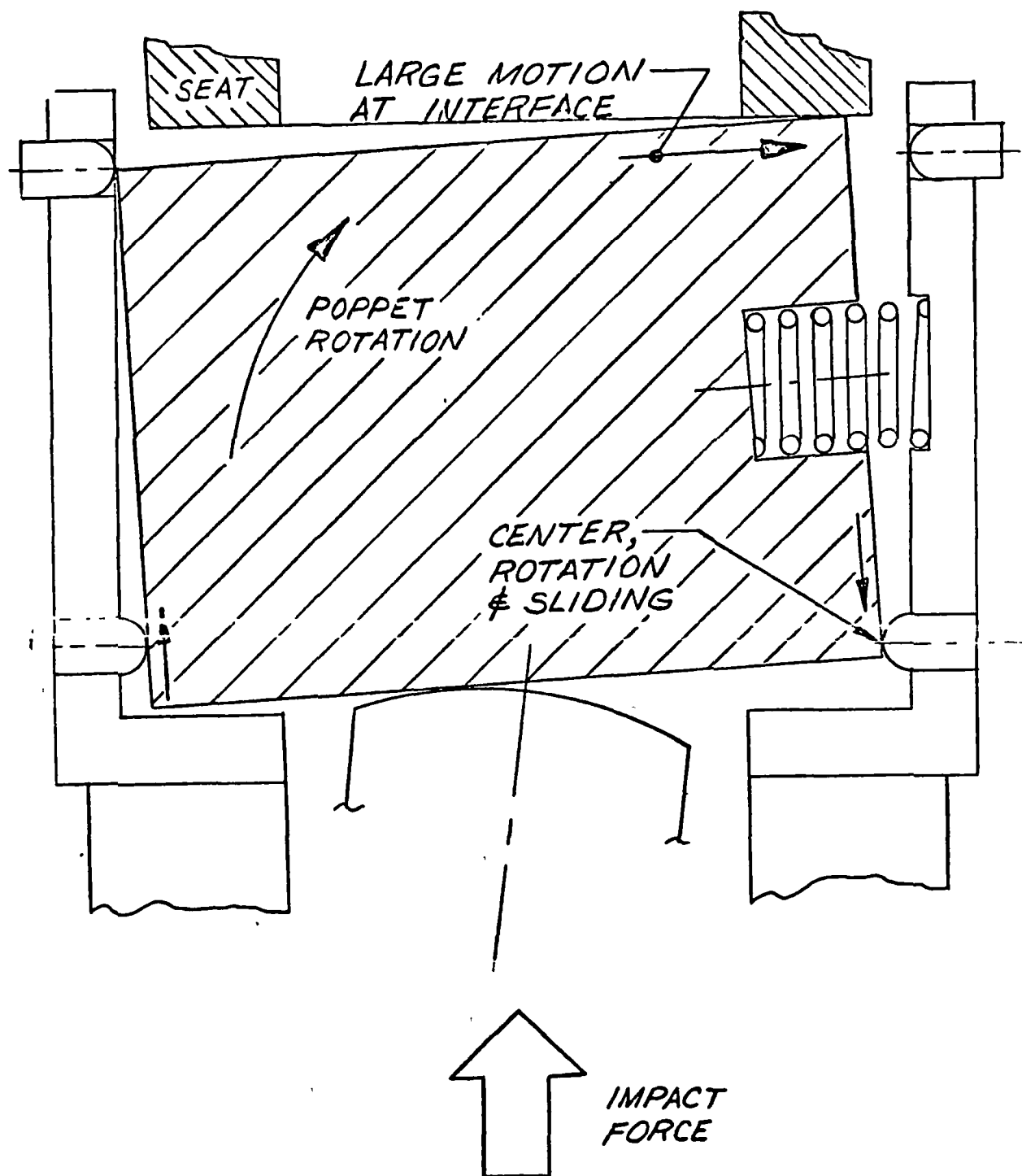


Figure B-3.

Page intentionally left blank

APPENDIX C

LAMINAR FLOW LEAKAGE CORRELATION

Experience with metal-to-metal valve seating (Ref. C-1) has shown that the predominant mode of valve seat leakage flow is laminar. Assuming a constant leak path geometry, leakage correlation of various fluids under a variety of conditions can be obtained by direct ratio between calculated leakage rates. Data published herein are computed for nitrogen, helium, hydrogen, and oxygen, and extend data published in Ref. C-2.

Real (computed) fluid properties were obtained from plots of Ref. C-3. Figures C-1 through C-4 display computed leakage data for a family of temperatures versus pressure for various fluids. Note that these curves define the state of the fluid (liquid or gas) flowing across the gap at a specific isothermal temperature (Ref. C-2 used saturated gas or liquid temperatures). The equations used, however, convert the leakage rates to the gaseous state at standard conditions (i.e., scim, cubic inches per minute at 14.7 psia, and 70 F), whether the leaking fluid is gas or liquid. Figure C-5 displays leakage ratios between helium gas at -320 F and liquid nitrogen at -320 F, hydrogen gas at -360 F, and liquid oxygen at -270 F for inlet pressures of 115 to 10,015 psia. It should be emphasized that the leak ratios are the leaking fluid converted to standard conditions (scim/scim). Any reference to temperature and fluid state refers to the fluid flowing across the gap. Figure C-5 also includes a plot of the leak ratio between helium leakage at -320 F and helium leakage at 70 F which provides for correlation with room temperature helium leakage.

Data for Fig. C-1 through C-4 are given in Table C-I. Real (computed) fluid properties were obtained from plots of Ref. C-3 at the average leak pressure $(P_1 + P_2)/2$. Data for Fig. C-5 are presented in Table C-II.

A summary of the derivation of the pertinent flow equations (presented in detail in Ref. C-2), together with a sample calculation, is presented below.

I. Flow Equations (See Ref. C-2 for detailed development).

The laminar flow equation for parallel plates is given by:

$$\omega = \frac{\rho W h_p^3 (P_1 - P_2)}{12 \mu L}$$

Where W , h_p , and L are determined by the leak path geometry, and ω is the mass leakage flow. The fluid properties ρ and μ are assumed to be taken at the average leakage pressure. Translating ω into an equivalent volumetric flow at standard temperature (70 F) and pressure (14.7 psia) yields an expression for volumetric leakage across the gap in scim, Q_s , as follows:

$$Q_s = \frac{\omega}{\rho_s}$$
$$\therefore Q_s = \frac{\rho W h_p^3 (p_1 - p_2)}{12 \mu L \rho_s}$$

where

ρ and ρ_s are given in lb/in.³

W , h_p , and L are given in inches

μ is given in lb-min/in.²

p_1 and p_2 are given in psia

The datum leak path specified the following geometry:

Seat Diameter, $D_s = W/\pi = 0.470$ inch

Parallel Plate gap, $h_p = 10 \times 10^{-6}$ inches

Leak Path Length, $L = 0.030$ inch

Substituting these in the above equation yields:

$$Q_s = \frac{4.1 \times 10^{-15} \rho (P_1 - P_2)}{\mu \rho_s} \quad (C-1)$$

If the assumption of a perfect gas is made, Eq. C-1 may be rewritten as follows:

$$\rho = \rho_{ave} = \frac{P_{ave}}{RT} = \frac{P_1 + P_2}{2} \cdot \frac{1}{RT}$$

$$\rho_s = \frac{P_s}{RT_s} = \frac{14.7}{R(530)}$$

$$\frac{\rho}{\rho_s} = \frac{(530) (P_1 + P_2)}{2 P_s T}$$

$$Q_s = \frac{(4.1 \times 10^{-15}) (5.3 \times 10^2) (P_1^2 - P_2^2)}{2 (14.7) \mu T}$$

$$Q_s = \frac{7.4 \times 10^{-14} (P_1^2 - P_2^2)}{\mu T} \quad (C-2)$$

Equation C-1 was used to calculate the leakage flow shown in Fig. C-1 through C-4. Equation C-2, accurate within the validity of the perfect gas assumption, was used to check the calculations, as applicable.

II. Sample Calculation

Fluid: Helium

Temperature: 70 F, 530 R

Pressure: $P_1 = 3015$ psia, $P_2 = 15$ psia, $P_{ave} = 1515$ psia

From Table C-1:

$$\rho = 5.85 \times 10^{-4} \text{ lb/in.}^3$$

$$\mu = 4.70 \times 10^{-11} \text{ lb-min/in.}^2$$

$$\rho_s = 0.0599 \times 10^{-4} \text{ lb/in.}^3 \text{ (from Ref. C-2)}$$

Using Eq. C-1:

$$Q_s = \frac{(4.1 \times 10^{-15}) (5.85 \times 10^{-4}) (3 \times 10^3)}{(4.7 \times 10^{-11}) (5.99 \times 10^{-6})}$$

$$Q_s = 25.6 \text{ scim}$$

Using Eq. C-2:

$$Q_s = \frac{(7.4 \times 10^{-14}) (3.03 \times 10^3) (3 \times 10^3)}{(4.70 \times 10^{-11}) (5.30 \times 10^2)}$$

$$Q_s = 27.0 \text{ scim}$$

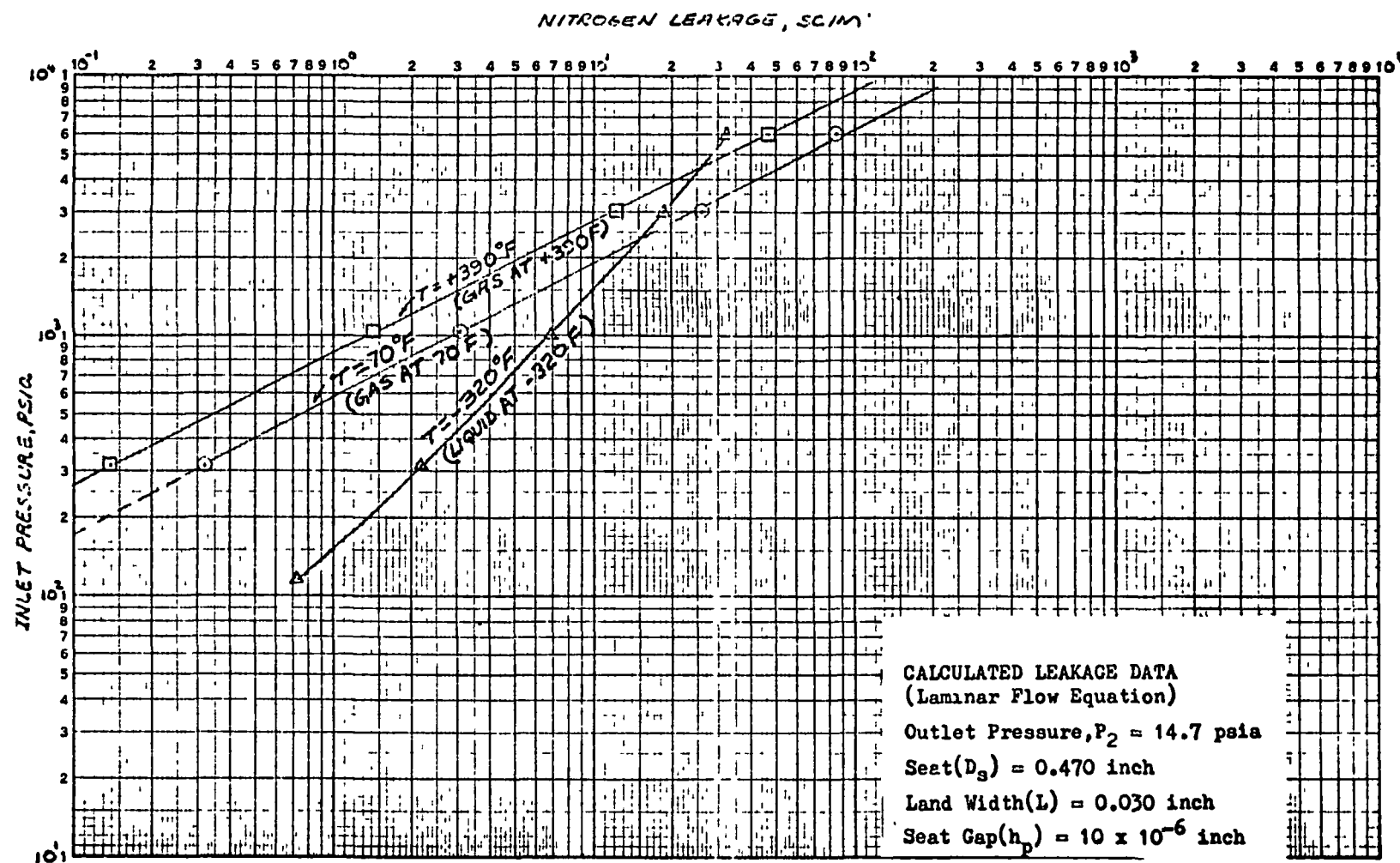


Figure C-1. Nitrogen Leakage

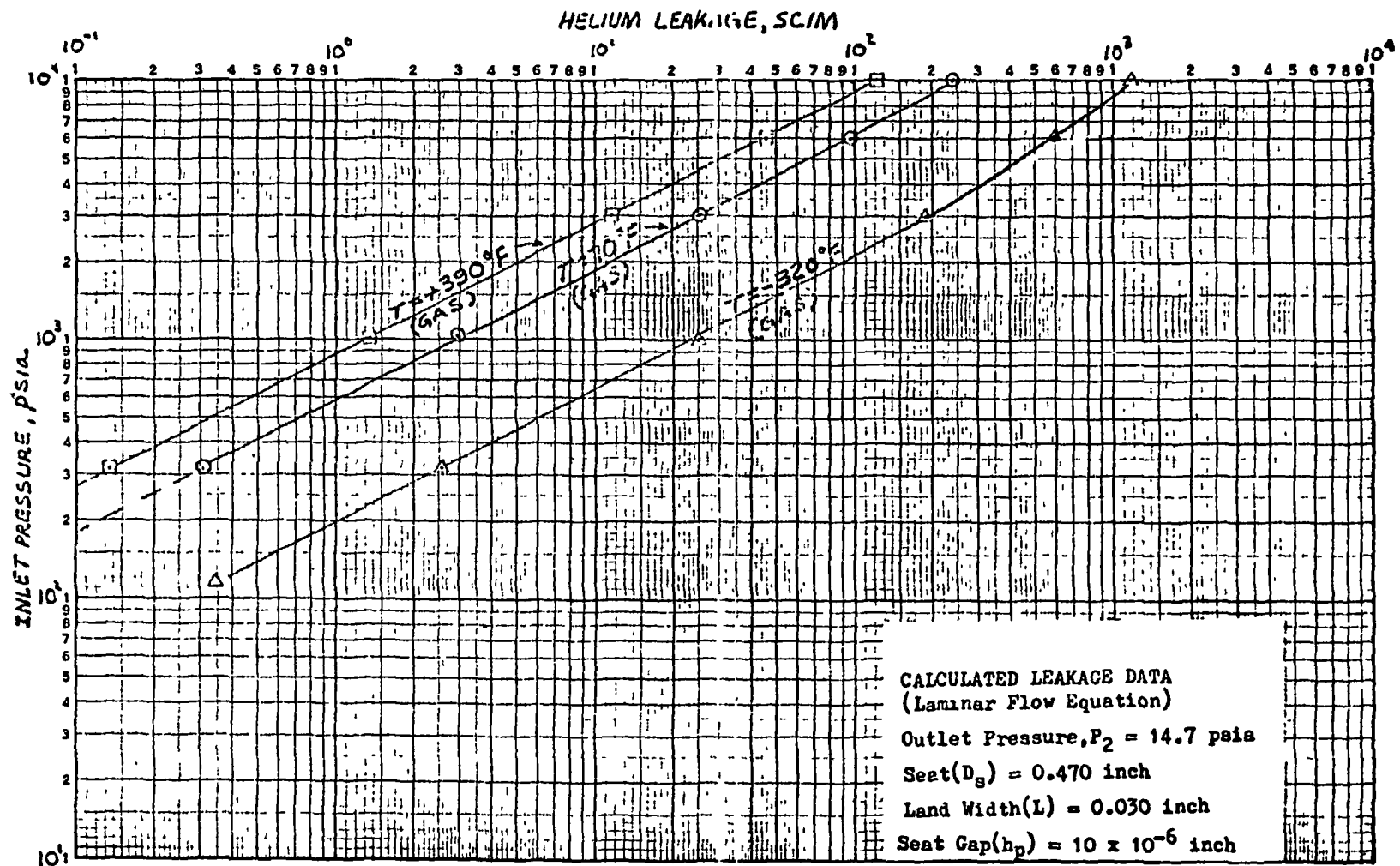


Figure C-2. Helium Leakage

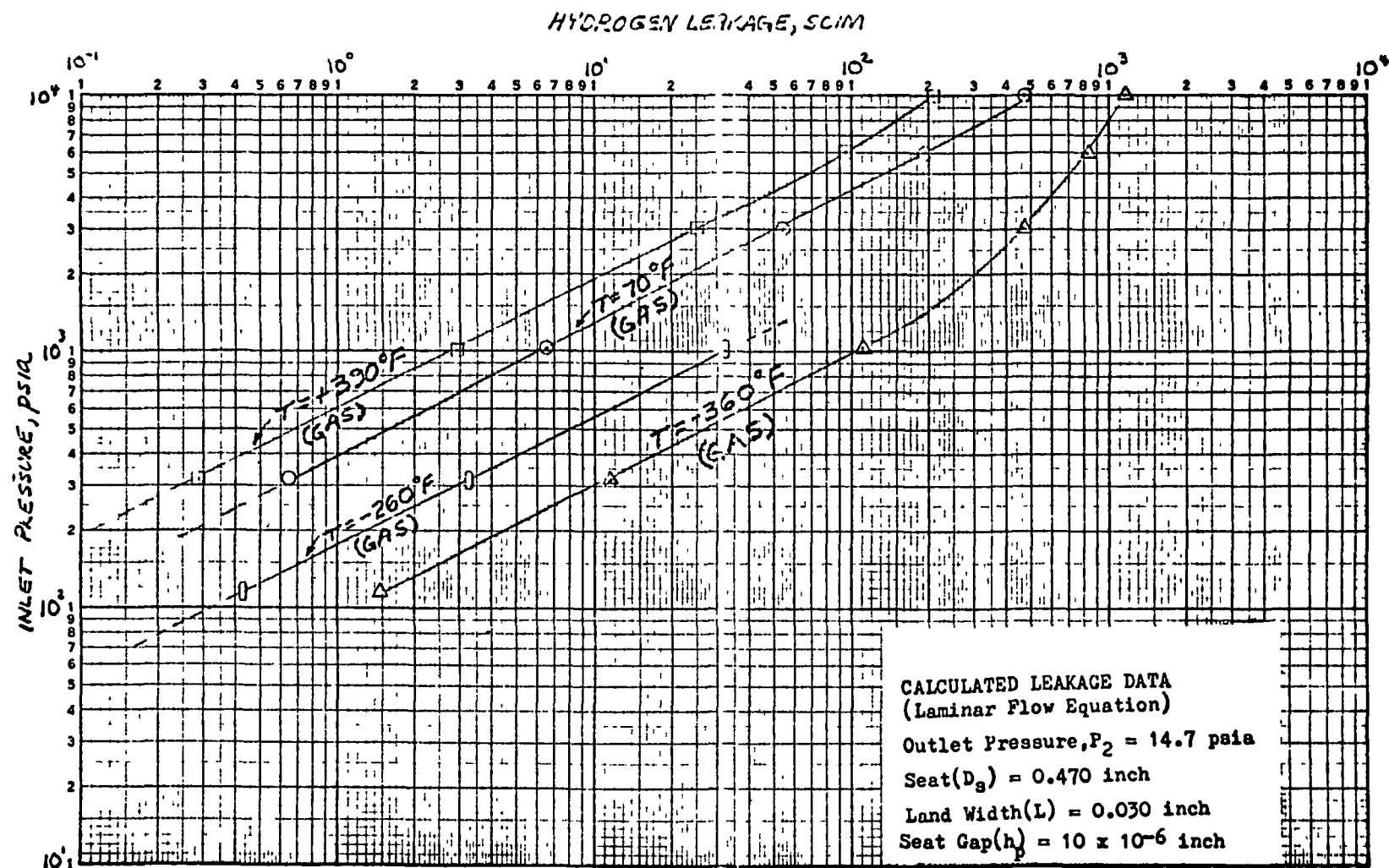


Figure C-3. Hydrogen Leakage

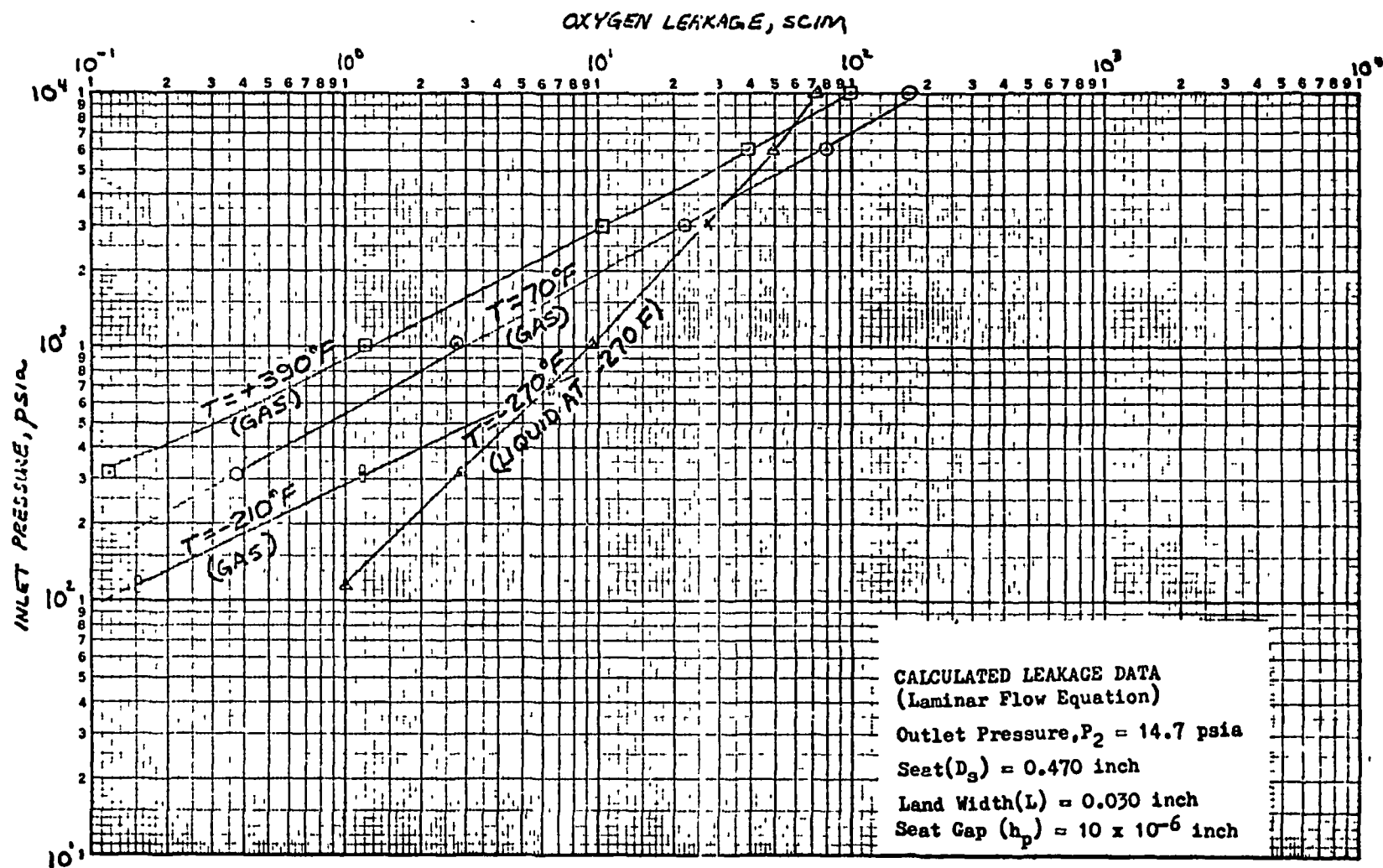


Figure C-4. Oxygen Leakage

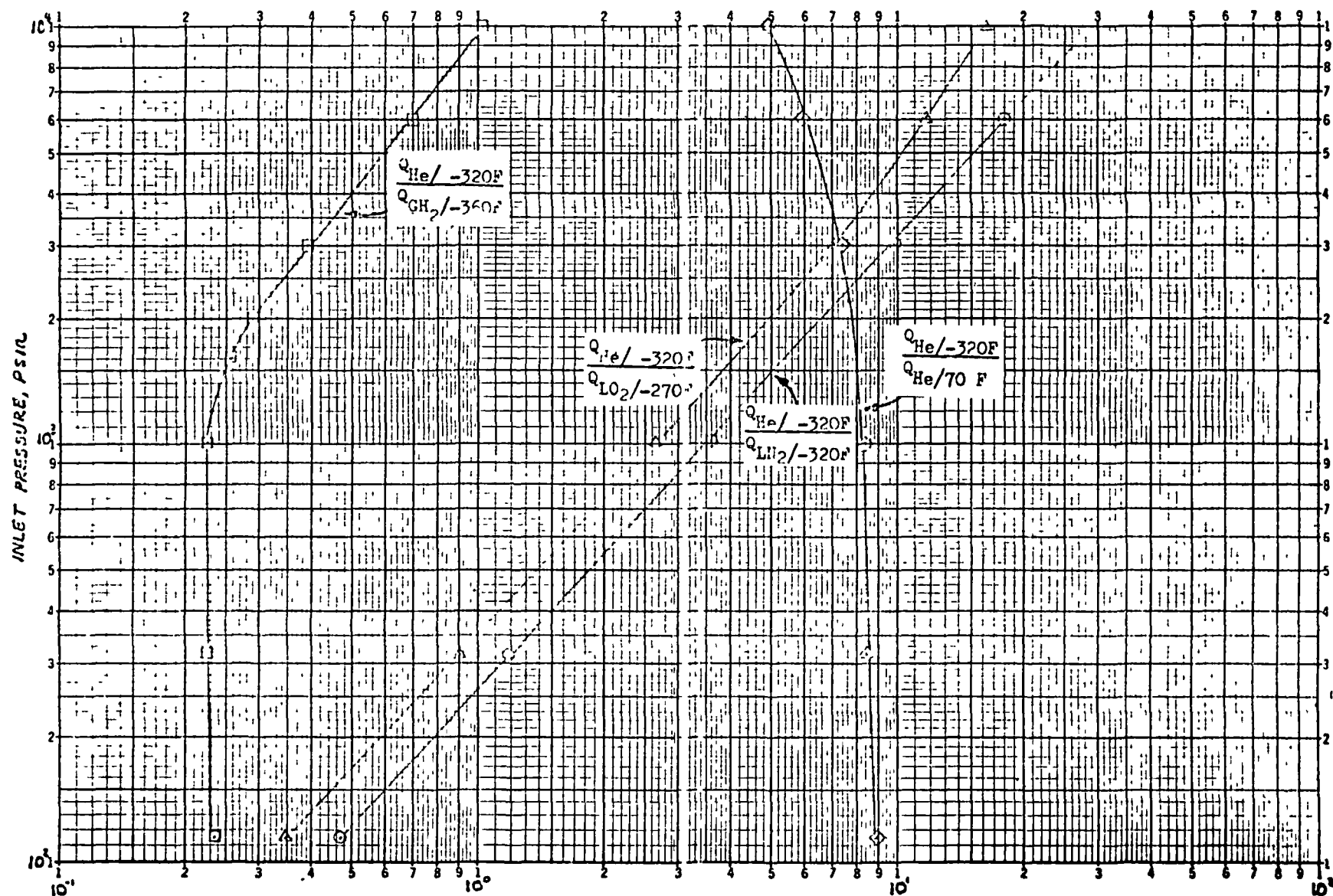


Figure C-5. Leakage Ratio, $Q_{\text{helium}}/Q_{\text{fluid}}$ (scim/scim)

TABLE C-I

FLUID	INLET PRESSURE (PSIA)	TEMPERATURE		GAS		LIQUID		LEAKAGE	
		°F	°R	ρ	μ	ρ	μ	Q_L	Q_R
				(FLUID PROPERTIES TAKEN AT P_A)					
NITROGEN	315	70	530	^{.61} 4.7	4.32	-	-	.320	-
	($P_A=165$)	-320	140	-	-	^{50.4} 292	39	-	2.2
		+390	850	2.93	6.2	-	-	.139	-
	1015	70	530	^{2.5} 14.5	4.62	-	-	3.08	-
	($P_A=515$)	-320	140	-	-	^{50.8} 294	41.5	-	6.94
		+390	850	9.13	6.3	-	-	1.42	-
	3015	70	530	^{74.5} 43.1	4.82	-	-	26.3	-
	($P_A=1515$)	-320	140	-	-	^{57.7} 299	46.5	-	18.9
		+390	850	26.9	6.5	-	-	12.2	-
	6015	70	530	¹⁴¹ 81.6	5.65	-	-	85.0	-
	($P_A=3015$)	-320	140	-	-	^{57.9} 306	56.0	-	32.2
		+390	850	53.5	6.75	-	-	46.7	-
HELIUM	315	70	530	^{.47} .70	4.70	-	-	.306	-
	($P_A=165$)	-320	140	^{.43} 2.5	1.98	-	-	2.59	-
		+390	850	^{213.5} .42	6.35	-	-	.136	-
	1015	70	530	^{.355} 2.05	4.70	-	-	2.99	-
	($P_A=515$)	-320	140	^{.3} 7.5	2.05	-	-	25.0	-
		+390	850	^{.317} 1.26	6.35	-	-	1.35	-
	3015	70	530	^{.101} 5.85	4.70	-	-	25.6	-
	($P_A=1515$)	-320	140	^{.24} 19.7	2.15	-	-	188.2	-
		+390	850	^{.63} 3.64	6.35	-	-	11.8	-
	6015	70	530	^{.141} 11.1	4.71	-	-	96.8	-
	($P_A=3015$)	-320	140	^{.5.8} 33.6	2.38	-	-	580.	-
		+390	850	^{.1.23} 7.12	6.35	-	-	46.0	-
	10015	70	530	^{.1.39} 17.0	4.83	-	-	241	-
	($P_A=5015$)	-320	140	^{.12} 47.5	2.72	-	-	1195	-
		+390	850	^{.1.46} 11.3	6.35	-	-	121	-

* Number in upper left represents density in lbs/ft³

ρ , density, given in lb/in³ $\times 10^4$

μ , viscosity, given in lb-min/in² $\times 10^{11}$

$$\text{NOTE: } P_A = \frac{P_1 + P_2}{2}$$

TABLE C-I (Continued)

FLUID	INLET PRESSURE (PSIA)	TEMPERATURE		GAS		LIQUID		LEAKAGE	
		°F	°R	* ρ	μ	* ρ	μ	Q_1	Q_2
				(FLUID PROPERTIES TAKEN AT P_A)					
HYDROGEN	115	-260	200	^{.061} 0.35	1.11	-	-	0.43	-
	($P_A=65$)	-360	100	^{.124} 0.72	0.67	-	-	1.46	-
	315	70	530	^{.658} 0.34	2.15	-	-	.646	-
	($P_A=165$)	-360	100	^{.33} 1.91	0.68	-	-	11.5	-
		+390	850	^{.820} .208	2.95	-	-	.289	-
		-260	200	^{.151} .89	1.12	-	-	3.24	-
	1015	70	530	^{.178} 2.05	1.03	-	-	6.5	-
	($P_A=515$)	-360	100	^{.116} 7.5	6.70	-	-	11.0	-
		+390	850	^{.11} 1.26	.637	-	-	2.92	-
		-260	200	^{.47} 2.70	1.15	-	-	32.0	-
	3015	70	530	^{.51} 2.95	2.21	-	-	54.5	-
	($P_A=1515$)	-360	100	^{.30} 17.4	1.48	-	-	480.	-
		+390	850	^{.32} 1.85	3.0	-	-	25.2	-
	6015	70	530	^{.94} 5.44	2.3	-	-	193.3	-
	($P_A=3015$)	-360	100	^{.40} 23.0	2.26	-	-	832.	-
		+390	850	^{.15} 3.56	3.07	-	-	94.6	-
OXYGEN	115	-210	250	^{.61} 4.7	2.65	-	-	.151	-
	($P_A=65$)	-270	190	^{.111} 6.42	2.10	^{.653} 378.	32.0	.260	1.00
	315	70	530	^{.93} 5.4	5.0	-	-	.276	-
	($P_A=165$)	-270	190	-	-	^{.662} 383	34.0	-	2.87
		+390	850	3.37	7.25	-	-	.119	-
		-210	250	^{.21} 12.7	2.75	-	-	1.178	-
	715	^{.58} 33.6	250	^{.58} 33.6	3.08	-	-	6.5	-
	1015	70	530	^{.292} 16.9	5.25	-	-	2.74	-
	($P_A=515$)	-270	190	-	-	^{.667} 386	34.4	-	9.5
		+390	850	10.5	7.4	-	-	1.20	-

* Number in upper left represents density in lbs/ft³

ρ , density, given in lb/in³ x 10⁴

μ , viscosity, given in lb-min/in² x 10¹¹

$$P_A = \frac{P_1 + P_2}{2}$$

TABLE C-I (Concluded)

FLUID	INLET PRESSURE (PSIA)	TEMPERATURE		GAS		LIQUID		LEAKAGE	
		°F	°R	* ρ	μ	* ρ	μ	Q ₁	Q ₂
				(FLUID PROPERTIES TAKEN AT P _A)					
OXYGEN	3015	70	530	⁸⁵ 49.2	5.7	-	-	22.03	-
(CONT'D)	(P _A =1515)	-270	190	-	-	⁶⁸ 393	37.4	-	26.7
		+390	850	30.9	7.7	-	-	10.23	-
	6015	70	530	⁸⁸ 104	6.6	-	-	80.4	-
	(P _A =3015)	-270	190	-	-	⁷⁰⁰ 405	42.0	-	49.7
		+390	850	61	8.0	-	-	39.2	-
	10015	70	530	²⁷⁹ 161.5	8.25	-	-	167	-
	(P _A =5015)	-270	190	-	-	⁷²⁰ 417	48.0	-	74
		+390	850	102	8.7	-	-	99.7	-
Helium	1615	-320	140	¹⁹⁵ 11.3	2.07	-	-	59.8	-
	(P _A =815)								
	2015	-320	140	²⁷⁴ 13.9	2.1	-	-	90.6	-
	(P _A =1015)								
HYDROGEN	1615	-360	100	¹⁹⁹ 11.0	1.03	-	-	233	-
	(P _A =815)								-
	2015	-360	100	²⁷³ 13.3	1.16	-	-	312	-
	(P _A =1015)								

*Number in upper left represents density
in lbs/ft³

ρ , density, given in lb/in³ x 10⁴

μ , viscosity, given in lb-min/in² x 10¹¹

$$P_A = \frac{P_1 + P_2}{2}$$

TABLE C-II

INLET PRESSURE	$\frac{Q_{He(-320)}}{Q_{LN_2(-270)}}$	$\frac{Q_{He(-320)}}{Q_{LN_2(-360)}}$	$\frac{Q_{He(-320)}}{Q_{LO_2(-270)}}$	$\frac{Q_{He(-320)}}{Q_{He(-270)}}$
(PSIA)				
115	0.47	0.236	0.344	8.91
315	1.18	0.225	0.902	8.46
1015	3.60	0.227	2.63	8.36
3015	9.96	0.392	7.05	7.35
6015	18.0	0.697	11.79	5.99
10015	—	1.025	16.15	4.96
1615			0.257	
2015			0.290	

APPENDIX D

VALVE SIZE TRADEOFFS

VALVE SIZE VARIATIONS

CALCULATE VALVE SIZE VARIATIONS FOR DIFFERENT ΔP 'S WITH $P_1 = 400$

$$\Delta P = 10 \quad \bar{R} = \frac{390}{400} = .975 \quad S = 1.2512$$

$$\Delta P = 15 \quad \bar{R} = \frac{385}{400} = .9625 \quad S = 1.5219$$

$$\Delta P = 20 \quad \bar{R} = \frac{380}{400} = .950 \quad S = 1.7450$$

$$\Delta P = 25 \quad \bar{R} = \frac{375}{400} = .9375 \quad S = 1.9371$$

$$A = \frac{w \sqrt{RT_1}}{C P_1 S}$$

$$w = .69 \text{ #/SEC}$$

REF:

$$R = 766.8$$

55E APS

$$T_1 = 540 R$$

VALVES D.S.

$$C = .62$$

($\Delta P = 5$, DIA WAS 1.6 IN)

$$P_1 = 400$$

$$A = \frac{(.69)(\sqrt{766.8 \cdot 540})}{(.62)(400)(5)} = \frac{1.7904}{5}$$

$\Delta P = 10$	$\Delta P = 15$	$\Delta P = 20$	$\Delta P = 25$
$A = \frac{1.7904}{1.2512}$	$A = \frac{1.7904}{1.5219}$	$A = \frac{1.7904}{1.7450}$	$A = \frac{1.7904}{1.9371}$
$A = 1.43 \text{ IN}^2$	$A = 1.176 \text{ IN}^2$	$A = 1.03 \text{ IN}^2$	$A = .9293$
$D = 1.35 \text{ IN}$	$D = 1.23 \text{ IN}$	$D = 1.15 \text{ IN}$	$D = 1.08 \text{ IN}$

VALVE SIZE VARIATIONS

CHECK SIZES WITH SAME ΔP 'S BUT $T_1 = 300^\circ R$

$$A = \frac{(69)(\sqrt{\frac{766.8 \cdot 300}{1.334}})}{(162)(400)(5)} = \frac{1.334}{5}$$

$\Delta P = 10$	$\Delta P = 15$	$\Delta P = 20$	$\Delta P = 25$
$A = \frac{1.334}{1.2512}$	$A = \frac{1.334}{1.5219}$	$A = \frac{1.334}{1.745}$	$A = \frac{1.334}{1.9371}$
$A = 1.066 \text{ in}^2$	$A = 0.876 \text{ in}^2$	$A = 0.764 \text{ in}^2$	$A = 0.6886 \text{ in}^2$
$D = 1.16 \text{ in}$	$D = 1.06$	$D = 0.99 \text{ in}$	$D = 0.93 \text{ in}$

CHECK ALSO $\Delta P = 5 \text{ PSI @ } 300^\circ R$ $S = .89$

$$A = \frac{1.334}{S} = \frac{1.334}{.89} = 1.498$$

$$D = 1.38 \text{ in}$$

CHECK WITH $T_1 = 200^\circ R$

$$A = \frac{(69)(\sqrt{\frac{766.8 \cdot 200}{1.334}})}{(162)(400)(5)} = \frac{1.09}{5}$$

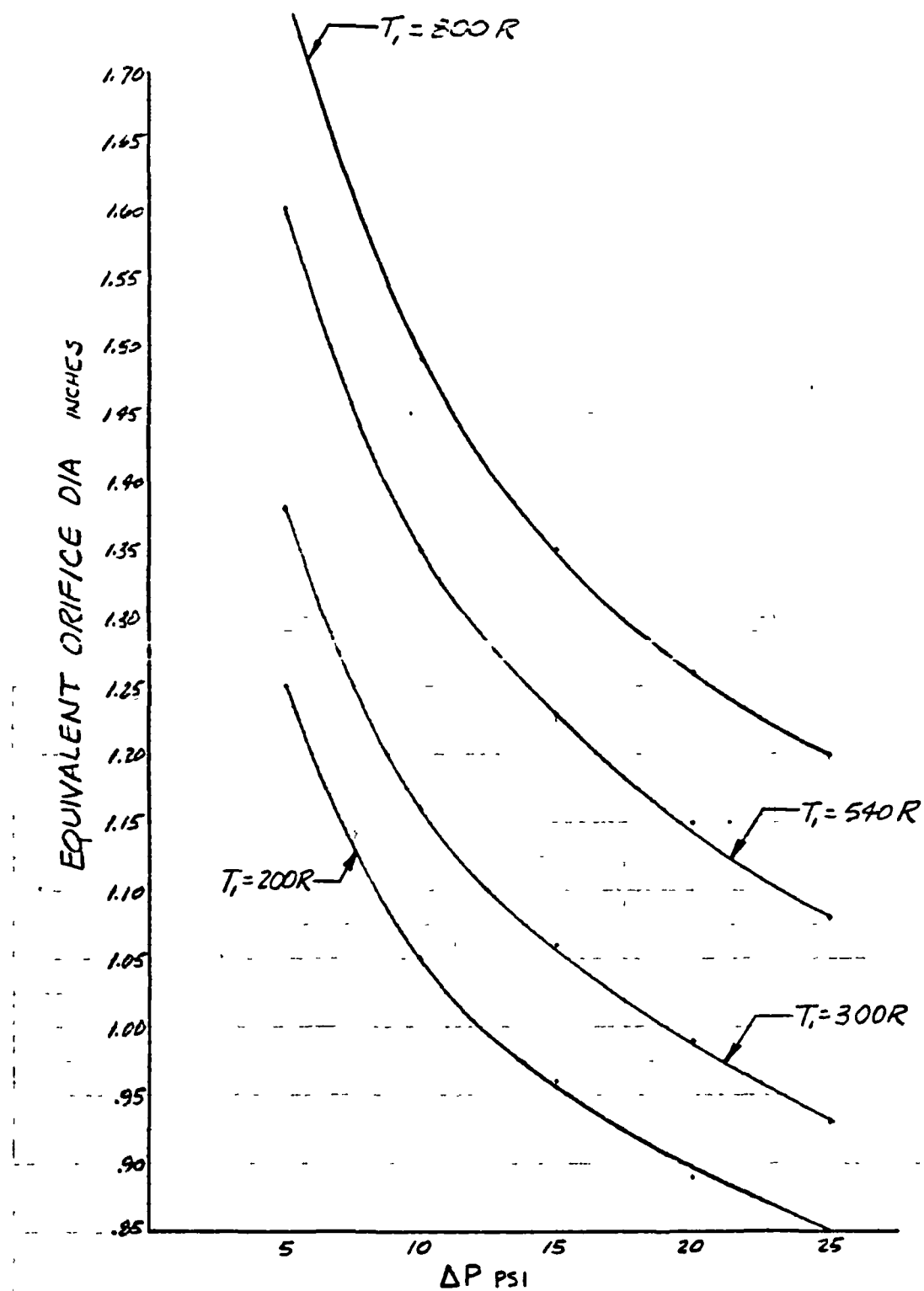
$\Delta P = 5$	$\Delta P = 10$	$\Delta P = 15$	$\Delta P = 20$	$\Delta P = 25$
$A = \frac{1.09}{.89}$	$A = \frac{1.09}{1.2512}$	$A = \frac{1.09}{1.5219}$	$A = \frac{1.09}{1.745}$	$A = \frac{1.09}{1.9371}$
$A = 1.224$	$A = 0.871$	$A = 0.716$	$A = 0.625$	$A = 0.563$
$D = 1.25 \text{ in}$	$D = 1.05 \text{ in}$	$D = 0.96 \text{ in}$	$D = 0.89 \text{ in}$	$D = 0.85 \text{ in}$

VALVE SIZE VARIATION

CHECK WITH $\bar{T}_1 = 800R$.

$$A = \frac{(0.69)(\sqrt{766.8 \cdot 800})}{(0.62)(900)(5)} = \frac{2.18}{5}$$

$\Delta P = 5$	$\Delta P = 10$	$\Delta P = 15$	$\Delta P = 20$	$\Delta P = 25$
$A = \frac{2.18}{0.89}$	$A = \frac{2.18}{1.2512}$	$A = \frac{2.18}{1.5219}$	$A = \frac{2.18}{1.745}$	$A = \frac{2.18}{1.9371}$
$A = 2.45$	$A = 1.74$	$A = 1.43$	$A = 1.25$	$A = 1.125$
$D = 1.76 IN$	$D = 1.49 IN$	$D = 1.35 IN$	$D = 1.26$	$D = 1.20 IN$



Valve Size Variation vs ΔP at Various Inlet Temperatures

Page intentionally left blank

APPENDIX E

DESIGN AND STATIC ANALYSIS, VALVE CONCEPT NO. 3

INTRODUCTION

The third of a series of preliminary layouts for the SS/APS has been completed. A layout depicting a piloted poppet valve concept and the static analysis for such a concept, complying with the high pressure design requirements, are presented herein.

The valve design is capable of accommodating any of the four types of closure concepts currently undergoing screening tests.

DISCUSSION

The preliminary layout (Fig. E-1) is of a piloted, 90-degree poppet valve which, like the conventional semibalanced poppet valve (concept No. 1), has some unique features to obtain long life. The valve is opened by venting the propellant pressure from the back side of the actuator piston. The valve is closed by opening (de-energizing) a pilot valve, allowing propellant pressure into the actuator and by the assistance of a helical spring.

All static seals in the valve are Teflon-coated metal O-rings. These were selected for their long service life (no age control required as with elastomer seals) and their resistance to corrosion. The piston seal, manufactured by Rudolf E. Krueger Co., was selected because of better wear characteristics than conventional lipseals and because it is able to compensate for thermal effects of the piston.

The poppet/seat arrangement, as shown on the layout, is a grooved gold seat with a flat poppet or a captive plastic poppet with a flat seat. These concepts are two representative types of those currently being tested under the closure screening test program. The seat assembly is an insert which "floats" on metal O-rings to compensate for temperature effects between the Inconel flange and aluminum body. This concept also flexes the sealing surface toward the poppet. The poppet seal is attached to the poppet shaft by means of a flexure disk which prevents the seat from scrubbing due to shaft movement.

Wear prevention and particle generation from rubbing are of prime concern for long-life characteristics. A Teflon bushing between the shaft and guide prevents metal to metal contact during valve actuation. Both concepts No. 1 and 2 utilize a thrust bearing to permit the poppet return spring to rotate on during compression, thus preventing particle generation from rubbing. Due to the low spring loads in this concept, the bearing was not required. To prevent scrubbing between the poppet and seat due to shaft rotation, two guide pins covered with Teflon bushings are used, like concept No. 2, on which the actuator piston is guided in a straight line motion.

The static analysis of the valve is included in the following pages. The valve was sized for a nominal pressure drop of 15 psi at 2.76 lb/sec oxidizer (gaseous oxygen) flow at 540 R with an inlet pressure of 400 psia, which determined the poppet seat and stroke. Providing sufficient actuator force for proper opening and closing control was a primary factor in this design.

SCHEMATIC

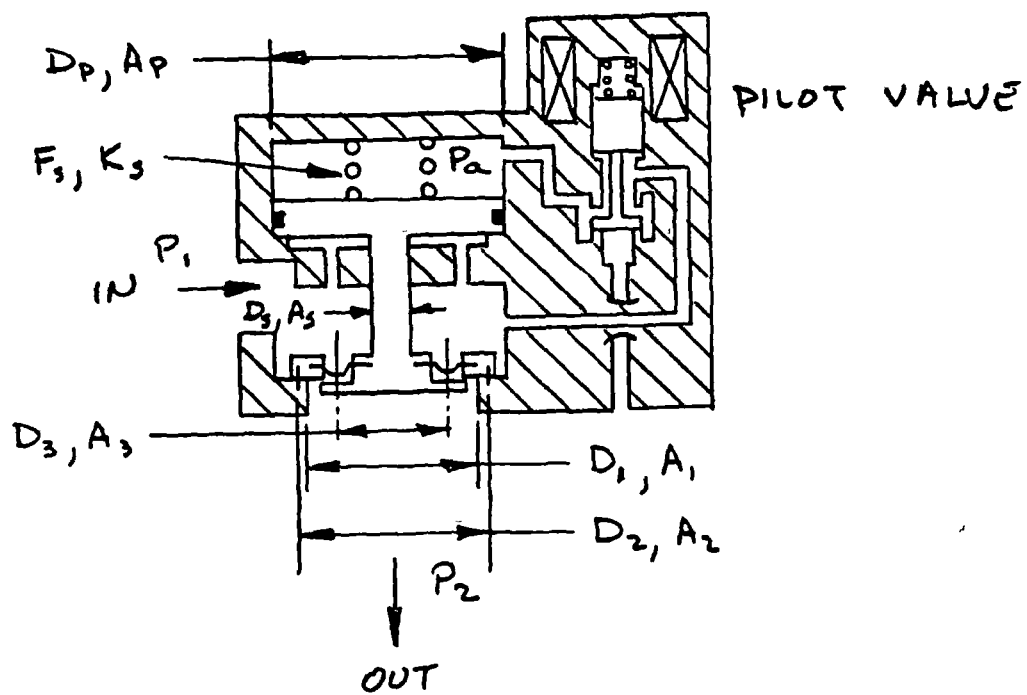


Figure E-1. Piloted Poppet Valve

SYMBOLS

A_1	= AREA OUTLET PORT	IN^2
A_2	= AREA POPPET SEAT	IN^2
A_c	= AREA SEAT CONTACT	IN^2
A_p	= AREA ACTUATOR PISTON	IN^2
A_s	= AREA POPPET SHAFT	IN^2
A_{sc}	= AREA SEAL CONTACT	IN^2
D_1	= DIAMETER OUTLET PORT	IN
D_2	= DIAMETER POPPET SEAT	IN
D_p	= DIAMETER ACTUATOR PISTON	IN
D_s	= DIAMETER POPPET SHAFT	IN
F_c	= SEAT CONTACT FORCE	LB
F_p	= ACTUATOR PISTON FORCE	LB
F_r	= FRICTION FORCE	LB
F_s	= INSTALLED SPRING LOAD	LB
K_s	= SPRING RATE	LB
K_T	= VALVE COEFFICIENT	—
l	= STROKE	IN
P_a	= ACTUATOR PRESSURE	PSIA
P_1	= INLET PRESSURE	PSIA
P_2	= OUTLET PRESSURE	PSIA
P_s	= SEAL PRESSURE	PSI
ΔP	= PRESSURE DROP ($P_1 - P_2$)	PSI
R	= SPECIFIC GAS CONSTANT	FT^2/OR
S_c	= SEAL STRESS	PSI
T	= TEMPERATURE	$^{\circ}\text{R}$
ρ	= DENSITY	LB/FT^3
μ	= COEFFICIENT OF FRICTION	—
\dot{w}	= FLOW RATE	LB/SEC (PPS)
A_3	= EFFECTIVE AREA DIAPHRAGM	IN^2
D_3	= EFFECTIVE DIAMETER DIAPHRAGM	IN

REQUIREMENTS

$$P_1 = 400 \text{ PSIA}$$

$$\Delta P = 15 \text{ PSI}$$

$$\dot{w}_{O_2} = 2.76 \text{ PPS (OXYGEN)}$$

$$\dot{w}_{H_2} = .69 \text{ PPS (HYDROGEN)}$$

$$K_T = 3.74$$

$$T = 540^\circ R$$

$$R_{O_2} = 48.3 \text{ FT}^2/\text{OR}$$

$$R_{H_2} = 766.8 \text{ FT}^2/\text{OR}$$

$$S_c = 2000 \text{ PSI (MIN)}$$

$$\rho_{O_2} = \frac{144 P_1}{RT} = \frac{144 (400)}{48.3 (540)} = 2.21 \text{ LB/FT}^3$$

$$\rho_{H_2} = \frac{144 (400)}{766.8 (540)} = .139 \text{ LB/FT}^3$$

VALVE INLET SIZE

$$D^2 = \frac{\dot{W}}{.525} \sqrt{\frac{K_T}{\rho \Delta P}}$$

$$D_{O_2} = \frac{2.76}{.525} \sqrt{\frac{3.74}{2.21(15)}} = 1.765$$

$$D_{H_2} = \frac{.69}{.525} \sqrt{\frac{3.74}{.139(15)}} = 1.760$$

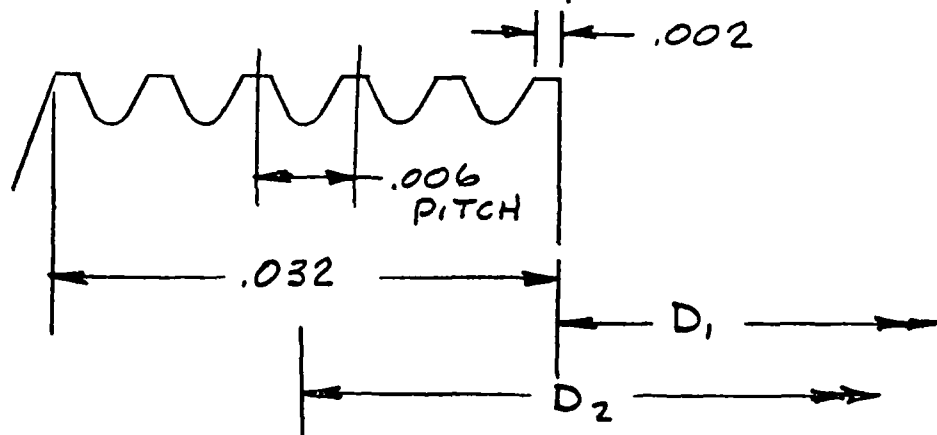
$$\text{USE } D^2 = 1.765$$

$$\therefore D_1 = \sqrt{1.765} = 1.330 \text{ IN}$$

$$A_1 = \frac{\pi}{4} (1.330)^2 = 1.382 \text{ IN}^2$$

POPPET SEAT SIZE

FOR GROOVED GOLD SEAT



$$D_2 = D_1 + .032 = 1.330 + .032 = 1.362 \text{ IN}$$

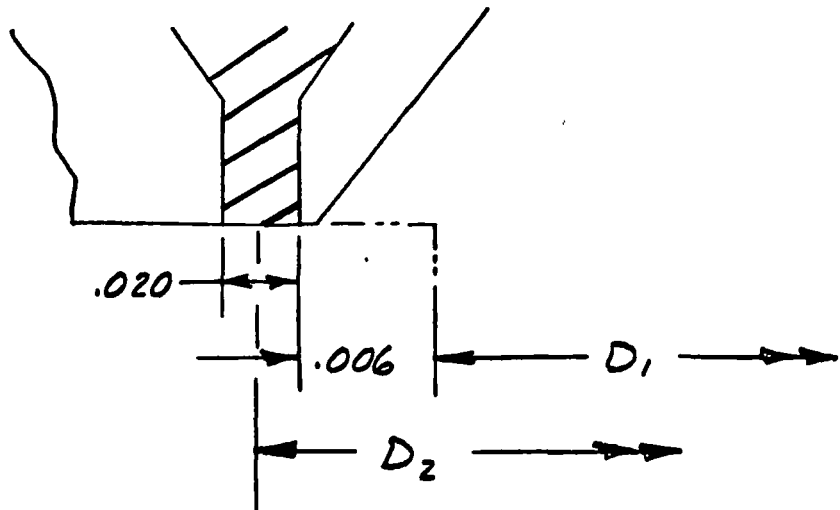
$$A_2 = \frac{\pi}{4} (1.362)^2 = 1.456 \text{ IN}^2$$

$$A_c = (1.362)(\pi)(6 \times .002) = .051 \text{ IN}^2$$

$$F_c = S_c A_c = 2000(.051) = 102 \text{ LB}$$

POPPET SEAT SIZE (CONT'D)

FOR CAPTIVE PLASTIC SEAT



$$D_2 = D_1 + 2 \times .006 + .020 = 1.362 \text{ IN}$$

$$A_2 = \frac{\pi}{4} (1.362)^2 = 1.456 \text{ IN}^2$$

$$A_c = (1.362)(\pi)(.020) = .085 \text{ IN}^2$$

$$F_c = S_c A_c = 2000(.085) = 170 \text{ LB}$$

\therefore 170 LB SEAT FORCE REQUIRED FOR ALL SEATS

SEAT STRESS

GROOVED GOLD

$$S_c = \frac{F_c}{A_c} = \frac{170}{.051} = 3333 \text{ PSI}$$

CAPTIVE PLASTIC

$$S = \frac{170}{.085} = 2000 \text{ PSI}$$

DIAPHRAGM SIZE

$$S_c = \frac{P_1 (A_2 - A_3)}{A_c}$$

$$A_3 = A_2 - \frac{S_c A_c}{P_1}$$

$$A_3 = 1.456 - \frac{2000}{400} A_c$$

$$A_3 = 1.456 - 5 A_c$$

FOR GROOVED GOLD

$$A_3 = 1.456 - 5(1.051) = 1.201 \text{ IN}^2$$

$$D_3 = \sqrt{\frac{4}{\pi}(1.201)} = 1.237 \text{ IN}$$

FOR CAPTIVE PLASTIC

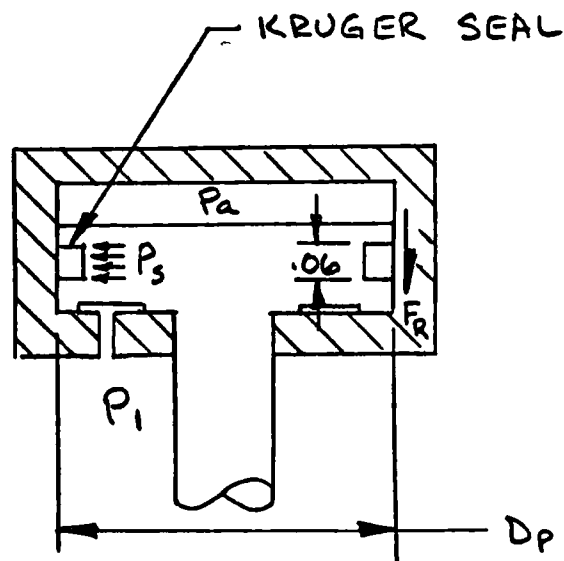
$$A_3 = 1.456 - 5(1.085) = 1.031 \text{ IN}^2$$

$$D_3 = \sqrt{\frac{4}{\pi}(1.031)} = 1.146 \text{ IN}$$

$$\text{USE } A_3 = 1.031 \text{ IN}^2$$

$$D_3 = 1.146 \text{ IN}$$

FRICTION



ASSUME $D_p = 1.750$ IN

$\mu = 0.1$ (TEFLON ON STEEL)

$P_a = 150$ PSIA

$$F_R = A_{sc} [P_s + (P_1 - P_a)] \mu = 1.750(\pi)(.06)(500 + 250)(0.1)$$

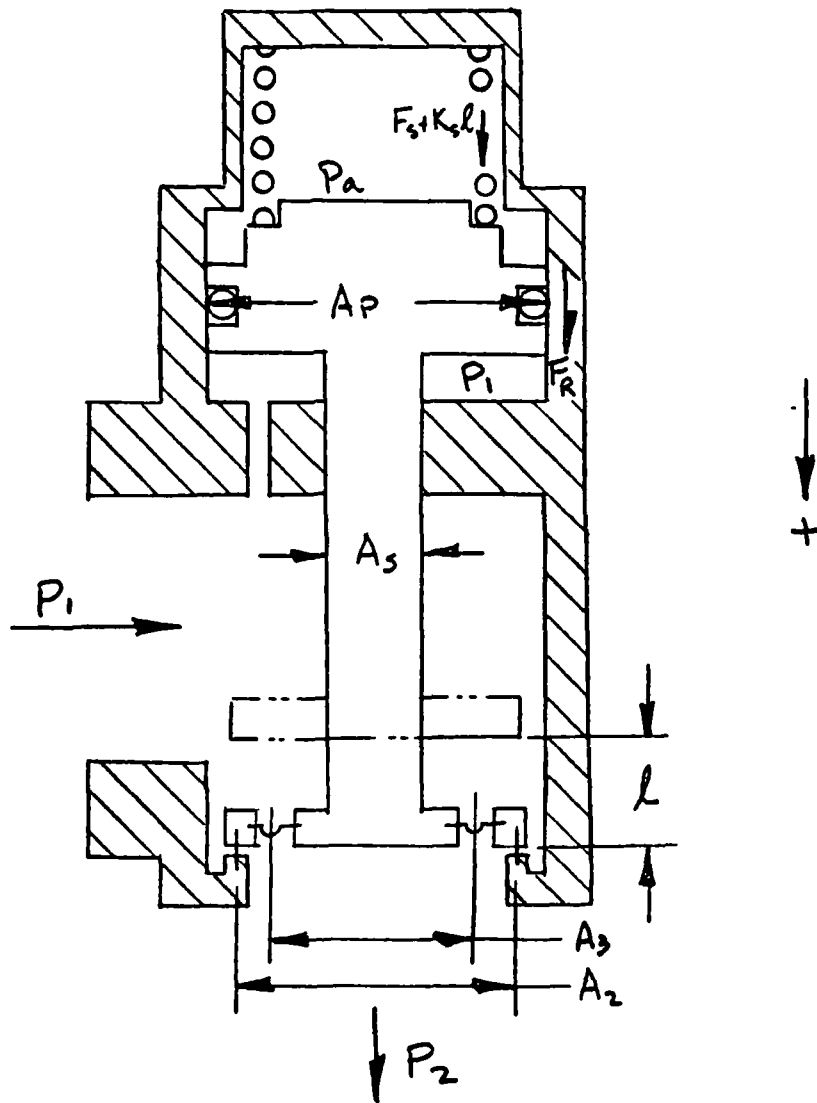
$$F_R = 24.7 \text{ LB (AT INITIATING OPENING)}$$

$$F_R = 1.750(\pi)(.06)(500 + 15)(0.1)$$

$$F_R = 17.0 \text{ LB (AT INITIATING CLOSING)}$$

USE $F_R = 50$ LB

FORCE BALANCE



GENERAL EQUATION FOR $0 < \ell < .332$

$$\sum F = 0$$

$$P_1(A_2 - A_5) - P_2 A_2 - P_1(A_P - A_5) + P_a A_P + F_R + F_S + K_S l = 0$$

FORCE TO INITIATE OPENING

$$P_1 = 400 \text{ PSIA}$$

$$P_2 = 0$$

$$F_R = 50 \text{ LB}$$

$$F_S = 50 \text{ LB}$$

$$A_2 = 1.456 \text{ IN}^2$$

$$P_1 (A_2 - A_s) - P_1 (A_p - A_s) + P_a A_p + F_R + F_S = 0$$

$$P_1 A_2 - P_1 A_s - P_1 A_p + P_1 A_s + P_a A_p + F_R + F_S = 0$$

$$582 - 400 A_p + P_a A_p + 50 + 50 = 0$$

$$A_p (400 - P_a) = 682$$

<u>A_p</u>	<u>D_p</u>	<u>P_a</u>
4.547	2.406	250
2.463	1.771	123

————— BASED ON
PRELIMINARY
DYNAMIC ANALYSIS

FORCE TO FULLY OPEN

$$P_1 = 400 \text{ PSIA}$$

$$P_2 = 385 \text{ PSIA}$$

$$F_R = 50 \text{ LB}$$

$$F_S = 50 \text{ LB}$$

$$A_2 = 1.456 \text{ IN}^2$$

$$K_S = 100 \text{ LB/IN (ASSUMED)}$$

$$l = \frac{D_1}{4} = \frac{1.330}{4} = .332 \text{ IN}$$

$$\Sigma F = P_1(A_2 - A_s) - P_2 A_2 - P_1(A_P - A_s) + P_a A_P + F_R + F_S + K_S l = 0$$

$$-P_a A_P = 582 - 385(1.456) - 400(2.463) + 50 + 50 + 100(.332)$$

$$P_a A_P = 831 \text{ LB} \quad , \quad P_a = \frac{831}{2.463} = 337 \text{ PSIA}$$

FORCE TO INITIATE CLOSING

$$P_1 = 400 \text{ PSIA}$$

$$P_2 = 385 \text{ PSIA}$$

$$F_R = -50 \text{ LB}$$

$$F_S = 50 \text{ LB}$$

$$K_S l = 33.2 \text{ LB}$$

$$A_s = 1.456 \text{ IN}^2$$

$$P_1(A_2 - A_s) - P_2 A_2 - P_1(A_P - A_s) + P_a A_P + F_R + F_S + K_S l = 0$$

$$582 - 560.6 - 985.2 + P_a(2.463) - 50 + 50 + 33.2 = 0$$

$$P_a = \frac{930.6}{2.463} = 377.8 \text{ PSIA}$$

SUMMARY

$$D_p = 1.771 \text{ IN}, \quad A_p = 2.463 \text{ IN}^2$$

$$D_s = 0.500 \text{ IN}, \quad A_s = .196 \text{ IN}^2$$

$$D_1 = 1.330 \text{ IN}, \quad A_1 = 1.382 \text{ IN}^2$$

$$D_2 = 1.362 \text{ IN}, \quad A_2 = 1.456 \text{ IN}^2$$

$$D_3 = 1.146 \text{ IN}, \quad A_3 = 1.031 \text{ IN}^2$$

$$K_s = 100 \text{ LB/IN}$$

$$l = .332 \text{ IN}$$

Page intentionally left blank

APPENDIX F

DAP4H ANALYSIS OF DESIGN CONCEPTS NO. 1, 2, AND 3

INTRODUCTION

Prior design studies led to the selection of three alternate valve design concepts for design layout. This report presents the results of a computerized analysis of each of those alternate concepts, and a comparative evaluation of their dynamic performance characteristics in support of a concept selection.

SUMMARY

Computer runs with mathematical models of each valve design concept, operating under identical propellant system conditions, were performed to investigate the effects of propellant gas properties (GH_2 or GO_2), inlet gas pressure, inlet gas temperature, pilot valve effective flow area, dashpot orifice effective flow area, and downstream volume. This report discusses the mathematical models and the analytical procedure, presents typical computer run graphic output data with interpretation of its significance, and summarizes the results of all computer runs performed.

CONCLUSIONS

In a design concept selection based on performance, the concept that is delineated in layout RS003934 (concept No. 3 in Fig. F-1) is the outstanding first choice. The design concept of layout RS003786 (concept No. 2 in Fig. F-1) has an intermediate rating, and the design concept of layout RS003524 (concept No. 1 in Fig. F-1) has the lowest rating.

DISCUSSION

The three valve design concepts that were investigated are illustrated in Fig. F-1.

The design schematic for concept No. 1 in Fig. F-1 is applicable to a hardware configuration that is delineated in design layout RS003524. When inlet pressure is applied to the valve in its normally closed condition, a poppet seating force is applied by inlet pressure acting against the differential area of the poppet seat cross section minus the smaller bellows effective area. The bellows is pressurized internally by valve outlet pressure. The actuator piston is spring biased in the valve closing direction, and the spring cavity is continuously vented. A solenoid-actuated, three-way pilot valve vents the active side of the actuator piston, when the solenoid is de-energized, and blocks inflow from main valve inlet pressure. When the pilot valve is actuated by energizing its solenoid, it ports inlet pressure to the active side of the piston to cause main valve actuation to its full-open position. When the pilot solenoid is subsequently de-energized, it vents the active side of the actuator piston, and the bias spring acts to close the main valve.

The design schematic for concept No. 3, and design layout RS003934, describes a poppet valve in which inlet pressure acts against the differential area of the poppet seat cross section minus the diaphragm effective cross section to provide a valve closing force. Inlet pressure is ported through the valve stem clearance and through an orifice into a piston cavity that is referred to as the actuator dashpot cavity. Inlet pressure is also ported through the solenoid-actuated, three-way pilot valve to the piston cavity containing the bias spring, when the solenoid is de-energized. The spring provides a valve closing force to assist unbalanced pressure forces. When the pilot valve is actuated by energizing its solenoid, it vents the spring cavity side of the actuator piston, and pressure in the dashpot cavity provides a motive force for opening the main valve. When the pilot solenoid is subsequently de-energized, it again ports valve inlet pressure into the spring cavity, and the combination of spring force and spring cavity pressure force acting on the actuator piston result in valve closing.

Analysis of the dynamic characteristics of each of the three valve design concepts of Fig. F-1 was performed using a Rocketdyne general purpose digital computer program that had been developed previously for use with an IBM 360 computer facility. The basic program is identified by the code name DAP4H (Dynamic Analysis Program Fortran IV, Level H). Rocketdyne report CER 7137-8021 is a user's manual that describes the program in detail. NASA Tech Brief 67-10523 is a summary of the user's manual. Information relative to this computer program may be obtained from COSMIC, Computer Center, University of Georgia.

DAP4H is a collection of subprograms represented by the blocks that are enclosed by a heavy-line rectangle in Fig. F-2. All programming related to input data acquisition, storing of computed data, printout, and graphic display of output data are complete and available for use in an analysis. Subprograms are available for recurrent forms of computations, such as those for pneumatic or hydraulic flowrates, pressure changes resulting from changes in flowrates and in volumes, accelerations and velocities in the presence of static and dynamic friction, and many others.

Subprogram CØNSYS, shown as a block in Fig. F-2, was formulated specifically for the analysis described in this report. It is a mathematical model of a physical system in which these propellant valves will operate. A test setup was simulated in which there is a constant supply pressure, a volume downstream from a propellant valve, and an orifice for flow from that volume to ambient pressure.

Three separate subprograms were formulated, indicated by blocks in Fig. F-2 as CØMPI, CØMP2, and CØMP3, as mathematical models of each of the three valve design concepts. Performance of each concept was analyzed under identical simulated test system conditions.

The analytical method used to investigate performance of the valve design concepts emphasizes realistic mathematical modeling of hardware physical features. Nonlinear phenomena are described by nonlinear equations, e.g., the computations for gas flowrates accommodate reversible subsonic or sonic flow conditions. Discontinuous phenomena are described by discontinuous equations, e.g., the computations for acceleration, velocity, and displacement accommodate static and dynamic friction, displacement limits, impact-rebound from mechanical stops, and

poppet separation from its lifting mechanism. Sliding-seal friction forces are computed as functions of variable applied pressure differentials. Overtravel in the poppet lifting mechanisms is accommodated.

A computer printout listing of the system subprogram CØNSYS is presented on pages F-29 through F-31 . A listing of a typical component subprogram (for valve concept No. 3) is presented on pages F-32 through F-37 . A sample of the input data printout for a typical computer run is shown on pages F-38 through F-40. A sample of the tabulated output data printout for a typical computer run is included on pages F-41 and F-42.

The most significant output data obtained in each computer run are displayed graphically in Fig. F-3a and F-3b. These graphs apply to valve design concept No. 1, but are presented primarily for a general discussion of computer output data.

Pilot valve and main valve actuator piston displacements are plotted in Fig. 3a as functions of time. The computer program is set up to simulate a 0.001-second ramp in pilot valve displacement at TIME = 0.005 and 0.040 second. Overtravel of 0.015 inch in the main valve-lifting mechanism is simulated. During an opening transient, the piston displaces through the overtravel and then pauses until the actuator pressure increases sufficiently to lift the main valve from its seat. During the closing transient shown in Fig. 3a, approximately 0.010 second reaction time is required for the actuator pressure to decay sufficiently to initiate piston motion in response to pilot valve displacement. In the vicinity of TIME = 0.060 second, there is a pronounced decrease in piston velocity because the valve outlet pressure exerts a force that opposes closing and, in this case, the valve closing response is affected by the rate of outlet pressure decay. (Review of other output data, such as that in Fig. F-3b, is required for verification of this explanation.) Notation in Fig. 3a indicates opening and closing impact velocities of 124 and 32 in./sec. These values were obtained from a tabulated data printout. The valve opened in 0.009 second and closed in 0.0255 second in response to pilot valve displacements. Pilot valve energize and de-energize response time lags are additive to the response times shown in Fig. 3a.

Valve inlet, outlet, and actuator pressures are plotted in Fig. 3b. During the opening transient, valve motion commences near TIME = 0.010 second under the influence of an increasing actuator pressure, P3. As the valve opens and outlet pressure, P2, increases the outlet pressure provides an assisting opening force. During the second half of the opening stroke, the piston was moving so rapidly that pressure P3 decreased because gas volumetric inflow through the pilot valve became less than the piston volumetric displacement. During the closing transient, the gas capacitance of a 100 cu in. volume at the valve outlet retards the decay of the outlet pressure, P2, and P2 exerts a valve force that opposes closing.

Figures F-3a and F-3b are labeled to identify the valve, the propellant (GH₂ or GO₂), the inlet gas temperature and pressure, the pilot valve equivalent orifice diameter, and the downstream volume.

Figure F-4 illustrates performance of valve design concept No. 1 with GH_2 at 200 R and 350-psia inlet conditions, and a pilot valve equivalent orifice diameter of 0.080 inch. During the valve closing transient, piston motion stopped for several milliseconds because during that time interval, the hold-open force exerted by the valve outlet pressure balanced the closing forces.

The computer run for Fig. F-5 was performed with conditions identical to those used in the run for Fig. F-4 except that a pilot valve equivalent orifice diameter of 0.110 inch was used. The use of a larger pilot valve effective flow area resulted in faster opening and closing response. The valve was almost closed when the outlet pressure introduced its delaying effect on closing.

Figure F-6 resulted from a computer run with conditions identical to those used in the run for Fig. F-5 except for a 450-psia inlet pressure. Comparison of Fig. F-5 and F-6 indicates significant variations in valve response as a result of variations in inlet pressure and, consequently, in outlet pressure.

Figure F-7 resulted from a computer run with conditions identical to those used in the run for Fig. F-5 except for a 10 cu in. downstream volume instead of a 100 cu in. volume associated with the valve outlet pressure. The valve opened 10 percent faster in Fig. F-7 because of a more rapid increase in outlet pressure as the valve opened. The valve closed 31 percent faster in Fig. F-7 because of a more rapid decrease in outlet pressure as the valve closed, and because of an unimpeded closing transient.

Figures F-8 and F-9 illustrate performance of valve design concept No. 2 with GH_2 at 500 R (midpoint of temperature range), inlet pressures of 350 and 450 psia (minimum and maximum specified pressures), and a pilot valve equivalent orifice diameter of 0.110 inch. The range of inlet pressures and the corresponding range of outlet pressures has negligible effect on valve response at 500 R.

Figures F-10 and F-11 illustrate performance of valve design concept No. 2 with GH_2 at an inlet pressure of 400 psia (midpoint of the inlet gas temperatures of 200 and 800 R (minimum and maximum specified temperatures), and a pilot valve equivalent orifice diameter of 0.110 inch. The closing transient trace in Fig. F-10 has inflections that indicate an outlet pressure retarding force with gas at 200 R, the condition for the slowest outlet pressure decay as the valve closes. Outlet pressure effects are not apparent in Fig. F-11, with gas at 800 R and the fastest outlet pressure response.

Figure F-12 illustrates performance of valve design concept No. 3 with GH_2 at 200 R and 350-psia inlet conditions, a pilot valve equivalent orifice diameter of 0.080 inch, and a dashpot equivalent orifice diameter of 0.063 inch. The dashpot equivalent orifice diameter is based on the combined effective flow areas of the piston rod bushing and the orifice that permit actuator dashpot cavity inflow and outflow. As illustrated, under these conditions there is excessive dashpot damping. The valve opened with an oscillatory, chugging motion. Valve closing was too slow.

The computer run for Fig. F-13 was performed with conditions identical to those used in the run for Fig. F-12 except that a dashpot equivalent orifice diameter of 0.080 inch was used, and the downstream volume was reduced from 100 to 50 cu in.

The run for Fig. F-14 also was performed with conditions identical to those used in the run for Fig. F-12 except that a dashpot equivalent orifice diameter of 0.080 inch was used, and the downstream volume was increased from 100 to 200 cu in.

The run for Fig. F-15 was performed with conditions identical to those used in the run for Fig. F-12 except that a dashpot equivalent orifice diameter of 0.125 inch was used.

Comparison of Fig. F-12 through F-15 indicates that concept No. 3 is insensitive to large changes in downstream volume and in dashpoint effective flow area, when there is sufficient dashpot effective flow area for avoidance of chugging.

Figure F-16 displays the dynamic response of valve design concept No. 3 operating with GH_2 at 800 R and 450-psia inlet conditions. Equivalent orifice diameters for the pilot valve and for the dashpot are both 0.080 inch. The downstream volume associated with the outlet pressure is 100 cu in.

Figure F-17 displays the dynamic response of valve design concept No. 3 operating with GO_2 at 800 R and 450-psia inlet conditions. Equivalent orifice diameters for the pilot valve and for the dashpot are both 0.160-inch (four times the effective flow areas in Fig. F-16). The downstream volume is 25 cu in. (one-fourth the downstream volume in Fig. F-16). Comparing Fig. F-16 and F-17, valve response is essentially identical, operating with GH_2 or GO_2 . The only changes in valve design parameters that are required to accommodate operation with GH_2 or GO_2 are in the pilot valve and dashpot orifice sizes.

The specific gas constant for GH_2 is 766.8 ft/R. The specific gas constant for GO_2 is 48.3 ft/R. Gas flowrates and pressure response time constants in volumes are inversely proportional to the square root of the specific gas constant $\sqrt{766.8/48.3}$. This factor of 4 is applied to pilot valve and dashpot effective flow areas in obtaining nominally identical valve response with GH_2 and GO_2 (larger areas for GO_2). This factor of 4 is applied to downstream volumes in obtaining nominally identical outlet pressure response with GH_2 and GO_2 (smaller volume with GO_2).

Figures F-18 and F-19 were obtained at minimum gas inlet temperatures and pressures. In comparing these two figures, the differences in response times and in impact velocities are related to $\sqrt{250/200}$, the square root of the ratio of the minimum GO_2 temperature and the minimum GH_2 temperature. Pilot valve and dashpot effective flow areas and downstream volumes are the same as for Fig. F-16 and F-17.

Gas flowrates and pressure response time constants in volumes are inversely proportional to the square root of the gas absolute temperature. For any given valve configuration, speed of response increases with $\sqrt{\text{Temp}}$. This relationship is approximate because of interrelationships among temperatures, pressures, valve displacement, and rate of change in valve displacement, but it is predominant in its effects on valve response.

Valve design concepts No. 1 and 2 have actuator piston cavities exposed to propellant vent pressures. Pilot valve exhaust ports and actuator drain or leakoff ports require tubing to route propellant flow to nonhazardous locations. Port, fitting, and tubing sizes must be large enough to prevent actuator vent pressure cavities from acting as dashpots that affect valve dynamic response. The use of valve design concepts with actuators exposed to vent pressures imposes limitations on the choice of vent disposal locations. Actuator vent cavities must be connected to vent disposal locations at pressures that do not vary sufficiently to affect actuator response. Dynamic response of an actuator with a piston cavity exposed to vent pressures may be significantly different at high altitudes from what it is at sea level.

In addition to the computer runs for the output data included in this appendix for a discussion of typical input and output data, computer runs were made for each of the three valve design concepts to investigate the effects of:

1. Propellant gas properties (GH_2 or GO_2)
2. Inlet gas pressure
3. Inlet gas temperature
4. Pilot valve effective flow area
5. Dashpot orifice effective flow area in concept No. 3
6. Downstream volume

The results are summarized in Fig. F-20 and evaluated in the dynamic performance rating chart of Fig. F-21. In a design concept selection based on performance, concept No. 3 is the outstanding first choice, concept No. 2 has an intermediate rating, and concept No. 1 has the lowest rating. The following factors influenced this order of preference.

Concept No. 3 can comply with the speed of response requirements with the smallest pilot valve effective flow areas. Thus, concept No. 3 can use a smaller pilot valve than is required for the other concepts, with faster pilot circuit response, allowing more time for main valve response with lower impact velocities, and least pilot valve weight.

The dashpot in the actuator of concept No. 3 results in this concept having the lowest opening and closing impact velocities of the three concepts, thereby contributing to extensive cycle life.

Concepts No. 2 and 3 are equally unaffected by variations in inlet pressures and in downstream volume effects on outlet pressure response. Concept No. 1 interacts with both inlet pressure level and outlet pressure transient response.

Of the three concepts, concept No. 3 is the only one in which vent pressures do not enter into the valve-and-actuator force balance. Therefore, concept No. 3 is the only one that will have response timing that is totally unaffected by ambient pressure or by pressure variations in a vent collection manifold or other vent discharge location.

VALVE SCHEMATICS

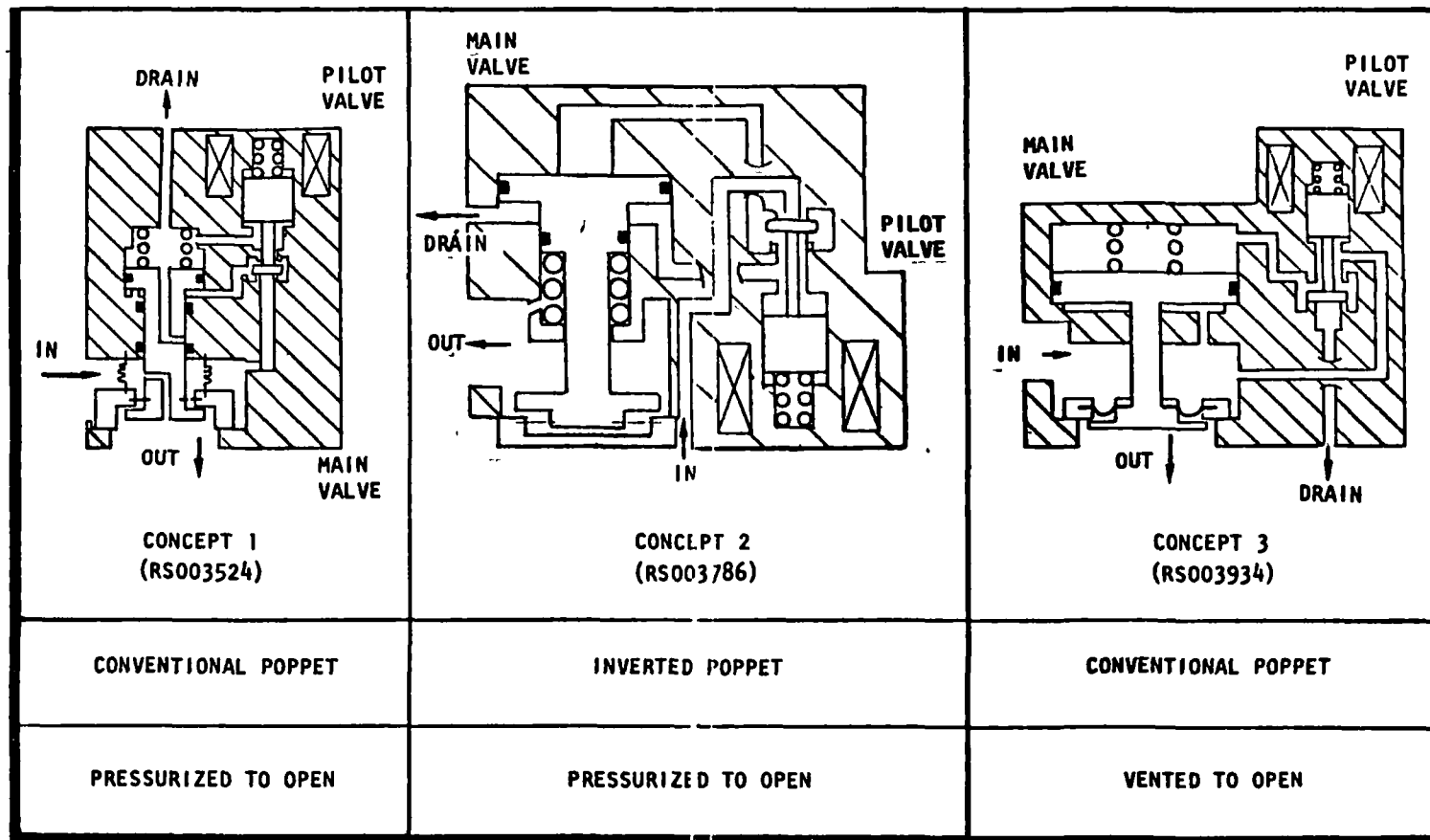


Figure F-1

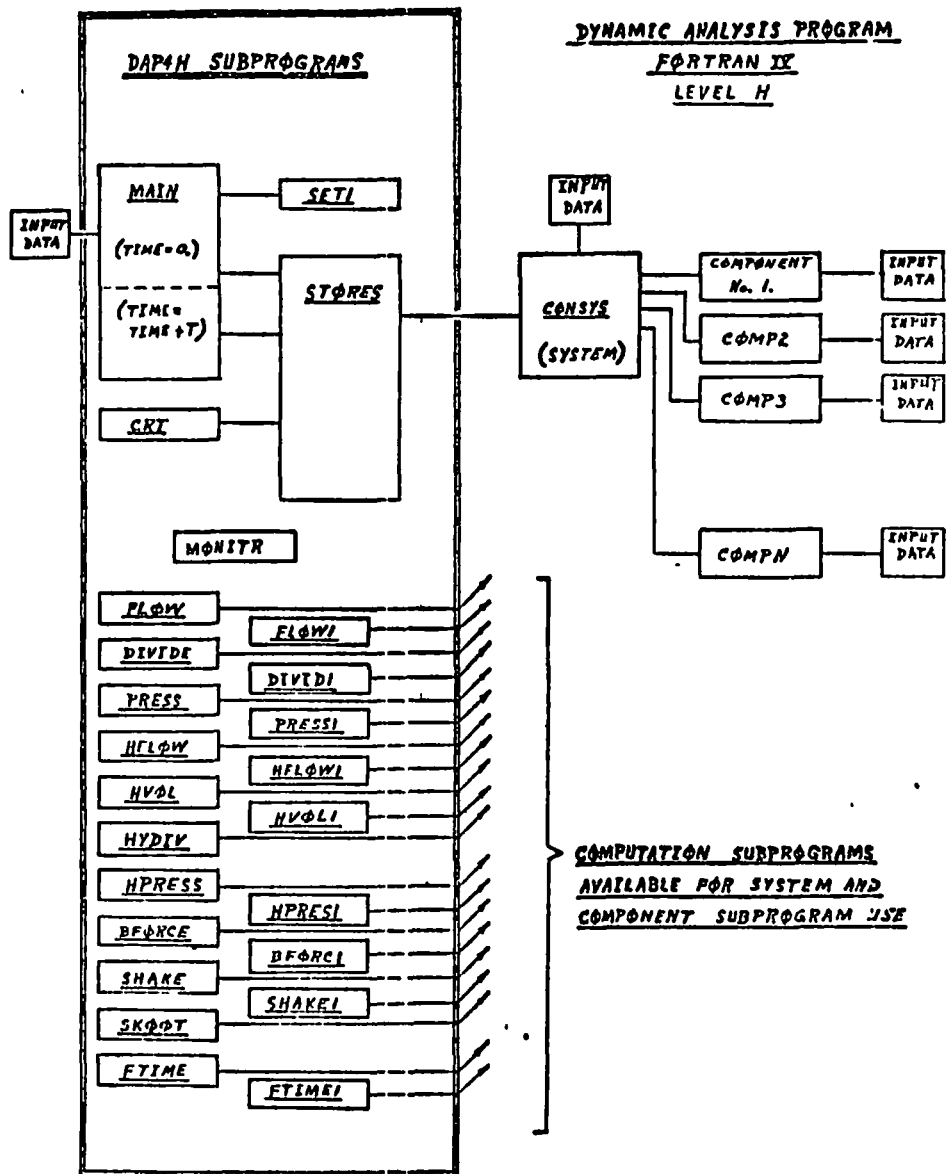


Figure F-2

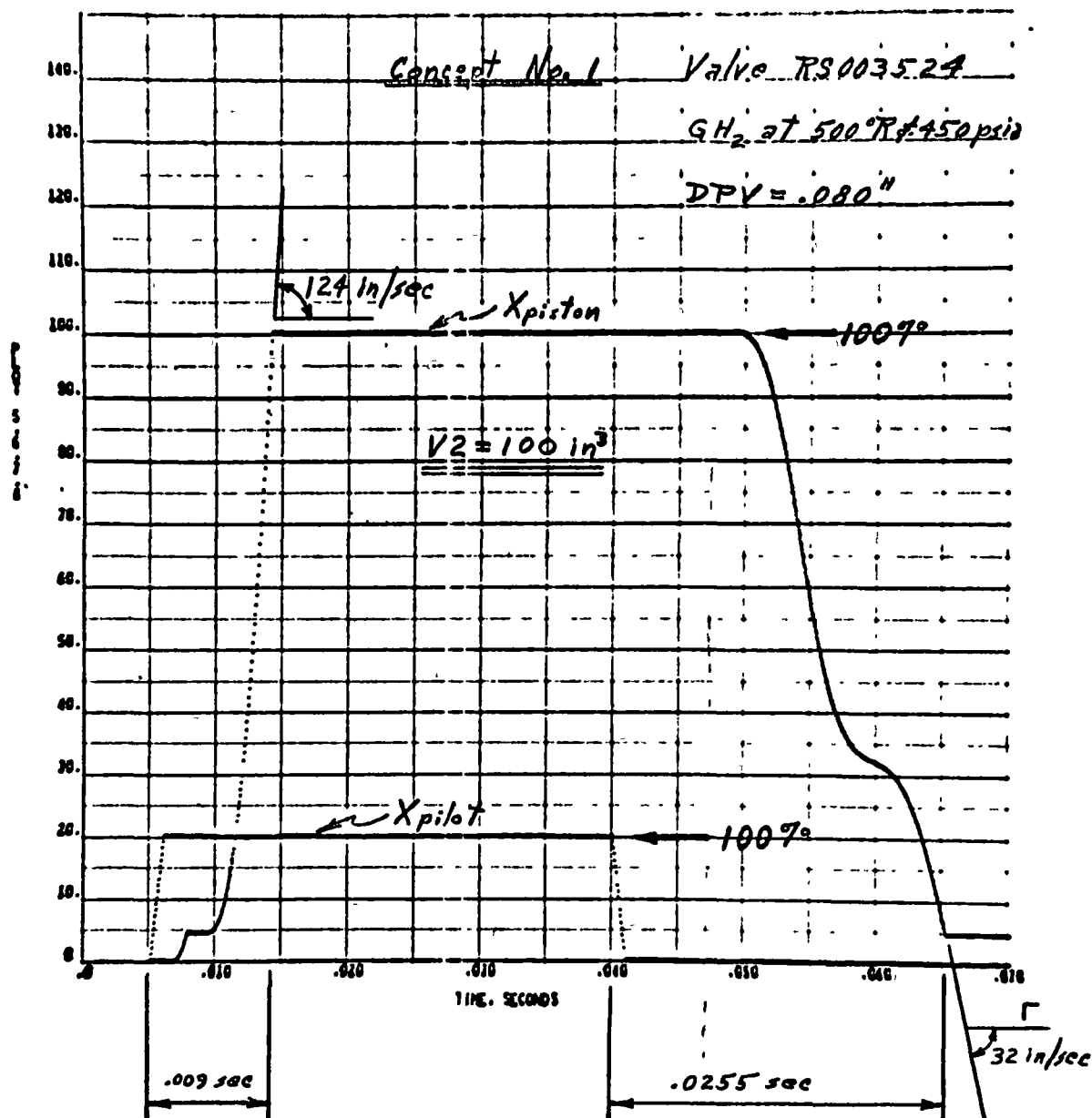


Figure F-3a

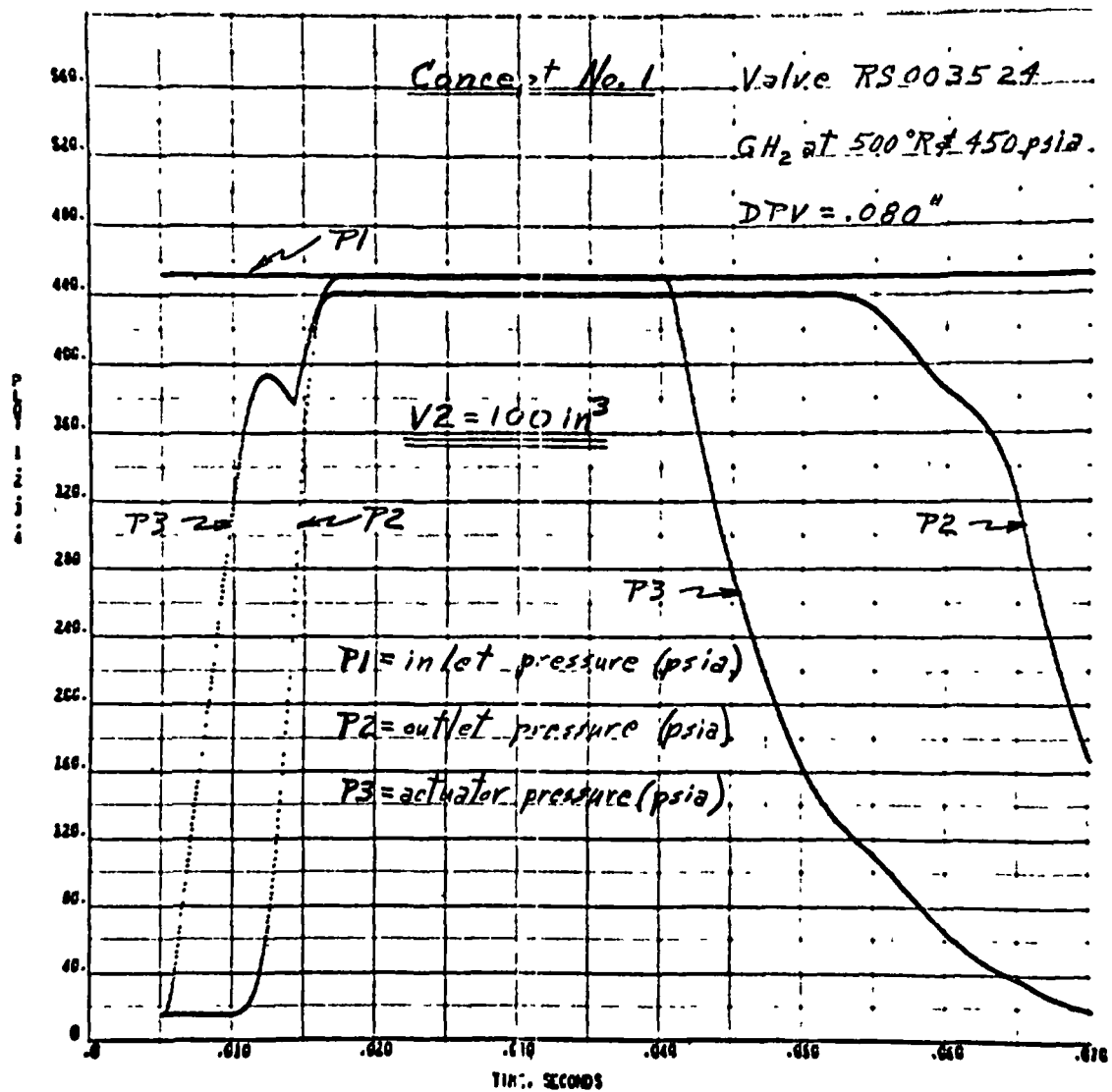


Figure F-3b

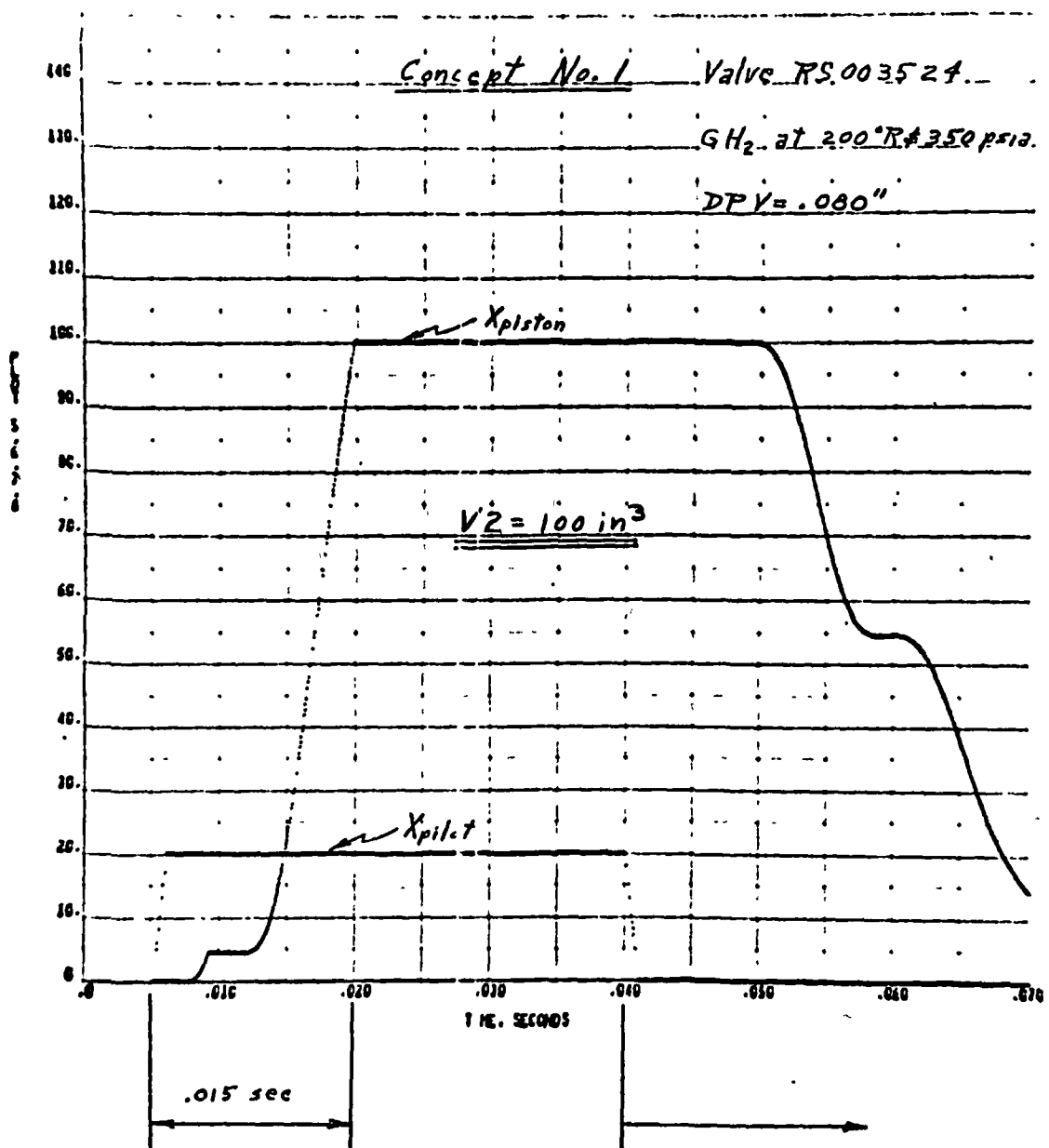


Figure F-4

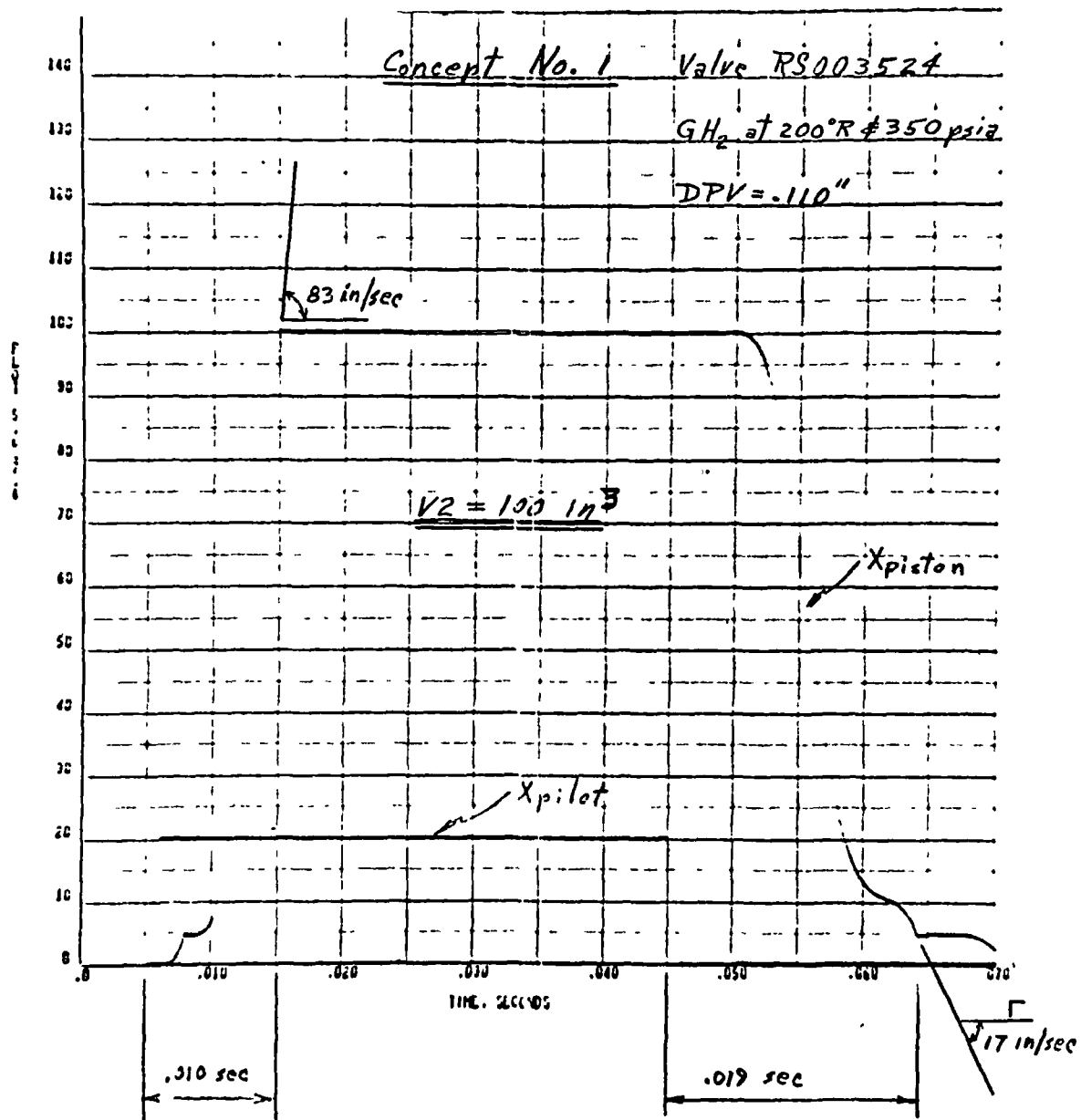


Figure F-5

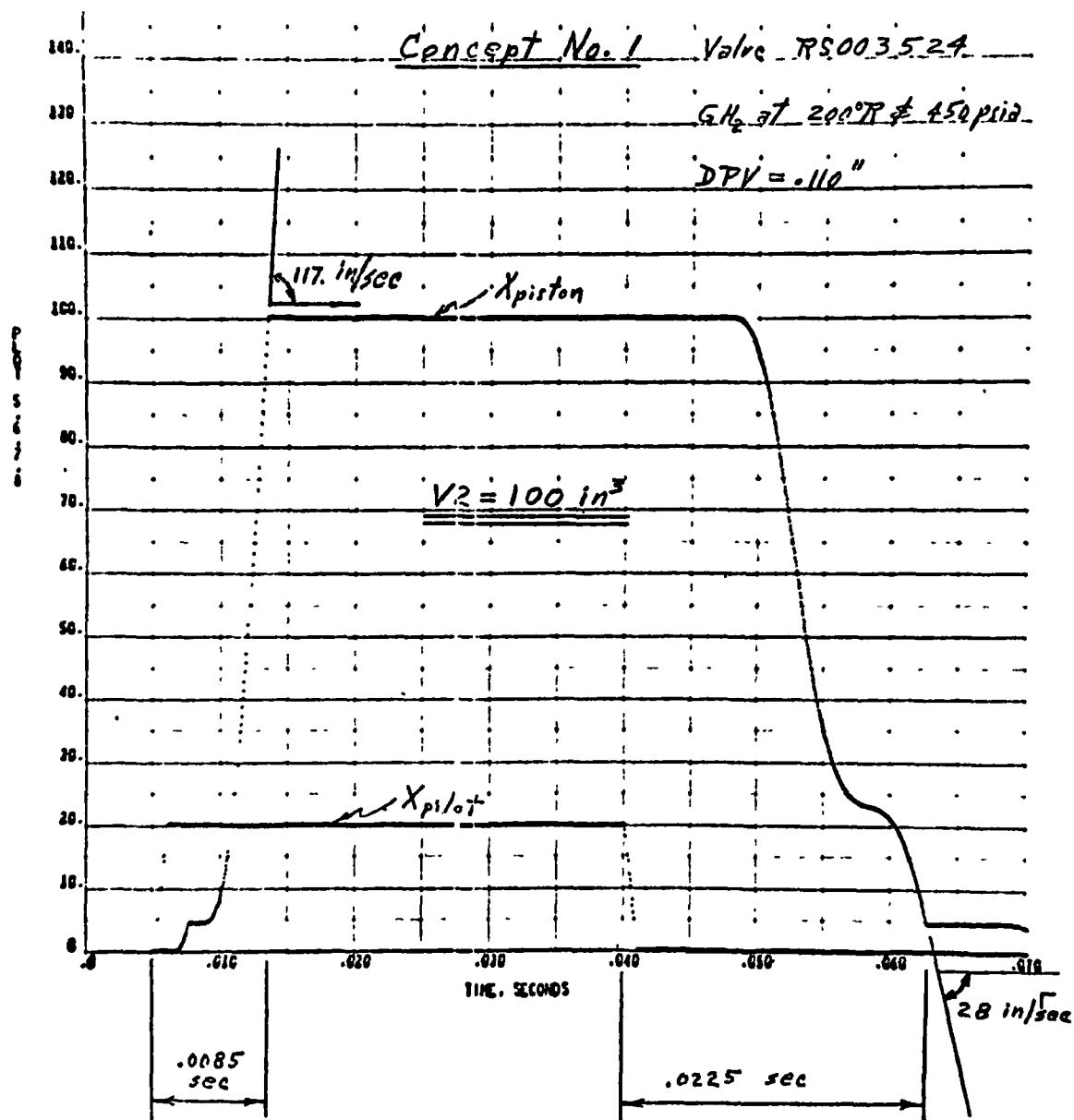


Figure F-6

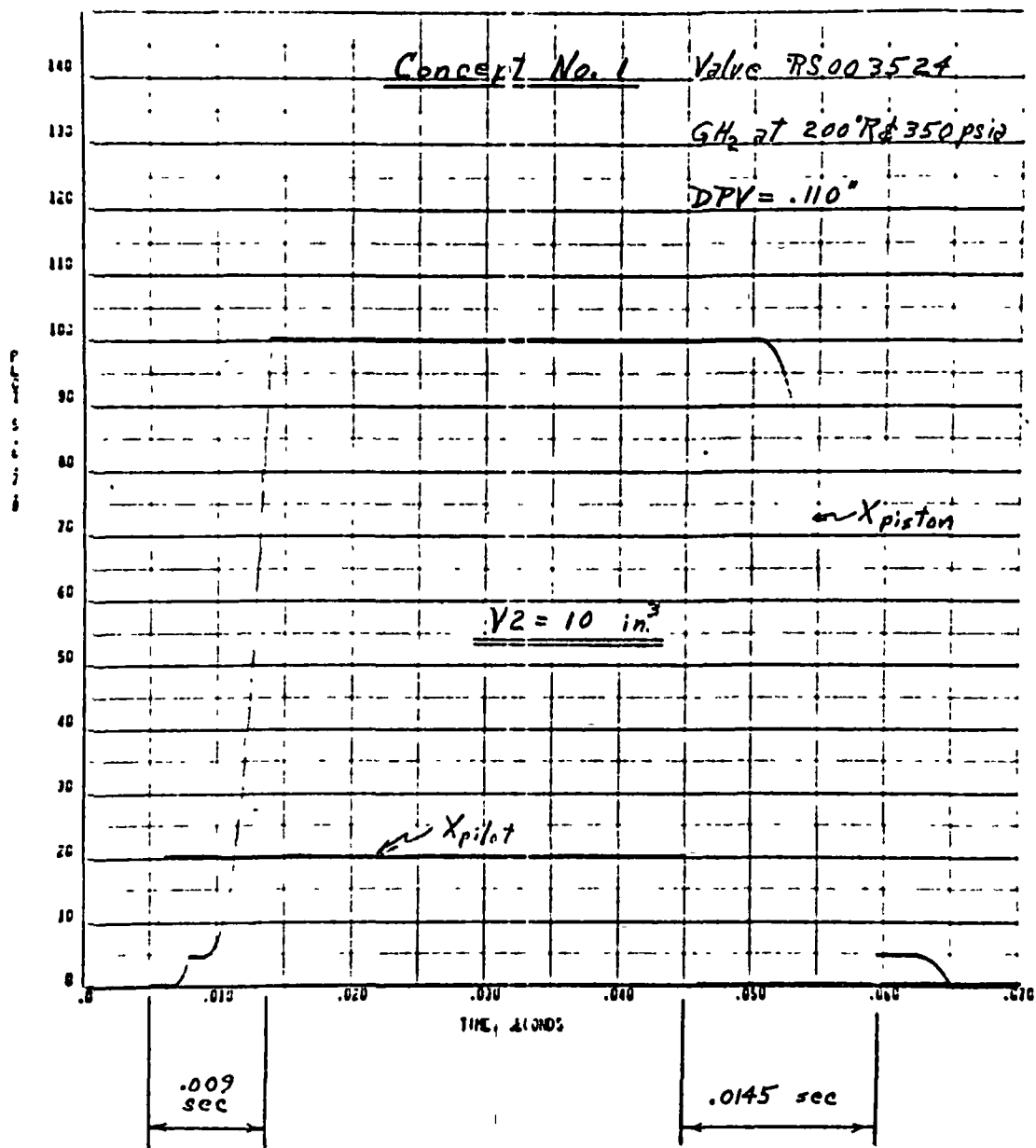


Figure F-7

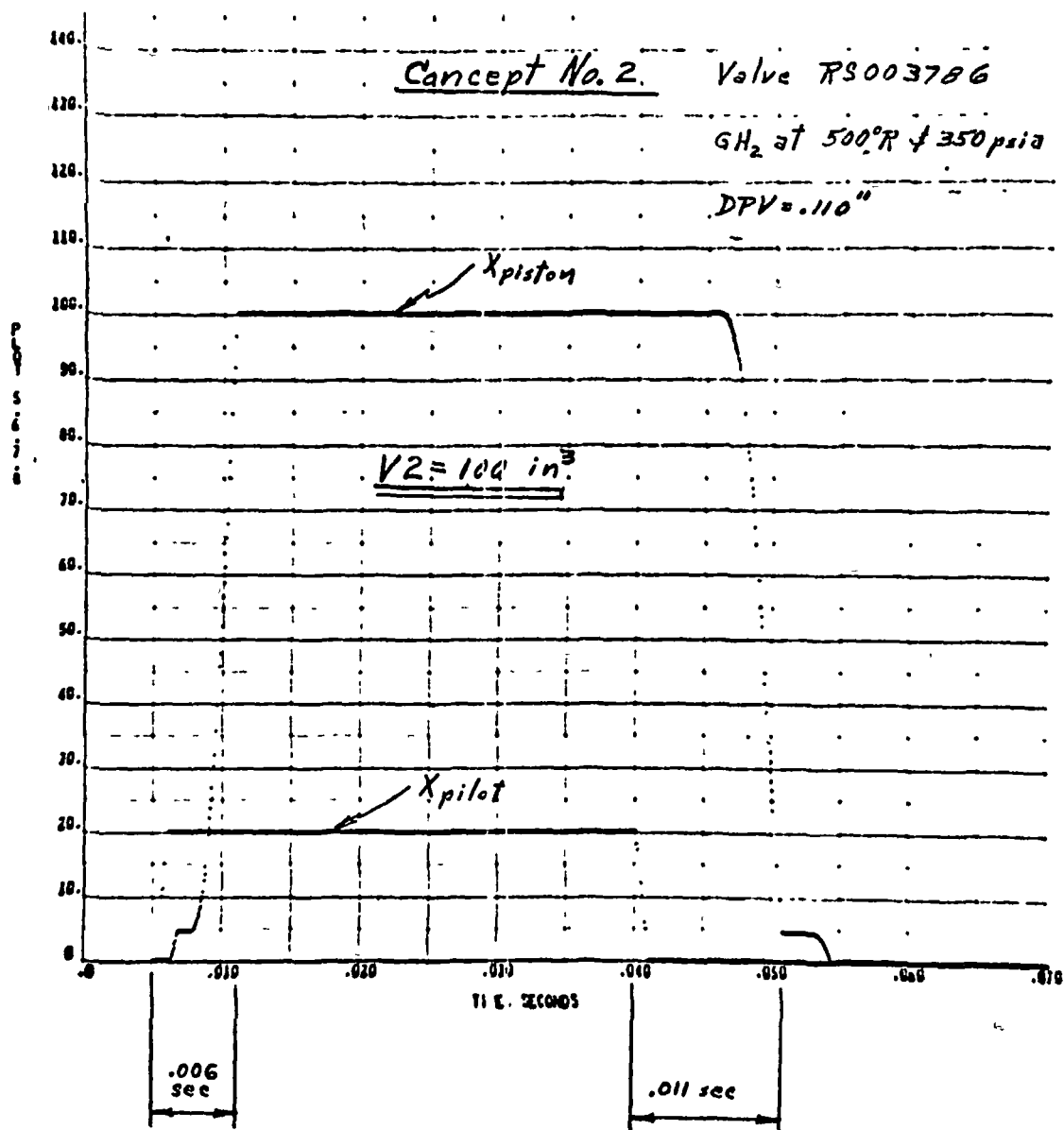


Figure F-8

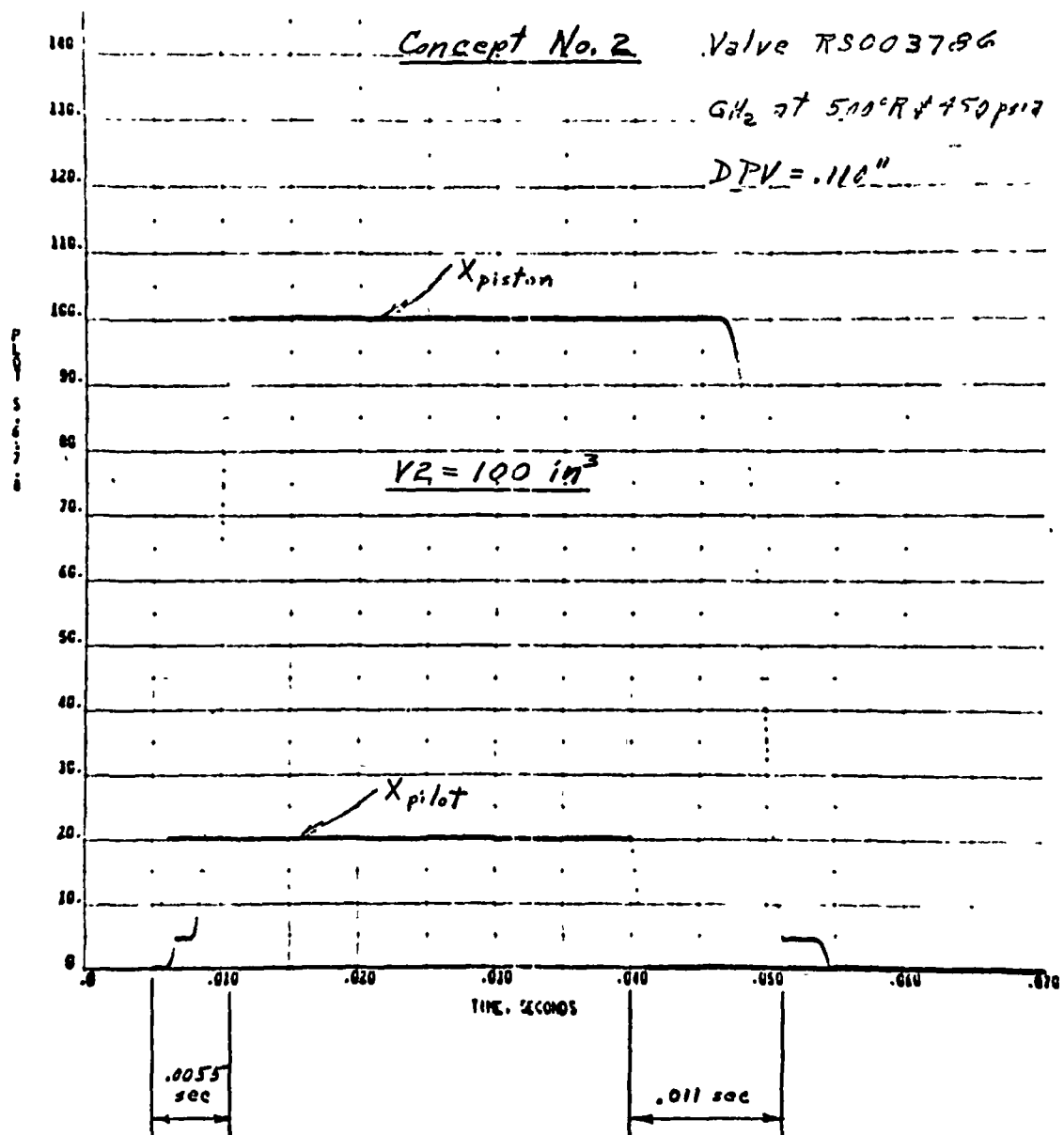


Figure F-9

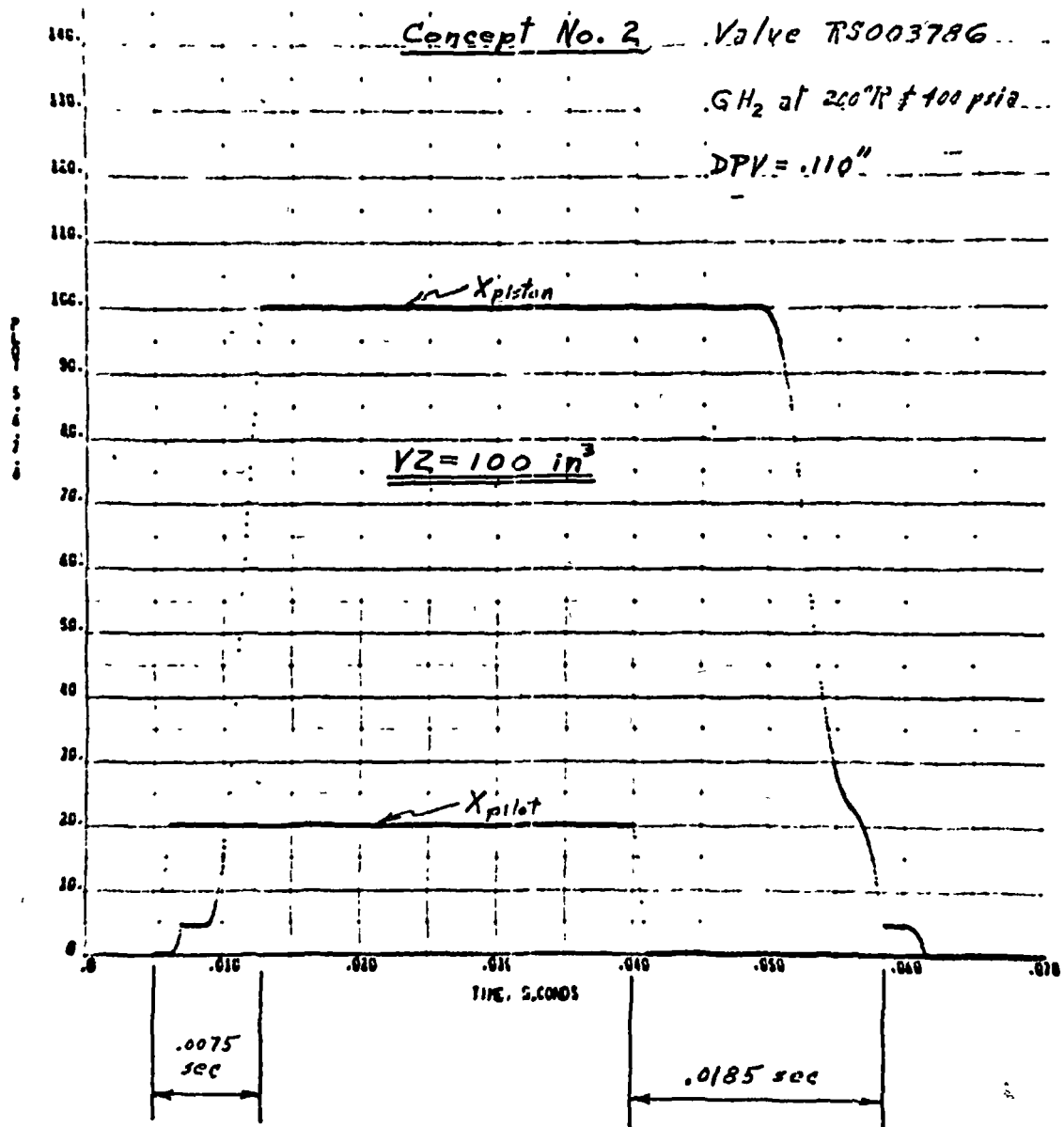


Figure F-10

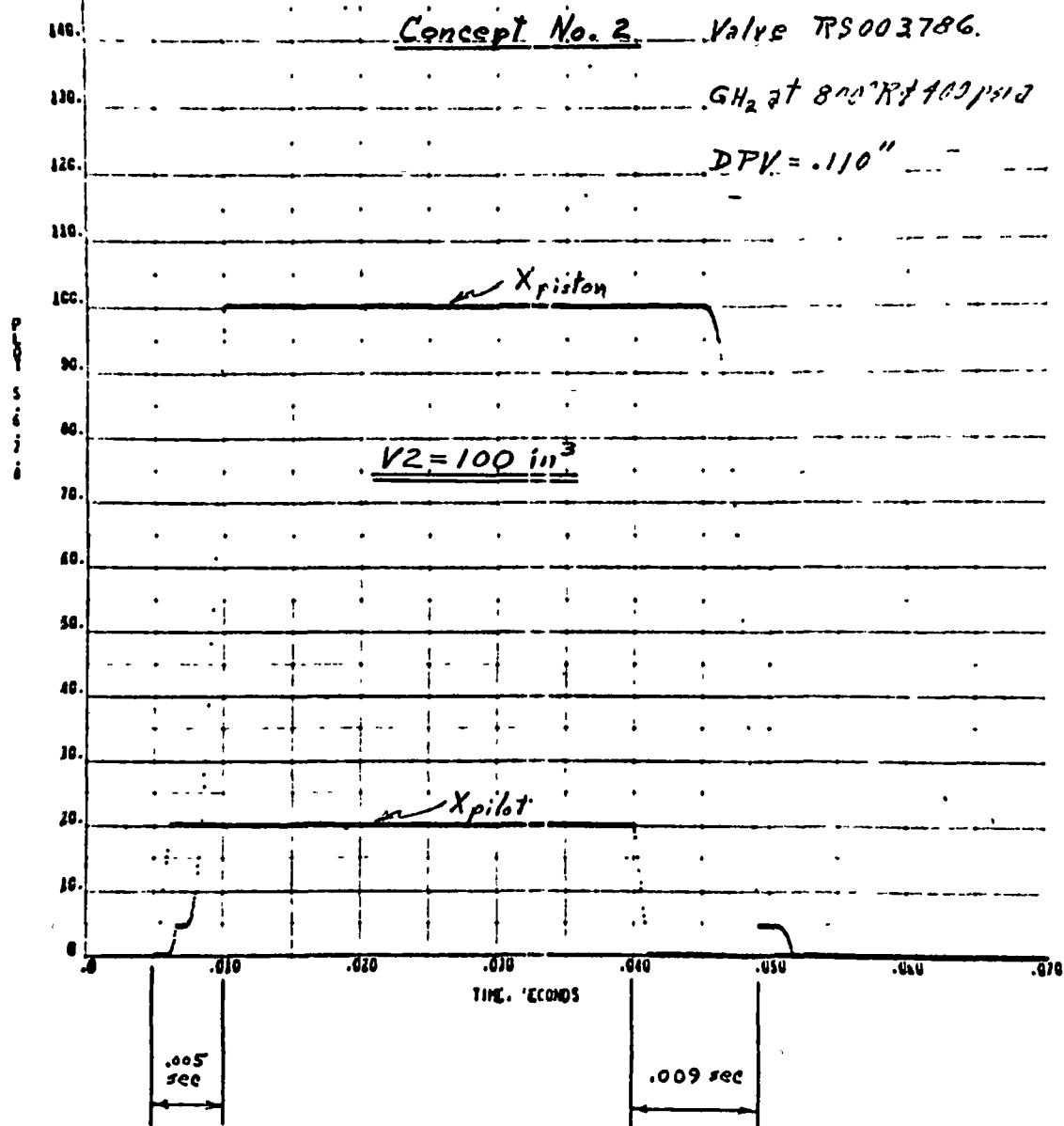


Figure F-11

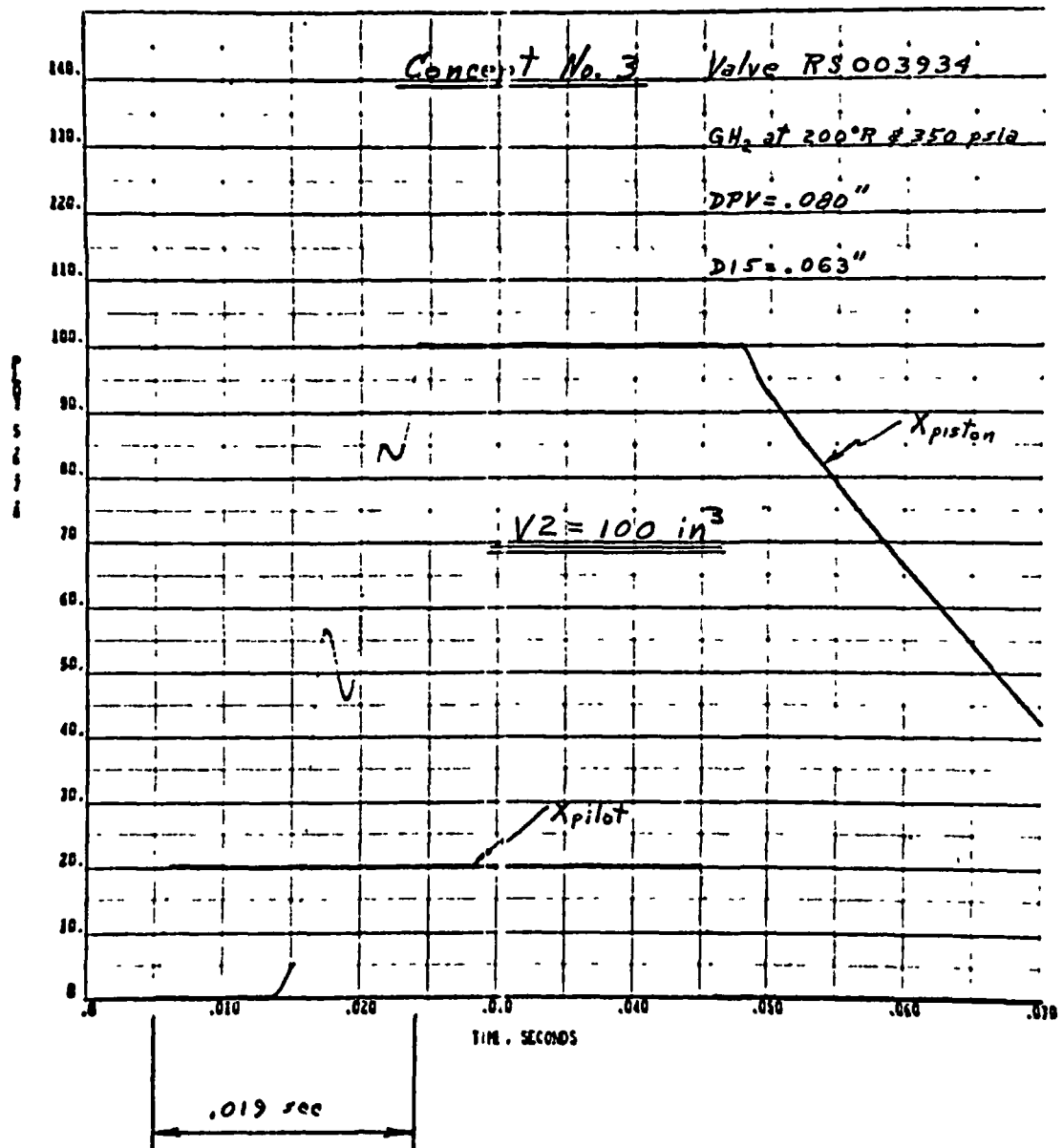


Figure F-12

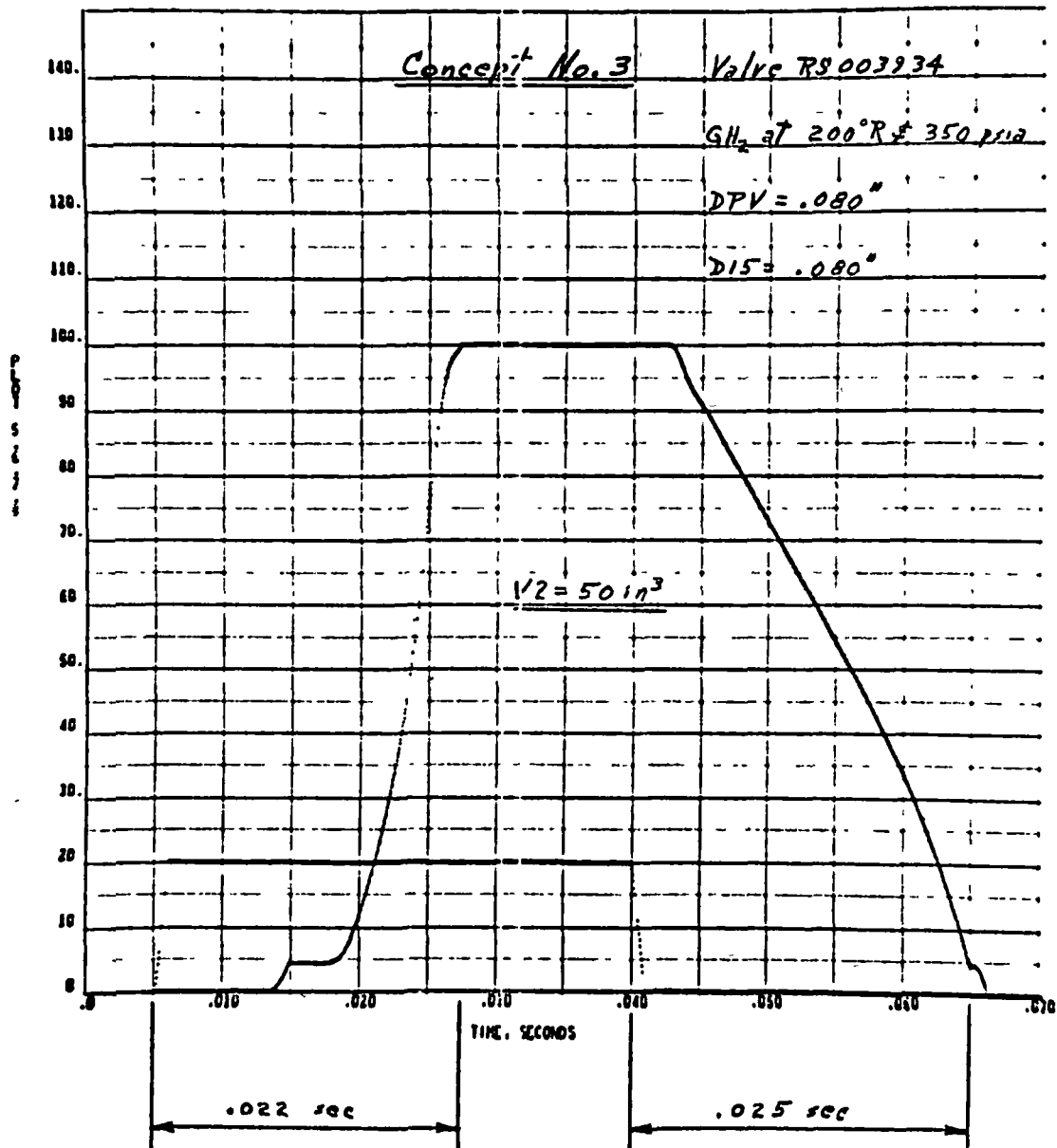


Figure F-13

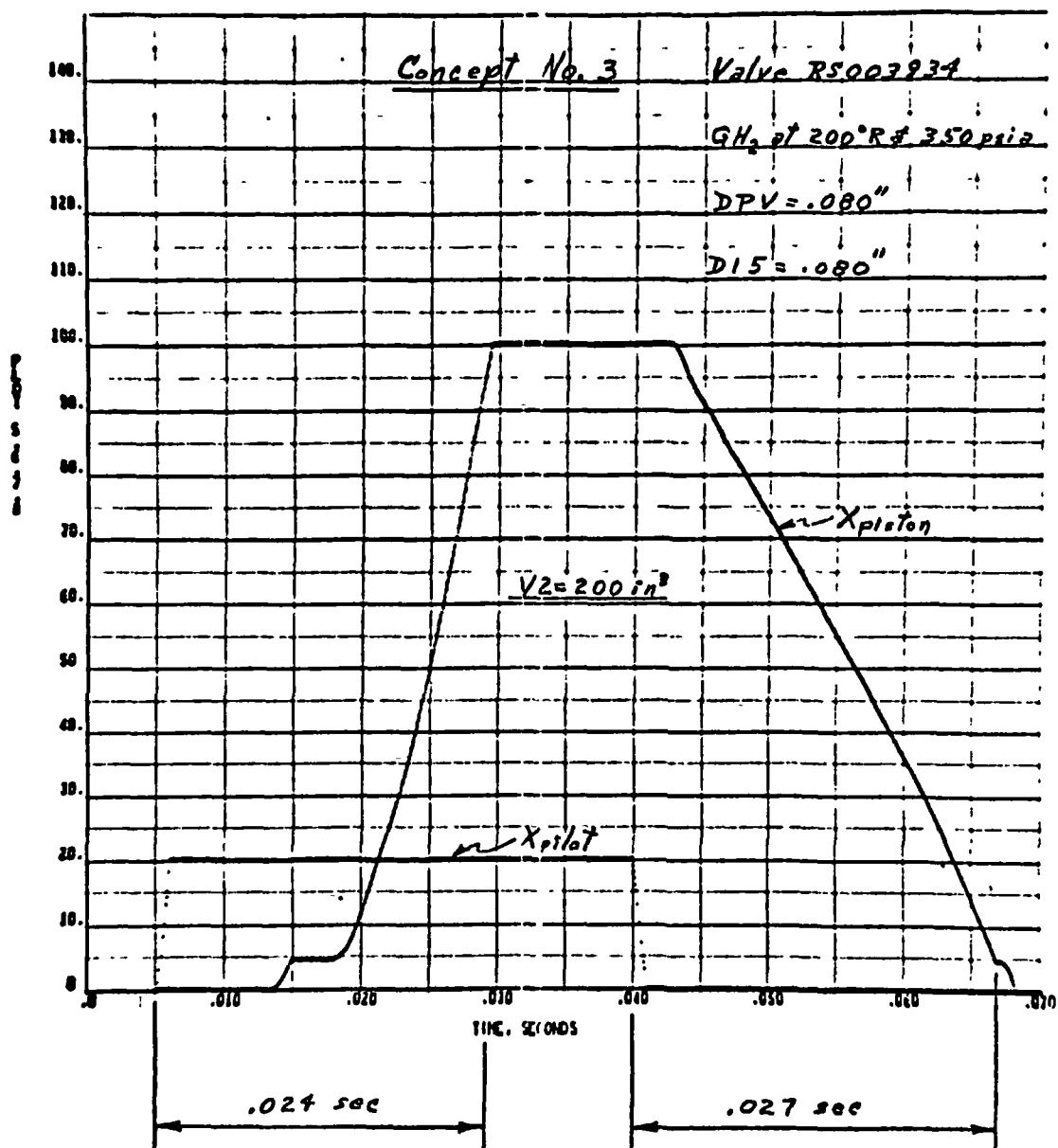


Figure F-14

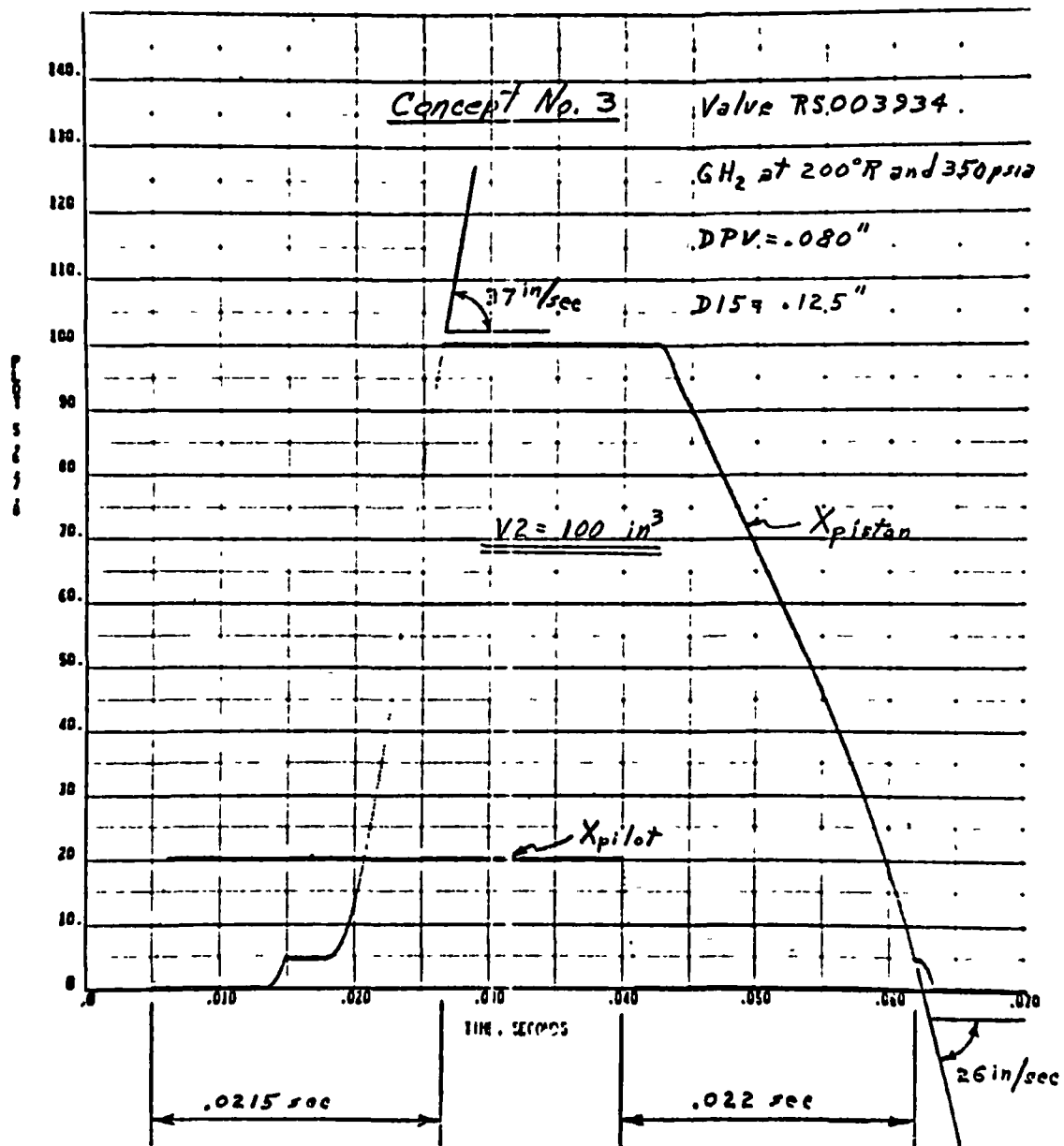


Figure F-15

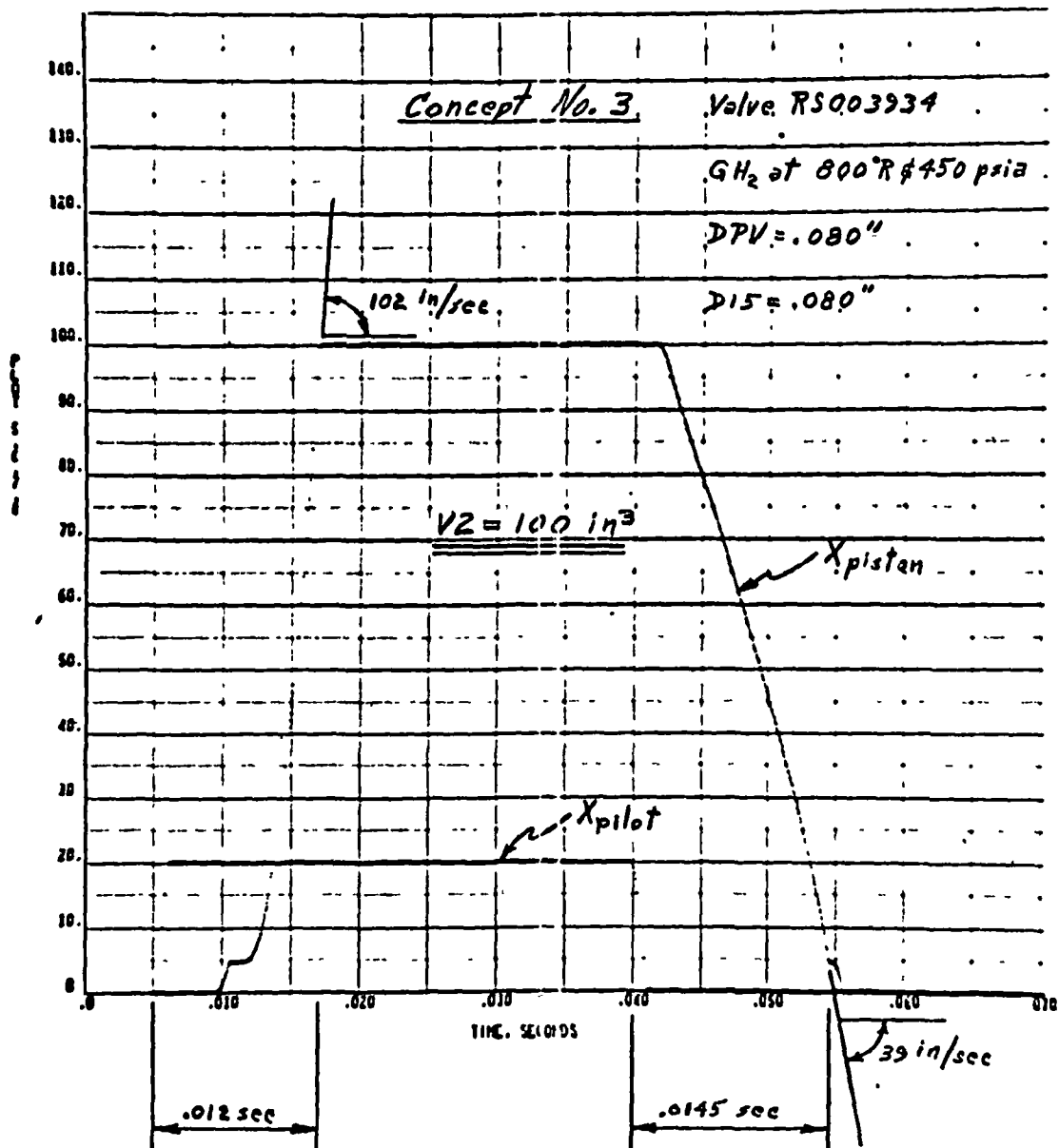


Figure F-16

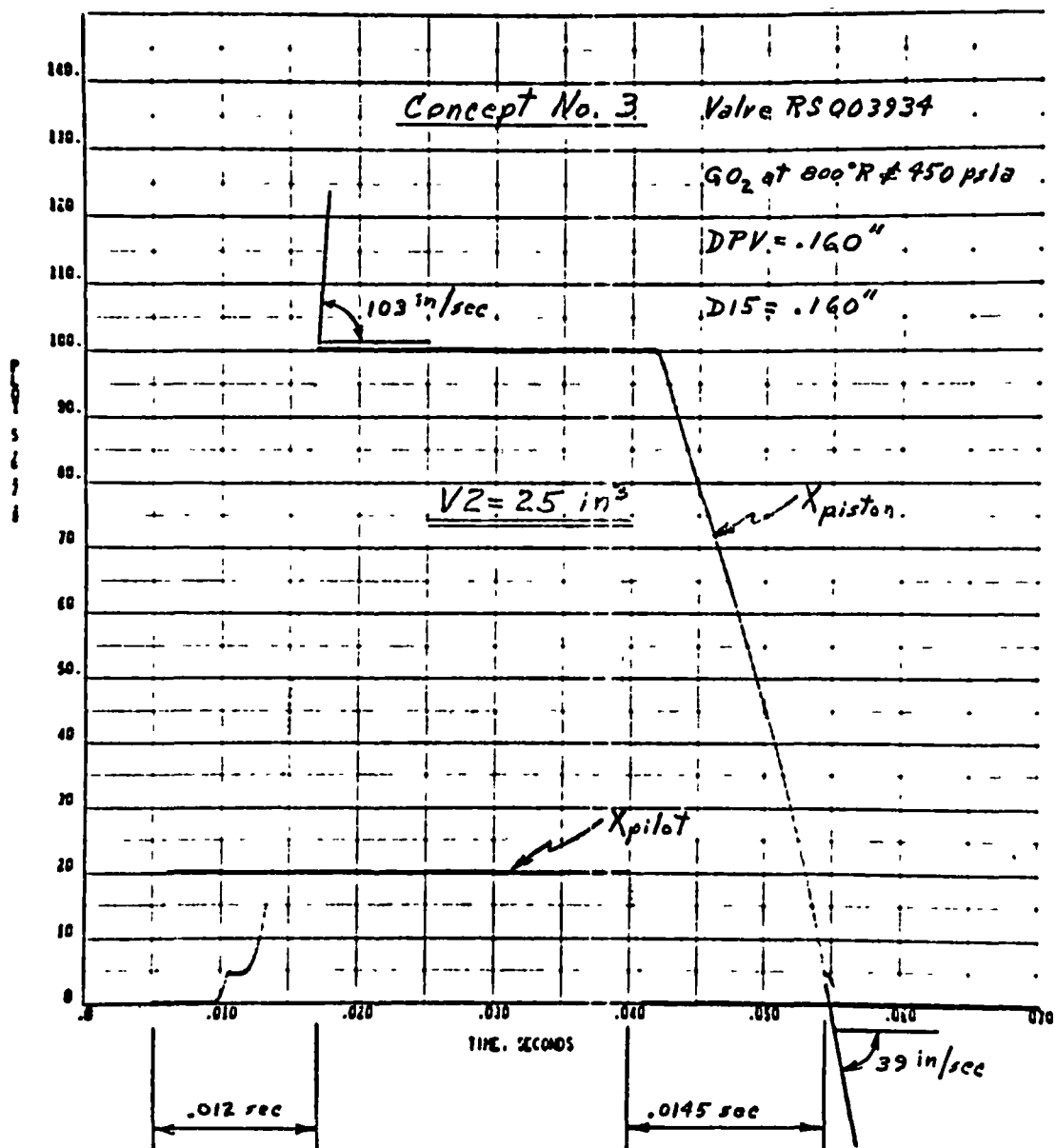


Figure F-17

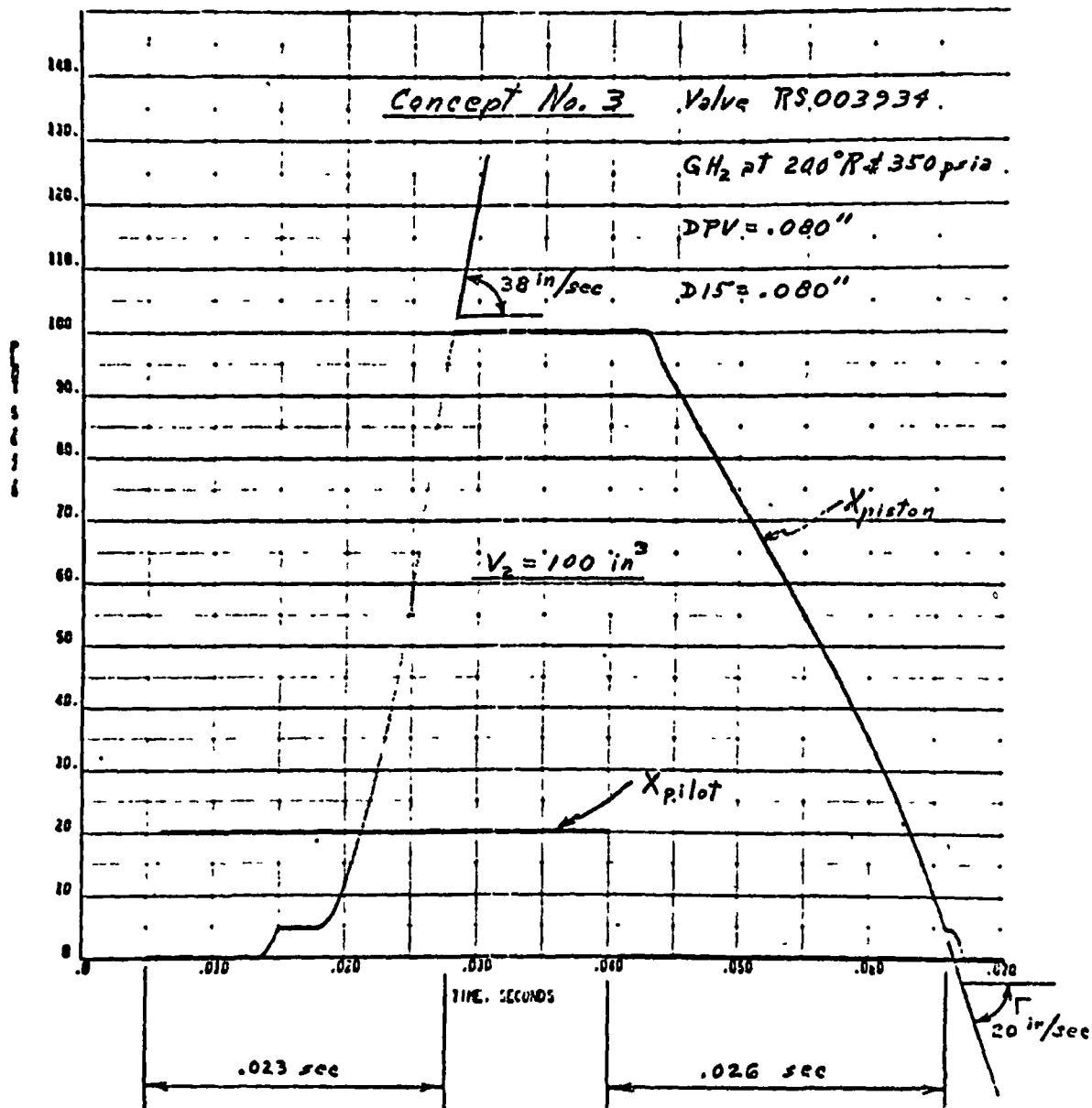


Figure F-18

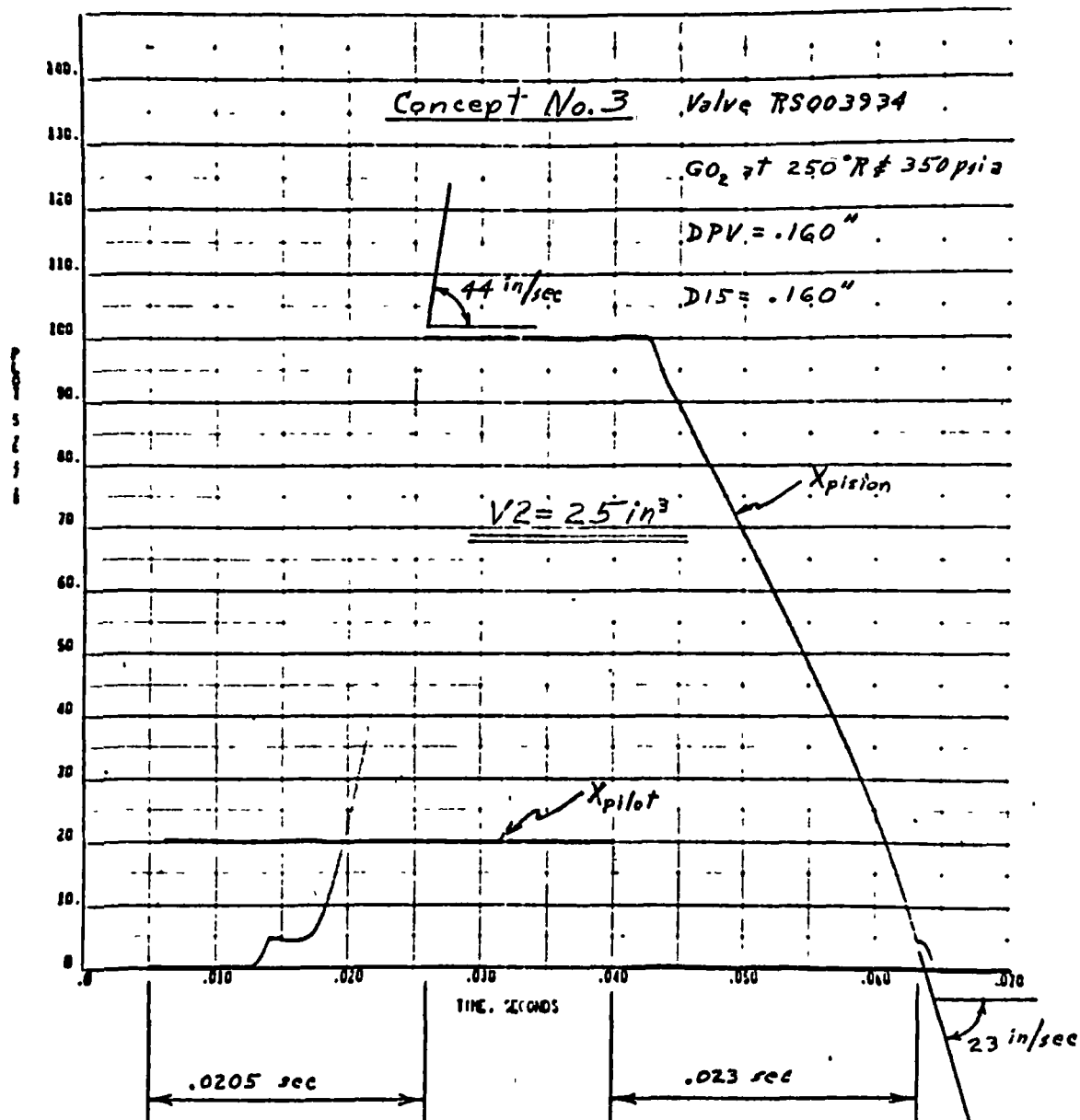


Figure F-19

SUMMARY OF COMPUTERIZED ANALYSES

Valve Concept No.	1	2	3
Pilot Valve Effective Flow Area (in ²) Oxygen Service Hydrogen Service	.0300 .0075	.0300 .0075	.016 .004
Valve Opening Time (sec)	.006-.010	.005-.008	.012-.023
Valve Closing Time (sec)	.009-.023	.009-.018	.014-.026
Opening Impact Velocity (in/sec)	133-83	212-90	102-38
Closing Impact Velocity (in/sec)	80-17	125-39	39-20

Figure F-20

DYNAMIC PERFORMANCE RATING

FEATURE CONCEPT	PILOT VALVE SIZE	CLOSING IMPACT VELOCITY	OPENING IMPACT VELOCITY	INLET PRESSURE EFFECTS	OUTLET PRESSURE EFFECTS	VENT PRESSURE EFFECTS	TOTAL POINTS
1	7	15	1	2	2	2	29
2	12	15	1	5	5	2	40
3	18	17	2	5	5	6	53
MAX. RATING POINTS	(20)	(20)	(2)	(6)	(6)	(6)	(60)

Figure F-21

LEVEL 18 (SEPT 69)

05/360 FORTRAN H

DATE 71.22

COMPILER OPTIONS - NAME= MAIN,OPT=01,LINECT=40,SOURCE,ERRORS,LIST,NOCHECK,LOAD,MAP,NOEDIT,IO,NXPR		
	C	C1001000
	C	C1002000
	C	C1003000
	C	C1004000
	C	C1005000
ISN 0002	C	C1006000
	C	C1007000
ISN 0003	C	C1008000
ISN 0004	C	C1009000
ISN 0005	C	C1010000
ISN 0006	C	C1011000
ISN 0007	C	C1012000
ISN 0008	C	C1013000
ISN 0009	C	C1014000
ISN 0010	C	C1015000
ISN 0011	C	C1016000
ISN 0012	C	C1017000
	C	C1018000
ISN 0013	C	C1019000
	C	C1020000
	C	C1021000
ISN 0014	C	C1022000
	C	C1023000
	C	C1024000
	C	C1025000
ISN 0015	C	C1026000
ISN 0016	C	C1027000
ISN 0017	C	C1028000
	C	C1029000
ISN 0018	C	C1030000
ISN 0019	C	C1031000
ISN 0020	C	C1032000
ISN 0021	C	C1033000
ISN 0022	C	C1034000
ISN 0023	C	C1035000
	C	C1036000
	C	C1037000
	C	C1038000
	C	C1039000
	C	C1040000

STI

ISN 0024	CD=0.8	C1034100
ISN 0025	A1=CD*PI4*DO1**2	C1034150
ISN 0026	AN=CD*PI4*DO**2	C1034200
	C	C1034600
	C	C1037000
	C	C1038000
ISN 0027	DEFINE INITIAL CONDITIONS	C1038050
	PS=AMAX1(PS,P1)	C1038060
ISN 0028	P1=AMAX1(PS,P1)	C1038100
ISN 0029	P2=PA	C1038130
ISN 0030	PC=PA	C1038150
ISN 0031	WDOT1=0.0	C1038160
ISN 0032	WDOT2=0.0	C1038200
ISN 0033	WDOT12=0.0	C1040000
	C	C1041000
	C	C1042000
	C	C1042100
ISN 0034	WRITE (6,15)	C1042110
ISN 0035	WRITE (6,16)	C1042200
ISN 0036	WRITE (6,20)P1,PA,STEP1,STEP2	C1043000
ISN 0037	WRITE (6,30)V2,DO,V1,DO1,PS	C1043100
ISN 0038	WRITE(6,40)VALVEN	C1044000
	C	C1045000
	C	C1045100
ISN 0039	IF (VALVEN-1.1) 90, 80, 80	C1045120
ISN 0040	80 IF (VALVEN-2.2) 92, 95, 95	C1046000
ISN 0041	90 CALL VALVE1(P1,P2,PA,WDOT12,STEP1,STEP2)	C1046100
ISN 0042	GO TO 98	C1046200
ISN 0043	92 CALL VALVE2(P1,P2,PA,WDOT12,STEP1,STEP2)	C1046300
ISN 0044	GO TO 98	C1046400
ISN 0045	95 CALL VALVE3(P1,P2,PA,WDOT12,STEP1,STEP2)	C1046500
ISN 0046	98 TIME=STEP1-T	C1055000
ISN 0047	GO TO 1000	C1056000
	C	C1056100
	C	C1056200
	C	C1057000
ISN 0048	100 CONTINUE	C1059000
	C	C1060000

	C	ITERATIVE COMPUTATIONS	C1060100
	C	*****	C1060200
	C		C1060300
ISN 0049		IF (VALVEN-1.1) 150, 110, 110	C1062020
ISN 0050	110	IF (VALVEN-2.2) 170, 170	C1062100
ISN 0051	150	CALL VALVE1(P1, P2, PA, WDOT12, STEP1, STEP2)	C1062200
ISN 0052		GO TO 200	C1062300
ISN 0053	160	CALL VALVE2(P1, P2, PA, WDOT12, STEP1, STEP2)	C1062400
ISN 0054		GO TO 200	C1062500
ISN 0055	170	CALL VALVE3(P1, P2, PA, WDOT12, STEP1, STEP2)	C1062600
	C		C1063050
	C		C1063075
	C		C1063080
	C	COMPUTE P2 AS FUNCTION OF VALVE OUTFLOW AND	C1063100
	C	SIMULATED INJECTOR FLOW	C1063110
ISN 0056	200	WDOT2C=FLOW(P2, PC, AQ, WDOT2C)	C1063200
ISN 0057		SUMW2=WDOT12-WDOT2C	C1063300
ISN 0058		CALL PRESS(V2, SUMW2, P2, P2DOT, 0., 0., 0)	C1063400
	C		C1070000
	C		C1072000
	C	COMPUTE P1 AS FUNCTION OF SUPPLY PRESSURE AND VALVE INFLOW	C1073000
ISN 0059		IF (V1-1.) 1000, 1000, 300	C1073050
ISN 0060	300	WDOTS1=FLOW(P1, P1, A1, WDOTS1)	C1073100
ISN 0061		SUMW1=WDOTS1-WDOT12	C1073200
ISN 0062		CALL PRESS(V1, SUMW1, P1, P1DOT, 0., 0., 0)	C1073300
	C		C1084000
ISN 0063	1000	RETURN	C1085000
ISN 0064		END	C1086000

LEVEL 18 (SEPT 69)		OS/360 FORTPAN H	DATE 71.22
COMPILER OPTIONS - NAME = MAIN,OPT=01,LINFCIT=40,SOURCE,FRCDIC,LIST,NODECK,LOAD,MAP,NODEIT,IO,NTRY			
	C		(4000000
	C		(4000100
	C		(4000200
	C		(4000300
	C		(4001000
	C		(4002000
	C	SLROUTINE FOR TIME RESPONSE OF PROPELLANT VALVE PS003934	(4003000
	C	***** ** ** ** ***** ** ***** ** *****	(4004000
	C		(4005000
ISN 0002	C	SUBROUTINE VALVE3(P1,P2,PA,WDOT12,STEP1,STEP2)	(4006000
	C		(4007000
	C		(4008000
	C		(4010000
	C		(4011000
ISN 0003		DIMENSION DUM1(28)	(4012000
ISN 0004		COMMON DUM1	(4013000
ISN 0005		COMMON TIME,T,T22,P1,P14,G,RT,XKRT1,RTI,XKRT1,RHO,GAMMA,FRULK	(4014000
ISN 0006		COMMON PHD1,GAMMA1,EPULK1,DUM2,DUM3	(4015000
ISN 0007		COMMON DUM4,DUM5,DUM6,DUM7,DUM8,XR,R,TEMP,XK1,R1,TEMP1	(4016000
ISN 0008		COMMON PLOT1,PLOT2,PLOT3,PLOT4,PLOT5,PLOT6,PLOT7,PLOT8	(4017000
ISN 0009		COMMON PLOT11,PLOT12,PLOT13,PLOT14,PLOT15,PLOT16,PLOT17,PLOT18	(4018000
ISN 0010		COMMON VAR1,VAR2,VAR3,VAR4,VAR5,VAR6,VAR7,VAR8,VAR9,VAR10,VAR11	(4019000
ISN 0011		COMMON VAR12,VAR13,VAR14,VAR15,VAR16,VAR17,VAR18,VAR19,VAR20	(4020000
ISN 0012		COMMON VAR21,VAR22	(4021000
	C		(4022000
	C		(4022100
	C		(4022200
ISN 0013	C	IF(TIME)1,1,100	(4023000
	C		(4024000
	C		(4024500
ISN 0014	C	1 CONTINUE	(4025000
	C		(4025100
	C		(4025200
	C		(4025300
	C		(4026000

C	NOMENCLATURE	04027000
C	*****	04028000
C	D1=PISTON DIAMETER (IN.)	04029000
C	D2=PISTON ROD DIAMETER (IN.)	04030000
C	D3=PUPPET DIAPHRAGM EFFECTIVE DIAMETER (IN.)	04031000
C	D4=PUPPET SEAT DIAMETER (IN.)	04032000
C	D4V=PILOT VALVE SEAT DIAMETER (IN.)	04033000
C	D4LV=PISTON TRAVEL WITH PUPPET SEATED (IN.)	04034000
C	F51=PISTON BIAS SPRING INSTALLED FORCE (LB.)	04035000
C	F51=PISTON BIAS SPRING RATE (LB./IN.)	04036000
C	F53=PUPPET FLEXURE INSTALLED FORCE (LB.)	04037000
C	F53=PUPPET FLEXURE SPRING RATE (LB./IN.)	04038000
C	STIC1=PISTON AND ROD STATIC FRICTION (LB.)	04039000
C	FRIC1=PISTON AND ROD DYNAMIC FRICTION (LB.)	04040000
C	P1=INLET PRESSURE (PSIA.)	04041000
C	P2=OUTLET PRESSURE (PSIA.)	04042000
C	P3=PISTON ACTUATION PRESSURE (PSIA.)	04043000
C	P4=VENT PRESSURE (PSIA.)	04044000
C	P5=PISTON DASHPOT PRESSURE (PSIA.)	04045000
C	PA=AMBIENT PRESSURE (PSIA.)	04046000
C	WT1=WEIGHT OF PISTON SUBASSEMBLY, EXCLUSIVE OF PUPPET (LB.)	04047000
C	WT2=WEIGHT OF PUPPET SUBASSEMBLY (LB.)	04048000
C	V2=SIMULATED INJECTOR VOLUME AT PRESSURE P2 (CU. IN.)	04049000
C	D0=SIMULATED INJECTOR ORIFICE DIAMETER (IN.)	04050000
C	V30=INITIAL VOLUME OF ACTUATOR CAVITY AT PRESSURE P3 (CU. IN.)	04051000
C	V50=INITIAL VOLUME OF ACTUATOR CAVITY AT PRESSURE P5 (CU. IN.)	04052000
C	D15=DIAMETER OF ORIFICE BETWEEN CAVITIES AT P1 AND P5 (IN.)	04053000
C	XP=PISTON DISPLACEMENT FROM CLOSED-POSITION STOP (IN.)	04054000
C	XV=PUPPET DISPLACEMENT FROM SEAT (IN.)	04055000
C	XDV=PILOT VALVE DISPLACEMENT FROM INLET SEAT (IN.)	04056000
C	XDOT, XVDOT=VELOCITIES (IN./SEC.)	04057000
C	XDDOT, XVDDOT=ACCELERATIONS (IN./SEC. SQUARED)	04058000
C	WDOT12=MAIN PUPPET PROPELLANT FLOWRATE (LB./SEC.)	04059000
C	WDOT13=GAS FLOWRATE TO ACTUATOR (LB./SEC.)	04060000
C	WDOT34=GAS FLOWRATE FROM ACTUATOR TO VENT (LB./SEC.)	04061000
C	WDOT15=GAS FLOWRATE TO CP FROM ACTUATOR DASHPOT CAVITY (LB./SEC.)	04062000
C	WDOT21=SIMULATED ENGINE INJECTOR PROPELLANT FLOWRATE (LB./SEC.)	04063000
C	STEP1=TIME AT WHICH PILOT VALVE BEGINS TO OPEN (SEC.)	04064000

	C	RAMP1=PILOT VALVE OPENING TRAVEL TIME (SEC.)	(4053000
	C	STFP2=TIME AT WHICH PILOT VALVE BEGINS TO CLOSE (SEC.)	(4054000
	C	RAMP2=PILOT VALVE CLOSING TRAVEL TIME (SEC.)	(4055000
	C	VALVEN=VALVE CONCEPT NUMBER	(4055100
	C		(4055200
	C		(4057000
	C	READ SUBROUTINE INPUT DATA	(4059000
ISN 0015		READ (5,10)D1,D2,D3,D4,D5	(4059000
ISN 0016		READ (5,10)F51,Y51,F53,Y53	(4060000
ISN 0017		READ (5,10)XPMAX,XVMAX,XPVMAX,D5LV	(4061000
ISN 0018		READ (5,10)WT1,WT2,V30,V50,D15	(4062000
ISN 0019		READ (5,10)RAMP1,RAMP2	(4063000
	C		(4064000
	C		(4064500
ISN 0020	10	FORMAT(6E12.5)	(4065000
ISN 0021	15	FORMAT(1H1 30X41H*****SUBROUTINE VALVE3 INPUT DATA*****)	(4065000
ISN 0022	16	FORMAT(37X2PH***** ***** ***/)	(4067000
ISN 0023	20	FORMAT(15X2HD1 15X2HD2 15X2HD3 15X2HD4 14X3HDPV/5F17.3//)	(4069000
ISN 0024	30	FORMAT(14X3HFS1 14X3HYS1 14X3HFS3 14X3HYS3/4F17.1//)	(4069000
ISN 0025	40	FORMAT(12X5HXPMA 12X5HXVMA 11X6HXPVMA 13X4HDELV/4F17.3//)	(4070000
ISN 0026	50	FORMAT(14X3HWT1 14X3HWT2 14X3HV3C 14X3HV50 14X3HD15/5F17.3//)	(4071000
ISN 0027	60	FORMAT(12X5HRAMP1 12X5HRAMP2/2F17.4//)	(4072000
ISN 0028	80	FORMAT(1H1 30X41H*****SUBROUTINE VALVE3 OUTPUT DATA*****)	(4072100
ISN 0029	82	FORMAT(37X2PH***** ***** ***/)	(4072200
ISN 0030	85	FORMAT(11X6HXVOUT1 11X6HXOVER1 11X6HXPOOT2 11X6HXVOUT2 11X6HXOVER2/6F17.3//)	(4072300
	1	12X5HTOVER/6F17.3//)	(4072400
	C		(4073000
	C		(4074000
	C	OFFLINE OR COMPUTE CONSTANTS	(4075000
ISN 0031		CO=0.8	(4076000
ISN 0032		SLUG1=WT1/G	(4080000
ISN 0033		SLUG2=WT2/G	(4081000
ISN 0034		SLUG12=SLUG1+SLUG2	(4082000
ISN 0035		XPMIN=0.0	(4083000
ISN 0036		XVMIN=0.0	(4084000
ISN 0037		XPVMIN=0.0	(4085000
ISN 0038		XPVDEL=XPVMA X-XPVMIN	(4085100
ISN 0039		CNFR=0.5	(4085150

ISN 0040	XLIM1=XPMAX-.015	04095160
ISN 0041	XLIM2=DELV+.015	04095170
ISN 0042	CONV=CD*PI*04	04096000
ISN 0043	CONPV=CD*PI*0PV	04097000
ISN 0044	CFN1=20./XPVMAX	04098000
ISN 0045	CFN2=100./XVMAX	04099000
ISN 0046	CFN3=100./XPMAX	04100000
ISN 0047	FF1=PI-CT*.06+.1	04101000
ISN 0048	T14E1=STFP1+RAMP1	04102000
ISN 0049	T14E2=STFP2+RAMP2	04103000
	C	04104000
	C	04105000
	C	04106000
	COMPUTE PRESSURIZED CROSS-SECTION AREAS	04107000
ISN 0050	AA1=PI4*D1**2	04108000
ISN 0051	AA2=PI4*D2**2	04109000
ISN 0052	AA3=PI4*D3**2	04110000
ISN 0053	AA4=PI4*D4**2	04111000
ISN 0054	AA12=AA1-AA2	04112000
ISN 0055	AA23=AA3-AA2	04113000
ISN 0056	AA34=AA4-AA3	04114000
ISN 0057	AA24=AA4-AA2	04115000
	C	04116000
	C	04117000
	C	04118000
	COMPUTE MAXIMUM EFFECTIVE FLOW AREAS AND COMPUTE FIXED EFFECTIVE FLOW AREAS	04119000
ISN 0058	A12MAX=CD*(AA4-AA2)	04120000
ISN 0059	A13MAX=CD*PI4*0PV**2	04121000
ISN 0060	A34MAX=0.9*A13MAX	04122000
ISN 0061	A11C5=CD*PI4*015**2	04123000
	C	04124000
	C	04125000
	C	04126000
	DEFINE INITIAL CONDITIONS	04127000
ISN 0062	P4=PA	04128000
ISN 0063	P3=P1	04129000
ISN 0064	P5=P1	04130000
ISN 0065	XV=XVMIN	04131000
ISN 0066	XP=XPMIN	04132000
ISN 0067	XPV=XPVMIN	04133000

ISN 0068	WDOT12=0.0	04110000
ISN 0069	WDOT13=0.0	04111000
ISN 0070	WDOT34=0.0	04112000
ISN 0071	WDOT15=0.0	04112100
ISN 0072	P3DOT=0.0	04113000
ISN 0073	P5DOT=0.0	04113100
ISN 0074	XPDOT=0.0	04114000
ISN 0075	XPDOT=(P5*AA12-P3*AA1-(P1-P2)*AA23-FS1-Y51*XP+FS3+P2*AA2)/SLUG1	04114050
ISN 0076	XVDOT=0.0	04114100
ISN 0077	N=Q	04114600
	C	04115000
	C	04116000
	C	04117000
	PPINT TABULATION OF SURRCUTINE INPUT DATA	04118000
ISN 0078	WRITE (6,15)	04119000
ISN 0079	WRITE (6,16)	04120000
ISN 0080	WRITE (6,20)D1,D2,D3,D4,DPV	04121000
ISN 0081	WRITE (6,30)FS1,Y51,FS3,Y53	04122000
ISN 0082	WRITE (6,40)XPMAX,XVMAX,XPVMAX,DELV	04123000
ISN 0083	WRITE (6,50)WT1,WT2,V10,V50,D15	04124000
ISN 0084	WRITE (6,60)RAMP1,RAMP2	04125000
	C	04126000
	C	04127000
ISN 0085	GO TO 1000	04128000
	C	04129000
	C	04130000
ISN 0086	100 CONTINUE	04131000
	C	04132000
	C	04133000
	C	04134000
	C	04135000
	C	04136000
	ITERATIVE COMPUTATIONS	04136100
	*****	04136120
	C	04136140
	COMPUTE PILOT VALVE DISPLACEMENT	04136160
ISN 0087	IF (TIME-STEP2)140,140,175	04136180
ISN 0088	140 IF (TIME-STEP1)150,150,155	04136200
ISN 0089	150 XPV=XPVMIN	04136220
ISN 0090	GO TO 155	04136240
ISN 0091	155 IF (TIME-TIME1)160,170,170	04136260
ISN 0092	160 XPV=XPVMIN+((TIME-STEP1)/RAMP1)*XPVDEL	04136280

ISN 0093	GO TO 195	(4136220
ISN 0094	170 XPV=XPVMAX	(4136240
ISN 0095	GO TO 195	(4136260
ISN 0096	175 IF (TIME-TIME2),180,150,150	(4136280
ISN 0097	180 XPV=XPVMAX-((TIME-STIP2)/RAMP2)*XPVDFL	(4136300
ISN 0098	195 CONTINUE	(4136320
	C	(4137000
	C	(4138000
	C COMPUTE DYNAMIC SEAL FRICTION FORCE	(4139100
	C ONE SEAL AT D1 EXPOSED TO P5-P3	(4139200
ISN 0099	FFIC1=(500.+P5-P3)*FF1	(4139300
ISN 0100	STIC1=FRIC1	(4139400
	C	(4139500
	C	(4140000
	C COMPUTE VARIABLE EFFECTIVE FLOW AREAS	(4141000
ISN 0101	A0102=AMIN1(A12MAX,CONPV*XPV)	(4142000
ISN 0102	A0103=AMIN1(A13MAX,CONPV*(XPVMAX-XPV))	(4143000
ISN 0103	A0104=AMIN1(A34MAX,CONPV*XPV)	(4144000
	C	(4146000
	C	(4147000
	C COMPUTE VARIABLE VOLUMES	(4148000
ISN 0104	V3=V30-AA1*XP	(4149000
ISN 0105	V5=V50+AA12*XP	(4150000
	C	(4151000
	C	(4152000
	C COMPUTE GAS WEIGHT FLOWRATES	(4153000
ISN 0106	WDOT12=FLOW(P1,P2,A0102,WDOT12)	(4154000
ISN 0107	WDOT13=FLOW(P1,P3,A0103,WDOT13)	(4155000
ISN 0108	WDOT34=FLOW(P3,P4,A0304,WDOT34)	(4156000
ISN 0109	SUMW3=WDOT13-WDOT34	(4157000
ISN 0110	WDOT15=FLOW(P1,P5,A0105,WDOT15)	(4158000
	C	(4159000
	C	(4160000
	C COMPUTE RATES OF CHANGE OF PRESSURES AND COMPUTE PRESSURES	(4161000
ISN 0111	CALL PRESS(V3,SUMW3,P3,P3DOT,AA1,XPDOT,1)	(4162000
ISN 0112	CALL PRESS(V5,WDOT15,P5,P5DOT,AA12,XPDOT,-1)	(4163000
	C	(4164000
	C	(4165000

*****MAIN PROGRAM INPUT DATA*****

T (SECONDS)	FINIS (SECONDS)	FRINT (SECONDS)	STOP (SECONDS)	HOP (--)	
0.00050	0.070	0.0	0.070000	21.00	
PLOT (SECONDS)	STOP1 (SECONDS)	SKIP (--)	FORMT (--)	FORMT1 (--)	
0.0	0.070050	1.00	6.0	0.0	
XK (CP/CV)	P (FT./DEG. R.)	TEMP (DEG. RANKINE)			
1.400	766.8	200.0			
XK1 (CP/CV)	R1 (FT./DEG. R.)	TEMP1 (DEG. RANKINE)			
1.005	0.0	0.5			
RHO (LB./FT. CUBED)	EBULK (PSI.)	RHO1 (LB./FT. CUBED)	EBULK1 (PSI.)		
0.0	0.0	0.0	0.0		
FRAMES (--)	TABS (--)				
2.0	1.0				
Y1MIN	Y1MAX	DY1	Y2MIN	Y2MAX	DY2
0.0	600.0000	20.0000	0.0	150.0000	5.0000
DX1 (SECONDS)	DX2 (SECONDS)				
0.0050	0.0050				
Y3MIN	Y3MAX	DY3	Y4MIN	Y4MAX	DY4
0.0	0.0	0.0	0.0	0.0	0.0
DX3 (SECONDS)	DX4 (SECONDS)				
0.0	0.0				

*****SUBROUTINE CONSYS INPUT DATA*****

P1
400.000

PA
14.700

STEP1
0.005

STEP2
0.040

V2
50.000

DN
0.705

V1
0.0

DC1
0.0

PS
400.000

VALVEN
3.0

*****SUBROUTINE VALVE3 INPUT DATA*****

D1 1.771	D2 0.500	D3 1.176	D4 1.362	DPV 0.080
-------------	-------------	-------------	-------------	--------------

FS1 50.0	YS1 100.0	FS3 5.2	YS3 344.0
-------------	--------------	------------	--------------

XPMAX 0.332	XVMAX 0.400	XPVMAX 0.020	DELV 0.015
----------------	----------------	-----------------	---------------

WT1 0.750	WT2 0.063	V3C 1.500	V50 0.500	D15 0.080
--------------	--------------	--------------	--------------	--------------

RAMP1 0.0010	RAMP2 0.0010
-----------------	-----------------

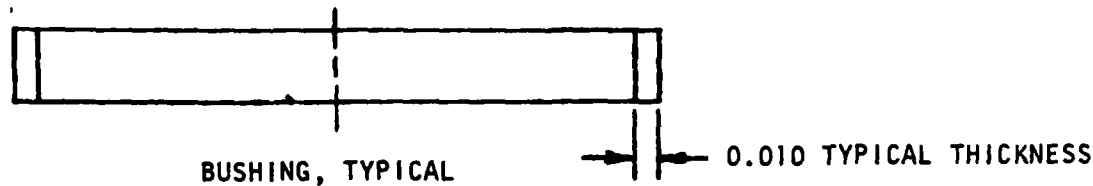
TIME	VAR1	VAR2	VAR3	VAR4	VAR5	VAR6	VAR7	VAR8	VAR9	VAR10	VAR11
0.004950	400.00	14.70	400.00	14.70	400.0000	0.0	0.0	0.0	0.0	-617.7422	0.0
0.006000	400.00	14.70	388.47	14.70	400.0000	0.0200	0.0	0.0	0.0	-557.1494	0.0
0.007050	400.00	14.70	364.02	14.70	400.0000	0.0200	0.0	0.0	0.0	-475.7754	0.0
0.008100	400.00	14.70	341.10	14.70	400.0000	0.0200	0.0	0.0	0.0	-399.4658	0.0
0.009150	400.00	14.70	319.62	14.70	400.0000	0.0200	0.0	0.0	0.0	-327.9622	0.0
0.010200	400.00	14.70	299.50	14.70	400.0000	0.0200	0.0	0.0	0.0	-260.9617	0.0
0.011250	400.00	14.70	280.64	14.70	400.0000	0.0200	0.0	0.0	0.0	-198.1775	0.0
0.012300	400.00	14.70	262.97	14.70	400.0000	0.0200	0.0	0.0	0.0	-139.7468	0.0
0.013350	400.00	14.70	246.41	14.70	400.0000	0.0200	0.0	0.0	0.0	-84.2254	0.0
0.014399	400.00	14.70	230.90	14.70	400.0000	0.0200	0.0	0.0	0.0	-32.5773	0.0
0.015449	400.00	14.70	216.36	14.70	400.0000	0.0200	0.0	0.0	0.0	0.0	0.0
0.016499	400.00	14.70	202.74	14.70	400.0000	0.0200	0.0	0.0	0.0	0.0	0.0
0.017549	400.00	14.70	191.09	14.70	357.7959	0.0200	0.0027	0.0	7.2440	28.8854	0.0
0.018599	400.00	14.70	184.06	14.70	389.2249	0.0200	0.0150	0.0	0.0	-100.7071	0.0
0.019649	400.00	14.70	172.19	14.70	400.0168	0.0200	0.0150	0.0	0.0	-33.6556	0.0
0.020699	400.00	14.70	161.08	14.70	400.0044	0.0200	0.0150	0.0	0.0	0.0	0.0
0.021749	400.00	14.70	150.69	14.70	359.5556	0.0200	0.0150	0.0	0.0	0.0	0.0
0.022799	400.00	14.70	140.97	14.70	400.0044	0.0200	0.0150	0.0	0.0	0.0	0.0
0.023849	400.00	14.83	132.44	14.70	358.7183	0.0200	0.0170	0.0020	5.2033	21.8566	0.0203
0.024899	400.00	17.51	126.88	14.70	350.9961	0.0200	0.0274	0.0124	14.5496	20.8211	0.1493
0.025949	400.00	28.31	124.03	14.70	379.2017	0.0200	0.0464	0.0314	21.2305	13.9941	0.3984
0.026999	400.00	51.91	123.15	14.70	366.3650	0.0200	0.0719	0.0569	27.8592	20.5226	0.7362
0.028049	400.00	91.48	125.23	14.70	348.8936	0.0200	0.1065	0.0915	38.8342	32.0400	1.1911
0.029099	400.00	152.07	132.87	14.70	323.5053	0.0200	0.1552	0.1402	54.6365	44.2111	1.8310
0.030149	400.00	241.28	151.32	14.70	252.4172	0.0200	0.2228	0.2078	74.7919	54.1662	2.6962
0.031198	400.00	349.21	194.07	14.70	258.4211	0.0200	0.3120	0.2970	92.6483	15.4856	2.7639
0.032248	400.00	390.40	188.50	14.70	276.5056	0.0200	0.3320	0.3170	0.0	152.9166	1.2937
0.033298	400.00	391.19	163.25	14.70	307.7805	0.0200	0.3320	0.3170	0.0	315.7007	1.2116
0.034348	400.00	391.19	141.39	14.70	335.9055	0.0200	0.3320	0.3170	0.0	458.3142	1.2115
0.035398	400.00	391.19	122.45	14.70	359.9028	0.0200	0.3320	0.3170	0.0	580.8320	1.2115
0.036448	400.00	391.19	106.05	14.70	378.5167	0.0200	0.3320	0.3170	0.0	682.0764	1.2115
0.037498	400.00	391.19	91.84	14.70	392.2312	0.0200	0.3320	0.3170	0.0	761.0952	1.2115
0.038548	400.00	391.19	79.54	14.70	399.2361	0.0200	0.3320	0.3170	0.0	817.0923	1.2115
0.039598	400.00	391.19	68.89	14.70	400.0002	0.0200	0.3320	0.3170	0.0	851.0254	1.2115
0.040648	400.00	391.19	72.63	14.70	400.0007	0.0070	0.3320	0.3170	0.0	839.7578	1.2115
0.041698	400.00	391.19	130.68	14.70	359.9990	0.0	0.3320	0.3170	0.0	666.1870	1.2115
0.042748	400.00	391.19	193.94	14.70	400.0007	0.0	0.3320	0.3170	0.0	477.1255	1.2115
0.043798	400.00	391.19	256.86	14.70	359.9993	0.0	0.3320	0.3170	0.0	289.0591	1.2115
0.044848	400.00	391.19	315.15	14.70	400.0007	0.0	0.3320	0.3170	0.0	114.8463	1.2115
0.045898	400.00	391.19	362.15	14.70	359.9990	0.0	0.3320	0.3170	0.0	0.0	1.2115
0.046948	400.00	391.19	385.70	14.70	402.2827	0.0	0.3320	0.3170	-11.6790	-46.8044	1.2115

TIME	VAR1	VAR2	VAR3	VAR4	VAR5	VAR6	VAR7	VAR8	VAR9	VAR10	VAR11
0.047998	400.00	391.19	377.00	14.70	412.7266	0.0	0.3093	0.2943	-19.5002	11.6830	1.2115
0.049047	400.00	390.46	377.74	14.70	415.7473	0.0	0.2937	0.2787	-9.9764	18.6764	1.1935
0.050097	400.00	389.75	385.48	14.70	412.1489	0.0	0.2842	0.2692	-10.5443	-15.3683	1.1943
0.051147	400.00	388.82	383.35	14.70	414.3640	0.0	0.2701	0.2551	-15.3228	-2.5455	1.1819
0.052197	400.00	387.47	381.40	14.70	416.6091	0.0	0.2549	0.2399	-12.7876	9.2499	1.1742
0.053247	400.00	386.10	383.73	14.70	415.0964	0.0	0.2427	0.2277	-11.4555	-3.1085	1.1710
0.054297	400.00	384.61	383.81	14.70	415.1711	0.0	0.2295	0.2145	-13.6188	-4.2248	1.1597
0.055347	400.00	382.65	382.36	14.70	416.6802	0.0	0.2149	0.1999	-13.6641	2.7772	1.1447
0.056397	400.00	380.31	382.45	14.70	416.7107	0.0	0.2011	0.1861	-12.8173	0.1085	1.1319
0.057447	400.00	377.60	382.46	14.70	416.7676	0.0	0.1874	0.1724	-13.6415	-2.9470	1.1145
0.058497	400.00	374.22	381.44	14.70	417.9939	0.0	0.1726	0.1576	-14.3956	-0.5842	1.0886
0.059547	400.00	369.92	380.54	14.70	419.1089	0.0	0.1574	0.1424	-14.4580	-0.4904	1.0570
0.060597	400.00	364.52	379.69	14.70	420.1890	0.0	0.1419	0.1269	-15.1357	-2.6217	1.0169
0.061647	400.00	357.56	378.21	14.70	422.2283	0.0	0.1254	0.1104	-16.2888	-2.7435	0.9600
0.062697	400.00	348.29	376.21	14.70	425.1052	0.0	0.1078	0.0928	-17.3787	-2.9316	0.8908
0.063745	400.00	335.76	373.76	14.70	428.5009	0.0	0.0888	0.0738	-18.9308	-4.7781	0.7704
0.064794	400.00	318.51	370.39	14.70	434.6877	0.0	0.0677	0.0527	-21.2390	-6.4032	0.6112
0.065843	400.00	294.28	365.85	14.70	443.5515	0.0	0.0440	0.0290	-24.1290	-7.8935	0.3814

TIME P1 P2 P3 P4 P5 XPV XP XV XPDT/7 XPDT/6 WDT/12

APPENDIX G

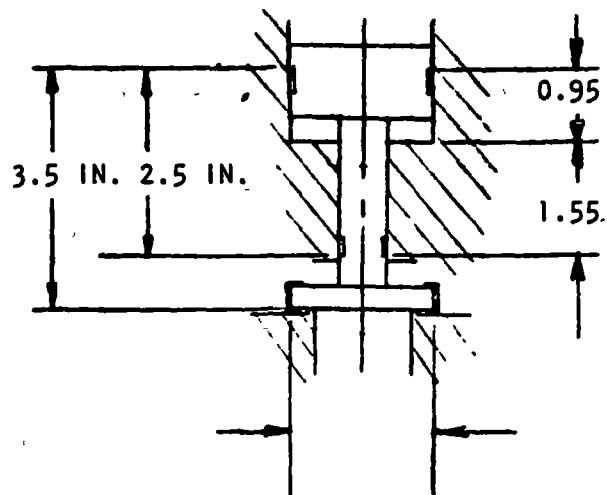
APS VALVE FIXTURE TOLERANCES



TFE Teflon ΔL = Change in Thickness, inches/inch
 ΔL , 70 to 390 F = +0.027 in./in.
 ΔL , 70 to -250 F = -0.0192 in./in.

Valve will be assembled at room temperature, with an interference fit, up to ~ 0.0007 -inch diametral between the piston bushing, shaft bushing, and their respective bores. The valve details will then be hot-soaked at +390 F to allow the Teflon to "cold-flow" to a zero clearance condition.

Pivotal Distances for
Calculating α Radians
of Clamshelling and
Scrubbing

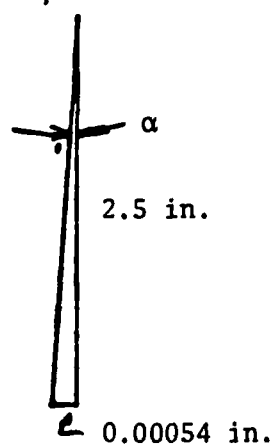


Screening Test Models 2α Clamshell = 0.0014 radian
 2α Scrubbing = 0.00216 radian

The scrubbing interface motion was 0.62α ; thus,
motion was $0.00216 \times 0.62 = 0.00134$ inches)

Clamshelling angle, worst case = 2α

Room Temperature: Assume pivot at top bushing, bottom bushing can travel a
 $\Delta L = 0.020$ bushing thickness times 0.027 in./in. (see page G-1)
 $\Delta L = 0.020 \times 0.027 = 0.00054$ in.



1. $\therefore \alpha$ (Bushing Clearance) = $\frac{0.00054}{2.5} = 0.000216$ radian
2. Body Parallelism, Actuator Surface to Seat Surface is 0.0002 in. over 3.438 inches = $\frac{0.0002}{3.438} = 0.000058$ radian
3. Bushing Perpendicularities to Actuator Surface (top) $\frac{0.0001}{0.95} +$ (bottom) $\frac{0.0001}{1.55} = 0.000105 + 0.0000645 = 0.000169$ radian
4. Shaft Lifter Normality $\frac{0.0001}{1.750} = 0.0000571$ radian
5. Poppet Carriage Parallelism $\frac{0.0001}{1.612} = 0.000062$ radian
 0.0001 over 1.612 inch
6. Parallelism of Seat Crests to Body Contact Area is $\frac{0.000010}{1.48} = 0.0000067$ radian
 0.000010 inch over 1.48 inch

7. Shaft to Piston Clearance, Radial $\frac{0.0005}{1.9} = 0.000131$ radian

Worst-Case Clamshell

Room Temperature, 2α	=	1.	0.000216
		2.	0.000058
		3.	0.000169
		4.	0.0000571
		5.	0.000062
		6.	0.0000067
		7.	0.000131

Room Temperature Clamshell, 2α
TOTAL

0.0007 radian

Increase in Radians at -250 F

$$\Delta L = 0.020 \times -0.0192 = -0.00038 \text{ inch} \quad \frac{0.00038}{2.5} = 0.000152 \text{ radian}$$

$$\text{-250 F Clamshell, } 2\alpha = 0.0007 + 0.000152 = 0.000852 \text{ radian}$$

Decrease in Radians at +390 F

$$\Delta L = 0.020 \times +0.027 = +0.00054 \text{ inch} = \frac{0.00054}{2.5} = 0.000216 \text{ radian}$$

$$\text{+390 F Clamshell, } 2\alpha = 0.0007 - 0.000216 = 0.000484 \text{ radian}$$

Scrubbing Angle, Worst Case = 2α

Scrubbing is purely a function of the bushing clearances multiplied by the ratio of top bushing-to-seat distance divided by top bushing-to-bottom bushing distance.

Room Temperature

Again, pivot about top bushing as on page G-2.

$$0.00054 \text{ in.} \times \frac{3.5 \text{ in.}}{2.5 \text{ in.}} = 0.000756 \text{ in.}$$

$$\text{Room Temperature Actual Angle } 2\alpha = \frac{0.00054}{2.5} = 0.000216 \text{ radian}$$

Increase in Scrubbing at -250 F (from page G-3)

$$0.00038 \text{ inch} \times \frac{3.5}{2.5} = 0.000532 \text{ inch}$$

$$\text{Increase in Actual Angle } 2\alpha = \frac{0.00038}{2.5} = 0.000152 \text{ radian}$$

$$\text{-250 F Actual Angle } 2\alpha = 0.000216 + 0.000152 = 0.000368 \text{ radian}$$

$$\begin{aligned} \text{Total Interfacial Motion} &= 0.000756 \\ &\quad \underline{+0.000532} \\ &= 0.001288 \text{ inch} \end{aligned}$$

This condition will exist only if the poppet is positioned against the carriage and the carriage is positioned against the shaft to cause all the scrubbing to be transmitted to the poppet.

The carriage-to-shaft diametral clearance is 0.002 to 0.004 inch, as is the carriage-to-poppet clearance; thus, the scrubbing could be zero, since the other motions would not necessarily be transmitted to the poppet.

SUMMARY

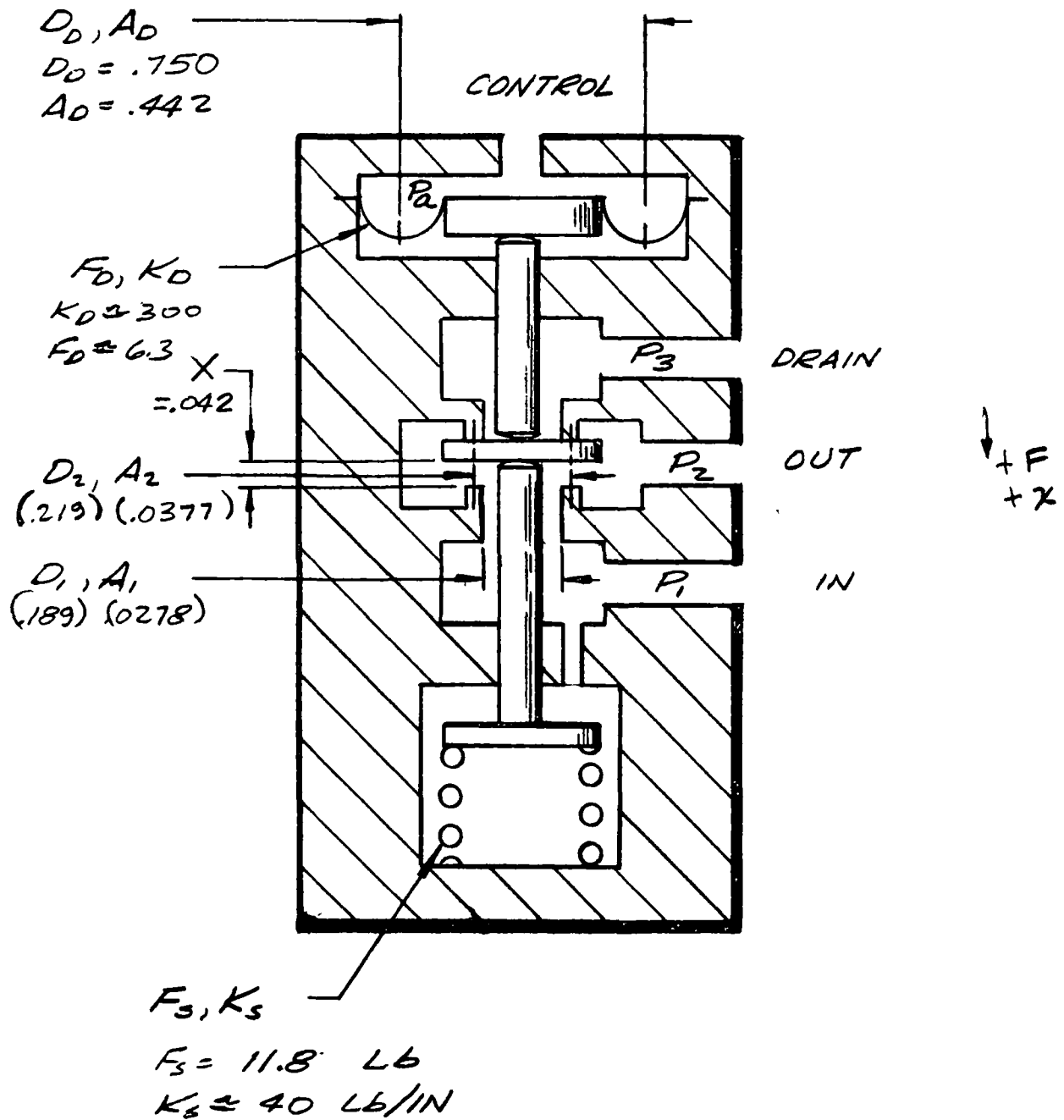
Worst-Case Clamshell = 0.000852 radian which is less than the 0.0014 radian tested

Worst-Case Scrubbing = 0.001288 inch motion which is less than the 0.00134 inch tested

APPENDIX H

APS PILOT VALVE DESIGN

PRESSURE ACTUATED PILOT VALVE DESIGN



• FLOW AREA AND SEAT DIMENSIONS:

.015 IN² EFFECTIVE AREA
REQUIRED (FROM ANALYSIS
OF CONCEPTS 1, 2 & 3)

$$C_d A = .015 \text{ IN}^2$$

USING A C_d OF 0.6

$$A = \frac{.015}{.6} = .025 \text{ IN}^2$$

WITH A PUSHROD OF .060 DIA,
.00283 IN²

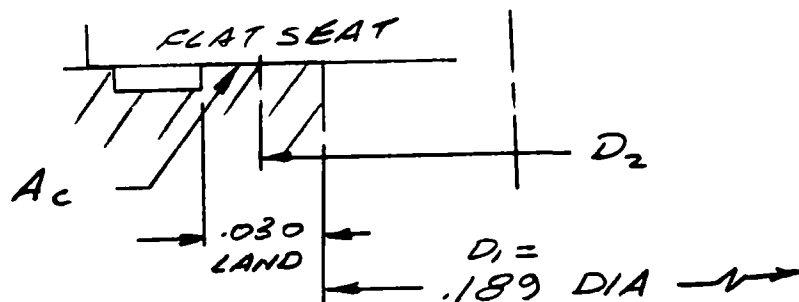
$$A_1 = .025 + .00283$$

$$A_1 = .0278 \text{ IN}^2$$

$$D_1 = \sqrt{.0354} = .189 \text{ IN}$$

$$X = \frac{.025}{(\pi)(.189)} = .042$$

WITH A SEAT STRESS OF 1000
PSI & THE SAME SEAT
DIMENSIONS AS ON TEST MODEL



$$D_2 = .030 + .189 = .219 \text{ IN}$$

$$A_2 = .0377 \text{ IN}^2$$

$$A_c = (.03)(.219)(\pi) = .0206 \text{ IN}^2$$

= SEAT CONTACT AREA

$$F_c = \text{MIN SEAT FORCE} = (1000)(.0206)$$

$$F_c = 20.6 \text{ LB MIN}$$

• FORCE BALANCE :

GENERAL FORCE BALANCE EQUATION.

$$\Sigma F = 0 = F_c + P_a A_D + F_D - P_1 A_2 + F_s$$

$$- (K_D + K_S) X$$

WITH THE DIAPHRAGM DEFLECTED
 $\frac{X}{2}$ WHEN $X=0$,

$$F_D = + \frac{X}{2} K_D = .021 K_D$$

$$\text{ASSUME } K_D = 455 \text{ LB/IN}$$

$$F_D = 9.6 \text{ LB}$$

$$\text{FOR } X=0, P_a = 0, P_1 = 400$$

$$F_s (\text{MIN}) = F_c + F_D - P_1 A_2$$

$$= 20.6 + 9.6 - (400)(.0377) \quad 15.12$$

$$F_s = 15.12 \text{ LB}$$

$$\text{ASSUME } K_S = 80 \text{ LB/IN}$$

$$\text{FOR } F_c = 0 \text{ \& } X=0$$

$$P_a A_D = F_s + P_1 A_2 - F_D$$

$$= 15.12 + (400)(.0377) - 9.6$$

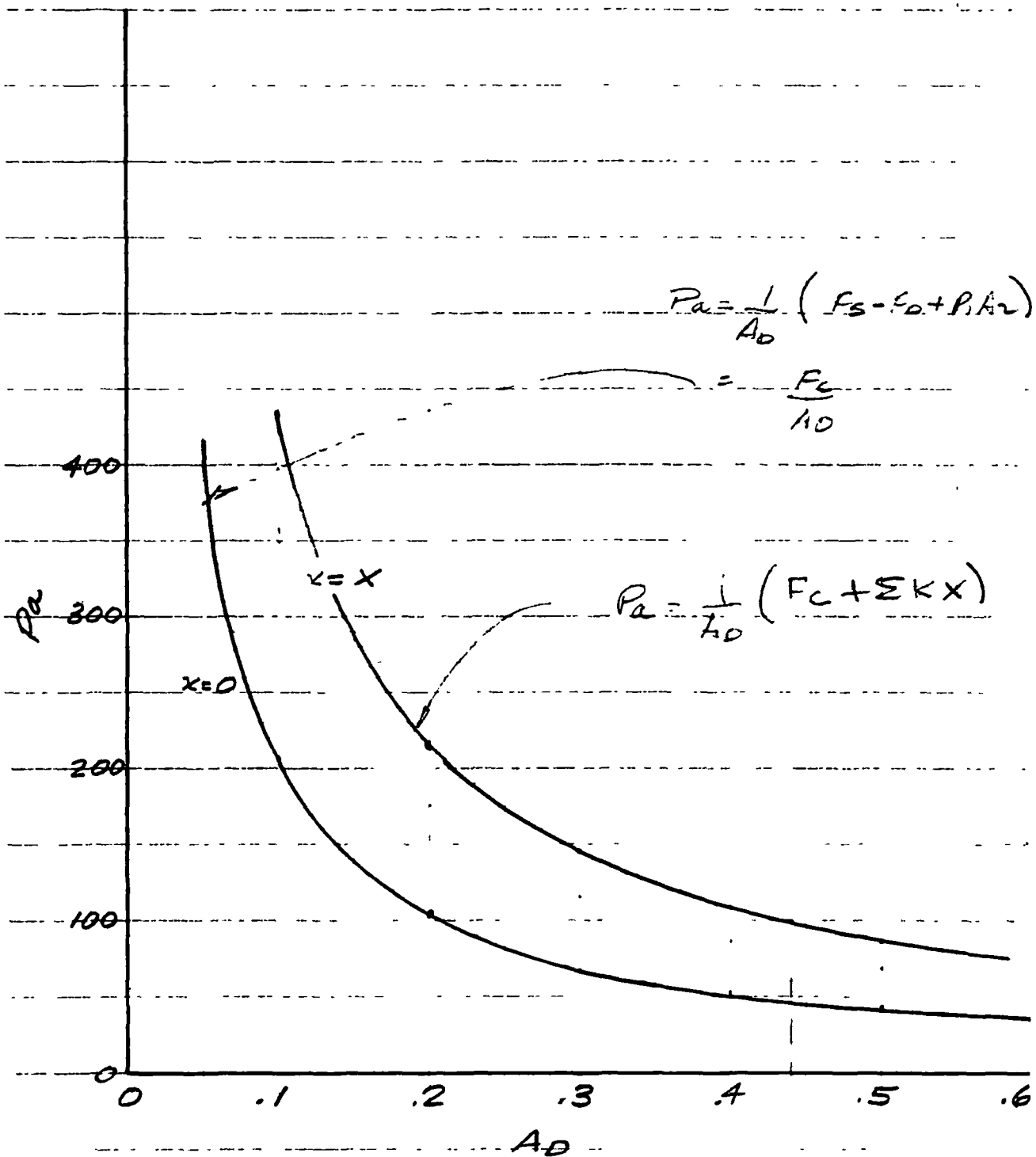
$$P_a A_D = 20.6$$

$$\text{IF } X = X = .042, P_a A_D = F_c + EKX$$

$$P_a A_D = 20.6 + (535)(.042) = 43.1$$

$$\text{IF } A_D = .196, P_a = \frac{43.1}{.196} = 219 \text{ PSI (FULL OPEN } P_a)$$

ACTUATION PRESSURE VS DIAPHRAGM AREA



$$F_c = 400A_D - 9.6 - 15.12 - 80 \times .042 - 15.08 = 400A_D - 43.16$$

$F_c = \text{SEAT CONTACT LOAD}$

$$F_c = P_a A_D + F_D - \Sigma KX - P_1 A_2 - F_s$$

F_c
 \oplus
 X
 $=$
 X

200

100

DES. POINT
 $A_D = .196$

$F_c = 36.66$

$F_c \text{ @ } X=0$

0

.1

.2

.3

.4

.5

.6

A_D

APPENDIX I

NEW TECHNOLOGY

A review of the work performed under this contract, NAS3-14350, revealed a number of new innovations, discoveries, and/or improvements. The appropriate title and the pages in this report which are applicable to the items are given below. For reader convenience, a copy of each Technology Utilization Disclosure is included in this Appendix.

<u>Title</u>	<u>Page</u>
Anti-Galling Bushings	149
Anti-Extrusion Rings for Compressed Plastic	170
Separable Seat with Flexible Ring Support	142
Self-Aligning Poppet	137
Captive Plastic Seal for Low Stress Levels	47
Fast Response, Propellant-Actuated Valve	135
Poppet Articulation Mechanism and Seat Tester	52

DISCLOSURE OF INNOVATION OR INVENTION

Title Anti-Galling Bushings

Docket No HN R81335

INNOVATOR OR INVENTOR	DEPT NO	SERIAL NO	PHONE NO	MAIL ADDRESS	SUPERVISOR
E. G. Spencer	596-135	192512	3431	AC32	C. G. Fargo

THE PROBLEM: Mechanical failure caused by metal parts rubbing against other metal parts.

DESCRIPTION OF SOLUTION: (Succinct statement of broad solution together with detailed description illustrated by sketches where appropriate, of the structure, operation, physical characteristics -- electrical, chemical, mechanical -- describing the new result. Attach additional material, preferably on Form 74-S)

Mechanisms with rubbing metal parts frequently fail due to galling or self-generated contamination. Some Rocketdyne valve designs for the J-2S engine incorporated machined plastic bushings to prevent metal-to-metal contact in both axial motion and vibration-induced radial motion applications. As a result, failures caused by galling and self-generated contaminants have been eliminated in valves incorporating this feature.

However, precision machined plastic bushings are expensive to machine to tight tolerances so lower cost means to achieve the same results were needed. Consequently, for the APS valve, shaft bushings were fabricated from heat shrinkable Teflon tubing. This method permits a close fitting Teflon sleeve to be applied to a shaft member without costly precision machining of either shaft or bushing. Commercially available expanded Teflon tubing of appropriate size is cut to length, heated to shrink it onto the mating shaft and, if necessary, machined only to size the final outside diameter.

1-4-72

Inventor: EUGENE G. SPENCER 10501 Laramie Pl., Chatsworth, Calif.
FIRST NAME INITIAL LAST NAME HOME ADDRESS DATE

Witnesses (Read and Understood By)

(1) Henry M. Smith 1-5-72
FIRST NAME INITIAL LAST NAME DATE

(2) Albert W. Olsen 1-5-72
FIRST NAME INITIAL LAST NAME DATE

(OVER)

FORM 74-S-1 REV. 11-69

DISCLOSURE OF INNOVATION OR INVENTION

11111 ANTI-EXTRUSION RING FOR COMPRESSED PLASTIC

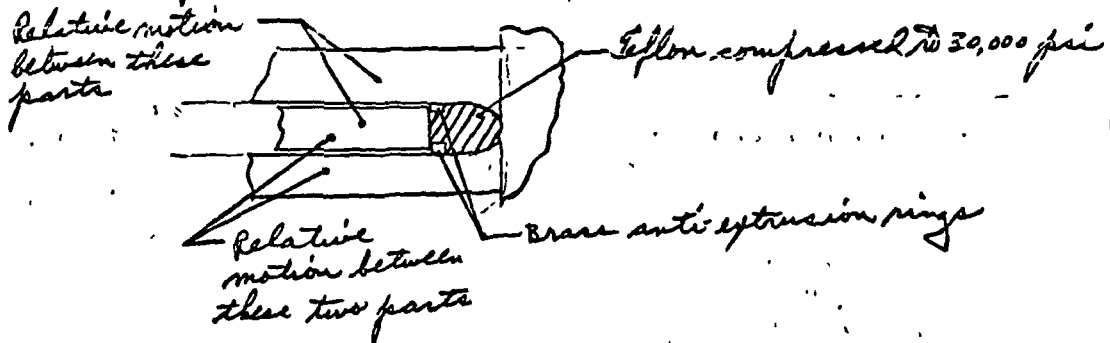
Docket No. NAR 81298

INNOVATOR OR INVENTOR	DEPT NO	SERIAL NO	PHONE NO	MAIL ADDRESS	SUPERVISOR
J. L. MONTGOMERY	578	303535	5636	SS11	D.M. CARPENTER

THE PROBLEM: Prevent extrusion of plastic material when compressed to high pressure and contained between two parts with relative motion

DESCRIPTION OF SOLUTION: (Succinct statement of broad solution together with detailed description, illustrated by sketches where appropriate, of the structure, operation, physical characteristics -- electrical, chemical, mechanical -- describing the new result. Attach additional material, preferably on Form 74-5)

To prevent the extrusion of a plastic material through the gap required between two metal parts with relative motion, a brass ring with a width greater than the gap width in the parts was installed. This prevents the extrusion, while still permitting motion between the metal parts.



INVENTOR: James L. Montgomery 7562 Charmide, Canoga Park 10/5/71
FIRST NAME INITIAL LAST NAME HOME ADDRESS DATE

Witnesses: (Read and Understood By:)

(1) E. Pano 1364 Audubon 10/5/71
FIRST NAME INITIAL LAST NAME DATE
(2) Clifford F. Walden 10/5/71
FIRST NAME INITIAL LAST NAME DATE

FORM 74-51 REV. 9-67

(OVER)

**DISCLOSURE
OF
INNOVATION OR INVENTION**

Title **SEPARABLE SEAT WITH FLEXIBLE RING SUPPORT**

Docket No. NAR 81297

INNOVATOR OR INVENTOR	DEPT NO	SERIAL NO.	PHONE NO	MAIL ADDRESS	SUPERVISOR
Willard A. Gillon, Jr.	596-135	302167	3431	AC32	D. F. Ferris

THE PROBLEM: Distortion and high impact loading of metal-to-metal flat seat

DESCRIPTION OF SOLUTION: (Succinct statement of broad solution together with detailed description, illustrated by sketches where appropriate, of the structure, operation, physical characteristics -- electrical, chemical, mechanical -- describing the new result. Attach additional material, preferably on Form 74-S)

Use of the hard sharp carbide seat concept for the SS/APS propellant valves requires flatness of the seat be maintained within 10 microinches to meet the leakage requirement of 0.1 scim helium at 450 \pm 50 psia over a temperature range of 200 to 850°R. Additionally, impact loads between the seat and poppet must be minimized to insure the operating life requirements of one million cycles. A separable seat, supported by a flexible ring* was used in the valve design to solve these problems. This flexible support isolates the seat from body and flange distortions that might arise from thermal and stress gradients. The elasticity of the flexible ring also reduces impact loads by absorbing kinetic energy that would be transmitted to a rigidly installed seat.

* Part number U-2212-01563-560 as shown on drawing R5004750X.

Inventor: Willard A. Gillon, Jr. 23032 Mobile St., Canoga Park 9-28-71
FIRST NAME INITIAL LAST NAME HOME ADDRESS DATE

Witnesses: (Read and Understood By)

(1) Joseph L. Ferris 9-28-71
(2) D. F. Ferris 9/29/71
FIRST NAME INITIAL LAST NAME DATE

FORM 74-S1 REV. 12-69

(OVER)

DISCLOSURE
OF
INNOVATION OR INVENTION

Title SELF-ALIGNING POPPET

Docket No. NAR 81296

INNOVATION OR INVENTOR	DEPT NO	SERIAL NO	PHONE NO	MAIL ADDRESS	SUPERVISOR
Willard A. Gillon, Jr.	596-135	302167	3431	AC32	D. F. Ferris

THE PROBLEM: Requirement for a propellant valve replaceable self-aligning poppet

DESCRIPTION OF SOLUTION: (Succinct statement of broad solution together with detailed description, illustrated by sketches where appropriate, of the structure, operation, physical characteristics -- electrical, chemical, mechanical -- describing the new result. Attach additional material, preferably on Form 74-S.)

Self-alignment, e.g., allowing the poppet sealing face to come into parallel contact with the seat face with a minimum amount of metal-to-metal scrubbing, was accomplished by placing the poppet inside a carriage so that it is not rigidly attached to the valve shaft. As the valve closes, the poppet comes to rest on the seat and the carriage continues to travel a specific distance so that the carriage and poppet are not in contact. To permit replacement of the poppet without disassembling the valve, tabs on the shaft are inserted into slots in the carriage, the shaft is then rotated 45° and released causing the pin in the carriage to engage the pin coupling slot in the shaft. The coil spring provides axial force between the poppet, carriage, and shaft keeping the pin from disengaging. The poppet is removed by compressing the coil spring and twisting the carriage 45°. The bowed ring maintains a small load between the carriage and shaft to prevent rattling of the carriage when the valve is closed.

Inventor: Willard A. Gillon, Jr. 23032 MOBILE ST. C.P. 9-28-71
FIRST NAME INITIAL LAST NAME HOME ADDRESS DATE

Witnesses: (Read and Understood By.)

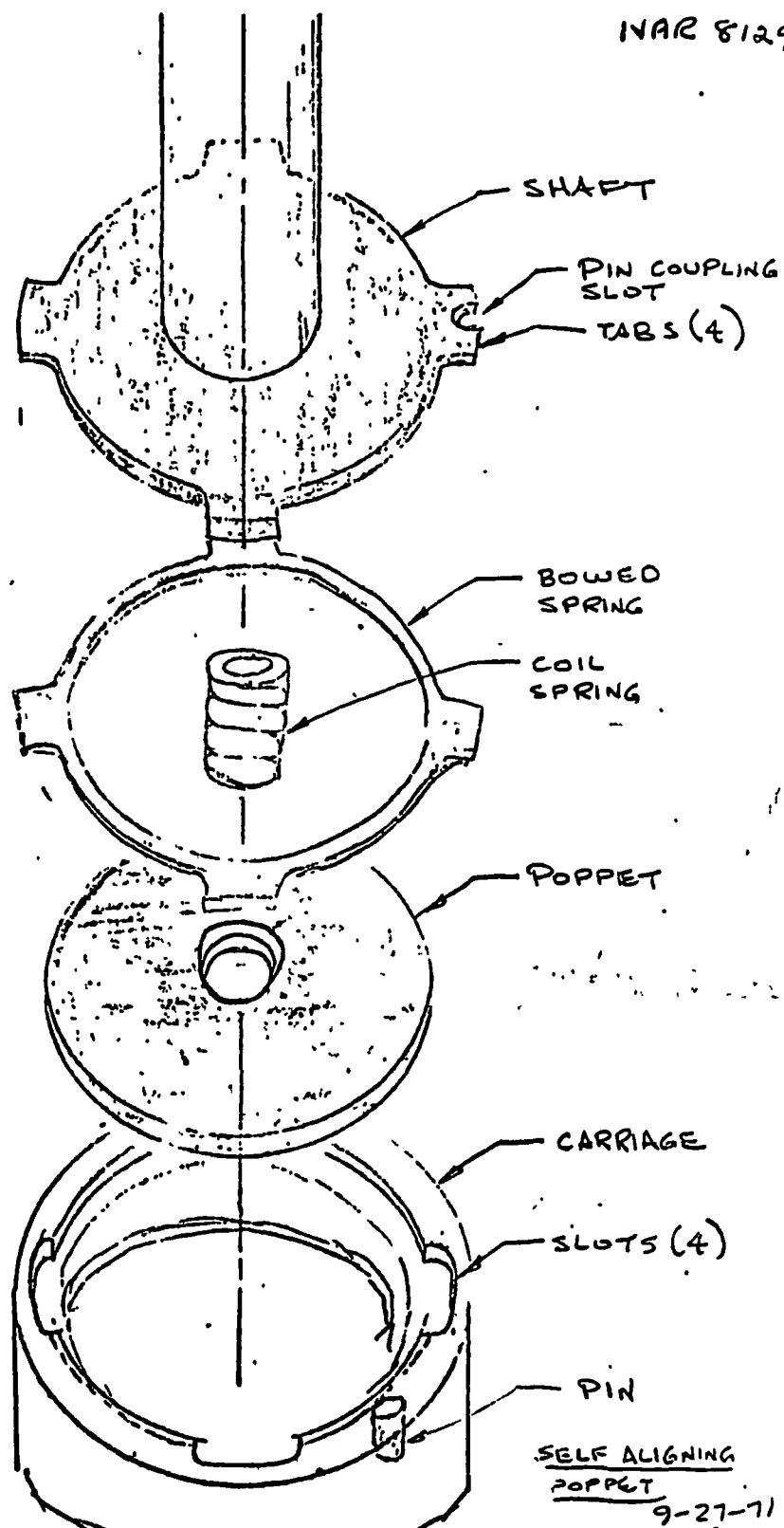
(1) Joseph E. Meister 9-28-71
FIRST NAME INITIAL LAST NAME DATE

(2) Mr. Larry F. Ferris 9/28/71
FIRST NAME INITIAL LAST NAME DATE

FORM 74-S-1 REV. 12-69

(OVER)

INAR 81296



DISCLOSURE OF INNOVATION OR INVENTION

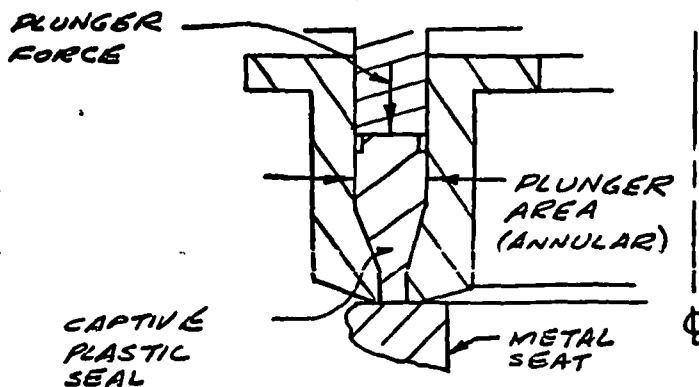
Title CAPTIVE PLASTIC SEAL FOR LOW STRESS LEVELS

Docket No. NAR 81295

INNOVATOR OR INVENTOR	DEPT NO	SERIAL NO	PHONE NO	MAIL ADDRESS	SUPERVISOR
Willard A. Gillon, Jr.	596-135	302167	3431	AC32	D. F. Ferris

THE PROBLEM: How to reduce load requirement of captive plastic seat design to values suitable for flight weight valves.

DESCRIPTION OF SOLUTION: (Succinct statement of broad solution together with detailed description, illustrated by sketches where appropriate, of the structure, operation, physical characteristics -- electrical, chemical, mechanical -- describing the new result. Attach additional material, preferably on Form 74-8.)



$$\text{PLASTIC STRESS} = \frac{\text{PLUNGER FORCE}}{\text{PLUNGER AREA}}$$

Previous use of the "captive plastic seat" design has been limited to plastic stresses from 15,000 to 35,000 psi. These stresses require large loads, and thus large actuators making this concept seem unsuitable for flight type valves. Recent testing of a captive plastic seat for the SS/APS valves program (NAS3-14350) has indicated that this seat concept can be used with very low stress levels (≈ 677 psi for .001 scim nitrogen leakage at 1000 psig inlet pressure). Successful testing at this stress level included purposely contaminating the seat with nickel balls and human hair, which proved the self-healing capability of this seat at low stress. This seat has since been incorporated into a prototype of a flight type valve and is illustrated on drawing RS004750X.

Inventor: Willard A. Gillon, Jr. 23032 MOBILE ST, C.P. 9-28-71
FIRST NAME INITIAL LAST NAME HOME ADDRESS DATE

Witnesses (Read and Understood By)

(1) Joseph L. Weston 9-28-71
FIRST NAME INITIAL LAST NAME DATE

(2) D. F. Ferris 9/19/71
FIRST NAME INITIAL LAST NAME DATE

FORM 74-81 REV 12-68

(OVER)

DISCLOSURE
OF
INNOVATION OR INVENTION

Title FAST RESPONSE, PROPELLANT-ACTUATED VALVE

Docket No. NAR 81292

INNOVATOR OR INVENTOR	DEPT NO	SERIAL NO	PHONE NO	MAIL ADDRESS	SUPERVISOR
E. G. Spencer	596-135	192512	3431	AC32	C. G. Fargo
A. W. Olsen	596-135	195373	3431	AC32	E. G. Spencer

THE PROBLEM: Design a fast response propellant actuated valve for use in gaseous oxygen and hydrogen.

DESCRIPTION OF SOLUTION: (Succinct statement of broad solution together with detailed description illustrated by sketches where appropriate, of the structure, operation, physical characteristics -- electrical, chemical, mechanical -- describing the new result. Attach additional material, preferably on Form 74-S.)

The valve is shown on the attached sketch. The design permits the valve to be opened and closed with a three-way normally open pilot valve using inlet pressure to assist both opening and closing. The valve is held closed by spring force and propellant inlet pressure acting on the closing side of the actuator in opposition to propellant inlet pressure acting on the opening side of the actuator. To open, closing pressure is vented through the pilot valve to the low pressure region of a venturi section downstream of the valve or overboard to ambient. To close, the closing pressure is applied with the pilot valve and the differential pressure force and the spring provide closing force. This valve concept and actuation method makes the valve opening and closing time independent of the propellant inlet pressure and minimizes the weight and complexity of the control system.

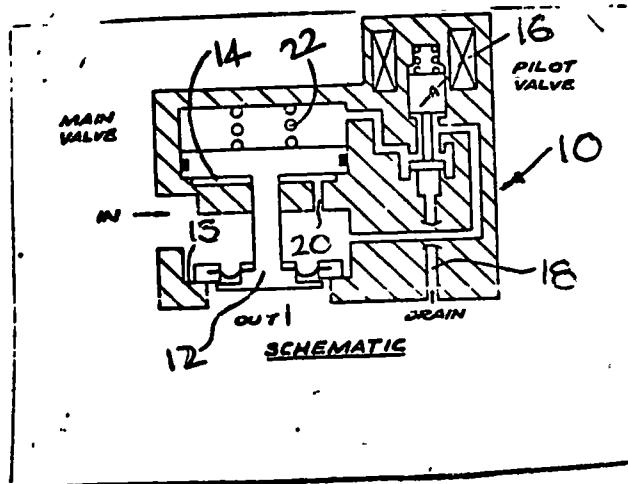
EC Spencer 10501 LARIMIC PL., CLATS WORTH, CALIF 91301
8/11/71

Inventor: Alfred W. Olsen 5453 Fenwood Ave, Woodland Hills 8/10/71
FIRST NAME INITIAL LAST NAME HOME ADDRESS DATE

Witnesses (Read and Understood By) Heard Homigphie 8-11-71
(1) _____
(2) David P. J. J. J. 8-11-71
FIRST NAME INITIAL LAST NAME DATE

FORM 74-S-1 REV 11-69

(OVER)



**DISCLOSURE
OF
INNOVATION OR INVENTION**

Title **Poppet Articulation Mechanism and Seat Tester**

Docket No **NAR 81291**

INNOVATOR OR INVENTOR	DEPT NO	SERIAL NO	PHONE NO	MAIL ADDRESS	SUPERVISOR
G. F. Tellier	596-135	238347	3431	AC32	E. G. Spencer

THE PROBLEM: Producing means for controlled testing of poppet to seat closure modes to evaluate wear and leakage versus cycles.

DESCRIPTION OF SOLUTION: (Succinct statement of broad solution together with detailed description illustrated by sketches where appropriate, of the structure, operation, physical characteristics -- electrical, chemical, mechanical -- describing the new result Attach additional material, preferably on Form 74-S)

Allowance must be made in valve closures for the sealing surfaces to achieve a continuous contact. Poppet type valves with soft seats obtain a seal by material deflection. Metal-to-metal seats, however, must be allowed to seek a sealing conformance with minimal external restraint, being loaded by inlet pressure or supplemental actuator force. Application of these forces at closure produces interfacial scrubbing during the last few thousandths inch which usually wear the sealing surface with attendant sealing degradation. Evaluation of this wear and sealing degradation has previously been limited to a phenomenistic approach with little, if any, attempt to control or measure the exact degree of scrubbing. The subject invention provides means for controlling both poppet closure scrubbing and impact cycling for millions of cycles. The feature of novelty in the design is the wobbler device in combination with the poppet holder and beam assembly which retain, guide and load the poppet. Complete description of the tester and results of design analysis are presented in IL0135-1003, pages 26 through 44. The tester has been built and successfully employed to perform screening tests in six closure designs, accumulating many millions of cycles.

A schematic of the wobbler concept is illustrated on the following page.

G. F. Tellier
Inventor: Gilbert F. Tellier 20223 Mobile Street 8/16/71
FIRST NAME INITIAL LAST NAME HOME ADDRESS DATE

Witnesses (Read and Understood By)

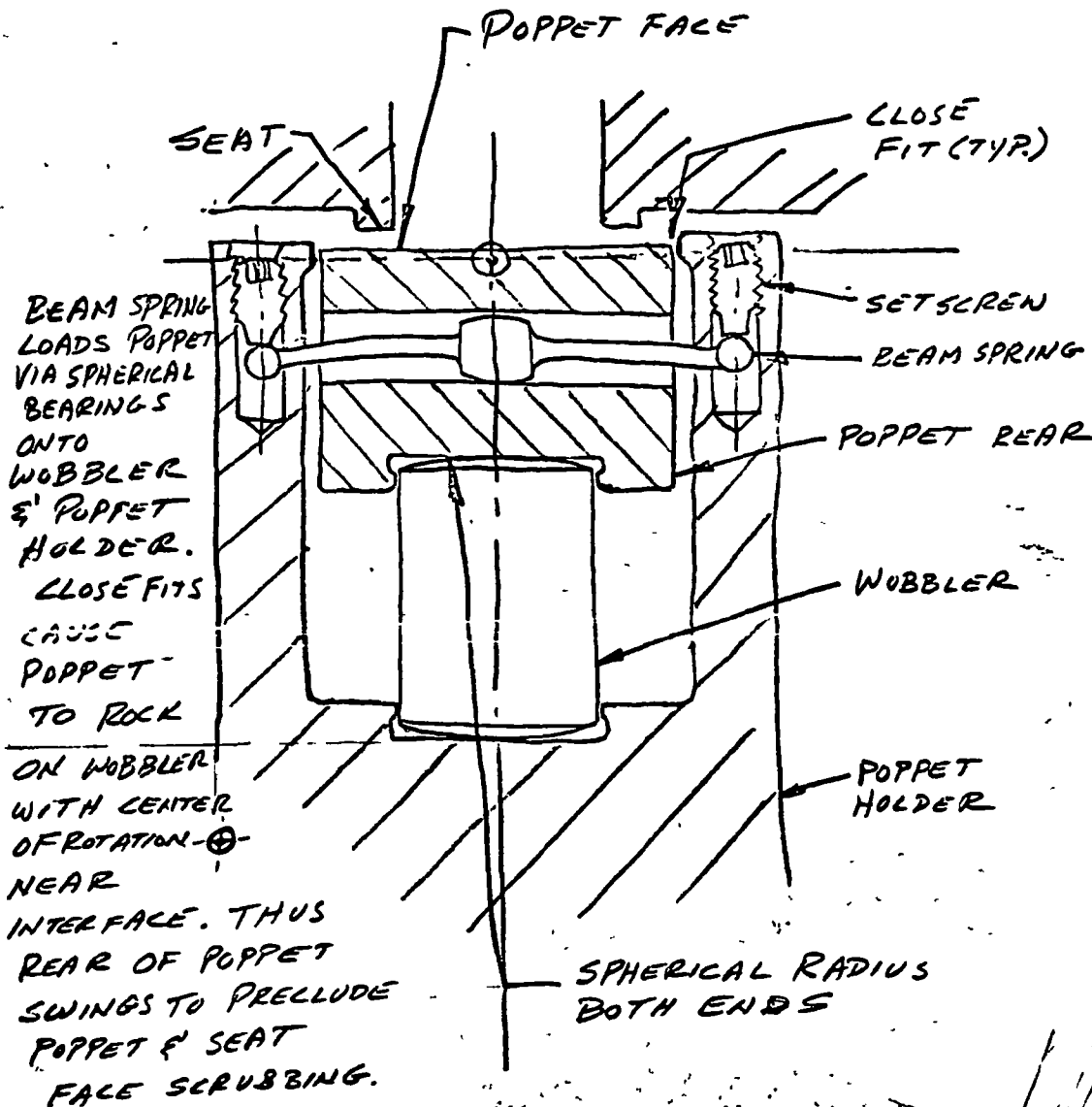
(1) Harry M. Smith 8/16/71
FIRST NAME INITIAL LAST NAME DATE

(2) James W. Jewell 8/17/71
FIRST NAME INITIAL LAST NAME DATE

(OVER)

FORM 74-S-1 REV. 11-69

[Describe (1) each new result obtained by the invention, (2) basic components, ingredients, or steps which are combined to obtain such results, and (3) the operation of the components, etc., which obtain such results. Provide sketches or flow diagrams if helpful in understanding the invention.]



Inventor: G. F. Tellier TELLIER 8/16/71
FIRST NAME INITIAL LAST NAME DATE

Read and

Page intentionally left blank

APPENDIX J

DISTRIBUTION LIST (NAS3-14390)

Report Copies <u>R D</u>	<u>Recipient</u>	<u>Designee</u>
	National Aeronautics & Space Administration Lewis Research Center 21000 Brookpark Road Cleveland, Ohio 44135	
1	Attn: Contracting Officer, MS 500-313	
5	E. A. Boarke, MS 500-205	
1	Technical Report Control Office, MS 5-5	
1	Technology Utilization Office, MS 3-16	
2	AFSC Liaison Office, 501-3	
2	Library	
1	Office of Reliability & Quality Assurance, MS 500-211	
1	J. W. Gregory, Chief, MS 500-203	
	R. E. Grey, Project Manager, MS 60-6	
1	N. T. Musial, MS 500-113	
1	I. E. Sumner, MS 500-203	
1	W. R. Dunbar, MS 500-103	
1	Director, Manned Space Technology Office, RS Office of Aeronautics & Space Technology NASA Headquarters Washington, D.C. 20546	
1	Director, Physics and Astronomy Programs, SG Office of Space Science NASA Headquarters Washington, D.C. 20546	
1	Director, Planetary Programs, SL Office of Space Science NASA Headquarters Washington, D.C. 20546	
2	Director Space Prop. and Power, RP Office of Aeronautics & Space Technology NASA Headquarters Washington, D.C. 20546	
1	Director, Launch Vehicles & Propulsion, SV Office of Space Science NASA Headquarters Washington, D.C. 20546	
1	Director, Materials & Structures Division, RW Office of Aeronautics & Space Technology NASA Headquarters Washington, D.C. 20546	

Report
Copies
R D

Recipient

Designee

1	Director, Advanced Manned Missions, MT Office of Manned Spaced Flight NASA Headquarters Washington, D.C. 20546	
1	National Aeronautics & Space Administration Ames Research Center Moffett Field, California 94035 Attn: Library	
1	National Aeronautics & Space Administration Flight Research Center P.O. Box 273 Edwards, California 93523 Attn: Library	
1	Director, Technology Utilization Division Office of Technology Utilization NASA Headquarters Washington, D.C. 20546	
1	Office of the Director of Defense Research & Engineering Washington, D.C. 20301 Attn: Office of Asst. Dir. (Chem. Technology)	
10	NASA Scientific and Technical Information Facility P.O. Box 33 College Park, Maryland 20740 Attn: NASA Representative	
1	Nation Aeronautics & Space Administration Goddard Space Flight Center Greenbelt, Maryland 20771 Attn: Library	
1	National Aeronautics & Space Administration John F. Kennedy Space Center Cocoa Beach, Florida 32931 Attn: Library	
1	National Aeronautics & Space Administration Langley Research Center Langley Station Hampton, Virginia 23365 Attn: Library	

Report
Copies
R D

Recipient

Designee

1	1	National Aeronautics & Space Administration	J. W. Akkerman
	1	Manned Spacecraft Center	J. W. Griffin
	1	Houston, Texas 77001	R. N. Tanner
	1	Attn: Library	Henry Pohl
1		National Aeronautics & Space Administration	Hans G. Paul
		George C. Marshall Space Flight Center	Leon J. Hastings
		Huntsville, Alabama 35912	James Thomas
	1	Attn: Library	Dale Burrows
			I. G. Yates
			Clyde Nevins
	1		J. Blumrich
			Kenneth Anthony
1		Jet Propulsion Laboratory	
		4800 Oak Grove Drive	
	1	Pasadena, California 91103	Duane Dippery
		Attn: Library	
1		Defense Documentation	
		Cameron Station	
		Building 5	
		5010 Duke Street	
		Alexandria, Virginia 22314	
		Attn: TISIA	
1		RTD (RTNP)	
		Bolling Air Force Base	
		Washington, D.C. 20332	
1		Arnold Engineering Development Center	
		Air Force Systems Command	
		Tullahoma, Tennessee 37389	
		Attn: Library	
1		Advanced Research Projects Agency	
		Washington, D.C. 20525	
		Attn: Library	
1		Air Force Missile Test Center	
		Patrick Air Force Base, Florida	
		Attn: Library	
1		Air Force Systems Command	
		Andrews Air Force Base	
		Washington, D.C. 20332	
		Attn: Library	

Report
Copies
R D

Recipient

Designee

1	Air Force Rocket Propulsion Laboratory (RPR) Edwards, California 93523 Attn: Library	
1	Air Force Rocket Propulsion Laboratory (RPM) Edwards, California 93523 Attn: Library	
1	Air Force FTC (FTAT-2) Edwards Air Force Base, California 93523 Attn: Library	
1	Air Force Office of Scientific Research Washington, D.C. 20333 Attn: Library	
1	Space & Missile Systems Organization Air Force Unit Post Office Los Angeles, California 90045 Attn: Technical Data Center	
1	Office of Research Analyses (OAR) Holloman Air Force Base, New Mexico 88330 Attn: Library RRRD	
1	U.S. Air Force Washington, D.C. Attn: Library	
1	Commanding Officer U.S. Army Research Office (Durham) Box CM, Duke Station Durham, North Carolina 27706 Attn: Library	
1	U.S. Army Missile Command Redstone Scientific Information Center Redstone Arsenal, Alabama 35808 Attn: Document Section	
1	Bureau of Naval Weapons Department of the Navy Washington, D.C. Attn: Library	

Report
Copies
R D

Recipient

Designee

1	Commander U.S. Naval Missile Center Point Mugu, California 93041 Attn: Technical Library	
1	Commander U.S. Naval Weapons Center China Lake, California 93557 Attn: Library	
1	Commanding Officer Naval Research Branch Office 1030 E. Green Street Pasadena, California 91101 Attn: Library	
1	Director (Code 6180) U.S. Naval Research Laboratory Washington, D.C. 20390 Attn: Library	
1	Picatinny Arsenal Dover, New Jersey 07801 Attn: Library	
1	Air Force Aero Propulsion Laboratory Research & Technology Division Air Force Systems Command United States Air Force Wright-Patterson AFB, Ohi 45433 Attn: APRP (Library)	
1	Annin Co. P.O. Box 22081 Los Angeles, California 90022 Attn: Library	
1	Space Division Aerojet-General Corporation 9200 East Flair Drive El Monte, California 91734 Attn: Library	
1	Antec/Calmec 5825 District Blvd. Los Angeles, California 90022 Attn: Library	

Report
Copies
R D

Recipient

Designee

1	Aerojet Liquid Rocket Company P.O. Box 15847 Sacramento, California 95813 Attn: Technical Library 2484-2015A	
1	Aeronutronic Division of Philco Ford Corp. Ford Road Newport Beach, California 92663 Attn: Technical Information Department	
1	Aerospace Corporation 2400 E. El Segundo Blvd. Los Angeles, California 90045 Attn: Library-Documents	
1	Arthur D. Little, Inc. 20 Acorn Park Cambridge, Massachusetts 02140 Attn: Library	
1	Astropower Laboratory McDonnell-Douglas Aircraft Company 2121 Paularino Newport Beach, California 92163 Attn: Library	
1	ARO, Incorporated Arnold Engineering Development Center Arnold AF Station, Tennessee 37389 Attn: Library	
1	Susquehanna Corporation Atlantic Research Division Shirley Highway & Edsall Road Alexandria, Virginia 22314 Attn: Library	
1	Battelle Memorial Institute 505 King Ave. Columbus, Ohio 43201 Attn: Library	
1	Beech Aircraft Corporation Boulder Facility Box 631 Boulder, Colorado Attn: Library	

Report
Copies
R D

Recipient

Designee

1	Bell Aerosystems, Inc. Box 1 Buffalo, New York 14240 Attn: Library	
1	Instruments & Life Support Division Bendix Corporation P.O. Box 4508 Davenport, Iowa 52808 Attn: Library	
1	Bellcomm 955 L'Enfant Plaza, S.W. Washington, D.C. Attn: Library	
1	Boeing Company Space Division P.O. Box 868 Seattle, Washington 98124 Attn: Library	
1	Chemical Propulsion Information Agency Applied Physics Laboratory 8621 Georgia Avenue Silver Springs, Maryland 20910	
1	Chrysler Corporation Missile Division P.O. Box 2628 Detroit, Michigan Attn: Library	
1	Chrysler Corporation Space Division P.O. Box 29200 New Orleans, Louisiana 70129 Attn: Library	
1	Curtiss-Wright Corporation Wright Aeronautical Division Woodridge, New Jersey Attn: Library	

Report
Copies
R D

Recipient

Designee

1	University of Denver Denver Research Institute P.O. Box 10127 Denver, Colorado 80210 Attn: Security Office	
1	Fairchild Stratos Corporation Aircraft Missiles Division Hagerstown, Maryland Attn: Library	
1	Crane Company Hydro-Aire Division 3000 Winoma Avenue Burbank, California 91504 Attn: Library	
1	Republic Aviation Fairchild Hiller Corporation Farmington, Long Island, New York	
1	General Dynamics/Convair P.O. Box 1128 San Diego, California 92112 Attn: Library	
1	Missiles and Space Systems Center General Electric Company Valley Forge Space Technology Center P.O. Box 8555 Philadelphia, Pa. 19101 Attn: Library	
1	General Electric Company Flight Propulsion Lab. Department Cincinnati, Ohio Attn: Library	
1	Grumman Aircraft Engineering Corporation Bethpage, Long Island, New York Attn: Library	
1	Hydraulic Research 25200 West Rye Canyon Road Valencia, California 91355 Attn: Library	

Report
Copies
R D

Recipient

Designee

1	Honeywell, Inc. Aerospace Division 2600 Ridgeway Road Minneapolis, Minnesota Attn: Library	
1	IIT Research Institute Technology Center Chicago, Illinois 60616 Attn: Library	
1	Kidde AeroSpace Division Walter Kidde & Company, Inc. 567 Main Street Belleville, New Jersey 07109	
1	Ling-Temco-Vought Corporation P.O. Box 5907 Dallas, Texas 75222 Attn: Library	
1	Lockheed Missiles and Space Company P.O. Box 504 Sunnyvale, California 94087 Attn: Library	
1	J. C. Carter Company 671 W. 17th Street Costa Mesa, California 92626 Attn: Library	
1	Lockheed Propulsion Company P.O. Box 111 Redlands, California 92374 Attn: Library, Thackwell	
1	Marquardt Corporation 16555 Saticoy Street Box 2013 - South Annex Van Nuys, California 91409	
1	Marotta Valve Corporation 2215 Standard Avenue Santa Ana, California 92707 Attn: Library	

Report
Copies
R D

Recipient

Designee

1	Denver Division Martin-Marietta Corporation P.O. Box 179 Denver, Colorado 80201 Attn: Library	
1	Orlando Division Martin-Marietta Corporation Box 5827 Orlando, Florida Attn: Library	
1	Western Division McDonnell Douglas Astronautics 5301 Belsa Avenue Huntington Beach, California 92647 Attn: Library	
1	McDonnell Douglas Astronautics Company P.O. Box 5941 Berkley, Missouri 63134 Attn: Library	
1	Rocketdyne Division Rockwell International 6633 Canoga Avenue Canoga Park, California 91304 Attn: Library, Department 596-306	
1	Space & Information Systems Division Rockwell International 12214 Lakewood Blvd. Downey, California Attn: Library	
1	Northrop Space Laboratories 3401 West Broadway Hawthorne, California Attn: Library	
1	Purdue University Lafayette, Indiana 47907 Attn: Library (Technical)	
1	Rocket Research Corporation Willow Road at 116th Street Redmond, Washington 98052 Attn: Library	

Report
Copies
R D

Recipient

Designee

1	Stanford Research Institute 333 Ravenswood Avenue Menlo Park, California 94025 Attn: Library	
1	TRW Systems, Inc. 1 Space Park Redondo Beach, California 90278 Attn: Tech. Lib. Doc. Acquisitions	
1	TRW TAPCO Division 23555 Euclid Avenue Cleveland, Ohio 44117	
1	United Aircraft Corporation Corporation Library 400 Main Street East Hartford, Connecticut 06108 Attn: Library	
1	United Aircraft Corporation Pratt & Whitney Division Florida Research & Development Center P.O. Box 2691 West Palm Beach, Florida 33402 Attn: Library	
1	United Aircraft Corporation United Technology Center P.O. Box 358 Sunnyvale, California 94038 Attn: Library	
1	Valcor Engineering Corp. 365 Carnegie Avenue Kenilworth, New Jersey 07033 Attn: Library	
1	Wallace O. Leonard, Inc. 373 Fair Oaks Avenue Pasadena, California 91504 Attn: Library	
1	Whittaker Corp., Controls Division 13035 Saticoy Street North Hollywood, California 91605 Attn: Library	

Report
Copies
R D

Recipient

Designee

1	A1Research Mfg. Division Garrett Corporation 402 South 36th Street Phoenix, Arizona 85034 Attn: Library	
1	E. I. DuPont Denemours and Company Eastern Laboratory Gibbstown, New Jersey 07036 Attn: Library	
1	Esso Research & Engineering Company Special Project Unit P.O. Box 8 Linden, New Jersey 07036 Attn: Library	
1	Commanding Officer U.S. Naval Underwater Ordnance Station Newport, Rhode Island 02844 Attn: Library	
1	FMC Corporation Chemical Research & Development Center P.O. Box 8 Princeton, New Jersey 08540	
1	Westinghouse Research Laboratory Beulah Road, Churchill Boro Pittsburgh, Pennsylvania 15235	
1	Cornell University Department of Materials Science & Engineering Ithaca, New York 14850 Attn: Library	